Weixing Cao
Jeffrey W. White
Enli Wang
Editors

Crop Modeling and Decision Support

TSINGHUA UNIVERSITY PRESS
Springer

Weixing Cao
Jeffrey W. White
Enli Wang

Crop Modeling and Decision Support

Weixing Cao
Jeffrey W. White
Enli Wang

Crop Modeling and Decision Support

With 175 figures

TSINGHUA UNIVERSITY PRESS

Springer

Editors
Weixing Cao
Nanjing Agricultural University
210095 Nanjing
P.R.China
E-mail: caow@njau.edu.cn

Jeffrey W. White
USDA ARS, ALARC
21881 N Cardon Lane
Maricopa, AZ 85238, USA
E-mail: jeffrey.white@ars.usda.gov

Enli Wang
CSIRO Land and Water
GPO Box 1666
Canberra ACT 2601
E-mail: enli.wang@csiro.au

ISBN 978-7-302-19333-3
Tsinghua University Press, Beijing

ISBN 978-3-642-01131-3 e-ISBN 978-3-642-01132-0
Springer Dordrecht Heidelberg London New York

Library of Congress Control Number: pending

Cover design: Frido Steinen-Broo, EStudio Calamar, Spain

Printed on acid-free paper

Springer is part of Springer Science + Business Media (www.springer.com)

Preface

Crop models and decision tools are increasingly affecting agriculture. Various forms of information technology are being adopted in agriculture as modern technology advances. To review research achievements and identify new directions in crop modeling and decision support, an international symposium on crop modeling and decision support was held in Nanjing, China in April, 2008. The main purposes of this symposium were to exchange the state-of-the art of current modeling and simulation approaches, as well as recent progress on crop models and decision support systems leading to on-farm applications; to explore future directions needed for advancement and potential opportunities for team collaboration.

The symposium was successfully held with a grand gathering of about 120 scientists and researchers from more than 20 countries. Over 100 abstracts and 40 papers were presented at the meeting, and selected papers were combined into this book as the symposium proceeding, in addition to some papers submitted for journal publication. Thus, the present book is a main output of the symposium, and should be useful for the scientists, graduate students and management specialists in the areas of crop modeling and decision support.

This proceeding book covers cutting-edge results on crop growth modeling, decision support system and model-based information technologies for crop growth prediction and production management. It covers the subjects of crop and soil process modeling, plant architectural modeling, climate change modeling, crop productivity modeling, simulation model development, model-based decision support systems (DSS), applications of crop models and DSS, integration of crop models with other information technologies.

We would like to express our gratitude to all the participants for their participations and presentations at the symposium. Great thanks go to the Academic Committee of the symposium for their great efforts and hard work, to Drs Qi Jing and Liang Tang as the secretaries of the symposium, and to Drs Yan Zhu, Yongchao Tian, XiaoJun Liu and Xia Yao for their hard work during the symposium. We also thank the sponsors for their generous supports making the symposium successful.

Editors

International Symposium on Crop Modeling and Decision Support (ISCMDS 2008)

April 19-22, 2008, Nanjing, China

Academic Committee

Dr. Senthold Asseng, CSIRO, Australia
Dr. Bas Bouman, International Rice Research Institute (IRRI)
Prof. Weixing Cao, Nanjing Agricultural University, China
Dr. Michael Dingkuhn, CIRAD, France
Prof. Graeme Hammer, University of Queensland, Australia
Dr. Toshihiro Hasegawa, Agro-Meteorology, NIAES, Japan
Prof. Gerrit Hoogenboom, University of Georgia, USA
Prof. Baoguo Li, China Agricultural University, China
Dr. Gregory S. McMaster, USDA-ARS, Fort Collins, Colorado, USA
Prof. John Porter, University of Copenhagen, Denmark
Prof. Herman van Keulen, Wageningen University, The Netherlands
Dr. Jan Vos, Wageningen University, The Netherlands
Dr. Enli Wang, CSIRO, Australia
Dr. Jeffrey W. White, Arid-Land Agricultural Research Center, USDA-ARS, USA
Dr. Xinyou Yin, Wageningen University, The Netherlands
Dr. Chunjiang Zhao, NERCITA, Beijing, China

Sponsors

Agricultural Production Systems Research Unit (APSRU), Australia
Agricultural Systems Research Unit, USDA-ARS
American Society of Agronomy
Australian Society of Agronomy
China Agricultural University
Chinese Academy of Agricultural Sciences
Chinese Society of Agronomy
Commonwealth Scientific and Industrial Research Organisation, Australia
European Society of Agronomy
Expert Group of Modern Agriculture, National Hi-Tech R&D Program of China
International Consortium for Agricultural Systems Applications
Modeling and Simulation Society of Australia and New Zealand (MSSANZ)
Nanjing Agricultural University
National Engineering Research Center for Information Technology in Agriculture
National Natural Science Foundation of China

Organizer

Nanjing Agricultural University

Contents

Whole Model Development and Applications

Modeling Time of Seedling Emergence of Spring Wheat

H. Wang[1,2], H. Cutforth[1], T. McCaig[1], G. McLeod[1], K. Brandt[1],
R. Lemke[1], T. Goddard[3], C. Sprout[3]

(1 Semiarid Prairie Agricultural Research Centre, Agriculture and Agri-Food Canada, Box 1030, Swift Current, Saskatchewan, S9H 3X2, Canada)
(2 Corresponding author. E-mail: wangh@agr.gc.ca)
(3 Alberta Agriculture and Food, #206, 7000 - 113 Street, Edmonton, Alberta, T6H 5T6, Canada)

Abstract: The timing of seedling emergence affects growth and yield of wheat (*Triticum aestivum* L.) greatly and a good growth model should predict it accurately. The Cropping System Model of The Decision Support System for Agrotechnology Transfer (DSSAT-CSM) is used worldwide for many different applications, but its simulation on the timing of seedling emergence of wheat is not satisfactory. In order to improve the prediction of seedling emergence, we incorporated a newly developed emergence model, Beta model, into DSSAT-CSM. Simulation performances were tested using observations of spring wheat (cv. Thatcher) from 24 sites across North America from 1930 to 1954 which totalled 244 site-years. Observed days from seeding to seedling emergence (DSE) ranged from 5 to 39 days. The unmodified DSSAT-CSM underestimated DSE in most cases (the mean difference (M) and root mean square error (RMSE) between simulated and measured DSE were -4.8 and 5.8 days, respectively). The modified DSSAT-CSM improved prediction of seedling emergence markedly. The performance of modified model using soil temperature at seeding depth was not as good as that using air temperature, which was caused by the inaccuracy of soil temperature simulation. Under some circumstances, the model also underestimated soil water content, which may cause an increase in simulated DSE. The modified model using simulated hourly air temperature was slightly better than that using daily temperature (M and RMSE were 0.3 and 3.3 days, respectively).

Keywords: seedling emergence, growth model, phenology, wheat, modeling

Abbreviations: days from seeding to seedling emergence (DSE); The Decision Support System for Agrotechnology Transfer-Cropping System Model (DSSAT-CSM)

1 Introduction

The timing of seedling emergence is an important factor in determining phenological development, growth and grain yield of wheat (*Triticum aestivum* L.) (Forcella et al., 2000; Gan et al., 1992). The accuracy of emergence prediction is also crucial for the performance of growth models.

The Decision Support System for Agrotechnology Transfer-Cropping System Model (DSSAT-CSM) is used worldwide for many different applications (Jones et al., 2003). In DSSAT-CSM, the seedling emergence of cereal crops is calculated by thermal time which is adjusted by a soil water factor, assuming that the adjusted thermal time is linearly related with the emergence process (Ritchie, 1991). The water factor for emergence is defined as the ratio of soil water potential at seeding depth to the upper limit on a scale from 0 to 1 with 0 being water stress that entirely inhibits the emergence process and 1 representing no water stress. Jame and Cutforth (2004), however,

indicated that the response of plant development rate to temperature is curvilinear. They developed a model (Beta model) to simulate seedling emergence of wheat under the effect of temperature using a series of beta functions. The Beta model predicted the time required for seedling emergence agreed reasonably well with the observed times under several controlled environments and field conditions (Jame and Cutforth, 2004).

Because the emergence process is directly affected by the soil environment, using soil temperature at seeding depth to simulate emergence is considered to be better than using air temperature by some authors (Jame and Cutforth, 2004; Lindstrom et al., 1976). McMaster and Wilhelm (1998), however, found that using soil temperature did not improve prediction of winter wheat phenology significantly when compared with that using air temperature.

Although many models use daily average temperature to simulate seedling emergence (McMaster and Wilhelm, 1998; Williams et al., 1989), modeling using a shorter time step is recommended by some authors (Shaykewich, 1995; Jame et al., 1999). Xue et al. (2004), however, found no significant improvement in the prediction of the Haun stage of winter wheat using hourly air temperature compared with using daily mean air temperature.

The objectives of this paper were to investigate if the modification of DSSAT-CSM by using the Beta model could improve seedling emergence prediction of a spring wheat cultivar under various environments in North America and to test if the model is improved by using simulated soil temperature at seeding depth or hourly air temperature as compared with that using daily air temperature to simulate seedling emergence.

2 Materials and Methods

Observations of seedling emergence

From 1930 to 1954, phenological development, including seedling emergence, heading and maturity, of a hard red spring wheat were observed at 32 sites across North America (Nuttonson, 1955). Among them were 24 sites where emergence was recorded for more than one year and weather data was available either on-site or within 100 km from the site. These 24 sites totalled 244 site-years of emergence observations that were used for this study (Table 1).

Table 1 Information of sites used in this study

Site	Province/State	Latitude ^{o}N	Longitude ^{o}E	Elevation m	Soil Zone
Fort Simpson	NW	61.9	121.4	169	Grey
Beaverlodge	AB	55.2	119.4	732	Grey
Edmonton	AB	53.6	113.4	671	Black
Melfort	SK	52.9	104.6	480	Black
Lacombe	AB	52.5	113.7	860	Black
Saskatoon	SK	52.2	106.8	501	Dark Brown
Indian Head	SK	50.6	103.7	586	Black
Regina	SK	50.5	104.6	577	Dark Brown
Swift Current	SK	50.4	107.9	825	Brown
Brandon	MB	49.9	100.0	363	Black
Morden	MB	49.2	98.1	297	Black
Langdon	ND	48.8	98.4	492	Black
Havre	MT	48.6	109.7	796	Brown

(Continued)

Site	Province/State	Latitude °N	Longitude °E	Elevation m	Soil Zone
Williston	ND	48.2	103.6	595	Brown
Moccasin	MT	47.0	109.8	1311	Brown
Fargo	ND	46.9	96.8	291	Black
Dickinson	ND	46.9	102.8	750	Brown
Mandon	ND	46.8	100.9	533	Brown
Bozeman	MT	45.7	111.1	1480	Brown
Sheridan	WY	44.9	106.9	1143	Brown
Brookings	SD	44.3	96.8	736	Black
Madison	WI	43.1	89.5	250	Black
Alliance	NE	42.2	102.9	1217	Brown
Lincoln	NE	40.9	96.6	491	Black

The cultivar was Thatcher, which was one of the first wheat cultivars specifically bred for stem rust resistance (Hayes et al., 1936) and was widely used as a resistant parent in subsequent breeding programs in North America (Humphreys et al., 2007; Kerber and Aung, 1999; Kolmer et al., 1991). Other physiological characteristics of Thatcher are standard height (Rashid and Halloran, 1984), vernalization insensitive (Flood and Halloran, 1986), photoperiod sensitive (Klaimi and Qualset, 1973) and, relatively short green flag leaf duration (Blake et al., 2007).

Because the information on crop management is limited (Nuttonson, 1955) we assume that ① the seedling emergence was defined to occur when the tip of the first leaf emerges from the soil surface for 50% of the plant population; ② the management was fallow-wheat rotation under conventional tillage; ③ the seeding depth was 5 cm; and ④ no fertilizer was added to the soil as latent fertility was thought to be adequate at that time.

The Beta Model

Jame and Cutforth (2004) separated the period between seeding and emergence of wheat into three consecutive processes: germination, subcrown internode elongation if seeding depth is deeper than 2.5 cm, and coleoptile elongation. The rates (DR) of germination (day^{-1}) and coleoptile elongation ($mm\ day^{-1}$) were calculated by the following beta function:

$$\mathrm{DR} = \mathrm{EXP}(\mu) \times (T - T_b)^{\alpha} \times (T_c - T)^{\beta} \quad (1)$$

where T is temperature in °C ($T_b < T < T_c$), T_b and T_c are base and upper critical temperatures, respectively, μ, α and β are the model parameters.

The rate of subcrown internode elongation ($mm\ day^{-1}$) was expressed as a function of temperature and the length of the subcrown internode (IL, mm):

$$\mathrm{DR} = A - B \times \mathrm{IL} \quad (2)$$

where

$$A = \mathrm{EXP}(\mu 1) \times (T - T_b)^{\alpha} \times (T_c - T)^{\beta} \quad (3)$$

$$B = \mathrm{EXP}(\mu 2) \times (T - T_b)^{\alpha} \times (T_c - T)^{\beta} \quad (4)$$

and

$$IL = \text{seeding depth (mm)} - 25 \quad (5)$$

Model Parameterization

Jame and Cutforth (2004) used data of two Australian cultivars (a winter type and a spring type) from Addae and Pearson (1992) and one Canadian cultivar, Neepawa, from Lafond and Baker (1986) to parameterize the equation of germination and used data of one Canadian cultivar, Canthatch, from de Jong and Best (1979) to parameterize equations of subcrown internode and coleoptile elongations. Both Neepawa (Campbell, 1970) and Canthatch (Campbell, 1963) are closely related to Thatcher (Hayes et al., 1936). According to Fig. 1 of Jame and Cutforth (2004) Neepawa clearly had lower germination rates than the Australian cultivars at temperature between 0 and 20 ^{o}C, indicating different temperature response curves between cultivars. We, therefore, only used data for Neepawa to fit the response curves of germination.

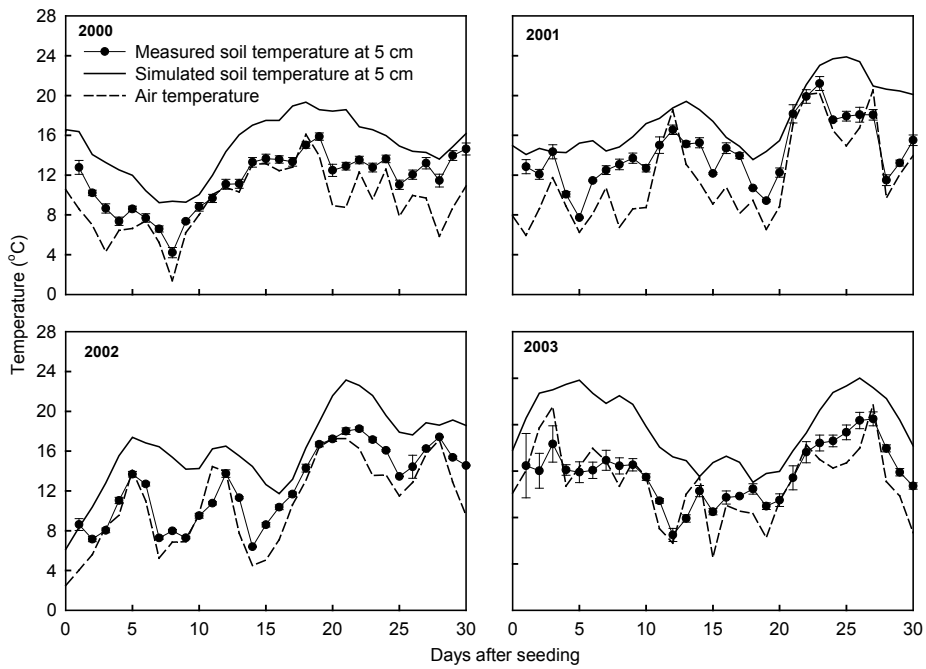

Figure 1 Measured and simulated soil temperatures at 5 cm under conventional tillage and air temperature. Bars are standard errors of measured soil temperature

The base temperature and T_c were set as 0 and 42℃, respectively, by Jame and Cutforth (2004). Many studies found that the T_b was above 0℃ (Addae and Pearson, 1992; de Jong and Best, 1979; Seefeldt et al., 2002; Angus et al., 1981). Although using 0℃ as T_b is often sufficient for most purposes (McMaster, 2005), it is not appropriate for identifying the cultivar difference in germination rate at low temperatures (Seefeldt et al., 2002). We used 1 and 39℃ as T_b and T_c, respectively, based on a Petri plate study for Neepawa (Wang and McCaig, unpublished data). The Beta model was re-parameterized using the same data used by Jame and Cutforth (2004) without the non-North American cultivars using nonlinear regression analysis (PROC NLIN, SAS Institute Inc., 1999).

Weather and Soil Data

The DSSAT-CSM requires weather data of daily maximum and minimum air temperatures, precipitation and solar radiation. Temperatures and precipitation for the United States of America

were downloaded from United States Historical Climatic Network available on the National Climatic Data Centre website (National Climatic Data Centre, 2008) while Canadian meteorological data were downloaded from the Agriculture and Agri-Food Canada (AAFC) Daily Climate Information website (Agriculture and Agri-Food Canada, 2006). Daily solar radiations were calculated using the Mountain Climate Simulator (Hungerford et al., 1989; Thornton et al., 2000). The hourly air temperature was calculated based on the maximum and minimum air temperatures and day length (Parton and Logan, 1981) in the subroutine HTEMP of DSSAT-CSM.

The DSSAT-CSM also requires soil physical and chemical properties of the soils the crops are to be grown on. These data were downloaded from the United States Department of Agriculture Natural Resources Conservation Service soil survey characterization data website (United States Department of Agriculture—Natural Resources Conservation Service 2008) and AAFC Soil Landscapes of Canada website (Agriculture and Agri-Food Canada, 2007).

Incorporation with DSSAT-CSM

The parameterized Beta model was incorporated into DSSAT-CSM to simulate the emergence of wheat. The simulated emergence rate was adjusted by the soil water factor calculated by DSSAT-CSM. The models were run by the sequence mode. For each site there were two sequence files, odd year wheat and even year wheat which allowed wheat to be simulated for each year under fallow-wheat rotations. Simulations started two years prior to the years with emergence observations in order to reduce the error of inputs of initial soil conditions. The original DSSAT-CSM and modified DSSAT-CSM using daily air temperature, soil temperature at seeding depth, hourly air temperature and hourly air temperature without the adjustment of the soil water factor, were run separately in order to compare their performances of emergence simulation.

Model Evaluation

Comparisons of the Beta model parameterizations between Jame and Cutforth (2004) and this study and comparisons of seedling emergence simulations among the various models mentioned above were assessed by their consistent errors (mean difference, *M*) (Addiscott and Whitmore, 1987), associations (Pearson's correlation, *r*) (Draper and Smith, 1966), and coincidences (root mean square errors, RMSE) (Loague and Green, 1991) between simulated and measured values using SAS (SAS Institute Inc., 1999).

Simulations of soil temperature and moisture with DSSAT-CSM were assessed because they may affect the performance of emergence prediction. Data were measured from wheat plots of a long-term experiment located on a Thin Black Chernozemic clay loam near Three Hills, Alberta (51°42' N, 113°13' W, 907 m) between 2000 and 2003. Details of this study have been reported by Wang et al. (2007). Soil temperatures at seeding depths (5 cm) were measured during the periods of seeding to emergence using TMC20-HA temperature sensors and were recorded by HOBO H8 data loggers (Onset Computer Corporation, Bourne, MA). Soil moistures at 0 – 15 cm in 2000 and at 0 – 6 cm in the other three years were measured by a travel time-based time domain reflectometry sensor, Trase BE probe (Soilmoisture Equipment Corp., California, U.S.A) and an impedance-based sensor, ML2 Theta probe (Delta-T Devices Ltd., Cambridge UK), respectively. Simulated daily soil temperature and moisture were compared with observations and their standard errors.

3 Results and Discussion

Table 2 showed that the parameterized Beta model using 1 and 39℃ as T_b and T_c, respectively, improved curve fittings for the all three emergence processes in term of the three indicators (lower *M* and RMSE and higher *r*) compared to using 0 and 42℃ as T_b and T_c, respectively, by Jame and Cutforth (2004).

Over all years and locations of this study, days from seeding to seedling emergence (DSE) ranged from 5 to 39 days and averaged 12.2 days. The unmodified DSSAT-CSM underestimated DSE in most cases (94% site-years) and averaged 4.8 days less than the observations (Table 3). The close correlation between measured and simulated DSE, however, indicates that the structure of the model is sound and could be improved (Smith et al., 1996).

Table 2 Parameters of the Beta model obtained by Wang et al. (2008)

Germination[1]	
μ	− 4.63
α	1.27
β	0.119
M (day^{-1})	− 0.0
r (n = 10)	0.99***
RMSE (day^{-1})	0.04
Coleoptile elongation[2]	
μ	− 1.0164
α	0.8207
β	0.26
M (mm day^{-1})	− 0.01
r (n = 4)	0.99***
RMSE (mm day^{-1})	0.24
Subcrown internode elongation[2]	
μ1	− 2.8681
μ2	− 7.8401
α	1.6
β	0.697
M (mm day^{-1})	0.03
r (n = 8)	0.99***
RMSE (mm day^{-1})	0.24

*** Significant at the 0.001 level.

M: mean difference, *r*: Pearson's correlation, RMSE: root mean square error.

The modified model using daily and hourly air temperature markedly improved simulations (Table 3). The modified model using simulated daily soil temperature at seeding depth also improved simulation in terms of *M* and RMSE (Table 3), but not as much as the model using air temperatures. It also tended to underestimate DSE in most cases (77%) and averaged 3.2 days less than observations. This is surprising, considering that soil temperature should better reflect seed environment than air temperature. Figure 1 showed that the model tended to overestimate soil temperature at seeding depth (5 cm). Although the air temperature tended to be lower than soil temperature at seeding depth, the difference of soil temperature at seeding depth from air temperature was often smaller than that from the simulated soil temperature. It seems that the relatively poor prediction of DSE by simulated soil temperature compared with that by air temperature is associated with the inaccuracy of soil temperature simulation.

Although the modified model using simulated hourly air temperature was only slightly better than that using daily temperature (Table 3), it is preferable because of the large diurnal variation in temperature and the nonlinear nature of the response of emergence process to temperature.

Table 3 Mean difference (*M*), Pearson's correlation (*r*), and root mean square error (RMSE) between simulated and measured days from seeding to seedling emergence

Module	*M* day	*r* (*n*=244)	RMSE day
DSSAT-CSM	– 4.8	0.59***	5.8
Beta model with daily soil temperature without water stress	– 3.5	0.59***	4.8
Beta model with daily soil temperature and water stress	– 3.2	0.56***	4.7
Beta model with daily air temperature without water stress	0.1	0.64***	3.3
Beta model with daily air temperature and water stress	0.5	0.64***	3.4
Beta model with hourly air temperature without water stress	– 0.1	0.66***	3.1
Beta model with hourly air temperature and water stress	0.3	0.64***	3.3

*** Significant at the 0.001 level.

Over the 244 site-years, calculated water stress for emergence occurred in 27 site-years (11%) which averaged 0.84. Obviously, soil temperature was the major factor controlling the simulated seedling emergence. The modified model using hourly air temperature without the adjustment of water factor achieved a little better simulation of emergence compared with other alternatives (Table 3). It is probably associated with the fact that wheat can germinate under relatively dry conditions. Previous studies found that soil moisture at or even below the permanent wilt point has little effect on rate of emergence of wheat (Owen, 1952; Lafond and Fowler, 1989). Another possible reason is that the simulation of soil moisture may not very accurate under certain circumstances. Figure 2 indicated that DSSAT-CSM simulated soil moisture during seedling emergence quite well in 2000 and 2001, but tended to underestimate soil water content in 2002 and 2003. When the underestimation of soil moisture at seeding depth is very large, it may reduce the water factor for seedling emergence significantly and increase the simulated DSE.

Figure 3 demonstrated that the modified model using hourly air temperature without consideration of water stress simulated wheat seedling emergence well at most sites. It seems that the model is

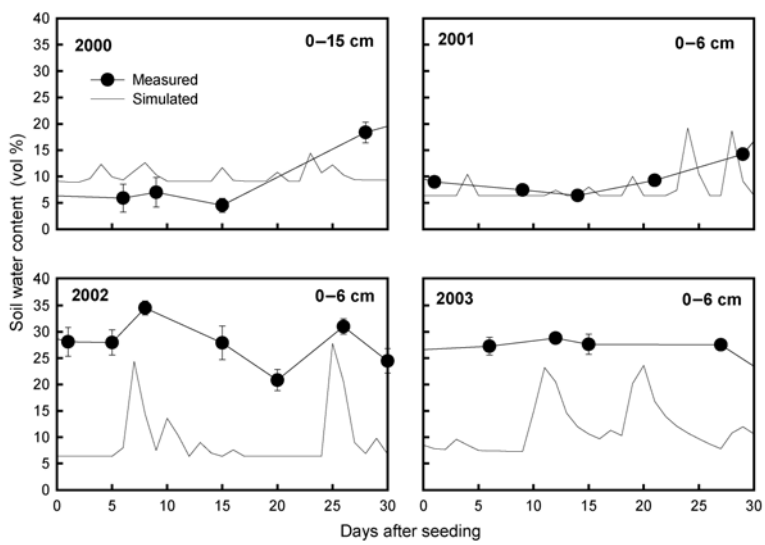

Figure 2 Measured and simulated soil water content under conventional tillage. In 2000, soil water was measured in the depth of 0 – 15 cm using a time domain reflectometry probe. In other years, soil water was measured at the depth of 0 – 6 cm with a Theta probe

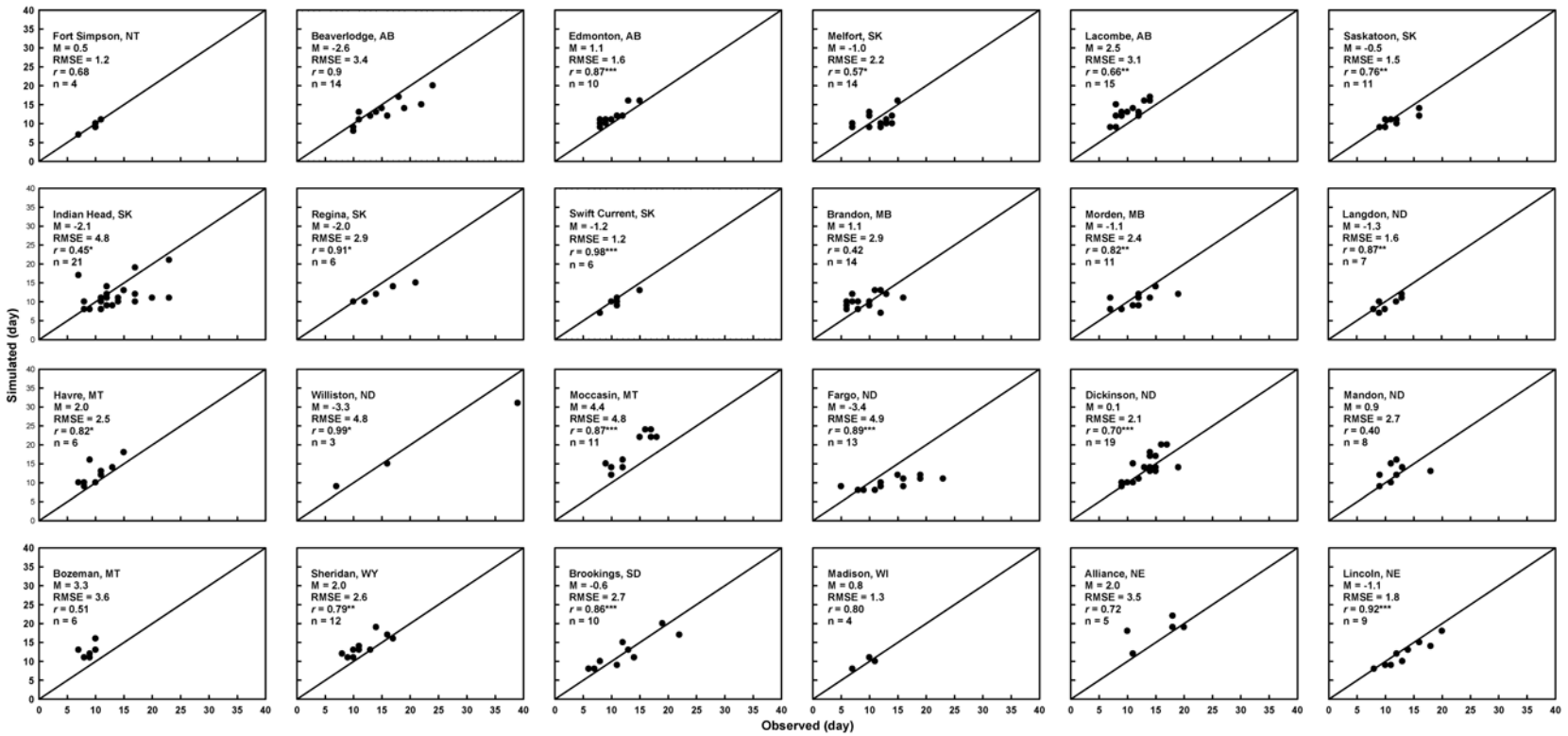

Figure 3 Observed vs. simulated days from seeding to seedling emergence of wheat at different sites. Simulations were done using DSSAT-CSM incorporated with Beta model using hourly air temperature without consideration of soil water stress. Solid lines are 1:1 lines. *M*: mean difference. RMSE: root mean square error. *r*: Pearson's correlation. *, **, *** Significant at the 0.05, 0.01 and 0.001, respectively

able to predict seedling emergence of wheat reasonably well under different weather and soil conditions. Relatively poor simulations were found, however, at two sites:

Indian Head, SK and Fargo, ND-where SEDs were not controlled by temperature or moisture. Other factors may affect the seedling emergence. The clay contents at seeding depth are relatively high at those two sites (67% at Indian Head, SK. and 37% at Fargo, ND), which could cause soil compaction (McGarry, 1987) and crusting (Sheldon, 1974) under certain conditions; and therefore, delay the seedling emergence. The DSSAT-CSM does not simulate the effect of seedbed condition on seedling emergence.

In conclusion, the DSSAT-CSM incorporated with Beta model improved the prediction of seedling emergence of wheat. Further work is needed to improve soil temperature and moisture simulations. Then, the model can use them to predict seedling emergence. Some other factors impacting seedling emergence such as soil surface properties should be added into the model.

Acknowledgements

The authors of this paper would like thank Drs. Gerrit Hoogenboom, Jeffrey White, Tony Hunt and Ken Boote for their help with the DSSAT-CSM. We also thank Alvin Anderson, Michael Bock and Wally Fraser from the Land Resource Unit with AAFC-AAC for their assistance with data collection. Special thanks go to our coop student Jae Hoon Saul for his help in data manipulation and model operation.

References

Addae PC and Pearson CJ (1992) Thermal requirements for germination and seedling growth of wheat. Aust. J. Agric. Res. 43: 585 – 594.

Addiscott TM and Whitmore AP (1987). Computer simulation of changes in soil mineral nitrogen and crop nitrogen during autumn, winter and spring. J. Agric. Sci. Camb. 109: 141 – 157.

Agriculture and Agri-Food Canada (2006). Daily Climate Information (Online) Available: http://sisintrpd.agr.gc.ca/cansis/nsdb/climate/wthr_query.html (2008 Jan. 04).

Agriculture and Agri-Food Canada (2007). Soil Landscapes of Canada Version 3.1.1 (Online) Available: http://sis.agr.gc.ca/cansis/nsdb/slc/v3.1.1/intro.html (2008 Feb. 14).

Angus JF, Cunningham MW and MacKenzie DH (1981). Phasic development in field crops. I. Thermal response in the seedling stage. Field Crops Res. 3: 365 – 378.

Blake NK, Lanning SP, Martin JM et al. (2007). Relationship of flag leaf characteristics to economically important traits in two spring wheat crosses. Crop Sci. 47: 491 – 494.

Campbell AB (1963). Registration of Pembina and Canthatch Wheats (Reg. Nos. 422 and 423). Crop Sci. 3: 457 – 458.

Campbell AB (1970). Neepawa hard red spring wheat. Can. J. Plant Sci. 50: 752 – 753.

de Jong, R. and Best, K. F. (1979). The effect of soil water potential, temperature and seedling depth on seedling emergence of wheat. Can. J. Soil Sci. 59: 259 – 264.

Draper NR and Smith H (1966). Applied Regression Analysis. Wiley and Sons, New York. 407 pp.

Flood RG and Halloran GM (1986). Genetics and physiology of vernalization response in wheat. Adv. Agron. 39: 87 – 125.

Forcella F, Arnold RLB, Sanchez R et al. (2000) Modeling seedling emergence. Field Crops Res. 67: 123 – 139.

Gan Y, Stobe EH and Moes J (1992) Relative date of wheat seedling emergence and its impact on grain yield. Crop Sci. 32: 1275 – 1281.

Hayes HK, Ausemus ER, Stakman ECet al. (1936) Thatcher wheat. Univ. of Minn. Agri. Experiment Station, Bull. No. 325.

Humphreys DG, Townley-Smith TF, Czarnecki E et al. (2007) Snowbird hard white spring wheat. Can. J. Plant Sci. 87: 301 – 305.

Hungerford RD, Running SW, Nemani RR et al. (1989) MTCLIM: A mountain microclimate extrapolation model. U.S. Forest Service. Res. Paper INT-414 52 pp.

Jame YW and Cutforth HW (2004) Simulating the effects of temperature and seeding depth on germination and emergence of spring wheat. Agric. For. Meteorol. 124: 207 – 218.

Jame YW, Cutforth HW and Ritchie JT (1999) Temperature response function for leaf appearance rate in wheat and corn. Can. J. Plant Sci. 79: 1 – 10.

Jones JW, Hoogenboom G, Porter CH, Boote et al. (2003) The DSSAT cropping system model. Eur. J. Agron. 18: 235 – 265.

Kerber ER and Aung T (1999) Leaf rust resistance gene Lr34 associated with nonsuppression of stem rust resistance in the wheat cultivar Canthatch. Phytopathology. 89: 518 – 521.

Klaimi YY and Qualset CO (1973) Genetics of heading time in wheat (*Triticum Aestivum* L.). I. The inheritance of photoperiodic response. Genetics 74: 139 – 156.

Kolmer JA, Dyck PL and Roelfs AP (1991) An appraisal of stem and leaf rust resistance in North American hard red spring wheats and the probability of multiple mutations to virulence in populations of cereal rust fungi. Phytopathology. 81: 237 – 239.

Lafond GP and Baker RJ (1986) Effects of temperature, moisture stress, and seed size on germination of nine spring wheat cultivars. Crop Sci. 26: 563 – 567.

Lafond GP and Fowler BD (1989) Soil temperature and water content, seeding depth, and simulated rainfall effects on winter wheat emergence. J. Agron. 81: 609 – 614.

Lindstrom MJ, Papendick RI and Koehler FE (1976) A model to predict winter wheat emergence as affected by soil temperature, water potential, and depth of planting. J. Agron. 68: 137 – 141.

Loague K and Green RE (1991) Statistical and graphical methods for evaluating solute transport models: overview and application. J. Contam. Hydrol. 7: 51 – 73.

McGarry D (1987) The effects of soils water content during land preparation on soil physical condition and cotton growth. Soil Till. Res. 9: 287 – 302.

McMaster GS and Wilhelm WW (1998) Is soil temperature better than air temperature for predicting winter wheat phenology? J. Agron. 90: 602 – 607.

McMaster GS (2005) Phytomers, phyllochrons, phenology and temperate cereal development. J. Agric. Sci. 143: 137 – 150.

National Climatic Data Centre. 2008. USHCN Daily Weather Data (Online) Available: ftp://ftp.ncdc.noaa.gov/pub/data/ushcn/daily [2008 Jan. 08].

Nuttonson MY (1955) Wheat-climatic relationships and the use of phenology in ascertaining the thermal and photothermal requirements of wheat. Washington, DC, American Institute of Crop Ecology. Washington, D.C. 388 pp.

Owen PC (1952) The relation of germination of wheat to water potential. J. Exp. Bot. 3: 188 – 203.

Parton, W. J. and Logan, J. A. (1981) A model for diurnal variation in soil and air temperature. Agric. Meteorol. 23: 205 – 216.

Rashid AH and Halloran GM (1984) Influence of photoperiod on culm elongation and apical development in semi-dwarf and standard-height wheats. Ann Bot. 54: 375 – 382.

Ritchie JT (1991) Wheat phasic development. p. 31 – 54. *In* Hanks, R.J., Ritchie, J.T. (Ed) Modeling Plant and Soil Systems. Agron. Monogr. 31, ASA, CSSSA, SSSA, Madison, WI.

SAS Institute Inc. (1999) SAS Procedures Guide, Version 8. SAS Institute Inc. Cary, NC, U.S.A.

Seefeldt SS, Kidwell KK and Waller JE (2002) Base growth temperatures, germination rates and growth response of contemporary spring wheat (Triticum aestivum L.) cultivars from the US Pacific northwest. Field Crops Res. 75: 47 – 52.

Shaykewich CF (1995) An appraisal of cereal crop phenology modeling. Can. J. Plant Sci. 75: 329 – 341.

Sheldon JC (1974) The behaviour of seeds in soil: III. The influence of seed morphology and the behaviour of seedlings on the establishment of plants from surface-lying seeds. J. Ecol. 62: 47 – 66.

Smith J, Smith P and Addiscott T (1996) Quantitative methods to evaluate and compare soil organic matter (SOM) models. p. 81–98. *In* D.D. Powlson et al. (ed.) Evaluation of soil organic matter models using existing long-term datasets. NATO ASI Series I, Vol. 38. Springer-Verlag, Heidelberg.

Thornton PE, Hasenauer H and White MA (2000) Simultaneous estimation of daily solar radiation and humidity from observed temperature and precipitation: an application over complex terrain in Austria. Agric. For. Meteorol. 104: 255 – 271.

United States Department of Agriculture—Natural Resources Conservation Service. (2008) National soil survey characterization data [Online] Available: http://ssldata.nrcs.usda.gov/querypage.asp (2008 Feb. 04).

Wang H, Lemke R, Goddard T et al.(2007) Tillage and root heat stress in wheat in Central Alberta. Can. J. Soil Sci. 87: 3 – 10.

Williams JR, Jones CA, Kiniry JR et al.(1989) The EPIC crop growth model. Trans ASAE. 32: 497 – 511.

Xue Q, Weiss A and Baenziger PS (2004) Predicting leaf appearance in field-grown winter wheat: evaluating linear and non-linear models. Ecol. Model. 175: 261 – 270.

Complete Parameterization of Photosynthesis Models —An Example for Barley

J. Müller, H. Braune, W. Diepenbrock

(Plant Systems Modeling and Ecophysiology Group Institute of Agricultural and Nutritional Sciences
Martin-Luther-University of Halle-Wittenberg Ludwig-Wucherer-Str. 2, D-06108 Halle/Saale,
Corresponding author E-mail: johannes.mueller@landw.uni-halle.de)

Abstract: Complete and robust parameterisation of biophysical CO_2 and H_2O gas exchange models is an essential requirement for its use as a sub-model of more complex crop models. Here, we address the following crucial points: ① effects of plant and leaf development and leaf insertion height on key model parameters (p), ② re-analysis of the parameters of the temperature response functions, ③ effects of leaf nitrogen content (N_a) and growth temperature (T_g) on p, and ④ required accuracy of parameter values and time resolution for calculating integrated daily carbon gain (IDC). With regard to these items, we developed an improved version of the LEAFC3-N model that was parameterised completely for barley. In particular, this version of the model accounts for effects of T_g on the parameters of the p–N_a relationships and on the activation energy parameter ΔH_a of the temperature response functions. Based on the derived p–N_a relationships, observed gas exchange patterns with respect to leaf senescence, leaf rank, and growth conditions were reproduced by the model fairly well. For calculating integrated daily carbon gain (IDC) with an accuracy of about ±5%, the accuracy of the slope of the V_{m25}-N_a and J_{m25}-N_a relationships should be of similar order, whereas an inaccuracy up to ±20% can be tolerated for the other parameters. With the given parameterisation, most accurate predictions of IDC will be obtained calculating net photosynthesis rate with high resolution in time (e.g., 1 to 15 min). However, up to a time step of about 1 to 2 h, the bias of IDC will not exceed 5%.

The analysis is part of a series of studies aiming to establish LEAFC3-N model versions adapted to different crop species. The parameters derived here for barley are close to those derived in our previous studies for leaves of wheat, leaves and pods of oilseed rape, and awns of barley. The model was successfully used as a sub-model of a canopy gas exchange model for oilseed rape and a Functional-Structural Plant Model for barley.

Keywords: leaf gas exchange, model parameterisation, C_3-plants, *Hordeum vulgare*

Symbols and abbreviations: A_g, A_n: gross or net photosynthesis rate (μmol m^{-2} s^{-1}); C_a: CO_2 concentration of ambient air (μmol mol^{-1}); BWB index: defined by A_g h_b / C_b; C_b: CO_2 concentration in the leaf-air boundary layer (μmol mol^{-1}); g_s, $g_{s,min}$: stomatal conductance or minimum g_s (mol m^{-2} s^{-1}); h_a: relative humidity of ambient air (%); h_b: relative humidity in the leaf-air boundary layer (decimal fraction); IDC: Integral daily carbon gain (mol C d^{-1}); J_{max}: light saturated rate of electron transport (μmol (e^-) m^{-2} s^{-1}); J_{m25}: J_{max} at 25 °C; m: slope of the relationship between g_s and BWB index (dimensionless); K_c, K_o: Michaelis-Menten constants of Rubisco for carboxylation and oxygenation of RuBP, respectively; N_a: leaf area based nitrogen content (g m^{-2}); $N_{a,min}$: minimum value of N_a, parameter in Eq. (1) (g m^{-2}); N_m: dry mass based nitrogen content (g g^{-1}); Q_i: incident photon flux density (μmol m^{-2} s^{-1}); R_{dark}: rate of mitochondrial respiration in the dark (μmol m^{-2} s^{-1}); RuBP: Ribulose-1,5-bisphosphate; Rubisco: Ribulose-1,5-bisphosphate carboxylase/oxygenase; s_{Na}: slope parameter in Eq. (1) (μmol g^{-1} s^{-1}); T_{air}: temperature

of ambient air (℃); T_g: growth temperature (℃); V_{cmax}: maximum carboxylation rate (μmol m^{-2} s^{-1}); V_{m25}: V_{cmax} at 25℃; I^*: CO_2 compensation concentration in the absence of mitochondrial respiration (μmol mol^{-1}); γ_{Na1}: parameter in Eq. (2) (mol (e^-) (mol (quanta))$^{-1}$); γ_{Na2}: parameter in Eq. (2) (m^2 g^{-1}); φ: quantum yield for electron transport (mol (e^-) (mol (quanta absorbed))$^{-1}$; ΔH_a: parameter related to activation energy (kJ mol^{-1}); δ_1: parameter of the θ–N_a relationship (m^2 g^{-1}); δ_2: parameter of the θ–N_a relationship (dimensionless); ε_1: coefficient in the parameter–T_g relationship ([unit of original parameter] K^{-1}); ε_2: coefficient in the parameter–T_g relationship (unit as original parameter); θ: curvature of the light dependence of electron transport rate (dimensionless).

1 Introduction

Including basic physiological, biochemical, and biophysical processes at organ or even cellular level into physiological submodels of complex crop growth models, modellers will have to deal with a large number of model parameters which often are difficult to determine. Thus, much more than with simple approaches like the radiation uses efficiency approach, over-parameterisation may become a problem and lead to difficulties in obtaining unique parameter solutions. Sophisticated numerical optimisation strategies may fail in solving such complex parameterisation problems (Mo and Beven, 2004). Thus, the only way to overcome these difficulties may be robust and, as far as possible, universal a-priori parameterisation of the individual sub-models included into comprehensive crop models.

In the present study we deal with a generalised parameterisation of the nitrogen-sensitive LEAFC3-N model of the coupled CO_2, H_2O, and radiation fluxes (Müller et al., 2005b). Previously, this model has been applied to leaves of winter wheat (*Triticum aestivum* L.) (Müller et al., 2005b), leaves and pods of oilseed rape (*Brassica napus* L.) (Müller and Diepenbrock, 2006), and awns of barley (*Hordeum vulgare* L.) (Braune et al., 2007). Here we discuss the complete parameterisation of this model for barley with special emphasis on the effects of leaf nitrogen content on key model parameters. The corresponding functions were included into the model since the variation of net photosynthesis rate with species, plant development, and growth conditions often was shown to be related to concurrent changes in leaf nitrogen content (e.g., Niinemets and Tenhunen, 1997; Medlyn et al., 1999; Meir et al., 2002). In addition, the effects of growth temperature on key model characteristics were analysed and included into the model. Finally, the conditions for using the model as a submodel of complex crop growth models will be discussed.

2 Model

LEAFC3-N is a nitrogen-sensitive extension of the generic steady-state flux model LEAFC3 (Nikolov et al., 1995) that couples major processes of CO_2 and H_2O gas exchange with stomatal function and the energy and mass transfer in the leaf-boundary layer.

The model core of LEAFC3 and LEAFC3-N combines the biochemical photosynthesis model of Farquhar et al (1980) (FCB model) and a stomatal conductance model as used also by several other advanced gas exchange models (e.g. Collatz et al., 1991; Harley et al., 1992; Friend, 1995; Leuning, 1995; Wohlfahrt et al., 1998). LEAFC3 and LEAFC3-N use the stomatal model of Ball et al. (1987) (BWB model). Here we will outline only main aspects of model formulation related to the present study. For more detail we refer to Nikolov et al (1995), Müller et al. (2005b) and Müller and Diepenbrock (2006). Main parameters of the net photosynthesis rate A_n (μmol m^{-2} s^{-1}) model part are: maximum carboxylation rate V_{cmax} (μmol m^{-2} s^{-1}), Michaelis-Menten constants of Rubisco for carboxylation and oxygenation of RuBP, K_c and K_o (μmol mol^{-1}), CO_2 compensation concentration

in the absence of mitochondrial respiration Γ^* (μmol mol^{-1}), light saturated rate of electron transport J_{max} (μmol (e$^-$) m^{-2} s^{-1}), quantum yield for electron transport φ (mol (e$^-$) (mol (quanta absorbed))$^{-1}$, curvature θ (dimensionless) of the light dependence of electron transport rate; and the rate of mitochondrial respiration in the dark R_{dark} (μmol m^{-2} s^{-1}). The parameters V_{cmax}, J_{max}, K_c, K_o, Γ^*, and R_{dark} are functions of temperature. The stomatal model part used by LEAFC3-N is a modified version of the BWB model and relates stomatal conductance g_s (mol m^{-2} s^{-1}) by a dimensionless scaling factor m to gross photosynthesis rate A_g (μmol m^{-2} s^{-1}) and to the ratio of air humidity and CO_2 concentration in the leaf boundary layer. Further, in the BWB model part a minimum value $g_{s,min}$ of g_s is considered.

In developing LEAFC3-N, parameter-nitrogen relationships were subjected to special analysis and included into the model for V_{cmax}, J_{max}, φ, θ, R_{dark}, and m.

3 Material and Methods

3.1 Experimental Design and Plant Material

From 2003 until 2005, spring barley (*Hordeum vulgare* L. cv. 'Barke') was grown in a series of 5 experiments (denoted as E1 to E5 hereafter). In E1 to E4, plants were cultivated in pots in an air-conditioned glasshouse (E1, uniculm plants, tillers removed) or in climatic chambers (E2-E4). In E5, plants were grown in field plots. In E1-E4, pots were filled with dry quartz sand mixed with water and nutrients (172 mg K as K_2SO_4, 42 mg Mg as $MgSO_4$, 31.4 g P as $Ca(H_2PO_4)_2$, 143 mg $CaCO_3$, 0.286 ml of $FeCl_3$ solution (7%), and 0.286 ml A-Z solution (a+b, after Hoagland and Snyder) per 1 kg dry sand). Nitrogen (N) fertilisation (as ammonium nitrate) was 200 mg N plant^{-1} (N200) in E1, 200 mg N plant^{-1} or 50 mg N plant^{-1} (N50) in E2, and 100 mg N plant^{-1} (N100) in E3 and E4.

In the glasshouse, average incident photon flux density (Q_i) at the top of the plants followed the typical seasonal pattern ($Q_{max} \approx 1000$ μmol m^{-2} s^{-1}), and CO_2 concentration, relative humidity and day/night temperatures of the air were maintained close to $C_a \approx 350$ μmol mol^{-1}, $h_a \approx 70\%$ and T_{air} = 22/16 ℃. In climatic chambers, plants were cultivated at 16 h photoperiod with Q_i = 380 μmol m^{-2} s^{-1} at plant height (Powerstar HQIT 250/D, OSRAM GmbH, München, Germany), relative air humidity (h_a) of 65 – 75%, average CO_2 concentration of the air $C_a \approx 350$ μmol mol^{-1}, and day/night air temperatures of 22°C/16℃ in E2, a constant growth temperature of 16℃ in E3, or three different growth temperature treatments of 13, 16, and 22 °C in E4. The pots were watered daily with deionized water to 60% of the maximum water holding capacity of the substrate. Pot positions were changed twice a week.

The field experiment (E5) was conducted at the experimental station Bad Lauchstaedt near Halle (Saale) in Central Germany (51°25′N, 11°45′E). The soil was a haplic Phaeozem. The seed was sown at the end of March; plant density after emergence was 280 plants m^{-2}. Nitrogen fertilisation was 0 (N0) or 60 kg N ha^{-1} (N60) (as calcium ammonium nitrate). The soil nitrogen content after winter was 60 kg ha^{-1} (soil layer 0 to 0.9 m). All other cultivation measures followed common practice. If required, plants were watered starting three days before the beginning of measurements (15 – 20 l m^{-2} day^{-1}).

3.2 Gas Exchange Measurements

CO_2 and water vapour exchange rates were measured with two infrared gas analyser leaf chamber systems (LI-6400, LI-COR, Inc., Lincoln, NE) on leaves of the main tiller (E1: leaf 3 to 10 (flag leaf); E2 and E5: leaf 4 and the leaf below the flag leaf, E3 and E4: leaf 4). In E1 and E2, we

measured maximum net photosynthesis rate ($A_{n,max}$) at saturating light (Q_i = 1500 µmol m^{-2} s^{-1}) and 380 µmol mol^{-1} CO_2 on 2 - 5 leaves, in E1-E5 additionally photosynthetic light response curves (A_n–Q_i curves) at Q_i = 0, 100, 250, 750, 1500 and 2500 (only E5) µmol m^{-2} s^{-1} and C_a = 380 µmol mol^{-1} and CO_2–response curves (A_n–C_i curves) at C_a = 70, 200, 300 and 400 µmol mol^{-1} in E1 and E2 or at 7 to 12 CO_2 steps from 50 to 1300 µmol mol^{-1} in E3-E5 at Q_i = 1500 µmol m^{-2} s^{-1} on 2 or 3 leaves. The other conditions were: h_a = 60 - 70%; T_{leaf} = 25℃ in E1 and E2, T_{leaf} = 10, 15 (only E3) 20, 25, 30, and 35℃ in E3 and E4 or 22℃ ±3 K in E5; O_2 = 21% and additionally 2% in E3-E5. The measurements were conducted once a week from leaf emergence until senescence. Leaves were adapted 15 minutes to chamber conditions; the equilibration time before data recording was 30 min in the dark, 25 min for every light step, and 60 – 180 s for every CO_2 step.

3.3 Supplementary Measurements

For the leaves used in gas exchange measurements we determined area, dry mass, and total dry mass based nitrogen content N_m[1] (g g^{-1}; Dumas combustion method; Vario EL, Elementaranalysensysteme GmbH, Hanau, Germany). From these data specific leaf mass (g m^{-2}) and leaf area based nitrogen content N_a (g m^{-2}) were calculated. Leaf chlorophyll content required as an input to the model for calculating absorbed photosynthetically active radiation was determined on intact leaves using the SPAD-502 spectral sensor (Minolta Co., Osaka, Japan) as described by Müller et al. (2005b).

3.4 Model Parameterisation

Photosynthesis Model Part

To estimate model parameters from data of E1 and E2, several basic parameters (in particular Γ^*, K_c, and K_o and the parameters of the temperature dependencies of V_{cmax}, J_{max}, K_c, K_o, Γ^*, and R_{dark} commonly assumed universal for C_3 plants were adopted from literature (Bernacchi et al., 2001; Leuning, 2002) as given in Müller et al. (2005b, table C1). Then, following Harley et al. (1992), Wohlfahrt et al. (1998), and Kosugi et al. (2003), V_{cmax}, φ, θ, and R_{dark} were estimated by fitting the related model equations to the A_n–Q_i and A_n–C_i response curve data for individual leaves as described previously (Müller et al., 2005b; Müller and Diepenbrock, 2006). In this procedure, J_{m25} was approximated by 2 V_{m25} (Leuning, 2002).

The data of E3 – E5 provided a basis to verify the assumptions made in E1 and E2 on Γ^*, K_c, and K_o and to estimate J_{max} as well as the activation energy coefficients of the temperature dependencies of V_{cmax}, J_{max}, K_c, K_o, Γ*, and R_{dark} (for detail, see (Braune, 2008)).

All parameter estimations were done using a numeric non-linear least-squares data-fitting approach (MATLAB® Optimisation Toolbox, The MathWorks, Inc., Natick, MA, USA, 2004). Then, from parameter values obtained this way for individual leaves with different nitrogen content, we estimated the coefficients of the parameter vs. N_a (p–N_a) relationships.

Stomatal Model Part

The parameters of the BWB model part, m and $g_{s,min}$, were specified as common from the linear regression of g_s on the so-called BWB index. The latter is defined here by $I_{BWB} = A_g\ h_b / C_b$, $I_{BWB} > 0$, were h_b and C_b are the relative humidity (decimal fraction) and the CO_2 concentration (µmol mol^{-1})

[1] Dr. K. Egle and Dr. H. Beschow, Institute of Agricultural and Nutritional Sciences, Group Plant Nutrition, Martin-Luther-University of Halle-Wittenberg, Halle (Saale), Germany.

in the leaf-air boundary layer, respectively (Ball et al., 1987; Collatz et al., 1991). In this analysis, the dependency of m on N_a was accounted for.

4 Results and Discussion

4.1 Parameter—Nitrogen Relationships

As shown by Fig. 1(a), the variation of maximum carboxylation rate V_{m25} (subscript 25: parameter at a reference temperature of 25°C) along with both leaf rank and leaf age could be attributed completely to concomitant changes in N_a. This correlation has a clear theoretical basis, since it is a well-known fact that most nitrogen in leaves is bound by Rubisco. The slope of the regression derived from the pooled data of E1 and E2 given in Fig. 1a amounted to 67 µmol (CO_2) g^{-1} (N) s^{-1} and thus in fact was similar to a theoretical estimate of 68 µmol (CO_2) g^{-1} (N) s^{-1} (cf. Müller et al, 2005). Unique p–N_a relationships were obtained also for the parameters φ (Fig. 1(b)) and θ (data not shown).

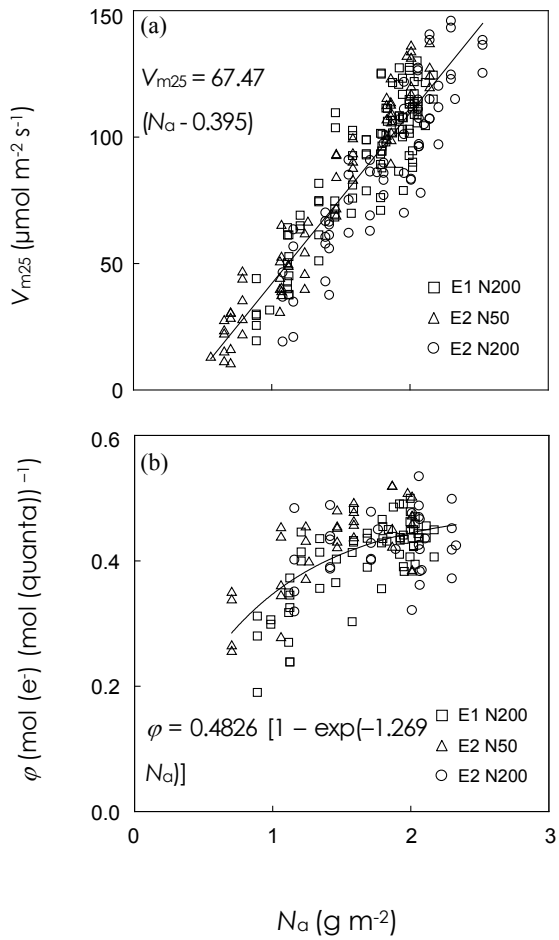

Figure 1 Nitrogen dependency of (a) maximum carboxylation rate V_{m25} and (b) maximum electron transport rate J_{m25}. The regressions were estimated from pooled data of E1 and E2

The above-discussed results were confirmed by recent measurements made in E3 to E5 (Braune, 2008). In that study, p–N_a relationships were derived also for J_{m25} and R_{d25} (R_{dark} at 25°C). In summarising the above-discussed experiments, the relationships between V_{m25}, J_{m25}, or R_{d25} and N_a can be expressed by the linear function:

$$p_{25} = \begin{cases} s_{Na}\left(N_a - N_{a,min}\right), & \text{if } N_a > N_{a,min} \\ 0, & \text{if } N_a \le N_{a,min}, \end{cases} \quad (1)$$

where p_{25} stands for V_{m25}, J_{m25}, or R_{d25}, s_{Na} (µmol g^{-1} s^{-1}) is the slope of the relationship, and $N_{a,min}$ is a minimum value of N_a at which p_{m25} approaches zero.
The φ–N_a relationship can be described by:

$$\varphi = \gamma_{Na1}\left[-\exp\left(-\gamma_{Na2}\ N_a\right)\right], \quad (2)$$

where γ_{Na1} (mol (e$^-$) (mol (quanta))$^{-1}$) is the value of φ at high N_a, and γ_{Na2} (m^2 g^{-1}) defines the curvature of the relationship. Note that in our previous analyses for wheat and rapeseed, due to the small number of data points, the φ–N_a relationship was approximated by a linear function (Müller et al 2005b; Müller and Diepenbrock 2006). However, that approximation neglected the fact that φ may be expected to tend to a maximum value slightly below 0.5 (mol (e$^-$) (mol (quanta))$^{-1}$ at high N_a (for further discussion, see Müller et al 2005b) and to zero if N_a equales zero as described correctly by Eq. (2). Summarising the results of E1-E5, appropriate parameter values recommended for use with Eqs. (1) and (2) and further parameter values discussed below were derived as given in Table 1.

Table 1 Recommended coefficients of the relationships between key model characteristics and leaf nitrogen content N_a or maximum carboxylation rate V_{m25}. The p–N_a or p–V_{m25} relationships may be used alternatively. For explanation see the list of used symbols and text

Relation	Equation	Parameter	Unit	Value
V_{m25} vs. N_a	1	s_{Na}	µmol g^{-1} s^{-1}	67
		$N_{a,min}$	g m^{-2}	0.3
J_{m25} vs. N_a	1	s_{Na}	µmol g^{-1} s^{-1}	151
		$N_{a,min}$	g m^{-2}	0.225
J_{m25} vs. V_{m25}	$J_{m25} = s_{Vc} V_{m25}$	s_{Vc}	mol (e$^-$) (mol (CO_2))$^{-1}$	2.2
φ vs. N_a	2	γ_{Na1}	mol (e$^-$) (mol (quanta))$^{-1}$	0.44
		γ_{Na2}	m^2 g^{-1}	2.3
R_{d25} vs. N_a	1	s_{Na}	µmol g^{-1} s^{-1}	0.6
		$N_{a,min}$	g m^{-2}	0.12
R_{d25} vs. V_{m25}	1	s_{Na}	–	0.006
		$V_{m25,min}$	µmol m^{-2} s^{-1}	0.3
θ vs. N_a	3	δ_1	m^2 g^{-1}	0.78
		δ_2	–	0.26
m vs. N_a	3	δ_1	–	15
		δ_2	–	0.56
g_s vs. BWB	cf. Fig. 2	$g_{s,min}$	mmol m^{-2} s^{-1}	50

Our former studies on wheat and rapeseed did not reveal any clear tendency of θ along with N_a, probably due to high scatter of the data. In contrast, all barley experiments yielded comparable patterns of the θ–N_a relationship that may be described by a descending power function (data not shown):

$$\theta = \delta_1 X^{-\delta_2} \; ; 0 \le \theta < 1 \, . \tag{3}$$

The value of the parameter δ_1 (m^2 g^{-1}) corresponds to the value of θ at N_a = 1 g m^{-2}. The parameter δ_2 (dimensionless) determines the curvature of the relationship. The curvature decreases for $\delta_2 \rightarrow 0$, where $\theta \rightarrow \delta_1$. The correlation between θ and N_a was higher for the climatic chamber experiment E3 ($R^2 = 0.47$) as compared to the field data ($R^2 \le 0.34$). Therefore, the parameter values derived from chamber data were recommended for use with the model (cf. Table 1).

Independent determinations of both J_{m25} and V_{m25} in E3 – E5 (Braune, 2008) were used to re-analyse the J_{m25} vs. V_{m25} relationship (Leuning, 2002) that was used in former versions of LEAFC3-N. For leaf 4 of plants grown at 13℃, 16℃, and 22℃ in a climatic chamber, the slope s_{Vc} of the J_{m25} vs. V_{m25} regression (absolute term forced to zero) approached 2.49, 2.10, and 1.82 mol (e^-) (mol (CO_2))$^{-1}$, respectively ($0.85 \le R^2 \le 0.94$), where the mean was 2.14 mol (e^-) mol (CO_2))$^{-1}$. In the field, measurements on both the fourth leaf and the leaf below the flag leaf yielded a mean value of s_{Vc} = 2.34 mol (e^-) (mol (CO_2))$^{-1}$ (R^2 = 0.86). These data fit fairly well into the range of (2.0 ± 0.6) mol (e^-) (mol (CO_2))$^{-1}$ derived for C_3 plants by Leuning (1997). Neglecting the effects of growth temperature on s_{Vc}, a mean value from climatic chamber and field data of E3 of s_{Vc}=2.2 mol (e^-) (mol (CO_2))$^{-1}$ can be derived that probably will satisfy most applications. However, note that the ratio of J_{m25} to V_{m25} may be affected by different factors (Delucia et al., 1985; Besford et al., 1990; Harley et al., 1992; Wong et al., 1985a,b; Evans, 1989; Leuning et al., 1991).

In order to retain the basic functions used in LEAFC3, the former wheat version of LEAFC3-N calculates R_{d25} proportional to V_{m25}, where this ratio was shown to decrease along with N_a (Müller et al., 2005b, their Fig. 5). The R_{d25} vs. N_a or V_{m25} relationships were re-analysed from data of E3 – E5 (Braune, 2008). In terms of Eq. (1), under chamber conditions the slope of the R_{d25} vs. N_a relationship, s_{Na1}, approached 0.621 µmol g^{-1} s^{-1} (R^2 = 0.6; n = 68), and the slope of the R_{d25} vs. V_{m25} relationship, s_{Vc}, 0.463 µmol g^{-1} s^{-1}. These correlations were less strong in the field due to a higher scatter of the data (R^2 = 0.2, n = 100). Therefore, the parameterisation derived from climatic chamber experiments here was accepted for further use (cf. Table 1).

The parameter m of the BWB stomatal model is given by the slope of the g_s vs. BWB index relationship (Fig. 2). The slope decreases non-linearly along with increasing N_a as shown in the small diagram included into the figure. This pattern means that at constant h_b and C_b and with descending N_a but similar ranges of A_n the stomatal conductance g_s will tend to lower values. In other words: comparing g_s for similar A_n values, stomata are wider open at low N_a than at high N_a. Note that a linear m–N_a relationship was found in a previous study for rapeseed leaves (Müller and Diepenbrock, 2006). The pattern observed here can be approximated by the power function defined by Eq. (3). Most accurate data on the m vs. N_a relationship were provided by the barley experiments E1 (N200) and E3-E5. The resulting parameter estimates were in close range, yielding for δ_1 and δ_2 values of about 17 and 0.68 from E1, 15 and 0.56 from E3 and E4, and 13 and 0.36 from E5, respectively. The value of the minimum stomatal conductance $g_{s,min}$ varied from about 30 mmol m^{-2} s^{-1} to 70 mmol m^{-2} s^{-1}, such that a mean value of 50 mmol m^{-2} s^{-1} is a good approximation. This value corresponds to about 7% of the maximum stomatal conductance of young leaves and to about 17% of that of senescent ones.

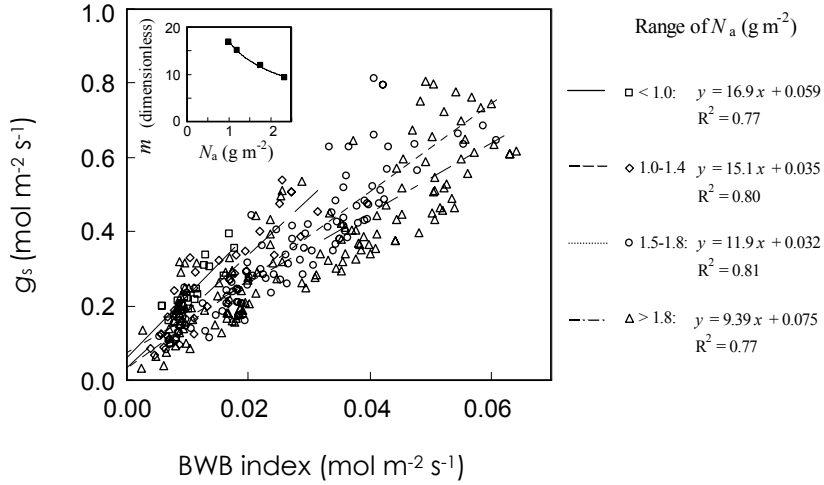

Figure 2 Stomatal conductance g_s vs. BWB index, experiment E1, N200, for different ranges of nitrogen concentration N_a. Included diagram: slope m as function of N_a, $m = 16.96\ N_a^{-0.6804}$; $R^2 = 0.99$

For the p–N_a relationships of Eqs. (1) – (3) and additional characteristics discussed above, the generalised parameter values for barley are summarised in Table 1 (for parameters not included see Table C1 in (Müller et al., 2005b). The values of the activation energy ΔH_a given there were confirmed for barley with slight modification by Braune (2008). In addition, that study revealed a dependency of s_{Na} and ΔH_a of key model characteristics on growth temperature T_g (Fig. 3 and Table 2) that may be included into the model depending on the required accuracy.

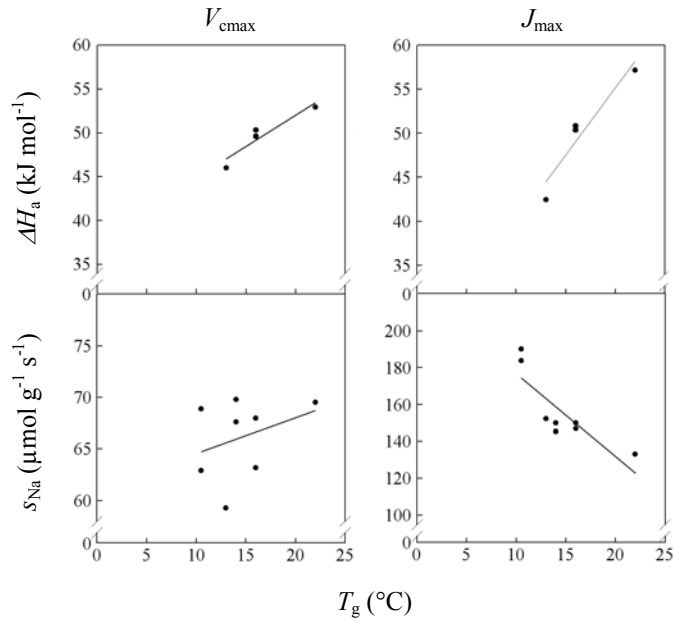

Figure 3 Dependency of activation energy ΔH_a and slope s_{Na} (cf. Eq. (1)) for V_{cmax} and J_{max} on growth temperature T_g. Parameter values and statistics see Table 2

Table 2 Slope ε_1 and absolute term ε_2 of the linear regression of key model parameters on growth temperature T_g. The data are given for the activation energy ΔH_a of both maximum carboxylation rate V_{cmax} and electron transport rate J_{max} and for the slope s_{Na} of the relationships between V_{cmax} or J_{max} and leaf nitrogen content N_a. The number of data points was 4 for ΔH_a and 8 for s_{Na}, respectively

Characteristic	Original parameter (unit)	ε_1 ([unit of original parameter] K^{-1})	ε_2 (unit as original parameter)	R^2
V_{cmax}	ΔH_a (kJ mol^{-1})	0.709	37.8	0.88
	s_{Na} (µmol g^{-1} s^{-1})	0.348	61.1	0.11
J_{max}	ΔH_a (kJ mol^{-1})	1.52	24.7	0.91
	s_{Na} (µmol g^{-1} s^{-1})	-4.50	222	0.70

4.2 Integration of the LEAFC3-N Model into Crop Models

LEAFC3-N can be integrated into crop models via an interface providing local environmental characteristics and organ-based or layer-based state variables (N, chlorophyll content, characteristic dimension of area elements, specific area). A former rapeseed version of LEAFC3-N was included into a multi-layer canopy gas exchange model for testing that model against diurnal and seasonal courses of canopy net photosynthesis and evapotranspiration rate measured by a canopy chamber system (Müller et al, 2005a). The barley version of LEAFC3-N was coupled to a 3D Functional-Structural Plant Model (Müller et al 2007; Wernecke et al, 2007). In that study, LEAFC3-N provides accurate estimates of carbon input of barley plants for simulating the combined carbon and nitrogen dynamics of the crop over the entire vegetation period. For further detail of these applications of the model, we refer to the above-cited papers.

With regard to the time step for using LEAFC3-N as submodel of a crop model, it must be pointed out that model calibration was derived from steady-state response curves of gas exchange rate and validated against diurnal time course data given with a measuring time interval of 15 s. In contrast, crop models usually operate with a daily time step that clearly cannot be taken as a basis for running a photosynthesis submodel for calculating reliable estimates of the integral daily carbon gain (IDC). Obviously, the accuracy will be best calculating IDC with high resolution in time and vice versa. However, very frequent calls of the photosynthesis model may greatly enlarge the overall computational time of the crop model. In addition, in many applications environmental inputs to the photosynthesis model may be available only for a limited number of time steps during the day. Therefore, we compared IDC obtained by running LEAFC3-N with input data acquired with different time steps ranging from 15 s up to 4 h or 3 times per day (light hours). The analysis was done for a number of days differing in the radiation conditions: clear sky, strong and rapid fluctuations of irradiance due to changes between short cloudy and clear periods, and overcast sky with slow variation of irradiance due to some change in cloudiness. The main conclusion that may be drawn from that analysis is that up to a time step of 1 h or even 2 h the error of the calculated daily carbon gain will not exceed 3 to 5% and thus probably will be tolerable for most applications. In contrast, using input data with a larger time step will lead to a considerable bias that must be corrected.

As mentioned above, complete and accurate model parameterisation is a rather time-consuming procedure. Thus, it would be useful to know which accuracy is needed in determining individual key model parameters. Clearly, this will depend on the envisaged use of the model. Here we will deal with this question from the viewpoint of applying the model as a submodel of a crop growth

model. For this purpose, we performed a sensitivity analysis for the key model parameters analysing the effect of a ±20% deviation of key model parameters on IDC, where the latter was computed from hourly data. The analysis was done choosing days with different characteristic radiation conditions as described above. As may be concluded from the results of the sensitivity analysis, among different parameters a variation of s_{Na} for V_{m25} and J_{m25} (cf. Eq. (1)) will have the most strong effect on IDC. Thus, to calculate IDC with an error < ±5%, the values of the parameter s_{Na} of V_{m25} and J_{m25} must be known with about the same accuracy as well. The sensitivity of IDC to inaccuracies of the remaining parameters above is much less. For those parameters, with inaccuracies in order of ±20% the resulting error in IDC will not exceed ±5%. Further, errors in the individual parameter values may be expected to have different signs and thus to compensate each other partially. A further consequence of this analysis is that species-specific determination of parameter values will be required only if the species-related differences in parameter values are expected to exceed the ranges given above.

5 Conclusion

In the current paper, we presented a generalised parameterisation of the LEAFC3-N model for barley to facilitate the use of the model by other researchers. In particular, parameter–nitrogen and parameter–growth temperature relationships were re-analysed. For barley and other C_3 species analysed in our previous parameterisation studies (wheat, oilseed rape), the parameter–N_a relationships mostly were in close range. The estimated value of the slope of the relationship of V_{m25} to area based leaf nitrogen content and the values of several other key parameters correspond well to the values theoretically expected. Nevertheless, it should be pointed out that further studies are needed to specify the effects of growth conditions and genetic factors on model parameters.
For calculating integral daily carbon gain from LEAFC3-N with an accuracy of at least ± 5%, the accuracy of the slope of the V_{m25}–N_a and J_{m25}–N_a relationships should be of similar order. With respect to the other parameters considered here, biases up to ± 20% or even higher can be tolerated for such calculations. The error of the calculated integral daily carbon gain will increase with increasing time step. Using a time step of about 1 to 2 h, there will be an overestimation of about 5%. The model was successfully tested as submodel of a multi-layer canopy gas exchange model for rapeseed and of a Functional-Structural Plant Model for barley.

Acknowledgements

The authors thank Dr. K. Egle and Dr. H. Beschow, Institute of Soil Science and Plant Nutrition, Martin-Luther-University of Halle-Wittenberg, for performing nitrogen analyses, and Dipl.-Ing. agr. A. Kahlau for performing gas exchange measurements of E1 and E2. The present study was funded by the German Research Association (Deutsche Forschungsgemeinschaft, DFG). The support of the state of Saxony-Anhalt is highly appreciated.

References

Ball JT, Woodrow IE, Berry JA (1987) A model predicting stomatal conductance and its contribution to the control of photosynthesis under different environmental conditions. In: Biggins J (ed), Progress in Photosynthesis Research. Proceedings of the VII. International Congress on Photosynthesis. Martinus Nijhoff Publishers, Dordrecht-Boston-Lancaster 4:221 – 224.

Besford RT, Ludwig LJ, Withers AC (1990) The greenhouse effect: Acclimation of tomato plants growing in high CO_2, photosynthesis and ribulose-1,5-*bis*phosphate carboxylase protein. J Exp Bot 41: 925 – 931.

Bernacchi CJ, Singsaas EL, Pimentel C et al (2001) Improved temperature response functions for models of Rubisco-limited photosynthesis. Plant Cell Environ 24 253 – 259.

Braune H (2008) Modellierung von Photosyntheseprozessen – Parametrisierung des Gas- und Energieaustauschmodells LEAFC3-N für Sommergerstenblätter (*Hordeum vulgare* L.). Ph.D. Thesis, Institut für Agrar- und Ernährungswissenschaften, Martin-Luther-Universität Halle-Wittenberg, Halle (Saale), Germany, 124 p.

Braune H, Müller J, Diepenbrock W (2007) Measurement and modeling of awn photosynthesis of barley (*Hordeum vulgare* L.) for Virtual Crop Models. Pflanzenbauwissenschaften (German Journal of Agronomy and Crop Science) 11:10 – 15.

Collatz GJ, Ball JT, Grivet C et al (1991) Physiological and environmental regulation of stomatal conductance, photosynthesis and transpiration: a model that includes a laminar boundary layer. Agric For Meteorol 54:107 – 136.

Delucia EH, Sasek TW, Strain BR (1985) Photosynthetic inhibition after long-term exposure to elevated levels of atmospheric carbon dioxide. Photosynth Res 7:175 – 184.

Evans JR (1989) Photosynthesis and nitrogen relationships in leaves of C_3 plants. Oecologia 78:9 – 19.

Farquhar GD, von Caemmerer S, Berry JA (1980) A biochemical model of photosynthetic CO_2 assimilation in leaves of C_3 species. Planta 149:78 – 90.

Harley PC, Thomas RB, Reynolds JF et al (1992) Modeling photosynthesis of cotton grown in elevated CO_2. Plant Cell Environ 15:271 – 282.

Leuning, R (1997) Scaling to a common temperature improves the correlation between the photosynthesis parameters J_{max} and V_{cmax}. J Exp Bot 48:345 – 347.

Leuning R (2002) Temperature dependence of two parameters in a photosynthesis model. Plant Cell Environ 25:1205 – 1210.

Leuning R, Cromer RN, Rance S (1991) Spatial distributions of foliar nitrogen and phosphorus in crowns of *Eucalyptus grandis*. Oecologia 88:504 – 510.

Medlyn BE, Badeck FW, De Pury DGG et al (1999) Effects of elevated [CO_2] on photosynthesis in European forest species: a meta-analysis of model parameters. Plant Cell Environ 22:1475 – 1495.

Meir P, Kruijt B, Broadmeadow M et al (2002) Acclimation of photosynthetic capacity to irradiance in tree canopies in relation to leaf nitrogen concentration and leaf mass per unit area. Plant Cell Environ 25:343 – 357.

Mo X, Beven K (2004) Multi-objective parameter conditioning of a three-source wheat canopy model. Agric For Meteorol 122:39 – 63.

Müller J, Behrens T, Diepenbrock W (2005*a*) Measurement and modeling of canopy gas exchange of winter oilseed rape (*Brassica napus* L.). Agric For Meteorol 132:181 – 200.

Müller J, Wernecke P, Diepenbrock W (2005b) LEAFC3–N: a nitrogen-sensitive extension of the CO_2 and H_2O gas exchange model LEAFC3 parameterised and tested for winter wheat (*Triticum aestivum* L.). Ecol Model 183:183 – 210.

Müller J, Diepenbrock W (2006) Measurement and modeling of canopy gas exchange of leaves and pods of oilseed rape. Agric For Meteorol 139:307 – 322.

Müller J, Wernecke P, Braune H et al (2007). Photosynthesis and carbon balance. In: Vos J, Marcelis LFM, de Visser PHB et al (eds): Functional-Structural Plant Modeling in Crop Production. Wageningen UR Frontis Series, Springer, Dordrecht, The Netherlands, 22:91 – 101.

Nikolov NT, Massman WJ, Schoettle AW (1995) Coupling biochemical and biophysical processes at the leaf level: An equilibrium photosynthesis model for leaves of C-3 plants. Ecol Model 80:205 – 235.

Niinemets Ü, Tenhunen JD (1997) A model separating leaf structural and physiological effects on carbon gain along light gradients for the shade-tolerant species *Acer saccharum*. Plant Cell Environ 20:845 – 866.

Vos J, Marcelis LFM, Evers JB (2007) Functional-structural plant modeling in crop production: Adding a dimension. In: Vos J, Marcelis LFM, de Visser PHB et al (eds): Functional-Structural Plant Modeling in Crop Production. Wageningen UR Frontis Series, Springer, Dordrecht, The Netherlands, 22:1 – 12.

Wernecke P, Müller J, Dornbusch T et al (2007) The virtual crop-modeling system 'VICA' specified for barley. In: Vos J, Marcelis LFM, de Visser PHB et al (eds): Functional-Structural Plant Modeling in Crop Production. Wageningen UR Frontis Series, Springer, Dordrecht, The Netherlands, 22:53 – 64.

Wong SC, Cowan IR, Farquhar GD (1985a) Leaf conductance in relation to rate of CO_2 assimilation. I. Influence of nitrogen nutrition, phosphorus nutrition, photon flux density, and ambient partial pressure of CO_2 during ontogeny. Plant Physiol 78:821 – 825.

Wong SC, Cowan IR, Farquhar GD (1985b) Leaf conductance in relation to rate of CO_2 assimilation. II. Influences of water stress and photoinhibition. Plant Physiol 78:830 – 834.

Studies on Photosynthesis Model of Mini-Cucumber Leaf in Greenhouse

Ping-Ping Li, Ji-Zhang Wang, Xin Chen, Wei-Hong Liu

(Key Laboratory of Modern Agricultural Equipment and Technology, Ministry of Education & Jiangsu Province, Jiangsu University, Jiangsu, 212013,China)

Abstract: Photosynthesis (Pn) is the most important parameters in greenhouse climate control system based on model. Temperature and radiation are important climate factors affecting crop photosynthesis rate. The purpose of this study is to quantitatively investigate the effects of both temperature and photosynthetically active radiation (PAR) on the cucumber Photosynthesis rate. Experiments with different weather were conducted in greenhouse of Jingkou Institute of Vegetable. The results show that under the fine and cloudy weather, the curve of photosynthesis had two peaks, with an obvious midday depression at 11:00am – 12:00am. But under the rainy weather, there is no depression. Based on experimental data, the relationship between photo-temperature and photosynthesis were established. The coefficient of determination (R^2) of the model is 0.953. And when temperature was 28.7℃, PAR was 1311 μ molm-2s-1, the photosynthesis would reach to a maximum value of 20.13 CO_2 μ $molm^{-2}s^{-1}$. The model developed in this study can predict photosynthesis with different temperature and radiation. And it also can give the optimum parameters of greenhouse climate control.

Keywords: greenhouse; photosynthesis model; cucumber

1 Introduction

Models for leaf photosynthesis were to describe and simulated the rate of leaf photosynthesis influenced by environmental conditions. It may be used in crop growth model, decision support system and greenhouse climate control. In order to estimate photosynthesis, Different version of modes has been established in computer simulations by many authors. It included descriptive and explanatory modeling of photosynthesis rate. Descriptive models usually contain few state variables, which is important to be used in on-line greenhouse climate control (GijZen, 1998). In HORTISIM, photosynthesis is the response curve of the initial light use efficiency(H), maximum rate of leaf photosynthesis(Pg,max) and absorbed radiation(ε) per leaf area. Actually, net photosynthesis is also influenced by CO_2 , temperature, radiation (Gifford, 1995; Li, 2001) and daily variation (Li, 2001).

In greenhouse climate control system, the main factors for control are temperature and radiation. In this paper, we established a mathematic model for greenhouse cucumber.

2 Materials and Methods

2.1 Materials

This test was performe in a multi-span glass greenhouse of jingkou Institute of vegetables in Zhenjiang from March to June in 2004. Cucumber used in test is called jasper. It is introduced from

the Netherlands. This variety of mature fruit is 15 to 20 cm long, 5 cm thick. Plants are put in the 100 cm × 30cm bag with Soilless cultivation method. Each bag has 4 plants as line spacing is 1600 cm. it is full of perlite irrigated nutrient solution.

2.2 Methods

2.2.1 Daily Variation of Photosynthesis

Photosynthesis was determined by the experimental device LI-6400 from the United States Company LI-COR .it is a portable photosynthesis system.In the medium-term of Cucumber growth, four normal plants owning similar condition are tagged; the fifth plant leaves (top-down) are chosen as objects. Each leaf is measured five data, and the average measured value is determined as the true value.

The test time of Photosynthesis is 7:00 to 5:00 pm, every one hour a measurement. Sunny, cloudy, cloudy weather chosen were respectively measured. During 4 months from March to June, photosynthetic of cucumber leaf change with the same trend, In this paper the data in May is cited to elaborate analysis

2.2.2 Light Response of Photosynthesis

To study photosynthesis rate on the response of the light intensity, LI-6400 photosynthesis system with automatic determination procedures of the light response was used to study temperature-response curve under the constant condition.

In order to study the relationship between the photosynthesis rate and environmental factors, photosynthetic rate was selected as a indicators, while temperature and light intensity factor selected for the test .Because they impact on the photosynthesis greatly. Using uniform test methods are designed for experiment, in which the temperature ranges -40℃ to 10℃, the light intensity ranges of $0-2000\mu molm^{-2}s^{-1}$.

2.2.3 Photosynthesis and Light and Temperature Factor Between the Statistical Models

The test was done in modern agricultural engineering laboratory of Jiangsu University in June 2004. Test equipment contains artificial climate room and LI-6400 photosynthesis measurement system. Environmental temperature and humidity values were set by artificial climate room. Humidity was kept at 80 percent. The LED light system of LI-6400 was used to set flux density. The experiment was performed as Table1.

Table 1 Experiment of photosynthesis model

ID	Temperature (℃)	PAR ($\mu mol/m^2/s$)
1	10	600
2	13	1600
3	16	1200
4	19	0
5	22	2000
6	25	400
7	28	1000
8	31	1400
9	34	200
10	37	1800
11	40	800

3 Results and Analysis

3.1 Daily Variation of Photosynthesis

Figure 1 is the result of sunny weather. Seen from the diagram, at 7:00 am of sunny weather in the morning, light intensity and temperature rose rapidly, at about 10:00 am photosynthetically active radiation (PAR) reached 950 μ mol/$m^{2/}$s, at the same time the temperature reached 34 ℃ While the photosynthetic rate peaked (21.9 CO_2 μmol/m^2/s). After 10:00 PAR continued to rise in 1180μmol/$m^{2/}$s, reached a maximum at 11:00, and the temperature reached a maximum at about 12:00. The photosynthetic rate gradually declined on after ten o'clock, forms a trough at 12:00, then starts to rebound from 13:00 and formed a second peak (18.7 CO_2 μmol/m^2/s) at 14:00, it is slightly lower than the first peak, and then gradually declining. It can be seen that the trend of changes in the photosynthetic rate is a typical double-peak curve, and there is an obvious "midday depression" phenomenon. This is a self-adaptive phenomenon that the plants avoid high-temperature, high light intensity, low humidity, and other adverse environmental conditions. During test, when photosynthetic rate is in a low value at 12:00, the temperature and flux density are in the vicinity of the peak, and around the leaves atmospheric relative humidity is only 31.8%, resulting in a cucumber leaf photosynthesis "midday depression".

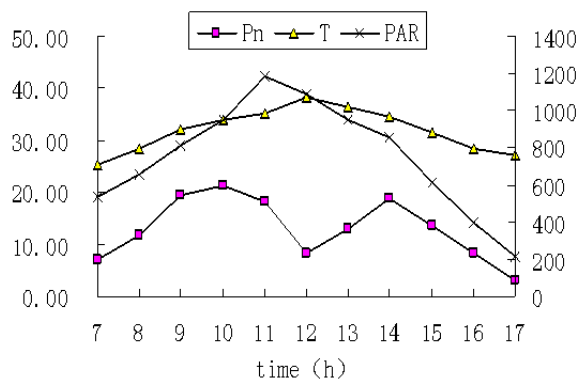

Figure 1 Daily variation of photosynthesis at cloudy weather

Figure 2 is the result of a typical cloudy weather. The PAR is decreased greatly, and appears the irregular changes, the temperature is also lower than sunny. Seen from diagram, photosynthesis variation has the same trend with the PAR changes, which shows that photosynthesis rate rises or

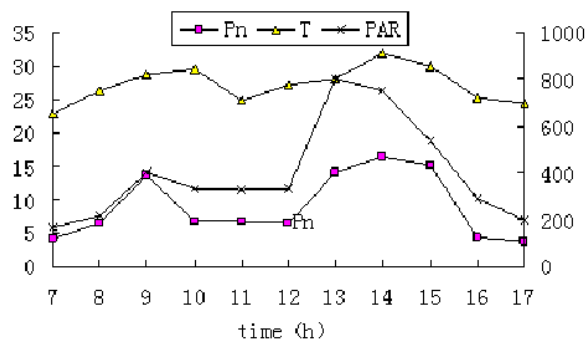

Figure 2 Daily variation of photosynthesis at cloudy weather

declines as PARs'. Around 9:00 the PAR is nearly 400μmol/m^2/s, forming a peak. Photosynthesis increased, forming the first peak (17.6 CO_2 μmol/m^2/s). At 13:00, PAR suddenly raised about 800μmol/m^2/s. Photosynthetic was slightly behind the light intensity, around 14:00 in the formation of a peak again (19.5 CO_2 μmol/m^2/s), because of strong significantly higher than this time in the morning, so photosynthesis peak slightly higher.

Figure 3 is the result of rainy. In rainy day PAR is lower, and change is gentler. At 13:00 in the afternoon the peak is only 50μmol/m^2/s, temperature changes smaller; in consistent with light intensity, so PAR is the main factor of photosynthesis.

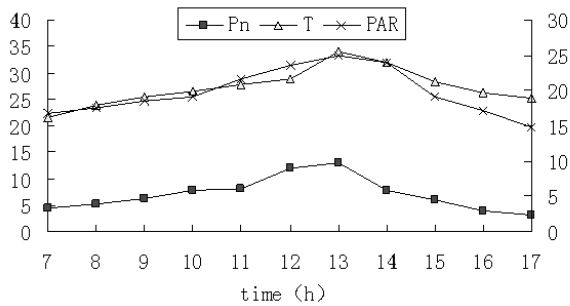

Figure 3 Daily variation of photosynthesis at rainy weather

3.2 Light Response of Photosynthesis

Figure 4 is the light fast response curve of cucumber photosynthesis on 30℃. As seen from Figure, when PAR is less than 1000 μmol/m^2/s, the change rate of photosynthesis is rapid, when PAR is more than 1000 μmol/m^2/s, the change rate of photosynthesis is slowly. Then its achieve the light saturation point. The quadratic equation of light and photosynthesis was achieved by regression method:

$$Y = -0.981 + 0.0333X - 1.148\text{E} - 05X^2 \ (R^2 = 0.93)$$

It can be seen that both of them have strong relevance, in the equation x = 1448, the maximum is 23.02, when x = 58.3, y = 0. The biological significance is the light saturation point is the 1448 μmol/m^2/s, while the corresponding photosynthesis intensity is 23.02 CO_2μmol/m^2/s, and light compensation point reaches 58.3 μ molm-2s-1, which match with light compensation point 51.0 μmol/m^2/s, light saturation point 1421.0 μmol/m^2/s,, and light-saturated photosynthesis intensity at 21.3 CO_2μmol/m^2/s, found by Zhang Zhenxian (1997).

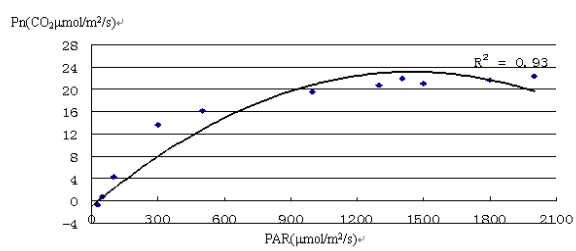

Figure 4 The result of light response of photosynthesis

3.3 Model of Photosynthesis

3.3.1 Data Analyze

The following equation is the result of quadratic regression method. It contains two variables (temperature(T) and PAR(L)):

$$P_n = -26.44 + 2.238T + 2.244\times10^{-2}L - 0.0479T^2 - 1.28\times10^{-5}L^2 + 3.881\times10^{-4}TL \quad (1)$$

the range of variable in the equation: $\begin{cases}10 \le T \le 40\\ 0 \le L \le 20\end{cases}$

Related test results are as follows: R = 0.953, which shows that be variable Pn is significantly related with variables L and T.

The variance analysis result about the Eq. (1) is in Table 2, which show that regression equation a high degree of marked property. Results of the regression coefficients in Table 3 show that the regression coefficient of all is notable in varying degrees.

Table 2 Result of variance analysis

	Sum of Squares	df	Mean Square	F	Sig. (α)
Regression	515.171	5	103.034	9.956	0.012
Residual	51.746	5	10.349		
Total	566.917	10			

Table 3 Result of Coefficients

	Std. Error	t	Sig. (α)
a	8.951	2.977	0.031
b	0.661	3.386	0.020
c	0.711	3.154	0.025
d	0.013	3.671	0.014
e	0.029	4.335	0.007
f	0.019	2.036	0.097

3.3.2 Model Validation

Make use of the model of in 30℃ was used to simulated response curve . The results are shown in Figure 5. As seen from the map, the light response curve and the actual measured value can inosculate well, which shows that the model can be used to describe the relationship of photosynthesis rate between temperature and PAR.

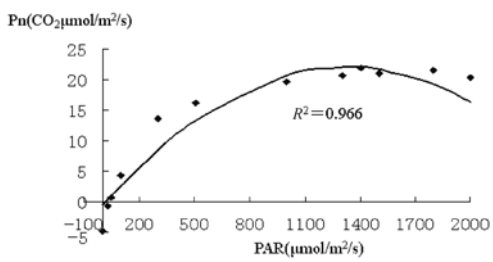

Figure 5 The result of photosynthesis model at 30℃

3.4 Model Analyses

According to the formula described in equation 1, photosynthetic rate model find optimal solution within the scope of the theory in its restrictive conditions, that is, to solve the equation extreme. In order to get the extreme value of equation 1, first step is to verify whether the model has extreme value, then, it must be determined it is the minimum or maximum value. It can be descibed as following:

$$\frac{\partial P}{\partial T} = \frac{\partial P}{\partial L} = 0 \tag{2}$$

The base station (28.67, 1311) was obtained the Eq. (2), then by Xue Halves specific methods judging extreme inequality,

$$D_1 = \left| \frac{\partial^2 P}{\partial^2 T} \right| = -9.58 \times 10^{-2} < 0 \tag{3}$$

$$D_2 = \begin{vmatrix} \dfrac{\partial^2 P}{\partial^2 T} & \dfrac{\partial^2 P}{\partial T \partial L} \\ \dfrac{\partial^2 P}{\partial L \partial T} & \dfrac{\partial^2 P}{\partial^2 L} \end{vmatrix} = \begin{vmatrix} -9.58 \times 10^{-2} & 3.881 \times 10^{-4} \\ 3.881 \times 10^{-4} & -0.256 \times 10^{-4} \end{vmatrix} = 2.28 \times 10^{-6} > 0 \tag{4}$$

Though Eqs. (3) and (4), it can be determined a maximum exists in Eq. (1), it means when temperature is 28.7℃ and the flux density is 1311μmol/m^2/s, the photosynthesis is the maximum value 20.13 CO_2μmol/m^2/s.

Acknowledgements

The authors gratefully acknowledge financial support from the National Natural Science Foundation of China (No: 30771259) and from Specialized Research Fund for the Doctoral Program of Higher Education of China (No: 20060299003) and from the Natural Science Foundation of Jiangsu Province (No: BK2006076) and from the Scientific Research Starting Foundation of Jiangsu University (No: 06JDG038).

References

GijZen H et al. (1998) HORTISIM: A model for greenhouse crops and greenhouse climate． Acta Horticulture. 456: 441 – 450.

Gifford RM et al. (1995)Whole plant and photosynthesis of wheat under increased CO2 concentration and temperature: long term vs. short term distinctions for modeling. Glob. Change Biol. 1,385 – 396.

Li Pingping; Hu Yongguang; Zhao Yuguo et al. (2001) Comprehensive Model on the Effect of CO_2 Enrichment on Lettuce Photosynthesis in Greenhouse. Transactions of The Chinese Society of Agricultural Engineering, 17(3):75 – 79.

Li Pingping; Hu Yongguang; Zhao Yuguo et al (2001) A Study on Daily Variation of Photosynthesis in Greenhouse Butterhead Lettuce. Acta Horticulturae Sinica, 28 (3) : 240 – 245.

Hao Xiuming, (1999), Effect of supplemental lighting and cover materials on growth, photosynthesis biomass partitioning, early yield and quality of greenhouse cucumber. Scientia Horticulturae, 80(1-2):1 – 18.

Zhang Zhenxian, Zhou Xuyuan, and Chen Liping (1997) The Characteristics of Photosynthesis and Transpiration in Major Vegetable Grops, Acta Horticulturae Sinica, 24 (2) :155 – 160.

Wu YY, Wu XM, Li PP et. al (2005) Comparison of photosynthetic activity of Orychophragmus violaceus and oil-seed rape ,Photosynthetic, 43(2): 229 – 302.

Finding a Suitable CO_2 Response Algorithm for Crop Growth Simulation in Germany

C. Nendel[1,*], K.C. Kersebaum[1], W. Mirschel[1], R. Manderscheid[2], H. J. Weigel[2] and K. O. Wenkel[1]

(1 Leibniz Centre of Agricultural Landscape Research; Institute of Landscape Systems Analysis, Eberswalder Str. 84; D-15374 Müncheberg, Germany; E-mail: nendel@zalf.de)
(2 Johann Heinrich von Thünen Institute (Federal Research Institute for Rural Areas, Forestry and Fisheries), Institute of Biodiversity, Bundesallee 50, D- 38116 Braunschweig, Germany.)
(Corresponding author. Tel.: +49 33432 82355; fax: +49 33432 82334.
E-mail: nendel@zalf.de (C. Nendel).)

Abstract: A soil-crop-environment model was used to describe the combined effects of atmospheric carbon dioxide concentration [CO_2], temperature and precipitation on different agricultural crop species. Within this model, a set of algorithms describing CO_2 response to photosynthesis and crop water use efficiency, which were different in complexity and parameter requirements, was tested for its suitability to explain crop growth responses and soil water dynamics observed over six years in a crop rotation (winter barley, sugar beet and winter wheat) with two cycles under normal and elevated atmospheric CO_2 levels (FACE experiment; Weigel and Dämmgen, 2000).

All algorithms were able to describe an observed increase in above-ground dry matter for all crops in the rotation, with Willmott's Index of Agreement (IoA) ranging between 0.93 and 0.99. Increasing water use efficiency with rising CO_2 was also successfully portrayed (IoA 0.80 – 0.86). A combination of a semi-empirical Michaelis-Menten approach, describing a direct impact of CO_2 on photosynthesis, and a Penman–Monteith approach with a simple stomata conduction model for evapotranspiration yielded the best simulation result. This combination is therefore considered suitable for the description of yield responses to rising [CO_2] at the regional level. However, the performance of all tested algorithms was only marginally different, at 550 ppm CO_2.

1 Introduction

The impact of climate change on food production is one of the key concerns of policy and research (Olesen and Bindi, 2002; Ziska and Bunce, 2007; Lobell et al., 2008). Global climate models (GCM) use the main processes that drive the earth's climate to calculate future climate scenarios under different preconditions (Watterson et al., 1995; Anderson et al., 2004; Stier et al., 2005; Johns et al., 2006). Regional climate models (Plummer et al., 2006; Jacob et al., 2007) or weather generators (Semenov and Barrow, 1997; Dubrovsky, 1997) downscale the GCM results to a meso-climate level, which can then be used to forecast climate effects on regional agriculture. This step is necessary since crop growth is very sensitive to radiation, temperature, soil moisture and other climate-derived variables, and crop growth modeling for yield prediction can only be carried out satisfactorily if local weather is predicted in the best possible way. Since landscape at the meso-scale has significant feedback relations to the development of local weather from global climate, the downscaling process needs to take a number of landscape characteristics (i.e. surface elevation, land use distribution) into account. Soil-crop-environment models are available to

calculate the growth of agricultural crops under consideration of site specifications and to predict yields using the downscaled weather data (Kersebaum et al., 2007).

Climate change is expected to affect crop growth mainly by increasing temperatures, a shifting distribution of precipitation, a changing amount of precipitation, and an increasing concentration of atmospheric carbon dioxide [CO_2]. Regional climates are expected to develop quite differently, including increasing rainfall in some areas (IPCC, 2007).

Describing the interactions of crop growth, soil processes and weather variables in a simulation model is the current state-of-art methodology to interpret downscaled GCM outputs for yield predictions. However, not all available models include the most important feedback relations. One of the processes included in agricultural process models was the impact of [CO_2] on crop growth (Acock et al., 1971; Farquhar et al., 1980; Farquhar and von Caemmerer, 1982). In detail, [CO_2] was found to mainly affect two processes: (i) In plants using the C3 mechanism of photosynthesis, an increasing [CO_2] would directly increase the photosynthesis rate (Gaastra, 1959). (ii) A higher [CO_2] would also lead to a decrease in stomatal conductance (e.g. Cowan, 1977) and thus to a higher water use efficiency (Manderscheid and Weigel, 2007).

The impact of [CO_2] on photosynthesis has been included in simulation models in different ways (Tubiello and Ewert, 2002). Simpler approaches use an empirical relation between [CO_2] and a crop-specific radiation-use-efficiency (RUE) factor (Ritchie and Otter-Nacke, 1985; Williams et al., 1989; Bindi et al., 1996; Jamieson and Semenov, 2000). Others employ a [CO_2]-dependency of the photosynthesis-light response curve (Hoogenboom et al., 1992; Porter, 1993; Goudriaan and van Laar, 1994). Only few approaches use leaf-level biochemical algorithms, which require extensive parameterisation and are therefore more applicable to biochemical process research (e.g. Rodriguez et al., 2001).

Leaf stomata control a crop's CO_2 intake for photosynthesis and water vapour exit (transpiration) by regulating the aperture. The stomatal opening, and hence the conductance for CO_2 and H_2O (g_s), is determined by light interception, [CO_2] and the plant's water status (Cowan, 1977). However, stomata regulation mechanisms are more complex, since dependency on photosynthesis activity is substantiated (Ball et al., 1987; Leuning, 1990; Leuning, 1995).

In this network of interactions, temperature affects a number of related processes. Photosynthesis itself reacts to temperature (Gaastra, 1959; Harley et al., 1985; Acock, 1991; Stanghellini and Bunce, 1993), as does crop transpiration, since the driving water vapour saturation deficit (D) is temperature-dependent. Moreover, a temperature relation is also known for the CO_2 compensation point (Γ), which describes [CO_2] when assimilation and dissimilation are at equilibrium (Bykov et al., 1981).

Coupled photosynthesis-transpiration models including stomatal conductance have been presented at different levels of detail. A pioneer modeling work was presented by Jarvis (Jarvis, 1976), using different coefficients to adjust stomatal conductance. The model of Ball et al. (1987), often referred to as the Ball-Berry model, assumes a linear relationship between stomatal conductance and photosynthesis, while Farquhar and Wong (1984) presented an empirical model on the basis of ATP. The Ball-Berry model was later refined by the works of Collatz (1991), Leuning (1990; 1995), Gui-Rui Yu (2001a; 2003) and Qiang Yu (2004). Dewar (1995; 2002), Gao et al. (2002) and Buckley et al. (2003), on the other hand, developed detailed biochemical models on the ideas of Farquhar and Wong (1984).

A soil-crop-environment model is currently under development for the simulation of climate change effects on typical agricultural crops produced in Northern Europe. In order to equip the model with the best available approach to describe CO_2 impact on crop growth, a number of selected algorithms were tested in the model framework against data from a Free Air Carbon

Enrichment (FACE) experiment (Weigel and Dämmgen, 2000). This paper presents the results of the simulations and discusses the usefulness of the different algorithms for regional yield predictions under climate change in Germany.

2 Material and Methods

2.1 The FACE Experiment

At the experimental station of the Johann Heinrich von Thünen Institute (vTI; formerly known as the Federal Research Agricultural Research Centre of Germany) at Braunschweig-Völkenrode, Germany (52°18' N, 10°26' E), a three-year crop rotation (winter barley, sugar beet and winter wheat) was grown over two cycles at normal and elevated [CO_2] (FACE experiment; Table 1). The crop rotation represents a typical cash crop sequence in Northern Germany. The crops were grown under optimum nutritional and hydric conditions. Standard crop protection was applied. A FACE system, consisting of six rings with a 20 m diameter, engineered by Brookhaven National Laboratory New York, USA, was set up (Lewin et al., 1992). Treatments included two rings equipped with blowers and enriched with CO_2, two rings operated with blowers and ambient air only and two rings without blowers. Target CO_2 concentration in the enriched rings during daylight hours was 550 ppm. In order to study the interaction between C and Nitrogen (N), the N supply was restricted to 50% (N50) of adequate N (N100) in a subplot within the six rings. The FACE experiment was described in detail by Weigel and Dämmgen (2000).

Table 1 FACE crop rotation details

Year		1999/00	2001	2001/02	2002/03	2004	2004/05
Crop		Winter barley	Sugar beet	Winter wheat	Winter barley	Sugar beet	Winter wheat
N-Fertiliser (100%)	kg N ha^{-1}	152	126	251	179	125	201
Irrigation	mm	69	107	60	63	84	121
Mean reference CO_2	ppm	370	370	370	378	377	379
Mean elevated CO_2	ppm	550	550	550	547	549	550

The soil at the experiment site is a luvisol with a loamy sand texture (69% sand, 24% silt, 7% clay), with 1.4% organic carbon (SOC) and a pH of 6.5. The soil texture allows a volumetric plant available water content (PAWC) of approx. 18% in the ploughed layer (0 – 30 cm), which decreases slightly with increasing profile depth. During the experiment, soil moisture contents were determined gravimetrically. Fresh and dry weights of individual plant organs (culm, leaves and ears or beet, respectively) were measured at intermediate harvests. At the final harvest, the cereal grain yield was also quantified. Crop phenology was surveyed. Daily weather data were recorded at a near-by weather station (at a distance of approx. 500 m).

2.2 The Model Framework

We used the HERMES model as a framework for testing the different CO_2 response algorithms. HERMES was designed to simulate crop growth, water and nitrogen uptake, and the nitrogen dynamics in the soil for applied purposes. This implies simple and robust model approaches, which are able to operate under restricted data availability. A more detailed description of the model is provided by Kersebaum and Beblik (2001) and Kersebaum (2007).

A capacity approach was used to describe soil water dynamics. The capacity parameters are

derived from German soil texture classifications and modified by soil organic matter content, bulk density and groundwater level (AG Bodenkunde, 1994). The reference evapotranspiration is calculated using the Penman-Monteith method, according to Allen et al. (1998), which requires the diurnal minimum and maximum temperature, water vapour pressure deficit, wind velocity and total global radiation. Crop-specific potential evapotranspiration is calculated using crop-specific factors (kc) during the growing season and bare soil factors between harvest and crop emergence. The kc factors are linked to the crops' developmental stages. Partitioning between evaporation and transpiration is a function of leaf area index (LAI), which is calculated by the crop growth model. The calculation of actual evaporation and transpiration considers the soil water status and vertical root distribution (Gerwitz and Page, 1974).

Daily net mineralisation of nitrogen (N) is simulated depending on temperature and soil moisture from two pools of potentially decomposable nitrogen (Richter et al., 1982), which are derived from the amount of soil organic matter and crop residues left from the previous crop. Denitrification is described using a Michaelis-Menten kinetic, which is dependent on soil nitrate content, water-filled pore space and temperature (Kersebaum, 1995).

Crop growth follows a generic approach, based on the SUCROS model (van Keulen et al., 1982). Daily net dry matter production by photosynthesis and respiration is driven by global radiation and temperature. Assimilates are partitioned, depending on the crop development stage, which is calculated from a thermal sum (degree-days) and modified, when appropriate, for each stage by day length and vernalisation. Root dry matter is distributed over depth according to Gerwitz and Page (1974), with the rooting depth increasing exponentially with the modified thermal sum. For cereals, the grain yield was estimated at harvest from the weight of the storage organ. With the crop residues, N, which was not previously exported with the product, is recycled.

Crop growth is limited by water and N stress. Drought stress is indicated by the ratio of actual to potential transpiration. Water and nitrogen uptake is calculated from the potential evaporation and crop N status, depending on the simulated root distribution and the availability of water and N in different soil layers (Kersebaum, 1995). Potential N uptake is reduced to actual N uptake if the soil mineral N supply is limited by a maximum uptake rate per root length. Nutrient transport to the roots is simulated using a simplified radial convection and diffusion approach (Kersebaum, 1995). The concept of critical N concentration in plants as a function of the crop's developmental stage (Kersebaum and Beblik, 2001) or of crop biomass (Greenwood et al., 1990) is applied to assess the impact of N shortage. Acceleration of crop ontogenesis by water and nitrogen stress is also considered for specific development stages.

The model under development will adopt many of the ideas originally developed and tested for the HERMES model (Kersebaum, 2007).

2.3 The CO_2 Response Algorithms

In order to equip the model with a suitable approach to describe CO_2 impact on crop growth, a number of algorithms were selected. Linear relationships (Bindi et al., 1996) were excluded from the panel of possible choices. On the other hand, detailed biochemical approaches (Dewar, 2002; Gao et al., 2002; Buckley et al., 2003) were also rejected, since the HERMES model computes daily time steps with a limited quality of input variables and parameters. The mechanistic and partly empirical character of the HERMES model determines the range of complexity the response algorithms have to match. The following approaches were selected for testing:

2.3.1 The Mitchell Approach for CO_2 Impact on Photosynthesis

Mitchell et al. (1995) presented a set of algorithms based on the ideas of Farquhar and von

Caemmerer (1982) and Long (1991), calculating the maximum photosynthesis rate

$$A_{\max} = \frac{(C_i - \Gamma^*) \cdot V_{c\max}}{C_i + K_c \cdot \left(1 + \frac{O_i}{K_o}\right)} \tag{1}$$

where C_i is the intercellular concentration of CO_2, Γ^* is the CO_2 compensation point of photosynthesis, referring to C_i in absence of dark respiration, O_i is the intercellular concentration of O_2, $V_{c\max}$ is the maximum Rubisco saturated rate of carboxylation, and K_C and K_O are the Michaelis-Menten constants for CO_2 and O_2. The temperature dependencies of C_i, O_i, K_c, K_0 and $V_{c\max}$ and their parameters were described by Long (1991).

Due to the nature of the testing environment, the Mitchell approach was modified such that the algorithms for subsaturating light intensities proposed by Mitchell et al. (1995) were not applied. Instead, $A_{\max}$ is adjusted for light interception according to Goudriaan and van Laar (1978). For the transition between photosynthetic quantum use efficiency and light saturated photosynthesis, Mitchell et al. (1995) suggested using

$$\varepsilon = \frac{0.37 \cdot (C_i - \Gamma^*)}{4.5 \cdot C_i + 10.5 \cdot \Gamma^*}. \tag{2}$$

This set of algorithms is characterised by a level of complexity comparable to the modeling environment.

2.3.2 The Nonhebel Approach for CO_2 Impact on Photosynthesis

A much simpler approach was extracted from the SUCROS87 model (Spitters et al., 1989), as proposed by Nonhebel (1996). Here, the RUE is directly affected by $[CO_2]$ as

$$\mathrm{RUE}_{CO_2} = \left(\frac{C_a - \Gamma}{C_a + 2\Gamma}\right) \cdot E_0, \tag{3}$$

where C_a denotes $[CO_2]$, Γ is the CO_2 compensation point of photosynthesis referring to C_a, and E_0 is the quantum use efficiency. Additionally, the maximum photosynthesis rate is influenced by $[CO_2]$ using

$$A_{\max(CO_2)} = \frac{C_a - \Gamma}{350 - \Gamma} \cdot A_{\max(350)} \tag{4}$$

2.3.3 The Hoffmann Approach for CO_2 Impact on Photosynthesis

An approach similar to Nonhebel's (1996) was chosen by Hoffmann (1995). Based on his own work with sugar beet and tree species and on data previously obtained by Gaastra (1959), he adjusted $A_{\max}$ by the factor

$$K_{CO_2} = \frac{\frac{C_a - \Gamma}{k_1 + C_a - \Gamma}}{\frac{C_{a0} - \Gamma}{k_1 + C_{a0} - \Gamma}} \tag{5}$$

where C_{a0} denotes the ambient [CO_2] and C_a is the elevated [CO_2]. Furthermore, k_1 = 220 + 0.158 · I_g and Γ = 80 – 0.0036 · I_g, where I_g is the global radiation [kJ m^2 d^{-1}].

2.3.4 The Allen/Yu Approach for CO_2 Impact on crop Transpiration

Only one approach was selected to describe crop transpiration. Evapotranspiration was calculated according to Penman and Monteith (Allen et al., 1998), using the stomata resistance calculated according to the suggestion by Yu et al. (2001b) as

$$r_s = \frac{C_s\left(1+\frac{D}{D_0}\right)}{a \cdot A_g} \tag{6}$$

where a is a constant, A_g denotes the gross photosynthesis rate, D/D_0 describes the air water vapour deficit and C_s is the ambient CO_2 concentration at leaf level, which in this case was set equal to C_a.

2.4 Model Calibration and Algorithm Testing

The HERMES model was calibrated to the data of the control treatment of the FACE experiment using the output variables of soil moisture (sum of 0 – 60 cm soil depth), above-ground crop dry matter and yield. Willmott's Index of Agreement (IoA) was used as a goodness-of-fit criterion (Willmott, 1981)

$$\mathrm{IoA} = 1 - \frac{\sum_{i=1}^{n}(P_i - O_i)^2}{\sum_{i=1}^{n}(|P_i - \overline{O}| + |O_i - \overline{O}|)^2} \tag{7}$$

where n denotes the number of experiments, P_i is the predicted value, O_i is the observed value and $\overline{O}$ is the observed mean.

To simulate the elevated [CO_2] treatments, the CO_2 response algorithms were incorporated. No further calibration was carried out. The Allen/Yu algorithm was tested in combination with the three approaches for CO_2 impact on photosynthesis.

3 Results

The Braunschweig FACE experiment revealed two important results: increased [CO_2] (i) enhanced crop growth for all investigated species and (ii) decreased the evapotranspiration rate of the canopies, resulting in higher soil moisture content (Weigel et al., 2005; Weigel et al., 2006). All algorithms tested within the HERMES model framework were able to adequately describe the observed crop growth and soil moisture dynamics under ambient and elevated [CO_2] (Table 2). Since the Nonhebel and Mitchell approaches also affected the method of calculating photosynthesis under ambient C_a (Fig. 1), simulation of the control treatment process yielded different results for all selected approaches. IoA yielded values of between 0.93 and 0.99 for the calibrated simulation of above-ground dry matter (including beet dry mass for sugar beet) and yield with a sufficient supply of N. However, the simulation performance was similar under limited N supply and elevated [CO_2]. For these variables, the Nonhebel approach performed slightly less adequately than

the others (Fig. 2). All algorithms were able to describe an observed increase in above-ground dry matter for all crops in the rotation under elevated C_a.

The simulation of LAI was already poor for the calibrated simulation (0.52 – 0.61) and further decreased under N limitation (0.49 – 0.55), elevated [CO_2] (0.51 – 0.57) and a combination of both (0.49 – 0.54).

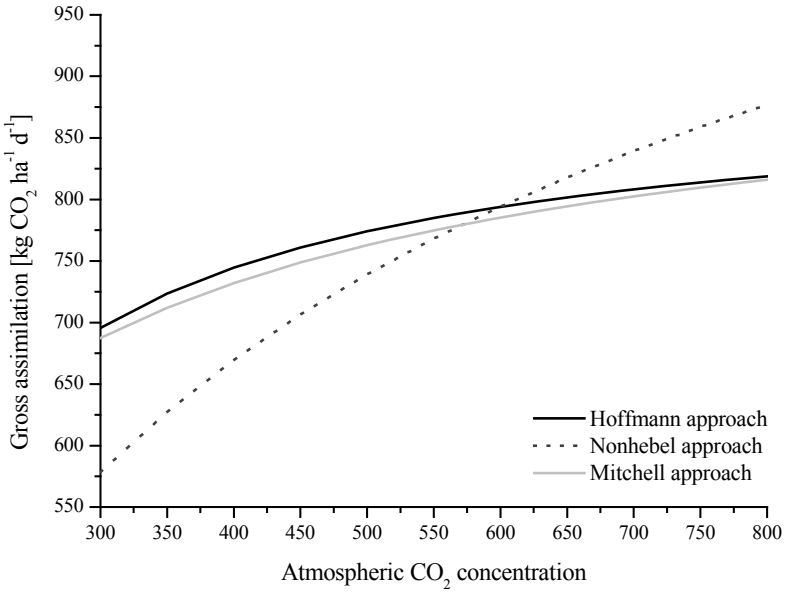

Figure 1 Gross assimilation simulated for a clear day (2150 J cm^2 d^{-1}) at Braunschweig, Germany, using three different approaches for the description of the CO_2 effect on photosynthesis: sensitivity analysis for atmospheric CO_2 concentration

Table 2 Index of Agreement (Willmott, 1981) as a goodness-of-fit criterion for the simulation of the crop rotation experiment, using different approaches for the description of CO_2 impact on crop growth

CO_2 level [ppm]	Ambient		550		Ambient		550	
N level [%]	100	50	100	50	100	50	100	50
	Hoffmann				**Hoffmann + Allen/Yu**			
Above-ground dry matter	0.99	0.98	0.99	0.99	0.99	0.99	0.99	0.99
Yield	0.98	0.96	0.97	0.94	0.98	0.98	0.97	0.97
Leaf area index	0.61	0.55	0.57	0.54	0.57	0.55	0.61	0.56
Soil moisture (0 – 60 cm)	0.82		0.80		0.86		0.85	
Mean IoA			**0.84**				**0.85**	
	Nonhebel				**Nonhebel + Allen/Yu**			
Above-ground dry matter	0.95	0.94	0.98	0.96	0.95	0.99	0.98	0.98
Yield	0.93	0.94	0.95	0.93	0.93	0.94	0.95	0.92
Leaf area index	0.66	0.58	0.55	0.52	0.66	0.59	0.55	0.54
Soil moisture (0 – 60 cm)	0.82		0.80		0.85		0.85	
Mean IoA			**0.82**				**0.83**	

(Continued)

CO_2 level [ppm]	Ambient		550		Ambient		550	
N level [%]	100	50	100	50	100	50	100	50
	Mitchell				**Mitchell + Allen/Yu**			
Above-ground dry matter	0.99	0.95	0.99	0.99	0.99	0.95	0.99	0.99
Yield	0.98	0.98	0.97	0.96	0.97	0.97	0.97	0.96
Leaf area index	0.52	0.49	0.51	0.49	0.52	0.50	0.52	0.50
Soil moisture (0 – 60 cm)	0.82		0.79		0.86		0.84	
Mean IoA	**0.82**				**0.82**			

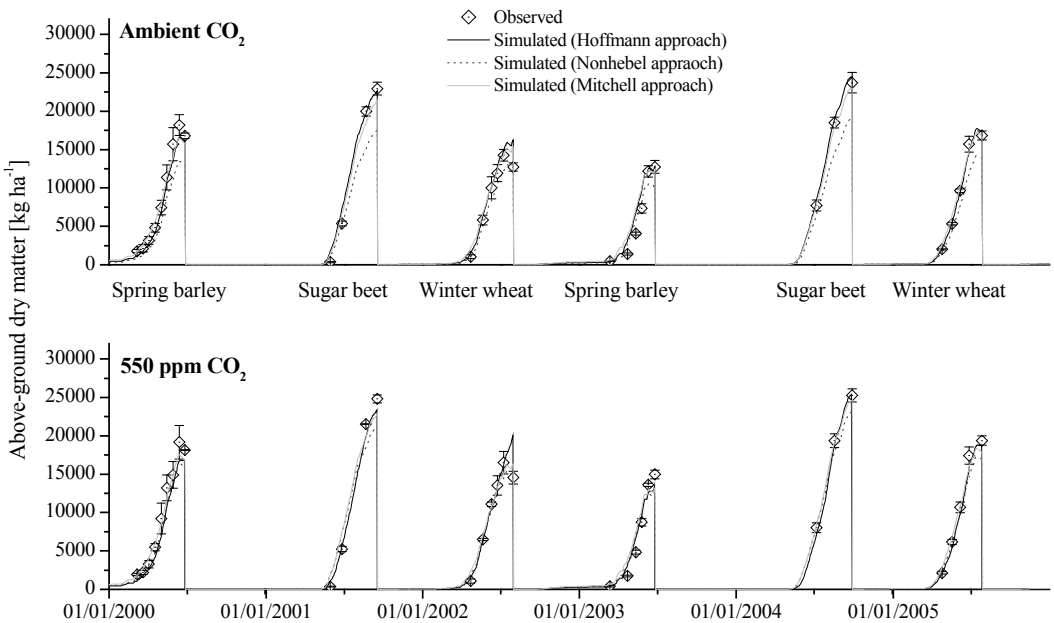

Figure 2 The Braunschweig FACE experiment: exemplary simulation of the above-ground dry matter (including tuber dry matter for sugar beet) using three different approaches for the description of the CO_2 effect on photosynthesis ◇ = observed above-ground dry matter (100% N treatment), —— = simulation using the Hoffmann (1993) approach —— = simulation using the Nonhebel (1996) approach and —— = simulation using the Mitchell (1995) approach

The simulation of soil moisture was compared to aggregated data (0 – 60 cm soil depth), revealing an IoA of 0.82 for calibrated conditions and 0.79 – 0.80 under elevated C_a. Measurements for the limited N treatment were not available.

The overall performance improved slightly when the CO_2 effect on transpiration was also taken into account (Table 2). The main reason for this improvement was the better performance of the soil moisture simulation for all approaches (Fig. 3). On the basis on above-ground dry matter, yield, LAI and soil moisture simulation, the Hoffmann approach to the CO_2 effect on photosynthesis in combination with the Allen/Yu approach to the CO_2 effect on transpiration performed best. Nonetheless, differences were marginal.

4 Discussion

A number of approaches have been published and tested against field or climate chamber data to describe the impact of [CO_2] on crop growth (Ewert et al., 2002). Although some empirical approaches on a linear basis have been used in climate change assessments (e.g. Bindi et al., 1996), most modeling approaches use algorithms that describe the CO_2 effect on photosynthesis in the asymptotic way it is observed in field and lab experiments (Gaastra, 1959).

A suitable approach to describe the CO_2 impact on crop growth within a soil-crop-environment model needs to consider all major feedback relations, as well as the semi-empirical character of the modeling framework. The model will calculate results in daily time steps with a limited number of input variables and parameters. Moreover, short computing times are required for future integration into a user-friendly decision support system. For these reasons, oversimplified and overelaborate approaches were not considered. The final selection included three different approaches of medium complexity, all sufficiently documented in the scientific literature. Testing these algorithms revealed that, at this level of detail, the choice of approach did not make much difference. All selected approaches enabled the model to adequately describe crop growth and yield, revealing an IoA ranging between 0.93 and 0.99. Such performances are often found for single season crop growth simulations (e.g. Eckersten and Jansson, 1991). However, for a six-year rotation with three different crops, this result is more than satisfactory (Kersebaum et al., 2007). The growth response to elevated [CO_2] as observed in the field experiment was also portrayed correctly by the model using the selected approaches. Although the Hoffmann approach performed best, the others were almost as good. However, the Nonhebel algorithm produced a steeper slope in the response curve than the other two algorithms (Fig. 1).

LAI simulation was less accurate; however, this was due to the insufficiency of the HERMES framework rather than the CO_2 response algorithms. Since in the HERMES model a LAI above 5.0 does not have any consequences on crop growth, this shortcoming can be ignored (van Keulen et al., 1982).

The similar performance for all tested algorithms is especially remarkable since the Hoffmann approach is given indirect preference under calibration: being the only algorithm not to affect any of the model framework's processes under ambient [CO_2], the calibration process yields the best performance for this approach *a priori*. Both Nonhebel and Mitchell algorithms affect a number of relations under ambient [CO_2]. Incorporating these algorithms already leads to lower quality simulation results than the Hoffmann approach for the ambient [CO_2] treatment. For the simulation of the elevated [CO_2] treatment, however, the preconditions were unbiased.

With regard to the sensitivity analysis depicted in Figure 1, the Hoffmann approach showed an assimilation response to [CO_2] resembling the Mitchell approach. This again is remarkable since the empirical Hoffmann approach is based on data from climate chambers obtained in the 1950s, while the Mitchell approach was developed from mechanistic considerations and data from both climate chambers and FACE experiments. The Nonhebel approach differs in the portrayed relation. However, at 550 ppm CO_2, all approaches yield a similar gross assimilation rate. Consequently, their simulation performance for this [CO_2] level is almost identical. The lower assimilation rate calculated using the Nonhebel approach for ambient [CO_2] consequently results in a lower simulated crop growth (Fig. 2). Expressed as the percentage of crop production at ambient [CO_2], the Hoffmann and Mitchell approaches predict an increase of approx. 10% at 550 ppm CO_2, which is in line with the findings of, e.g. Kimball et al. (1995) and Weigel et al. (2006).

Simulation of the soil moisture dynamics yielded acceptable results for the ambient [CO_2] treatment. The sugar beet was irrigated during the experiment and developed only a shallow rooting system. This had an impact on the simulation of the depth distribution of soil moisture (not shown)

since the default parameters for sugar beet assume a non-irrigated crop. For this reason, we chose a method of displaying the data as bulk percentage of field capacity to show that within the soil depth of 60 cm at least the overall amount of water in the soil was correctly simulated (Fig. 3). Under elevated [CO_2], a higher soil moisture level was observed in the field. Using the CO_2 response algorithm for transpiration this effect was correctly described by the model. Even if the details of water movement in individual years were not adequately simulated, the difference between the two CO_2 treatments expressed as the sum over six years corresponded well with the observed mean difference in actual evapotranspiration of approx. 20 mm water per year (data not shown). This performance is acceptable for use as a multi-year simulation tool for climate impact assessment. With regards to feedback relations in ecological simulation models, it has to be emphasised that adding the CO_2 response algorithm for crop transpiration improved not only the simulation of soil moisture dynamics, but also the simulation of crop growth, albeit slightly.

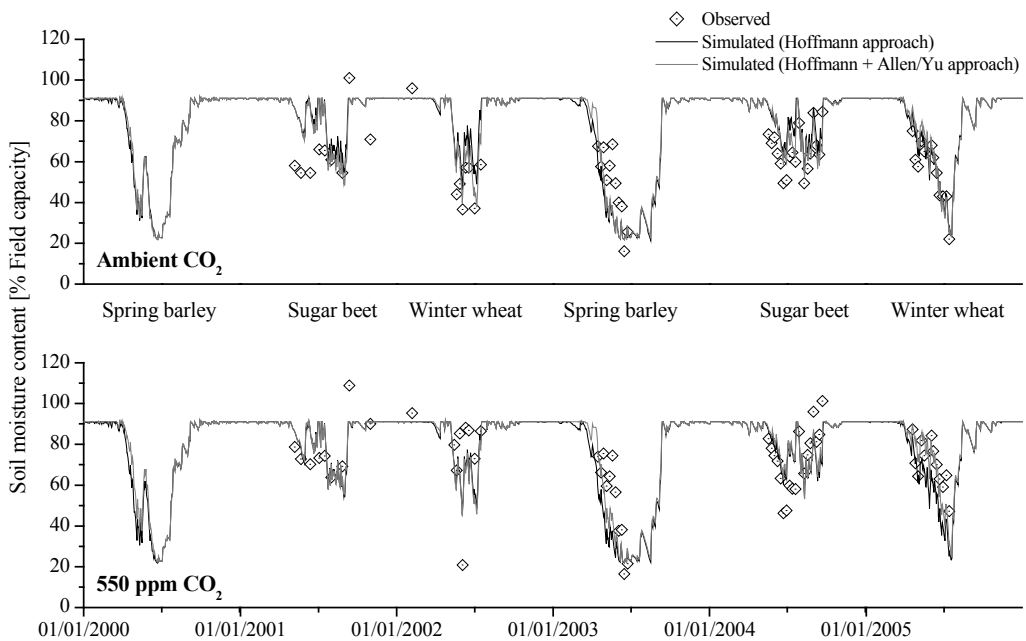

Figure 3 The Braunschweig FACE experiment: exemplary simulation of the soil moisture content using the Hoffmann approach for CO_2 impact calculation on photosynthesis with and without consideration of the CO_2 effect on crop transpiration according to Allen et al. (1998) and Yu et al. (2001b) for ambient atmospheric CO_2 concentration (top) and 550 ppm CO_2 level (bottom). ◇ = observed soil moisture, —— = simulated soil moisture using only the CO_2 effect on photosynthesis, —— simulated soil moisture using the CO_2 effect on photosynthesis and transpiration

The temperature effects on crop growth and feedback relations to CO_2 impact have been incorporated into the background of this investigation. This was due to the fact that temperature effects were not explicitly investigated in the FACE experiment. However, temperatures were recorded and used as input variables to drive the HERMES model, which simulates actual photosynthesis and respiration, dependent on temperature. With the temperature effects on soil water (evapotranspiration) and N (net mineralisation, denitrification) dynamics, the major modes of action for temperature in the investigated system are considered. For the Nonhebel and Mitchell approaches, temperature also affects the calculation of the CO_2 compensation point, while for the Hoffman approach the CO_2 compensation point is related to global radiation.

A model equipped with the top performer of the tested CO_2 response algorithms should be able to adequately simulate yield responses to the expected change of [CO_2], temperature and precipitation regime at the regional level to predict the future of agricultural crop production, where wheat, barley and sugar beet play a dominant role. The potential of such a model can be used in decision support platforms that aim to advise farmers and policy-makers on how to develop adaption strategies to meet the risks and potentials of climate change (LandCaRe2020; http://www.landcare2020.de/index.html).

5 Conclusions

To simulate expected climate change effects on regional agriculture, an algorithm was found to successfully describe the combined effects of [CO_2], temperature and moisture regime in a typical agricultural crop rotation in Northern Europe. Together with major feedback algorithms that were previously introduced in other simulation models, the important network of feedback relations between the above-mentioned climate variables makes the resulting model a powerful tool for climate impact assessment at regional and sub-regional levels.

Acknowledgements

The authors gratefully acknowledge funding from the German Federal Ministry of Education and Research (BMBF) within the “klimazwei” research program.

References

Acock, B. (1991) Modeling canopy photosynthetic response to carbon dioxide, light interception, temperature and leaf traits. p. 41-55. *In* K.J. Boote and R.S. Loomis (ed.) Modeling crop photosynthesis - from biochemistry to canopy. Crop Science Society of America, American Society of Agronomy, Anaheim, California, USA.

Acock, B., J.H.M. Thornley, and J.W. Wilson. (1971) Photosynthesis and energy conversion. p. 43-75. *In* Wareing P.F.and Cooper J.P. (ed.) Potential crop production. Heinemann Educational Publishers, London, UK.

Bodenkunde AG. (1994) Bodenkundliche Kartieranleitung. E. Schweizerbartsche Verlagsbuchhandlung, Hannover.

Allen, R.G., Pereira L.S., Raes D.et al. (1998) Crop evapotranspiration. Guidelines for computing crop water requirements. FAO Irrigation and Drainage Paper 56, Roma.

Anderson, J.L., Balaji V., A.J. Broccoli, et al.Global Atmospheric Model Dev. (2004) The new GFDL global atmosphere and land model AM2-LM2: Evaluation with prescribed SST simulations. J. Clim. 17 (24):4641 – 4673.

Ball, J.T., Woodrow I.E., and Berry J.A.. (1987) A model predicting stomatal conductance and its contribution to the control of photosynthesis under different environmental conditions. p. 221 – 224. *In* I. Biggins (ed.) Progress in photosynthesis research. Martinus Nijhoff Publishers, The Netherlands.

Bindi, M., Fibbi L., Gozzini B., et al.(1996) Modeling the impact of future climate scenarios on yield and yield variability of grapevine. Clim. Res. 7:213 – 224.

Buckley, T., Mott K., and Farquhar G.D..(2003) A hydromechanical and biochemical model of stomatal conductance. Plant Cell Environ. 26 (10):1767 – 1785.

Bykov, O.D., Koshkin V.A., and Catsky J.(1981) Carbon dioxide compensation concentration of C-3 and C-4 plants - Dependence on temperature. Photosynthetica 15 (1):114 – 121.

Collatz, G.J., Ball J.T., Grivet C.,et al.(1991) Physiological and environmental regulation of stomatal conductance, photosynthesis and transpiration - A model that includes a laminar boundary layer. Agric. For. Metorol. 54 (2-4):107 – 136.

Cowan, I. (1977) Stomatal behaviour and environment. Adv. Bot. Res. 4:117 – 228.

Dewar, R.C. (1995) Interpretation of an empirical model for stomatal conductance in terms of guard cell function. Plant Cell Environ. 18 (4):365-372.

Dewar, R.C. (2002) The Ball-Berry-Leuning and Tardieu-Davies stomatal models: synthesis and extension within a spatially aggregated picture of guard cell function. Plant Cell Environ. 25 (11):1383 – 1398.

Dubrovsky, M. (1997) Creating daily weather series with use of the weather generator. Environmetrics 8 (5):409 – 424.

Eckersten, H., Jansson P.E.(1991) Modeling water flow, nitrogen uptake and production of wheat. Fert. Res. 27:313 – 329.

Ewert, F., Rodriguez D., Jamieson P., et al.(2002) Effects of elevated CO_2 and drought on wheat: testing crop simulation models for different experimental and climatic conditions. Agr. Ecosyst. Environ. 93 (1 – 3):249 – 266.

Farquhar, G.D., S. von Caemmerer. (1982) Modeling of photosynthetic response to environmental conditions. p. 549-587. *In* O.L. Lange et al. (ed.) Encyclopedia of plant physiology. New series. Volume 12B. Physiological plant ecology. II. Water relations and carbon assimilation.

Farquhar, G.D., S. von Caemmerer, and J.A. Berry. (1980) A biochemical model of photosynthetic CO_2 assimilation in leaves of C-3 species. Planta 149 (1):78 – 90.

Farquhar, G.D., Wong S.C.(1984) An empirical model of stomatal conductance. Austr. J. Plant Physiol. 11 (3):191 – 209.

Gaastra, P. (1959) Photosynthesis of crop plants as influenced by light, carbon dioxide, temperature, and stomatal diffusion resistance. Mededel. Landbouwhogesch. Wageningen 59 (13):1 – 68.

Gao, Q., Zhao P., Zeng X., et al. (2002) A model of stomatal conductance to quantify the relationship between leaf transpiration, microclimate and soil water stress. Plant Cell Environ. 25 (11):1373-1381.

Gerwitz, A., Page E.R.(1974) An empirical mathematical model to describe plant root systems. J. Apl. Ecol. 11:773 – 781.

Goudriaan, J., H.H. van Laar. (1978) Relations between leaf resistance, CO_2 concentration and CO_2 assimilation in maize, beans, lalang grass and sunflower. Photosynthetica 12 (3):241 – 249.

Goudriaan, J., H.H. van Laar. (1994) Modeling potential crop growth processes. Kluwer Academic Publishers, Dordrecht, The Netherlands.

Greenwood, D.J., D.A. Stone, and A. Draycott. 1990. Weather, nitrogen supply and growth rate of field vegetables. Plant Soil 124 (2):297 – 301.

Harley, P.C., Weber J.A., and Gates D.M. (1985) Interactive effects of light, leaf temperature, CO_2 and O_2 on photosynthesis in soybean. Planta 165 (2):249 – 263.

Hoffmann, F. (1995) Fagus, a model for growth and development of beech. Ecol. Mod. 83 (3):327 – 348.

Hoogenboom, G., Jones J.W., and Boote K.J. (1992) Modeling growth, development, and yield of grain legumes using Soygro, Pnutgro, and Beangro - A review. Trans. ASAE 35 (6):2043 – 2056.

IPCC. (2007) Climate Change 2007: The Physical Science Basis. Contribution of Working Group I to the Fourth Assessment Report of the Intergovernmental Panel on Climate Change. Cambridge University Press, Cambridge, United Kingdom and New York, NY, USA.

Jacob, D., L. Barring, O.B. Christensen, et al.(2007) An inter-comparison of regional climate models for Europe: model performance in present-day climate. Clim. Change 81:31 – 52.

Jamieson, P.D., M.A. Semenov. (2000) Modeling nitrogen uptake and redistribution in wheat. Field Crops Res. 68 (1):21 – 29.

Jarvis, P.G. (1976) Interpretation of variations in leaf water potential and stomatal conductance found in canopies in field. Philosophical Transactions of the Royal Society of London Series B-Biological Sciences. 273 (927):593 – 610.

Johns, T.C., Durman C.F., Banks H.T. et al.(2006) The new Hadley Centre Climate Model (HadGEM1): Evaluation of coupled simulations. J. Clim. 19 (7):1327 – 1353.

Kersebaum, K.C. (2007) Modeling nitrogen dynamics in soil-crop systems with HERMES. Nutr. Cycl. Agroecosys. 77 (1):39 – 52.

Kersebaum, K.C. (1995) Application of a simple management model to simulate water and nitrogen dynamics. Ecol. Mod. 85:145 – 156.

Kersebaum, K.C., Beblik A.J. (2001) Performance of a nitrogen dynamics model applied to evaluate agricultural management practices. p. 549-569. *In* M.J. Shaffer et al. (ed.) Modeling carbon and nitrogen dynamics for soil management. Lewis, Boca Raton, FL, USA.

Kersebaum, K.C., Hecker J.-M., Mirschel W. et al..(2007) Modeling water and nutrient dynamics in soil-crop systems: a comparison of simulation models applied on common data sets.-in press. *In* K.C. Kersebaum et al. (ed.) Modeling water and nutrient dynamics in soil crop systems. Springer, Stuttgart.

Kimball, B.A., Pinter P.J., Garcia R.L., et al.(1995) Productivity and water use of wheat under free-air CO_2 enrichment. Global Change Biology 1 (6):429 – 442.

Leuning, R. (1995) A critical appraisal of a combined stomatal-photosynthesis model for C-3 plants. Plant Cell Environ. 18 (4):339 – 355.

Leuning, R. (1990) Modeling stomatal behavior and photosynthesis of Eucalyptus-Grandis. Austr. J. Plant Physiol. 17 (2):159 – 175.

Lewin, K.F., Hendrey G.R., and Kolber Z. (1992) Brookhaven National Laboratory Free-Air Carbon-Dioxide Enrichment Facility. Crit. Rev. Plant Sci. 11 (2-3):135 – 141.

Lobell, D.B., Burke M.B., Tebaldi C. et al. (2008) Prioritizing climate change adaptation needs for food security in 2030. Science 319:607 – 610.

Long, S.P. (1991) Modification of the response of photosynthetic productivity to rising temperature by atmospheric CO2 concentrations - Has its importance been underestimated. Plant Cell Environ. 14 (8):729 – 739.

Manderscheid, R., Weigel H.J. (2007) Drought stress effects on wheat are mitigated by atmospheric CO_2 enrichment. Agron. Sust. Dev. 27 (2):79 – 87.

Mitchell, R.A.C., Lawlor D.W., Mitchell V.J. et al. (1995) Effects of elevated CO_2 concentration and increased temperature on winter-wheat - Test of ARCWHEAT1 simulation model. Plant Cell Environ. 18 (7):736 – 748.

Nonhebel, S. (1996) Effects of temperature rise and increase in CO_2 concentration on simulated wheat yields in Europe. Clim. Change 34 (1):73 – 90.

Olesen, J.E., Bindi M.. (2002) Consequences of climate change for European agricultural productivity, land use and policy. Eur. J. Agron. 16 (4):239 – 262.

Plummer, D.A., Caya D., Frigon A. et al. (2006) Climate and climate change over North America as simulated by the Canadian RCM. J. Clim. 19 (13):3112 – 3132.

Porter, J. (1993) AFRCWHEAT2: a model of the growth and development of wheat incorporating responses to water and nitrogen. Eur. J. Agron. 2 (2):69 – 82.

Richter, J., Nuske A., Habenicht W.et al. (1982) Optimized N-mineralization parameters of loess soils from incubation experiments. Plant Soil 68:379 – 388.

Ritchie, J.T., Otter-Nacke. S. (1985) Description and performance of CERES-Wheat: a user-orientated wheat yield model. ARS Wheat Yield Project, Washington D.C.

Rodriguez, D., Ewert.F., Goudriaanet J.et al (2001) Modeling the response of wheat canopy assimilation to atmospheric CO_2 concentrations. New Phytol. 150 (2):337 – 346.

Semenov M.A., Barrow E.M. (1997) Use of a stochastic weather generator in the development of climate change scenarios. Clim. Change 35 (4):397 – 414.

Spitters C.J.T., van Kraalingen D.W.G and van Keulen. H. (1989) A Simple and Universal Crop Growth Simulator: SUCROS 87. p. 145 – 181. *In* : Rabbinge R et al. (ed.) Simulation and Systems Management in Crop Protection. Pudoc, Wageningen, The Netherlands.

Stanghellini, C., Bunce. J.A. (1993) Response of photosynthesis and conductance to light, CO_2, temperature and humidity in tomato plants acclimated to ambient and elevated CO_2. Photosynthetica 29 (4):487 – 497.

Stier, P., Feichter J., Kinne S. et al. (2005) The aerosol-climate model ECHAM5-HAM. Atmos. Chem. Phys. 5:1125 – 1156.

Tubiello, F.N., Ewert. F. (2002) Simulating the effects of elevated CO_2 on crops: approaches and applications for climate change. Eur. J. Agron. 18 (1 – 2):57 – 74.

van Keulen, H., Penning de Vries F.W.T, and Drees. E.M. (1982) A summary model for crop growth. p. 87 – 97. *In:* Penning de Vries F.W.T. and van Laar H.H. (ed.) Simulation of plant growth and crop production. PUDOC, Wageningen.

Watterson, I.G., Dix M.R., Gordon H.B. et al.. (1995) The CSIRO 9-Level Atmospheric General Circulation Model and its equilibrium present and doubled CO_2 climates. Aust. Meteorol. Mag. 44 (2):111 – 125.

Weigel, H.J., Dämmgen. U. (2000) The Braunschweig Carbon Projekt: atmospheric flux monitoring and free air carbon dioxide enrichment (FACE). J. Appl. Bot. 74:55 – 60.

Weigel, H.J., Manderscheid R., Burkart S. et al. (2006) Responses of an arable crop rotation system to elevated [CO_2]. p. 121 – 137. *In* : Nösberger J. et al. (ed.) Managed ecosystems and CO_2 case studies, processes, and perspectives. Ecological Studies, Vol. 187.

Weigel, H.J., Pacholski A., Burkart S. et al. (2005) Carbon turnover in a crop rotation under free air CO2 enrichment (FACE). Pedosphere 15 (6):728 – 738.

Williams, J.R., Jones C.A., Kiniry J.R. et al.(1989) The EPIC crop growth model. Trans. ASAE 32 (2):497 – 511.

Willmott, C.J. (1981) On the validation of models. Phys. Geogr. 2:184 – 194.

Yu, G.R., Kobayashi T., Zhuang J.E. et al.(2003) A coupled model of photosynthesis-transpiration based on the stomatal behavior for maize (Zea mays L.) grown in the field. Plant Soil 249 (2):401 – 416.

Yu, G.R., Zhuang J., and Yu. Z.L. (2001a) An attempt to establish a synthetic model of photosynthesis-transpiration based on stomatal behavior for maize and soybean plants grown in field. J. Plant Physiol. 158 (7):861 – 874.

Yu, Q., Goudriaan J., and Wang T.D. (2001b) Modeling diurnal courses of photosynthesis and transpiration of leaves on the basis of stomatal and non-stomatal responses, including photoinhibition. Photosynthetica 39 (1):43 – 51.

Yu, Q., Zhang Y., Liuet Y. et al. (2004) Simulation of the stomatal conductance of winter wheat in response to light, temperature and CO_2 changes. Ann. Bot. 93 (4):435 – 441.

Ziska, L.H., Bunce J.A. (2007) Predicting the impact of changing CO_2 on crop yields: some thoughts on food. New Phytol. 175 (4):607 – 617.

Bringing Genetics and Genomics to Crop Simulations: Experiences with Wheat, Sorghum and Common Bean in Solving the GEM-to-P Problem

J. W. White

(US Arid Land Agricultural Research Center, USDA-ARS, 21881 North Cardon Lane, Maricopa, AZ 85239, USA E-mail: jeffrey.white@ars.usda.gov)

Abstract: Genetics and genomics offer avenues to reduce model uncertainty by improving descriptions of cultivar differences and of individual plant processes. Ultimately, this should greatly enhance our ability to integrate data on genotypes (G), environment (E) and management (M) in order to quantitatively predict phenotypes (P), which can be termed the GEM-to-P problem. This paper reviews use of genetics and genomics with emphasis on wheat (*Triticum aestivum*), sorghum (*Sorghum vulgare*) and common bean (*Phaseolus vulgaris*). Cultivar specific parameters, such as for photoperiod sensitivity or grain size, are often problematic because their values are determined empirically from field studies and because the assumed physiology is inaccurate. Genotypic data should be more reliable than phenotypic data, since environmental effects are minimized. Using the Cropping System Model (CSM) for bread wheat, sorghum and common bean, coefficients were estimated through linear functions of gene effects. For all three crops, simulations using gene-based coefficients were similar to those from conventional coefficients. The main constraint to wider use of this approach is the limited number of loci that have been characterized for readily modeled traits. However, emerging genomic tools allow rapid, robust characterization of genes such as the *Vrn* and *Ppd* series in wheat, and data limitations are diminishing. Genomics can also improve how processes are modeled. Examples include determining the end of the juvenile phase, characterizing interactive effects of temperature on photoperiod sensitivity, improving how tiller development is modeled, and estimating carbon costs of low-lignin traits for bioenergy crops. Realizing the potential of crop genetics and genomics, however, will not happen spontaneously. Modelers must broaden their understanding of genomics and related fields, while developing effective collaborations with the plant biology community.

Keywords: QTL, quantitative trait loci

1 Introduction

Process-based ecophysiological models are powerful tools for predicting how plant performance (the phenotype) vary in response to genetic makeup of the plants (G), the biophysical environment (E) they grow in, and how the plants are managed (M). Cooper et al. (2002) described this prediction problem as the genotype to phenotype or GP problem, but it is more accurately termed the GEM-to-P problem, recognizing the contributions of environment and management. While we are far from solving the GEM-to-P problem, ecophysiological models are widely used both as research and decision support tools.

Uncertainty erodes confidence in crop simulations but can be decreased by accurately specifying inputs and improving how individual processes are represented. Genetics and genomics offer

avenues to benefit both aspects of modeling (White and Hoogenboom, 2003). The simplest and most immediately practicable opportunities relate to improved estimation of model parameters used to represent cultivar differences, such as for photoperiod sensitivity or grain size. These parameters are often problematic because their values are determined empirically from field studies and because the assumed underlying physiology is inaccurate. Further opportunities reside in using information from genomics and related fields to improve representations of specific physiological processes.

This paper reviews use of genetics and genomics to improve models with emphasis on experiences from bread wheat (*Triticum aestivum*), sorghum (*Sorghum vulgare*), and common bean (*Phaseolus vulgaris*). Table 1 describes six levels of genetic detail that models may implement, ranging from non-species specific, generic models to models that seek to describe processes by scaling up from gene-sequences or gene products and eventually, to major physiological processes or even an entire plant. These six levels provide a useful framework for our discussion. Current widely-used models such as the Cropping Systems Model (Jones et al., 2003), which is distributed with the Decision Support System for Agrotechnology Transfer for (DSSAT) software (Hoogenboom et al., 2004), and APSIM (McCowan et al., 1996) are at level 3 (Table 1), where genetic differences are specified through empirically adjusted coefficients affecting traits like photoperiod sensitivity, leaf appearance rate, and characteristic leaf or grain sizes. Emphasis is given here to improvements in modeling per se. The ultimate goal, of course, is to benefit applications ranging from ideotype specification to cultivar adaptation to climate change (Hoogenboom et al., 2004).

Table 1 Six levels of genetic detail in crop simulations models (after White and Hoogenboom, 2003)

1. Generic: no consideration of difference among species
2. Species-specific: species described but no cultivar differences recognized
3. Cultivar specific parameters used to describe cultivar differences
4. Cultivar differences represented by genotypes with linear model parameters
5. Cultivar differences expressed through processes described using knowledge of gene expression and gene products
6. Full representation of gene regulators, gene-products, etc. in networks

2 Gene-Based Estimation of Model Parameters

The most immediately practicable approach for employing genetic information is to estimate cultivar parameters as a function of the alleles present at known loci, corresponding to level 4 in Table 1. An essential first step is to assemble field data for a large set of germplasm known to vary for loci of interest. This can be problematic since breeding nurseries typically deal with materials of similar adaptation and may show limited variation. In the case of sorghum, near-isogenic lines for maturity loci had been tested in a wide range of environments, providing a valuable data resource for model development (White et al., 2007b). The field data are then used to calibrate the cultivar coefficients using the conventional approach of adjustment and comparison of measured vs. simulated data on phenotypes. With the coefficient values in hand, one can then proceed to estimate the effects of known loci.

In the simplest case, where only dominant and recessive alleles are known and cultivars are pure, inbred lines, the alleles can be scored with a value of 1 if dominant and 0 if recessive, and their effects estimated through linear regression. Thus, for two alleles affecting a cultivar parameter P, one might have:

$$P = a + bL_1 + cL_2$$

where a, b and c are regression coefficients (estimated through ordinary least squares), and L_1 and L_2 are scores for two loci. Interactions among loci (genetic epistasis) are incorporated by multiplying loci effects (e.g., $L_1 \times L_2$), as done for the *Ppd* and *Hr* loci affecting photoperiod sensitivity in common bean (White and Hoogenboom, 1996). Applied to wheat, the estimating equation for the effect of the *Ppd-D1* locus on the photoperiod sensitivity coefficient P1D thus was:

$$\text{P1D} = 39.9 - 13.9\ \textit{Ppd-D1} \qquad R^2 = 0.42^{**}$$

where *Ppd-D1* indicated the effect of the corresponding locus. Note that dominance (*Ppd-D1* = 1) reduces the value of P1D, reducing photoperiod sensitivity, which agrees with the described effect of the locus.

Selection of alleles used to estimate a parameter should emphasize physiological rationales. For example, based on our knowledge of action of the *Rht* loci in wheat, one might expect them to influence leaf size but not photoperiod sensitivity. Tests for significance of coefficients can be used to reject loci whose effects are too small or uncertain to merit inclusion in a given regression, but physiological understanding (or at least firm hypotheses) should lead variable (locus) selection.

Estimation through linear regression has been used successfully for common bean, soybean (*Glycine max*), sorghum and wheat (White and Hoogenboom, 1996; Hoogenboom et al., 1997; Stewart et al., 2003; Messina et al., 2006; White et al., 2007b; White et al., 2008). Fig. 1 shows simulations of days to flowering using gene-based approaches for sorghum and wheat, using independent evaluation datasets. For both crops, simulations of flowering dates were similar to those obtained with conventional cultivar coefficients (White et al., 2007b and 2008).

Table 2 Comparisons of results for conventional and gene-based simulation models of time to flower for sorghum (White et al., 2007b), and wheat (White et al., 2008). Evaluation datasets are independent from calibration sets, predominantly involving different locations. The variation that was explained by assuming no differences among cultivars was tested by evaluating simulations based on a single generic cultivar

Crop	Dataset	*N*	Model type	Mean	R^2	Slope	RMSE
Sorghum	Calibration	108	Generic	64	0.23**	0.76	12.5
			Conventional	67	0.61**	0.76	8.8
			Gene-based	67	0.55**	0.73	9.5
	Evaluation	74	Generic	58	0.31**	1.41	8.8
			Conventional	61	0.60**	0.91	6.7
			Gene-based	61	0.61**	0.97	6.6
Wheat	Calibration	540	Generic	208	0.95**	0.95	9.7
			Conventional	209	0.98**	0.95	6.6
			Gene-based	208	0.96**	0.92	8.6
	Evaluation	1499	Generic	214	0.89**	1.02	10.4
			Conventional	213	0.92**	1.00	9.0
			Gene-based	214	0.90**	0.99	9.9

** Significant at the $P < 0.01$ level.

Table 2 summarizes results of simulations of time to flowering in sorghum and wheat using conventional and gene-based modeling. In testing effects of genotypes, the effect of a “generic” cultivar was included in order to provide a more meaningful basis for comparison. For each species,

parameter values for the generic cultivar were estimated as the mean values for all cultivars being examined (the modal value could also be used). For sorghum, the generic cultivar performed poorly compared to the conventional and gene-based models, but in wheat, the generic cultivar was surprisingly effective (Table 2). One interpretation of these results is that for the wheat dataset, there were very large differences among environments that a generic cultivar was capable of representing, whereas in sorghum cultivar differences were large relative to environmental differences. Regression analysis and related techniques provide valuable tool for exploring the relative ability of models to explain genotype, environment and management effects (White et al., 2007a).

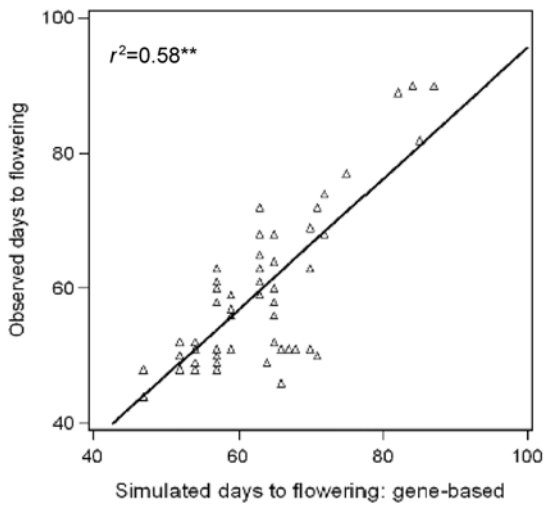

(a)

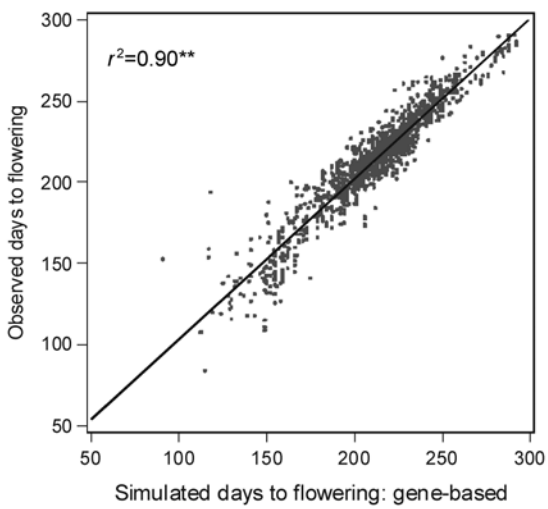

(b)

Figure 1 Comparison of observed vs simulated days to flowering using gene-based model parameters. Both datasets were independent of calibration data. (a) For sorghum recombinant inbred lines varying for *Ma* loci (White et al., 2007b). (b) For 30 wheat cultivars of the IWWPN (White et al., 2008)

In GeneGro, the common bean model that first used gene-based estimation, genotypes were input directly into the model, and gene effects were specified as part of the model code. Subsequently, we realized that since the gene effects were only used to specify model parameters, the calculations

should be external to the model code: the gene-based estimates of cultivar parameters can simply replace the conventionally estimated parameters. Thus for wheat and sorghum, we estimated gene-effects externally and inputted the values to the model through alternate files containing gene-based estimates of the cultivar parameters. Additional minor innovations in the basic approach have included consolidating effects of three loci with similar effects (*Vrn-A1, Vrn-B1,* and *Vrn-D1* in wheat) through a single variable for number of dominant alleles present (White et al., 2008) and accounting for the three alleles of the sorghum Ma_3 locus by scoring values of 1.0, 0.5 and 0 based on estimates of the relative effect of each allele (White et al., 2007b).

The main constraints to gene-based estimation of cultivar parameters probably are that many modelers are not familiar enough with crop genetics to implement the approaches, that very few loci are sufficiently characterized to permit efficient modeling, and that even if loci are well characterized in terms of their effects and underlying physiology, few cultivars have been genotyped for loci of interest. Reducing the first constraint requires effort from the modeling community. The latter two constraints are diminishing rapidly as genomic tools facilitate characterization of cultivars for loci such as the *Vrn* and *Ppd* series in wheat as well as accelerate identification of new loci. Illustrating this progress, CIMMYT is now capable of genotyping wheat lines for photoperiod sensitivity (*Ppd-B1, Ppd-D1*), vernalization (*Vrn-A1, Vrn-B1, Vrn-D1*) and plant height (*Rht-B1, Rht-D1*), at a cost per locus of $2.00 US (S. Dreisigacker, 2008, personal communication).

In this transition period when characterization of loci affecting physiological traits limits progress in modeling, a complementary strategy is to use molecular markers to identify quantitative trait loci (QTL), and then use loci effects to estimate model parameters. In GeneGro (White and Hoogenboom, 1996), this approach was implicitly used since the three hypothetical loci for seed mass were inferred mainly from QTL studies. QTL-based estimation has been used in simulating barley growth and yield (*Hordeum vulgare*; Yin et al., 2000), sorghum phenology (Chantereau et al., 2001) and leaf growth in maize (Reymond et al., 2003). Traditional QTL studies based on populations of inbred lines have numerous limitations, but these problems are being overcome through approaches combining high throughput marker systems such as Diversity Array Technology (Wenzl et al., 2004) with association mapping (Janink and Walsh, 2002; Crossa et al., 2007).

3 Improved Physiology

In a sense, simple linear models of gene action imply partial knowledge of the underlying physiology. Specifying that the bean *Ppd* locus only affected photoperiod parameters implicitly assumed that the photoperiod response is independent of traits related to growth such as intrinsic leaf size or potential leaf photosynthetic rate. However, such trivial examples represent minimal advances in our understanding of physiology. Better integration of plant science and ecophysiological modeling is still needed (Hammer et al., 2004; Yin et al., 2004; White, 2006) in order to move to level 5 of Table 1. Four cases are explored illustrating the potential benefits to modeling.

Onset of flowering in many plant species depends on activation of the meristem identity gene APETALA1 (*AP1*), which initiates the conversion of the shoot apex to a reproductive state (Murai et al., 2003; Imaizumi and Kay, 2006). The photoperiod system inhibits *AP1*, but to model the photoperiod effect, one needs to specify time of onset and end of photoperiod sensitivity. The onset of sensitivity is considered to represent the end of the juvenile phase and usually is determined with experiment manipulations. Plants of a sensitive genotype are grown under both short and long day regimes, and individual plants are transferred from one regime to the other every few days. Analysis of days to flowering (or other stages) should reveal a date prior to which the plants can be grown in either photoperiod with no effect on development, indicating that this date corresponds to the end of the juvenile phase (e.g., Alagarswamy et al., 1998). Besides being labor intensive and requiring

large numbers of plants, the experiments may not reveal a clear transition (see Figs. 2 and 3 (in Alagarswamy et al., 1998)). Genomic tools should allow tracking the activity of the photoperiod system as manifested in levels of specific gene-products and ultimately provide reliable criteria for measuring the end of the juvenile phase, as well as the end of photoperiod sensitivity much later in development.

Warmer temperatures increase photoperiod sensitivity in many crops, and there are genetic differences among cultivars for this effect (e.g., Quinby et al., 1973; Cao and Moss, 1989; White et al., 1996). Presumably due to uncertainty over its physiological description, however, few models consider this interaction. Genomics offers the possibility of clarifying the underlying response mechanisms. Simply improving characterization of genotypes would facilitate testing alternative approaches to model the interaction, but genomics might determine whether the response involves a specific, independent temperature sensor or simply results from generic effects of temperature on metabolic rates.

Modeling effects of tillers is also problematic. Many models work well for high population densities and narrow row spacings, but they underestimate the growth and yield of tillers when interplant competition is low. The *Tin* locus inhibits tillering in wheat (Richards, 1988) and provides one entry point for molecular-level dissection of tillering. Tiller production involves phytochrome B as part of the shade avoidance syndrome, and advances in understanding of this system (Franklin and Whitelam, 2005) are another source of information for modeling tiller development.

A fourth example involves estimating the carbon costs of novel traits. Changes in plant composition are actively sought as a means to improve the digestibility of cereal straw for cellulosic ethanol production (Sarath et al., 2008). Lignins, as complex polymers of phenolic compounds, are not fermentable, and breeding seeks to manipulate their levels by means such as the brown midrib mutants of maize and sorghum (Sarath et al., 2008). In cereals, lignins typically represent 15 to 20% of stem dry weight, so reducing their levels should reduce the net growth respiration. The pioneering work of F. Penning de Vries suggested that the cost of biosynthesis of lignins is approximately 2.2 g glucose per 1 g lignin vs. 1.2 g g^{-1} for cellulose (Penning de Vries et al., 1983). These values allow a rough estimation of the impact of reduced lignin concentration on growth respiration, but more precise estimates would require a detailed understanding of the metabolic pathways affected—information obtainable through genomics and metabalomics. Of course, the metabolic benefit of lowering lignin concentration should be considered in the light of possible adverse effects such as reduced stem strength. Note that consideration of costs of biosynthesis should have broad applications in assessing possible trade-offs for crop improvement efforts that seek to radically alter plant structure or composition, regardless of whether the changes are through application of molecular or conventional breeding.

4 Plant Systems Biology

The sixth and highest level of complexity in modeling approaches is to explicitly represent biochemical networks of genes and gene products to achieve what is sometimes termed the "in silico plant" (Minorsky, 2003). Various software systems can simulate complex metabolic pathways (e.g., Hoops et al., 2006; Takahashi et al., 2004), and the Systems Biology Markup Language (SBML) was established to facilitate this research (Hu et al., 2005). Welch et al. (2003 and 2005) have probably advanced the furthest in applications that are relevant to crop modeling through their efforts to model control of flowering in Arabidopsis with simplified networks, although other flowering models also consider biochemical pathways (e.g., Locke et al., 2005).

5 How Well Can We Solve the GEM-to-P Problem?

While the arguments outlined above support optimism for improved ability to predict phenotypes from genotypes, environment and management, there is value in considering the potential limits to model prediction, especially using genetic data as inputs. For a given quantitative trait, one might ask what percent of variation can ultimately be explained by models that integrate the best available knowledge about genetics, physiology and the environment (Fig. 2). Certainly there has been progress since Reaumur (1735) first proposed concepts that provided the foundation of quantitative modeling of plant development, but if we look to 2050 or beyond, how much further improvement can we expect?

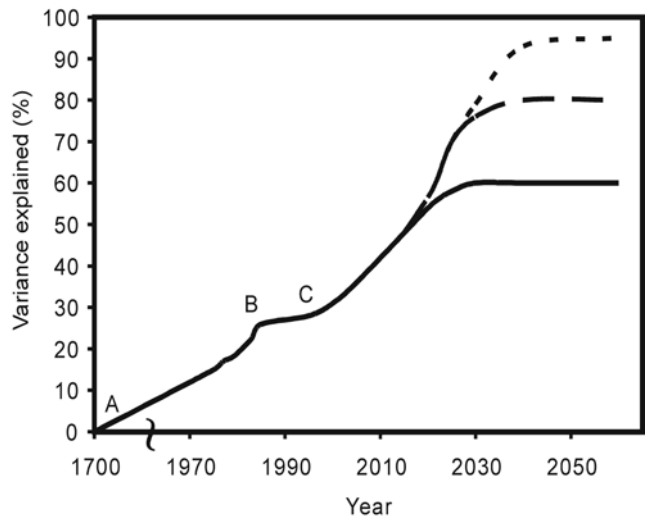

Figure 2 Hypothetical plot of progress in simulation of an arbitrary trait (e.g., flowering date). Note interrupted axis between 1700 and 1970. The three points correspond to the following events: A. First conceptualization of accumulated temperature affecting phenology by Reaumur (1735). B. Expansion of simple developmental models to consider photoperiod. C. First attempts to introduce genetic information into models

When the Arabidopsis genome was sequenced in 2000 (The Arabidopsis Genome Initiative, 2000), the genome was estimated to contain 25,000 genes. Subsequent progress in genomics suggests that the notion of "gene" is more complex than expected. MicroRNAs have proven to have important signaling roles, complicating the "one gene, one enzyme" paradigm (Axtell et al., 2007). Similarly, alternate splicing patterns of pre-messenger RNA mean that a single gene sequence can result in multiple transcripts and hence, multiple proteins (Reddy, 2007). And demonstration of important epigenetic effects imply that gene sequences are sometimes less important in regulating transcription than how DNA is physically packaged (Bender, 2002).

Taking 25,000 genes as a lower estimate of the potential complexity of a single species, one might argue that the prospects for major improvements in predictive ability are poor. However, counter-arguments in favor of additional simplifications exist. Many gene-systems may primarily affect disease or pest resistance and have minimal direct relevance to processes considered in ecophysiological models. Additionally, the genetic systems for pollination, fertilization and early embryo development may have limited relevance except as they relate to specific stress responses. In many cases, signaling systems, such as from roots to shoots, may not require complete description: it should suffice to know that a sensor exists and that a message is transmitted to a receptor. The simplified gene network model of Welch et al. (2005) for phenology exemplifies this "middle way."

The possible limits of crop modeling to solve the GEM-to-P problem also relates to the broader issue of whether evolution is driven by slow accumulation of micro-adaptations, which would favor arguments for genetic complexity, or whether most mutations are essentially neutral, and only occasionally do mutations cause major, step-like changes in phenotypes. The first hypothesis implies that we must ultimately model massively complex regulatory networks, while the latter favors a view that major simplifications are possible. The increasing availability of genome sequence data allows more rigorous testing of the nature of evolution (e.g., *Drosophila* 12 Genomes Consortium, 2007), including for crop domestication (Wright et al., 2005). To date, the evidence mainly suggests that the genomic rate of adaptive evolution differs greatly among species (Eyre-Walker, 2006).

Prospects for bringing genetics and genomics to ecophysiological modeling, and solving the GEM-to-P problem, appear excellent. However, the required research is surrounded with uncertainty that may ultimately require solving fundamental issues of plant evolution and function. Furthermore, realizing this potential will not happen spontaneously. Modelers must broaden their understanding of genomics and related fields, while developing effective collaborations with the plant biology community.

References

Alagarswamy, G., Reddy D.M., and Swaminathan G. (1998) Durations of the photoperiod-sensitive and -insensitive phases of time to panicle initiation in sorghum. Field Crops Res. 55:1 – 10.

Arabidopsis Genome Initiative. (2000) Analysis of the genome sequence of the flowering plant *Arabidopsis thaliana*. Nature (London) 408:796 – 815.

Axtell, M.J., Snyder J.A., and Bartel. D.P. (2007) Common functions for diverse small RNAs of land plants. Plant Cell 19:1750 – 1769.

Bender, J. (2002) Plant epigenetics. Current Biol. 12:R412-R414.

Chantereau,J, Trouche G,Rami J.F, et al.(2001) RFLP mapping of QTLs for photoperiod response in tropical sorghum. Euphytica 120:183 – 194.

Cooper, M.,Chapman S.C., Podlich D.W et al. (2002) The GP problem: quantifying gene-to-phenotype relationships. In Silico Biol. 2:151 – 164.

Crossa, J., Burgueno J., Dreisigacker S. et al.(2007) Association analysis of historical bread wheat germplasm using additive genetic covariance of relatives and population structure. Genetics 107:1889 – 1913.

Drosophila 12 Genomes Consortium. (2007) Evolution of genes and genomes on the *Drosophila* phylogeny. Nature 450:203 – 218.

Franklin, K.A., andWhitelam. G.C. (2005) Phytochromes and shade-avoidance responses in plants. Ann. Bot. 96:169 – 175.

Hammer, G.L., Sinclair, T.R, Chapman, S.C.,et al.(2004) On systems thinking, systems biology, and the in silico plant. Plant Phys. 134:909 – 911.

Hoogenboom, G., Jones J.W, Wilkens P.W,et al.(2004b) Decision Support System for Agrotechnology Transfer Version 4.0 [CD-ROM]. University of Hawaii, Honolulu, HI.

Hoogenboom, G., and White. J.W. (2003) Improving physiological assumptions of simulation models by using gene-based approaches. Agron. J. 95:82 – 89.

Hoogenboom G., White.J.W, Acosta-Gallegos J., et al.(1997) Evaluation of a crop simulation model that incorporates gene action. Agron. J. 89:613 – 620.

Hoogenboom, G., White J.W, andMessina C.D. (2004a) From genome to crop: integration through simulation modeling. Field Crops Res. 90:145 – 163.

Hoops, S., Sahle S., Gauges R.,et al.(2006) COPASI- A COmplex PAthway SImulator. Bioinformatics 22: 3067 – 3074.

Hucka, M., Finney A., Sauro H.M.,et al. (2003) The systems biology markup language (SBML): a medium for representation and exchange of biochemical network models. Bioinformatics 19:524 – 531.

Imaizumi, T., and Kay S.A. (2006) Photoperiodic control of flowering: not only by coincidence. Trends Plant Sci. 11:550 – 558.

Jannink, J.-L. andWalsh. J.B.(2002) Association mapping in plant populations. In: Kang M.S. (ed.) Quantitative Genetics, Genomics and Plant Breeding, edited by CABI, Wallingford, UK.

Jones, J.W., Hoogenboom G., Porter C.H, et al.(2003) The DSSAT Cropping System Model. Eur. J. Agron. 18:235 – 265.

Locke, J.C.W., Southern M.M, Kozma-Bognar L, et al.(2005) Extension of a genetic network model by iterative experimentation and mathematical analysis. Mol. Syst. Biol. 1:2005.0013.

McCowan, R.L., Hammer G.L., Hargreaves J.N.G, et al.(1996) APSIM: a novel software system for model development, model testing and simulation in agricultural systems research. Agric. Sys. 50:255 – 271.

Messina, C.D., Jones J.W, Booteet K.J,et al. (2006) A gene-based model to simulate soybean development and yield responses to environment. Crop Sci. 46:456 – 466.

Minorsky, P.V., (2003) Achieving the in silico plant. Systems biology and the future of plant biological research. Plant Physiol. 132, 404 – 409.

Quinby, J.D., Hesketh J.D, and Voigt. R.L. (1973) Influence of temperature and photoperiod on floral initiation and leaf number in sorghum. Crop Sci. 13:243 – 246.

Reaumur, R.A.F.d. (1735) Observations du thermometre, faites a Paris pendant I'annee 1735, compares avec celles qui ont ete faites sous la ligne, a l'lsle de France, a Alger et en quelques-unes de nos isles de I'Amerique. Mem. Acad. des Sci., Paris 545 – 576.

Reddy, A.S.N. (2007) Alternative splicing of pre-messenger RNAs in plants in the Genomic Era. Annual Rev. Plant Biol. 58:267 – 294.

Reymond, M., Muller B., Leonardi A.,et al. (2003) Combining quantitative trait loci analysis and an ecophysiological model to analyze the genetic variability of the responses of maize leaf growth to temperature and water deficit. Plant Physiol. 131:664 – 675.

Richards, R. (1988) A tiller inhibitor gene in wheat and its effect on plant growth. Austral. J. Agric. Res. 39:749 – 757

Sarath, G., Mitchell R, Sattler S, et al. Opportunities and roadblocks in utilizing forages and small grains for liquid fuels. J. Industr. Microbiol. Biotech: 10.1007/s10295-007-0296-3.

Stewart, D.W., Cober E.R.,and Bernard R.L.(2003) Modeling genetic effects on the photothermal response of soybean phenological development. Agron J 95:65 – 70.

Takahashi, K., Kaizu K, Hu B,et al.(2004) A multi-algorithm, multi-timescale method for cell simulation. Bioinformatics 20:538 – 546.

Welch, S.M., Roe J.L., and Dong Z..(2003) A genetic neural network model of flowering time control in *Arabidopsis thaliana*. Agron. J. 95:71 – 81.

Welch, S.M., Roe J.L, Das S.,et al. (2005) Merging genomic control networks and soil-plant-atmosphere-continuum models. Agric. Syst. 86:243 – 274.

Wenzl, P., Carling J., Kudrna D.,et al. (2004) Diversity Arrays Technology (DArT) for whole-genome profiling of barley. PNAS 101:9915 – 9920.

White, J.W., Kornegay J., and Cajiao C. (1996) Inheritance of temperature sensitivity of the photoperiod response in common bean (*Phaseolus vulgaris*). Euphytica 91:5 – 8.

White, J.W. (2006) From genome to wheat: Emerging opportunities for modeling wheat growth and development. Eur. J. Agron. 25:79 – 88.

White, J.W., and Hoogenboom. G. (1996) Simulating effects of genes for physiological traits in a process-oriented crop model. Agron. J. 88:416 – 422.

White, J.W., and Hoogenboom. G. (2003) Gene-based approaches to crop simulation: past experiences and future opportunities. Agron. J. 95:52 – 64.

White, J.W., Boote K.J, Hoogenboom G., et al. (2007a) Regression-based evaluation of ecophysiological models. Agron. J. 99:419 – 427.

White, J.W., Hoogenboom G., and Ottman M. (2007b) Modeling phenology of sorghum based on known maturity (*Ma*) loci. P. 83-85. In: Farming Systems Design 2007. Proc. Int. Conf., Catania, Italy. 10-12 Sept. 2007. http://www.iemss.org/farmsys07/uploads/Main/Field_farm_scale_CD.pdf (verified 31 March 2008).

White, J.W., Herndl M., Hunt L.A, et al.(2008) Simulation-based Analysis of Effects of *Vrn* and *Ppd* Loci on Flowering in Wheat. Crop Sci. 48: 678 – 687.

Yin, X., Chasalow S.D, Dourleijn C.J, et al.(2000) Coupling estimated effects of QTLs for physiological traits to a crop growth model: predicting yield variation among recombinant inbred lines in barley. Hered. 85:539 – 549.

Yin, X., Struik P.C, and Kropff M.J. (2004) Role of crop physiology in predicting gene-to-phenotype relationships. Trends in Plant Sci. 9:426 – 432.

Establishment of Dynamic Model for the Nutrient Uptake and Development about Tomato in Greenhouse

Jin-Xiang Chu, Zhong-Fu Sun, Ke-Ming Du, Qian Jia, Shuang Liu

(Institute of Environment and Sustainable Development in Agriculture, Chinese Academy of Agricultural Sciences, Beijing 100081, China, Correspondence author, E-mail: sunzf@263.net)

Abstract: Nutrient supply is of utmost importance in many crops. It is not well-understood and is one of the weakest features in crop simulation models. After studied nutrient dynamics of greenhouse tomato, a simulation model of nutrient uptake was established. First, daily N diamond of crop and daily N supply of soil are simulated. Then, the proportion about former to latter was calculated. The proportions about P and K were calculated in the same way. These proportions had obviously relationships with daily dry matter accumulation. So, after relationships mentioned above had been built, dynamically simulation model of nutrient uptake was established. Compared simulation data to experiment data, its reliability in simulating growth course and yield of greenhouse tomato was validated. At the same time, its sensitivity in simulating the nutrient lack and excessive was analyzed. With soil nutrient date in different area, growth on base soil nutrient supply was analyzed.

Keywords: nutrient, dynamically model, greenhouse tomato

The study about crop growth model was started at 1960's, now it goes to a practical period (Wang et al., 2002; Li et al., 2000; Li et al., 2006). Because it was based of growth mechanism and take good care of relations about crop，air, soil and environment (Lin et al., 2003; Xie et al., 2001), dynamic simulating crop growth model has been to the most effective tool in agricultural research. Several levels of limit factors were introduce into crop growth model study, for example, light and temperature level, water level, nutrition level, etc. More limit factor equals to less yield (Wang et al., 2005; Xie et al., 2003). The first two levels have been well studied, but the nutrition level hasn't. For the nutrition level, only field crops such as wheat, maize, rice, and cotton had been studied, studies about greenhouse crops was very lack (Wu et al., 2007; Li et al., 2007).

TOMSIM was designed by E. Heuvelink at 1992 in Holland, and was perfected continuously, now it is one of the most typical greenhouse crop models[10], which was developed with a universal structural design and could be extended to other crops through making some modification and improvement. It is mainly composed of a sub-model of dry matter production and a sub-model of dry matter partition. The loop of the calculating dry matter production is in one hour. Dry matter partition is absolutely independent to dry matter production. It was adjusted by sink strength. On the base of mechanism about TOMSIM, a new N,P and K uptake model was build, which can be used to simulate the crop growth and NPK uptake in greenhouse.

1 Model Establishment

1.1 Sub Model of NPK Uptake

(1) Substantial uptake simulate

Daily substantial uptake of NPK in different growing stage is calculated. Uptake of *N* is taking as

an example in this article.

Daily substantial uptake of N ($U_{S,N}$) can be expressed as a function of N concentration and N uptake capability around root surface.

$$U_{S,N} = 2\pi r_1 \alpha C_N L_v \tag{1}$$

where $U_{S,N}$ means daily substantial uptake of N (kgm^{-2}d^{-1}), r_1 means root semidiameter (cm), α is a coefficient of N uptake capability (cmd^{-1}), C_N means N concentration around root surface, L_v is root length density (cmcm^{-3}).

By the same way, daily substantial uptake of P ($U_{S,P}$) and K ($U_{S,K}$) can be calculated.

(2) Potential uptake simulate

Daily potential uptake of NPK is calculated by different growing stage. Potential N uptake is also taken as an example. Potential N uptake [$U_{P,N}$ (kgm^{-2}d^{-1})] has relation with utmost N concentration in root, stem and leaf. N is offered directly by root, stem and leaf, not absorbed from soil.

$$U_{P,N} = N_{r,\max}\Delta W_r(in) + N_{s,\max}\Delta W_s(in) + N_{l,\max}\Delta W_l(in) \tag{2}$$

in which, $N_{r,\max}$, $N_{s,\max}$ and $N_{l,\max}$ mean utmost concentration in root, stem and leaf (kgkg^{-1}). $\Delta W_r(in)$, $\Delta W_s(in)$ and $\Delta W_l(in)$ mean daily biomass growth of root (kg), stem and leaf. By the same way, daily potential uptake of P ($U_{P,P}$) and K ($U_{P,K}$) can be calculated.

1.2 Sub Model of Crop Growth

(1) Growing phase simulate

In the model, growth time is calculated by physiological growth day, which is influenced by the variety of tomato. When current physiological growth days accumulated enough, it goes to the next growth stage automatically. In this article, tomato growth is divided into five phases: germinating phase, sprouting phase, flowering-fruit bearing phase, fruit phase and harvest phase. Physiological development time is calculated according to:

$$\text{PDT} = \text{SUM(PDE)} \tag{3}$$

where PDE is daily physiological development efficiency.

Daily physiological development efficiency (PDE) is determined by daily relative thermal efficiency (RTE):

$$\text{PDE} = \text{RTE} \tag{4}$$

Relative thermal efficiency (RTE) is calculated according to:

$$\text{RTE} = \begin{cases} P^{-(T-T_0)^2} & T_L < T \le T_0 \\ P^{-\left\{\frac{T_0-T_L}{T_H-T_0}\right\}(T-T_0)^2} & T_0 < T < T_H \\ 0 & T \le T_L, T \ge T_H \end{cases} \tag{5}$$

in which, P means a uncertain parameter more than 1. T_L is the lower developmental temperature(℃),

T_H is the upper developmental temperature(℃), T_O is the optimum developmental temperature(℃), T is the daily average temperature(℃). T_L, T_O and T_H in different growing phases for tomato can be found on table 1.

Table 1 T_L, T_O and T_H in different growing phases for tomato

	T_L (℃)	T_O (℃)	T_H (℃)
Germinating phase	10	29	35
Sprouting phase	10	27	33
Flowering-fruit bearing phase	15	25	35
Fruit phase	15	25	35
Harvest phase	15	25	35

(2) Photosynthetic uptake simulate

Daily photosynthetic uptake [P_{ud} （g m^{-2} d^{-1}）] can be calculated by an integral equation of crop gross photosynthetic rate:

$$P_{ud} = \int_{T_1}^{T_2} P_{gc}(x)\mathrm{d}x \tag{6}$$

in which, P_{gc} is crop gross photosynthetic rate (g m^{-2} s^{-1}), T_1 is the start time of photosynthesis, T_2 is the stop time of photosynthesis.

P_{gc} is calculated as:

$$P_{gc} = P_{gc.\max}\left[1-\mathrm{Exp}\left(-\varepsilon\times\frac{\mathrm{PAR}}{P_{gc.\max}}\right)\right]\cdot\left[\mathrm{Min}\left(\frac{U_{S,N}}{U_{P,N}},\frac{U_{S,P}}{U_{P,P}},\frac{U_{S,K}}{U_{P,K}}\right)\right]^2 \tag{7}$$

where $P_{gc.\max}$ is the largest crop gross photosynthetic rate (g m^{-2} s^{-1}). ε is the crop photochemical efficiency(gJ^{-1}). PAR is the photosynthetically active radiation(Wm^{-2}). $\mathrm{Min}\left(\frac{U_{S,N}}{U_{P,N}},\frac{U_{S,P}}{U_{P,P}},\frac{U_{S,K}}{U_{P,K}}\right)$ is the minimum value of $\frac{U_S}{U_P}$ about *N*, *P* and *K*.

(3) Respiration consume simulate

Respiration for the whole crop in different temperature is calculated from the weights of the plant organs:

$$R_m(T) = (\mathrm{MAINT}_{LV}W_{LV} + \mathrm{MAINT}_{ST}W_{ST} + \mathrm{MAINT}_{FR}W_{FR} + \mathrm{MAINT}_{RT}W_{RT})Q_{10,C}^{[0.1(T-T_1)]} \tag{8}$$

in which $R_m(T)$ is the maintenance respiration rate (g$m^{-2}$$d^{-1}$) at temperature T (℃), MAINT is the maintenance respiration rate (g$m^{-2}$$d^{-1}$) at reference temperature T_1 (℃), and W is the organ dry weight per unit of greenhouse area (gm^{-2}) with the subscripts referring to leaves, stem, roots and fruits, respectively. $Q_{10,C}$ represents the sensitivity to temperature.

(4) Dry matter accumulation simulate

Daily dry matter production is calculated according to:

$$\mathrm{d}W / \mathrm{d}t = C_f (P_{g.d} - R_m) \tag{9}$$

in which $\mathrm{d}W / \mathrm{d}t$ is the crop growth rate ($gm^{-2}d^{-1}$), C_f the conversion efficiency from assimilates to dry matter, $P_{g.d}$ the crop gross assimilation rate per unit ground area ($gm^{-2}d^{-1}$) and R_m the maintenance respiration rate ($gm^{-2}d^{-1}$).

(5) Dry matter partition simulate

The fraction of dry matter partitioned to the fruits (F_{fruit}) may be calculated by sink strength.

$$F_{\text{fruit}} = \frac{N_f}{N_f + \mathrm{SS}_{\text{veg}} / \mathrm{SS}_{\text{fruit}}} \tag{10}$$

in which N_f is the number of fruit, SS_{veg} is the vegetative sink strength, $\mathrm{SS}_{\text{fruit}}$ is the fruit sink strength.

(6) Yield simulate

Tomato yield [Y(kgm^{-2})] can be calculated by dry matter partitioned to the fruits (F_{fruit}) (kg) and ratio of dry weight to fresh weight (RDF).

$$Y = \frac{F_{\text{fruit}}}{\mathrm{RDF}} \tag{11}$$

2 Model Validation

NPK uptake and growth experiments were implemented on greenhouse tomato experiments in Daxing district(E116.33, N39.73) of Beijng from 2006 to 2007, 1 plot was chosen to validate the model in each year. NPK experiments are designed to be 3 factors, 4 levels and 14 disposals. The compare of measured and simulated values in 2006 and 2007 are shown in Fig. 1 and Fig. 2.

3 Conclusions and Discussion

In this article, greenhouse tomato growth and development are simulated by synthetically thinking over of NPK uptake and its influence to photosynthesis. By improvement and validation, now the model can simulate NPK uptake and tomato growth very well.

There are some experiential parameters in the model, such as Q_{10}, which has good stability in temporal and regional region. But there are also some parameters such as root length density and LAI, which need to adjust by actual circumstance.

In fact, NPK uptake is very complicated, which is restricted by many factors, such as soil, temperature and water etc. In this article, the simulation of NPK uptake is very simple, further study and accomplishment are strongly needed.

From Fig. 1, relative coefficient (R) between simulated yield in 2006 and 1:1 line is 0.8493. Standard error is $1.6532 kgm^{-2}$. From Fig.2, relative coefficient (R) of simulated yield in 2007 and 1:1 line is 0.9676. Standard error is $1.5669 kgm^{-2}$. So, simulation in 2006 was not very good, and by the improvement in 2007, it gets a good achievement. Now, the model can simulate NPK uptake and tomato growth very well.

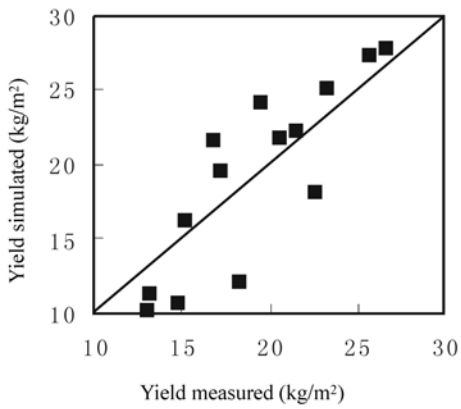

Figure 1 Compare of yield measured and yield simulated in 2006

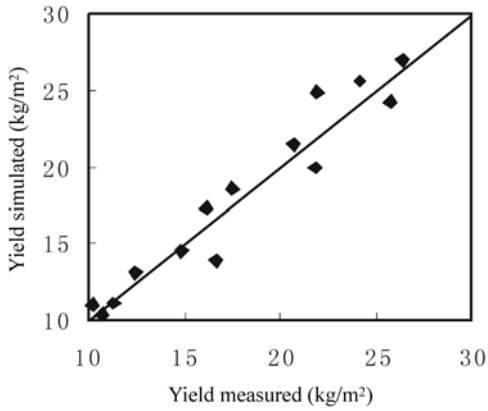

Figure 2 Compare of yield measured and yield simulated in 2007

Acknowledgements

This work is supported by the National Natural Science Foundation of China (No.30671211), the National Hi-tech Research and Development Program of China '863' (No.2006AA10Z218) and the National Scientific Support Program of Eleventh Five Year Plan (No.2006BAD04B08).

References

Wang K, Shen RK, Wang FQ (2002) Simulation of biomass formation and nitrogen uptake in winter wheat under different water and nitrogen suppl. Irrigation and Drainag 21(1):6 – 10.

Li FS and Lu SN (2000) Study on the fertigation and its application. Plant Nutrition and Fertilizer Scienc 6(2):233 – 240.

Li YF, Li JS, and Rao MJ (2006) Effects of drip fertigation strategies on root distribution and yield of tomato. Transactions of the CSAE 22(7):205 – 207.

Lin ZH, Mo XG, and Xiang YQ (2003) Research advances on crop growth models. Acta Agronomica Sinica 29(5): 750 – 758.

Xie ZJ, Cao WX, Luo WH (2001) Applications and prospects of crop growth simulation modes in precision agriculture and intellectualized greenhouse in Shanghai. Acta Agriculture Shanghai 17(2):17 – 21.

Wang YL and He LY (2005) A review on the research and application of crop simulation model. Journal of Huazhong Agricultural University 24(5): 529 – 535.

Xie Y and James RK (2002) A review on the development of crop modeling and its application. Acta Agronomica Sinica 28(2):190 – 195.

Wu DL, Mao HP, and Li PP (2007) Progress on the growth model of horticultural crops in greenhouse in China. Journal of Changjiang Vegetables 2007.2 Special report.

Li D et al. (2007) Crop Growth Simulated System and its Application in Equipment Hor ticultural Production. Journal of Anhui Agri 35(11) : 3141 – 3142, 3145.

Heuvelink EP (1997) TOMSIM: a dynamic simulation model for tomato crop growth and development. http://lib rary.wur.nl /WebQuery/wurpubs/37973 Wageningen University and Research center Publications.

CANON: A Canonical Composition for Building Plant Shoots From the Bottom Up

J. N. G. Hargreaves[1], G. S. McMaster[2]

(1 CSIRO Sustainable Ecosystems/APSRU, Toowoomba, Queensland Australia.
E-mail: John.Hargreaves@csiro.au)
(2 USDA-Agricultural Research Service, Agricultural Systems Research Unit, Fort Collins, Colorado U.S.A. E-mail: Greg.McMaster@ars.usda.gov)

Abstract: The phytomer concept has been useful for understanding plant development and architecture. Commonly the phytomer has been viewed as a vegetative unit consisting of a leaf, node, internode, and axillary bud, with this unit repeated within and among shoots. This definition can be extended to the inflorescence structure. Based on available knowledge and objectives, models may not fully incorporate phytomer concepts, rather some phytomers may be aggregated into a single component such as a grain component. The continuing development of object-oriented (OO) design and associated programming languages is providing opportunities for better incorporating phytomer concepts into models. For instance, the use of a Composite Pattern in an object-oriented (OO) design facilitates implementation of different scales from the phytomer to a mixture of single and aggregated phytomers for different plant components. The objectives of this paper are to use winter wheat (*Triticum aestivum* L.) to illustrate ① how plants build their canopies by the appearance, growth, and abortion/senescence of phytomer units, and ② present a conceptual prototype for translating this botanical abstraction into an OO design of a plant model, CANON, so called because the interplay of repeating phytomers is analogous to the repeating melodies of a musical composition called a canon.

In CANON OO design, the canopy is built by the addition of phytomer units that have a consistent type of communication with adjoining phytomers. This communication matches the OO structural composite design pattern described, where objects are represented in part-whole hierarchies by tree structures, with uniform treatment of individual objects and compositions of objects. At any point, the following sub-hierarchy is viewed as a single entity thus allowing parts of the hierarchy to be replaced with a single object, without affecting the preceding part of the hierarchy. This approach allows specification of sub-models of different levels of detail which could be selected at implementation or run-time. Initial implementation of the proof-of-concept using winter wheat (*Triticum aestivum* L.) vegetative phytomers is presented.

Keywords: organ development, *Triticum aestivum* L., wheat, phytomer, phyllochron, canopy architecture, object-oriented design, object-oriented phytomer model, CANON, phytomer composite pattern, scaling

1 Introduction

When Grey presented the concept of the phytomer in 1879, he presented a concept that has proven to be a useful botanical abstraction for providing a foundation to understand plant development and architecture. In this conceptualization of canopy development, canopies are built by the addition,

growth, and abortion/senescence of basic building blocks (i.e., phytomers) that is repeated within and among all shoots on a plant.

Plant simulation models have varied considerably in their conceptualisation and approach for modeling plant canopy development and architecture. Extensive developmental knowledge and building canopies by phytomer units for some species such as wheat has been known from the earliest days of crop simulation modeling. However because of limited knowledge or due to the objectives of the model, few models have fully incorporated phytomer concepts.

Early efforts in simulating phytomer construction of plant canopies include use of L-systems and developmental-based simulation models using structured programming languages (e.g., SHOOTGRO, McMaster et al., 1992; Wilhelm et al., 1993; Rickman et al., 1996). More recent work on functional-structural modeling (e.g. Vos et al., 2007) has provided considerable detail on phytomer construction of canopies.

Many initial efforts at object-oriented (OO) design of plant growth models did not reflect how the plant canopy actually develops by phytomer units. A common approach was to view the plant from the concept that it consists of leaf, stem, root, and seed components (e.g., APSIM, McCown et al., 1996; APSIM-Plant, Wang et al., 2002; Sequeira et al., 1991; 1997). In this design, the phytomer unit components are split into these generic plant components. With advances in OO design and application of OO Design Pattern, new possibilities for capturing botanical knowledge of the phytomer into simulation models is possible. The Composite Design Pattern has not received much recognition in many OO designs for crop simulation models. This design pattern can be utilized for plant models based on phytomer concepts so that the phytomer concepts can be aggregated into lower levels of resolution (such as entire shoots or inflorescences) or different conceptualizations of the plant such as mentioned above.

The objectives of this paper are to use winter wheat as a case study to ① discuss how plants build their canopies by the appearance, growth, and abortion/senescence of phytomer units and extend the phytomer concept into the inflorescence, and ② translate this botanical abstraction into an OO design based on the Composite Design Pattern and provide initial implementation efforts (CANON).

2 Phytomer Unit and Building Plant Canopies

While various definitions of phytomers have been proposed (Wilhelm and McMaster, 1995), most commonly the phytomer is viewed as a unit consisting of a leaf, node, internode, and axillary bud, with this unit being repeated within and among shoots (Fig. 1). This basic definition has been extended to include the nodal root buds (Klepper et al., 1984), and is considered a “vegetative” phytomer. The plant builds its canopy by the addition, growth, and abortion/senescence of these vegetative phytomer units on a shoot, with the same process for each shoot (Rickman and Klepper, 1995). The vegetative phytomer unit concept can be extended for building the spike inflorescence using “reproductive” phytomers, where both the spikelet and floret parts of the wheat inflorescence have analogs to the vegetative phytomer leaf and axillary buds. The main axis of the wheat spike (i.e. the rachis) is built by the sequential addition of phytomers consisting of spikelets (=leaf), with the other similar phytomer components of the node, internode, and axillary bud. In turn, the main axis of each spikelet (i.e., the rachilla) is built by the sequential addition of phytomers consisting of florets (=leaf), and the node, internode, and axillary bud. Others have recognized this pattern of repeated phytomers for barley (*Hordeum vulgare* L.). For instance, Bossinger et al (1992) described a phytomer concept for barley including spikelet components, roots, tillers and branches which Forster et al. (2007) extended to all elements of the barley plant. The resulting model was entirely composed of phytomers to describe the whole canopy architecture. This dynamic interplay

of phytomers within and among plant components can be viewed as analogous to a composition of music called a canon (a familiar simple form being a round) where individual phytomers repeat a part against and with other phytomers as do the melodies of a canon. This analogy led to the naming of our proof-of-concept OO design as CANON.

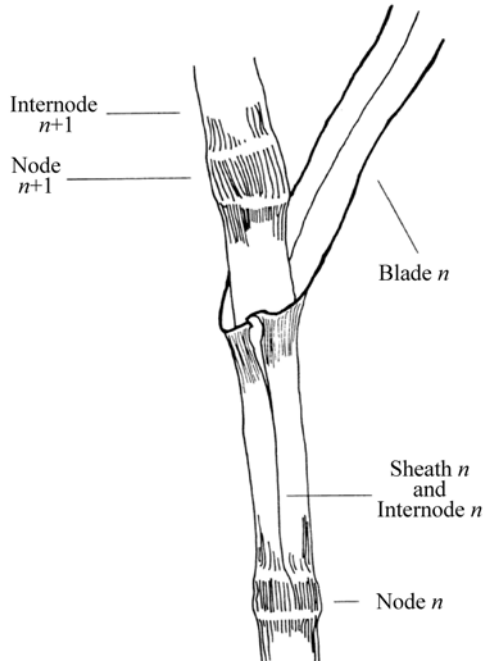

Figure 1 Common definition of a vegetative phytomer unit (From McMaster et al., 1991)

Considerable data are available for certain species, particularly wheat, to quantify the orderly development of the plant canopy by the dynamic interplay of phytomers. Using wheat as a case study, each vegetative phytomer can be considered to be initiated when either the leaf primordium is formed on the shoot apex or when the leaf primordium further differentiates and grows resulting in the appearance of the leaf. Since the primordia and leaves are produced sequentially with a fairly consistent pattern related to thermal time (Rickman and Klepper, 1995; McMaster, 2005), the production of vegetative phytomers on a shoot is quite predictable. In a similar manner, the production of each spikelet primordium on the rachis of the spike is analogous to the production of vegetative phytomers, and generally is 2 to 3 times faster than the rate of leaf primordia production (Hay and Kirby, 1991; Kirby, 1974). On the axis of the spikelet, floret primordia production is also quite consistent with thermal time. Therefore, the general concept of building a canopy by the addition of phytomers within a shoot can be quantified for winter wheat. The timing of new axes, or shoots, can be well related to thermal time, and has been successfully correlated with main stem leaf number (Klepper et al., 1982; 1984). Therefore, the building of an entire wheat canopy by the addition of phytomers has been quantified by numerous scientists (e.g. Rickman and Klepper, 1995).

A similar understanding of the orderliness and predictability of the growth of each component of the phytomer has been developed over time. For instance, an increase in leaf dimensions and biomass of successive leaves on a shoot has been studied (Hay and Wilson, 1982). The internode component of the first few vegetative phytomers is negligible, and appreciable internode elongation does not begin until shortly before the developmental stage of jointing. As with leaves, successive internodes of vegetative phytomers increase in length (McMaster et al., 1991). Kernel growth normally follows a sigmoidal pattern, and a common pattern of final kernel size tends to be

observed within the inflorescence ((McMaster, 1997) cites many references).

Similarly, considerable knowledge of the senescence or abortion of phytomer components is available, such as numerous studies of tiller and kernel abortion cited in McMaster (1997). Of critical importance is predicting the timing of developmental events, or phenology, necessary to simulate the state of each phytomer and phytomer component. Wheat phenology has been successfully simulated in many crop simulation models such as APSIM (Keating et al., 2003), ARCWHEAT1/2 (Porter, 1984; 1993; Weir et al., 1984), Sirius (Jamieson et al., 1995; 1998), and DSSAT (Ritchie and Otter, 1985; Ritchie, 1991; Hunt and Pararajasingham, 1995; Jones et al., 2003; Hoogenboom et al., 2004).

3 Translation of Phytomer Concept into OO Design

With the botanical conceptualization of a phytomer as a starting point, the fundamental components of a phytomer unit were identified for our OO design. In summary, for our proof-of-concept purposes, a plant consists of two basic types of components each built using phytomer units. One component is a vegetative component consisting of stems or axes with leaves and internodes and the other a reproductive component (a spike) consisting of axes with spikelets and internodes. A vegetative phytomer has components which, for our proof-of-concept purposes, are a leaf, an internode, an axillary axis and a root while a reproductive phytomer has components of spikelet, internode and axillary axis. Phytomers are arranged in sequence to form an axis (a generic term we use in the prototype for a culm or tiller or shoot).

A phytomer can be described in terms of its properties (e.g. its component parts such as leaf, internode, axillary axis, root, its state such as growing, senescing, its age, etc.), processes (e.g. growth and senescence, ageing and change of state) and messages to its adjoining phytomers and its own components (e.g. collecting information such as leaf area of all leaves along the hierarchy from this phytomer, or signalling a whole plant event such as death). This description can be viewed in OO terms as an object that has data (properties), methods (processes) and a consistent interface for the passing of messages to other phytomer objects and its own component part objects (e.g. communication by signalling and movement of resources). A series of recursive and like phytomers form a plant component such as a vegetative axis, with the phytomer properties describing their type and function. To form a different type of component such as a reproductive spike of phytomers or an aggregate axis (reproductive or vegetative), the phytomers or their aggregate change to a new set of properties describing their new functionality. Thus a plant component can be viewed as either a composite set of recursive phytomers or as an aggregation of phytomers into a single plant component. Many functional-structural models are based on this conceptualization, using a phytomer approach for vegetative (culm and canopy) development and an aggregated organ approach for root and reproductive (grain) development (Vos et al., 2007). Tomlinson et al (2007) use this approach for clonal bunchgrasses.

In this model, a phytomer has a consistent type of communication with adjoining phytomers, regardless of the hierarchical structure that follows. This matches the object-oriented, structural composite design pattern described by Gamma et al. (1994), where objects are composed into tree structures to represent part-whole hierarchies, in which individual objects and compositions of objects are treated uniformly by each preceding object in the hierarchy (parent object). At any point in the tree structure of a composite pattern, the following sub-hierarchy is treated as a single entity. This enables parts of the hierarchy to be replaced with a single simple aggregated object, without affecting the preceding part of the hierarchy. For example, the phytomeric inflorescence sub-hierarchy of the structure could be replaced with a simpler sub-hierarchy or a single object. This replacement strategy can be used for any logical group in the hierarchy. This approach allows specification of sub-models of different levels of detail which can be selected at run-time, without

altering the object design.

The phytomer model we use is a modification of the common vegetative model of leaf+sheath, node+internode, and axillary bud (Fig. 1) by the addition of a root bud and extending the model to describe the reproductive structure (Fig. 2).

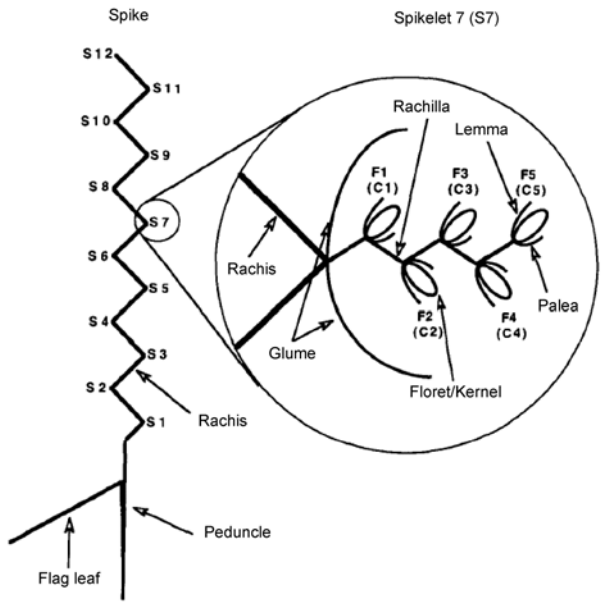

Figure 2 Reproductive phytomers consisting of spikelets (=leaf) on the main axis (=rachis) and florets (=leaf) on spikelet axis (=rachilla) (From Wilhelm and McMaster, 1996)

This model is extended further by Forster et al. (2007) who describe every organ in terms of a basic phytomer unit. Complex plant growth and development models are commonly built out of simple specialised plant components. A simple implementation could define OO classes for simple structures such as grain, stem, leaf and root. This approach does not consider the biological significance of the phytomer as a building block of plant growth and development. A phytomer approach to modeling plant architecture produces a botanical abstraction of a phytomer in an object-oriented (OO) design. Commonly, phytomers are incorporated into a model design by defining the phytomer as a class with a stem class acting as a container class for all the stem phytomers, keeping inflorescence (grain), leaf and root as simple classes (Fig. 3). In turn the main stem and each tiller could be defined as larger container classes for the leaf, stem, grain and root, and the whole plant in turn defined as a still larger container class for the main stem and tillers, similar to the functional-structural model of Tomlinson et al. (2007).

To implement the approach described by Forster et al. (2007), phytomers build each component of the plant, so different classes could be defined for the phytomers in each organ. Container classes would then be defined for all phytomers of each type and so on as described before.

Gamma et al. (1994) point out that the problem with this approach is that client code that uses these classes has to treat the simple and container classes differently, even though each can have the same basic properties and processes. To overcome this, they define a Composite Design Pattern (Fig. 4) which describes how to use recursive composition so that the client code doesn't need to make a distinction between simple and container classes and treats all objects in the composite structure uniformly. Thus a simple object has no children, while a composite object has children which could be simple or composite objects.

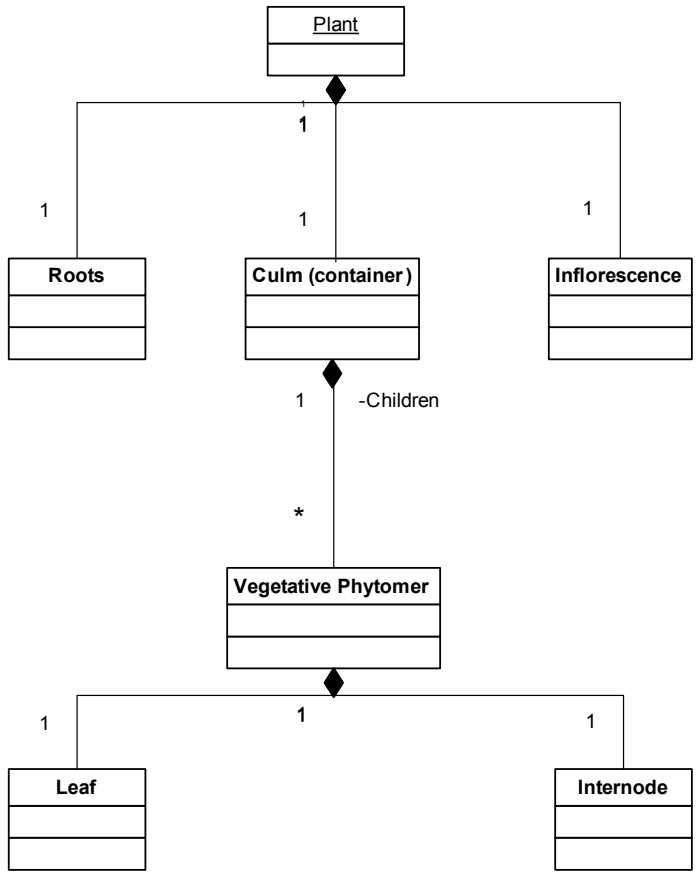

Figure 3 A basic phytomer model with a culm containing vegetative phytomers consisting of a leaf and internode, and simple components for the roots and reproductive inflorescence

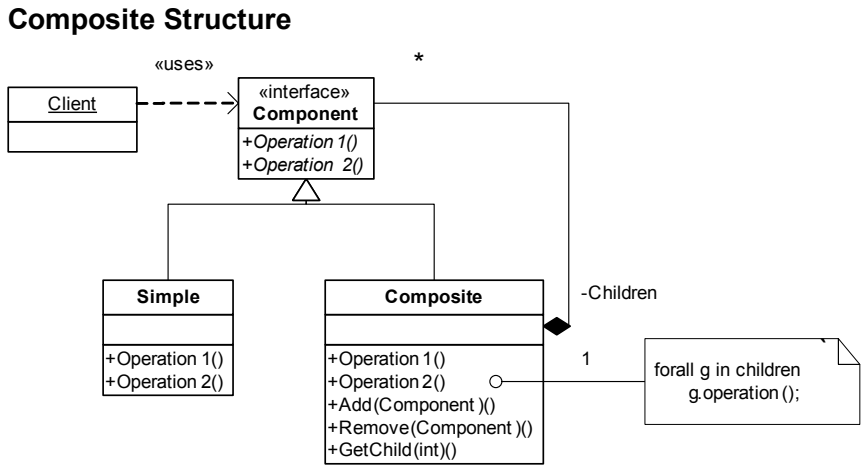

Figure 4 Composite Pattern Structure. Both Composite and Simple classes derive from a common Component class which provides the standard interface. The composite class contains a component list of its children which it loops through, sending a common message to each, not distinguishing between simple or composite class children. The client code communicates through the common Component class, again not distinguishing between simple or composite classes. A Simple class is a Component and Composite class is a Component. A Composite class also has a Component (one or more) which are its children

Figure 5 shows the simplicity of a basic composite phytomer plant model matching that of Forster et al. (2007). This can be extended to match other phytomer models as described by Bossinger et al. (1992), Tomlinson et al. (2007) and in this paper, so a "simple phytomer" class could represent either a phytomer or an aggregate component such as the spike.

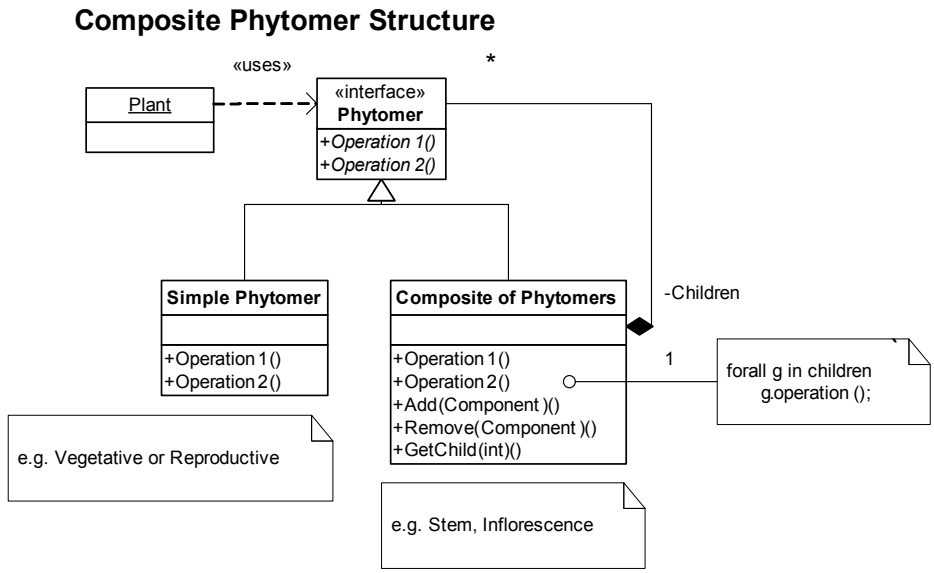

Figure 5 Composite Phytomer Model. Plant is the client that communicates with the phytomer hierarchy through the Phytomer class which provides a standard interface to all components in the hierarchy. A simple phytomer represents a single phytomer, either vegetative or reproductive, or an aggregation of phytomers into a single component. A composite of phytomers represents a collection of phytomers such as a stem (axis) or inflorescence (spike)

4 Initial Implementation Efforts of OO Design

Proof-of-Concept Development

While these concepts could apply to any species, we have chosen to implement the design using winter wheat (*Triticum aestivum* L.) because information for this species is readily at hand and it is conceptually very simple. For proof-of-concept simplicity, our initial implementation is constrained to the vegetative phytomers (not including nodal roots). Figure 6 shows the class diagram of this initial implementation. In the next development phase, we will introduce reproductive phytomers.

We are beginning the implementation of our OO design into a proof-of-concept (CANON) using the C++ programming language. In this implementation, we are initiating phytomers, growing phytomer sub-components, senescing phytomer components, and repeating this process for new axes, or shoots. Many of the rules for the methods are being derived from the SHOOTGRO model (McMaster et al., 1992) and using winter wheat as the model plant. As a proof-of-concept we are assuming optimal growing conditions (McMaster et al., 1991; 1992; Wilhelm et al., 1993). Initial tests are showing the OO design principles outlined in this chapter are able to be implemented into a plant growth simulation model. There are a number of alternative implementations of the phytomer design. A phytomer, upon creation, could be populated with dormant buds for all of its components, which can then be activated by nominated events. In our implementation, we have chosen not to form an axillary bud, but initiate a new axillary axis when the bud begins to elongate, which is signaled by a phenological event. Similarly, we do not form a node and initiate the internode when its elongation begins.

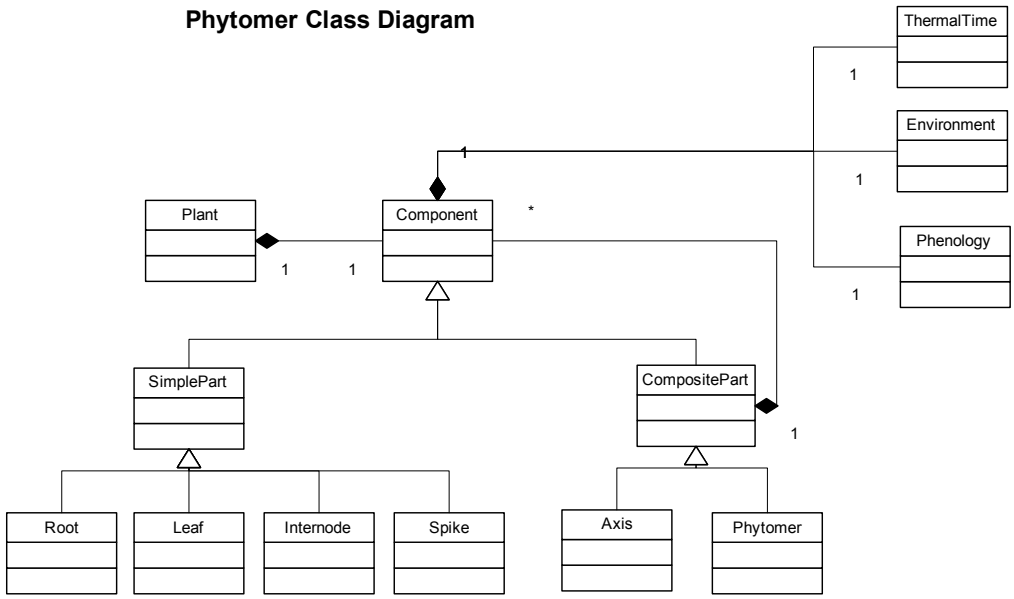

Figure 6 Class diagram of CANON phytomer model. This shows the prototype class relationship structure of vegetative phytomers with their components (root, axis, internode and leaf). Here each Root, Leaf, Spike and Internode class is a SimplePart, each Axis and Phytomer is a CompositePart, each SinglePart and CompositePart is a Component and Plant has a Component. CompositePart also has one or more Components. The Component class has service classes for thermal time, environment (weather) and phenology which are inherited for use by all its sub-classes

Figure 7 shows our implementation of phytomers on a wheat plant with a main stem, primary tiller (T1), and spikelet/reproductive phytomers. The internode of each phytomer is developed while the other buds are suppressed or developed. Along the main axis or stem, the root bud of Phytomer 0 is developed while the leaf and axillary buds are suppressed. The next phytomer to develop on the main axis, Phytomer 1, has the root bud suppressed with the leaf developed and axillary bud developed into a secondary axis or branch. Phytomer 1 is followed by vegetative phytomers until the terminal phytomer which suppresses the leaf and develops its axillary bud into an axis of reproductive phytomers in which the reproductive organ is developed and the leaf and root buds suppressed. The secondary vegetative axes begin with a Phytomer 0 consisting solely of an internode and develop similarly to the main axis.

5 Discussion

The Conundrum—Multiple and Variable Scales

Limited knowledge and application objectives determine the levels of detail or scale used within a model. For example, a model may be built with three simple components viz. vegetative, reproductive and root, to meet a project's simulation requirements. As knowledge improves and objectives change, the vegetative component may be developed to a more detailed sub-model constructed with phytomers, while light capture by the canopy may be adequately simulated at the whole plant level. This illustrates simulation at three scales within the model, with leaf growth and development at phytomer levels (detailed phytomer level), with leaf area being aggregated at plant canopy level for light interception (whole of plant level), while the reproductive spike is simulated as a single grain component (aggregated organ level). Another application may need the spike component

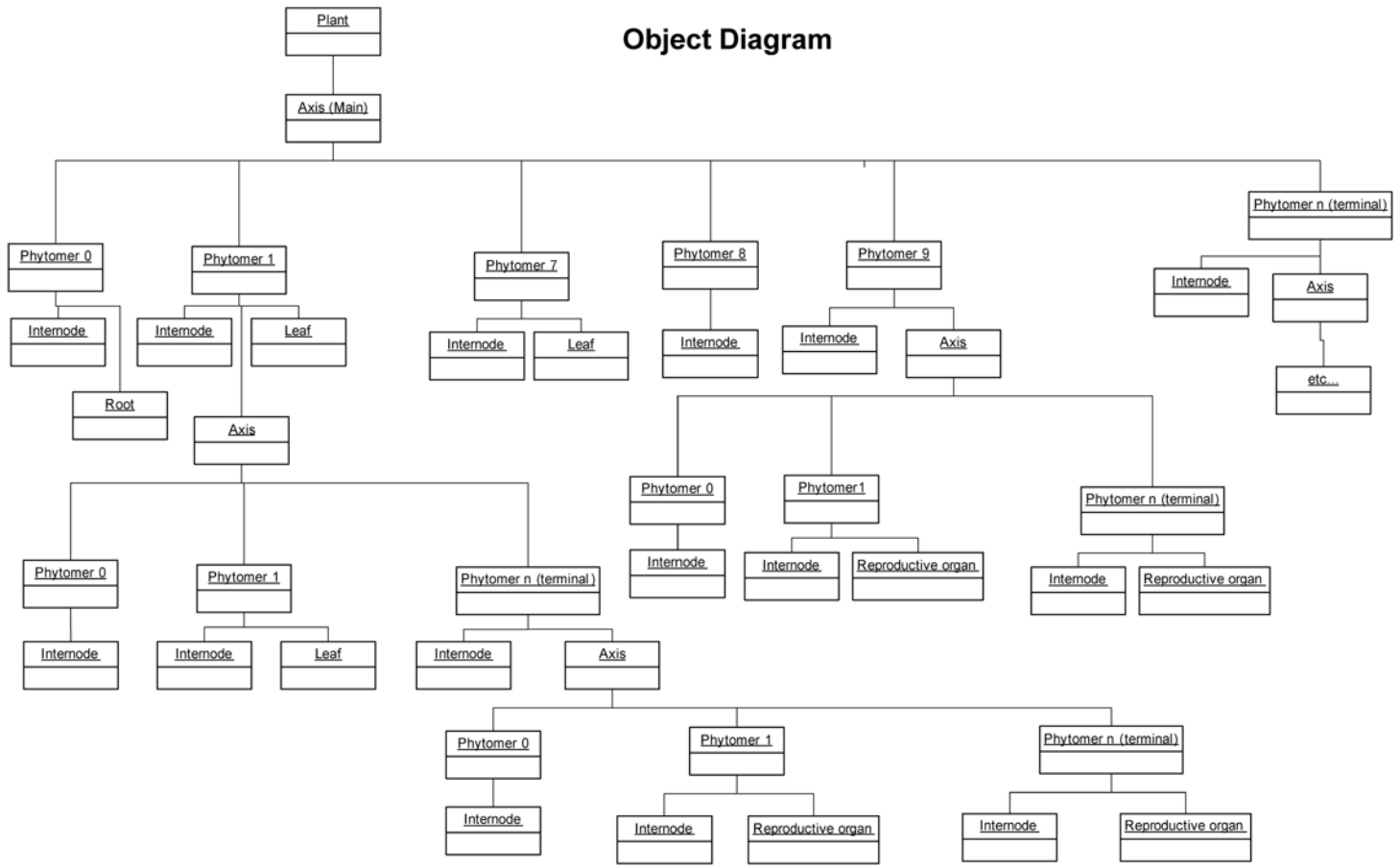

Figure 7 Object diagram of CANON phytomer model. This demonstrates a potential structure of vegetative and reproductive phytomer objects with their components (root, axis, internode, leaf and grain)

to be simulated at phytomer levels. The challenge is to facilitate the incorporation of multiple levels of scale into a model with runtime selection of these scales while providing for the addition of new expanded or reduced scales as knowledge increases and application requirements change. Any change in configuration due to scales produces essentially a different model which will have associated changes in model performance and validation. In this paper, we are primarily interested in providing a simple design which facilitates easy opportunities for simulating at any level of resolution.

In summary, the requirements for our proof of concept model are: ① ability to replace a logical group of phytomers with a single component or vice versa, ② ability for some processes to operate at whole plant level, using the collective information of more detailed components and distributing new information to the more detailed components, and ③ ability of components, such as phytomers to represent different types or classes of plant components, such as vegetative and reproductive. An additional objective is for components to be respecified to represent other species.

Advantages of the Composite Design Pattern

The OO Composite Design Pattern underpins our solution to the conundrum by satisfying the three main requirements identified above that must be demonstrated in our proof of concept. There are a number of important effects the Composite Pattern has on the code. It defines hierarchies of simple objects and composite objects. The simple objects can be composed into compound or composite objects, which can be composed in turn into compound objects and so on, in a recursive manner. This enables simple and composite objects to be indistinguishable to the code that uses these objects. The advantage of this is the code is simplified as both simple and composite objects are treated alike and the code doesn't know or care if it is using a simple or composite object. The code is simplified as it doesn't need to distinguish between the types of objects (e.g. leaf or axis). A very important advantage of this behaviour is that it makes it easier to expand the hierarchy by adding new kinds of single or composite components and or to collapse sub-hierarchies into a simpler composite component or even further into a single simple component.

Application to Plant Modeling

Implementing a plant model based on the Composite Design Pattern can simplify the code and reduce the potential for errors. The recursive nature of the pattern allows indeterminate or determinate plant development to be easily implemented. Phytomers or their aggregate replacement in the hierarchy can be implemented to be self configuring, based on the phytomer or component type (e.g., vegetative or reproductive).

Depending on the type, development of phytomeric components can be switched on or off, such as the root bud. Axillary buds can be switched on to form a new tiller or secondary branch axis or left off to remain dormant. The generality of this design allows modeling at various scales as appropriate for the problem being studied. It also allows the phytomer model to be applied to other monocots and dicots as described in McSteen and Leyser (2005) by re-specification of the phytomer and component parameters.

OO plant simulation models that have leaf, stem, grain and root objects (e.g. APSIM-Plant, Wang et al., 2002) could be adapted to this design which would then provide the flexibilities described earlier.

Acknowledgements

The authors thank the following organizations for their support of this work: Grains Research and Development Corporation (GRDC; http://www.grdc.com.au) by providing a Grains Industry

Visiting Fellowship, USDA-Agricultural Research Service, Agricultural Systems Research Unit (http://www.ars.usda.gov), and CSIRO Sustainable Ecosystems (http://www.cse.csiro.au)

References

Bossinger G, Rohde W, Lundqvist U, Salamini F (1992) Genetics of barley development: mutant phenotypes and molecular aspects. In: Shewry, P.R. (ed) Barley: Genetics, Biochemistry, Molecular Biology and Biotechnology, pp 231–264. Wallingford: CAB International.

Forster BP, Franckowiak JD, Lundqvist U, Lyon J, Pitkethly I, Thomas WTB (2007) The Barley Phytomer. Ann Botany 100:725 – 733.

Gamma E, Helm R, Johnson R, Vlissides J (1994) Design Patterns: Elements of Reusable Object-Oriented Software. Addison-Wesley.

Gray A (1879) Structural Botany New York: Ivsion, Blakeman, Taylor and Company.

Hay RKM, Kirby EJM (1991) Convergence and synchrony – A review of the coordination of development in wheat. Aust J Agric Res 42:661 – 700.

Hay RKM, Wilson GT (1982) Leaf appearance and extension in field-grown winter wheat plants: The importance of soil temperature during vegetative growth. J Agric Sci (Camb) 99:403 – 410.

Hoogenboom G, Jones PW, Wilkens JW, Porter CH, Batchelor WD, Hunt LA, Boote KJ, Singh U, Uryasev UO, Bowen WT, Gijsman AJ, du Toit A, White JW, Tsuji GY (2004) Decision Support system for agrotechnology transfer, version 4.0 [CD-ROM]. Univ Hawaii, Honolulu.

Hunt LA, Pararajasingham S (1995) CROPSIM-WHEAT: A model describing the growth and development of wheat. Can J Plant Sci 75:619 – 632.

Jamieson PD, Brooking IR, Porter JR, Wilson DR (1995) Prediction of leaf appearance in wheat: A question of temperature. Field Crops Res 41:35 – 44.

Jamieson PD, Semenov MA, Brooking IR, Francis GS (1998) Sirius: A mechanistic model of wheat response to environmental variation. Eur J Agron 8:161 – 179.

Jones JW, Hoogenboom G, Porter CH, Boote KJ, Batchelor WD, Hunt LA, Wilkens PW, Singh U, Gijsman AJ, Ritchie JT (2003) The DSSAT cropping system model. Eur J Agron 18:235 – 265.

Keating BA, Carberry PS, Hammer GL, Probert ME, Robertson MJ, Holzworth D, Huth NI, Hargreaves JNG, Meinke H, Hochman Z, McLean G, Verburg K, Snow V, Dimes JP, Silburn M, Wang E, Brown S, Bristow KL, Asseng S, Chapman S, McCown RL, Freebairn DM, Smith CJ (2003) An overview of APSIM, a model designed for farming systems simulation. Eur J Agron 18:267 – 288.

Kirby EJM (1974) Ear development in spring wheat. J Agric Sci (Camb) 82:437 – 447.

Klepper B, Belford RK, Rickman RW (1984) Root and shoot development in winter wheat. Agron J 76: 117 – 122.

Klepper B, Rickman RW, Peterson CM (1982) Quantitative characterization of vegetative development in small cereal grains. Agron J 74:789 – 792.

McCown RL, Hammer GL, Hargreaves JNG, Holzworth DP, Freebairn DM (1996) APSIM: a Novel Software System for Model Development, Model Testing and Simulation in Agricultural Systems Research. Agric Sys 50: 255 – 271.

McMaster GS (1997) Phenology, development, and growth of the wheat (*Triticum aestivum* L) shoot apex: a review. Adv Agron 59:63 – 118.

McMaster GS (2005) Phytomers, phyllochrons, phenology and temperate cereal development. J Agric Sci (Camb) 143:137 – 150.

McMaster GS, Klepper B, Rickman RW, Wilhelm WW, Willis WO (1991) Simulation of shoot vegetatiave development and growth of unstressed winter wheat. Ecol Modell 53:189 – 204.

McMaster GS, Morgan JA, Wilhelm WW (1992) Simulating winter wheat spike development and growth. Agric Forest Meteorol 60:193 – 220.

McSteen P, Leyser O (2005) Shoot branching. Annu Rev Plant Biol 56:353 – 374.

Porter JR (1984) A model of canopy development in winter wheat. J Agric Sci (Camb) 102:383 – 392.

Porter JR (1993) AFRCWHEAT2: A model of the growth and development of wheat incorporating responses to water and nitrogen. Eur J Agron 2:64 – 77.

Rickman RW, Klepper B (1995) The phyllochron: Where do we go in the future? Crop Sci 35:44 – 49.
Rickman RW, Waldman SE, Klepper B (1996) MODWht3: A development-driven wheat growth simulation. Agron J 88:176 – 185.
Ritchie JT (1991) Wheat phasic development. In: Hanks J, Ritchie JT (ed) pp 31-54 Modeling plant and soil systems. ASA-CSSA-SSSA, Madison, WI.
Ritchie JT, Otter S (1985) Description and performance of CERES-Wheat: A user oriented wheat yield model. In: Willis WO (ed) Wheat yield improvement. USDA-ARS Publ 38 National Technical Information Serv, Springfield, VA.
Sequeira RA, Olson RL, McKinion JM (1997) Implementing generic, object-oriented models in biology. Ecol Modell 94:17 – 31.
Sequeira RA, Sharpe PJH, Stone ND, El-Zik KM, Makela ME (1991) Object-oriented simulation: Plant growth and discrete organ to organ interactions. Ecol Modell 58:55 – 89.
Tomlinson KW, Dominy JG, Hearne JW, O'Connor TG (2007) A functional-structural model for growth of clonal bunchgrasses. Ecol Modell 202:243 – 264.
Vos J, Marcelis LFM, de Visser PHB, Struik PC, Evers JB (eds) (2007) Functional-Structural Plant Modeling in Crop Production. Springer Publishing, Netherlands.
Wang E, Robertson MJ, Hammer GL, Carberry PS, Holzworth D, Meinke H, Chapman SC, Hargreaves JNG, Huth NI, McLean G (2002) Development of a generic crop model template in the cropping system model APSIM. Eur J Agron 18:121 – 149.
Weir AH, Bragg PL, Porter JR, Rayner JH (1984) A winter wheat crop simulation model without water or nutrient limitations. J Agric Sci (Camb) 102:371 – 382.
Wilhelm WW, McMaster GS (1995) Importance of the phyllochron in studying development and growth in grasses. Crop Sci 35:1 – 3.
Wilhelm WW, McMaster GS (1996) Spikelet and floret naming scheme for grasses with a spike inflorescence. Crop Sci 36:1071 – 1073.
Wilhelm WW, McMaster GS, Rickman RW, Klepper B (1993) Above-ground vegetative development and growth of winter wheat as influenced by nitrogen and water availability. Ecol Modell 68:183 – 203.

A Quantitative Analysis on Leaf Curvature Characteristics in Rice

Liang Tang, Chun-Lin Shi, Yan Zhu, Qi Jing, Wei-Xing Cao

(Hi-Tech Key Laboratory of Information Agriculture of Jiangsu Province, Nanjing Agricultural University, Nanjing 210095, Jiangsu, China; Corresponding author: caow@njau.edu.cn)

Abstract: With rapid development of computer graphics and crop simulation, virtual crop study that can intuitionally express crop growth on computer has attracted great attention from many scientists in the world, with significant progress on visualization of crop plants. In virtual crop modeling, leaf shape is a very important character, and has been described with empirical curves derived from field experiments in the previous studies. The fitting curves are helpful for understanding organ morphogenesis, but the parameters obtained from the specific leaves and environments are not well adapted to changing growth processes of leaves. So it is critical to develop a dynamic model for simulating the leaf morphology under different growth conditions.

Organ morphogenesis of plant is associated with its forces. From force analysis on a rice leaf, the gravity fraction in leaf normal direction keeps equilibrium with elasticity, then a dynamic leaf curvature equation was deduced with some assumptions. The equation included the synthetic effects of leaf blade length, leaf blade width, initial leaf angle, specific leaf weight and deformation coefficient on leaf space shape. Then the equation was solved with parameterization. The sensitivity analysis showed that the equation could well reflect the integrated effects of leaf length, leaf width, specific leaf weight and leaf deformation coefficient, consistent with rice plant architecture in practice.

A field experiment was conducted at the Nanjing Agricultural University using two rice cultivars (SU63 and WYG7). At jointing and booting stages of rice, the 3-dimension coordinates of several points along leaf midrib were measured with the 3D digitizer, and at the same time leaf blade length, width, initial leaf angle were obtained. Then simulation analyses on the equation were conducted for comparison with the experiment data. The results indicated that the leaf curvature equation could dynamically and reliably describe the change pattern of leaf shape characteristics of rice under different conditions, including different leaf angles and specific leaf weights.

Keywords: rice; leaf shape; leaf curvature; quantitative modeling; virtual crop

1 Introduction

By visually simulation of plant growth in 3-dimention space on computer, virtual plant is extensively applied to the fields of plant structure analysis, plant architecture design, and teaching assistance with computer. In recent years, virtual crop study is under rapid development with the application of plant structure simulation technology. Many scholars have studied the virtual growth of cotton, maize, rice and wheat by simulating plant structure and established the technique of visual structure realization in 3-dimention space. However, the architecture and spatial structure construction remain to be analyzed dynamically and expressed virtually.

Leaves are main photosynthetic organs in crop plants. The architecture of leaves affects utilization of light energy by plant and also is key external character of different genotypes. So

spatial architecture of leaves is important for study of crop growth simulation. Leaf spatial architecture can be represented by the spatial curves of leaf midrib, which is often positioned with the coordinates and influenced by different parameters and coefficients. Yet the influence of leaf length, leaf width and specific leaf weight on the leaf curve coefficients has not be determined. So this study was undertaken to derive a dynamic equation of leaf curve on the basis of leaf force analysis, and to test if the leaf curve equation can simulate the spatial leaf shape under different conditions. This work would provide key technique for modeling morphogenesis and realizing virtual growth in rice.

2 Materials and Methods

2.1 Experiment and Measurement

The field experiment was conducted at the campus experiment station of Nanjing Agricultural University. Two japonica cultivars were used to compare the morphological differences among genotypes, including SU63 of droopy leaf and WYJ7 of erect leaf. The seeds were sow in dry-bed on May 20 and seedlings were transplanted on June 20, with spacing of 13.3cm and 25cm. The experiment was repeated 3 times with plot size of 1m× 1m. Water and nutrients were supplied according to a routine rice management. At jointing and booting stages, the 3-dimension coordinates of 6 to 7 points from the leaf ring to the leaf tip along leaf midrib were measured with the 3D digitizer (Fastrak, USA). Then the relative coordinates of the measurement points were calculated with the leaf ring as the origin point, which transferred the 3D coordinates into the 2-D coordinates on the plane of leaf curve.

2.2 Deduction of Leaf Curve Equation

The rice leaves are not twisted normally. The leaf curve can be expressed on a 2-D plane by the coordinate transformation. The leaf curve can be regarded as first derivative differentiable, second derivative continuity if the leaf is not broken. As illustrated in Figure 1, the tiny cell with the length of dl is affected by the gravity force *G*, deformation restoring ability *F*, and pull force from 2 ends. Each force of an immobile object keeps equilibrium with each other at different directions according to Newton's kinatics principle. So the gravity force keeps equilibrium with deformation restoring ability in leaf normal direction. It is shown as the Eq. (1), in which θ represents the average leaf curve angle in the leaf section.

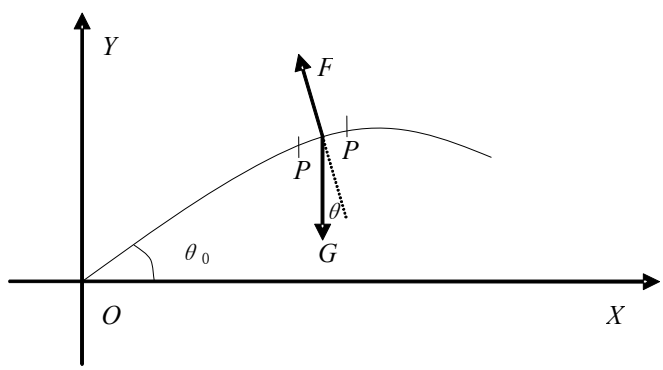

Figure 1 Leaf curvature and force analysis in rice

$$G \cdot \cos\theta = -F \tag{1}$$

The deformation restoring ability F generally keeps direct ratio with the degree of deformation, which can be expressed with the tangent angle difference of 2 end points in leaf tiny cell, as shown in Eqs. (2) and (3).

$$y'(x+\mathrm{d}x) = \tan(\theta+\mathrm{d}\theta) \text{ and } y'(x) = \tan(\theta)$$

$$F = k(l) \cdot \mathrm{d}\theta \tag{2}$$

$$\mathrm{d}\theta \approx \cos^2\theta \cdot (y'(x+dx) - y'(x)) \tag{3}$$

In Eq. (2), $k(l)$ represents average deformation parameter as restoring ability when the leaf bends one unit angle, l represents length between the tiny cell and the leaf ring, and $\mathrm{d}\theta$ represents the difference between the points P and P'.

In the Eq. (3), x and x+dx represent the x coordinates of P and P' points, respectively, $y'(x)$ represents the slope of P point.

The weight of leaf tiny cell is the product of the specific leaf weight and the area of tiny cell, which is equal to the product of leaf length and leaf width. $\sqrt{1+y'^2} \cdot \mathrm{d}x$ is for the length of leaf tiny cell. So the weight of leaf tiny cell G is shown as Eq. (4), in which SLW is the specific leaf weight, $w(l)$ is leaf width and dl is the length of leaf tiny cell PP'.

$$G = \mathrm{SLW}(l) \cdot w(l) \cdot \mathrm{d}l = \mathrm{SLW}(l) \cdot w(l) \cdot \sqrt{1+y'^2} \cdot \mathrm{d}x \tag{4}$$

Equation (5) is then obtained from combining the Eqs. (1) to (4)

$$\mathrm{SLW}(l) \cdot \sqrt{1+y'^2} \cdot \mathrm{d}x \cdot w(l) \cdot \cos\theta = -k(l) \cdot \cos^2\theta \cdot (y'(x+\mathrm{d}x) - y'(x)) \tag{5}$$

The leaf curve equation could be obtained on the basis of the upper equations and $y' = \tan(\theta)$ and $y'' \approx [y'(x+dx) - y'(x)]/\mathrm{d}x$.

The leaf curve morphology is correlated to the specific leaf weight, leaf length, leaf width and leaf deformation parameter. Therefore, the change patterns of the specific leaf weight, leaf width and leaf deformation parameter along with the leaf length must be determined before the leaf curve equation is resolved.

2.3 Resolution of Leaf Curve Equation

In general, the specific leaf weight slightly differed with the changing time and space in the process of leaf growth. The temporal and spatial change of the leaf special weight is affected by leaf lengthening, leaf expansion and dry matter output at different stages. Yet in this paper the specific leaf weight was set to a constant value for simplifying the present study. The leaf deformation parameter $k(l)$ is affected by vein thickness and moisture content. The moisture is usually enough during rice growth, so the vein thickness is the primary factor of $k(l)$. If the thickness of vein is linear with leaf length, the cross section of leaf vein changes in the 2nd power. So the characterization of $k(l)$ could be shown as the Eq. (7), in which l is the distance between the point and the leaf ring, LL is the maximum leaf length, and k_0 is deformation parameter at the leaf ring.

$$k(l) = k_0 \cdot (1 - l^2/\mathrm{LL}^2) \tag{7}$$

Based on the upper hypothesis, the specific leaf weight and deformation parameter at the leaf ring may be regarded as the ratio of restoring ability to weight and deformation angle, as shown in the Eq. (8). So the ratio of deformation parameter to the specific leaf weight in the Eq. (6) may be marked as a variable *K*.

$$k_0 / \mathrm{SLW} = K \tag{8}$$

The rule of the leaf width change along with leaf length is expressed in the Eq. (9), in which $W_{\max}$ is the maximum leaf width, LL is the maximum leaf length, β is the ratio of the leaf length at the maximum leaf width to the maximum leaf length, *e* is the ratio of the leaf width at the leaf ring to the maximum leaf width, *l* is the distance between the point and the leaf ring, $w(l)$ is the leaf width at the distance *l* from the leaf ring.

$$\frac{w(l)}{W_{\max}} = \begin{cases} 1-(1-e)\cdot(l-\beta\cdot \mathrm{LL})^2/(\beta\cdot \mathrm{LL})^2 & 0 \le l < \beta\cdot \mathrm{LL} \\ 1-(l-\beta\cdot \mathrm{LL})^2/(\mathrm{LL}-\beta\cdot \mathrm{LL})^2 & \beta\cdot \mathrm{LL} \le l \le \mathrm{LL} \end{cases} \tag{9}$$

The Eq. (6) could be resolved with the limited factor, y=0 and $y' = \tan(\theta_0)$ when x=0. The answers of Eq. (6) are related to the specific leaf weight, leaf length, leaf width and leaf deformation parameter. So it is rather difficult to be obtained, and needs the method of numerical value analysis.

In the Eqs. (6) and (9), the leaf length and width are related to cultivation managements, the environmental factors and cultivars, β and e are related to leaf position and cultivars, θ_0 related to leaf age. Their values could be obtained from a separate leaf morphology model, which will be presented in another article.

3 Results and Analysis

3.1 Sensitivity Analysis of Leaf Curve Equation

For verifying the reliability of leaf curve equation and its parameterization, the sensitivity of the leaf curve equation parameter was tested and the results were shown in Figs. 2 and 3. The leaf shape changed from erect shape to droopy shape when the initial leaf angle, leaf length, and leaf width increased, which is consistent with the phenomenon that the leaf of indica rice is droopier than the leaf of japonica rice. Moreover, the leaf shape gradually became droopy when the angle between the leaf and sheath increased in the course of leaf growth, which follows the biological pattern of leaf development in rice. It can be also seen from the Fig. 3 that the leaf shape became droopy when *K* value decreased. When the curly force was generated in the curly leaf, leaf deformation parameter *K* increased, so the leaf got to erect. These results indicate that the present leaf curve equation could dynamically and reasonably describe the change patterns of leaf curves under different conditions.

3.2 Simulation Analysis of Leaf Curve Equation

The leaf curve equation was simulated for comparison with the 3-D coordinates of rice leaf veins at jointing and booting stages obtained in the experiment, as shown in the Fig. 4. The leaf length, maximum leaf width and leaf width were all from measurements. The quality deformation parameter *K* ranged between 33 cm^2 and 100 cm^2. The simulation results indicated that the leaf

curve shapes of different leaf positions and cultivars varied greatly with changing leaf length, leaf width and initial leaf obliquity, but the leaf curve equation could reliably simulate the spatial changes of rice leaves (Fig. 4).

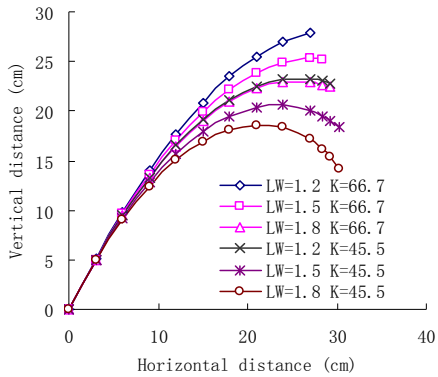

Figure 2 The effects of leaf length and initial angle on leaf curvature with leaf width of 1.5cm and *K* value of 45cm^2

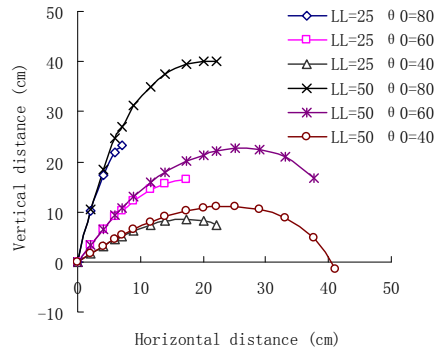

Figure 3 The effects of leaf width and *K* on leaf curvature with leaf length of 40cm and initial leaf angle of 60°

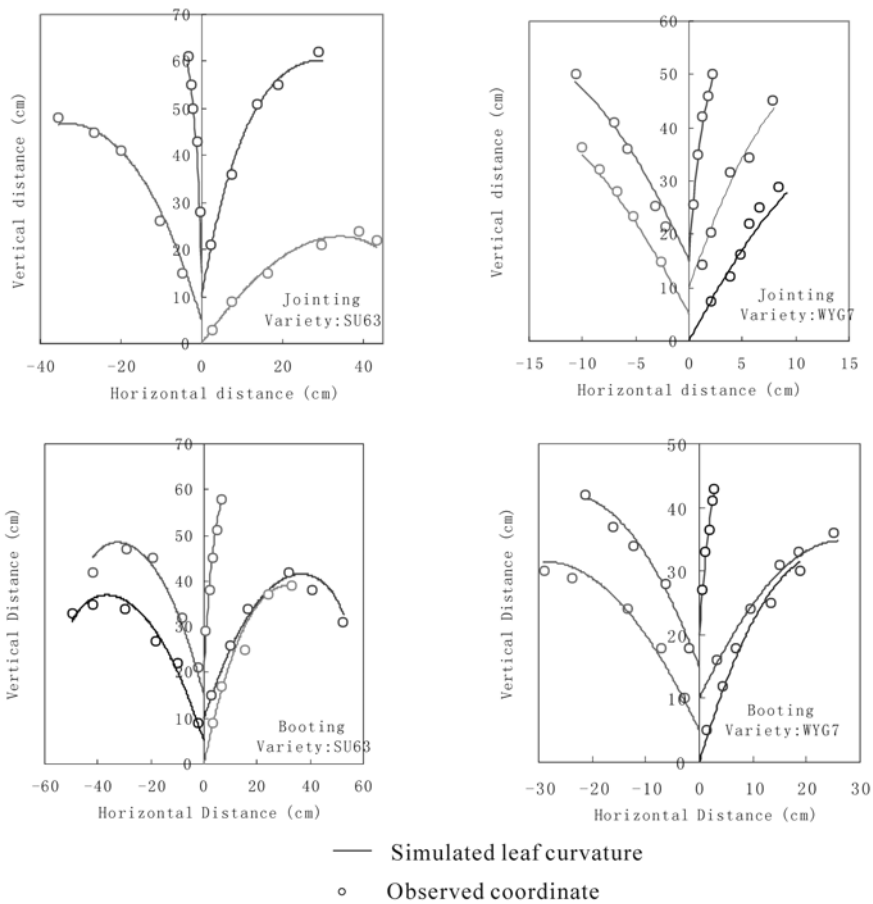

Figure 4 Comparison of simulated with observed values of leaf curvature at jointing and booting stages of two rice genotypes

4 Discussion

The virtual crop technology is to translate the digital information into the image information in essence, which is helpful for visually understanding the dynamic processes of crops growth. The studies on virtual crop focused on realizing the model and visualizing architecture, shape and reflection of crop plant in 3-dimension. Since the traditional technology for leaf curve simulation can not reveal the impact of the leaf length, leaf width, leaf obliquity, specific leaf weight and leaf deformation parameter on leaf curve, we established the dynamic leaf curve model that is adapted to the leaf obliquity and leaf weight through quantitative analysis. It can well reflect the influences of leaf length, leaf width and leaf deformation parameter on leaf curve characters and represent the leaf curves of different plant types. This study has laid a foundation for leaf shape simulation in rice and improved the current methodology of leaf curve analysis in crops. However, this study has mainly considered the gravity force and deformation force in the leaf direction, whereas the leaf erecting force of lodging plants and leaf curling force under drought are not analyzed. In addition, the specific leaf weight is not simulated dynamically in the process of equation resolution. Thus, the present leaf curve equation need to be further refined and improved in future studies.

References

Guo Y, Li B G (2001) Advances in virtual plant. Chinese Sci Bull 46(4): 373 – 380.

Room PM, Hanan JS (1995) Virtual cotton: a new tool for research, management and training. In: Constable GA. Proceedings of the World Cotton Research Conference. I. Challenging the Future. Melbourne: CSIRO Australia, 40 – 44.

Fournier C, Andrieu B (1998) A 3D architectural and process-based model of maize development. Ann Bot, 81: 233 – 250.

Watanabe T, Room PM, and Hanan JS (2001) Virtual rice: simulating the development of plant architecture. Intern Rice Res Notes, 26(2): 60 – 62.

Song Y-H, Guo Y, Li BG, Philippe de Reffye (2003) Virtual maize model. I. biomass partitioning based on plant topological structure. Acta Eco Sinica, 23(11): 2333 – 2341.

Hanan J S, Hearn AB (2003) Linking physiological and architectural models of cotton. Agric Sys, 75: 47 – 77.

Edmeades GO, Daynard TB (1979) The relationship between final yield and photosynthesis at flowering in individual maize plants. Can J Plant Sci, 59: 585 – 601.

Prevot L, Aries F, Monestiez P (1991) Modelisation de la structure geom.etrique du mais. Agronomie, 11: 491 – 03.

Stewart DW, Dayer LM (1993) Mathematical characterization of maize canopies. Agric For Meteorol, 66: 247 – 265.

Guo Y, Li BG (1999) Mathematical description and three dimensional reconstruction of maize canopy. China J App Ecol, 10(1): 39 – 41.

Zhang JE, Huang R, Liu CS, ea al (2001) 22Preliminary study on the visualization modeling of maize leaf structure. J of South China Agric Univ (4): 5 – 7.

Mi XC, Ao HJ, Zou YB, Shi JC, Cai S (2003) Application of visualization technology, model-document-view architecture in crop simulation. Trans CSAE, 19(4): 164 – 167.

Yan H, Kang M, de Reffye P, Dingkuhn M (2004) A dynamic architectural plant model: simulating resource-dependent growth. Ann Bot, 93: 591 – 602.

Guo Y, de Reffye P, Song Y, Zhan Z, Dingkuhn M, Li B (2003) Modeling of biomass acquisition and partitioning in the architecture of sunflower. In: B G Hu, Marc Jaeger (ed) Plant Growth Modeling and Applications, Beijing: Tsinghua Univ Press, 271 – 284.

Chen GQ, Zhu Y, Cao WX (2005) Modeling leaf sheath and internode growth dynamics in wheat. J Trit Crops, 25(1): 71 – 74.

The Response of Canopy Direction Reflectance Spectrum for the Wheat Vertical Leaf Distributing

Chun-Hua Xiao [1,2], Shao-Kun Li [1,2], Ke-Ru Wang [1,2] , Yan-Li Lu [2], Jun-Hua Bai [2], Rui-Zhi Xie [2] , Shi-Ju Gao [2] , Xiao-Jun Li [2] , and Hai-Zhen Tan [1,2]

(1 Key Laboratory of Oasis Ecology Agriculture of Xinjiang Construction Crop/The Center of Crop High-Yield Research, Shihezi 832003, Xinjiang, China)
(2 Institute of Crop Science, Chinese Academy of Agricultural Sciences, / National Key Facility for Crop Gene Resources and Genetic Improvement, NFCRI, Beijing 100081)
(Corresponding author, Address: Department of Crop Culture, Institute of Crop Science, Chinese Academy of Agricultural Sciences, Beijing 100081, P. R. China, Tel: +86-010-68918891, E-mail: lishk@mail.caas.net.cn)

Abstract: The accurate information access and analysis of crop canopy are the basis of quantitative research on crop information.This experiment was conducted using two winter-wheat (*Triticum aestivum*)cultivars P7(leaf erect) and ZY9844(leaf horizontal). The wheat canopy direction spectral reflectance over 350-2 500nm with view angles of 0°, 30°, 60°, 90°, 120°, 150°and 180°to the vertical line to wheat row were measured, using delamination slice method from underlayer of the wheat canopy to upside at milking stage, and compared the direction spectral characteristic of removing difference leaf layer. The contributions of different layers to Canopy Direction Spectra (CDS) were preliminarily defined, which are obviously different at 300 – 700 nm, 800 – 1300 nm and 1400 – 1800 nm. Compared the traditional 90° observational angle, the spectral information observed at the 0° angle mainly revealed the information of upper canopy and the lower layer had little impact on their spectra. However, the spectral information observed at 30° and 60° angles reflected the whole canopy information and the status of the lower layer of canopy had great effect on their spectra. Variance analysis indicated that ear layer of canopy and the first top leaf blade made greater contributions to CDS. The reflectance spectra of upper leaves for ZY9844 had less impact than that of P7. The canopy spectral information was effected by the observation angles. It is a method to improve crop canopy spectral estimation precision that changed the measured angle for different canopy structure.

Keywords: wheat canopy, leaf distribute, direction spectral, view angle

1 Introduction

The spectral characteristics of crop canopy were determined by biophysical and biochemical, it is primarily a function of tissue optical properties, for example, leaf, woody stem, and standing litter. Plant structural attributes drive variation in canopy reflectance characteristics by orienting the scatterers of leaves and stems in three-dimensional space, providing a means for photons to interact with multiple surfaces such as leaves, woody material, and soils. Leaf optical properties are a function of leaf structure, water content, and the concentration of biochemical.

The crop composition and structure are difficult to assess by traditional spectral measurement with vertical canopy direction but represent imgportant information needed to guide crop management. The direction spectrum includes a great deal of crop canopy information, Multiangle

data significantly improved the accuracy of recovering forest parameters when inverting 3-D optical models (Kimes et al., 2002) , forest vertical structure can not be captured accurately using only the 4 spectral bands in the nadir view or all view angles with a single spectral band(D.S. Kimes et al.,2006).It has been shown that the directional radiances in or near the principal plane of the sun provides information that leads to more accurate prediction of canopy structure parameters than from other azimuth planes (Gobron et al., 2000). For satellite data the directional views deviate from the principal plane of the sun. Consequently, the authors believe that the accuracies for predicting forest structure measures may decrease as the deviation from the solar plane increases.Canopy emissivity was an increasing with increasing view angle, due to the greater proportion of vegetation observed at off-nadir view angles, when the proportion of leaves is lower than that of soil, canopy emissivity grows with increasing view angle (Sobrino et al., 2005).

It should be noted that these models assume a Lambertian behaviour for soil and vegetation surfaces. Despite the fact that vegetation surfaces show a near Lambertian behaviour, bare soil surfaces do not show this behaviour, and the angular variation on emissivity can not be neglected. Lidars, multiangle radiometers, radars and imaging spectrometers have been identified as systems that can capture information in the vertical dimension. This requires a capability to remotely measure the vertical and spatial distribution of forest structural parameters that are needed for more accurate models of energy, carbon, and water flux over regional, continental, and global scales, so we examined the utility of hyperspectral datd for quantitative characterization of vertical wheat structure.

The most remote sensing system provided the image of the horizontal scope, but can't provide the vertical information of crop canopy biochemical distribute, causing the lower accuracy of resume, but mul-angle datas can increased the precision of the forest parameter (Kimes et al., 2006).

The tissue distribution of crop canopy have certainly characteristic, biochemical distribution were different because of matter transferring during grow stage. The leaves of wheat canopy is composed with under layer, middle layer, upper layer and ears layer (Wang Z J, et al.2004).The spectral characteristic was different for canopy leaves because of the different reflection and scatter, so their effect for canopy spectral was different (Wang, et al., 2004).

Various biochemical (foliar lignin and nitrogen)and biophysical factors influencing canopy reflectance signatures have been studied in previous work, it was showed the information of biochemical precision extracted were importance, the multi-angle spectral include the different direction information, it can more exact prediction the biochemical parameter.

To date, no studies showed the relative importance of wheat leaves vertical distribution that determines canopy reflectance across the shortwave (350 – 2500nm) spectrum; the contribution of each leaves layer relative to all other factors has not been adequately addressed. Yet, it is the interaction of these factors, including their potential covariance or unique behavior, that must be understood if advances in remote sensing are to be achieved.

In this paper, the leaves slice method was used by the characteristics of wheat canopy, studied the spectral response of leaf vertical distribution in wheat canopy, determine the characteristic of spectral curve for different leaves layers, develop a methodology for prediction the biochemical of canopy.

2 Materials and Methods

2.1 The Training Experiment

An outdoor field-culture experiment was conducted in Experimental Station of Institute of Crop Science of Chinese Academy of Agricultural Sciences (39º57'55" N, 116º19'46" E) in the 2005 – 2006 growing season at Chinese Academy of Agricultural Sciences Experiment Station, Beijing China(39°57'55" N, 116°19'46" E). The soil was a silt clay loam with organic matter 1.16%,

alkali-hydrolysis N 42.6 mg kg^{-1}, available phosphorus 26.5 mg kg^{-1} and available potassium 139.4 mg kg^{-1} which were determined by ASI method (Hunter, 1980).

Two winter wheat cultivars were investigated in this experiment: P7, a erect leaves plant-type and Zhongyou9844, a lax leaves plant-type. Four N fertilizer treatments were set up with four randomized replications for each cultivar:N0, no N fertilization, N1, 150 kg hm^{-2} pure N fertilization, N2, 300 kg hm^{-2} (rationally fertilized),N3, 450 kg hm^{-2} (excessively fertilized). The N rates were applied with three splits at pre-sowing (50% of the total amount), reviving stage (25% of the total amount) and jointing stage (25% of the total amount). All the treatments were fertilized with the same amount of P (P_2O_5, 144 kg hm^{-2}) and K (K_2O, 75 kg hm^{-2}) at pre-sowing.

The leaves slices method of wheat canopy: the wheat sample of length 0.5m width 0.8m were choose, based on the vertical distribution of wheat canopy, the sample were measured off whole wheat canopy(WWC), ear layer of canopy (ELC), inverse first leaves layer of canopy(ILLC-1), inverse second leaves layer of canopy(ILLC-2), inverse third leaves layers of canopy(ILLC-3), inverse fourth leaves layer of canopy(ILLC-4). The layers of canopy were wipe off by scissors from under to upper.

2.2 Measured Traits and Methods

All canopy spectral measurements were taken from a height of 1.3 m above ground (the height of the wheat is 90 cm at maturity), under clear sky conditions between 10:00 and 14:00 (Beijing local time), using an ASD FieldSpec Pro spectrometer (Analytical Spectral Devices, Boulder, CO,USA) fitted with a 258 field of view fiber optics, operating in the 350 – 2500 nm spectral region with a sampling interval of 1.4 nm between 350 and 1050 nm, and 2 nm between 1050 and 2500 nm, and with spectral resolution of 3 nm at 700 nm,10 nm at 1400 nm. A 40 cm ×40 cm BaSO4 calibration panel was used for calculation of reflectance, The spectral were measured with view angles of 0°, 30°,60°,90°,120°, 150°, and 180°to the vertical line to wheat row using the Simple multi-angle spectral measured equipment (Fig. 1 and Fig. 2) after every layer were wiped off.

Plant samplings were taken almost synchronously with the spectral measurements. Measurements were conducted at anthesis, milky stages.

Figure 1 Simple multi-angle spectral measured equipment

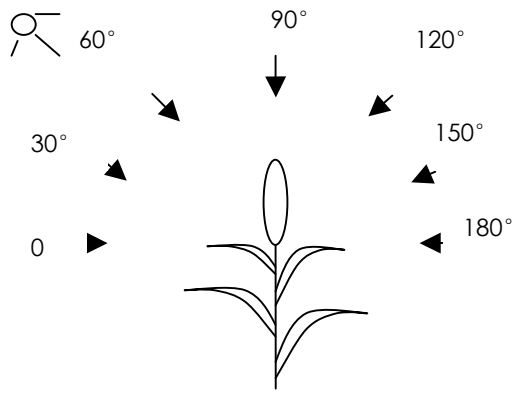

Figure 2 Sketch map of measured method

2.3 Data Analysises

The hyperspectral data used the Matlab6.5 software, statistic analysis used the Microsoft Excel 2000 and the SPSS10.0 software . The data were tested using an analysis of variance (ANOVA) procedure.

3 Results

3.1 The Spectral Curve Responses for Wiped off Different Leaves Layers

The under leaves of canopy changed the spectral reflectivity (Fig. 3, part data) with different view angle at 350 – 700nm, 800 – 1300nm, 1400 – 1800nm wavelength. It is important for pigment content with the visible wave band (350 – 700nm). The reflectivity of near infrared(800 – 1300nm) is influence by canopy characteristic. The wavebands (1400 – 1800nm) is the water content information. In this paper, we analyzed the characteristics of visible (350 – 700nm) and near infrared (800 – 1300nm) wavebands Compared the direction spectral characteristic of two wheat canopy, the spectral response of P7 variety with different view angle was more significant than that of ZY9844 at visible and near infrared wavebands, the max reflectivity of P7 at 350 – 700nm was 31% higher than that of ZY9844, was 22.4% higher at 800 – 1300nm.

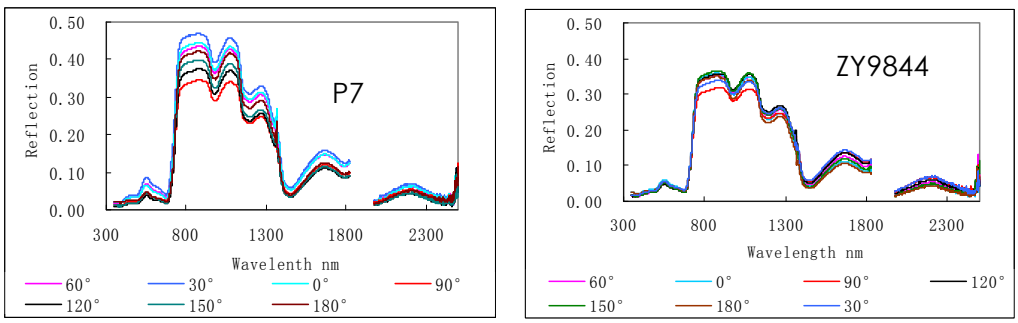

Figure 3 The spectral of removing reciprocal 4 leaf layer at different angles for P7 and ZY9844 wheat

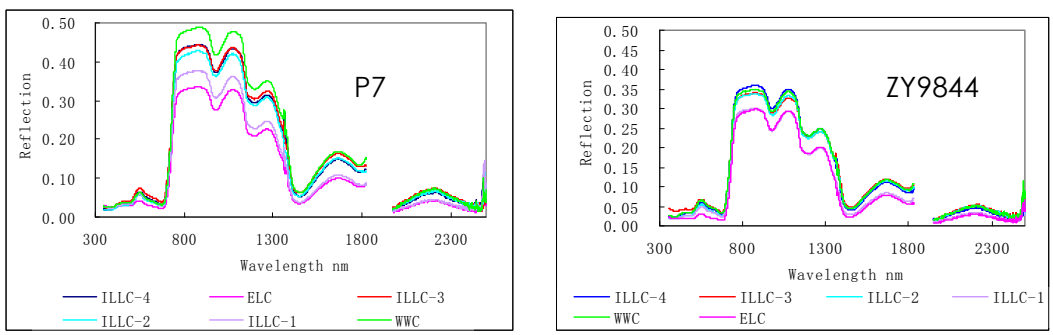

Figure 4 The spectral of removing different leaf layers at 60° angles for P7 and ZY9844

The spectral curve of doing away different leaves at 60° view angle showed the leaf influenced the curve of visible and near infrared waveband(Fig.4), the change of P7 was more significant than ZY9844, the spectral reflectivity of P7 at 350 – 700nm was 11.2% higher than that of ZY9844, was 26.8% higher at 800 – 1300nm.

In order to further analysis the relation between canopy spectral and leaves, we chose the six spectral reflectivities at 450, 550, 670, 980, 1090, 1200nm.

3.2 The Analysis of Layers Spectral Reflectivity Characteristic at Different View Angles

As showed in Fig.5, for P7 variety, the spectral reflectivity of whole canopy were similar with the wiping off ILLC-4, doing away with ELC and ILLC-1, the reflectivity were most lower.

The reflectivity changes of 550nm was more obvious than that of 450, 670 nm in visible wave bands, it was evident for 980, 1090,1200nm in near infrared wave bands. At different view angle, the reflectivity of 90° view angle was most lower, with away from the vertical measured, the reflectivity were increasing, it was more obvious in visible wave bands than that of near infrared. The reflectivity changes of wiping off ILLC-1 and ELC were more obvious than that of other leaves layers.

The reflectivity change of wiping off ILLC-3 for 1090nm was 8.8% at 0° view angle, was 48.6% for ILLC-1, At 90° view angle, the change was 5.6% and 40.7%, At 30°, was 12.9% and 27.7%, At 60°, was 12.2% and 34%. The change was less at 180°,150°,120° view angle. The results showed: compared the 90° view angle, the reflectivity of 30° and 60° had more information of under leaves, the under leaves were important for reflectivity of canopy, the reflectivity of 0° included more information of upper leaves, the upper leaves were important.

The canopy spectral reflectivity of ZY9844 were lower than P7(Fig.6), for 1090nm, the reflectivity of wiping off ILLC-3 at 0° view angle changed 4.4%, ILLC-1 was 14.7%; at 90° view angle, they were 5.9% and 46.8%, at 30° view angle, were 16.9% and 44.4%, at 60° view angle, were 16.8% and 41.2%. Compared the traditional 90° view angle, the under leaves were important for canopy spectral at 30° and 60° view angle, the upper leaves were important at 0° view angle, the upper leaves of ZY9844 were less influenced for canopy spectral than that of P7.

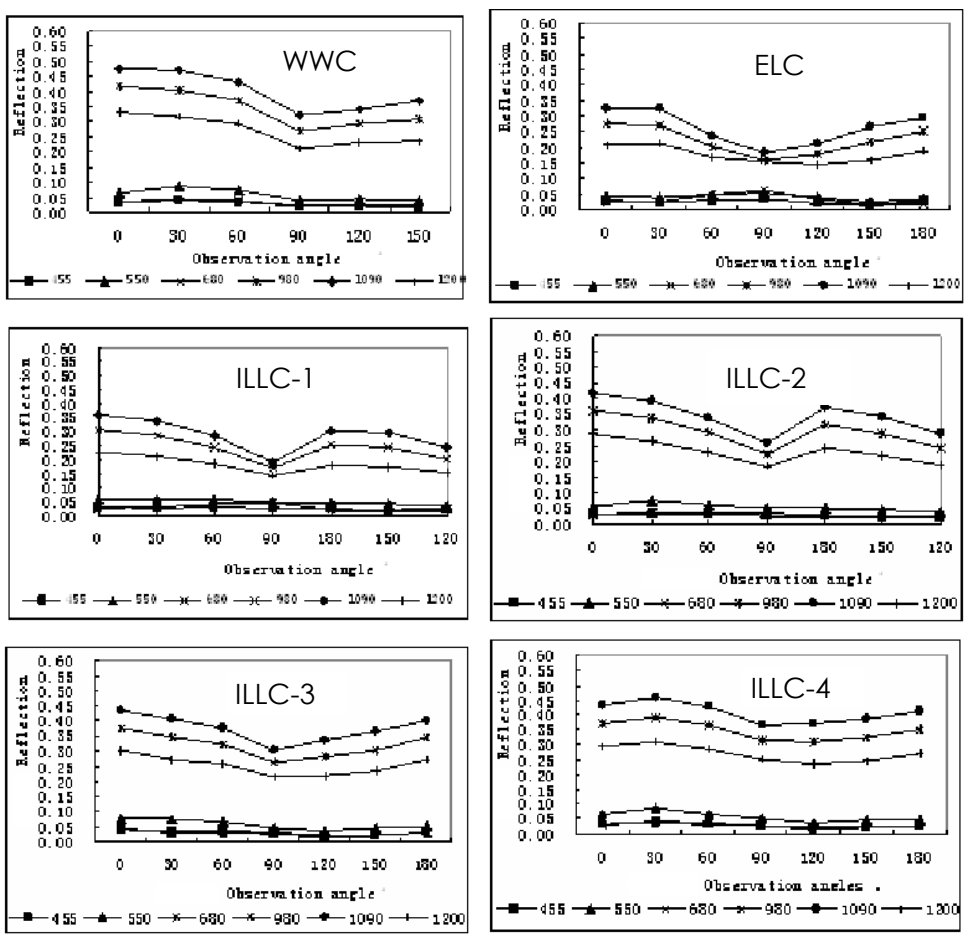

Figure 5 The spectral characteristic comparision at removing different leaf layer for P7

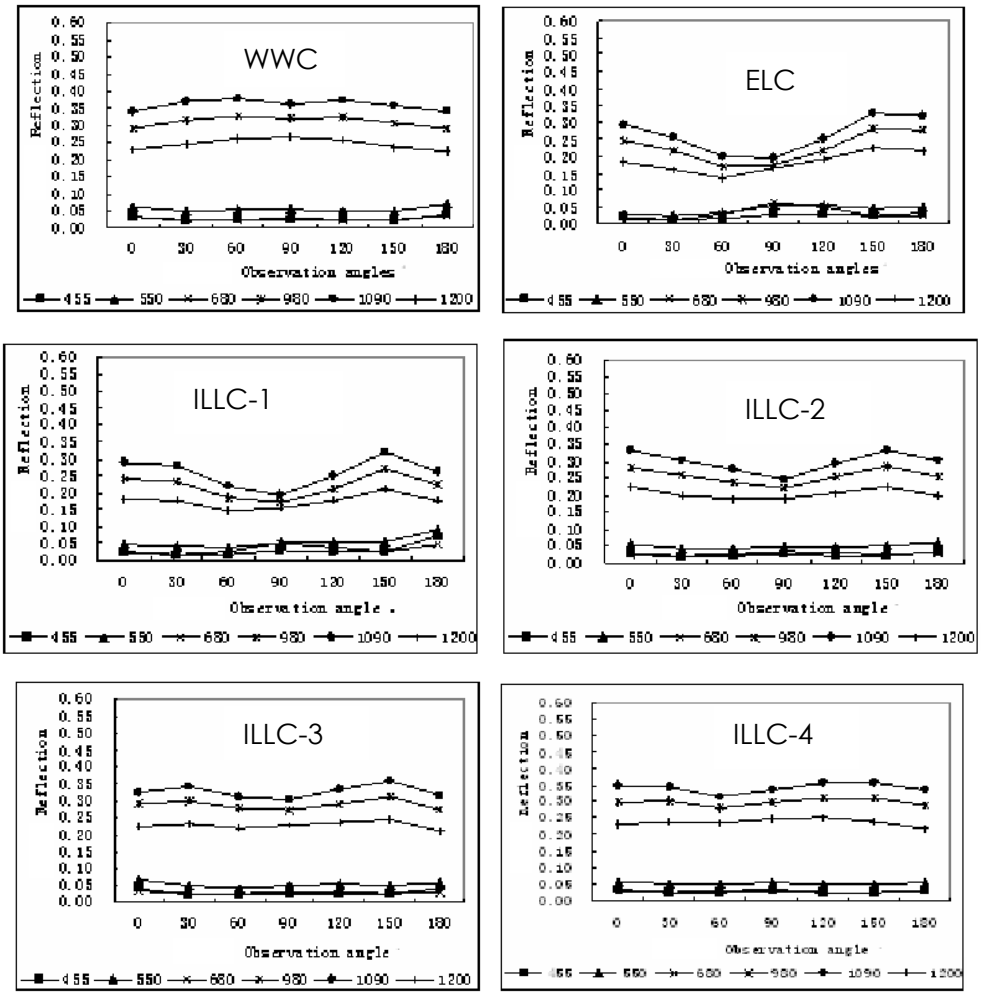

Figure 6 The spectral characteristic comparision at removing different leaf layer for ZY9844

3.3 The ANOVA Analysis of Spectral Reflectivity for Different Leaves Layers

The ANOVA analysis of six wavelength reflectivity average show the reflectivity of P7 were lower than that of ZY9844(Table 1), For P7, the response of canopy spectral with wiping off ILLC-1 and ELC were significant at 0° view angle, at 30°, wiping off ELC, ILLC-1, ILLC-2 and ILLC-3 were significant, 60° and 30° were similar, at 90°, the ELC and ILLC-1 were important, at 120°, 150° and 180° view angle, the ELC and ILLC-1 were significant. The ELC and ILLC-1 were important for canopy spectral, the influence of under leaves were less; for different view angle, at 0°, 90°, 120°, 150°, 180° view angle, the under leaves were less influence, at 30° and 60°, the response of under leaves were significant.The canopy spectral response of different leaves for ZY9844 were different from P7, at 0° and 90° view angle, the ELC and ILLC-1 were significant, at 30° and 60°, the ELC, ILLC-1, ILLC-2 were significant.

At the same view angle, the ELC and ILLC-1 were more importance than that of under leaves.

The spectral response of under leaves were relation to the view angle, with vertical and horizontal measured, the influence of under leaves were less than that of others view angle.

Table 1 The significance analysis of canopy spectral characteristic at removing leaf layers for P7 and ZY9844

Angle	Treatment	The Average Value					
		P7			ZY9844		
0°	WWC	0.2254	a	A	0.1657	a	A
	ILLC-3	0.2110	a	A	0.1643	a	A
	ILLC-4	0.2046	a	AB	0.1662	a	A
	ILLC-2	0.1974	ab	AB	0.1573	a	A
	ILLC-1	0.1690	bc	BC	0.1354	b	B
	ELC	0.1508	c	C	0.1308	b	B
30°	WWC	0.2265	a	A	0.1713	a	A
	ILLC-4	0.2196	ab	A	0.1646	a	AB
	ILLC-3	0.1951	bc	AB	0.1619	ab	AB
	ILLC-2	0.1886	c	AB	0.1398	bc	BC
	ILLC-1	0.1591	d	BC	0.1276	cd	C
	ELC	0.1487	d	C	0.1143	d	C
60°	WWC	0.2064	a	A	0.1784	a	A
	ILLC-4	0.2021	a	A	0.1553	ab	A
	ILLC-3	0.1816	ab	AB	0.1503	ab	AB
	ILLC-2	0.1645	bc	ABC	0.1323	bc	ABC
	ILLC-1	0.1412	bc	BC	0.1052	c	BC
	ELC	0.1225	c	C	0.0974	c	C
90°	WWC	0.1588	a	A	0.1766	a	A
	ILLC-4	0.1726	a	AB	0.1657	a	AB
	ILLC-3	0.1451	ab	AB	0.1532	abc	AB
	ILLC-2	0.1292	ab	AB	0.1276	abcd	AB
	ELC	0.1081	b	B	0.1137	bcd	B
	ILLC-1	0.1040	b	B	0.1084	d	B
120°	WWC	0.1645	a	A	0.1765	a	A
	ILLC-4	0.1642	a	A	0.1692	ab	AB
	ILLC-3	0.1511	ab	AB	0.1616	abc	AB
	ILLC-2	0.1341	abc	AB	0.1432	bcd	AB
	ILLC-1	0.1139	bc	AB	0.1255	d	AB
	ELC	0.1051	c	B	0.1325	cd	B
150°	ILLC-4	0.1734	a	A	0.1679	ab	A
	ILLC-3	0.1637	ab	AB	0.1692	a	A
	ILLC-2	0.1547	abc	AB	0.1568	bc	A
	WWC	0.1454	abc	ABC	0.1672	ab	AB
	ILLC-1	0.1325	cd	BC	0.1515	c	AB
	ELC	0.1166	d	C	0.1555	c	B
180°	WWC	0.2254	a	A	0.1678	a	A
	ILLC-4	0.1879	ab	AB	0.1599	a	A
	ILLC-3	0.1883	ab	ABC	0.1555	a	A
	ILLC-2	0.1725	bc	BC	0.1464	a	A
	ILLC-1	0.1388	c	BC	0.1461	b	B
	ELC	0.1360	c	C	0.1537	b	B

Note: minuscule indicate significant differences at 5%; majuscule indicate significant differences at 1%.

4 Discussion

The crop canopy have tridimensional structure characteristics, canopy structure is determined by several factors, including species composition and the three-dimensional distribution of leaves.

The biochemical content have certain distribution regulation on the canopy space.The traditional spectral measurement method of vertical canopy plane was supposed by the homogeneous canopy, the information of point can representative the characteristics of canopy, the biochemical content can been extracted using the canopy spectral reflectivity.

Under nature state, the ray not only has the absorption, much reflectivity, but also includes much dispersion in canopy, it is very complicated, so the spectral measured of characteristics of canopy was difficulty. Leaf is the mainly organ of crop canopy, the distribution of leaves and state influenced the incept of radiation and direction, the canopy spectral were changed by the view direction, so it is important to research the spectral response of leaves for improving the spectral prediction precision.

In this paper, two different plant-type wheat varieties were chosen, using leaves layers slice method, analyzing the spectral changing for different leaves layers at different view angle in the plane of vertical wheat line, the result showed:

(1) The spectral characteristics were varied in 300 – 700nm, 800 – 1300nm, 1400 – 1800nm wave bands because of wiping off leaves layers and different view angle, the change of visible wave bands was less near infrared wave bands, P7 was less ZY9844.

(2) Compared with the traditional 90° view angle measured, the spectral information of under leaves were more at 30° and 60° view angle than that of angles, that of upper leaves at 0° view angle were more . For two wheat, the spectral influence of ZY9844 upper leaves at 0° view angle were less than that of P7. The upper leaves of lax leaves plant-type wheat capture much radiation because the upper leaves were horizontal, the proportion of upwards lay was bigger than that of downwards; the erect leaves plant-type was opposite, the radiation characteristics were complicated.

It is important for precise agriculture to accurate measured the state of crop growing using remote sensing technique, in this paper, we analysis the canopy spectral characteristic of the two plant-type wheat, the result showed the canopy spectral were influence by the leaves layer and view angle, the spectral response of under leaves were varied with different view angle. The quantitative study of different leaves layer and spectral was need for crop precise manage.

That result was obtained only in the region of Peking, using the two different plant-type wheat varieties, more experiments should been studied.

Acknowledgements

The research was supported by grant 2006AA10Z207, 2006AA10A302 from the National High Tech R&D Program and 30760109 National Natural Science Fundation of China.

References

Dorigo WA, Zurita-Milla R, de Wit AJW, Brazile J, Singh R, Schaepman ME (2006) A review on reflective remote sensing and data assimilation techniques for enhanced agroecosystem modeling. International Journal of Applied Earth Observation and Geoinformation. 5:1 – 29.

Kimes DS, Ranson KJ, Sun G, Blair JB (2006) Predicting lidar measured forest vertical structure from multi-angle spectral data. Remote Sensing of Environment, 100:503 – 511.

José A.Sobrino,Juan C.Jiménez-Muñoz,Wout Verhoef (2005) Canopy directional emissivity: comparison between models. Remote Sensing of Environment, 99:304 – 314.

O'Neill AL, Kupiec JA, Curran PJ (2002) Biochemical and reflectance variation throughout a sitka spruce canopy. Remote Sensing of Environment. 80:134 – 142.

Wang ZJ, Wang JH, Huang WJ, Ma ZH, Wang BH, Zhao CJ, Zhao M (2004) The properties of temporal and spatial distributions relationship between leaf nitrogen and grain quality leaf nitrogen and the winter wheat. Acta Agronomica Sinica, 7:700 – 707(in Chinese).

Wang JH, Wang ZJ, Huang WJ, Ma ZH, Liu LY, Zhao CJ (2004) The vertical distribution characteristic and spectral response of canopy nitrogen in different layer of winter wheat. Journal of Remote Sensing, 7:309 – 315(in Chinese).

Lee F.Johnson (2001) Nitrogen influence on fresh-leaf NIR spectra. Remote Sensing of Environment, 78:314 – 320.

Lydia Serrano, Josep Peñuelas, Susan L. Ustin (2002) Remote sensing of nitrogen and lignin in mediterranean vegetation from AVIRIS data: decomposing biochemical from structural signals. Remote Sensing of Environment. 81:355 – 364.

Moses Azong Cho, Andrew K. Skidmore (2006) A new technique for extracting the red edge position from hyperspectral data: The linear extrapolation method. Remote Sensing of Environment, 101: 181 – 193.

Li Y X, Zhu Y, Tian Y C, Yao X, Qin X D, Cao W X (2006) Quantitative relationship between leaf nitrogen accumulation and canopy reflectance spectra in wheat. Acta Agronomica Sinica, 2:203 – 209 (in Chinese).

Xue L H, Cao W X, Luo W H, Jiang D, Meng Y L, Zhu Y (2003) Diagnosis of nitrogen status in rice leaves with the canopy spectral reflectance. Scientia Agricultura Sinica, 36(7):807 – 812(in Chinese).

Lu Y L, Wang J H, Li S K, Xie R Z, Gao S J ,Ma D L (2005) Identification of wheat canopy structure using hyperspectral data. Scientia Agricultura Sinica, 4(9): 668 – 672.

Bai J H, Li S K, Wang K R, Zhang X J, Xiao C H, Sui X Y (2007) The response of canopy reflectance spectrum for the cotton LAI and LAI inversion. Scientia Agricultura Sinica, 40(1):63 – 69(in Chinese).

Liu Wei-dong, Xiang Yue-qin, Zheng Lan-fen, Tong Qing-xi, Wu Chang-shan (2000) Relationships between rice LAI, CH.D and hyperspectra data. Journal of Remote Sensing, 4(4):279 – 283(in Chinese).

Wu Chang-shan, Xiang Yue-qin, Zheng Lan-fen, Tong Qing-xi (2000) Estimating chlorophyll density of crop canopies by using hyperspectral data. Journal of Remote Sensing, 4(3):228 – 232(in Chinese).

Zhang Xia, Liu Liang-yun, Zhao Chun-jiang, Zhang Bing (2003) Estimating wheat nitrogen concentration with high spectral resolution image. Journal of Remote Sensing, 7(3):176 – 181(in Chinese).

Jean-Luc Widlowski , Bernard Pinty, Thomas Lavergne, Michel M. Verstraete, Nadine Gobron (2006) Horizontal radiation transport in 3-D forest canopies at multiple spatial resolutions: Simulated impact on canopy absorption. Remote Sensing of Environment, 103: 379 – 397.

E. A. Walter-Shea, J. Privette, D. Cornell. M. A. Mesarch, and C. J. Hays (1997) Relations between directional spectral vegetation indices and leaf area and absorbed radiation in alfalfa1. Remote Sensing of Environment, 61:16 – 177.

Andres Kuusk and Tiit Nilson (2000) A directional multispectral forest reflectance model. Remote Sensing of Environment, 72: 244 – 252.

Fraser Gemmell and Adrian J. McDonald (2000) View zenith angle effects on the forest information content of three spectral indices. Remote Sensing of Environment, 72:139 – 158.

Laurent Bousquet, Sophie Lachérade, Stéphane Jacquemoud, Ismaë Moya (2005) Leaf BRDF measurements and model for specular and diffuse components differentiation. Remote Sensing of Environment, 98: 201 – 211.

Gao F, Zhu Q J (1997) The advance in multi-angle remote sensing of vegetation canopy. Scientia Geographica Sinica, 11:346 – 355.

Lu Y L, Li S K, Wang K R, Xie R Z, Gao S J, Wang G (2006) Prediction of grain protein content using ear layer spectral reflectance data. Acta Agron Sin, (32)2:232 – 236.

Lu Y L, Li S K, Wang J H (2005) Prediction of grain protein content of wheat based on the ear level spectrum25th Anniversay IGARSS (International Geoscience and Remote Sensing Symposium) 25-29 July, 2005, Seoul. Korea.

Xiao C H, Li S K, Wang K R, Lu Y L, Xie R Z, Gao S J (2007) Prediction canopy leaf nitrogen content of winter wheat based on reflectance spectra in different directions. Acta Agron Sin, 33(7):1141 – 1145.

Modeling Leaf Sheath and Internode Growth Dynamics in Wheat

Yan Zhu, Liang Tang, Zi-Hui Tan, Guo-Qing Chen, Wei-Xing Cao

(Hi-Tech Key Laboratory of Information Agriculture of Jiangsu Province, Key Laboratory of Crop Growth Regulation of Ministry of Agriculture, Nanjing Agricultural University, Nanjing 210095, China, Corresponding author: caow@njau.edu.cn)

Abstract: Based on extensive observations and quantitative analyses on leaf sheath and internode growth processes with different variety types, a dynamic model was developed to simulate time-course growth characters of leaf sheath and internode in wheat. The growth dynamics of leaf sheath and internode were described using the Logistic model, the internode length was simulated with the relationship between leaf sheath length and corresponding internode length, and the internode thickness was quantified using the relationship between internode thickness and corresponding internode length. The results of model validation showed that the mean RMSEs of leaf sheath length, internode length and thickness were 1.34 cm, 1.71 cm and 0.06cm, respectively, which indicated a good performance of the model in prediction of leaf sheath and internode growth dynamics in wheat.

Keywords: wheat, leaf sheath growth, internode growth, dynamic model

1 Introduction

Crop morphological model is the important part of crop simulation model. Recently, with the application of information technology in agriculture, the research of virtual crop has become popular area in plant growth modeling and information agriculture. Many morphological models have been developed (Song et al., 2000; Guo et al., 2001), yet most of them are static models adapted to a given set of conditions (Guo et al., 1999; Zhan et al., 2001; Prusinkiewicz et al., 1994) while the process-based models are seldom in literature. In particular, how to describe the time-course growth of morphology in cereal crops is a difficult task. In the processes of morphological growth in wheat, the growth dynamics of leaf sheath and internode are key aspects for describing vertical development of morphological architecture in wheat. Thus, this research was undertaken to develop a dynamic simulation model on time-course growth characters of leaf sheath and internode in wheat, including the dynamic length of leaf sheath and internode and thickness of internode. This work would help to provide a technical basis for building virtual growth system of wheat plant.

2 Material and Methods

2.1 Experiment Design

The experiment was conducted with five winter wheat cultivars (Xumai 26, Yumai 34, Ninmai 9, Yangmai 9, Yangmai 10) with different morphological styles on the field experiment station of Nanjing Agricultural University, China (118°42' E, 32°03' N) from 2002 to 2003. The seeding rate was $1.2*10^6$ seeds ha^{-1}, and other field managements followed local practices for high yield wheat.

2.2 Measurement

From emergence, time-course measurements were taken on dynamic growth characters of leaves in wheat. At each observation, the same three plants in each plot were chosen for continuous observations. Since appearance of the first leaf sheath, each leaf sheath was consecutively surveyed for length once every three days until the leaf length was fixed. From jointing, the length of internode was measured once every two days. The internode thickness was measured at three points of the same internode (terminal, middle, base).

2.3 Data Use

The actual data collected in Xumai 26, Yumai 34, Ninmai 9 and Yangmai 9 were used to develop a dynamic model for simulating time-course growth characters of different leaf sheath and internodes on wheat plant, while the data from Yangmai 10 were used for validation of the model. The following statistic method, root mean square error (RMSE), was used to calculate the fitness between the estimated results and observed data.

$$\mathrm{RMSE} = \sqrt{\frac{\sum_{i=1}^{n} (\mathrm{OBS}_i - \mathrm{SIM}_i)^2}{n}}$$

where SIM_i and OBS_i are predicted and observed values, respectively, and n is the number of samples. The RMSE gives a measure of relative difference between the simulated versus observed data. The prediction is considered better if RMSE is smaller.

2.4 Model Description

2.4.1 Leaf Sheath Growth Dynamic

The leaf sheath growth pattern generally follows S-shaped growth curve, well fitting a Logistic equation:

$$\mathrm{SHLen}_n(\mathrm{GDD}) = \frac{\mathrm{SHLen}_n}{1 + \mathrm{SHPa} \times \mathrm{e}^{-\mathrm{SHPb} \times (\mathrm{GDD\text{-}SHIGDD}_n)}} \quad (1)$$

$$\mathrm{SHIGDD}_n = 102 + n \times \mathrm{PHYLL} \quad (2)$$

where n is the leaf number; GDD is growth degree days; SHLen_n(GDD) is the length of leaf sheath n at a certain GDD; SHIGDD_n is a GDD at initial appearance of the leaf sheath n and linearly related to PHYLL, which is the thermal interval for the adjacent two leaves to emerge, and largely a genetic factor as defined by Yan et al. (2001); 102 is the GDD value needed from seeding to emergence; SHPa and SHPb are the coefficients of the model, set as 4 and 0.08; SHLen_n is the final length of leaf sheath n (cm). The final length of leaf sheath increases exponentially with the leaf number, as in Eq. (3).

$$\mathrm{SHLen}_n = \mathrm{SHa} \times \mathrm{e}^{\mathrm{SHb} \times n} \quad (3)$$

where SHa and SHb are equation parameters. The value of SHa was set as the length of the first leaf sheath (FSHLen, cm), which is variety dependent and little influenced by environments, and

thus defined it as a genetic parameter. The SHa and SHb are significantly correlated with r^2 of 0.9945, with the equation calculated as follows:

$$\mathrm{SHb} = 0.5199 - 0.2428 \times \mathrm{SHa} \tag{4}$$

2.4.2 Internode Length Dynamic

The growth pattern of internode is similar to that of leaf sheath and generally followed a S-shaped growth curve, well fitting a Logistic equation:

$$\mathrm{INLen}_n(\mathrm{GDD}) = \frac{\mathrm{INLen}_n}{1 + \mathrm{INPa} \times \mathrm{e}^{-\mathrm{INPb} \times (\mathrm{GDD} - \mathrm{INIGDD}_n)}} \tag{5}$$

where n is the internode number; $\mathrm{INLen}_n(\mathrm{GDD})$ is the length of internode n at a certain GDD; INPa and INPb are the equation parameters, set as 4 and 0.6, respectively; INIGDD_n is the GDD when internode n begins to appearance, and calculated as follows:

$$\mathrm{INIGDD}_n = \mathrm{GDD}_j + (n-1) \times \mathrm{PHYLL} \tag{6}$$

where GDD_j is the GDD at jointing calculated by wheat growth model (Liu et al., 2001).

It was found that the ratio of leaf sheath length to corresponding internode length is arithmetical series. Thus the length of internode can be calculated as follows:

$$\mathrm{INLen}_n = \frac{\mathrm{SHLen}_n}{\mathrm{SHINRatio}_n} \tag{7}$$

where SHLen_n is the length of leaf sheath n; $\mathrm{SHINRatio}_n$ is the ratio of the length of leaf sheath n to the length of the corresponding internode, calculated as follows:

$$\mathrm{SHINRatio}_n = \mathrm{SHINRatio}_n + (n-1) \times 0.2484 \qquad \mathrm{INN} \geq n \geq 1 \tag{8}$$

where $\mathrm{SHINRatio}_n$ is the ratio of the length of flag leaf to the length of the corresponding internode, which is similar among different cultivars, and thus set as a mean value of 0.686.

2.4.3 Internode Thickness Dynamic

The thickness of internodes increases very slowly in the process of wheat growth,and is assumed to increase linearly with GDD:

$$\mathrm{INTh}_n(\mathrm{GDD}) = a + \frac{\mathrm{INTh}_n}{b} \times (\mathrm{GDD} - \mathrm{INIGDD}_n) \tag{9}$$

where $\mathrm{INTh}_n(\mathrm{GDD})$ is the thickness of internode n at a certain GDD; INIGDD_n is a certain GDD when the internode begins to elongate; a is the thickness of internode when the internode begins to elongate, set as 0.24(cm); b is the GDD interval from elongation to thickness fixing of an internode, set as 98 (℃); INTh_n is the final thickness of internode n (cm), correlated to length of internode, calculated as:

$$\mathrm{INTh}_n = \frac{\mathrm{INLen}_n - 45.2}{\mathrm{ThP}a} \tag{10}$$

where $INLen_n$ is the final length of internode n; ThPa is the model coefficient and calculated as:

$$\text{ThP}a = \frac{INLen_{max} - INLen_{min}}{c} \tag{11}$$

where $INLen_{max}$ and $INLen_{min}$ is the length of longest and shortest internode (cm), respectively, which can be calculated by Eq. (5); c is the thickness difference between the maximum thickness and minimum thickness among different internodes, and set as a mean value of 0.15 with slight variation in different cultivars.

3 Model Validation

The observed data of Yangmai 10 experiment in 2002 and 2003 were used to validate the model of the length of leaf sheath, the length and thickness of internode. The RMSE was calculated to reflect the statistic differences between the simulated and observed values. From the first leaf sheath to 10th, the RMSE were 0.41, 0.28, 0.43, 0.60, 1.00, 1.15, 1.77, 2.60, 3.06, 2.07 cm, respectively, with the average RMSE as 1.34 cm (Table1). The RMSE values of internodes length were 0.48, 1.60, 2.43, 1.52, 2.51 cm, respectively, with the average value as 1.71 cm (Table 2). The RMSEs of internode thickness were 0.07, 0.05, 0.04, 0.07, 0.05 cm, respectively, with the average value as 0.056 cm (Table 3). Overall; plotting of 1:1 relationships exhibited a good fit between the simulated and observed values in leaf growth dynamics (Figs. 1 and 2).

Table 1 Prediction errors for individual leaf sheath length in Yangmai 10

Replication	Absolute Prediction Errors (cm)									
	1st	2nd	3rd	4th	5th	6th	7th	8th	9th	10th
1	– 0.05	0.03	0.43	– 0.40	0.44	0.81	1.02	1.31	4.82	
2	– 0.05	0.53	0.73	– 0.20	– 0.06	0.31	2.02	3.81	2.32	– 0.48
3	– 0.55	– 0.17	0.13	0.10	1.94	– 1.69	2.52	-3.19	– 2.68	– 3.98
4	– 0.60	0.03	– 0.07	1.10	– 0.06	1.31	1.02	0.81	1.32	– 0.98
RMSE	0.41	0.28	0.43	0.60	1.00	1.15	1.77	2.60	3.06	2.07

Table 2 Prediction errors for length of different internodes in Yangmai 10

Replication	Absolute Prediction Errors (cm)				
	1st	2nd	3rd	4th	5th
1	0.70	– 0.87	– 3.84	0.30	1.10
2	0.50	0.13	– 0.84	0.60	2.10
3	1.50	– 2.87	0.16	– 2.90	– 4.40
4	0.40	1.13	– 2.84	0.60	– 0.40
RMSE	0.89	1.60	2.43	1.52	2.51

Table 3 Prediction errors for thickness of different internodes in Yangmai 10

Replication	Absolute Prediction Errors (cm)				
	1st	2nd	3rd	4th	5th
1	0.07	– 0.01	– 0.02	– 0.03	– 0.02
2	0.07	0.04	– 0.02	– 0.03	– 0.05
3	0.10	0.04	– 0.06	– 0.14	– 0.09
4	– 0.05	– 0.07	– 0.02	– 0.10	– 0.04
RMSE	0.07	0.05	0.04	0.07	0.05

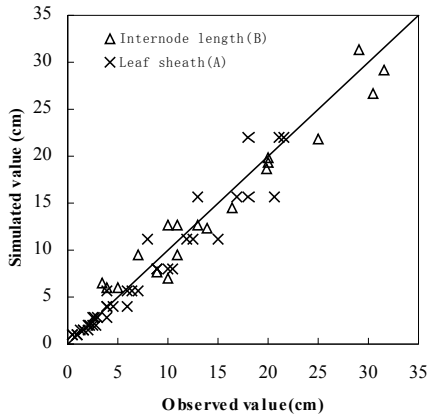

Figure 1 Comparison of simulated with observed values of individual leaf sheath length (A) and internode length (B) in Yangmai 10

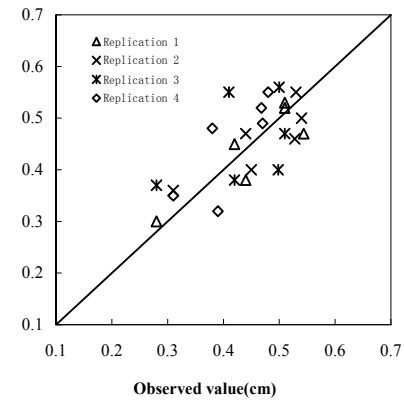

Figure 2 Comparison of simulated with observed stem thickness in Yangmai 10

4 Summary and Discussion

By integrating the experiment and simulation researches and following the biological patterns of morphological development in wheat, a dynamic simulation model on leaf sheath and internode growth was established, including the time course changes of leaf sheath length and internode thickness and length. Validation of the model with the observed data indicated that the model could give a good prediction on dynamic characters of leaf sheath and internode growth. This model provides a foundation for establishing process-based morphological model and constructing virtual growth system of wheat plant.

The present model quantified the dynamic characters of leaf sheath and internode in winter wheat with several algorithms from detailed growth analysis. Using Logistic model to describe the time course growth of the leaf sheath and internode fit with the biological rules of wheat growth dynamic. Simulating dynamic internode length with the ratio of leaf sheath length to corresponding internode length reduced number of the parameters and improved the applicability of the model. The result of the validation proved the assumption that the internode thickness is linear with GDD. The model appeared to be well adapted to normal field managements. Yet, further studies are necessary for adding the effects of water and nitrogen levels to the model and testing the model over a range of climatic and production conditions.

References

Cury R B, Chen L H (1971) Dynamic simulation of plant growth, I. Development of a model. ASAE Trans, 14(5): 946 – 959.

Guo Y, Li B G (1999) Mathematical description and three 2 dimensional reconstruction of maize canopy. Chin J Appl Ecol, 10(1):39 – 41.

Guo Y, Li B G (2001) New advances in virtual plant research. Chin Sci Bull, 46(11): 888 – 894.

Li S K, Wang C T (1997) The methods of obtaining and expressing information of crop plant shape and population structure. J Shihezi Univ (Natural Science), 3:250 – 256.

Liu T M, Cao W X, Luo W H, Pan J. Yan M H, Guo W S (2001) Simulation on wheat tillering dynamic. J Huazhong Agric Univ, 20(5): 416 – 421.

Prusinkiewicz P, Remphrey W R, Davidson C G (1994) Modeling the architecture of expanding Fraxinus pennsylvanica shoots using L-systems. Can J Bot, 72: 701 – 714.

Smith G S, Curtis J P, Edwards C M (1992) A method for analyzing plant architecture as it relates to fruit quality using three-dimensional computer graphics. Ann Bot, 70: 265 – 269.

Song Y H, Jia W T, Guo Y, LI B G (2000) A review virtual crop research. Computer and Agriculture, 6: 6 – 8.

Yan M C, Cao W X, Luo W H, Wang S H (2001) A simulation model of above-ground organ formation in wheat. Acta Agronomica Sinica, 27(2): 221 – 229.

Zhan Z G, Wang Y M, Reffye P, Hu B G (2001) Morphological architecture-based growth model of winter Wheat. Transactions of the Chinese Society of Agricultural Engineering. 5: 6 – 11.

Zhang L D, Li S K, Zhao M, Wang S A (1998) Statistical model about geometric characters of maize plant shape. Acta Agronomica Sinica, 24(5): 635 – 638.

Modeling Fruit Morphological Formation on Muskmelon

Li-Ying Chang, Ming-Han Chi, Dan-Feng Huang

(School of Agriculture and Biology, Shanghai Jiaotong University, 800 Dongchuan Road, Shanghai, 200240, P. R. China)

Abstract: Modeling fruit morphological formation on muskmelon is of significant importance for realizing virtual and digital plant growth. Two experiments were carried out for data acquisition, involving different organic fertilizer rates and cultivars. Time-course observations were made on fruit morphological properties (fruit size, color and netted) on muskmelon plant under different experiment conditions. The results showed that the fruit swelling process (vertical diameter and horizontal diameter) of muskmelon exhibited a slow-rapid-slow pattern, which could be well described with a logistic curve against growing degree-days (GDD); Fruit color changes based on the RGB values could be represented quadratic relationship to cumulative GDD; The fruit netted changes over growth progress could be partitioned into 3 phases according to before and after pollination 30 and 40 days. The first phase was the process from pollination 1 day to after pollination 30 days, in which the vertical stripe becomes at fruit middle part and the horizontal stripe at fruit handles and hilum part. The second phase was the process from pollination 30 to 40 days, in which the horizontal stripe becomes at fruit middle part and the netted formed. The third phase was the process of after 40 days, in which the netted breadth and thick are gradually increased. The model was validated with the independent experiment data involving different muskmelon cultivars, and the mean RMSEs of fruit were 0.28 cm and 0.19 cm, respectively, for vertical diameter and horizontal diameter, 12.6 for fruit color, 0.13 cm for stripe length and diameter at varied GDD. Thus the present model had a good performance in predicting morphological growth of muskmelon fruit, which should be useful for further realizing virtual expression of fruit growth dynamics in muskmelon plant.

Keywords: growth dynamic, vertical diameter, horizontal diameter, fruit color, muskmelon, vertical stripe, horizontal stripe

1 Introduction

Virtual crop growth modeling has long been known as the most important parts of agriculture information technique plays a vital role in output of visualization express result and digital agriculture (Prusinkiewicz, 2004). During the past years, many scholars have paid much attention to this study. The previous studies have mainly focused on the morphological re-building of leaf, leaf sheath, internode, panicle and root in soybean (Hanan, 1997), corn (Andrieu et al., 1995; Fournier and Andrieu, 1998; Fournier 1999; Zhang et al., 2001), wheat (Zhan et al 2001; Chen et al 2004), barley (Buck-Sorlin 2000, 2002), sorghum (Kaitaniemi et al., 2000), rice (Watanabe et al., 2005; Shi et al., 2006) and cotton (Hanan and Hearn, 2003). Recently, CIRAD has made great progress in the field of plant growth mechanistic model, which was included in the software of AMAP. (Zhao et al., 2001) proposed a dual-scale automaton model, and then developed the plant model of GreenLab and established a virtual plant growth and visualization system. Meanwhile (Hanan et al., 2003) analyzed cotton structure model on the basis of the growth model. (Wang et al., 2005)

simulated the spatial distribution of radiation in the upper layers of corn. Essentially, the above studies have built the preliminary models of virtual structures based on the relationships between structure and function of crop growth, by combining morphogenesis model and mechanism model and then deducing the geometrical parameters of organs. In the area of plant morphological simulation in agronomic crops, the studies were directed toward the field crops, whereas the horticulture crops were seldom reported, such as muskmelon, are involved rarely.

Fruit as the harvest organ of muskmelon and its shape is one of the most distinct characteristic of plant morphological formation. Thus, modeling the fruit spatial shape is a key task for virtual muskmelon research. At present, the study on fruit shape mainly emphasized on fruit quality and aimed at characteristics heredity analysis (Hector et al., 2007; Xu et al., 2007). Even less attempt has revealed dynamic characteristics of fruit shape process so that the fruit growth processes at different times are yet to be elucidated. Since muskmelon, as a horticulture crop, has complex and beautiful fruit shape, it is difficult to quantitatively describe the characteristics of fruit shape changes, which is of key importance for dynamic simulation and virtual expression of muskmelon plant.

The objectives of this study were to characterize the change patterns of fruit growth characters with plant development progress, and to model morphological formation of fruit in muskmelon plant, on the basis of time-course observations and analyses on the dynamics of fruit vertical diameter, horizontal diameter, fruit color, vertical stripe and horizontal stripe in muskmelon plant under different organic fertilizer rates and cultivar types. The expected information would lay a foundation for further realizing virtual and digital expression of fruit growth on muskmelon plant with a comprehensive simulation system.

2 Materials and Methods

2.1 Experiment Design

Two experiments were carried out for data acquisition to build and test model, organic fertilizer rates and cultivar types in muskmelon.

Exp. 1: The experiment was conducted with four organic fertilizer rates at the membrane and multispan greenhouse of experiment farm at School of Agriculture and Biology, Shanghai Jiaotong University, China in 2007. The muskmelon cultivar included Wanglu, Jinlu and Dongfangmi 1 were planted on 11 August, and transplanted on 29 August with three seedlings per substrate bag. Organic fertilization was applied at 0.4, 0.8, 1.2 and 1.6 kg per substrate bag. The experiment was arranged in a randomized complete block design with three replications for each treatment. Each substrate bag was drip irrigated independently. Other field managements followed local practices for conventional methods.

Exp. 2: The experiment was conducted with four cultivars in substrate bag simultaneously with Exp. 1 at the membrane and multispan greenhouse of experiment farm at School of Agriculture and Biology, Shanghai Jiaotong University in 2007. Three muskmelon cultivars, Wanglu, Jinlu and Dongfangmi 1 were grown in the experiment. The organic fertilizer rate and the cultural management was the same as in Exp. 1.

2.2 Observation Method

To observe the dynamic processes of fruit growth, three replicate plants per substrate bag were used for measuring vertical diameter, horizontal diameter, chlorophyll content, stripe length, stripe diameter of all individual fruit with sensor. The measurements were taken normally at the 30 min every day interval. During the experiment periods, new leaves on plants were marked continuously to distinguish from the old ones.

During the whole growth period, the temperature changes of each day were measured every half hour with a hand-carried automatic weather station, HOBO-21, which is made in America. The data were downloaded every month and used for calculating growing degree-days (GDD) as a basic driving factor of fruit growth in muskmelon.

2.3 Data Analysis and Utilization

Statistical analyses were conducted with means of three observations for each substrate bag in each experiment. To fully built and test the robustness of the model, the data from exp. 1 was used to build the model, and data from and exp. 2 were used to test the model performance under different cultivar types. The fitness between the simulated and observed values was verified with root mean square error (RMSE). The lower RMSE value indicated the greater reliability of the model. The RMSE was calculated as follows, where OBS_i and SIM_i are observed and simulated values, respectively, and n is the number of samples.

3 Results and Analysis

3.1 Growth Dynamic of Fruit Size (Vertical Diameter and Horizontal Diameter)

The results of this study indicated that the growth process of vertical diameter and horizontal diameter of muskmelon fruit exhibited the S pattern change rules, which well fit with a logistic pattern as shown in Fig. 1. Thus, the whole process of vertical diameter and horizontal diameter changes over growth progress could be partitioned into 3 phases in muskmelon fruit. The first phase was the process from pollination to after pollination five days, in which the vertical diameter and horizontal diameter gradually increased. The second phase was the fruit inflating stage from after pollination five to twenty-five days, in which the vertical diameter and horizontal diameter were increased rapidly. The third phase was the process from after twenty-five days to fruit harvest, in which the vertical diameter and horizontal diameter were growth gradually slower.

Thus, the fruit growth process of vertical diameter and horizontal diameter in muskmelon could be described quantitatively with Eq. (1):

$$\mathrm{FL}\,(\mathrm{GDD}\,) = \mathrm{FL}\,/1 + \mathrm{Fa} \times \mathrm{e}^{-\mathrm{Fb}\times(\mathrm{GDD}\,-\mathrm{FAGDD}\,)} \tag{1}$$

where GDD (℃·d) is growing degree-days, calculated in Eq. (2); FL (GDD) (cm) is the vertical diameter and horizontal diameter of fruit at GDD; FL (cm) is final vertical diameter and horizontal diameter of fruit, and a cultivars parameter; Fa and Fb are the equation coefficients and set as 8.302 and 0.044 from our test analyses, respectively; FAGDD (℃·d) is the initial GDD when the fruit begins to grow, calculated in Eqs. (3) and (4).

$$\mathrm{GDD} = \sum(\mathrm{Ti} - \mathrm{Tb}) \tag{2}$$

where Ti (℃) is the average daily temperature; Tb (℃) is the base temperature for muskmelon growth.

$$\mathrm{FAGDD} = \mathrm{LAGDD}_{\mathrm{LN}+1} \tag{3}$$

$$\mathrm{LAGDD}_n = 68 + \mathrm{PHYLL}\times(n-1) \qquad n = 1, 2, \cdots, \mathrm{LN} \tag{4}$$

where LAGDD_n is the emergence GDD of leaf n and have linearity relationship with PHYLL;

PHYLL is the thermal time interval of joined leaf emergence on muskmelon stem, and a specifically heredity parameter; LN is the final leaf number, and a cultivars parameter; 68 is the GDD required from sowing to seedling emergence.

3.2 Growth Dynamic of Fruit RGB Color

The color of a fruit is a combination of various colors, the ratio between chlorophyll for green and carotenoid for yellow determines the overall color, several color systems could be used to describe colors in nature. In general, there are RGB (Red, Green, Blue), HLS (Hue, Lightness, Saturation) and CMYB (Cyan, Magenta, Yellow, Black). RGB presents color through mixing red, green, blue together in different ratios, often used in displaying system. HLS can describe colors in terms of quantity. It uses hues to show color in order to distinguish this color from another; it uses saturation for color thickness, lightness for the bright sense of color.

The results showed that the color character distilled through RGB system was affected greatly by ray, and rule not evidence. For embodied exactly and sufficiently the change rule of fruit color, the RGB color character were all treated with a normalization procedure, thus could be wipe off the effect of illumination and shadow partly. *r*, *g*, *b* were normalization component of three colors, respectively, and showed as Eqs. (5) – (7).

$$r=R/(R+G+B) \tag{5}$$

$$g=G/(R+G+B) \tag{6}$$

$$b=B/(R+G+B) \tag{7}$$

After normalization procedure, executed reverse change, displayed as Eqs. (8) – (10).

$$R=r\times 255 \tag{8}$$

$$G=g\times 255 \tag{9}$$

$$B=b\times 255 \tag{10}$$

The results indicated that the change of *R*, *G* and *B* value with GDD could be described with a quadratic curve, respectively, and quantified as Eq. (11).

$$\mathrm{FR,FG,FB(GDD)} = \mathrm{Fa}\times \mathrm{TimeS}^2 + \mathrm{Fb}\times \mathrm{Times} + \mathrm{Fc} \tag{11}$$

where FR, FG, FB (GDD) are *R*, *G*, *B* value at GDD; Fa, Fb, Fc are coefficients and set as -0.0055, 1.238, 6.049 respectively, from our experiments; TimeS is temporal variable as described in Eq. (12).

$$\mathrm{TimeS} = \mathrm{GDD} - \mathrm{FAGDD} \tag{12}$$

3.3 Growth Dynamic of Fruit Netted (Stripe Length, Stripe Diameter)

The observation indicated that the fruit surface already have stripe after pollination 20 days, and more vertical stripe at fruit middle part, and that horizontal stripe at fruit handles and hilum part. The vertical stripe at fruit middle part is increased 1 cm after pollination 25 days and horizontal stripe are not happened. The stripe at fruit surface already becomes netted connection after pollination 30 days.

The mostly becomes netted after pollination 35 days. The netted breadth and thick increased and it becomes very beautiful.

Thus, the whole process of netted changes over growth progress could be partitioned into 3 phases according to before and after pollination 30 and 40 days. The first phase was the process from pollination 1 day to after pollination 30 days, in which the vertical stripe becomes at fruit middle part and the horizontal stripe becomes at fruit handles and hilum part. The second phase was the process from pollination 30 to 40 days, in which the horizontal stripe becomes at fruit middle part and the netted formed. The third phase was the process of after 40 days, in which the netted breadth and thick increased. The dynamic changes of fruit netted on muskmelon plant could be expressed in Eq. (13).

$$\text{FNetted(GDD)} = \begin{cases} \text{FNa} \times \text{Ln(TimeS)} + \text{FNb} & 0 \leqslant \text{TimeS} \leqslant 5 \times \text{PHYLL} \\ \text{FNc} \times \text{Ln(TimeS)} + \text{FNd} & 5 \times \text{PHYLL} \leqslant \text{TimeS} \leqslant 6.6 \times \text{PHYLL} \\ \text{FNe} \times (\text{TimeS})^{\text{FNf}} & \text{TimeS} > 6.6 \times \text{PHYLL} \end{cases} \tag{13}$$

where FNetted(GDD) (cm) is the vertical and horizontal stripe length at GDD; FNb is initial vertical and horizontal stripe length after fruit emergence, similar for different fruit in muskmelon and can be averaged as 0.3 from our experiments; FNd, FNe, FNf are equation coefficients, and set as -1.828, 0.063, 0.769 from our experiments, respectively; FNa and FNc are described in Eqs. (14), (15) and (16), respectively.

$$\text{FNa} = -0.004/\text{TF}_{\max} \tag{14}$$

$$\text{TF}_{\max} = 5 \times \text{PHYLL} \tag{15}$$

$$\text{FNc} = 0.011 \times \text{TF}_{\max} \tag{16}$$

where $\text{TF}_{\max}$ is the time for the vertical and horizontal stripe length reaches the maximum value.

3.4 Test of Fruit Vertical Diameter, Horizontal Diameter, RGB Color and Netted

The submodels of fruit vertical diameter, horizontal diameter, RGB color and netted were all validated with the independent data sets from experiments 2, and the results indicated a high consistency and accordance between the simulated and observed values. Figures 1 and 2 display the 1:1 relationship for fruit vertical diameter and horizontal diameter at varied GDD and the model could well simulate the time-course changes of fruit vertical diameter and horizontal diameter dynamics. The statistical analysis gave the RMSEs of fruit vertical diameter and horizontal diameter at varied GDD as 0.28 cm and 0.19 cm, respectively.

Similarly, the 1:1 relationship between the observed and simulated fruit color at varied GDD were exhibited in Fig. 3. Overall, the present model had good prediction ability to estimate the changes of fruit color for muskmelon. The statistical analysis showed that RMSEs of fruit color at varied GDD was 12.6.

Figure 4 was a comparison of the simulated with observed vertical and horizontal stripe length of netted at varied GDD. The change rule is vertical stripe happen earlier than horizontal stripe. This pattern was well predicted by the present model, with RMSEs of 0.13 cm for vertical and horizontal stripe at varied GDD on muskmelon.

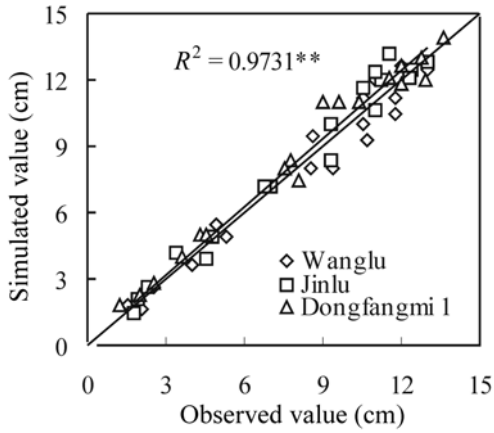

Figure 1 Comparison of simulated with observed values for the vertical diameter of muskmelon fruit at varied GDD under different cultivars

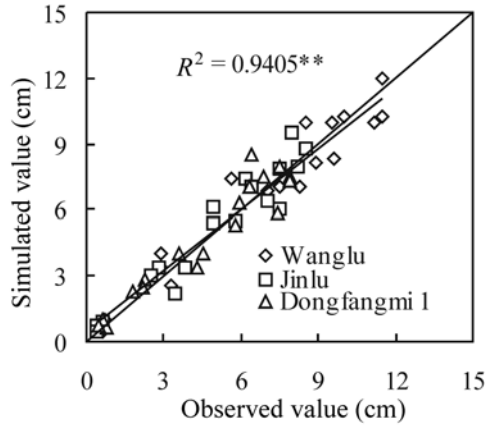

Figure 2 Comparison of simulated with observed values for the horizontal diameter of muskmelon fruit at varied GDD under different cultivars

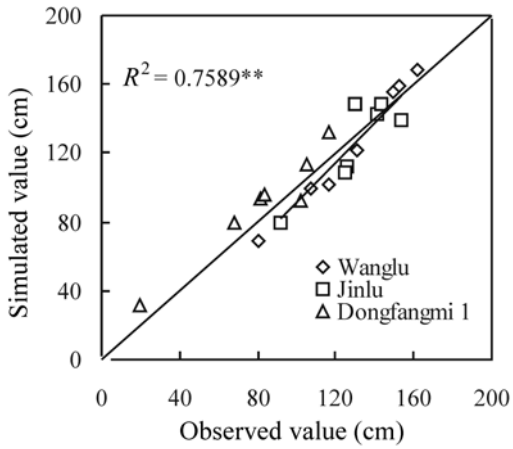

Figure 3 Comparison of simulated with observed values of R on muskmelon fruit under different cultivars

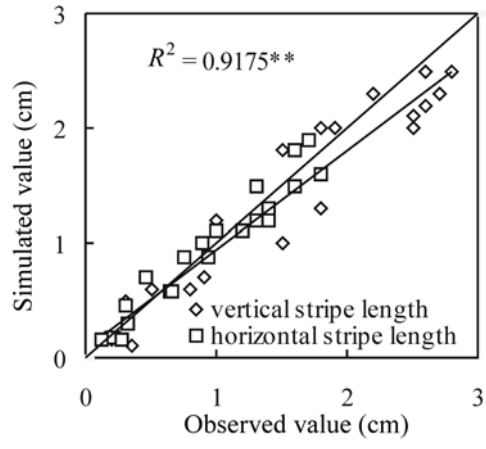

Figure 4 Comparison of simulated with observed values for the vertical and horizontal stripe length of Wanglu at varied GDD

4 Discussions

The present study analyzed the dynamic change patterns of fruit morphology (vertical diameter, horizontal diameter, fruit color and netted) with growth progress under different organic fertilizer rates, and then developed a process-based simulation model for quantitative description of fruit growth dynamics on muskmelon plant. This model was validated with the independent experiment data and could well predict the time-course morphological formation of muskmelon fruit under different cultivars. This work should lay a reliable foundation for describing the muskmelon fruit in a 3-D space by integrating with the morphogenesis models of leaf, stem and root within the framework of plant topology.

In the field of morphological modeling, (Chen et al., 1993) established the simulation model of poplar tree and simulating the spatial distribution of leaves and its obliquity, (Feng and Yang, 2000)

built the fractal discrimination model of plant roots, (Tomonari et al., 2005) studied the plant shape model of rice, (Shi et al., 2006) described the leaf curve dynamic change of rice. The previous studies have mainly focused on field crop models, and thus hardly involved horticulture crop. In this study, the simulation model was developed by observing and analyzing the time-course fruit morphological characters and the dynamic relationships of vertical diameter, horizontal diameter, fruit color, vertical and horizontal stripe length. The detailed experiment data generated a comprehensive description of fruit growth dynamics with limited geometrical parameters.

It should be noted that this study is not involved in the different conditions. In addition, the fruit growth in muskmelon is affected by factors such as nitrogen rates; water regimes, phosphorus and potassium, and thus the present model should be expanded to enhance its applicability under diverse growing conditions. At the same time, the morphological model should be further coupled with growth model so that morphological simulation and physiological simulation could be coordinated, mechanism of the fruit growth dynamics strengthened, and reliability of the simulation system improved.

Acknowledgements

We acknowledge the financial support of the National Hi-tech R&D Plan of China (2006AA10A311), National Hi-tech R&D Plan of China (2006AA10Z221) and Shanghai Leading Academic Discipline Project, Project Number: B209.

References

Andrieu B, Ivanov N, Boissard P (1995). Simulation of light interception from a maize canopy model constructed by stereo plotting. Agric. For. Meteorol. 75: 103 – 119.

Buck-Sorlin G H, Bachmann K (2000). Simulating the morphology of barley spike phenotypes using genotype information. Agron. J. 20: 691 – 702.

Fournier C (1999). ADEL-maize: a L-system-based model for the integration of growth processes from the organ to the canopy. Application to regulation of morphogenesis by light availability. Agron. J. 19: 313 – 327.

Fournier C, Andrieu B (1998). A 3D architectural and process-based model of maize development. Ann. Bot. 81: 233 – 250.

Hanan J S (1997). Virtual plants – integrating architectural and physiological models. Environ. Model. Softw. 12: 35 – 42.

Hanan J S, Hearn A B (2003). Linking physiological and architectural models of cotton. Agric. Sys. 75: 47 – 77.

Hector G N, Donald J H, Harry J K et al (2007). Fruit ripening characteristics in a transgenic 'Galia' male parental muskmelon (Cucumis melo L. var. reticulatus Ser.) line. Postharvest Biology and Technology. 44: 95 – 100.

Kaitaniemi P, Hanan J S, Room P M (2000). Virtual sorghum: visualisation of partitioning and morphogenesis. Comp. Electron. Agric. 28: 195 – 205.

Prusinkiewicz P (2004). Modeling plant growth and development. Curr. Opin. Plant Biol. 7: 79 – 83.

Shi C L, Zhu Y, Cao W X et al (2006). Dynamic simulation of rice canopy structure. Acta. Agron. Sin. 32: 1831 – 1835 (In Chinese).

Watanabe T, Hanan J S, Room P M et al. (2005). Rice morphogenesis and plant architecture: measurement, specification and the reconstruction of structural development by 3D architectural modeling. Ann. Bot. 95: 1131 – 1143.

Xu J H, Yang X P, Jiang J et al. (2007). Analysis of combining ability of main characters of muskmelon fruit. China Vegetables. 1: 15 – 17 (In Chinese).

Zhao X, de Reffye P, Xiong F L et al. (2001). Dual-Scale automaton model for virtual plant development. Chin. J. Comp. 6: 608 – 615 (In Chines).

Shape Modeling of Organs and Structures Generating for Crops

Sheng-Lian Lu, Xin-Yu Guo, Chun-Jiang Zhao, Chang-Feng Li

(National Engineering Research Center for Information Technology in Agriculture, Beijing 100097, China)

Abstract: We present a modeling method that allows easy generation of various crop organs including leaves, fruits, caudexes, petioles and even nonbotanical things. B-splines curve has been used to describe the skeleton of these organs, then the geometry of an organ is generated from its skeleton. The model can be modified interactively by editing the shape of the skeleton and the silhouette in 3-D to control the overall shape of an organ. The users get immediate feedback on what they've created model. Realistic appearance of the generated organ is improved by using texture mapping and including hairs that cover many plant organs. We demonstrate that our method handles the complexity of most real plant organs. Basing on these organs models, we develop a simple but efficient method for constructing crop structure. An interactive modeler has been developed to help users to model, edit the organs and crop structure quickly. We demonstrate the flexibility of our approach by creating different organs and crops structure.

Keywords: modeling plant shape, crop, interactive design, visualization

1 Introduction

The simulation of natural scenes is an important branch in computer graphics. Due to the diversity of species and irregularity of morphogenesis in plant, it is a challenge to create vivid plant model. The motivation for plant modeling comes mainly from two aspects, one is the requirement rooted in agricultural and forestry research, the other aims to generate only visually pleased shapes of plants. The first tries to describe and visualize the real growth and development of plant in computer, it emphasis that the desired plant morphology should be "faithful" to the underlying physiology process of the plant. While the second efforts just seek to achieve vivid appearance in vision. Up to day many methods have been proposed to model the architecture of tree, generally which focus on the overall structure. The structure of horticultural crops, however, is less developed. Our method focuses on the second goal and tries to give users a flexible tool for creating a wide range of structure in crops.

Specifically, we aim to provide a general method and program for modeling geometry of crops, in which various crop organs can be generated using a same describing method. Also, from the practicability point of view, we hope the tool providing flexible interaction, and users can design the shape of plant organs with a fashion of "what you see is what you get". Our approach for generating geometry of an organ can be divided into two steps. Firstly, we describe the skeleton of a crop organ with B-splines curves. Secondly, a triangular mesh of the organ is generated basing on the skeleton. Basing on the base of organs, we allow the users generating crops structure with intuitive interaction.

2 Related Work

Pioneering work on plant geometry generation by Lindenmayer and later by Smith and Prusinkiewicz give a general method known as L-systems to describe the structure and topology of plants (Prusinkiewicz, 1993). L-system-based plant modeling packages, L-studio, has been developed to leverage the power of L-system to model the structures and development processes of plants with visual results (Karwowski et al., 2004). L-studio is powerful for simulating the growth of plants. However, due to its highly abstract, controlling directly the global aspects of the shape is difficult, and describing the detail aspects of the plant organs still proves a challenge, which has become a focus to enhance the realism of L-systems (Fuhrer, 2005).

Lintermann and Deussen presented a general approach to model the wide range of features in plant imaging, each organ being developed as a component, using parameterized interaction (Lintermann et al., 1999). Their method worked at a more direct way and provided vivid shape of plants, even animation of plant growth. However, it was mostly restricted to trees. There is a great number of efforts have been done to model the structure of trees, including static shape and dynamic motions, review of this topic can be found in (Mantler, et al., 2003) and (Taylor-Hell, 2005).

There are also many methods in realistic modeling and/or rendering plant organs, we will mention them in the relevant section. While we listed above we want to stress that most of existing plant models focus on modeling trees, in which the branching structures are more important than the details of an organ, since tree is always big and tall. Although there is a long history in modeling horticultural crops (Fournier et al., 1999; Ding, et al., 2005), for example corn, tomato and so on, these simulators act mostly on biological functions. The quantitative accuracy is the most important goal, instead of visual realism. The visualization was usually missed, or the geometry of organs in these models was often represented with simple polygons.

3 Modeling Crop Organs

Due to the diversity of species and irregularity of morphogenesis in plant organs, it is a challenge to create precise and vivid geometric models for plant organs. In computer graphics, complex objects are generally abstracted as a skeleton, a skeleton may be a line section, or a branch structure consists of several line sections. To provide a common method for generating shape of various crop organs, we use a skeleton description of organs shape and create the geometry of an organ from its skeleton. With this model users can create a wide range of crop organs with highly realistic shape. In this section, we will detail our approach in creating the skeleton and modeling the geometry of crop organs.

3.1 Skeleton Description and Generation

A skeleton may be a line section, or a branch structure consists of several line sections. To handle the diversity of morphogenesis in plant organs, we use different skeleton representation for different organs according to its outside shape. In particular we classify these skeletons as three categories: axis skeleton, silhouette-axis skeleton and double silhouette-axis skeleton, as Fig. 1 shows. Axis skeleton is used to model organs which have cylinder shape, such as caudex, petiole and tendril; silhouette-axis skeleton is consists of an axis and a silhouette curve, it is used to model organs with irregularity silhouette and approximately symmetrical shape, such as fruit of watermelon; while the third skeleton is used to described main shape of a leaf or petal, these organs can be seen as a complex surface.

For representing these skeletons in computer, we use B-splines curve. B-splines curve is one of the common used curves, it provide much convenience for describing outline of irregular objects.

As shows in Fig.1, each axes and silhouette is represented as a B-splines curve, and each B-splines curve consists of several control points. Basing on B-splines curves, we aim to develop a general model for describing the geometry of various crop organs.

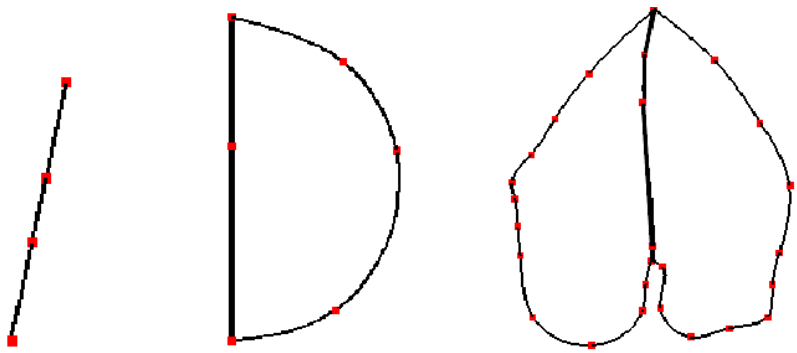

Figure 1 Organ skeleton categories: (a) axes skeleton, (b) silhouette-axes skeleton, (c) double silhouette-axes skeleton

To obtain the control points of B-splines curves in an organ skeleton, several methods can be used. For the silhouette curve, the boundary of the silhouette can be recovered from the scanned image of a real organ, such as a leaf, by using common techniques for edge detection and boundary simplification. Then these control points can be extracted from the boundary. As a substitute, the axes and the silhouette of an organ skeleton can be initiated automatically with some parameters in our modeler. Based on the initiated skeleton, the user can edit the skeleton interactively. They can drag the control points in 3D space to fit the desired curve. Further, users can insert new control points into the skeleton. A variety of shape of organs can be fit by this way.

3.2 Generating Geometry of Organs

Different methods are used for generating geometry of organs based on these skeletons mentioned above. We will detail the used techniques in the following.

3.2.1 Generating Geometry of Organs from Axis Skeleton

We have mentioned that axis skeleton is used the model organs like caudex, petiole and tendril. These organs have a character that their cross-section all are approximately an ellipse. Therefore, the geometry of these kind organs can be seen as the result of a series of line with defined radius rotating around the axis skeleton. For simplification, a sequence of point set in the cross-section are generated along the medial axis, these points are then triangulated later to form the outline of the organ. In this case the rotation radius can be provided as a parameter corresponding to the radius of the generated organ. Fig. 2 shows the process with two examples.

3.2.2 Generating Geometry of Organs from Silhouette-Axis Skeleton

Silhouette-axis skeleton is used mainly to generate geometry of fruit organs. Similar to caudex and petiole, the geometry of a fruit can be seen as the result of a silhouette curve rotating around a medial axis. We do this similar as generating the geometry of organs from axis skeleton. The difference is that the rotation radius has been given by the silhouette. Fig. 3 illustrates the process.

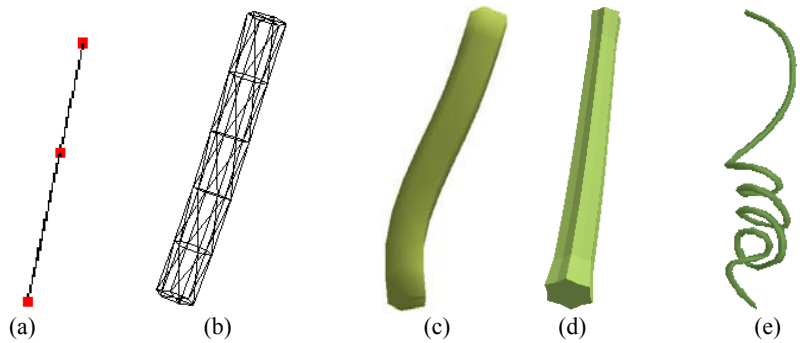

Figure 2 Generating geometry from axes skeleton: (a) the medial axis; (b) the triangulation forms the outline; (c), (d) two examples of caudex geometry; (e) an example of tendril

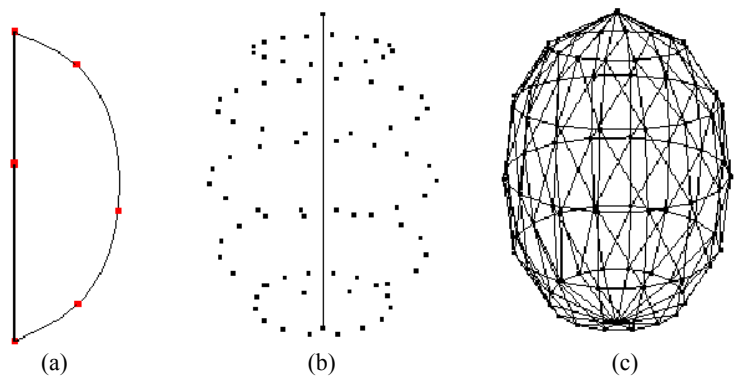

Figure 3 Geometry definition of a fruit: (a) the skeleton; (b) point sets are defined as cross-section; (c) the triangulation forms the outline

3.2.3 Generating Geometry of Organs from Double Silhouette-Axis Skeleton

The double silhouette-axis skeleton can be used to create geometry of organs with a surface, such as leaf and petal. It is a challenge to model the geometry of these organs for the variety of their outline, which may vary from species to species, from seedling stage to ripe stage. Up to day several methods has been proposed for modeling the geometry of leaves, with accurate geometric representation and/or realistic effects (Mündermann, MacMurchy, Pivovarov et al. 2003; Loch, 2004; Runions, Fuhrer, Lane et al. 2005; Sung, Simpson, and Gladimir, 2005). But none of these methods can handle the diversity and irregularity in the outline of plant leaf and petal.

So we use the double silhouette-axis skeleton as an abstract representation of a leaf, while the silhouette and axes is described by B-splines curves, which is flexible enough to handle the diversity and irregularity in the outline of plant leaves. And the surface of a leaf can be generated from the skeleton. To generate the geometric surface surrounded by the axis and two silhouette curves, which may include concave areas in the generated polygon, we apply Delaunay triangulation to mesh the area. Delaunay triangulation is used extensively in computer graphics. Fig. 4(b) shows the result of Delaunay triangulation of a leaf skeleton demonstrated in Fig. 4(a). Because the double silhouette-axis skeleton may be made in 3D, a subdivision and refinement process are applied to the initial triangulation mesh for generating smoother surface. Our method for subdivision and refinement is similar to Loop's method (Smith, 2006). Figure 4(c) and (d) show the results of subdivision and refinement respectively.

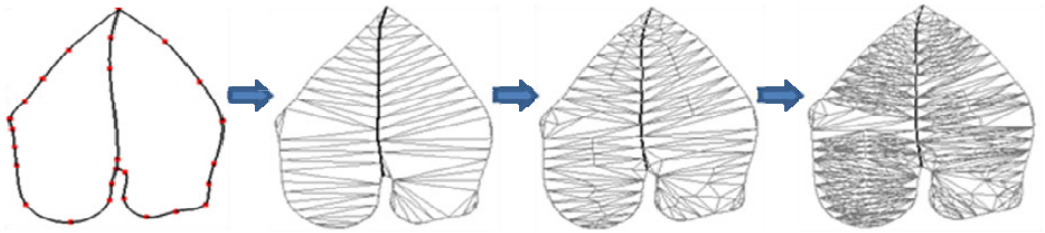

Figure 4 Process of generating surface of a leaf from a double silhouette-axis skeleton: (a) skeleton; (b) the Delaunay triangulation; (c) a subdivision mesh of (b); (d) the refinement mesh of (c)

3.3 Details Description

The geometric surface generated by using above methods just describes the spacial shape of an organ, but lack of facial details, such as texture. We use texture mapping and hairs generating techniques to improve the realistic effects of the generated organ models.

3.3.1 Texture Mapping

In computer graphics, one of popular methods for obtaining realistic effects is texture mapping. We use texture mapping in leaf and fruit models. To leaf model, the scanned image for obtaining silhouette information of a leaf also provides texture source material. Specifically the texture coordinates of each vertex $v(x, y, z)$ in the leaf mesh are calculated with the following formula:

$$\begin{aligned} \text{TexCoordX} &= (v.x - \text{minX})/(\text{maxX} - \text{minX}) \\ \text{TexCoordY} &= (v.y - \text{minY})/(\text{maxY} - \text{minY}) \end{aligned} \tag{1}$$

where maxX and minX are the maximum and minimum of x coordinate in all vertices of the mesh respectively, while the maximum and minimum of y coordinate are stored in maxY and minY. To prevent the background from showing up near the boundaries of the leaf in case of inaccuracies in the texture mapping, we also take advantage transparency channel to make all pixels outside the leaf surface transparent.

To fruit model, the texture coordinates are calculated in the process of generating the outline triangulate mesh.

3.3.2 Hairs Generating

Many organs of crops are covered by fine hairs, especially in their early stage of growth. Realistic hairs stands on the surface of an organ can be hardly obtained by simple texture mapping. We use a geometric representation of individual hair for modeling hairs of organs. Individual hair is represented as a curve or cylinder, and users can adjust the shape of a hair interactive. This method employs Poisson-disk pattern to assign the distribution of hairs on the surface of an organ, while the density of hairs is adjusted based on the area of organ surface. Individual hairs are then mapped onto the organ surfaces according to the generated attachment point. Hair properties including length, radius, direction and density are specified and adjusted according to positional information of the organ surface. This allows generating a wide range of hairs plant styles. Figure 5 illustrates organ shapes with hairs.

(a) (b)

Figure 5 Organs with hairs: (a) hairy leaf petiole; (b) hairy vine and fruit of watermelon

3.4 Compound Organ

We have detailed methods for modeling shape of individual organ. In real kingdom of crops, most of crops consisted of compound organs. For example, flower is often composed of pedicel, sepal, petal and bud. Our system allows the user to create compound organs with individual organs freely. The leaf and flower image shown in Fig. 5 give two examples of compound organ.

3.5 Examples of Organs Shape

We have created a modeling and deforming interface for creating geometric models of crop organs. Different organ models can be created in less than 5 minutes, including creating the skeleton, generating triangulate mesh and using texture mapping or hair generation. To demonstrate our approach, we recreated surfaces of several crop organs. In particular, we model a leaf of corn, model and texture map several fruits shape. Figures 6 and 7 show the results.

(a) (b) (c)

Figure 6 Modeling corn leaf: (a) skeleton; (b) mesh surface; (c) rendered surface

4 Interactive Generating Crop Structure

Generating the structure of a crop is an interactive process in our system. We have developed various kinds of organs geometric models, including individual and compound organs. In real kingdom of plant, even in a same crop, the shape of a same kind of organs may be different extremely. For example, the shape of a young leaf is different from of an old leaf. So how to construct vivid crop structure from these organ models is a challenge. In the rest of this section, we will detail our solution to these issues.

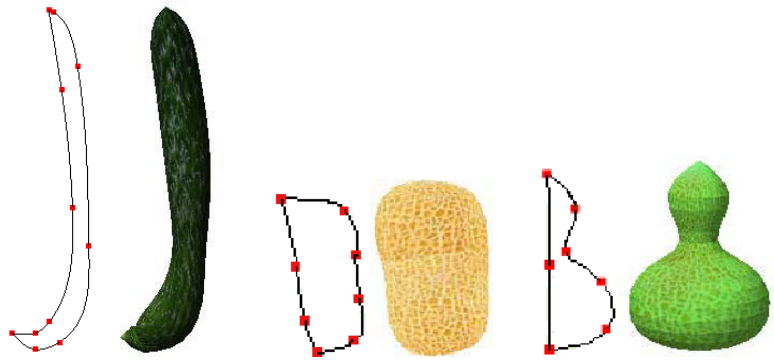

Figure 7 Examples of fruit geometry (with texture mapping): (a) skeleton and the geometry of cucumber fruit; (b) example of muskmelon; (c) example of calabash

4.1 Templates of Organ and Morphing

Since our method of modeling organs is general for modeling individual organ, such as leaf, fruit, caudex and so on. Users can use these modelers to create different kinds of organs for different kinds of crop, and save as templates. Furthermore, template is available to deal with the problem of the same kind of organ holding different shape in a same crop. Figure 8 shows four templates of watermelon leaf which correspond to four growth stages of the real leaf respectively. We can obtain a series of shapes of the leaf in between each two leaves templates by using a morphing technique or a scale parameter.

Figure 8 Templates of a watermelon leaf

4.2 Guidance for Constructing Crop Structure

Our system provides guidance for generating the structure of a crop, the guidance includes four steps. In first step, the user defines a series of parameters, including number of caudex and its average length, number of branch, and so on. Then an initial structure of the crop is generated (Fig.9(a)). The initial structure just gives the user an overview about the crop, and do not includes details such as flowers and fruits. In next step the user edit the main vine of the crop to create natural structure (Fig.9(b)). Then user can define the number of flower, fruit and tendril in each caudex, and the angle of between these organs and the main vine (Fig.9(c)). The system generates automatically the structure lastly. An interface (Fig.9(d)) is provided for editing the generated crop interactively, including editing the shape of an organ, modifying the parameters of organs.

Figure 10 gives three examples of the generated crop structure, including cucumber, watermelon and tomato respectively. Four leaf templates are used both in the cucumber structure and the watermelon structure.

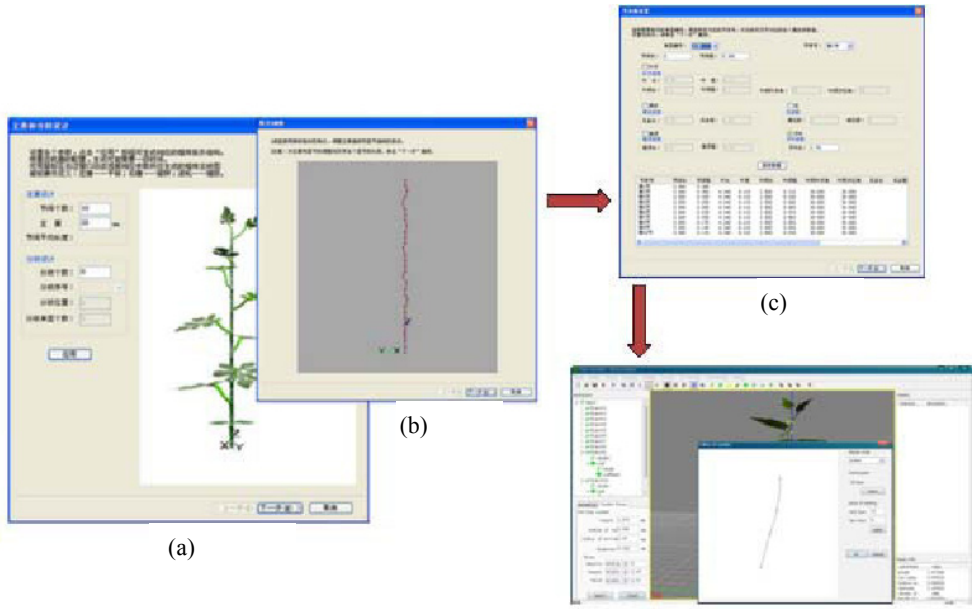

Figure 9 Guidance for generating a crop structure: (a) defining parameters; (b) designing the main vine; (c) defining detail parameters; (d) interactive editing

Figure 10 Examples of generated crop structure

5 Conclusions

We presented methods and a framework for constructing organs shape and generating structure of crops interactively. The proposed methods allow users design a wide variety of crop organs by mostly intuitive mechanisms. Moreover, it can construct complex plant organs such as lobed leaves and free-from deformed organs.

An interactive modeler has been developed to help users to model, edit the organs and crop structure quickly as well as easily. Interactive manipulation of the skeleton model and real-time rendering with OpenGL API are two important characteristics of the modeler. We demonstrated the flexibility of our approach by constructing several organs and crops structure. This flexibility results from the pipeline architecture of procedural operations.

In the near future, several open research problems are in our plan to address. Most crop organs have detail of features except hairs, such as wrinkle, edge of saw tooth. These details are desired to cover in a close-up realistic modeling. We also plan to develop better interface and combine our model with functional modeling.

In addition, multi-resolution organ shape modeling is attractive. Although the number of nodes in an organ mesh model used in this paper is at most two hundreds, in general there are hundreds of thousands such organs in a virtual garden. Therefore, it is almost impossible to use the organ mesh model with several hundred nodes in ecosystem scale. Multi-resolution mesh models, where the mesh complexity varies depending on the level of detail, are commonly used to alleviate this problem.

Acknowledgements

This work is supported by National High Tech R&D Program of China under grant No. 2007AA10Z224, National Nature Science Foundation of China under grant No. 30700493 and Beijing Natural Science Foundation under grant No. 4081001.

References

Prusinkiewicz P (1993) Modeling and visualization of biological structures. p. 128-137. Proceeding of Graphics Interface ’93. 19-21 May 1993.Toronto, Ontario.

Karwowski R, Prusinkiewicz P (2004) The L-system-based plant-modeling environment L-studio 4.0. In: Godin C, Hanan J, Kurth W, et al (ed). Proceedings of the 4th International Workshop on Functional-Structural Plant Models. 07-11 June 2004, Viala Montpellier, France.

Fuhrer M (2005) Hairs,textures, and shades: improving the realism of plant models generated with L-systems. Master’s thesis, University of Calgary.

Lintermann B, Deussen O (1999) Interactive modeling of plants. IEEE Computer Graphics and Applications. 19(1):56 – 65.

Mantler S, Tobler RF, Fuhrmann AL (2003) The state of the art in real-time rendering of vegetation. VRVis Certer for Virtual Reality and Visualization.

Taylor-Hell J (2005) Biomechanics in botanical trees. Master’s thesis, University of Calgary.

Fournier C, Andrieu B (1999) ADEL-maize: an L-system based model for the integration of growth processes from the organ to the canopy. Application to regulation of morphogenesis by light availability. Agronomie. 19: 313 – 327.

Ding WL, Xiong FL, Cheng Z (2005) Study and implementation of the expert system for greenhouse tomato planting. p.325-329. Proc. of 3rd Int. Con. on Information Technology and Applications. July 2005. Sydney, Australia.

Mündermann L, MacMurchy P, Pivovarov J, et al (2003) Modeling lobed leaves. p.60 – 67. Proceedings of Computer Graphics International, CGI (ed.). 2003. Tokyo, Japan.

Loch BI (2004) Surface fitting for the modeling of plant leaves. Ph.D thesis, University of Queensland, Australia.

Runions A, Fuhrer M, Lane B et al (2005) Modeling and visualization of leaf venation patterns. ACM Trans. on Graphics, 24(3): 702 – 711.

Sung MH, Simpson B, Gladimir VGB (2005) Interactive venation-based leaf shape modeling. Computer Animation and Virtual Worlds. 16(3-4): 415 – 427.

Smith C (2006) On vertex-vertex systems and their use in geometric and biological modeling. Ph.D. thesis, University of Calgary.

Modeling Shoot and Root Biomass of Lucerne Crops—New Insights on the Seasonality of Dry Matter Partitioning and Root Maintenance Respiration

Edmar I. Teixeira, Derrick J. Moot*, Hamish E. Brown, David P. Monks

(Agriculture and Life Sciences Division, Lincoln University, Canterbury, New Zealand.
*Corresponding author:E-mail: moot@lincoln.ac.nz)

Abstract: Lucerne crops (*Medicago sativa* L.) are an important source of energy and protein for grazing and confined livestock in temperate and tropical countries. In contrast with annual crops, the modeling of above ground biomass of lucerne crops is often inaccurate when light interception (R_i) and radiation use efficiency (RUE) are used to estimate assimilation. The reason is that a large fraction of total assimilates are allocated to the root system and the pattern of partitioning differs in response to seasonal environmental stimuli. This dynamic has not been accurately quantified in lucerne models. In this study, a simple framework for a lucerne model to address the dynamics of shoots and roots is tested. Simulation results are compared with 2 years of field data from Lincoln University, Canterbury, New Zealand. The model incorporates recent findings on RUE, R_i and dry matter partitioning to roots in response to environmental factors. Shoot biomass and vegetative development were accurately simulated. In contrast, the model showed a systematic offset between simulated and measured root biomass caused by assuming constant rates of root maintenance respiration (Rm). A new hypothesis was tested by using the model as a tool to indicate the most appropriate rates of Rm to improve fits and resemble the seasonality of root and shoot biomass dynamically. Results indicated a systematic pattern of change in Rm from 3.5% in summer to <0.5% in winter that is consistent with the differences in metabolic processes that involve storage and translocation of carbon and nitrogen reserves.

1 Introduction

Frequently, lucerne (*Medicago sativa* L) models calculate shoot biomass accumulation as the product of intercepted radiation (R_i) and radiation use efficiency for above ground biomass (RUE_{shoot}) (Confalonieri et al., 2004; Robertson et al., 2002). This framework was developed for annual crops and does not explicitly address dry matter partitioning dynamics to roots (Monteith, 1972). This is a drawback for perennial crops such as lucerne because a large amount of daily accumulated biomass is allocated to the root system, particularly in autumn (Teixeira et al., 2007b). In spring, these root reserves are mobilized to support shoot regrowth (Avice et al., 1997). The lack of understanding and incorporation of root biomass in lucerne models was suggested as an important explanation for the lower accuracy of shoot yield predictions observed during spring and autumn regrowth cycles (Monks et al., 2008). In this paper, we propose that by explicitly addressing the seasonal dynamics of root biomass partitioning and using radiation use efficiency for total biomass (RUE_{total}) together with empirical partitioning coefficients (Teixeira et al., 2007a), the accuracy of shoot yield predictions may be systematically improved in lucerne models. To achieve this, the framework of a simple lucerne model that incorporates recent quantitative knowledge on lucerne physiological responses to environmental stimuli is presented and the model is tested with datasets from a 2-year field experiment in which shoot and root biomass were measured.

2 Materials and Methods

The model was constructed using the software ModelMaker version 4.0 (Cherwell Scientific Publishing, Ltd, UK) and runs in daily time-steps by assessing weather data: T_{max}, T_{min} and T_{mean} (℃, maximum, minimum and mean daily temperatures respectively), *Radn* (daily total solar radiation, MJ/m^2), Ph (photoperiod, h), Ph_dir (photoperiod direction of change) and T_{soil} (°C, soil temperature at 100 mm depth). Weather data were obtained from Broadfields Meteorological Station, 3 km north from Lincoln University (43°38' S and 172°28' E) in which the field experiments used to test the model were performed (Teixeira et al., 2007b).

In the model, each day dry matter assimilation is calculated as the intercepted amount of PAR (PAR_i, MJ PAR/m^2) multiplied by the total RUE for total biomass (RUE_{total}, g DM/MJ PAR), which is adjusted for temperature (Brown et al., 2006; Monteith, 1977). This new daily assimilated dry matter is integrated into DM_{total} and then partitioned to shoots (DM_{shoot}) or to root dry matter (DM_{root}) as controlled by the fractional coefficient of partitioning to roots (p_{root}, dimentionless) that ranges from 0 to 1. The p_{root} was empirically derived from the relationship between soil and air temperature (T_{soil}/T_{mean}) for Canterbury conditions (Teixeira et al., 2007a). The DM_{shoot} is partitioned into DM_{leaf} or DM_{stem}, according to the partitioning coefficient to leaves (p_{leaf}). The p_{leaf} declines exponentially with DM_{shoot} as a function of the allometric growth of these organs (Lemaire et al., 1992; Teixeira, 2006). The maintenance respiration of the root biomass ($Rm_{root,}$ g DM/ha/day) is discounted daily from DM_{root} and is sensitive to soil temperature. A graphical representation of the relationships used is given in Fig. 1. Detailed explanation of quantification of each relationship was previously published (Teixeira et al., 2007a; Teixeira et al., 2007c).

Measured data for testing model predictions were from a field experiment at Lincoln University, Canterbury, New Zealand. Methodologies and procedures for this experiment were presented in detail in previous publications (Teixeira et al., 2007b). In brief, we use a subset of measured data for lucerne crops grazed for 4 days and spelled for 38 days, grown under unconstrained conditions of water and mineral supply were used.

3 Results and Discussion

Simulation for leaf area index, count of expanded leaves and shoot yield gave a RMSD (root mean square deviation) ranging from 13 to 24% of the mean when compared with two years of field data (Table 1). This is an improvement in relation to previous simulations in which only shoot RUE and R_i were used (Monks et al., 2008). This improvement in the accuracy of simulation indicated that the assumed relationships for phyllochron, leaf area expansion, RUE_{total} and DM partitioning coefficients more mechanistically captured the seasonality of light interception, conversion of light into total biomass and further retention of DM in the aerial biomass.

Table 1 Statistics for the comparison of simulated and measured leaf area index (LAI), number of primary leaves per shoot (leaves) and shoot dry matter yield of lucerne crops grown at Lincoln University, Canterbury, New Zealand

	LAI	Number of Leaves	Shoot Yield
RMSD	0.6 m^2/m^2	0.9 leaves/shoot	0.3 t/ha
RMSD (% mean)	24	13	20

Note: Values represent statistics for two years (15 growth cycles).

Throughout the season, the seasonality of shoot dry matter accumulation was captured by the model. With the exception of an underestimation of 1.0 t/ha in the April 2003 cycle, all other 14 cycles were closely predicted by the model (Fig. 2).

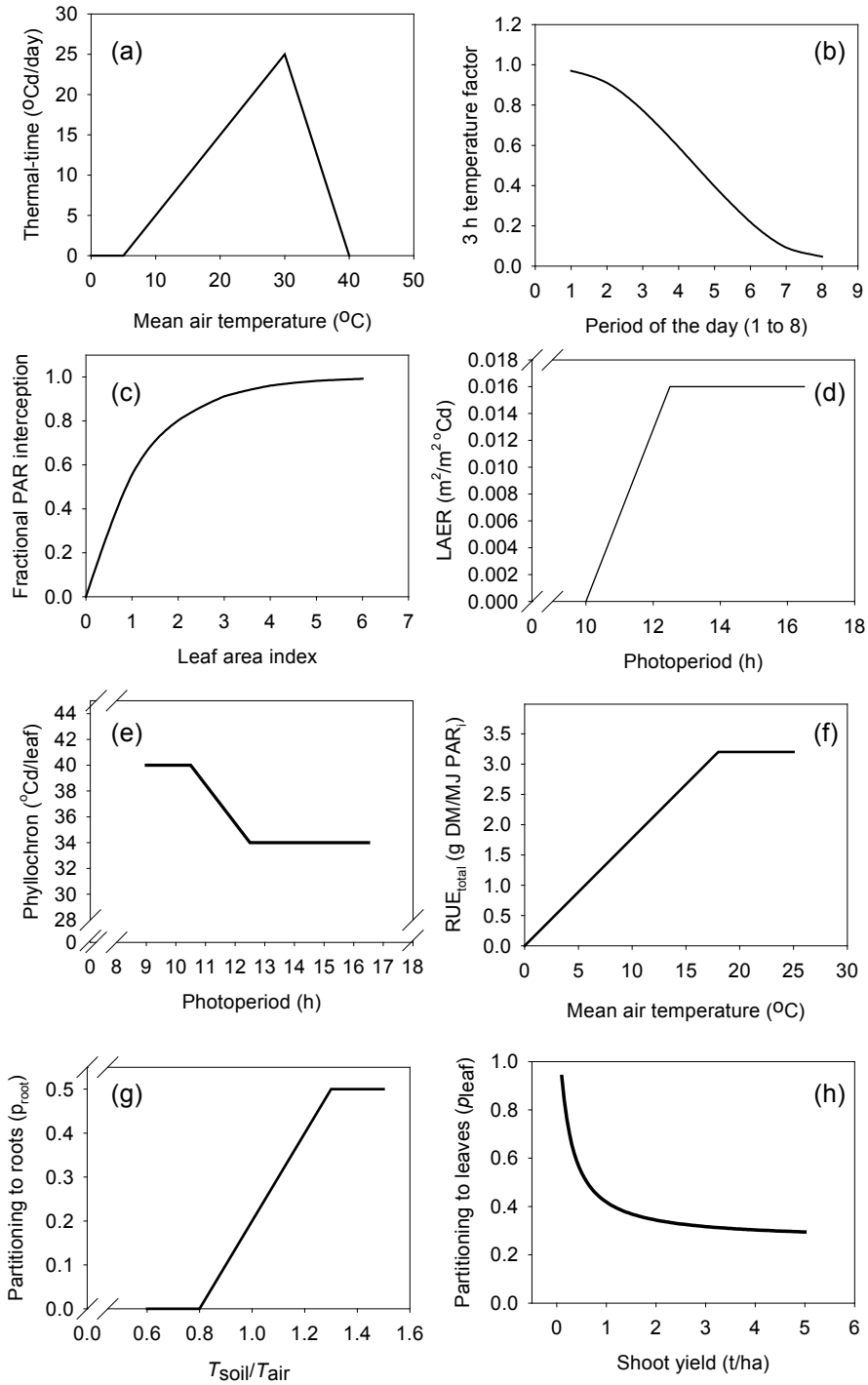

Figure 1 Summary of relationships used to calculate vegetative development, biomass accumulation and partitioning in the lucerne simulation model

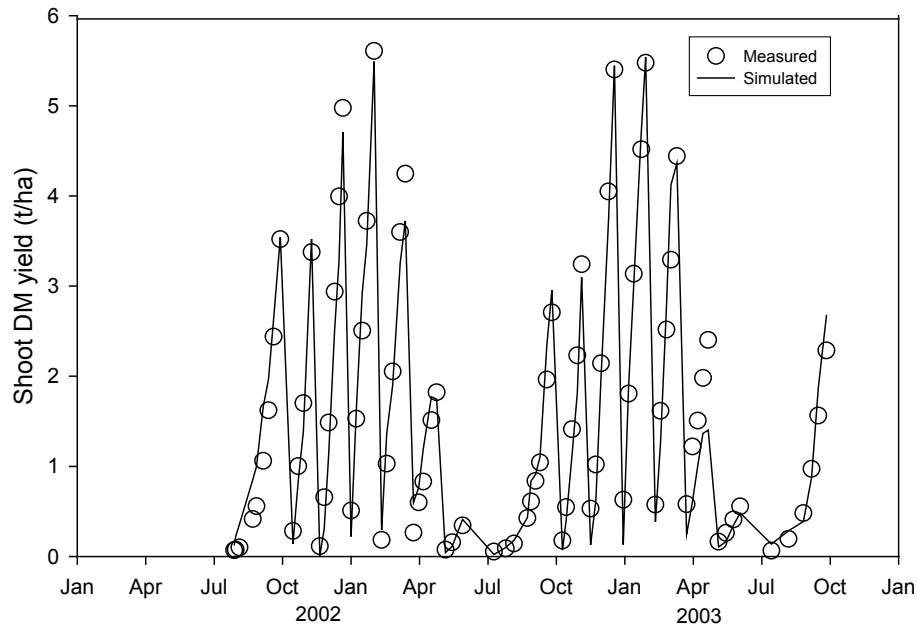

Figure 2 Comparison of simulated and measured shoot yield for lucerne crops subjected to a 42-day cycle defoliation regime in the 2002/03 and 2003/04 growth seasons at Lincoln University, Canterbury, New Zealand
Note: Statistics for the fit are given in Table 1

After confirming that biomass retention in shoots was, accurately captured by the model, measured and simulated root biomass were compared. Conceptually, the difference between total accumulated biomass and the biomass retained into shoots was partitioned to roots. The seasonal measured root biomass was then compared with simulated values using a range of possible values for a conservative rate of root maintenance respiration (Rm), the only additional parameter which modulated root biomass dynamics (Fig. 3).

The seasonal pattern of root biomass was mirrored by simulations (Fig. 3). Nevertheless, the sensitivity analysis showed that regardless of the assumed value of a conservative Rm (i.e. only modulated by temperature using a Q_{10} of 1.8), there was always an offset between simulated and measured values (Fig. 3).

To explore possible reasons for such a systematic offset, a new hypothesis assuming that the value of Rm were not constant throughout the cycle, but differed seasonally (Bouma et al., 2000), was then tested. This was done by running the model assuming that Rm values shifted at the start of seasons until a best fit with measured data was achieved (i.e. lowest RMSD).

The 'best fit' Rm value showed the same seasonal pattern in both years ranging from <0.05% DM in winter to ~3.5% DM in early summer (Fig. 4).

Using a seasonal pattern of Rm improved the fit with measured data from a RMSD of >35% of the mean to 14% of the mean (Fig. 5). This pattern of a seasonal Rm was also found in other perennial crops (Bouma et al., 1997). In lucerne this would be in agreement with the metabolic activities involved with storage and mobilization of carbohydrates and proteins in the root system that occur from early spring to late autumn (Avice et al., 2001). Recent studies (Teixeira et al., 2007b) showed that the fastest rates of DM accumulation in roots occured in mid-summer, in agreement with the highest estimated values of Rm.

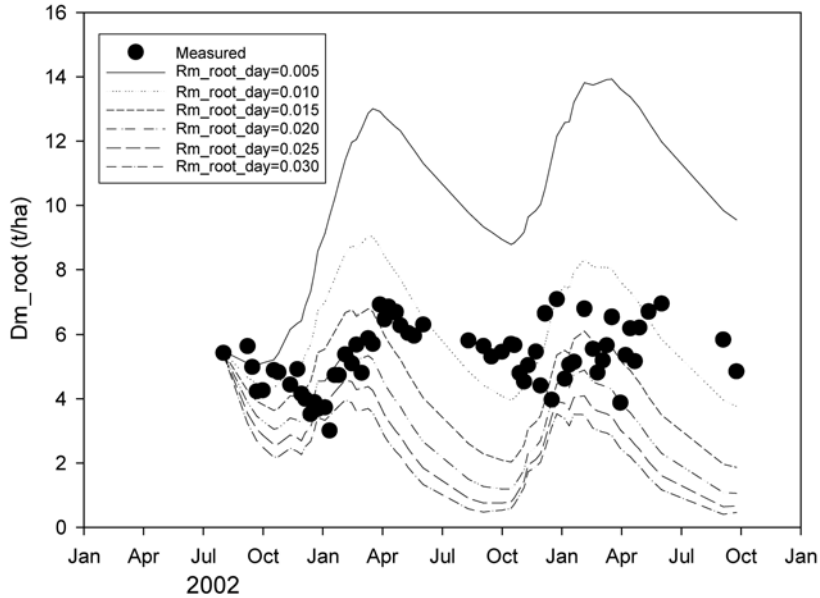

Figure 3 Testing of six values of maintenance respiration rates of root DM (0.005-0.030 DM/day) for lucerne crops subjected to a 42-day cycle defoliation regime in the 2002/03 and 2003/04 growth seasons at Lincoln University, Canterbury, New Zealand

Note: Rm_root_day is the fractional daily maintenance respiration rate of root DM.

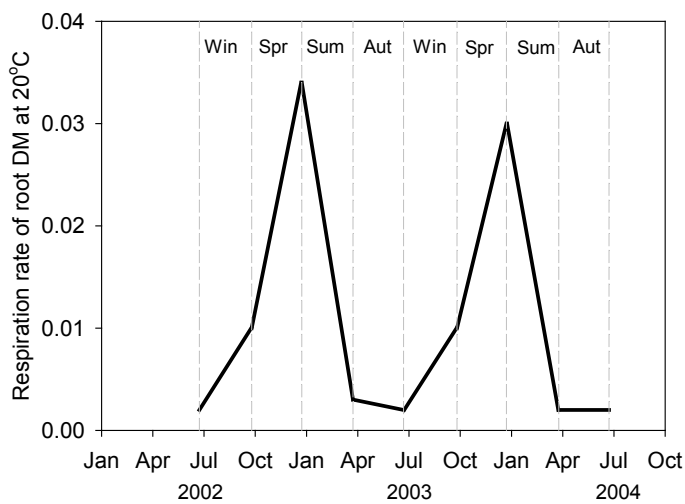

Figure 4 Seasonal pattern of root maintenance respiration rates selected to give the best fit (lowest RMSD) between simulated and measured Rm of lucerne crops grazed at 42-days regrowth cycles at Lincoln University, Canterbury, New Zealand

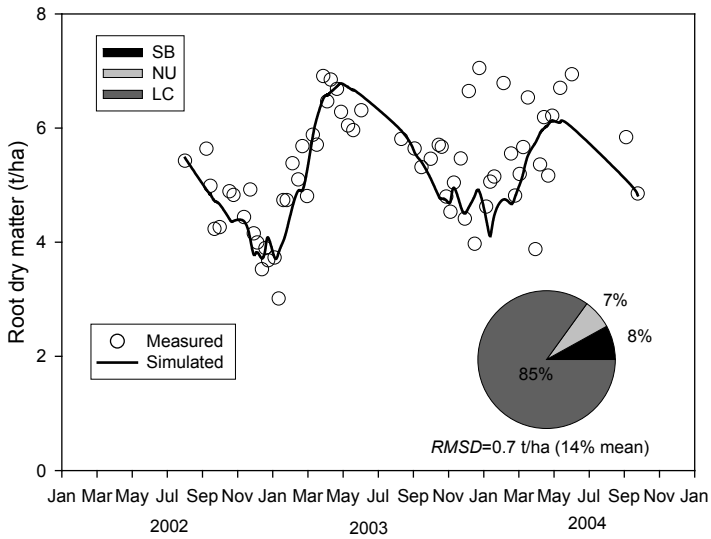

Figure 5 Adjusted fit of root dry matter simulation for lucerne crops grazed at 42-days regrowth cycles at Lincoln University, Canterbury, New Zealand
Note: SB, NU and LC are the three independent additive components of the mean squared deviation (MSD) which percent is shown in the pie graphs. RMSD is the root mean squared deviation.

In conclusion, the seasonality of shoot and root biomass of lucerne crops may be more realistically simulated if the concept of total RUE (RUE_{total}) is used (i.e. instead of RUE_{shoot}) together with empirical coefficients of DM partitioning and a seasonal value of root maintenance respiration. These hypotheses may be confirmed by targeted field and laboratory experimentation which can be guided by model results as presented here.

References

Avice JC, Lemaire G, Ourry A, Boucaud J (1997) Effects of the previous shoot removal frequency on subsequent shoot regrowth in two *Medicago sativa* L. cultivars. *Plant and Soil* 188, 189 – 198.

Avice JC, Louahlia S, Kim A, Morvan-Bertrand A, Prudhomme MP, Ourry A, Simon JC (2001) Influence des reserves azotees et caerbonees sur la repousse des especes prairiales. *Fourrages* 165, 3 – 22.

Bouma TJ, Bryla DR, Yadong L, Eissenstat DM (2000) Is maintenance respiration in roots constant? In 'The supporting roots of trees and woody-plants: form, function and physiology.' (Ed. A Stokes) pp. 391-396. (Kluwer Academic Publishers: Dordrecht, The Netherlands).

Bouma TJ, Nielsen KL, Eissenstat DM, Lynch JP (1997) Estimating respiration of roots in soil: interactions with soil CO_2, soil temperature and soil water content. *Plant and Soil* 195, 221 – 232.

Brown HE, Moot DJ, Teixeira EI (2006) Radiation use efficiency and biomass partitioning of lucerne (*Medicago sativa*) in a temperatre climate. *European Journal of Agronomy*, doi:1016/j.eja.2006.1008.

Confalonieri R, Bechini L (2004) A preliminary evaluation of the simulation model CropSyst for alfalfa. *European Journal of Agronomy* 21, 223 – 227.

Lemaire G, Khaiti M, Onillon B, Allirand JM, Chartier M, Gosse G (1992) Dynamics of accumulation and partitioning of N in leaves, stems and roots of lucerne (*Medicago sativa* L.) in a dense canopy. *Annals of Botany* 70, 429 – 435.

Monks DP, Moot DJ, Brown HE, Teixeira EI (2008) APSIM-lucerne validation in the temperate climate of New Zealand. In 'ISCMDS'. Nanjing, China.

Monteith JL (1972) Solar radiation and productivity in tropical ecosystems. *Journal of applied ecology* 9, 747 – 766.

Monteith JL (1977) Climate and the efficiency of crop production in Britain. *Philosophical Transactions of the Royal Society of London - B.* 281, 277 – 294.

Robertson MJ, Carberry PS*, et al.* (2002) Simulation of growth and development of diverse legumes species in APSIM. *Australian Journal of Agricultural research* 53, 429 – 446.

Teixeira EI (2006) Understanding growth and development of lucerne crops (*Medicago sativa* L.) with contrasting levels of perennial reserves. Ph.D. Thesis, Lincoln University.

Teixeira EI, Moot DJ, Brown HE (2007a) Defoliation frequency and season affected radiation use efficiency and dry matter partitioning to roots of lucerne (*Medicago sativa* L.) crops. *European Journal of Agronomy* 28, 103 – 111.

Teixeira EI, Moot DJ, Mickelbart MV (2007b) Seasonal patterns of root C and N reserves of lucerne crops (*Medicago sativa* L.) grown in a temperate climate were affected by defoliation regime. *European Journal of Agronomy* 26, 10 – 20.

Teixeira EI, Moot DJ, Pollock KJ, Brown HE (2007c) How does defoliation management affect yield, canopy forming processes and light interception in lucerne (*Medicago sativa* L.) crops? *European Journal of Agronomy* 27:154 – 164.

A Morphogenetic Crop Model for Sugar-Beet (Beta vulgaris L.)

S. Lemaire[1,2,3], F. Maupas[1*], P. H. Cournède[4], P. de Reffye[2]

(1 Institut Technique de la Betterave, Paris, 75008 France)
(2 CIRAD, UMR AMAP, Montpellier, 34000 France)
(3 AgroParisTech, UMR EGC, Grignon, 78000 France)
(4 Ecole Centrale Paris, Laboratoire MAS, Châtenay Malabry, 92295, France)

Abstract: This paper is the instructions for the proceeding of the International Symposium on Crop. Sugar beet crop models have rarely taken into account the morphogenetic process generating plant architecture despite the fact that plant architectural plasticity plays a key role during growth, especially under stress conditions. The objective of this paper is to develop this approach by applying the GreenLab model of plant growth to sugar beet and to study the potential advantages for applicative purposes.

Experiments were conducted with husbandry practices in 2006. The study of sugar beet development, mostly phytomer appearance, organ expansion and leaf senescence, allowed us to define a morphogenetic model of sugar beet growth based on GreenLab. It simulates organogenesis, biomass production and biomass partitioning. The functional parameters controlling source-sink relationships during plant growth were estimated from organ and compartment dry masses, measured at seven different times, for samples of plants. The fitting results are good, which shows that the introduced framework is adapted to analyse source-sink dynamics and shoot-root allocation throughout the season. However, this approach still needs to be fully validated, particularly among seasons.

Keywords: sugar beet, functional structural plant models, GreenLab, parametric identification from experimental data

1 Introduction

For healthy and unstressed crops of sugar beet, the total amount of dry matter is proportional to the amount of radiation intercepted by the canopy during the growth (Jaggard and Qi, 2006). The leaf area controls the interception of radiation and its expansion is particularly important until full leaf cover is reached. In sugar beet, a leaf area index of about 3.0 is needed for maximal interception (Malnou et al., 2008). Therefore, any factor restricting the speed of leaf surface expansion directly reduces the final production. Increase in leaf area index depends on the rate at which new leaves appear and expand, on their final sizes and on how long they are retained by plants. All these factors are strongly influenced by the environment (climate, irrigation, fertilization) (Milford et al., 1985a). In stress situations, there is a strong interaction between plant growth and architectural development (Werker et al., 1999) and classical crop models are not able to predict accurately root biomass and sugar content. In a context of sustainable agriculture and low input crop management, it is important to better understand plant physiology under stressed conditions and a model that takes into account plant morphogenesis could be a useful tool. In this prospect, this paper aims at

introducing a morphogenetic model of sugar beet growth and study how this model can help understanding the shoot-root interaction during plant growth.

Functional-Structural plant growth models combine the description of the architectural development of plants and of the ecophysiological processes governing resource acquisition and repartition. We refer to Sievänen et al. (2000) for the presentation of general concepts and reviews or de Reffye et al. (2008) for the presentation of the most recent progresses.

GreenLab is such type of model. It takes its origin in the AMAP architectural models (de Reffye, 1988) but its ecophysiological concepts are inspired from those classically used in process-based models (Monteith, 1977; De Wit, 1978; Howell and Musick, 1985; Marcelis et al., 1998 or Qi et al., 2005 for sugar beet), except that the dynamics of source-sink interaction is described at the level of organs according to their rhythm of appearance, see de Reffye and Hu (2003). The model does not claim to be fully mechanistic with regards to physiological and biophysical processes and fluxes involved in plant growth but a particular care is taken to follow empirically the dynamics of the carbohydrate budget, production and allocation, see (Yan et al., 2004).

Its mathematical formulation as a discrete dynamical system (Cournède et al., 2006) and the relative low number of parameters makes it suitable to identification from experimental data, in order to test its predictive capability. The model parameters have already been estimated for several plant species: sunflower (Guo et al., 2003), maize (Guo et al., 2006; Ma et al., 2008), cucumber (Mathieu et al., 2008), tomato (Dong et al., 2008) among others. Model predictive ability was studied in details in (Ma et al., 2007).

For this reason, it seemed interesting to use this model in order to describe the dynamics of source sink interaction during the growth of sugar beet, more precisely the balance between the vegetative part and the root system.

This paper begins with a quick presentation of the main concepts underlying the GreenLab model and of its adaptation to the sugar beet plant. The experimental protocol carried out in 2006 in order to collect the experimental data necessary for the model calibration is then described. In the second part of the article, we present the main results of the study. With the data collected at different stages during plant growth, the parameters of the GreenLab model can be estimated, which allows quantifying precisely the source-sink dynamics. Finally, these results are discussed in order to open new research perspectives with the objective to develop new tools for yield prediction and optimization.

2 Materials and Methods

In this section, we briefly recall the basic concepts underlying the GreenLab model and the adapted experimental protocol for its parametric identification. The experimental data collected in 2006 are then given. A more detailed presentation of the model can be found in de Reffye and Hu (2003) and Yan et al. (2004).

A source-sink model with a common pool of reserves

The main hypothesis to compute the functional growth is that the biomass produced by each leaf is stored in a common pool of reserves and redistributed among all organs according to their sink strengths. The initial seed and the leaves are sources. Petioles, blades and the root system are sinks.

The time unit to compute the ecophysiological functioning (resource acquisition and allocation) is chosen to coincide with the time unit of the morphogenetic sequence based on phytomer appearance. This time unit is called growth cycle (GC) and is thus classically given in thermal time by the phyllochron, that is to say the sum of degree-days necessary for a new phytomer to develop, cf. Dale and Milthorpe (1983).

Therefore, the individual plant is described as a discrete dynamical system.At growth cycle *n*, the empirical equation of neat dry matter production Q_n is given by

$$Q_n = \mathrm{PAR}_n \, \mu S^p \left(1 - \exp\left(-k \frac{S_n}{S^p}\right)\right) \tag{1}$$

- PAR_n denotes at cycle *n* the incident photosynthetically active radiation. It is assumed to equal 0.48 times the global incident radiation (RG), *cf.* Gallagher (1978), Varlet-Grancher (1989)
- μ is an empirical coefficient related to the Radiation Use Efficiency
- S^p is an empirical coefficient corresponding to a characteristic surface (related to the two-dimensional projection of space potentially occupied by the plant onto the x-y plane)
- S_n is the total leaf surface area of the plant at cycle *n*
- *k* is the Beer-Lambert extinction coefficient

In our equation, the ratio $\frac{S_n}{S^p}$ can be seen as a "local Leaf Area Index", see Cournède et al. (2008).

At every growth cycle, the biomass thus produced is allocated to organs individually according to their relative demands called sink strengths. The sink strength of an organ depends on its type (blade, petiole and root in sugar beet) and varies from its initiation to maturity which corresponds to the end of its expansion. For an organ of type o (o=b,p,r for blade, petiole and root respectively), the sink variation P_o is given classically in GreenLab (*cf.* de Reffye and Hu, 2003) as a function of its age *j* (in terms of growth cycles) as follows:

$$P_o(j) = p_o f_{a_o,b_o}(j) \quad \text{for} \quad 0 \le j < T_o \quad \text{and} \quad P_o(j) = 0 \quad \text{otherwise.} \tag{2}$$

with f_{a_o,b_o} a normalized beta distribution and T_o the time (in growth cycles) necessary for the organ to reach its maximal size from its initiation and named "expansion time". However, in sugar beet, the expansion time widely varies from one blade to another, from one petiole to another. As a consequence, it is necessary to determine experimentally the expansion times of each blade and each petiole according to their rank *k*: $T_{b,k}$ and $T_{p,k}$. Moreover, we also had to adapt the sink variation function in order to take this phenomenon into account. Several tests and trials led us to choose for $P_{o,k}(j)$, the sink variation of an organ of type *o*, of rank *k* and of chronological age *j*:

$$P_{o,k}(j) = p_o f_{a_o,b_o}\left(\frac{T_o}{T_{o,k}} j\right) \tag{3}$$

and

$$f_{a_o,b_o}(j) = \frac{1}{M_o}\left(\frac{j+0.5}{T_o}\right)^{a_o-1}\left(1-\frac{j+0.5}{T_o}\right)^{b_o-1} \tag{4}$$

with M_o chosen such that: $\sup f_{a_o,b_o}(j) = 1$ and $T_o = \max_k T_{o,k}$.

A specific change in biomass allocation at canopy closing led us to consider a variable petiole sink:

$$P_{p,k}(j) = \left(p_p + q_p I_k\right) f_{a_o,b_o}\left(\frac{T_o}{T_{o,k}} j\right) \tag{5}$$

where I_k denotes a competition index at growth cycle k and is given by the ratio of the leaf interception surface area to the total leaf area:

$$I_k = \frac{S^p\left(1-\exp\left(-k\frac{S_n}{S^p}\right)\right)}{S_n} \tag{6}$$

At each growth cycle n of its expansion period, an organ of age i receives a biomass increment $\Delta q_o(n,i)$:

$$\Delta q_o(n,i) = P_o(i)\frac{Q_n}{D_n} \tag{7}$$

and its accumulated biomass $q_o(n,i)$ is thus given by the sum of all these increments since its appearance:

$$q_o(n,i) = \sum_{j=0}^{i} \Delta q_o\left(n-i+j, j\right) \tag{8}$$

If we assume a constant specific blade mass (SBM), the surface area of a given leaf is directly deduced by dividing by SBM the accumulated biomass of its blade. The total green leaf area S_n used in the production equation is the sum of the surface areas of all the non senescent leaves. It implies determining for all phytomers the leaf life-span, that is to say the number of growth cycles between appearance and senescence. $T_{s,k}$ will denote the life-span (in growth cycles) of the leaf borne by the phytomer of rank k. If the phyllochron, expansion duration ($T_{b,k}$, $T_{p,k}$, T_r), life-span ($T_{s,k}$) and specific blade mass can be observed experimentally, it is not the case for the parameters: μ , S^p , $(p_o, a_o, b_o)_{o=r,p,b}$. They will be estimated from experimental data by model inversion, as detailed by Guo et al. (2006).

Field Experiments

Field experiments were conducted in 2006 to investigate the sugar beet development of leaves and the growth of organs (root, blades and petioles). The experiments were carried out in 2006 in the Beauce plain near Pithiviers, France N48°10'12", E2°15'7". A commercial sugar beet variety, Radar was sown on March 20 in husbandry conditions. The most uniform sections within a large sugar beet field were selected for the trials after plant emergence. This emergence stage (corresponding to the date when 80% of the final population is reached) occurred on April 8, corresponding to 150℃ days (base temperature: 0℃) after sowing. The final population was estimated to be 9.6 plants per m^2. Daily mean values of air temperature (℃), solar radiation ($MJ.m^{-2}$), relative humidity (%) as well as total daily rainfall (mm) were obtained from French meteorological advisory services (Météo France) 5 km away from the experimental site. Thermal time was calculated by daily integration of air temperature (base temperature: 0℃) cumulated from emergence. The final harvest was carried out on October 3. The plants were given adequate water and fertilisers and were kept from pests and diseases.

Development Measurements

Leaf development (appearance, expansion and senescence) was measured weekly non-destructively on the same groups of seven representative and adjacent plants. Coloured rings were placed around

the petioles of the 1st, 5th, 15th and 20th leaves as markers.

Leaf appearance and phyllochron: the phyllochron is defined as the thermal time interval that separates the emergence of successive leaves, each corresponding to a phytomer (the two cotyledons forming the first phytomer). We consider a leaf as emerged when its length is above 10mm.

Expansion: blade lengths and widths as well as petiole lengths were measured to determine expansion kinetics. The curve giving the product of blade length by blade width as a function of the thermal time was fitted with a logistic equation with three parameters.

$$f(x) = \frac{B}{1 + \exp\left(\frac{b - x}{a}\right)}$$

with x the thermal time from emergence.

Let $T_{i,k}$ be the thermal time corresponding to the appearance of phytomer k. Since, the parameter b corresponds to the inflexion point and since the curve is symmetrical, the expansion times for blades and petioles is: $T_{b/p,k} = 2(b - T_{i,k})$.

Senescence: a leaf was supposed senescent when its entire surface had yellowed. We thus determined $T_{s,k}$ for all k.

Biomass Measurements

Biomass measurements were carried out at seven different stages during the growing period: May 12 (423℃days), May 17 (499℃days), May 24 (597℃days), June 15 (989℃days), July 11 (1538℃ days), August 8 (2178℃days) and October 3 (3168℃days). At each date, seven individual plants were selected (randomly) in a group of fifteen adjacent plants and the dry mass of every individual organ (blades, petioles and root storage) was measured. Dry matter was obtained by drying for 48h at 75°C. Every leaf was digitalized in order to estimate length and width of its blade and petiole, and blade surface area. In each group of fifteen, the eight other plants were measured at the level of organ compartments: total dry mass of blades, that of petioles and that of root. The final stage of measurements corresponds to harvest. For this date, the seven plants fully described (at the level of organs) are those for which the development scheme was established with non-destructive measurements.

These biomass measurements are the experimental data from which the model parameters are estimated, *cf*. Guo et al. (2006) for the details of the calibration procedure.

3 Results and Discussion

Analysis of experimental data of sugar beet development and growth

Dry matter production and allocation

The total dry matter per square meter is shown to be proportional to the amount of photosynthetically active radiation intercepted by the crop (PARi), *cf.* Fig. 1, with at growth cycle n:

$$\mathrm{PAR}i_n = 0.48\,\mathrm{RG}\left(1 - \exp\left(-k\,\mathrm{LAI}_n\right)\right)$$

RG is the amount of global solar radiation.

LAI_n, the leaf area index at cycle n, is obtained by multiplying the average of the observed leaf area per plant by the crop density (9.6 plants per m^2). The ratio of dry matter production to intercepted PAR is defined as the Radiation Use Efficiency (RUE). It is widely used in crop models since Monteith (1977). For our experiments, the radiation use efficiency is found to be 3.36 $g.MJ^{-1}$.

It is comparable to Damay's result (1993) who found 3 to 3.8 g.MJ^{-1}. Jaggard (2006) obtained an equivalent RUE of 3.66.MJ^{-1}.

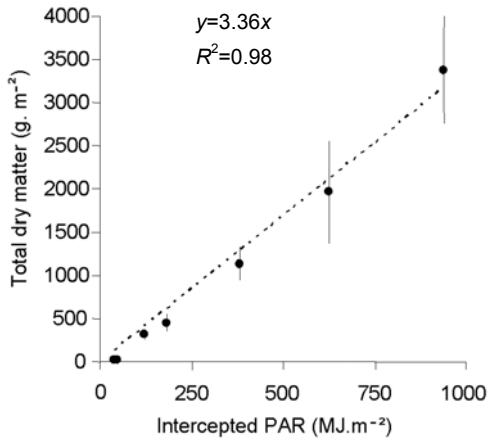

Figure 1 Dry matter production against accumulated intercepted PAR

Figure 2 (a) shows the observed total dry matter accumulated in the three compartments (roots, blades, petioles). After 750 to 800℃days, most assimilates are allocated to the storage root. In Fig. 2 (b), the ratio of blade dry matter to petiole dry matter against thermal time since emergence illustrates the partition between exchange organs (blades) and structural organs (petioles). At the first stages of growth, with little competition for light, exchange surface (leaf surface area) is privileged. With increasing intra- and inter- plant competition, allocation to petioles relatively increases in order to face competition effects.

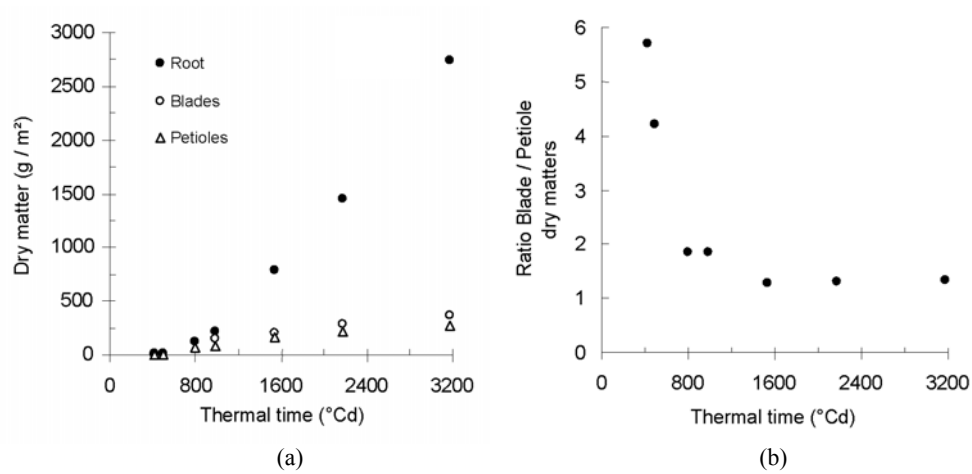

(a) (b)

Figure 2 Dry matter repartition between the different compartments against thermal time since emergence. (a) Accumulated dry mass of roots (closed dots), blades (open dots) and petioles (open triangles); (b) Ratio of accumulated blade dry mass to petiole dry mass

Phytomer Emission and Phyllochron

Growth pattern of successive leaves depend on both ontogeny and temperature. The effect of temperature can be integrated by expressing leaf appearance and expansion as linear functions of thermal rather than chronological time (Milford, 1985a). The first pair of leaves (cotyledons)

unfolds from the apex together; subsequent leaves appear individually on a 5:13 phyllotaxis, as described by Stehlik, 1938 and Milford, 1985b. We thus consider that the pair of cotyledons forms the first phytomer and each subsequent leaf corresponds to a phytomer. For all the seven plants, plotting the number of phytomers against thermal time since emergence reveals a piecewise linear relationship, with two distinct intervals, *cf.* Fig. 3. The linear relation indicates that the temperature is the main determinant of the rate of leaf appearance and this rate is constant for each phase. The inverse of the slope is the phyllochron, *i.e.* the thermal time interval between the visual appearances of two successive phytomers (Milford et al., 1985; Granier et al., 1998).

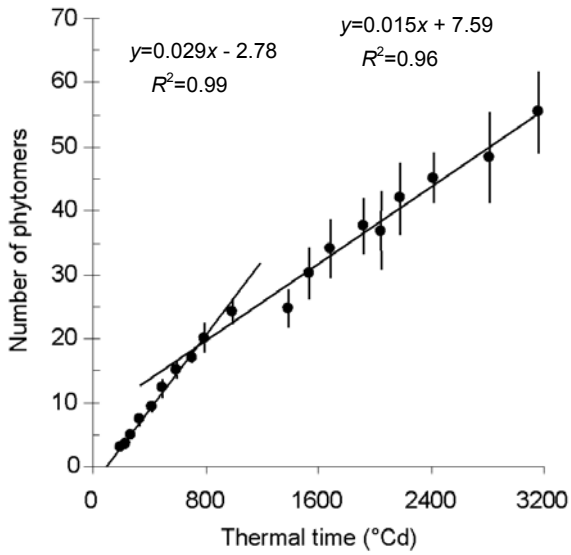

Figure 3 Number of phytomers as a function of thermal time (base temperature: 0℃) since emergence. The dots correspond to the average number of phytomers for the 7 measured plants; error bars indicate standard deviations

The regression slopes vary significantly for the seven plants, see Table 1.

Table 1 Phyllochrons of the two development phases for the extremes seven measured plants. The last line corresponds to the regression of the average number of phytomers at each measurement stage

	First Phase Phyllochron (℃days)	R^2	Second Phase phyllochron (℃days)	R^2
Minimum	29.9	0.98	56.8	0.94
Maximum	38.5	0.99	78.1	0.95
Average Plant	34.4	0.99	66.7	0.97

This change in phyllochron after approximately 20 leaves was already observed by Milford (1985a,b). He showed that the phyllochron of the first phase was constant among seasons and experimental treatments applied to the crop (sowing dates, N-content or plant density). Nevertheless, for these various treatments, the thermal duration of this early phase was variable, from 285 to 883℃days (thermal time from sowing with a base temperature of 1℃day). In the second phase, the leaf appearance is slower (66.7℃days against 34.4℃days). Many hypotheses were suggested by Milford to explain the curve bending: base temperature that changes when the plant gets older, photoperiodic factor, trophic competition, that is to say the competition for assimilates between the developing storage root and vegetative organs. This competition may slow down the rate of leaf appearance. In our

experiments, this rate starts decreasing at the beginning of the linear phase of root growth (Fig. 4.). This stage also corresponds to the observed canopy closing. Caneill (1994) also pointed out that there was important modification in assimilate partitioning between leaves and roots at canopy closing.

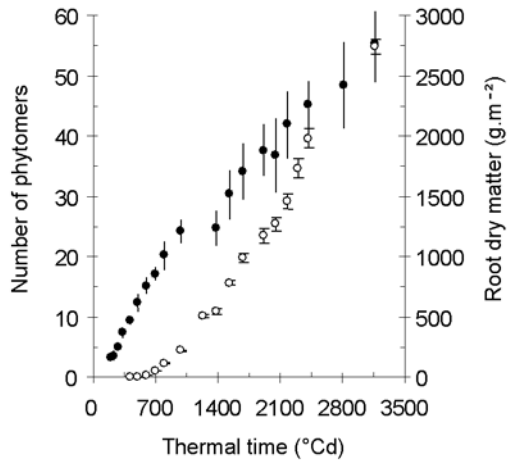

Figure 4 Comparison of phytomer appearance (closed dots) and increase in root dry matter (open dots) as functions of thermal time since emergence. Arrows indicate the time of the observed canopy closing, which corresponds to the decrease of the rate of leaf emission and the beginning of the linear phase of root growth

Organ Expansion and leaf Senescence

To control the dynamics of sources and sinks, it is necessary to determine the duration of the expansion phase for all organs (which says how long they are sinks) and the life-span of all leaves (which says how long they are sources). Figure 5 compiles the thermal time since emergence of appearance, end of expansion and senescence for the leaves of all phytomers. There is again a change of incline, for both end of expansion and senescence, at canopy closing.

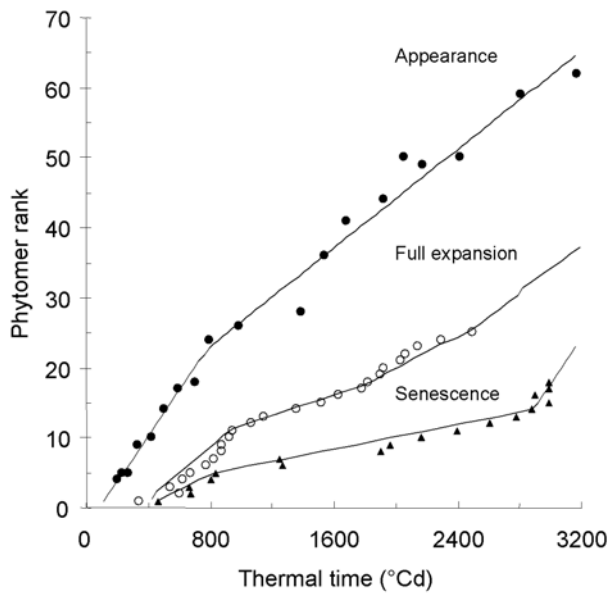

Figure 5 Leaf development scheme

The expansion durations of petioles are really close to those of blades and are thus considered identical. In previous studies (unpublished data), the observation of root growth over two years gave us an expansion duration of 3900℃days for the root storage.

Specific Blade Mass

The specific blade mass is defined as the ratio between blade dry mass and blade surface area. Plotting one variable against the other for all measured data (different plants at different ages), *cf.* Fig. 6, shows that the linear relation is pretty good, even though the dispersion increases for bigger leaves.

The specific blade mass thus obtained is 0.0080g.cm^{-2}. It is useful in the GreenLab model to deduce the production of blade surface area from the accumulated biomass. Our results do not confirm a possible increase in specific blade mass when leaves get older, phenomenon underlined by Ann Clark and Loomis (1978).

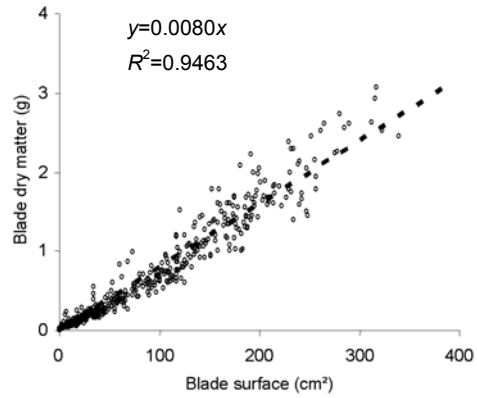

Figure 6 Blade dry mass against blade surface for all measured data and results of the linear regression

Identification of the morphogenetic model and source-sink dynamics

The preliminary analysis of our experimental data helped us construct the morphogenetic model of growth based on GreenLab. First, the time step for model computation (also called Growth Cycle) is chosen as the smallest phyllochron observed. It allows that no phytomer emission is missed for any plant. Even after the increase of the phyllochron at canopy closing, the model time step remains the same but a new phytomer is not generated at every growth cycle in the model. A new phytomer appears or not according to the theory of discrete lines (Reveilles, 1991), which ensures that at every growth cycle the number of phytomers is the best possible approximation of the continuous reality.

The expansion durations and life-spans for all organs according to their ranks which were obtained in thermal time are given their corresponding values in growth cycles. Some other parameters are measured (specific blade mass) or obtained in the literature (the Beer-Lambert extinction coefficient $k = 0.7$ according to (Andrieu et al., 1997)). The environmental input PAR_n is given by the cumulated photosynthetically active radiation at each growth cycle.

The other parameters are estimated from our experimental data. Note that since sink values are barycentric coefficients, one of these values must be fixed. For this reason, we impose that the blade sink strength is equal to 1. For the root sink strength, any important value would do since after some time the most important part of matter is allocated to the root.

Table 2 gives the results of the estimation procedure (achieved with Digiplante software, developed at Centrale Paris, *cf.* Cournède et al., 2006).

Table 2 Parameters of the GreenLab model of sugar beet growth

Parameter	Description	Estimated (E) Measured (M) or Fixed (F)	Value	Unit
μ	Empirical coefficient related to the radiation use efficiency	E	1.23	$g.MJ^{-1}$
k	Beer-Lambert extinction coefficient	M	0.7	-
S^p	Empirical coefficient corresponding to a characteristic surface	E	0.021	m^2
SBM	Specific blade mass	M	0.008	$g.cm^2$
p_r	Root sink strength	F	400	-
p_b	Blade sink strength	F	1 (reference value)	-
p_p	Petiole sink strength	E	0.4916	-
q_p	Petiole sink correction	E	0.3894	-
T_r	Root expansion duration	M	130	GC
$T_{b,k}$	Blade expansion duration	M	Function of phytomer rank	GC
$T_{p,k}$	Petiole expansion duration	M	Function of phytomer rank	GC
$T_{s,k}$	Leaf life span	M	Function of phytomer rank	GC
a_r	Parameter for beta law	E	3.13	-
b_r	Parameter for beta law	E	1.15	-
a_b	Parameter for beta law	E	3.56	-
b_b	Parameter for beta law	E	2.22	-
a_p	Parameter for beta law	E	2.56	-
b_p	Parameter for beta law	E	1.67	-

In Figs. 7 and 8, are shown the differences between the (averaged) experimental data and the model output obtained for the estimated parameters. The different stages of growth are satisfactorily reproduced at the level of organs, which proves that not only the global balances of biomass allocation are described but also the precise dynamics of source-sink interaction.

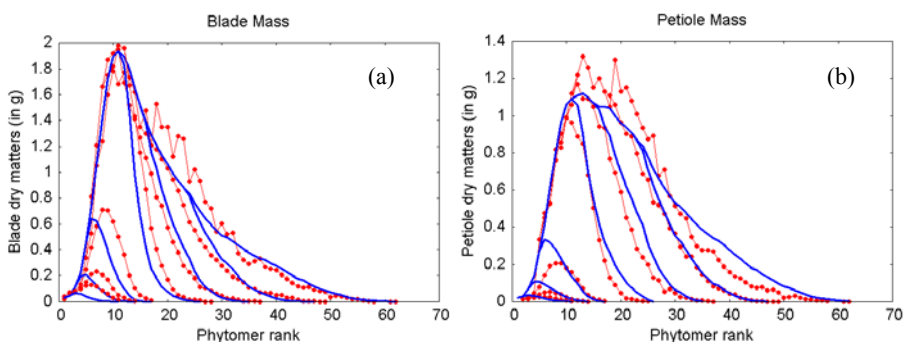

Figure 7 Average plants at organ level: experimental data (open dots) and simulated data (lines) (a) Blade dry masses and (b) petiole dry masses according to phytomer ranks , at 423, 499, 597, 989, 1538, 2178 and 3168℃ days after emergence

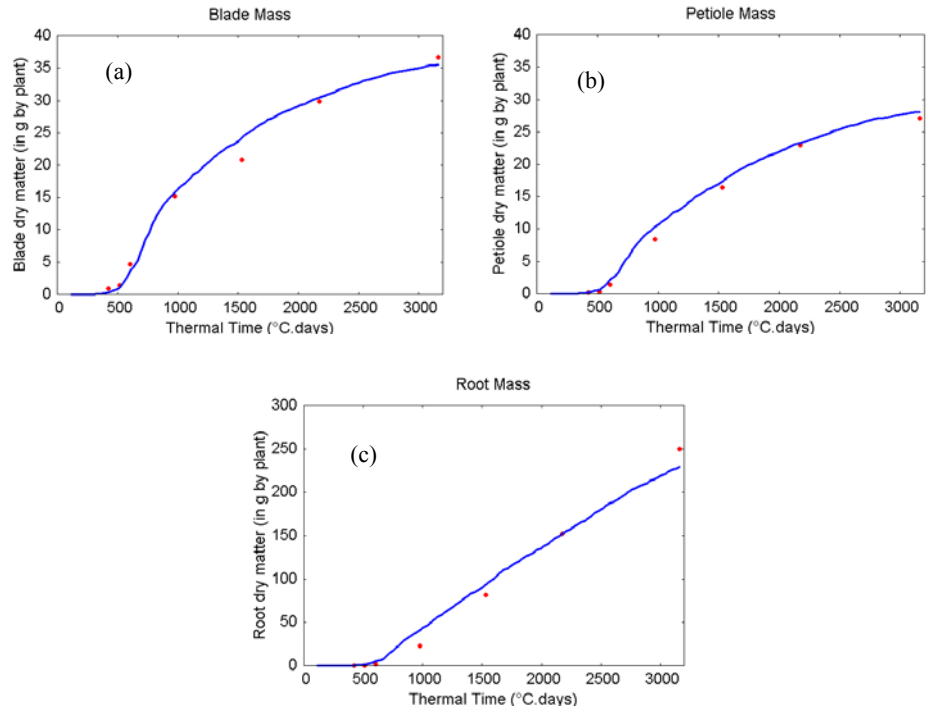

Figure 8 Average plants at compartment level: experimental data (red dots) and simulated data (blues lines) (a) Blade compartment dry mass (b) Petiole compartment dry mass and (c) Root dry mass as functions of thermal time since emergence

Figure 9 shows the biomasses allocated to blades, petioles and root at every growth cycle. We clearly see the rapid increase of the allocation to the root compartment after 500℃days since emergence with a maximal proportion of assimilates distributed to root storage at 700℃days after emergence, which corresponds to the maximal biomass production. This stage may be related to the linear phase of root growth and phyllochron change above-mentioned (*cf.* Fig. 4). In Fig. 10 are shown the simulated proportions of biomass allocated to shoot and to root throughout the season. The observed tendencies are very classical and correspond to those given by the SUCROS model (Spitters et al., 1989).

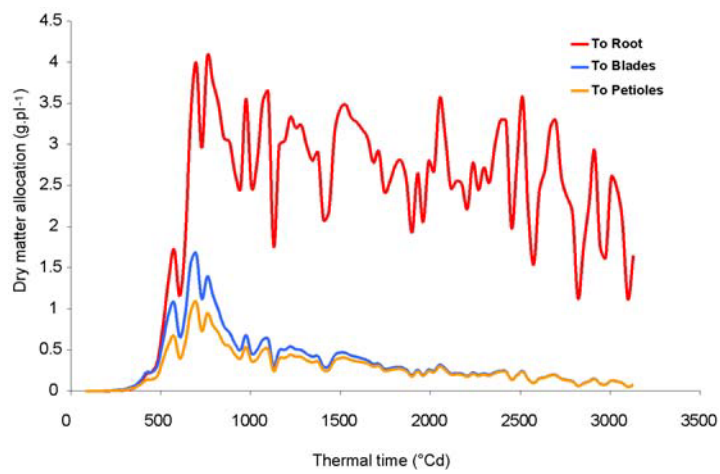

Figure 9 Biomass allocation between blade, petiole and root compartments simulated by the GreenLab model

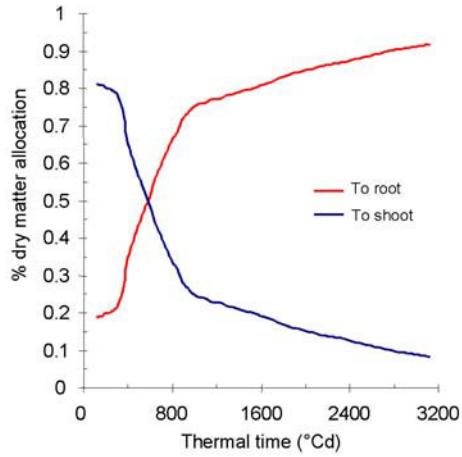

Figure 10 Proportions of biomass allocated to shoot and to root throughout the season

4 Conclusion

The experimental study of sugar beet development, mostly phytomer appearance, organ expansion and leaf senescence, allowed us to define a morphogenetic model of sugar beet growth based on GreenLab. The functional parameters controlling source-sink relationships during plant growth were estimated from organ and compartment dry masses, measured at seven different times, for samples of plants. The fitting results are good and the dynamics of source-sink interactions is precisely described by the model throughout the season.

We believe such a simulation tool may be useful in a general context of input reduction in agricultural practices. The impacts of low input management need to be quantified. Estimation of losses in sugar yield resulting from stress is important for growers who need to make decisions for a rational use of inputs. If the relationship between root dry matter yield at harvest and light energy intercepted during growth is generally good, it shows limitations when plants are affected by stress, particularly water stress (Werker and Jaggard 1998). As foliage is the main determinant of root yield, it is important to precisely control leaf development and its interaction with root growth. Pests or water and nutrient limitations can cause sugar beet leaves to prematurely end their expansions or wilt. It entails a decrease of crop photosynthetic efficiency and, consequently, of root mass and sugar content.

Moreover, in sugar beet plants, there are numerous exchanges of carbohydrates between leaves and root storage, which are strongly modified when plant undergo stress. Therefore, it is important to better understand relationships between leaf development and growth throughout the growth season. Since the GreenLab model provides a dynamic description of matter allocation at the level of organs, changes in leaf development mechanistically impact the source-sink ratio (biomass production and allocation), and thus root growth. For this reasons, we believe the modeling framework introduced is a good candidate to help understand how stress affects the balance between sinks, more particularly the shoot-root allocation dynamics.

Likewise, the morphogenetic model proposed may help determine characteristic physiological phases in sugar beet growth. Caneill (1994) proposed a description of different phases of sugar beet development depending on the priorities of biomass allocation among organs. He defined four particular stages according to the ratio between root dry matter and shoot dry matter. However, the thermal time necessary to reach these stages was not stable, in particular for the 3rd stage, which corresponds to the beginning of the linear root growth. The GreenLab model is potentially able to

help determine these physiological phases, under different growing conditions including stress, density effects, sowing dates ...

However, the preliminary results of this study simply prove that the introduced framework is adapted to analyse source-sink dynamics and shoot-root allocation. This approach still needs to be fully validated, particularly among seasons. More particularly, the leaf development scheme of several seasons and several stress conditions has to be studied. What are the system stabilities and what variables are strongly impacted? In such experimental conditions, how is the source-sink dynamics affected? New experiments were conducted in 2007 (including nitrogen stress and water stress) and in 2008 (4 different densities). The results are in the process of analysis.

Acknowledgements

This work was supported by the French Sugar-beet Technical Institute (ITB). We thank A. de Silans, P. Houdmon, H. de Balathier, A. Nioche and M. Allart of ITB for technical assistance.

References

Andrieu B, Allirand JM, Jaggard KW (1997) Ground cover and leaf area index of maize and sugar beet crops. Agronomie 17:315 – 321.

Ann Clark E, Loomis RS (1978) Dynamics of leaf growth and development in sugar beets. J. Amer. Soc. sugar beet technologists 20:97 – 112.

Caneill J, Fleury A, Ferre F (1994) L'élaboration du rendement de la betterave sucrière. In: Combe L, Picard D (eds.) Un point sur l'élaboration du rendement des principales cultures annuelles. INRA éditions, Paris

Cournède PH, Kang MZ, Mathieu A, Barczi JF, Yan HP, Hu BG, de Reffye P (2006) Structural factorization of plants to compute their functional and architectural growth. Simulation 82:427 – 438.

Cournède PH, Mathieu A, Houllier F, Barthélémy D, de Reffye P (2008) Computing competition for light in the Greenlab model of plant growth: a contribution to the study of the effects of density on resource acquisition and architectural development. Ann. Bot. 101:1207 – 1219.

Dale JE, Milthorpe FL (1983) General features of the production and growth of leaves. In: Dale JE, Milthorpe FL (eds.) The Growth and Function of Leaves. Cambridge University Press.

Damay N and Le Gouis J (1993) Radiation use efficiency of sugar beet in Northern France. Eur. J. Agron. 2:179 – 184.

de Reffye P, Edelin C, Françon J, Jaeger M, Puech C (1988) Plants models faithful to botanical structure and development. Comput. Graphics 22:151 – 158.

de Reffye P, Hu BG (2003) Relevant qualitative and quantitative choices for building an efficient dynamic plant growth model: GREENLAB case. In: Hu BG and Jaeger M (eds.) Plant Growth Modeling and Applications. Proc. PMA03' Int. symp. on plant growth modeling, simulation, visualization and their applications, Beijing, China, October 13-16, 2003. Tsinghua University Press and Springer.

de Reffye P, Heuvelink E, Barthélémy D, Cournède PH (2008) Modeling plant growth and architecture. In: Jorgensen S (ed.) Encyclopedia of Ecology, Elsevier.

de Wit CT et al (1978) Simulation of assimilation, respiration and transpiration of crops. Simulation. Wiley, New York

Dong QX, Louarn G, Wang YM, Barczi JF, de Reffye P (2008) Does the structure-function model GREENLAB deal with crop phenotypic plasticity induced by plant spacing? A case study on tomato. Ann. Bot. 101:1207 – 1219.

Gallagher JN, Biscoe PV (1978) Radiation absorption, growth and yield of cereals. J. Agric. Sci. Camb. 91:47 – 60.

Granier C, Tardieu F (1998b) Is thermal time adequate for expressing the effects of temperature on sunflower leaf development? Plant, Cell and Env. 21:695 – 703.

Guo Y, de Reffye P, Song YH, Zhan ZG, Dingkuhn M, Li BG (2003) Modeling of biomass acquisition and partitioning in the architecture of sunflower. In: Hu BG and Jaeger M (eds.) Plant growth modeling and

applications. Proc. PMA03' Int. symp. on plant growth modeling, simulation, visualization and their applications, Beijing, China, October 13-16, 2003. Tsinghua University Press and Springer.

Guo Y, Ma YT, Zhan ZG, Li BG, Dingkuhn M, Luquet D, de Reffye P (2006) Parameter optimization and field validation for the functional-structural model GREENLAB for maize. Ann. Bot. 97:217 – 230.

Howell TJ, Musick JT (1985) Relationship of dry matter production of field crops to water consumption. In: Perrier A and Riou C (eds.) Proc. Int. Conf. Les besoins en eau des cultures. Paris, France, INRA editions.

Jaggard K W, Qi A (2006) Crop physiology and agronomy. In: Draycott AP (ed) Sugar Beet. Blackwell Publishing, Oxford.

Ma YT, Li BG, Zhan ZG, Guo Y, Luquet D, de Reffye P, Dingkuhn M (2007) Parameter stability of the functional–structural plant model GREENLAB as affected by variation within populations, among seasons and among growth stages. Ann. Bot. 99:61 – 73.

Ma YT, Wen MP, Guo Y, Li BG, Cournède PH, de Reffye P (2008) Parameter optimization and field validation of the functional-structural model GREENLAB for maize at different population densities. Ann. Bot. 101:1185 – 1194.

Malnou CS, Jaggard KW, Sparkes DL (2008) Nitrogen fertilizer and the efficiency of sugar beet crop in late summer. Eur. J. Agron. 28:47 – 56.

Marcelis LFM, Heuvelink E, Goudriaan L (1998) Modeling biomass production and yield of horticultural crops: a review. Sci. Hort. 74:83 – 111.

Mathieu A, Zhang B, Heuvelink E, Liu S, Cournède PH, de Reffye P (2008) Calibration of fruit cyclic patterns in cucumber plants as a function of source-sink ratio with the GreenLab model. In: Hanan J and Prusinkiewicz P (eds.) Proc. of the 5th international workshop on FSPM.

Milford GFJ, Pocock TO, Riley J (1985a) An analysis of leaf growth in sugar-beet. I. Leaf appearance and expansion in relation to temperature under controlled conditions. Ann. Appl. Biol. 106:163 – 172.

Milford GFJ, Pocock TO, Riley J (1985b) An analysis of leaf growth in sugar beet. II. Leaf appearance in field crops. Ann. Appl. Biol. 106:173 – 185.

Monteith JL (1977) Climate and the efficiency of crop production in Britain. Proc. of the Royal Society of London. B. 281:277 – 294.

Qi A, Kenter C, Hoffmann C, Jaggard KW (2005) The Broom's Barn sugar beet growth model and its adaptation to soils with varied available water content. Eur. J. Agron. 23:108 – 122.

Reveilles JP (1991) Géométrie discrète, calcul en nombres entiers et algorithmique. PhD thesis, Univ. of Strasbourg.

Sievänen R, Nikinmaa E, Nygren P, Ozier-Lafontaine H, Perttunen L, Hakula H (2000) Components of functional-structural tree models. Ann. Forest. Sci. 57:399 – 412.

Spitters CJT, van Keulen H, van Kraalingen DWG (1989) A simple and universal crop growth simulator: SUCROS87. In: Rabbinge R *et* al. (eds.) Simulation and Systems Management in Crop Protection. Simulation Monographs 32. Wageningen, Pudoc.

Stehlik V (1938) La feuille de betterave sucrière. In: Communication au VIIIème congrès de.l'IIRB, janvier 1938.

Varlet-Grancher C, Gosse G, Chartier M, Sinoquet H, Bonhomme R, Allirand JM (1989) Mise au point : rayonnement solaire absorbé ou intercepté par un couvert végétal. Agronomie. 9:419 – 439.

Werker AR, Jaggard KW, Allison MF (1998) Dependence of sugar beet yield on light interception and evapotranspiration. Agric. Forest Met. 89:229 – 240.

Werker AR, Jaggard KW, Allison MF (1999) Modeling partitioning between structure and storage in sugar beet: Effects of drought and soil nitrogen. Plant Soil 207:97 – 106.

Yan HP, Kang MZ, de Reffye P, Dingkuhn M (2004) A dynamic, architectural plant model simulating resource-dependent growth. Ann. Bot. 93:591 – 602.

Coupling Process-Based Models and Plant Architectural Models: A Key Issue for Simulating Crop Production

P. de Reffye[1,2], E. Heuvelink[3], Yan Guo[4], Bao-Gang Hu[5] and Bao-Gui Zhang[4]

([1] CIRAD UMR AMAP, A-51/PS2, Boulevard de la Lironde, 34398 Montpellier cedex, France)
([2] INRIA Saclay, Digiplante Project, ECP Laboratoire MAS, Chatenay Malabry, F-92295, France)
([3] Wageningen University, Horticultural Supply Chains group, The Netherlands)
([4] College of Resources and Environment, China Agricultural University, Beijing 100193, China, Corresponding author : email : zhangbg@cau.edu.cn)
([5] LIAMA, Institute of Automation, Chinese Academy of Sciences, Beijing 100080, China)

Abstract: Process-Based Models (PBMs) can successfully predict the impact of environmental factors (temperature, light, CO_2, water and nutrients) on crop growth and yield. These models are used widely for yield prediction and optimization of water and nutrient supplies. Nevertheless, PBMs do not consider plant architecture as a determinant of yield, thus they often lack the flexibility to follow plant plasticity. Leaf area index (LAI), flower and fruit abortion are usually not predicted very well, because PBMs operate at the level of plant compartment (e.g. all leaves together) and unit area of crop instead of the phytomers where the feedback between plant growth and plant architecture operates. Functional Structural Plant Models (FSPMs) use the architecture as the support of functioning, integrate properly the action of the environmental conditions at the phytomer level that gives the plant its full plasticity: feedback between biomass production and biomass partitioning for both development (functioning of meristems) and growth (sink strength and variation, allometry of organs). These kinds of models suffer from the drawbacks that data acquisition is very heavy and model parameter estimations rely on numeric simulation that demands thousands of iterations as no analytical solution is available. Coupling PBM and FSPM, as done in the GreenLab model, is an important step to improve yield prediction not only with respect to its quantity but also to its quality (number and size of organs, branching pattern in ornamental plants). In the GreenLab model biomass production depends on PAR (photosynthetically active radiation) and LAI, a common pool of biomass is assumed and partitioning of biomass among organs is based on their relative sink strength. Plant architecture is simulated dynamically and the organ functioning is modified continuously during growth according to various environmental conditions. Such mathematical models could provide better yield prediction, as crop production depends on the functioning of the plant architecture, and parameter identification is more accurate with inverse methods. Some examples addressing the above-mentioned issues are presented in this paper using the GreenLab model.

Keywords: plant growth, crop production, model, Process-Based Models, Functional Structural Plant Models

1 Introduction

For yield prediction of cultivated plants, nowadays the use of process-based models is common (Marcelis et al., 1998). Such models integrate environmental factors (climate: light, temperature, CO_2; soil conditions: water and nutrient availability etc.), by using compartment data, such as total leaf surface and harvest index. Hardly any information about the architecture is taken into account,

because these models focus on yield per unit of ground surface area and not on the individual plant functioning. They are generally considered as sufficient for practical use in agronomy, but far from satisfying for eco-physiologists who are interested in the mechanisms of crop production, for which more details are required about the plant microclimate and the plant functioning relying on the source and sink processes that work inside the plant architecture. Functional structural plant models (FSPMs) (Sievanen et al, 2000) have been developed in order to get a deeper understanding in plant physiology. Nowadays powerful computer algorithms exist to simulate with accuracy the 3D plant structure, but they deal only with the plant geometry for computer graphics. Integration of physiological knowledge in such geometrical models that provide the structural support of the functioning is a challenge. Light interception by individual leaves needs to be computed, as well as the production, transport and partitioning of assimilates during short periods of time within the network of the plant architecture. FSPMs are dedicated to simulate in detail all these processes with a mechanistic approach. Heavy computations are needed at all the steps of these different processes. Study of the mechanisms of the plant functioning, is certainly of great academic interest, but it remains doubtful whether FSPMs can work as well as PBMs in agricultural application for several reasons:

- The data acquisition is much heavier.
- Parameter identification from real plants presents a serious problem, as parameters are numerous, and for their estimation, numeric simulations such as simulated annealing algorithms that demand thousands of iterations have to be used for lack of analytical solutions that rely upon derivation of powerful mathematical methods (e.g. Gauss-Newton). Moreover, most of the parameters of the models come from literature instead of estimation by inverse methods.

In the domains where PBMs work properly, Ockham's razor indicated FSPMs should not do better, as the good simplifications have been found by the agronomists.

Nevertheless in some cases where the PBMs reach a bottle neck, the plant architectural approaches seem necessary as will be discussed later. That implies not to give up all the sensible methodology and to change completely their approach, as it exists a relevant way to use the plant architecture concepts, keeping all know-how of the PBMs. The GreenLab model presented here is an attempt to improve when necessary, the efficiency of PBMs.

2 Advantages and Limitations of PBMs and FSPMs

Below we list the most relevant advantages and limitations of PBMs and FSPMs and propose a possible way to improve PBMs formalism.

Plant architecture is the result of both development and growth phenomena put together with geometrical rules.

- Development concerns the functioning of meristems creating new organs and also expansion of these organs depending on the so called "thermal time". Linked to geometrical operations, development is sufficient to simulate a 3D virtual plant.
- Growth concerns biomass production and biomass partitioning among the competing organs.
- Architecture is the 3D structure of the plant as a stack of organs (internodes, leaves, root, fruits, etc.) that is transformed in mesh in the computer memory.

PBMs have the advantage of being simple for plant growth modeling and measurements.

- No detailed references to plant development are required. This avoids numerous measurements on the plant to follow the organogenesis depending of the thermal or calendar time.
- Light interception is calculated efficiently according to the Lambert–Beer law by using LAI instead of a cumbersome plant canopy structure description; Intercepted light is converted into biomass with light use efficiency (LUE); influence of the environmental conditions (radiation, temperature, CO_2 concentration) is taken into account using empirical functions.

- Using a common pool of biomass (transport resistance for assimilates is neglected), the biomass is allocated to organs according to their relative sink strength.
- Sources and sinks have no significant direct interactions.

Limitations of the PBMs are obvious in some cases as no information is available at the level of organs or phytomer which consists of an internode, a leaf and an auxiliary bud.

- For ornamental plants, a 3D output is necessary to assess the resulting plant architecture, this is not possible with PBMs simulations as no information is available about the plant development and its architecture.
- A lack of prediction of the specific leaf weight in different environmental conditions (climate, density) prevents a good estimation of the leaf area.
- Organ abortion in crops such as cucumber, tomato, sweet pepper and the harvest index of cereals are not well predicted.
- No stochastic variations of yield is taken into consideration, thus it is impossible to assess the quality of simulated output.
- PBMs fail to simulate girth growth which is essential for the stem diameter of trees.

FSPMs are dedicated to follow plant development and growth by introducing the physiological knowledge at the level of organs and even cells (e.g. stomata, xylem vessels etc.). They rely upon computer performance and can model and simulate both plant development and growth

- The plant development, using growth grammars (e.g. L-systems) that are able to follow in parallel the behaviour and the fate of thousands of meristems.
- The plant growth, calculated from the light interception by the plant canopy (using radiosity or ray-tracing methods) and the biomass production at the level of individual leaves.
- The biomass transportation and partitioning through the complex network of the plant structure right down to individual competing organs.

This is certainly of academic interest for computer scientists and physiologists, but is less suitable for farmers and agronomists who are interested in accurate crop yield predictions. Furthermore, FSPMs suffer from the following drawbacks :

- Complex data acquisition on the plant structure is necessary (e.g. AMAPmod (Godin et al., 1997). It is doubtful to convince practitioners to invest in such method.
- Heavy computations for both the development and the growth are not only time consuming but also prevent the use of inverse methods.

Being aware of the advantages and limitations of the two approaches, and keeping in mind “not to throw the baby out with the bath water”, we should take the advantage of the simplicity of PBMs and make necessary improvements in case of above-mentioned limitations. Although FSPMs consider the detailed architectural structure and heterogeneity of microclimate inside the plant system, relevant simplification can considerably reduce computing and measuring costs without reducing the precision in prediction of biomass production and partitioning. The model GreenLab (Fig. 1) is an attempt to couple both approaches:

- It maintains the ecophysiological part of PBMs with their simplifications on light interception, biomass production and partitioning. This is sufficient in most applications in agriculture, and there is no reason to complicate something that works well.
- Plant development is presented in a more efficient way. Here we must underline that plant development is not plant architecture. In general, the later is not required for yield prediction. Counting the number of similar organs produced by a plant is less difficult than recording their individual locations into the plant topological structure. For each compartment, recording the cumulative biomass and the number of organs in that compartment is sufficient, with the ratio being the weight of individual organs.

- It works at the level of a phytomer instead of the compartment. The number of different kinds of organs is equal to the number of the corresponding compartments. So the complexity of the system is not increased. A compartment is made of the sum of organs sharing the same chronological and physiological ages. Growth rate of an organ is a simple function of its age, its sink value, the total sink of all organs together (demand) and the available biomass (supply). These are computed by equations and no more by numerical simulations. Organ size is deduced from allometric relationships between weight and volume.

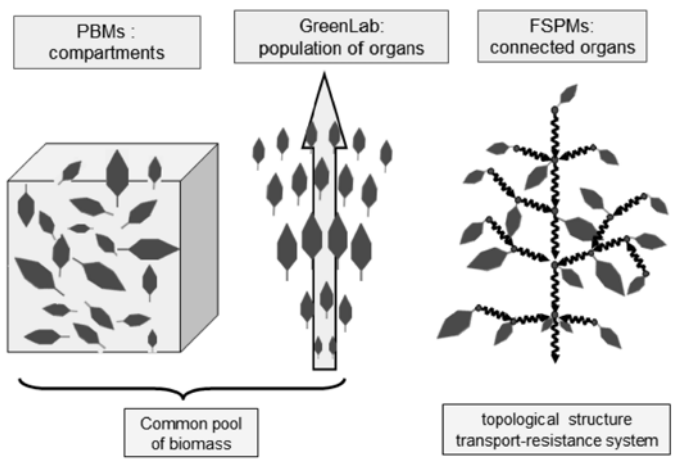

Figure 1 Different approaches for biomass partitioning in the three types of models. PBMs pool all organs of the same kind in one compartment, regardless of their chronological ages. FSPMs are a network of source and sink connected organs. In GreenLab, organs are classified in sub-compartments depending on the time of their creation. Each compartment gets a number of organs and a weight that gives the biomass of the individual organ. History of growth is stored along the series of compartments

3 Modeling Plant Development

Plant development is the result of the meristem functioning (growth, death, branching processes). The same average organ number can be produced by different branching patterns (Fig. 2), moreover in stochastic cases multiple combinations are possible.

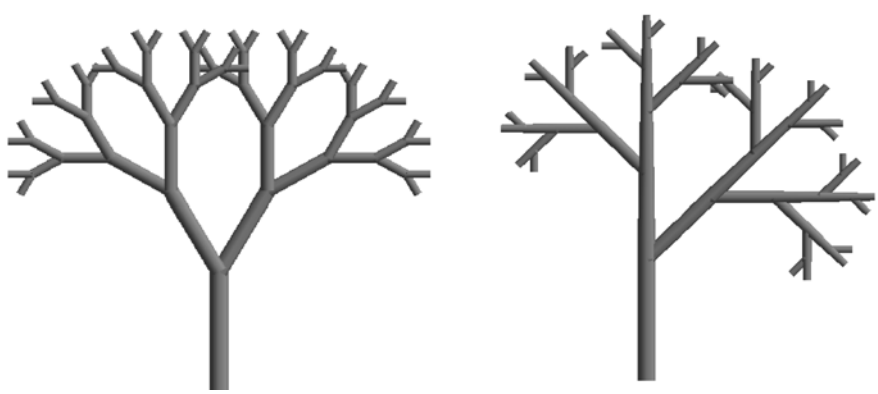

(a) (b)

Figure 2 Example of similar development with different architecture. Binary trees with either sympodial (a) or monopodial (b) branching. Both architectures produce the same number of organs

Case of PBMs

As mentioned above, PBMs do not consider plant development in detail. The advantage is that it is not necessary to follow the organogenesis or measure the duration of organ expansion, although in some of them e.g. Tomsim (Heuvelink, 1999), a part of the development is taken into account (evolution of the fruit number).

Case of FSPMs

The strong point of FSPMs is to simulate with a maximum of detail the plant development which is totally coupled with the plant architecture construction. Plant architectural models have been designed by botanists, (Hallé et al., 1978), and improved recently (Barthélemy and Caraglio, 2007). They provide all the necessary information to follow the plant development that will be simulated accurately thanks to a grammar (L-system) by computer scientists. Simulated development is a topological structure serving for the support of plant functioning and which is a guide for the construction of the geometrical structure. The time to simulate the plant development is proportional to the number of organs to create and this is clearly a bottleneck of FSPMs for trees.

Phyllochron and duration of organ expansion have to be measured properly which may need a lot of observations. The first generation of FSPMs forced the number and the size of organs to be controlled by the thermal time in ADEL (Fournier and Andrieu, 1999); GRAAL (Drouet and Pagès, 2003); AMAPsim (Barczi et al., 2008). Moreover, organ expansion has to be measured according to its specific rank position on the stem. The organs are 3D shapes whose sizes depend on expansion according to their chronological age and their position inside the plant (Fig. 3). Volume of organs depends on the incoming biomass, but their relative sizes seem to be stable and can be assessed from a simple function of the rank. A drawback is that it fails to simulate plant plasticity and

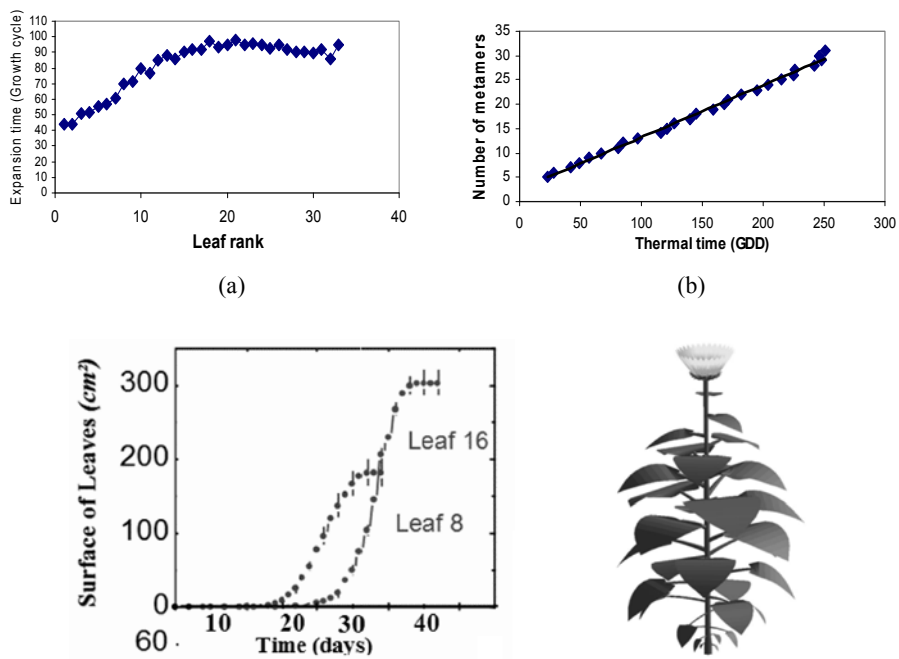

Figure 3 Sunflower development and simulation of the plant architecture as a function of thermal time with AMAPsim software (adapted from Rey et al., 2007). (a) Phyllochron expressed as thermal time. (b) Leaf expansion duration as a function of leaf rank. (c) Leaf expansion for leaf 8 and 16. (d) Simulation of the plant architecture driven by thermal time

everything is forced. The plant architecture is obtained by coupling the rules of organ production with the geometrical rules needed for the 3D plant construction (organ size, phyllotaxy, branching angles...). The 3D models build by the FSPMs provide meshes that are used to simulate light interception by leaf polygons, resistance to sap transportation biomechanics by finite elements.

Case of Coupling PBMs and Architectural Models

It is not always necessary to couple architecture and development excepting that if the 3D output is needed. If only organ numbers, biomass production and its partitioning among organs are required for yield prediction, there is no need to build a topological and a geometrical structure.

In GreenLab model, a dual scale automaton (Hu et al., 2003, Fig. 4) works with the physiological age notion from botany (Barthélémy and Caraglio, 2007), it allows a powerful factorization of the organogenesis. Computing the development is no more proportional to the number of organs to create, but only to the plant age. This provides a faster computing of the organ production. The plant demand, i.e. the sum of the individual sinks, is thus computed with a faster algorithm. The automaton can be deterministic or stochastic. In the latter case the formalism allows to compute means and variances of the production depending on the probabilities associated with growth, death, branching and state transitions.

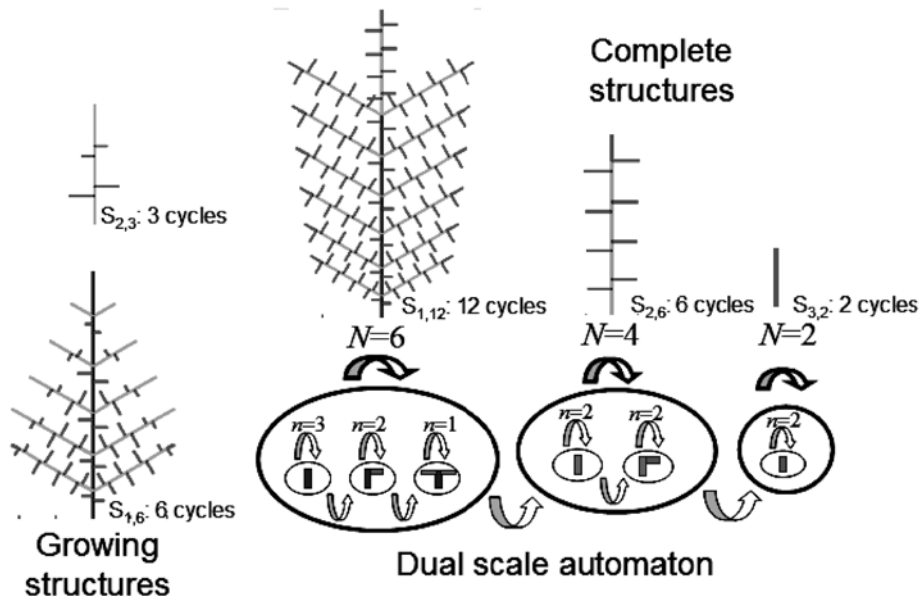

Figure 4 Construction of plant architecture in GreenLab model.
A dual scale automaton controls the growth and the branching of the meristems (Hu et al. 2003). A first level builds the phytomers and a second the growth units composed of phytomers and the basic element of the branches. In the figures, architecture with elements of 3 physiological ages is illustrated

Measurement on the plant to assess the phyllochron and expansions of organs are still required as for FSPMs, but category of organs may be sorted according to their chronological and their physiological ages and gathered into a sub-compartment. No more consideration about their location in the plant structure is necessary. This greatly simplifies the introduction of plant development.

Moreover, the size of the different sets of organ populations can be fitted with an automaton that adjusts the cumulated number of organs in the corresponding compartments according to their physiological and chronological ages. Every automaton that fulfils the goal is convenient, with the simplest being the better.

4 Modeling the Biomass Production

The light interception by the plant foliage is an important aspect of biomass production. The overlapping of leaves makes that photosynthesis is no longer linearly proportional to the plant population area. At high plant density, hardly any light will reach the ground surface.

Case of PBMs

The leaf compartment as a whole is concerned and not individual leaves. The plant community is considered at the m² level.

The growth rate Q_n (/m²/day) of a plant population is written as:

$$Q_n = \mathrm{LUE} * \mathrm{PAR}_n * I_n \tag{1}$$

Where n is the time (calendar or thermal)**,** LUE is the light use efficiency (g/MJ), PAR (MJ/m^2.day), is the amount of incident photosynthetically active radiation and I is the fraction of light intercepted by the plant canopy.

Spatial distributions and leaf orientations are assessed to calculate the light interception according to the Lambert-Beer law (that assumes a spatial Poisson-distribution of leaves).

$$I_n = 1 - \exp(-k * \mathrm{LAI}_n) \tag{2}$$

Formalism of light interception relies upon the leaf area index (LAI), which is the total functioning leaf area for a unit surface area of ground covered by the plant population. Parameter k, the extinction coefficient, is related to leaf size and leaf orientation. This assumption is usually robust and tolerates some shift from reality. Special improvements can be done in the case of clumping due to particular plantation densities. Limitations occur when densities are low, because Eq. (2) assumes a homogenous distribution of leaves, whereas at low planting densities leaves are clustered. In those situations, a crop coefficient K_c may be introduced to take account only of the ground area covered by plants.

Equation (2) is used by most of the process-based models, both for light interception and transpiration of the plant populations. Advantage is its fast computation. LAI can be more or less complicated to assess, especially in the case of water stress. For a young plant canopy I is almost proportional to the leaf area, and when LAI is larger than 3, more than 90% of the light is intercepted.

LAI depends on the leaf biomass and the SLW (specific leaf weight). However, LAI can be modelled as a function of thermal time. This works well when daily temperature and radiation are closely correlated, but it is no longer valid for greenhouses or winter crops (winter wheat). In PILOTE (Maihol et al., 1997), an empirical mathematical function fits the observed LAI at different growth stages (Fig. 5), and is used as a fixed input for Eq. (2)

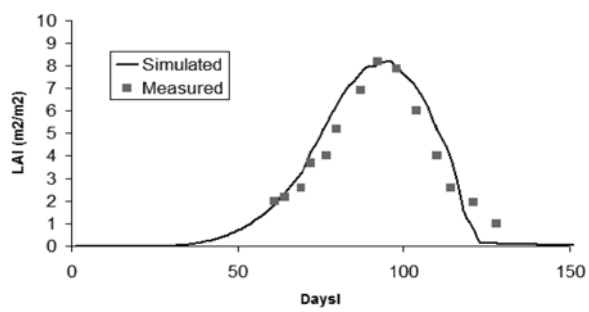

Figure 5 PILOTE System from Cemagref (Maihol et al., 1997) Fitting the evolution of the LAI in a wheat plantation

In Fig. 5 the measured data are calculated from light interception measurements and fitted with the equation:

$$LAI_{(j)} = LAI_{max}\left[\left(\frac{TT_{(J)} - Ts}{t_f}\right)^{\beta} \exp\left\{\frac{\beta}{\alpha}\left(1 - \left(\frac{TT_{(j)} - Ts}{t_f}\right)^{\alpha}\right)\right\}\right]$$

TT is the temperature sum at day J, t_f the development duration and Ts the accumulated temperature until emergence. LAI_{max} is the maximum value of LAI; α and β are regression parameters.

Case of FSPMs

Here the interest is focused on the heterogeneity of microclimate surrounding individual leaves to understand more about the plant functioning at the phytomer level. The 3D structure can be obtained by digitalizing the plant architecture (Fig. 6) or by simulating the 3D architecture from the plant development coupled with the geometry of plant organs with L-systems (Fournier and Andrieu, 1999) or automaton (AMAPsim; Barczi et al., 2008).

Figure 6 Digitalized architectures of Maize, Sunflower and Cotton (from Guo and Li, 2001)

Digitalized architectures though accurate, give only a static view of the plant structure but no information about the growth process. On the other hand, 3D structures generated from FSPMs must be matched first to the reality. They provide a support to compute the microclimate step by step. This is called phylloclimate (Chelle, 2005).

Modeling light interception requires using ray-tracing or radiosity methods acting on the canopy as a result of a population of 3D plants described by a set of polygons (Fig. 7). The cost of such computations is heavy and makes it less suitable than PBMs for field applications. Not only the data acquisition is complex, but coupling a phylloclimate model with a FSPM adds complexity over complexity. Such works to determine plant phylloclimate have been carried out by Chelle (2005) and Dauzat et al. (1996, 1998).

New generations of FSPMs perform the full loop of biomass production, that creates leaf organs that in turn creates new biomass etc. such as AMAPhydro (Reffye et al., 1996; Soler et al., 2003), GRO-IMP (Kniemeyer et al., 2006); LIGNUM (Perttunen et al., 1996; Wernecke et al., 2000), L-PEACH (Allen et al., 2005), CANONICAL MODELS (Renton et al., 2006). Photosynthesis is calculated at the level of each leaf or even at each polygon belonging to the triangular mesh that makes up the leaf surface, and is then integrated.

Once the phylloclimate is determined, a local module computes the photosynthesis of each leaf and hence its contribution to the whole plant biomass production. Although these FSPMs work at the phytomer level they are still far from calibration on real plants at this level. They simulate

growth using parameter values coming from literature. For example, the sink strength of individual organs is not identified from the plant architecture but taken from literature. The VICA model (Wernecke et al., 2000) deals with the inverse problem (estimation of parameters from measurement data) but fits the result of the simulation with the real plant at the compartment level, whereas this should be done at organ level for a real FSPM. A good fitting at compartment level does not imply a good fitting of the competing organs for their biomass, according to their location in the plant architecture. For VICA fitting at organ level will be part of the new version (Wernecke et al., 2007).

(a) (b)

Figure 7 Simulations of light interception and transpiration. (a) Light interception in a simulated 3D structure of Sunflower; (b) Transpiration of a digitalized coffee tree depending on light and temperature. Color from blue to red indicates gradient of increasing light intensity and temperature (From Dauzat et al, 1996, 1998)

Case of Coupling PBMs and Architectural Models

We take advantage of the sensible and efficient simplifications of PBMs for light interception and biomass production. Here we assume that a virtual plant exists with similar architecture compared to the real one (that undergoes various phylloclimates for each different leaf), whose leaf functioning is homogeneous at the cm² level. This assumption is relevant, since if the common pool concept works well, even if individual leaves have distinct functioning, the average functioning by leaf surface unit multiplied by the total leaf area, will give the same total biomass production.

Nevertheless, Eq. (2) must be adapted at the plant architecture level, because the LAI concerns the total leaf surface of plants per unit surface occupied. We adapt this formula for a single plant, thus light interception becomes:

$$I = \mathrm{Sp}\left(1 - \exp\left(-k\frac{\mathrm{Sl}}{\mathrm{Sp}}\right)\right) \tag{3}$$

Sl is the surface of functioning leaves of the plant and parameter Sp is called the "projection surface" of the plant. Eq. (1) then becomes:

$$\mathrm{Qp} = \mathrm{LUE} * \mathrm{PAR} * \mathrm{Sp}\left(1 - \exp\left(-k\frac{\mathrm{Sl}}{\mathrm{Sp}}\right)\right) \tag{4}$$

Qp is the growth rate per plant (g/m²/GC). The growth cycle (GC) is usually the observed phyllochron expressed in thermal time. Advantage of this formulation is that in real experiments Qp and Sl are

known (Qp can be deduced from the plant weight), so there is always a given Sp, solution of Eq. (4). the ratio Sl/Sp can be considered as "apparent LAI per plant" giving the best fit between observed and measured biomass production.

For a given population of plant density *d,* the area available per plant is Sd=*1/d.*

Equation (1) can be written as well as:

$$Q = \mathrm{LUE} * \mathrm{PAR} * d * \mathrm{Sd}\left(1 - \exp\left(-k\frac{d*\mathrm{Sl}}{d*\mathrm{Sd}}\right)\right)$$

We retrieve Eq. (1) for a plant population, where LAI =*d**Sl/(*d**Sd) by definition. But when the density is low, there is no guarantee that we get Sp = Sd meanwhile Eq. (4) still operates. We can deduce in this case that generally Sd > Sp, because the leaves are gathered around the stem and follow no longer the Poisson distribution. Sp plays a role similar to *Kc,* but at level of individual, it is an unknown parameter that has to be identified by the inverse method from the data. For tomato (Dong et al., 2006), and Maize (Guo et al., 2006; Ma et al., 2006) this method has been used successfully in planting density experiments. Results are as expected: for high densities we find: $\mathrm{Sp} \approx \mathrm{Sd}$ (Table 1).

We can see from the following array that for high density Sp is quite close to Sd that means the Lambert-Beer law works well. For low density (here for tomato) we have Sd > Sp. The GreenLab model here captures well the auto-shadow effect into the plant. It is a nice result that the model can assess by inverse method the projection surface Sp and consequently the spatial competition of a given plant, from the behaviour of its architecture.

Table 1 Comparison between the surface per plant calculated from planting density and the computed projection surface Sp optimized by GreenLab according to formula (4)

Crop at Different Densities	Surface/Plant (Sd =1/Density)	Surface/Plant Sp Computed
Tomato	1	0.2
Tomato	0.37	0.16
Tomato	0.089	0.085
Maize	0.36	0.30
Maize	0.18	0.23
Maize	0.09	0.13

We can consider two cases:

- For crops with high planting density, a constant Sp works well, because at the beginning the growth is independent of Sp and quickly, the canopy will get closed and Sp plays then the same role than Sd that is fixed.
- For low planting densities, we can assess that Sp is a function of Sl. We assume an allometric relationship between these two parameters: $\mathrm{Sp} = \mathrm{Spo} * \mathrm{Sl}^{\alpha}$.

This can follow a smooth LAI/plant evolution. Studies about the consequence of this Sp formulation, show that both Sp and consequently growth rate Qp still reach a limit if $\alpha < 1$.

Parameters Spo and α can be assessed from the growth process by inverse method, provided that there is at least two measured growth stages!

5 Modeling Biomass Transport and Partitioning

The biomass produced in the leaves is shared by the different competing organs and this is done in a different way according to PBMs and FSPMs.

Case of PBMs

The common pool of biomass (Fig. 8) makes all organs directly connected with the source and biomass transportation resistance is ignored (Heuvelink, 1999). Cost of respiration (depending of temperature), is often ignored, only net photosynthesis is taken into account.

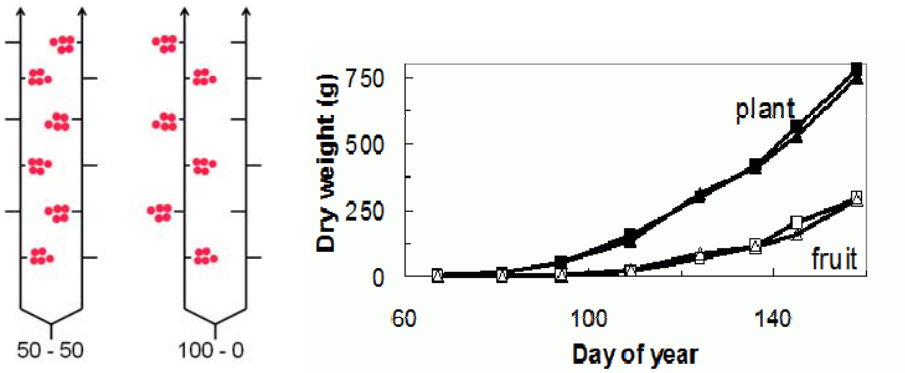

Figure 8 The common pool of biomass as illustrated by the effect of source-sink distance on the biomass partitioning. Tomato fruits located on one stem (triangle) or on two stems (square) on 2 plants with 50% of trusses removed. Both experiments give same biomass production and partitioning (Heuvelink, 1995)

So PBMs can focus directly on biomass partitioning. Sinks correspond usually to the demand of the compartments (stem, fruits) for the biomass. Only the relative sink strength is important. Biomass partitioning can be computed fast in this way. Some PBMs separate the vegetative compartment (stem + leaves + roots) from individual fruit (trusses) whose sink function is assessed by direct measurement of the potential growth rates (Heuvelink, 1999).

The growth rate of the organ *k*-aged in thermal time can be written as:

$$q_k = \frac{s_k}{\sum_i s_i} Q \tag{5}$$

It is proportional to the organ sink value s_k at the stage of growth *k*, the biomass supply available from the plant, and inversely to the plant demand (sum of sinks).

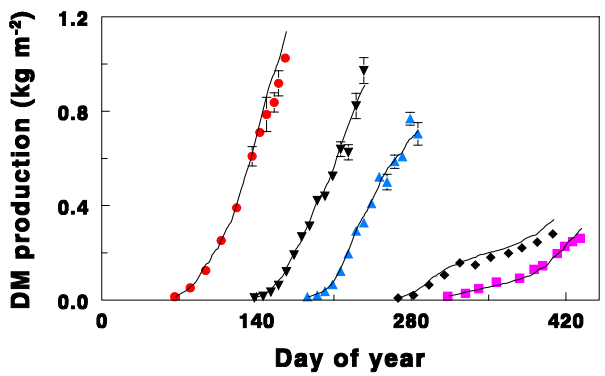

Figure 9 Tomato biomass prediction for different planting dates calculated by the TOMSIM model (Heuvelink, 1999)

Such PBMs work successfully and can compute for instance the yield of a tomato crop at different periods of the year, corresponding to very different climate conditions in the greenhouse (Fig. 9).

Under resource-limited conditions, PBMs must take into account also effects of water and/or nutrient stress (Maihol, 1997).

Case of FSPMs

Unlike the common assimilate pool in PBMs, the mechanistic approach of FSPMs endeavours to propagate the biomass production of each individual leaf, step by step through the geometrical network of the plant until each sink organ. Here architecture represents a transport-resistance system and according to a concentration gradient, the biomass will be shared between all the competing sinks until equilibrium is reached (Michin, 1996). For this, calculations on a complex network system need to be performed, in which both time and plant geometry are involved. Examples of such software are GRO-IMP (Kniemeyer et al., 2006; Wernecke et al., 2000), VICA (Wernecke et al., 2000) and L_PEACH (Allen et al., 2005). At present, in these models the inverse problem is not solved at organ level and these models cannot yet cope with real plants for yield prediction. Moreover, the number of "hidden" parameters (can not be measured directly) to compute is quite large. Biomass partitioning as underlined by Sievanen et al. (2006) can increase until 8 times the computing time needed to establish the plant development, because the geometrical structure must be explored during several iteration steps.

In theory, FSPMs have no limitations to simulate the plant functioning. For instance they integrate the neighbouring of source and sink organs as well as the phylloclimate. Particularly, modeling girth growth that is an important sink in trees cannot be computed by PBMs that do not simulate geometry. Fortunately crops have very little girth growth. Software as Lignum, L_peach and Grogra can deal with girth growth, although identifying sink strength remains a problem (inverse method can not be used).

Case of Coupling PBMs and Architectural Models

In coupling PBMs and architectural models, the assumption of a common pool of biomass used in PBMs is maintained. Equation (5) is used to calculate the growth rate of organs. An improvement is to define Eq. (4) as the form of a dynamical system. Leaf surface depends on the incoming biomass that ensures leaf growth. Geometry can be eliminated. For GreenLab, it takes the form of a dynamical system with several equations:

Computing plant development

$$\left[N_t^k\right] = t \cdot \left[u_k\right] + \sum_{i=1}^{t-1} \sum_{j=k+1}^{m} \left(n_{k,j} \cdot \left[N_i^j\right]\right) \quad (6)$$

(k varies from m to 1)

Equation (6) expresses the production of the dual scale automaton according to its parameterization (Fig. 4). m is the maximum physiological age found in the plant and n_{kj} is the number of axillary meristems with physiological age j, on a phytomer with physiological age k (botanical data). This equation computes the number $[\boldsymbol{N}_t^k]$ of organs having the physiological ages from k+1 $\rightarrow m$, when the plant has the chronological age $\boldsymbol{t}$. It uses the factorization of the architecture in substructures. The knowledge of $\left[\boldsymbol{N}_t^k\right]$, gives the information about plant development i.e. the number of produced organs. The computing time of development is then proportional to the chronological age.

Computing plant demand

$$D(i) = \sum_{o} \sum_{j=1}^{i} N_0(i-j+1)\, p_o(j) \quad (7)$$

The plant demand is a scalar product between all the population of organs according to both physiological and chronological ages with their corresponding sinks values.

Computing biomass of organs

$$q_o(n,i) = \sum_{j=i}^{n} p_o(j-i+1) * \frac{Q_m(j-1)}{D(j)} \tag{8}$$

The biomass of an organ is the sum of the organ growth rates, computed based on the proportional sink strengths. Functions p_o in GreenLab are Beta law shaped. This fulfils the biomass partitioning.

Computing the leaf surface area

$$S(n) = \frac{1}{\mathrm{e}} \sum_{i=n-ta+1}^{n} N_a(i).q_a(n,i) \tag{9}$$

The leaf area S is calculated as the sum of individual leaf biomass divided by the SLW (e in Eq. (9)).

Computing the biomass production of an individual plant

$$Qp(n) = \frac{\mathrm{LUE.PAR}(n).\mathrm{Sp}}{k}\left(1-\exp\left(-k\frac{S(n)}{\mathrm{Sp}}\right)\right) \tag{10}$$

Eventually Eq. (10) is similar to Eq. (1).

Dynamical equation of GreenLab

$$Qp(n) = \frac{E(n)\mathrm{Sp}}{r.k}\left(1-\exp\left(-\frac{k}{e.\mathrm{Sp}}\sum_{i=n-t_a+1}^{n} N_a(i)\sum_{j=i}^{n}\frac{p_a(j-i+1)Qp(j-1)}{D(j)}\right)\right) \tag{11}$$

Combining Eqs. (6) up to (10) results in a calculation of plant growth rate depending only on the previous growth rates and developments without any references to plant architecture like Eq. (11)! r is a calibration coefficient and $E(n)$=LUE*PAR(n) represents the converted light energy for the date n.

This equation is very useful for various purposes and allows studying the model behaviour, the sensitivity to parameters, and performing efficient optimization thanks to the derivations of the formula. Moreover linked to geometrical rules, equation (11) allows rebuilding the 3D plant architecture if needed.

The Inverse Problem

The plant is a set of organs whose individual biomasses are a target for the model. Each population of organs of same category has a corresponding growth rate given by Eq. (8) for the average individual one.

Hidden parameters are the parameters of the sink functions Po and the projection surfaces Sp. The generalized least square method running on the Eqs. (6) to (10) finds easily the optimized parameters that fit best the model to the real plant. This has been done successfully on all the studied plants with GreenLab model (Kang and De Reffye, 2006). Plants are measured for several

growth stages and all organ biomasses are fitted simultaneously with the matching output values computed by the model according to the optimized parameters. These parameters are few (less than 12) and belong to the source and sink functions.

It is not necessary to measure all the organs of the plant. In the first stages, measurements can be at the compartment level (aggregated data) to capture the growth and the last one at the phytomer level (Figs. 10 and 11, Ma et al., 2006).

It is important to see that the history of growth is carved in the plant architecture and one plant is theoretically sufficient to trace back the functioning story, meanwhile compartments give only punctual information on a stage of growth. Practically speaking it is better to get intermediate stages because it decreases the variances linked to the hidden parameter estimations, more over, it controls that one set of constant parameters, explains the dynamical growth. It is not possible to assess the sink variation function from measurements at compartment level alone. Constant sink strengths are sufficient at organ level to fit compartments. Introducing architecture allows capturing the sink variation because the same organ is present at different positions in the plant architecture.

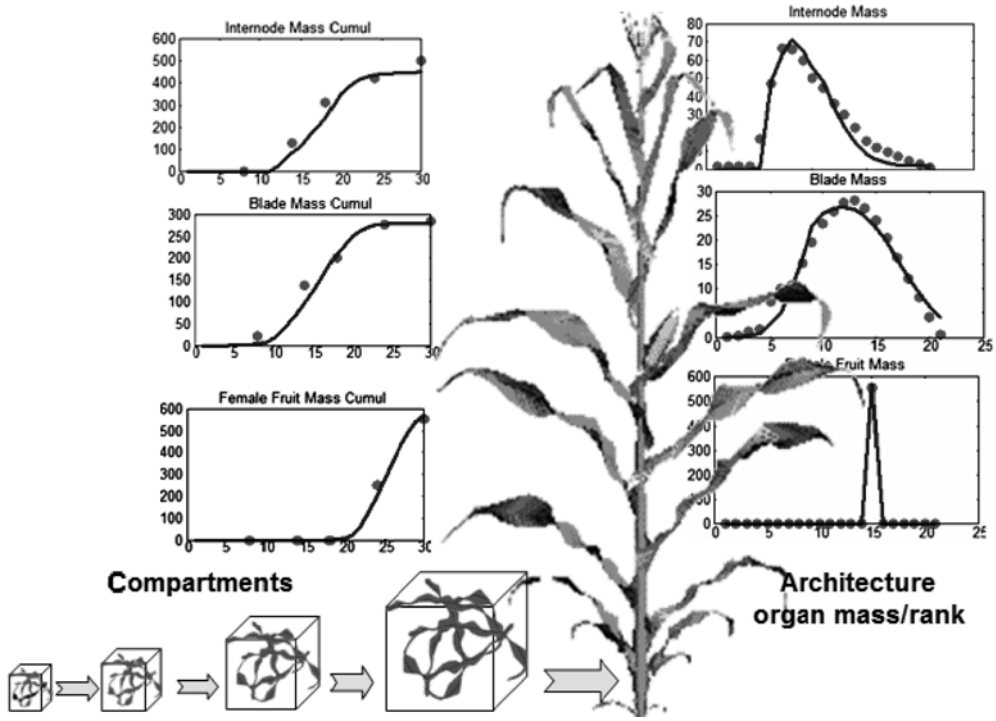

Figure 10 Fitting the growth of maize with sparse data using GreenLab (Ma, 2006)

Yield Prediction

Coupling PBMs and architectural models is expected to work at least better. To test this, Ma (2007) studied the prediction of maize yield in several years (Fig. 11). Yield predictions agreed well with observed yields and the estimated parameters were constant over the years (except SLW).

Girth Growth

For calculation of girth growth, plant structure is needed and PBMs can not do it. Nevertheless in fact, it is not necessary to use the plant architecture for the biomass transportation. It is still possible to keep the common pool and to build the stack of rings inside branches and trunk. It is known that

the ring thickness of a branch inside the tree architecture is proportional to the leaf area seen above. The factorization in GreenLab allows knowing the volume of the canopy above any point of a given substructure. Thus a powerful algorithm can build the stack of rings of any branch in the tree depending of the sink for girth growth (Fig. 12). It can also assess the proportion of assimilates going down to the roots or climbing to the crown at a branching point.

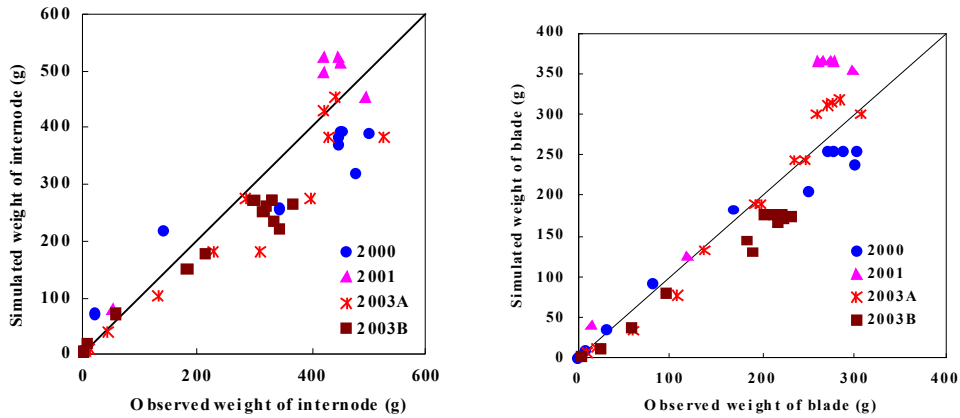

Figure 11 A four year experiment on Maize. Parameters are computed for the year 2000. These values are used to predict the yield in the following years. Evapo-transpiration is computed with climatological data, and is converted to biomass using WUE. Specific leaf weight had to be adjusted as it changes according to climate or density (Ma, 2007)

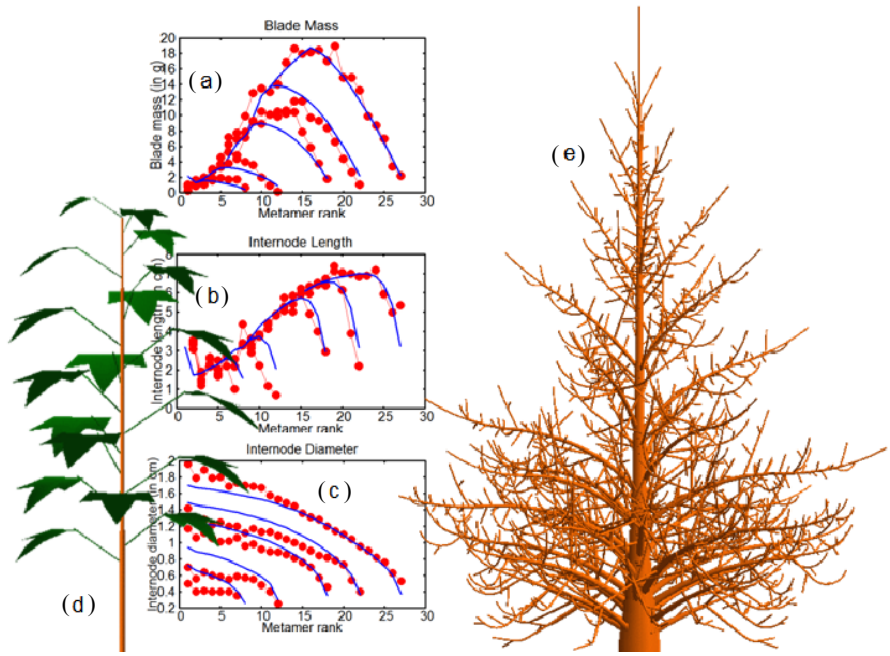

Figure 12 Simulation of girth growth with GreenLab
(a), (b), (c), (d): fitting of a single cotton stem (Zhan 2003). Leaf and internode parameters are determined from fitting on data of 5 growth stages. Length and diameter of the pith depends on allometry, and internode diameter is the sum of the stack of rings width and pith diameter at any phytomer from the stem. The simulated shoot is presented in (d). The tree (e) shows the results of girth growth according to GreenLab algorithm on a complex structure

6 Conclusion: Why Architecture for Plant Growth Models?

The reason for architecture in plant growth models is not only to obtain a 3D visualisation, as for crops external quality is not important, except for ornamentals.

Although PBMs give good yield prediction for most crops, they provide little information on the yield components that are hidden in the parameters of the plant development and those of the source-sink functioning at organ level. Parameter identification is of major interest for genetics and agricultural sciences because these parameters can provide orientations for selection in breeding (QTLs (Letort et al., 2006) and optimization for planting density (Cournède et al., 2006), irrigation (Wu et al., 2005). Plant architecture is necessary to understand not only the yield components of the crop, but also the plant functioning, as the data contain information necessary for retracing the history of growth and development that the compartment data fail to provide.

This article aims to show that between the simple PBMs that follows the main traits of plant growth depending of environment and LAI, and the complex FSPMs that try to mimic the internal mechanisms of growth and development using the plant architecture as a support, it exists a middle way to use plant architecture for models in agronomy.

Moreover, until now FSPMs do not deal with crop production and focus on the details of plant functioning. They do not address the interactions between plant functioning and architecture.

Integrating plant architecture could improve PBMs, giving them the strong features of FSPMs without introducing too much complexity that would prevent applications in agriculture. This is the result of introducing a factorization in the plant development that authorized a fast computing of the plant demand, and keeping the common pool of biomass and not introducing transport resistance.

The GreenLab model is summarized by a set of powerful dynamic equations, it allows computing quickly the biomass production and partitioning, and moreover it makes the inverse problem, (i.e. the computation of the hidden parameters for development and growth that control the yield), rather easy. These equations allow for derivatives and thus differential mathematics, optimizations and optimal control.

GreenLab can not only provide accurate growth and yield predictions as PBMs do, but also provides the main features of FSPMs without giving up the PBMs philosophy. Introducing plant development is necessary if obtaining the sizes of individual organs and control of their growth rates step by step is needed. Size of organs also contributes to the quality of the yield; often the weight of the compartment of interest is not sufficient to assess the economical value.

In the model, populations of individual organs of the same category are pooled in compartments both for number of organs and biomass. Because it is not necessary to record the plant structure (i.e. the organ position in the architecture), measurement is easy. The number, weight and age of organs of the same kind must be known and this allows sensible sampling in complex structures. It is encouraging to use this model for agricultural issues, as for PBMs users the extra information needed on plant development is limited compared to FSPMs.

A drawback of PBMs pointed out previously has already been overcome by the GreenLab model: stochastic cases (Kang et al. 2008), feedbacks between growth and development (fruit abortions, rhythmic growth, (Mathieu 2007) and eventually 3D visualization of cultivated ornamental crops as chrysanthemum (Kang et al 2006). The passage from the individual plant functioning to the stand functioning is implicit in this model that eventually provides the same kind of output than PBMs but from a lower scale of observation. Greenlab combines the strong points of both PBMs and FSPMs and we expect GreenLab can be used successfully as a tool for crop physiologists and geneticists.

References

Allen M, Prusinkiewicz P, and DeJong T (2005) Using L−systems for modeling source−sink interactions, architecture and physiology of growing trees: the L−PEACH model. New Phytol. 166: 869 – 880.

Barczi J F Rey H, Caraglio Y et al. (2008) AmapSim: A Structural Whole-plant Simulator Based on Botanical Knowledge and Designed to Host External Functional Models. Ann Bot 101: 1125 – 1138.

Barthélémy D, and Caraglio Y (2007) Plant Architecture: A Dynamic, Multilevel and Comprehensive Approach to Plant Form, Structure and Ontogeny. Ann Bot 99: 375 – 407.

Chelle, M (2005) Phylloclimate or the climate perceived by individual plant organs: what is it? how to model it? what for? New Phytol 166:781 – 790.

Cournède P-H, Mathieu A, Houlier F, et al (2008) Computing Competition for Light in the GREENLAB Model of Plant Growth: A Contribution to the Study of the Effects of Density on Resource Acquisition and Architectural Development. Ann Bot 101:1207 – 1219.

Dauzat J, Eroy NM (1996) Simulating light regime and intercrop yields in coconut based farming systems, Eur J Agron 7 : 63 – 74.

Dauzat J, Rapidel B, Berger A (1998) Simulation of leaf transpiration and sap flow in virtual plants : description of the model and application to a coffee plantation in Costa Rica. Agric For Met 109: 143 – 160.

Dong QX, Louarn G, Wang YM et al. (2006) Modeling the phenotypic plasticity of the tomato crop (*Lycopersicon esculentum* Mill.) in response to light and planting density using the structural-functional model GreenLab. PMA06: *The Second International Symposium on Plant Growth Modeling, Simulation, Visualization and Applications*, 13-17 November. Beijing, P. R. China. Poster.

Drouet JL and Pagès L (2003) GRAAL: a model of GRowth, Architecture and carbon Allocation during the vegetative phase of the whole maize plant: model description and parameterisation. Ecol Model 165:147 – 173.

Fournier C and Andrieu B (1999) Adel-maize: an L-system based model for the integration of growth processes from the organ to the canopy. Agronomie 19:313 – 327.

Godin C, Guedon Y, Costes E, Caraglio Y (1997) Mesuring and analysing plants with the AMAPmod software. in: Michalewicz MT (Ed), Plants to Ecosystems:Advances in *Computational Life Sciences I*, CSIRO Publishing, Melbourne, 1997, pp 63 – 94.

Guo Y and Li BG (2001) New advances in virtual plant researches. Chinese Sci Bul 46: 888 – 894.

Guo Y, Ma Y, Zhan Z, Li B et al (2006) Parameter optimization and field validation of the functional-structural model GREENLAB for maize. Ann Bot , 97: 217 – 230.

Hallé F, Oldeman R A A and Tomlinson P B (1978) *Tropical Trees and Forests*. Springer Verlag, Berlin, Heidelberg, New-York, 441p.

Heuvelink E (1995) Dry matter partitioning in a tomato plant: One common assimilate pool? J Exp Bot 46: 1025 – 1033.

Heuvelink E (1999) Evaluation of a dynamic simulation model for tomato crop growth and development. Ann Bot 83: 413 – 422.

Hu BG, de Reffye P, Zhao X Yan HP and Kang, M.Z (2003) GreenLab: a new methodology towards plant functional-structural model - Structural aspect. In: B.G. Hu et M. Jaeger (Eds) *Plant growth modeling and application - Proceedings - PMA03*. Beijing, Chine: Tsinghua University Press, Springer, pp. 21 – 35.

Kang MZ Cournède PH De Reffye P, Auclair D and Hu BG (2008) Analytical study of a stochastic plant growth model: Application to the GreenLab model. Mathematics Computers Simulation 78: 57 – 75.

Kang MZ, Heuvelink E, and de Reffye P (2006) Building virtual chrysanthemum based on sink-source relationships: Preliminary results. Acta Hort, 718:129 – 136.

Kang MZ, de Reffye P (2006) A mathematical approach estimating source and sink functioning of competing organs In: Functional-Structural Plant Modeling in Crop Production (eds.: J. Vos, L. F. M. Marcelis, P. H. B. deVisser, P. C. Struik, J. B. Evers). Proceedings of a workshop held in Wageningen (NL), 5.-8. 3. Kluwer, Dordrecht.

Kniemeyer O, Buck-Sorlin G, Kurth K (2006) GroIMP as a platform for functional-structural modeling of plants. In: Vos J, Marcelis L F M, deVisser P H B, Struik P C, Evers J B (eds.) Functional-Structural Plant Modeling in Crop Production, Kluwer, Dordrecht.

Letort V, Mahe P, Cournède P-H, Reffye P, and Courtois B (2007) Quantitative Genetics and Functional–Structural Plant Growth Models: Simulation of Quantitative Trait Loci Detection for Model Parameters and Application to Potential Yield Optimization. Ann of Bot 1–12, doi:10.1093/aob/mcm197.

Ma Y, LI BG, Zhan ZG et al. (2007) Parameter stability of the functional-structural plant model GreenLab as affected by variation within populations, among seasons and among growth stages. Ann Bot 99: 61 – 73.

Ma Y, Wen M, Guo Y et al. (2006) Evaluation of functional-structural model GreenLab-Maize with sparse experimental data, PMA06: *The Second International Symposium on Plant Growth, Modeling, Visualization and Applications*, 13-17 novembre 2006, Beijing, P.R. China.

Mailhol JC, Olufayo A A, Ruelle P (1997) Sorghum and sunflower evapotranspiration and yield from simulated leaf area index. Agric Water Manag. 35: 167 – 182.

Marcelis LFM, Heuvelink E, Goudriaan J (1998) Modeling biomass production and yield of horticultural crops: a review. Sci Hort 74 : 83 – 111.

Mathieu A, Cournède P-H , Barthelemy D and DE Reffye P (2008) Rhythms and Alternating Patterns in Plants as Emergent Properties of a Model of Interaction between Development and Functioning. Ann Bot 1–10, 2008 (in press). doi:10.1093/aob/mcm171.

Minchin, PEH and Thorpe, MR (1996) What determines carbon partitioning between competing sinks? J Exp Bot, 47:1293 – 1296.

Perttunen J, Sievänen R, Nikinmaa E et al (1996) LIGNUM: a tree model based on simple structural units, Ann Bot 77: 87 – 98.

Renton M, ThornbY D, Hanan J (2006) Canonical modeling In: Functional-Structural Plant Modeling in Crop Production (eds.: J. Vos, L. F. M. Marcelis, P. H. B. deVisser, P. C. Struik, J. B. Evers). Proceedings of a workshop held in Wageningen (NL), 5.-8. 3. 2006. Kluwer, Dordrecht.

Rey H, Dauzat J, Chenu K, et al. (2007) Using a 3D virtual sunflower to simulate light capture at organ, plant and plot levels : contribution of organ interception, impact of heliotropism and analysis of genotypic differences. Ann Bot 101 :1139 – 1151.

Sievanen R, Nikinmaa E, Nygren P, et al. (2000) Components of functional-structural tree models. Ann For Sci 57: 399 – 412.

Soler C, Sillion F, Blaise F, de Reffye P (2003) An Efficient Instantiation Algorithm for Simulating Radiant Energy Transfer in Plant Models ACM Transactions On Graphics 22: 204 – 233.

Wernecke P, Muller J, Dornbusch T et al. (2007) The virtual crop-modeling system 'VICA' specified for barley. In : Functional-structural plant modeling in crop production. Vos J, Marcelis M, de Visser P, Struik P, Evers J, eds. Kluwer Academic Publishers. Wageningen UR Frontis Series. pp53 – 64.

Wernecke P, Buck-Sorlin G. and Diepenbrock W (2000) Combining process- with architectural models: the simulation tool VICA. Sys An Model Sim 39:235 – 277.

Wu L, Le Dimet F, Hu B G et al. (2005) A Water Supply Optimization Problem for Plant Growth Based on GreenLab Model. ARIMA Journal, 194 – 207.

Zhan Z G, de Reffye P, Houllier F, Hu B G (2003) Fitting a structural-functional model with plant architectural data. In: Hu BG, Jaeger M (eds.). *Proc. Plant Growth Modeling and Applications (PMA'03)*, Beijing, China. Tsinghua University Press and Springer, 236 – 249.

A Functional-Structural Plant Model—Theories and Its Applications in Agronomy

Meng-Zhen Kang [1], Paul-Henry Cournède [2], Amélie Mathieu [2], Véronique Letort [2], Rui Qi [1,2], Zhi-Gang Zhan[3]

(1 LIAMA, Institute of Automation, Chinese Academy of Sciences, 100080, Beijing, China)
(2 Laboratory of Applied Mathematics, Ecole Centrale Paris, 92295 France)
(3 College of Resources and Environmental Sciences, China Agricultural University, 100094, Beijing, China)

Abstract: Functional-structural plant models (FSPM) simulate plant development and growth, usually accompanied with visualization of the plant 3D architecture. GreenLab is a generic and mechanistic FSPM: various botanical architectures can be produced by its organogenesis model, the growth rate is computed from leaf area, and the biomass partitioning is governed by the sink strength of growing individual organs present in plant structure. A distinguished feature of GreenLab model is that, the plant organogenesis (in terms of the number of organs) and growth (in terms of organ biomass) are formulated using dynamic equations, aside simulation software. This facilitates analytical study of model behaviour, bug-proof of simulation software, and application of efficient optimization algorithm for parameter identification and optimal control problems.

Currently several levels of GreenLab model exist: ① the deterministic one (GL1): plants have a fixed rule for development without feedback from the plant growth; ② the stochastic level (GL2): pant development is probabilistic because of bud activities, which has influence on plant growth; ③ the feedback model (GL3): the plant development is dependent on the dynamic relationship between biomass demand and supply (and in turn the environment).

This paper presents the typical GreenLab theories and applications in past ten years: ① calibration of GL1 for getting sink and source functions of maize; ② features of GL2 and its application on wheat plant; ③ rebuilt of the rhythmic pattern of cucumber using GL3;④ optimization of model parameters for yield improvement, such as wood quantity (for trees); ⑤ the possible introduction of genetic information in the model through detection of quantitative trait loci for the model parameters; ⑥ simulation of plant competition for light.

Keywords: GreenLab, FSPM, GL1, GL2, GL3, plant optimization, QTL, plant competition

1 Introduction

In past years, Functional-Structural Plant Models (FSPMs) were attracting interest from plant modellers (Vos et al., 2007). GreenLab methodology, began to develop around ten years ago, have been applied for several different kinds of crops, including maize (Guo et al., 2006; Ma et al., 2007; Ma et al., 2008), tomato (Dong et al., 2008), chrysanthemum (Kang et al., 2006), pine tree (Guo et al., 2007), arabidopsis (Letort et al., 2007), and wheat (Kang et al., 2008). Other undergoing GreenLab-based application for various purposes includes modeling on beech tree, rice, cotton, cucumber, sweet pepper, etc. On the other hand, theoretical work on GreenLab went on in parallel, includes the formalism of the organogenesis model (de Reffye et al., 2003), structure factorization of complex

plant structure for fast computation (Cournède et al., 2006), analytical computation of mean and variance of stochastic model (Kang et al., 2007), generation of rhythmic pattern of branch or fruits from GreenLab dynamic system (Mathieu et al., 2007), link between GreenLab parameters and QTL (Letort et al., 2008), computation of inter-plant competition (Cournède et al., 2008). Software based on GreenLab model has been developed for simulation and parameter identification, including CornerFit (for single-stem plants), GreenScilab (open-source and generic), and DigiPlante (generic and efficient). In this paper, we review the general form of GreenLab model, present its different levels, and its applications on real plants. Three theoretical works are presented to show future possible applications.

2 General Presentation

A time step (a growth cycle, GC) in GreenLab model corresponds to the temperature sum it takes to generate a growth unit (GU), being a metamer for crops or an annual axis for trees. The plant development is simulated using automaton (Zhao et al., 2001). All organs (leaf blade and petiole, internode pith, layer, female and male organs, root system) are sinks that share biomass from a common pool. The sink strength of an organ can vary with time. The biomass of each organ is a result of biomass competition in each GC. From its biomass, the size of each organ is computed. Beside the seed that provide biomass in initial GCs, leaf is the main source organ. The production of a plant is a function of green leaf area.

The number of GC since the appearance of an organ or a branch is called chronological age (CA). Another property of organs or buds/branches is physiological age (PA). PA is expressed in integer values too, being one for main stem. Branches are physiologically older than its parent axis, except the case of reiteration. The tip of an axis can mute into another physiological age. The maximum PA in plant is noted as P_m. Organs of the same CA and PA are supposed to have the same sink strength and thus the same biomass (except for internodes that can have secondary growth). Based on the notion PA, using substructure decomposition (Cournède et al., 2006), the number of organs in each GC can be computed with equations without resorting to simulation.

A highly compact form of GreenLab model can be expressed as in Eq. (1):

$$\begin{aligned} \boldsymbol{N}_{\mathbf{o}} &= f(P_{\mathbf{d}}, \boldsymbol{Q}, T) \\ \boldsymbol{Q} &= f(\boldsymbol{N}_{\mathbf{o}}, \boldsymbol{P}_{\mathbf{g}}, E) \end{aligned} \tag{1}$$

In Eq. (1), $\boldsymbol{N}_{\mathbf{o}}$ are the number of new organs of each CA and PA in plant structure at each growth cycle, O=B (blade), S (sheath), pith (P), layer (L), female (F), male (M), or root (R). $\boldsymbol{P}_{\mathbf{d}}$ is the vector of development parameters that define the plant topology, including the number and PA of leaves, buds, flowers and axillary buds in each kind of GU, the repetition times of GU in an axis before mutate into another PA, etc. T is the air temperature. In the model, the development speed of the plant, or number of days per GC, is mainly decided by the air temperature. $\boldsymbol{Q}$ include the biomass of a part of plant at each growth cycle: those of individual organs, a certain type of organs (say fruits), or the whole plant. E is the environmental data. $\boldsymbol{P}_{\mathbf{g}}$ is the vector of growth parameters that control the biomass production and partitioning among organs, includes:

(1) the relative sink strength of organs (P_O^p), p being PA of organs. That of blade in main stem is set to one as the reference, i.e. $P_B^1=1$;

(2) parameters of sink variation function (φ_O^i) that describe the change of sink strength of individual organs, i being CA of organs. The actual sink strength of an organ of PA p and CA i is thus $P_O^p \varphi_O^i$;

(3) the empirical parameters of source function (β and γ *in* Eq. (3));

(4) the functioning duration (t_f) and expansion duration (t_x) of organs;

(5) internode allometric parameters and specific leaf weight (e).

The total demand for biomass of plant at GC n is computed as sum of sink strength of all growing organs, as in Eq. (2):

$$D_n = \sum_{\mathrm{O}} \sum_{p=1}^{P_m} \sum_{i=1}^{t_{xo}} N_{\mathrm{O}}^{p,n-i+1} P_{\mathrm{O}}^{p} \varphi_{\mathrm{O}}^{i} \tag{2}$$

$N_{\mathrm{O}}{}^{p,n\text{-}i+1}$ is number of organ O of PA p and CA i at plant age n. A commonly used biomass production function of GreenLab is inspired by the Beer-Lambert law of light extinction:

$$Q_n = E_n \beta (1 - \exp(-\gamma S_n)) \tag{3}$$

Where β, γ are empirical model parameters estimated by model inversion, S_n is the total green leaf area of the plant at growth cycle n.

The biomass increment of an organ is a function of biomass supply and demand:

$$\Delta q_{\mathrm{O},n}^{p,i} = P_{\mathrm{O}}^{p} \varphi_{\mathrm{O}}^{i} \frac{Q_{n-1}}{D_n} \tag{4}$$

The biomass of an organ is the sum of increment since its appearance:

$$q_{\mathrm{O},n}^{p,i} = \sum_{j=1}^{i} \Delta q_{\mathrm{O},n-j+1}^{p,j} = \sum_{j=1}^{i} P_{\mathrm{O}}^{p} \varphi_{\mathrm{O}}^{j} \frac{Q_{n-j}}{D_{n-j+1}} \tag{5}$$

From Eq. (5), it can be seen that the biomass of an organ depends on the ratio (Q/D) during its life span. Although organs of the same type and PA have the same sink strength in the model, their final biomasses are not necessary the same if they appear at different moments. In this sense, the organ architecture records the growth history of the plant.

3 Three Levels of the GreenLab Model and Their Applications

Different levels of GreenLab model have been developed, namely GL1, GL2, and GL3. Among them, GL1, the deterministic level, is the common part. An important issue of model application is parameter identification. Part of the parameters can be observed directly, such as specific leaf weight, internode allometric parameter, development parameters (case of deterministic model), functioning and expansion time of organs. Organ sink strength, sink expansion functions, and empirical parameters for biomass production, are difficult to measure directly. These (hidden) parameters can be estimated using optimization algorithms aiming at minimizing the model output and measured data. Below we present the parameterizing in GL1, and extra features in GL2 and GL3.

3.1 GL1 and Parameter Identification for Maize

GL1, the basic version, has been applied to simulate many plants: maize (Ma et al., 2007), pine tree (Guo et al., 2006), arbidobisis (Letort et al., 2008), chrysanthemum (Kang et al., 2006), etc. In GL1, the plant development (and consequently the number of organs) is not influenced by the biomass

supply, but follows a fixed rules. The form of GL1 is thus differs from Eq. (1):

$$\begin{aligned} \boldsymbol{N}_{\mathbf{O}} &= f(\boldsymbol{P}_{\mathbf{d}}, T) \\ \boldsymbol{Q} &= f(\boldsymbol{N}_{\mathbf{O}}, \boldsymbol{P}_{\mathbf{g}}, E) \end{aligned} \tag{6}$$

In the case that the plant is of single stem structure, the numbers of organs are easy to compute, and one can concentrate on the identification of sink-source parameters. For field plants, the plant growth rate Q_n, and organ growth rate $\Delta q_{o,n}$ are internal and transient variables, which are technically difficult to be directly measured. Therefore, the source and sink functions cannot be separately determined by using classical fitting methods. On the other hand, the plant architecture and organ biomass are accumulative results of the dynamical processes since the plant emergence, including plant growth and organ development. From the modeling point of view, since GreenLab model output variables (number, size and mass of organs) implicitly and nonlinearly depend on the hidden parameters in the recursive simulation process, these parameters can be identified through inverse modeling, i.e., the parameter values are determined by minimizing the differences between observed and simulated data. When this is achieved, GreenLab model can fit best to plant morphological and architectural data observed at several points of time. There are several different optimization algorithms available to minimize the proposed objective function, for example, the Levenberg-Marquardt method, genetic algorithms, or stochastic methods. The Levenberg-Marquardt method is practically proved more efficient than the others in terms of computation time.

For maize, under moderate density, the final structure of the maize plant consists of four types of organs: the main stem, the leaf sheathes and blades, a tassel (the male organ) at top, and one or several ears (the female organs) set at different nodal positions along the stalk. For maize, the variation of sink strength of individual organs was taken as the form of Eq. (7):

$$\varphi_{\mathrm{O}}^{i} = \begin{cases} g_{\mathrm{O}}^{i} / \mu_{\mathrm{O}} & 1 \le i \le t_{x\mathrm{O}} \\ 0 & i > t_{x\mathrm{O}} \end{cases}$$

where

$$g_{\mathrm{O}}^{i} = \left(\frac{i-0.5}{t_{x\mathrm{O}}}\right)^{\alpha_{\mathrm{O}}-1} \left(1-\frac{i-0.5}{t_{x\mathrm{O}}}\right)^{\beta_{\mathrm{O}}-1} \tag{7}$$

$$\mu_{\mathrm{O}} = \max\{g_{\mathrm{O}}^{i} \mid 1 \le i \le t_{x\mathrm{O}}\}, \mathrm{O} = \mathrm{B,S,I,F,M}$$

There are 12 parameters to be estimated for maize plants, including two empirical parameters of the source function (β and γ in Eq. (3)), and ten parameters of the sink functions (P_{O} in Eq. (2) and α_{O} in Eq. (7), o = B, S, I, F, M, denoting leaf blade, sheath, internode, ear and tassel, respectively, $\alpha_{\mathrm{O}} + \beta_{\mathrm{O}} \equiv 5$ for all organs).

During the course of plant development and growth, plants were regularly sampled and measured in detail, including size (length, diameter, area) and fresh or dry mass of each organ. The data were stored in a specified structure according to the position, type and attribute of organs. From these data the target was constructed for the model to fit. In order to get an estimate of the source and sink parameters, we use the weighted least-square criterion:

$$\phi(\boldsymbol{\theta}) = (\boldsymbol{Z} - F(\boldsymbol{\theta}))^{\mathrm{T}} \boldsymbol{W} (\boldsymbol{Z} - F(\boldsymbol{\theta})) \tag{8}$$

where $\boldsymbol{Z}$ is the target vector consisting of measurement data on plant samples at several stages; $\boldsymbol{\theta}$ is

the parameter vector to be estimated, a subset of $\boldsymbol{P}_g$; $F(\boldsymbol{\theta})$ is a vector function (i.e., the recursive simulation equations) with respect to $\boldsymbol{\theta}$, whose components are simulated data corresponding to $\boldsymbol{Z}$; $\boldsymbol{W}$ is a positive definite matrix which weights the various observations.

GL1 model were fitted to three stages of maize plants. The fitting results are shown in Fig. 1. Based on the calibrated parameters, the model was tested against independent data from different years (Ma et al., 2007) and different population densities (Ma et al., 2008).

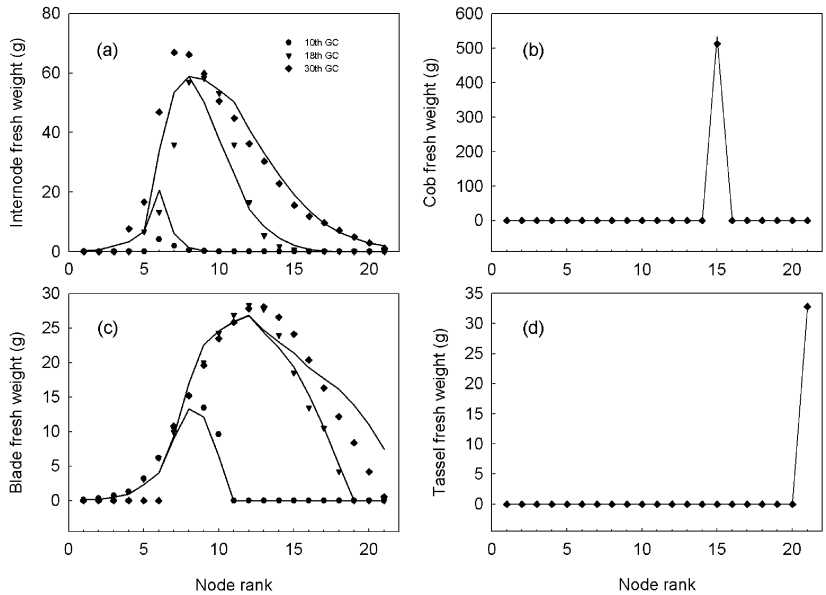

Figure 1 Simultaneous fitting of GL1 to measured data at three ages (i.e., 10, 18, and 30 GC) for maize plants. Target data are organ fresh weights (a) for internode, (b) for the cob, (c) for leaf blade, and (d) for the tassel. Leaf sheath weights were also fitted (data not shown). Data are from YunTao Ma, China Agricultural University

3.2 GL2 and Case Study on Wheat

GL2 is a stochastic functional-structural plant model, having the same form as Eq. (6), whereas N_O are stochastic variables. It take into account the topology variations and its effect on plant functioning. The randomness of plant structures in GL2 is caused by bud activities, such as bud dormancy and bud death, which had been introduced for realistic visual simulation twenty years ago (de Reffye et al., 1988). For individual plants, N_O can be counted in Monte-Carlo simulation. For a plant population, however, it is time consuming to simulate thousands of samples to obtain an estimation of the mean and standard deviation. The solution is to use the analytical results through theoretical study on the model, as done in (Kang et al., 2007). Figure 2 shows three simulated stochastic trees at age 20; the mean and standard deviation of number of organs were computed through formula. The second step is to compute the biomass production Q in the context of GL2. As Q is a complex nonlinear function of N_O, a reasonable choice of computing its analytical mean and variance is to use differential statistics (Kang et al., 2007). The same computation need to be taken when the functional parameter, P_g, are also stochastic variables. Parameterizing of GL2 then concerns no more than fitting the analytical output of the model with the corresponding data, using the methods as for GL1.

GL2 feature is interesting for plants that show strong randomness in topology. First try of application was on wheat plant. Through introducing tiller bud outgrowth probability and tiller survival probability, the number of phytomers in tillers and the final remaining tillers were well fitted, as shown in Fig. 3. This prepared the second step of model calibration concerns fitting on biomass

production. The average plant, instead of individual plants, is fitted, representing the common plant among those of various topologies.

Figure 2 Stochastic tree simulated using a single set of functional and developmental parameters. Analytical mean and standard deviation of number of phytomers are 15120.1 and 3765.8 respectively

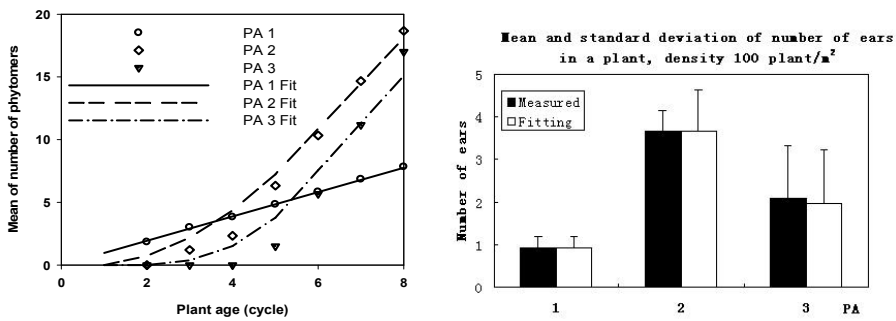

Figure 3 The number of phytomers and remaining ears in main stem (PA 1), primary tillers (PA 2), secondary tillers (PA 3) of a wheat plant, with population density 100 plants m^{-2} (data from CWE group, Wageningen University)

3.3 GL3 and Sweet Pepper

GL3 is a feedback version, having the same form as Eq. (1) regarding the biomass production but the topological events of the plant are assumed to be controlled by the ratio of biomass (Q; Eq. (3)) to demand (D; Eq. (2)), that is to say that the numbers of the different type of organs $\boldsymbol{N_O}$ are computed as functions of this ratio. It allows reproducing the plant phenotypic plasticity as the number of organs depending on the plant vigour.

As an example, this GL3 model can be used to simulate the cyclic patterns of fruits that have been observed in the sweet pepper plant (Marcelis et al., 2004) or in the cucumber plant (Marcelis, 1992). Fruit abortion can occur within the first days after fruit anthesis. In the GL3 model, we assume that if the ratio of biomass to demand (Q/D) is under a given threshold a few growth cycles after the fruit appearance, then the one will abort. Otherwise it will continue growing. This model was calibrated on pruned cucumber plants where the fruit growth is not limited by fruit initiation (Mathieu et al., 2008). Figure 4 shows the differences between the plant measurements and the model simulation. Fruits appeared on the plant when the ratio of biomass to demand exceeds a

threshold (Fig. 5) which explains the two waves of fruits on the stem. The cyclic patterns of fruits are explained as a consequence of the assimilate competition between organs.

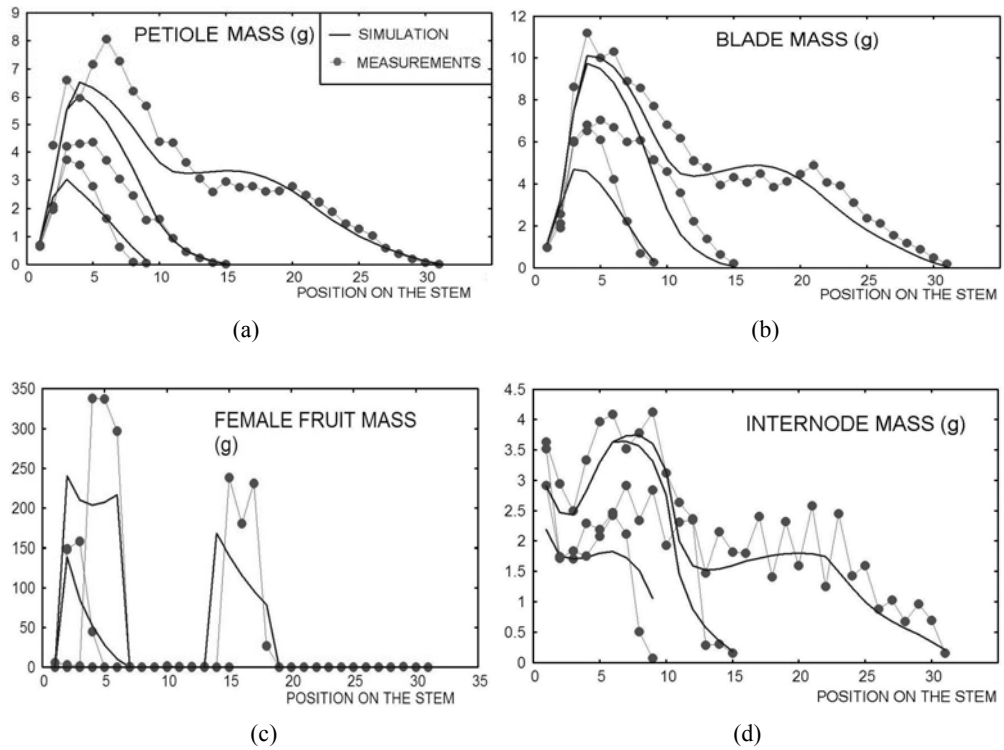

Figure 4 Simulation and measurement for a cucumber plant at three different ages (9GC, 15 GC, 31 GC). We used a multifitting procedure with the same set of source-sink parameters. The variations in the phytomer profile along the stem are a consequence of the competition between sinks

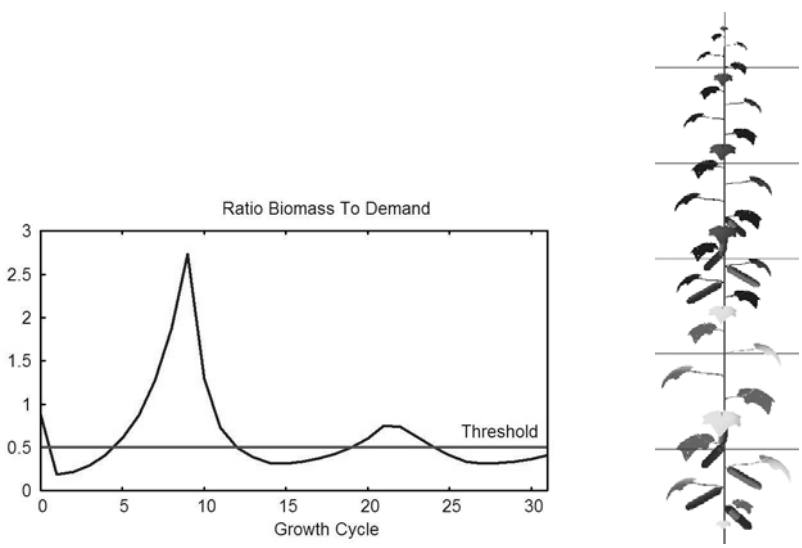

Figure 5 Ratio of biomass production to demand as a function of growth cycles and corresponding plant. Horizontal line represents threshold value (a). When the ratio exceeds this value, fruits grow on the main stem. Two timeframes in which fruit set can take place are observed (b)

4 Theoretical Study

The virtual plant itself as described by GreenLab model is a complex dynamic system. As it can behave close to real plants through model calibration, it is meaningful to do virtual experiment on GreenLab plants. The theoretical studies present here are experiments done in computer. These works may pioneer the future applications.

4.1 Possible Link with Quantitative Trait Loci (QTL)

In maize (Ma et al., 2007) and tomato (Dong et al., 2007), although the relative sink strength (of pith and fruit) vary, their expansion function remain the same for plants grown under different population densities. Consequently, it can be hypothesized that some of GreenLab parameters are species-specific and gene-based. Let Y denote the vector of these 'genetic' parameters. Introducing genetics in the model allows simulating plant reproduction and studying the evolution in time of a virtual population without requiring to time- and space- consuming experiments. In our model, the genotype of the plant is defined as a set of two vectors C_1 and C_2, representing the chromosomes (for sake of simplicity, only pairs of chromosomes are considered, although maize is generally haploid). The components of these vectors (alleles) are positive real numbers representing the parameter variation around a reference value Y_{ref}. An application f defines the rules of allele expression (dominance or additivity) and then the 'genetic' vector of GreenLab parameters Y is calculated as a product of matrices:

$$Y = C \times A \times f(C_1, C_2) \tag{9}$$

A is a matrix defining the influence of genes on each parameter, including pleiotropic rules (one gene has an influence on several parameters) or combinations of several gene effects on one parameter. C is a diagonal matrix introduced to ensure that the coefficients of Y are of the same order range (similar to barycentre calculation). Reproduction between two plants is simulated with realistic rules (Poisson law) driving the probability of crossing-over occurrences, see Letort et al. (2007) for details. It allows generating a virtual mapping population (recombinant inbred lines) to simulate the procedure of quantitative trait loci (QTL) detection, as done by geneticists on real plants (de Vienne, 2003). Their goal is to localize the chromosomal segments (called QTL) that contain genes of interest (influencing the yield, for instance). In our model, QTL detection is analogous to determination of the coefficients of matrix A that drives the link between the plant genotype and the model parameters. Results shown in Fig. 6 are consistent with the opinion defended in several recent papers that underlined the potential benefits of introducing physiological knowledge into breeding programs (e.g. Chapman et al., 2003; Hammer et al., 2006; Tardieu et al., 2003; Yin et al., 2003). Our study illustrated that QTL detection on model parameters is more accurate on model parameters than on the classical morphological data such as cob weight (Fig. 5). We conclude that this method is worthy to be tested on real plant populations. GreenLab parameters provide new criteria to renew the breeding process and to characterize model-based ideoptypes.

4.2 Yield Optimization

As GreenLab is a mathematical model, it is possible to apply various optimization algorithms. Optimization on plants helps revealing the relationship between sources and sinks, and guiding us the direction in cultivation and genetic operation.

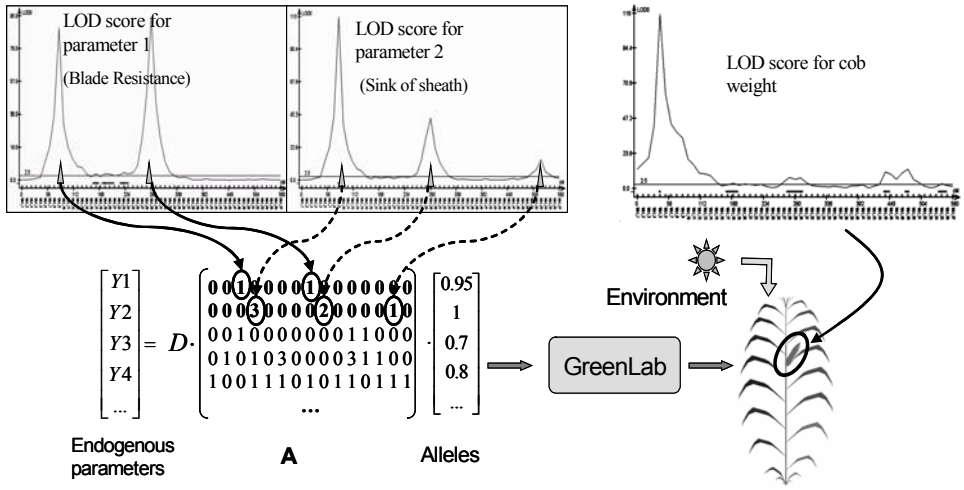

Figure 6 Simulation of QTL detection: GreenLab parameters (Y) are determined through a simple genetic model (matrix multiplication D, A) from the allele values. The graphs represent the results of QTL detection using a virtual mapping population when traits are model parameter compared to the case where the trait is cob weight

The optimization applications on GreenLab can be classified into two categories. If the parameters on which we optimize are related to genetic factors, such as sink variation of organs, their positions, etc, this kind of optimization problems belong to the classical multivariate optimization problem. If the variables to optimize are related to cultivation methods, such as water supply strategy (Wu et al., 2005), pruning strategy, etc, this kind of problems belongs to optimal control problem. Here we present several optimization problems of different aims based on GreenLab model.

There are two basic optimization problems: optimization with or without constraints. Most optimization problems for plant growth can be classified to constrained ones. For example, in the domain of forestry, the volume (quantity) and quality of wood are of primary importance, from both economic and mechanic point of view. In GreenLab model, wood quantity is impacted by the sink strength for cambial growth and a coefficient that determines how biomass for cambial growth is allocated to each internode. Optimization on these two parameters gives the best yield of wood. On the other hand, wood quality is related to the geometrical shape of a bole and branches, which is controlled by mechanical parameters. Given the total biomass for cambial growth, if too much biomass is allocated to the branches, the biomass partitioned to the bold is not sufficient. Otherwise, if allocation is too much for the bole, the load of the bole will be too heavy and fall down easily, see Fig. 7. As a result, besides maximizing the bole weight, the angle of the bold at the top is limited under a threshold. The optimization problem on wood quantity and quality for a tree is the classical optimization problem with constraints.

Pruning is a common cultivation action in agriculture or forestry, in order to make plants growing better and to get better yield. For example, most of side branches of tomatoes are removed to make sure fruit yield. Obviously the behavior of plant is modified if pruning is done during plant growth. A special case is to prune leaves, such as tea plant. Here leaf plays double roles: it is not only the source organs the provide biomass to whole plant, but also the yield. For this problem, we add a control variable that represents the proportion of number of leaves pruned among the living leaves. With the objective being maximizing pruned leaves, it is an optimal control problem. An ongoing optimization issue concerns the relationship among palm tree, insects and parasites. In this system, leaves produce biomass through photosynthesis, insects eat leaves and parasites suppress the population growth of insects. The optimization problem is complex because of interaction

among the three actors. It is necessary to study the population growth of insects and parasites, both affect significantly the growth behaviour of the palm tree. In addition, to avoid destroying leaves, pesticide is used. Considering the fact that pesticide kills not only insect adults but also parasite adults, and the price of pesticide is very expensive, in order to reduce the cost and increase its use efficiency (kill only insect adults), it is important to decide when pesticide is put to palm tree. This is again an optimal control problem.

(a) (b)

Figure 7 3D illustration of wood quality and quantity, for a 40 years old virtual tree. (a) trunk weight 5.04E+4g (b) trunk weight 2.45E+5g

4.3 Plant Competition

GreenLab is an individual-based plant growth model. However, for applications in agriculture and forestry, it has to be extended to the scale of plant population. For this purpose, inter-plant competition for light is taken into accounted, see Cournède et al. (2008).

For high density crops at full cover, the model should be equivalent to the classical equation of field crop production. For example, Howell and Musick (1985) showed that biomass production is proportional to crop transpiration T. It is driven by the potential evapotranspiration, the soil water content and the exposed green leaf surface area, evaluated using Beer-Lambert's extinction law. If at cycle n, E_n denotes the product of the potential evapotranspiration modulated by a function of the soil water content, k is the Beer-Lambert extinction coefficient related to leaf angular deviation and LAI_n is the leaf area index, T_n is estimated as:

$$T_n = E_n(1-\exp(-k\mathrm{LAI}_n)) \tag{10}$$

Finally, the biomass production per unit surface area Q_n^c is:

$$Q_n^c = \mu\ T_n = E_n\mu\ (1-\exp(-k\mathrm{LAI}_n)) \tag{11}$$

where μ is the Water Use Efficiency. From the individual plant production equation of GreenLab (Eq. 3) and in the case of a homogeneous crop of density d, the biomass production per unit surface area is directly deduced:

$$Q^c{}_n = E_n\,\beta\,d\,\left(1-\exp\left(-\eta S_n\right)\right) \tag{12}$$

Let $S_d=1/d$. For a homogeneous crop, $LAI_n = S_n/S_d$, by identifying (11) and (12), the empirical parameters β and η are thus given by $\beta=\mu S_d$ and $\eta=\mu/S_d$. This analogy helps us derive a general formulation for the individual plant production equation:

$$Q(n) = E(n)\,\mu\, S_p \left(1 - \exp\left(-k\, S(n)/\, S_p\right)\right) \tag{13}$$

S_p is a reference surface, such that $S_p=S_d$ in the case of homogeneous high density crops (see the application to maize for different densities in Ma et al., 2008). In the case of spatially heterogeneous crops (like rapeseed fields), a Voronoi tessellation can help determine the S_p of all individuals in the population. For tree communities, things can get far more complex. First, the reference surface can not be taken as a constant: it increases along plant growth. Cournède et al. (2008) proposed to model it as a function of the leaf surface: $S_p(n)=S_p^0(S_n/S_p^0)^\tau$. Simulation results are shown in Fig. 8, which shows the impact of density on tree architecture. Moreover, a generalized Poisson model of leaf repartition inside the canopy was proposed by Cournède and de Reffye (2007) to compute plant production for individuals in heterogeneous and potentially multi-specific tree stands. Although the simulation results are encouraging, this model still lacks field validation.

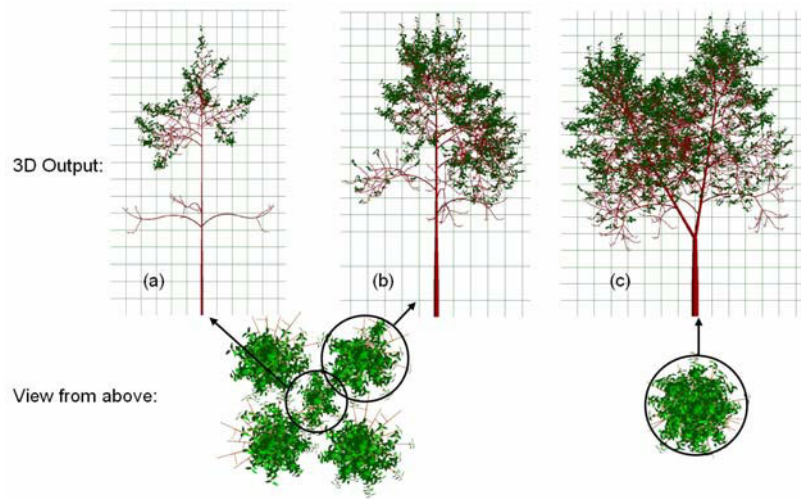

Figure 8 Simulation and visualization of trees (of the same species) growing in different conditions of competition: in a clump for individuals (a) and (b) and in open-field conditions for (c)

5 Conclusion and Discussion

The GreenLab model catches the main growth processes of plant by integrating the competition and production of assimilate inside plant structure. It is proved to be generic for plants of various architectural models through calibration study. Here it is worthy to mention that the success of model parameterizing is based on using the plant architecture, which records the growth history of the plant itself. To calibration the model is similar to solve a set of equations using the plant architecture as known values.

A good model helps in integrating knowledge, raising hypothesis and better understanding the object itself. GreenLab-based virtual plants serve these roles through model calibration, verification and optimization. When difference is discovered between model behaviour and the experimental data, it may reveal lack of certain important ecophysiological process in the model; further experimental studies may be required to provide knowledge or to verify hypothesis. On the other hand, pure

theoretical work pioneers the experiments by exploring into the field that is out of the limit of the real experiment, such as optimization of the parameters presented in this paper. In a spiral way, through interaction between theory and experiment, knowledge on plant can be increased. Such work is highly inevitably multi-disciplinary.

Although the shining future is to make realistic plant in computers that can serve fundamental and decision-making studies, this dream has not yet true. It is not because the techniques of computer graphics are not sufficient to render visually nice plants; instead, such techniques have much developed in past years. The challenge is from the kernel: the model. For GreenLab, to step forward this goal, the direction is the combination of GL2 and GL3, leading to a stochastic functional-structural plant model with interaction (GL4). The demand of this new generation has come already from plants in study, including sweet pepper, wheat, cucumber, etc.

In GreenLab, there are still several parameters that lack explicit physiological meanings. To stand on sound basis, it is necessary to link them with actual measurable values, to make it easier to compare the parameters of plants under different condition, or different species. Linkage between GreenLab and traditional process-based models is also worthy to be made to benefit each other.

Acknowledgements

Special thanks to the father of GreenLab, Dr. Philippe de Reffye. Thanks to Dr. Ma YunTao from China Agricultural University who provided data of maize. The work is supported in part by Natural Science Foundation of China (#60703043), Chinese 863 program (#2008AA10Z218 and # 2006AA10Z229).

References

Chapman S, Cooper M, Podlich D, Hammer G (2003) Evaluating plant breeding strategies by simulating gene action and dryland environment effects. Agron J 95: 99 – 113.

Cournède PH, Kang MZ, Mathieu A, et al (2006) Structural factorization of plants to compute their functional and structural growth. Simul 82: 427 – 438.

Cournède PH, de Reffye P (2007) A generalized Poisson model to estimate inter-plant competition for light. In: Fourcaud T, Zhang XP (eds) proc PMA06 - Plant growth model, simul, vis and their appl. IEEE Computer Society, Los Alamitos, California: 11 – 15.

Cournède PH, Mathieu A, Barthélémy D, et al (2008) Computing competition for light in the GreenLab model of plant growth: a contribution to the study of the effects of density on resource acquisition and architectural development. Ann Bot 101: 1207 – 1219.

Dong QX, Louarn G, Wang YM et al (2008) Does the structure-function model GREENLAB deal with crop phenotypic plasticity induced by plant spacing? A case study on tomato. Ann Bot 101:1195 – 1206.

Guo Y, Ma YT, Zhan ZG, et al (2006) Parameter optimization and field validation of the functional-structural model GreenLab for maize. Ann Bot 97: 217 – 230.

Hammer G, Cooper M, Tardieu F, et al (2006) Models for navigating biological complexity in breeding improved crop plants. Trends Plant Sci 11: 587 – 593.

Guo H, Letort V, Hong LX, et al (2007) Adaptation of the GreenLab model for analyzing sink-source relationships in Chinese Pine saplings. In: Fourcaud T, Zhang XP (eds) proc PMA06 - Plant growth model, simul, vis and their appl. IEEE Computer Society, Los Alamitos, California: 236 – 243.

Kang MZ, Heuvelink E, de Reffye P (2006) Building virtual chrysanthemum based on sink-source relationships: preliminary results. Acta Hortic 718: 129 – 136.

Kang MZ, Cournède PH, de Reffye P, et al (2007) Analytic study of a stochastic plant growth model: application to the GreenLab model. Mat Comput Simul 78: 57 – 75.

Kang MZ, Evers JB, Vos J, et al (2008) The derivation of sink functions of wheat organs using the GreenLab model. Ann Bot 101: 1099 – 1108.

Letort V, Cournède PH, Lecoeur J, et al (2007) Effect of topological and phenological changes on biomass partitioning in Arabidopsis thaliana inflorescence: a preliminary model-based study. In: Fourcaud T, Zhang XP (eds) proc PMA06-Plant growth model, simul, vis and their appl. IEEE Computer Society, Los Alamitos, California: 65 – 69.

Letort V, Mahe P, Cournède PH, et al (2008) Quantitative genetics and functional-structural plant growth models: simulation of quantitative trait loci detection for model parameters and application to potential yield optimization. Ann Bot 101: 1243 – 1254.

Ma YT, Li BG, Zhan ZG, et al (2007) Parameter stability of the functional-structural plant model GREENLAB as affected by variation within populations, among seasons and among Growth Stages. Ann Bot 99: 61 – 73.

Ma YT, Wen M, Guo Y, et al (2008) Parameter optimization and field validation of the functional structural model GreenLab for maize at different population densities. Ann Bot 101: 1185 – 1194.

Marcelis LFM (1992) The dynamics of growth and dry matter distribution in cucumber. Ann Bot 69: 487 – 492.

Marcelis LFM, Heuvelink E, Baan Hofman-Eijer LR, et al (2004) Flower and fruit abortion in sweet pepper in relation to source and sink strength. J Exp Bot 55: 2261 – 2268.

Mathieu A, Cournède PH, Barthélémy D, et al (2007) Conditions for the generation of rhythms in a discrete dynamic system. Case of a functional structural plant growth model. In: Fourcaud T, Zhang XP (eds) proc PMA06-Plant growth model, simul, vis and their appl. IEEE Computer Society, Los Alamitos, California: 26 – 33.

Mathieu A, Cournède PH, Barthélémy D, et al (2008) Rhythms and alternating patterns in plants as emergent properties of a model of interactions between development and functioning. Ann Bot 101: 1233 – 1242.

de Reffye P, Edelin C, Francon J, et al (1988) Plant models faithful to botanical structure and development. Computer Graphics 22: 151 – 158.

de Reffye P, Goursat M, Quadrat J, et al (2003) The dynamic equations of the tree morphogenesis GreenLab model. Research Report, INRIA-Rocquencourt, n^{o} RR – 4877.

Tardieu F (2003) Virtual plants: modeling as a tool for the genomics of tolerance to water deficit. Trends Plant Sci 8: 9 – 14.

de Vienne D (2003) Les marqueurs moléculaires en génétique et biotechnologies végétales. INRA Editions

Vos J, Marcelis LFM, de Visser PHB, et al (ed) (2007) Functional-structural plant modeling in crop production. Springer, Dordrecht

Wu L, Le Dimet FX, Hu BG, et al (2005) A water supply optimization problem for plant growth based on GreenLab model. ARIMA J: 194 – 207.

Yin X, Stam P, Kropff MJ, et al (2003) Crop modeling, QTL mapping, and their complementary role in plant breeding. Agron J 95: 90 – 98.

Zhao X, de Reffye P, Xiong FL, et al (2001) Dual-scale automaton model of virtual plant growth. Chin J Comput 24: 608 – 615.

New Approach for the Study of Source-Sink Dynamics on Maize

Rui Qi[1,2*], Yun-Tao Ma[2,3], Bao-Gang Hu[2], P. de Reffye[4,5], Paul-Henry Cournède[1]

(1 Ecole Centrale Paris, Laboratory of Applied Mathematics, 92295 Chatenay-Malabry, France)
(2 Institute of Automation, Chinese Academy of Sciences, LIAMA, Beijing 100080, China)
(3 China Agricultural University, Key Laboratory of Plant-Soil Interactions, Ministry of Education, College of Resources and Environment, Beijing 100094, China)
(4 INRIA-saclay, Parc Orsay Universite, 91893 Orsay cedex, France)
(5 CIRAD montpellier, AMAP, 34398, France)

Abstract: The objective of our work is to investigate the source-sink dynamics by applying the optimization methods to mathematical plant growth models. As a test case, maize is selected since it is one of the most widely cultivated cereals all over the world. An optimization problem with a single objective function on maximization of cob weight is investigated. The variables we optimized are specific parameters of the plant growth model related to plant genetics: cob sink variation. Promising observations can be obtained from the investigations. Firstly, the optimal results of our optimization problem revealed the dynamic interactions between sources and sinks. Secondly, the interaction between plant architecture and plant functioning is well established through optimization. Numerical study confirms that the proposed optimization approach could be a useful tool for genetic analysis and management control.

Keywords: GreenLab, functional-structural model, *Zea mays*

1 Introduction

Maize (*Zea mays* L., DEA cultivar) is one of the most widely cultivated cereals all over the world. Commonly, it is used as human diet in both fresh and processed forms. We can benefit from cob weight from an economical point of view. Therefore, a single optimization problem of maximization of cob weight is investigated in this study. It is acknowledged that final cob weight of maize depends on the relationship between cob sink and availability of assimilates resulting from the biomass production of the plant, cob weight is highly dependent on growth conditions during the early stages of grain filling, and the final cob weight reflects the source-sink dynamics of the entire grain filling period (Borras et al., 2002). Thus, the optimized variables are specific parameters of the plant growth model related to plant genetics: cob sink variation. In addition, the impact of cob position on the cob weight is studied.

It becomes widely accepted that plant growth models may provide efficient tools to study plant growth behavior, since they complement field experiments. As there exist critical relationships between plant architectures and physiological processes during the growth of plant (Sievänen et al., 2000; Mathieu et al., 2008), functional-structural models were developed (Perttunen et al., 1998; Kurth, 2000; Allen et al., 2005; Cournède et al., 2008) which combined the description of organogenesis, photosynthesis and biomass partitioning.

As the effect of cob position on cob weight is investigated in this work, we need to consider both topological information and physiological process of plant growth and therefore turn towards

functional-structural models. The GreenLab model is chosen here because of its mathematical formulation as a dynamic system, which makes it suitable for solving optimization problems. It is used to simulate the growth behavior of maize and to calibrate parameters from experimental data obtained at three growth stages. A heuristic optimization algorithm, Particle Swarm Optimization (PSO), is used to maximize cob weight. The optimal results revealed the importance of the source-sink dynamics. Moreover, the interaction between plant architecture and plant functioning is investigated through optimization.

2 Materials and Method

GreenLab is a functional-structural plant growth model combining the descriptions of plant architecture and physiological processes of plant growth, in interaction with its environment (light, water, temperature and density, etc). The dynamic mechanisms to generate plant architecture (organogenesis), plant biomass production and partitioning to the organs are introduced in details in (De Reffye and Hu, 2003; Yan et al., 2004; Cournède et al., 2008). The model was validated on maize cultivar 'ND108' and the estimated parameters showed stability within different environmental conditions (Ma et al., 2007; Ma et al., 2008). Here, only a brief introduction was adopted.

In the usual cultivation conditions, maize is a single stem crop. Thermal time was always used as the prediction of the phytomer appearance. The model time step, also called growth cycle (GC), is the time interval between two successive phytomers (phyllochrone). The topology is simplified as follows. First six phytomers with short internodes appeared. They are followed by 15 phytomers with longer internodes. The last one bears the male flower (tassel). Even though several phytomers bear female flowers (cobs), Guo et al (2006) chose to gather all these cobs in only one (corresponding to the one at the 15th internode with maximal weight, which occupied more than 95% biomass of the total cob). This simplification was proved very effective for plant calibration and we adopt it. Figure 1 illustrates the organogenesis mechanism for maize in GreenLab and the 3D representation of maize at the 33rd growth cycle.

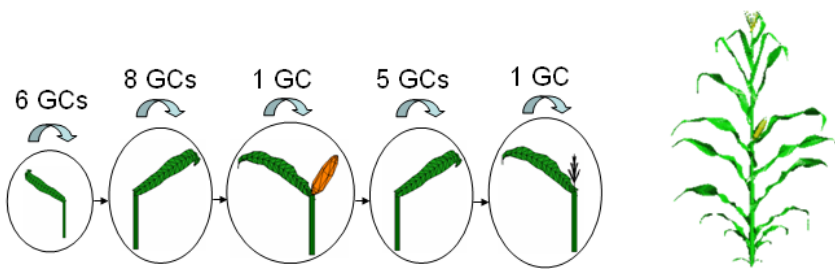

Figure 1 (a) Illustration of the organogenesis mechanism for maize in GreenLab (b) 3D representation of maize at the 33rd growth cycle

The functional processes of growth are described by a source-sink model, with a theory of a common pool for biomass. At growth cycle n, the equation of biomass production Q_n for an individual plant is as Eq. (1). It depends on the green leaf surface area at growth cycle n (S_n), on environmental factors gathered in the function E_n and on empirical parameters β (linked to energetic efficiency) and γ (linked to light interception):

$$Q_n = \beta E_n \left(1 - \exp\left(-\gamma S_n\right)\right) \tag{1}$$

All living organs are sinks among which biomass is distributed according to their sink values. The

total demand of the plant at growth cycle n, denoted by D_n, is given by:

$$D_n = \sum_o \sum_{j=1}^{\min(n, t_{x\_o})} p_o(j) \tag{2}$$

$p_o(j)$ is the sink value of organ o at the jth expansion time, o representing blade (a), sheath (s), internode (e), female (f) and male (m) organs; t_{x_o} is the expansion time of organ o.

The biomass increment of an organ o with age j at growth cycle i is proportional to its sink value and the ratio between biomass production Q and the total demand of the plant D, as Eq. (3).

$$\Delta q_o(i, j) = p_o(j) \frac{Q_{i-1}}{D_{i-1}} \tag{3}$$

The accumulated biomass for an organ o is given by:

$$q_o(i, j) = \sum_{k=1}^{j} \Delta q_o(i - j + k, k) \tag{4}$$

As a consequence, the green leaf surface area at growth cycle n, denoted by S_n, is

$$S_n = \frac{\sum_{j=1}^{t_a} q_a(n, j)}{e} \tag{5}$$

t_a is the functioning time of blades, and e is the specific leaf weight of blades. Leaf area index (LAI) is given by S_n multiplied by maize density.

The sink of an organ depends on its chronological age. Beta function was chosen to describe this empirical sink strength variation, modulated by the sink amplitude (also called sink strength) P_o:

$$f_o(j) = \begin{cases} g_o(j) / M_o & (1 \le j \le t_{x\_o}) \\ 0 & (j > t_{x\_o}) \end{cases}$$

with

$$g_o(j) = (j - 0.5)^{a_o - 1} \cdot (t_{x\_o} - j + 0.5)^{b_o - 1} \tag{6}$$

and

$$M_o = \max_j (g_o(j), 1 \le j \le t_{x\_o})$$

The sink value of organ o with age j, denoted by $p_o(j)$ is

$$p_o(j) = P_o f_o(j) \tag{7}$$

a_o and b_o are the coefficients of the sink variation function (Beta function). By adjusting these two coefficients, various shapes of sink variations can be obtained. An illustration of a sink variation example is given in Fig. 2.

Maize cultivar 'ND108' (*Zea mays* L., DEA cultivar) was used in this study, and was sown at the China Agricultural University (39°50' N, 116°25' E). The detailed information about the irrigation and measurements was described in Guo et al. (2006) and Ma et al. (2007). The form of the sink variation function here is slightly improved compared to the one described in Guo et al. (2006) and

Ma et al. (2007). Thus, the corresponding calibrated parameters values which are listed in Table 1 are different and are refitted by a generalized least square method.

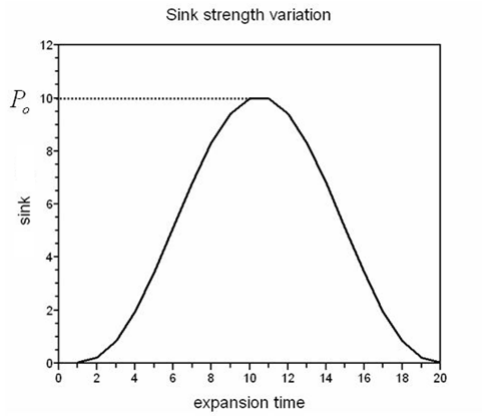

Figrue 2 Example of sink variation, with sink strength P_o = 10, a_o = 4, b_o = 4 and t_{x_o} = 20

Table 1 Calibrated parameters values

Parameters		Value
P_a	(Sink strength of blade)	1 (fixed)
a_a / b_a	(Coefficients of beta function for blade)	3.59 / 5.38
P_s	(Sink strength of sheath)	0.6
a_s / b_s	(Coefficients of beta function for sheath)	3.05 / 3.69
P_e	(Sink strength of internode)	1.4
a_e / b_e	(Coefficients of beta function for internode)	3.34 / 1.65
P_f	(Sink strength of cob)	806.47
a_f / b_f	(Coefficients of beta function for cob)	8.34 / 2.60
P_m	(Sink strength of tassel)	4.23
a_m / b_m	(Coefficients of beta function for tassel)	1 / 1
K_e	(Coefficient of sink strength for short internode)	0.20
β	(Energetic efficiency)	12.36
	(Light interception coefficient)	1.90E-4

The parameters on which we optimized are supposed to be linked to plant genetics and therefore should be representative of some physiological process. As it is acknowledged that final cob weight of maize depends on the relationship between cob sink and biomass production (Borras et al., 2002), we choose cob sink variation to do our research. The related parameters are the cob sink strength P_f and the two coefficients of the beta function, $a_f$and b_f. The effect of cob position on cob weight is also studied.

The optimization problem revealed non-convex and we therefore turned to heuristic optimization algorithms. Our preference led us to consider population-based methods, which usually allows obtaining fast acceptable solutions after one iteration. Compared to other population-based heuristic optimization algorithms, Particle Swarm Optimization (PSO) (Kennedy and Eberhart, 1995) has high convergence rate for a wide range of optimization problems (Kennedy and Eberhart, 2001). Therefore, PSO (He et al., 2004) was used in our study in order to solve our optimization problem, where the maximal number of iteration is 500, the population size is 100 and the other parameters in PSO are set as recommended by He et al. (2004).

3 Results

3.1 Maximization of Cob Weight with Fixed Expansion Duration

The optimization result of maximization of cob weight associated with cob position is illustrated in Fig.3(a). The cob expansion duration is restricted to 19 growth cycles as observed, wherever the cob is. From Fig.3(a), we found that the threshold of cob position is 15. The cob weight increases monotonously with the cob position increasing, until the cob appears at the 15th internode. It is the result of different competition time of cob for biomass with other organs. Cob development strategy can be revealed by its sink strength variation. The corresponding optimal cob sink strength variations of three randomly selected examples where the cob is at the 1st, 5th and 13th internode on the stem are illustrated in Fig.3(b), respectively. Comparing the optimal sink strength variations, we found that, in order to get the maximal cob weight with respect to cob position, the sink value is almost 0 at the beginning of cob development to let leaf area index increase as illustrated in Fig.3(c) and thus more biomass was produced by photosynthesis. And then, the cob sink value increases very quickly at the last short period of its expansion duration where nearly all the biomass is distributed to the cob as illustrated in Fig.3(d). When the cob stops getting biomass, the biomass of plant will

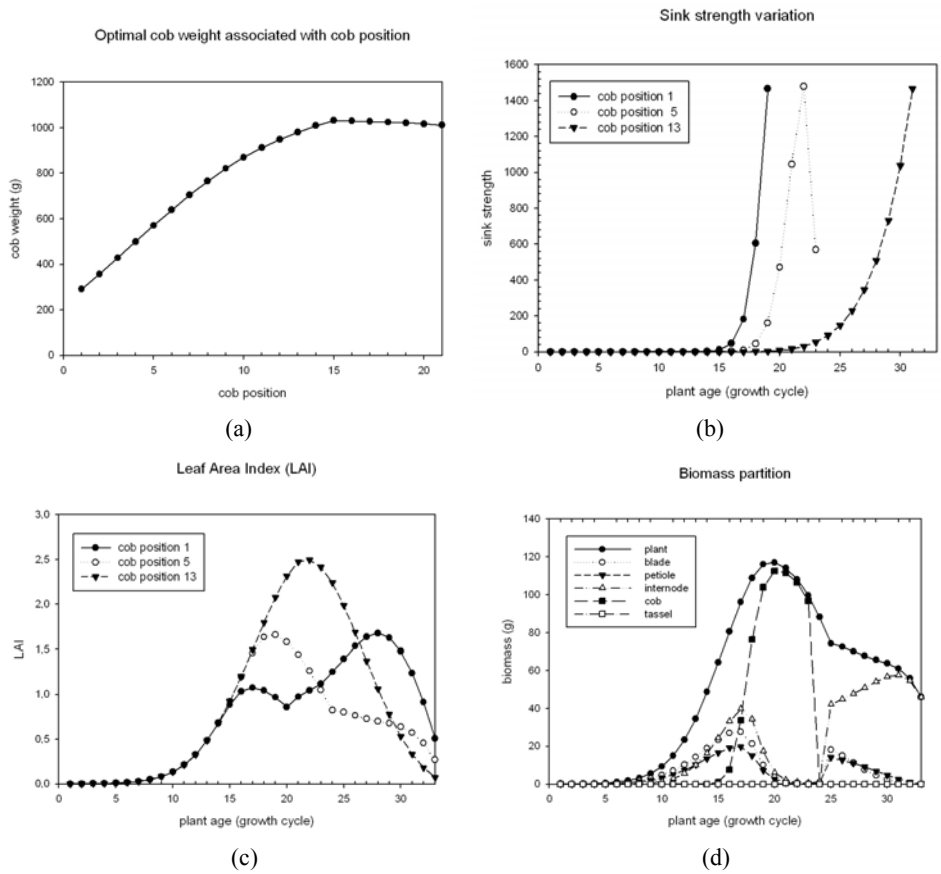

Figure 3 (a) Maximal cob weight associated with cob position (b) Three randomly selected examples of the optimal cob sink strength variations where the cob is at the 1st, 5th and 13th internode on the stem (c) Leaf Area Index (LAI) of maize where the cob is at the 1st, 5th and 13th internode on the stem, with the optimal cob sink strength variations (d) Biomass partition to each kind of organs associated with the optimal sink strength variation, where the cob is at the 5th internode on the stem

only be distributed to leaves and internode, or tassel in the following growth cycles. Comparing Fig.3(a) and Fig.3(b), we found that the cob at the 1st internode developed earlier than the cob at the 5th internode. However the optimal cob weight with cob at the 1st internode is lower than the one with cob at the 5th internode. It is because, on one hand, the cob at the 1st internode competes for biomass with source organs (leaves) too earlier when the leaf area index is small and the plant biomass is not too much. On the other hand, the plant growth is suppressed if the cob develops too early, due to the larger cob sink amplitude comparing with the other organs, especially leaves which are the source organs used to produce biomass through photosynthesis.

When the cob position is higher than the 15th internode, the cob weight begins to decrease. As observed, the cob expansion duration is set to be 19 growth cycles. To guarantee that the cob expands for 19 growth cycles where the plant is 33 growth cycles, the highest position of cob is at the 15th internode on the stem. If the cob position is higher than the 15th internode, it will miss the potential ability to obtain biomass. The higher the cob is, the more potential ability missed. Therefore, the maximal cob weight with respect to cob position decreases where the cob position is higher than the 15th internode.

3.2 Maximization of Cob Weight with Variable Expansion Duration

To make sure that the cob has enough time to develop, and to avoid missing its potential ability to obtain biomass, the cob expansion duration varies according to its position. The cob will have possibilities to obtain biomass until maize plant stops growing. For instance, if the cob is at the 1st position, its expansion duration is 33 growth cycles, where the plant age is 33 growth cycles. From Fig.4(a), we can see that there is no significant difference among the optimal cob weights associated with different cob positions. It is because they have similar sink strength variation wherever the cob is. The average optimal sink strength variation is shown in Fig.4(b). In order to obtain the maximal yield of biomass, the sink value of cob keeps extremely small, almost zero, so that leaf can obtain more biomass and leaf surface area can increase. When light interception, and thus biomass production, is high enough, the cob begins absorbing biomass significantly and cob biomass quickly increases till the last stages of growth cycle where nearly all the available biomass goes to the cob. The corresponding Leaf Area Index (LAI) is given in Fig.4(c), and we can see that cob weight start increasing when the light interception ratio is above 80%. Fig.4(d) gives the result of the biomass production of maize and biomass partition into each kind of organs, with the average optimal cob sink variation in Fig.4(b).

4 Discussions

Particle Swarm Optimization is applied to a functional-structural plant growth model GreenLab as a dynamic discrete system containing mathematical formulas. It is a population-based heuristic optimization algorithm. As it has high convergence rate and better searching accuracy and doesn't require derivative information of the objective function, it is used to solve our non-convex multimodal optimization problem: maximization of cob weight of maize cultivar 'ND 108' (*Zea mays* L., DEA cultivar) modelled by GreenLab.

The optimal results of cob sink strength variation on which we optimized implied the source-sink dynamics. In order to obtain the maximal yield of cob, the cob keeps dormant and doesn't develop to let leaf surface area increase and to have more biomass production via photosynthesis. At the last short period of its development, it becomes the strongest competitor for biomass against the other organs, where the cob absorbs nearly all the available biomass. This phenomenon can be derived from the monotonously increasing cob sink strength variation as illustrated in Fig.3(b) and Fig.4(b).

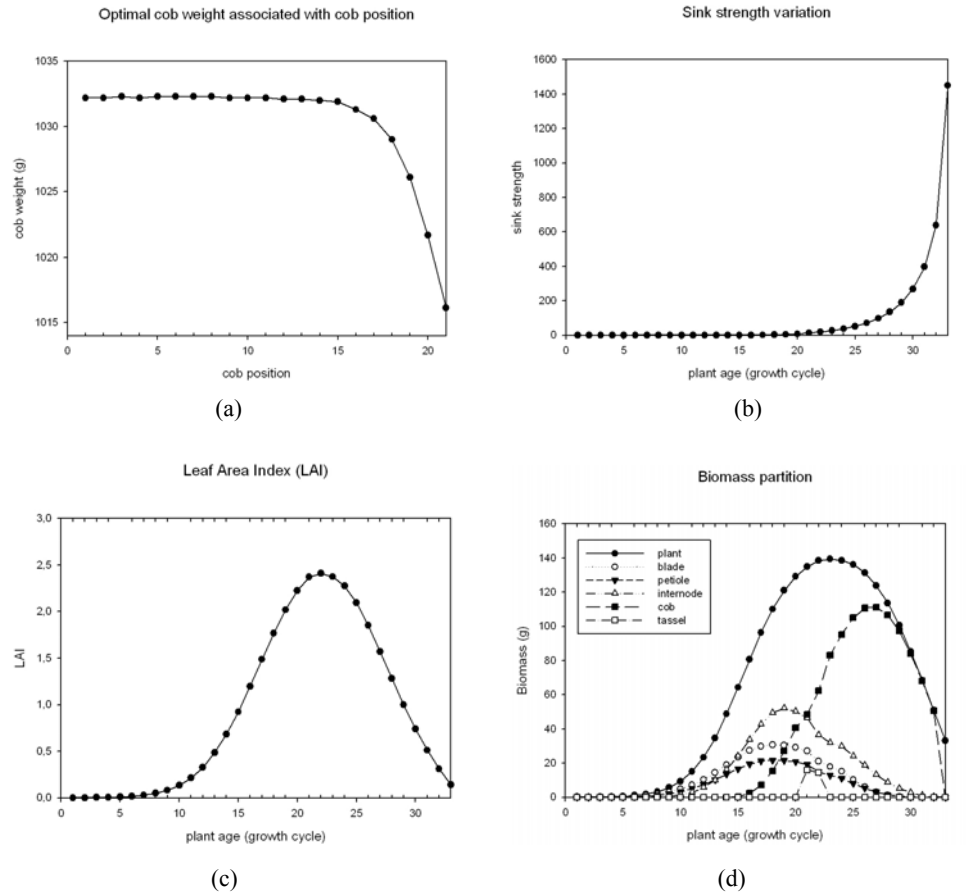

Figure 4 (a) Maximal cob weight associated with cob position (b) the optimal average cob sink strength variation (c) Leaf Area Index (LAI) of maize with the optimal average cob sink strength variation (d) Biomass partition to each kind of organs associated with the optimal average cob sink strength variation

The difference among the maximal cob weights associated with cob position reveals the relationship between plant architecture and plant functioning. Under the condition of fast development of cob, i.e. cob expansion duration is 19 growth cycles, the plant growth behaviour changes when the cob position varies, even though the cob grows with the similar development strategy. The difference of plant architecture results in the change of the competition relationship between sources and sinks. Early appearance of sink organs with larger sink strength, i.e. fruit, will strongly decrease the growth of source organs, i.e. leaves, and results in less leaf surface area (Fig.3(c)).

The relative stability of GreenLab model parameters in a wide range of environmental conditions (Ma et al., 2007; Ma et al., 2008) leads us to consider a probable link of the model parameters to the genotype of the species. Letort et al. (2008) explored the possibility to link GreenLab to a genetic model in order to design new breeding strategies. In this paper, we restrict ourselves to the optimization of GreenLab parameters for given purposes. The cob position is important for the plant harvest. If the cob is high, it is difficult to pick it up; if the cob is low, there is a risk to be eaten by animals. Therefore, to avoid these drawbacks, the cob can be controlled at an appropriate position and breeding strategies can be improved according to the optimal results in order to get the maximal cob weight. The optimal results could be a guide for genetic analysis and management control.

Acknowledgements

This work is supported partly by Natural Science Foundation of China (60073007, 60703043), Chinese 863 program (2008AA10Z218), and French embassy in China.

References

Allen M, Prusinkiewicz P, DeJong T (2005) Using L-systems for modeling source-sink interactions, architecture and physiology of growing trees: the L-PEACH model. New Phytologist 166:869 – 880.

Borras L, Cura J A, Otegui M E (2002) Maize Kernel Composition and Post-Flowering Source-Sink Ratio. Crop Sci. 42:781 – 790.

Cournède P-H, Mathieu A, Houllier F, Barthelemy D, De Reffye Ph (2008) Computing Competition for Light in the GREENLAB Model of Plant Growth: A Contribution to the Study of the Effects of Density on Resource Acquisition and Architectural Development. Ann. Bot. 101:1207 – 1219.

Guo Y, Ma Y T, Zhan Zh G, Li B G, Dingkuhn M, Luquet D, De Reffye Ph (2006) Parameter Optimization and Field Validation of the Functional–Structural Model GREENLAB for Maize. Ann. Bot. 97:217 – 230.

He S, Wu Q H, Wen J Y, Saunders J R, Paton R C (2004) A particle swarm optimizer with passive congregation BioSystems 78:135 – 147.

Kennedy J, Eberhart R C (1995) Particle swarm optimization. p. 1942–1948. In Proc. IEEE Conf. on Neural Networks, IV, Piscataway, NJ.

Kennedy J, Eberhart R C (2001) Swarm Intelligence. Morgan Kaufmann Publishers.

Kurth W (2000) Towards universality of growth grammars: Models of Bell, Pagès, and Takenaka revisited. Ann. For. Sci. 57:543 – 554.

Letort V, Mahe P, Cournède P-H, De Reffye Ph, Courtois B (2008) Quantitative Genetics and Functional-Structural Plant Growth Models: Simulation of Quantitative Trait Loci Detection for Model Parameters and Application to Potential Yield Optimization. Ann. Bot. 101:1243 – 1254.

Ma Y T, Li B G, Zhan Zh G, Guo Y, Luquet D, De Reffye Ph, Dingkuhn M (2007) Parameter Stability of the Functional-Structural Plant Model GREENLAB as Affected by Variation within Populations, among Seasons and among Growth Stages. Ann. Bot. 99:61 – 73.

Ma Y T, Wen M P, Guo Y, Li B G, Cournède P-H, De Reffye Ph (2008) Parameter Optimization and Field Validation of the Functional-Structural Model GREENLAB for Maize at Different Population Densities. Ann. Bot. 101:1185 – 1194.

Mathieu A, Cournède P-H, Barthélémy D, De Reffye Ph (2008) Rhythms and Alternating Patterns in Plants as Emergent Properties of a Model of Interaction between Development and Functioning. Ann. Bot. 101:1233 – 1242.

Perttunen J, Sievänen R, Nikinmaa E (1998) LIGNUM: a model combining the structure and the functioning of trees. Ecological Modeling 108:189 – 198.

De Reffye Ph, Hu B G (2003) Relevant qualitative and quantitative choices for building an efficient dynamic plant growth model: GreenLab Case. p. 87-107. In Hu, B.G., Jaeger, M., (eds.) Plant Growth Modeling and Applications. Proceedings - PMA03, Tsinghua University Press and Springer, Beijing, China.

Sievänen R, Nikinmaa E, Nygren P, Ozier-Lafontaine H, Perttunen J, Hakula H (2000) Components of functional-structural tree models. Ann. For. Sci. 57:399 – 412.

Yan H P, Kang M Zh, De Reffye Ph, Dingkuhn M (2004) A Dynamic, Architectural Plant Model Simulating Resource-dependent Growth. Ann. Bot. 93:591 – 602.

A Review of Research on the Virtual Plants

Lin Hu, Guo-Min Zhou, Yun Qiu, Jing-Chao Fan, Jian Wang

(Agricultural Information Institute of CAAS, Beijing 100081, P .R. China)

Abstract: The plant growth model is an important content for many subjects. There are needs for more accurate model for simulating plant growth in the area of biology, ecology, computer science, and the video & film, but the numeric growth equation cannot description. more realistic and more vivid description were needed, with the relationship between plants and their environment factors could be probed in depth In the area of biology, and not only the more realistic static plant model but also the dynamic growth model are needed in the area of the video & film. The virtual plant is the combination of the science and the art, and it was developed in the environment with the developing of the botany and the technology of the computer. In the data collection, the laser scanner and the close-shot, taken the place of the manual methods, improve the efficiency and the precision of the modeling. The integration of the structure and the picture was used to descript the grow procedure developed from the structure model and the picture model. There are two main kinds of models, one is the functional model and the other is the non-functional model. the multi-item have been researched in the physiology and ecology, which have transcend the application in the ecology, even more, now the model research has been used to explore the affection of the gene on the plant growth, and the virtual plant have been probed into from the three level, i.e., micro level, individual level and the macro level.

Keywords: virtual plant, data collection, model kinds, research view

1 Definition and Signification of the Virtual Plants Research

1.1 Definition of Virtual Plants

Virtual plant is the simulation of the construction and growth of the plants in 3D space (Liu Fei and Zhu Yuye, 2007; Liu Xiuhai et al., 2006; przemyslaw Prusinkiewicz, 2004). The meaning of the virtual plants is different in different area. The appearance of the plants must be much alike in the video area, while it does not concern with the contents of the plants ecology and the physiology. However, it is not only to purchase the visual effecting, but also to model the plants based on the principle of the morphology, physiology and ecology of the plants. Meanwhile, the practical methods used in video area have been adopted in biological model. Virtual plant is the combine of the art and the science(przemyslaw Prusinkiewicz, 2004).

Though the major consideration of the virtual plant is the simulation of the plant form and the growth, its research area can be extended to others, such as the relationship between the leaf color and plant pest and disease; the affection of the lighting on the plant; the gene and the development; the morphogenesis and the plant hormone or the other substance of the metabolism (Peter Room et al., 1996; Zhengge Huang et al., 2006; Bedrich Benes and Juan Miguel, 2004).

The research on the virtual plant has been developed into a new stage with the application of the virtual reality technology in the virtual plant research. The research object is to reveal the form and the mechanism of the plant. The virtual plant is the reflection of the real plant in the computer

world, it can simulate the birth, development, getting old and death realistically based on the morphology, ecology and physiology strictly.

1.2 Research Signification

Plants are the best partner of the mankind. People have been want to know the plants from many aspects with different means, to descript it with text, picture and video in art circle, with morphology, taxonomy and physiology in science circle. The classical description with the numerical formulation cannot meet the needs of the science research now, such as to research the relationship between the leaf color and the pest damage. Therefore, the virtual plant is the necessary outcome of the plant research.

The fields of the research on the virtual plants can be divided from deferent views.

Horizontally, the virtual plant is the main research object, the individual as the research base, extended at the micro and the macro level. On micro level, research the relationship between the structure and the form, on macro level, the relation between the individual even the community and the ecological system.

Vertically, virtual plant model could be implied in every aspect, such as the specie design, fertilizes test and the pest control (Wu Lin et al., 2004; Mialet-Serra et al., 2001; Jim Hanan et al., 2002; JiJoon Kim and Member, 2006).

The virtual plant model has a broad application in art and other area. Simulating the plant growth in the video and teaching the related knowledge in school with the model.

The virtual plant model will be the important media in plant research, knowledge imparting and skill training. Therefore, the virtual model is the necessary and has theory and application value.

Virtual plants model is the consequence of the computer visual research. The virtual plants model research will be focused gradually.

2 Research Situation of the Virtual Plants

2.1 Research Status

The plants model research has been several procedures, from the numeric formula, visual presentation and virtual reality technology. The plant visualization begins at the Ulam and Cohen's research on the branching model, develops at the L system decrypting the cell production prompted by Lindenmayer, a Hungary botanist, this system have been formed an important tool to descript plant morphology, and is implied broadly. L system has been developed by prusinkiewicz, a profession of the Calgary University, and a plant fractal generator and a software virtual laboratory is developed. AMAP is a software system developed by the national agriculture research institute, French. The system divided the whole plants into 24 basic constructors, using the picture gallery to design plants.

De Reffye and his team, a professor at International agricultural development and corporation center of French, develop AMAP software. On the basis of this model, institute of Automation of Academia of Chinese science academy corporate with the CIRAD to develop a function-structure model, greensciLab. The function model could be divided into five kinds; they are the model based on the process, stem form model, L system, fractal model and the light transfer model in the canopy. Their present model are separately COTTON model (the model integrate of the GOSSYM and the L system), LIGNUM (descript the relationship between the stem and the leafs, the application is limited), L system (developed greatly, now it is used to descript the plants contracture, and are used to implied in the research on the root structure, plant pest and disease and the insect behavior. Diggle developed open L-system in 1988, which is a model presenting the mutual between the

plants and the environment.), fractal model (according to the fractal theory, the fractal model include the Iteration Functional System, branching matrix, particle system) and the light transfer model (including the dickmann's ECOPHYS, Celine leroy's ARCHIMED based on the AMAP and the Percy & Yang's YPLANT) (Qiu Jianjun and Xiao Yinnan, 2000; Xie yun and James R Kiniry, 2002; Sun Ning 2002; Celine Leroy et al., 2005; Pearcy R.W and Yang W.M, 1996)

2.2 Virtual Plants Technology

Virtual plant is a discipline integrating the mathematics, computer vision, ecology, etc. it needs mastering a serial of technologies including the data acquisition, analysis and presentation, the key of these is the virtual reality technology.

2.2.1 Virtual Plant Model

There are three kinds of model at present; they are the L-system, the AMAP and a virtual model created by Queensland University. L system is fit to descript the little plants, the AMAP to descript the big plants, especially the big trees. Integrating the environment model, a virtual model based on L system has been developed by the CPAI of the Queensland University. It is a model generated from real data measured from the real plants with 3D digitizer (including the generate rules of the new organ and the varying rules of the geometry outer).

L-system is a rewriting symptom system in essence, that is to rewriter an initial object step by step according to a rule and to form a complex object. There are different edition software due to its platform, the L studio on Windows and the virtual laboratory on UNIX.

AMAP is developed by a team headed by de Reffy in 1980s. It is a common used as landscape design software, but not a research tool. In order to make up its shortcoming, a greenscilab has been developed(Cournede P.H et al., 2005). Comparing with the video model, neither the L studio nor the AMAP can present the plants vividly. Therefore, it is necessary to enhance the research in the future (Tang Weidong and Li Pingping, 2006; Hu Baogang et al., 2001).

2.2.2 Instruments for Virtual Plants Research

Instruments is important to the research, even play a key role, decide whether a research can be possible. The model is more accurate, with the means from manual to automatic.

Collecting data and modeling manually, the accuracy cannot meet the work due to the coarse data.

The digitizer improves the accuracy and the collecting speed to some extent, but it only can collect one point data each time, so its speed is low and it only is as a progress tool.

Three-dimension scan and photography are two automatic ways to collecting data, which are adopted in many fields, such as ancient builds modeling, historical relics modeling and industrial design.

The main types of the laser scanner which are used to collect the plant data are the fastscan made by polhemus corp. of U.S.A and T-scan made by Leica corp. of Switzerland. Fastscan is portable, but it is interfered by the environmental light. It should be used in fields at down or morning when the direct light is not too strong. The plant organ which is measured should be preprocessed for the laser wave can be absorbed by the plants. Leica corp. is famous for its image process products. T-scan is one of its products. It is not affected by environmental light, and could be used to measure the large plants(Grigore C. Burdea and Philippe Coiffet, 2005; Visser et al., 2002).

There are two methods to reconstruct the model using pictures. One of these is the profile, the other is the photogrammetry. Software based on the profile is the 3DSOM pro developed by Creative Dimension Software Corporation (Ma Yuntao et al., 2006), software based on the photogrammetry is the imagemodeler developed by Realviz Corporation which is a subsidiary of the Autodesk. The former

is fit to model the small plants, while the later one is fit to model the large building and the big trees.

There are different characteristics to reconstruct 3D model between the scanner and photo. It is more quick and easy to model regular object with scanner than camera, however, the form of the plants is not regular, and it is difficult to model the plants with scanner. The photo can be used to model the plants graphic, but it is less accurate now.

2.2.3 Main Research Body

The famous research bodies those studies the virtual plants are mainly distributed in European, American, Oceania and Asian. They are the CIRAD of the France, Goettingen University of German, Westminster University of English and the Wageningen University of Holland (de visser P.H.B et al., 2002). The main research object is the contracture model, and one of their research results is the AMAP (Christophe Godin and Yann Guedon). One of the main research tasks of the Wageningen University is to research the plants ecology and physiology using the virtual plants. Bedrich Benes of the Czech Technical University has researched the growth direction of the virtual plants (Bedrich Benes, 1997). Based on the Lendenmayer's research, Calgary University developed virtual plants software which is named the virtual laboratory on UNIX and the L studio on Windows (Pavol Federl and Przemyslaw Prusinkiewicz, 1999; Mech R et al., 1997). It is the Queensland University in Oceania (Hanan J,1997). There are many research bodies in Asian, such as the Osaka University in Japan (Katsuhiko Onishi, et al., 2003), and the Chinese Agriculture University (), the automatic research Institute of Chinese scientific academy research, Chinese Agricultural science academy, Nanjing Agricultural University, Beijing Agriforest science academy and Taiwan University in china.

2.3 Difficulties in the Virtual Plants Research

There are many research work have been done, and the advantage and the disadvantage will be coexistence for a very long time of the numeric model, visual model and the virtual plants model. The main problem is as the fellows in the virtual plants research.

(1) Backward research means

There are still many research institutes whose research means are traditional manual, which does not match the requirements of the modern research. Due to the great labor, data error and long work cycle, the model based on such data has low accuracy. The automatic is the direction of the development of the data collection, analysis and the presentation. The more scientific methods should be adopted to improve the research efficiency in virtual plants researches.

(2) Insufficient research accumulate

The research of the virtual plants is still on the initial stage. The appearance of the plant model is lack of the realness; the mechanism of the plants growth still cannot be applied in the models, so the models cannot support the research of the physiology and the ecology of plants. The relationship between the plants colony and the morphology should be enhanced in future.

(3) Weakness of the model presentation

The virtual plants models is only able to descript the simple plants, it is still difficult to present the complex plants. It is lack of the power to present the single organ detail such as the flower, fruit and the root, especially for those plants which appearance are change greatly.

(4) Lacking of unity

There is not a model to present the whole plants completely yet.

The application of virtual plants model is not frequent used except the AMAP as a landscape model. In the enhanced realism research, some video model could be referenced, such as the verdant of the digital element corporation, the xfrog of the greenworks, etc...

3 Conclusions

The study of the virtual plants can be summarized as the application of the computer simulation in the plant growth model. The progress of the plant model research is the image of the computer simulation technology. All we can believe that the virtual plants model will and must make great progress. The research of the virtual plants model is the direction of the plant growth model research, and is a complex integrates of the plants science. The research of the virtual plants will improve the development of the plants science and the computer simulation science; meanwhile, it will provide a platform for the communication and development.

References

Bedrich Benes(1997). Fast Estimation of Growth direction in Virtual Plants Simulation. WSCG'97. Vol: Ⅰ, 1-10. University of west Bohemia Press.

Bedrich Benes, Juan Miguel (2004.). Clustering in virtual plant ecosystems. WSCG'2004.

Celine Leroy, Marilyne Laurans, Jean Dauzat, etc (2005). Simulation of light transmission under Acacia mangium wild. and Tectona grandis L. canopies and comparision with in situ measurements.International Consultation Workshop 18-21 August 2005, Malang, Indonesia.

Christophe Godin, Yann Guedon. AMAPmod, introduction and reference Manual. see http://www.cirad.fr/amapmod/referman18/couverture.html.

Cournede PH, Yan HP, Kang MZ, Barczi JF et al. (2005). A Review on the structural Factorization of plants in GreenLab Model. OICMS.

de visser P.H.B, Marcelis L.F.M, Van der Heijden G.W.A.M, et al. (2002). 3D modeling of plants: a review, report of the virtual plant Network Wageningen. plant research international. see http://www.plant.wageningen-ur.nl.

Grigore C. Burdea, Philippe Coiffet (2005). Virtual reality technology [M]. Beijing, Publishing House of Electronics Industry (PHEI).

Hanan J.(1997). Virtual plants - Integrating architectural and physiological models. Environmental Modeling & Software. 12, 35-42, Elsevier, Oxford.

Hu Baogang, Zhao xing, Yan Hongping, et al.(2001). Review and outlook of the plant growth model and simulation[J].Journal of automation. 27(6):816 – 835.

JiJoon KIM, Member (2006). A growth Model for Root system of Virtual Plants with soil and Moisture Control. IEICE TRANS. INF. & SYST., VolE89-D,No,5 ,1743 – 1750.

Jim Hanan, Przemyslaw Prusinkiewicz, Myron Zalucki, et al. (2002). Simulation of insect movement with respect to plant architecture and morphogenesis. computers and Electronics in agriculture, 35:255 – 269.

Katsuhiko Onishi,Shoichi Hasuike, Yoshifumi Kitamura, Fumio Kishino(2003). Interactive Modeling of Trees by using Growth Simulation. in Proc. of the ACM symposium on Virtual Reality software and Technology.

Lao Fei, Zhu Yuye(2007). Application of the virtual reality technology in Agriculture [J]. ANHui Agricultural science. 35(14):4375 – 4376.

Liu Xiuhai, Xiao Baixiang, Zheng Wengang, et al. (2006). Review on the virtual maize[J]. maize science. 14(2):164 – 167.

Ma Yuntao, Guo Yan, Zhan Zhigan, et al. (2006). Assessment on the GreenLab-Maize model. Plants Journal, 32(7):956 – 963.

Mech R, Prusinkiewicz P, Hanan J(1997). Extensions to the graphical interpretation of L-systems based on turtle geometry. see http://algorithmicbotany.org/lstudio/graph.pdf.

Mialet-Serra, Dauzat J Auclair D(2001). Using plant architectural models for estimation of radiation transfer in a coconut agroforestry system. agroforestry system. 53:141 – 149.

Pavol Federl and Przemyslaw Prusinkiewicz (1999). Virtual Laboratory: an interactive software environment for computer graphics. In Proceedings of Computer Graphics International, pp.93 – 100.

Pearcy R.W, Yang W.M(1996). A three-dimensional crown architecture model for assessment of light capture and carbon gain by understory plants. Oecologia. 108: 1 – 12.

Peter Room, Jim Hanan, Przemyslaw Prusinkiewicz.(1996.) Virtual plants: new perspectives for ecologists, pathologists and agricultural scientists[J]. Trends in Plant Science. Vol. 1, pp. 33-38.

przemyslaw Prusinkiewicz. (2004.) Art and Science for life: Designing and Growing Virtual Plants with L-systems. In c. Davidson and T. Fennandez (Eds:) Nursery Crops: Development, Evaluation, Production and use: Proceedings of the XXVI International Horticultural Congress. Acta Horticulturae 630, pp. 15 – 28.

Qiu Jianjun, Xiao Yinnan(2000). Research pregress on the cotton growth model of American_GOSSYM[J].world agriculture.4:21 – 22.

Sun Ning(2002). Application of the plants simulation technology in the research of the influence of clime change on the agriculture production[J]. Geography frontier. 9(1).

Tang Weidong, Li Pingping(2006). Research on the visualization of the plant growth model based on the state machine[J].Journal of agricultural machines. 37(7):104 – 108.

Visser, P H B, De, et al.(2002).3D modeling of plants: a review[R]. Wageningen(Netherlands): plant research international.

Wu Lin, Le Dimet FX, Hu B.G, et al. (2004). A Water Supply Optimization Problem for Plant Growth Based on GreenLab Model. Cari 101 – 108.

Xie yun,James R Kiniry(2002). Review of the plant growth model abroad [J]. Journal of the plants. 28(2):190-195.

Zhengge Huang, Yao Zheng, Lijun Xie, et al. (2006.) A Virtual Plant Ecosystem Featuring Parallel Computing and Distributed Visualization. IMSCCS'06. VOL.1, 424 – 429.

Concepts and Applications of AquaCrop: The FAO Crop Water Productivity Model

P. Steduto[1*], Dirk Raes[2], Theodore C. Hsiao[3], Elias Fereres[4], Lee K. Heng[5], Terry A. Howell[6], Steven R. Evett[6], Basilio A. Rojas-Lara[3], Hamid J. Farahani[7], Gabriella Izzi[1], Theib Y. Oweis[8], Suhas P. Wani[9], Jippe Hoogeveen[1], Sam Geerts[2]

(1 Land and Water Division, FAO United Nation, Rome, Italy)
(2 Department of Earth and Environmental Sciences, K.U. Leuven University, Belgium)
(3 Department of Land, Air and Water Resources, University of California, Davis, CA)
(4 IAS-CSIC and University of Cordoba, Spain)
(5 Joint FAO/IAEA Division of Nuclear Techniques in Food and Agriculture, IAEA, Vienna, Austria)
(6 USDA-ARS, Bushland, TX)
(7 Department of Agric. & Biol. Engr., Clemson University, Edisto Research & Education Center, Blackville, SC)
(8 ICARDA, Aleppo, Syria)
(9 ICRISAT, Anhdra Pradesh, India)
(* Corresponding author)

Abstract: Predicting attainable yield under water-limiting conditions is an important goal in arid, semi-arid and drought-prone environments. To address this task, FAO has developed a model, *AquaCrop,* which simulates attainable yields of the major herbaceous crops in response to water. Compared to other models, *AquaCrop* has a significantly smaller number of parameters and attempts to strike a balance between simplicity, accuracy, and robustness. Root zone water content is simulated by keeping track of incoming and outgoing water fluxes. Instead of leaf area index, *AquaCrop* uses canopy ground cover. Canopy expansion, stomatal conductance, canopy senescence, and harvest index are the key physiological processes which respond to water stress. Low and high temperature stresses on pollination and harvestable yield are considered, as is cold temperature stress on biomass production. Evapotranspiration is simulated separately as crop transpiration and soil evaporation and the daily transpiration is used to calculate the biomass gain via the normalized *biomass water productivity*. The normalization is for atmospheric evaporative demand and carbon dioxide concentration, to make the model applicable to diverse locations and seasons, including future climate scenarios. *AquaCrop* accommodates fertility levels and water management systems, including rainfed, supplemental, deficit, and full irrigation. Simulations are routinely in thermal time, but can be carried out in calendar time. Future versions will incorporate salt balance and capillary raise. *AquaCrop* is aimed at users in extension services, consulting firms, governmental agencies, NGOs, farmers associations and irrigation districts, as well as economists and policy analysts in need of crop models for planning and assessing water needs and use of projects and regions.

Keywords: crop modeling, water-driven growth-engine, transpiration and biomass, water stress

1 Introduction

The complexity of crop responses to water deficits has often led to the use of empirical production functions as the most practical option to assess crop yield response to water. Among the empirical

function approach, FAO *Irrigation & Drainage Paper* 33 (Doorenbos and Kassam, 1979) has been a landmark in predicting the yield response to water of annual and perennial crops, through the following equation:

$$\left(\frac{Y_x - Y_a}{Y_x}\right) = k_y \left(\frac{\mathrm{ET}_x - \mathrm{ET}_a}{\mathrm{ET}_x}\right) \quad (1)$$

Where Y_x and Y_a are the maximum and actual yields, ET_x and ET_a are the maximum and actual evapotranspiration, and k_y is the proportionality factor between relative yield loss and relative reduction in evapotranspiration. Different forms of Eq. (1) may be found in the literature (Stewart et al., 1974; Tanner and Sinclair, 1983).

Theoretical and experimental advances in crop-water relations from 1979 to date, along with the strong demand for improving water productivity as one of the major approaches to cope with water scarcity, have prompted FAO to revise its *Paper* 33. This was carried out through a consultative process with experts from major scientific and academic institutions and governmental organizations worldwide. The consultation led to a revision framework that treats field and vegetable crops separately from tree crops because of the different level of knowledge and the additional complexities involved in yield determination of the latter. For herbaceous crops, the decision was to develop a simulation model of proper structure based on concepts traceable to Eq. (1), for use in planning, management and scenario analysis. The model is named *AquaCrop*, which attempts to strike a balance between accuracy, simplicity, robustness, and ease of use.

This paper describes the conceptual framework, structure, algorithms, and distinctive features of *AquaCrop*, along with the performance evaluation for a few crops grown under variable water availability.

2 Model Description

2.1 Model Growth-Engine and Flowchart

Conceptually, *AquaCrop* is an expression of Eq. (1) but with refinements. The crop evapotranspiration (ET) is separated into soil evaporation (E) and crop transpiration (Tr) to avoid the confounding effect of the non-productive consumptive use of water (E). This is particularly important when canopy cover of the ground is incomplete and soil E may be the major component of ET. The harvestable yield (Y) is expressed as a function of biomass (B) and harvest index (HI) to distinguish between environmental stress effects on B from those on HI. The separation of these two kinds of effects, which differ fundamentally, makes it possible to introduce functional links based on underlying physiological processes. The changes described led to the following equations at the core of the *AquaCrop* growth engine:

$$B = \mathrm{WP} \cdot \Sigma \mathrm{Tr} \quad (2)$$

And,

$$Y = B \cdot \mathrm{HI} \quad (3)$$

Where WP is the water productivity parameter in units of kg (biomass) m^{-2} (land area) mm^{-1} (water transpired). Stepping from Eq. (1) to Eq. (2) makes the model more robust and more applicable, due to the conservative behavior of WP when normalized for climatic conditions (Steduto et al.,

2007), although both equations are expressions of a *water-driven growth-engine* in terms of crop model design (Steduto, 2003). In Eq. (2), *AquaCrop* introduces daily time steps to account for dynamic changes in water supply, soil evaporation, crop transpiration and air temperature, in contrast to the use of Eq. (1) to compute production over long periods (weeks to months).

Other important refinements include a novel way to simulate canopy growth, the separation of effects of stress on canopy growth, stomatal conductance, canopy senescence, and pollination and other aspects of HI, as will be described below.

Similarly to other models, *AquaCrop* has a structure that overarches the soil-plant-atmosphere continuum. It includes the *soil*, with its water balance; the *plant*, with its development, growth and yield processes; and the *atmosphere*, with its thermal regime, rainfall, evaporative demand and carbon dioxide concentration. In terms of *management*, the model emphasizes irrigation, but also considers soil fertility, especially nitrogen, and aspects related to water such as soil bounds and mulches, as they affect the soil water balance, crop development and growth. Cuttings of forage crops are also specified under management. Pests, diseases, and weeds are not considered.

The functional relationships between the different model components are depicted in Fig. 1.

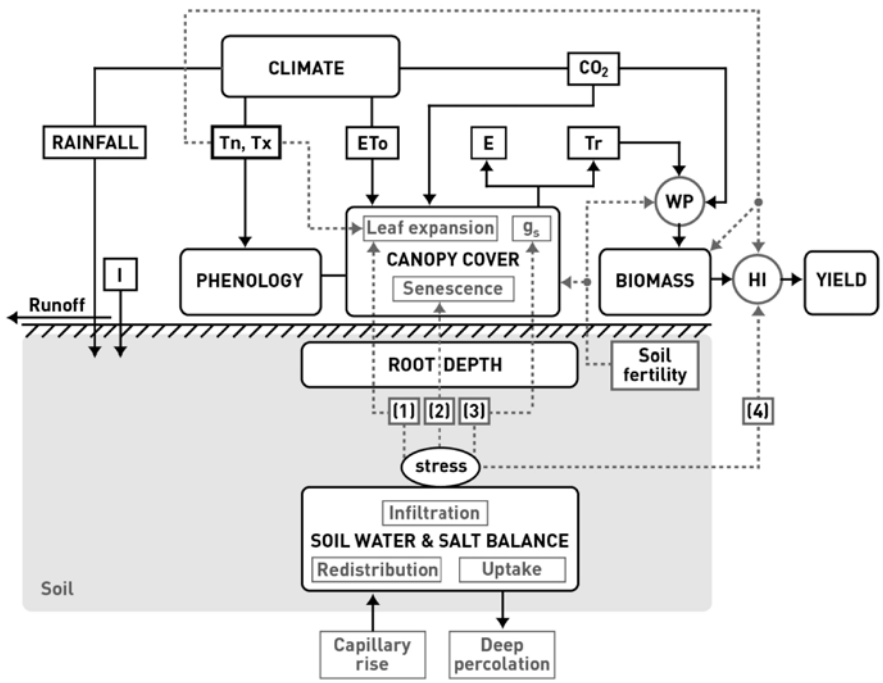

Figure 1 Chart of AquaCrop indicating the main components of the soil-plant-atmosphere continuum and the parameters driving phenology, canopy cover, transpiration, biomass production and final yield (I – Irrigation; Tn – Min air temperature; Tx – Max air temperature; ETo – Reference evapotranspiration; E – Soil evaporation; Tr – Canopy transpiration; gs – Stomatal conductance; WP- Water productivity; HI – Harvest Index; CO_2 – Atmospheric carbon dioxide concentration; (1), (2), (3), (4) – different water stress response functions). Continuous lines indicate direct links between variables and processes. Dashed lines indicate feedbacks. For explanation, see processes description

Following is a brief description of the model, which consists of 4 components: the atmosphere, the crop, the soil, and management. Only algorithms largely distinctive to *AquaCrop* are presented, while those in common with existing models are only mentioned, with reference to the literature. For further insight into the model components and software, the reader is referred to Steduto et al. (2008) and Raes et al. (2008a,b).

2.2 The Atmosphere

The atmospheric environment of the crop is described in the *climate* component of *AquaCrop* (Fig. 1) as 5 weather input variables: daily maximum and minimum air temperatures, daily rainfall, daily evaporative demand of the atmosphere, expressed as ET_o, and the mean annual carbon dioxide concentration in the bulk atmosphere. While the first 4 are obtained or derived from data of agro-meteorological stations, the CO_2 concentration uses the Mauna Loa Observatory records in Hawaii.

ET_o should be calculated from daily solar radiation, temperature, humidity, and wind data following the procedures described in the FAO *Paper* 56 (Allen et al., 1998). When not all the required input variables for ET_o are available, *Paper* 56 describes the methods for their estimation. *AquaCrop* does not include the routines for calculating ET_o, but a separate software program (named *ETo Calculator*) based on *Paper 56* is provided for such purposes. When daily weather data are not available, 10-day or monthly records are processed by *AquaCrop* into daily values using the downscaling procedure of Gommes (1983). This flexibility allows the use of *AquaCrop* in areas of limited weather records. The model also has a sub-routine to estimate *effective* rainfall from 10-day or monthly data through two options, the USDA Soil Conservation Service method (SCS, 1993), or by setting effective rainfall as a percentage of total rainfall.

As illustrated in Fig. 1, temperature plays a role in influencing crop development (phenology, biomass production and pollination); the rainfall and ET_o are inputs for the water balance of the soil root zone; and the CO_2 concentration of the atmosphere influences the canopy growth rate and the water productivity (WP).

2.3 The Crop

The crop system has 5 major components (Fig. 1): phenology, green canopy cover, rooting depth, biomass production and harvestable yield. The crop grows and develops through the ontogenetic stages of its cycle by expanding, maintaining, and senescing its canopy, deepening its rooting system, flowering, and accumulating above-ground biomass, partly in the yield organ. The dynamic responses to water stress associated to the various crops components are discussed later.

2.4 Canopy Development

The canopy is a crucial feature of *AquaCrop*. Through its expansion, ageing, changes in conductance, and senescence (Fig. 1), it determines the amount of water transpired, which in turn determines the amount of biomass produced. One of the key features of *AquaCrop* distinguishing it from existing models is the expression of crop surface for transpiration (hence for biomass production) as the fractional green canopy ground cover (CC) and not via leaf area index (LAI). This simplifies the simulation significantly, reducing the overall canopy expansion to a growth function and allowing the user to enter actual values of CC, even those estimated by eye. Moreover, CC may be easily obtained also via remote sensing. One important feature of the equations developed to simulate CC is that they account directly for the effects of plant density, within the commonly encountered density range. Beyond CC, where differences due to canopy architecture and height may exert influence, the effects are implicitly incorporated when parameterizing the crop coefficient for transpiration of each crop species.

For non-stress conditions, the canopy expansion from emergence to full canopy development follows a sigmoid-type curve constructed with an exponential function for the first half of the development, and an exponential decay function for the second half, according to the equations:

$$CC = CC_o e^{CGC \cdot t} \tag{4}$$

$$CC = CC_x - (CC_x - CC_o) \cdot e^{-CGC \cdot t} \quad (5)$$

Where CC is the canopy cover at time t in growing degree day (GDD) or calendar day, CC_o is the initial canopy cover (CC at t=0), CGC is the canopy growth coefficient in fraction per GDD (or per day), and CC_x is the maximum canopy cover, or canopy cover at t=∞. CC_o represents the initial canopy cover once the seedlings are established and is equal to the plant density times the mean initial canopy cover per seedling. The latter is a crop-specific parameter provided in *AquaCrop* for each of the major crops.

After its full development, the canopy can have a variable duration before entering the senescence phase. For the fully developed canopy and before senescence, an ageing effect is applied to account for the slight reduction in the overall canopy transpiration capacity over time (e.g., 0.3% reduction per day). Once senescence starts in the late season, CC enters a declining phase following the equation:

$$CC = CC_x \left[1 - 0.05 \left(\exp^{\frac{CDC_t}{CC_x}} - 1 \right) \right] \quad (6)$$

Where t is time since the start of canopy senescence, and CDC is a canopy decline coefficient that reflects the speed of decline up to maturity.

2.5 Biomass and Yield

The green canopy represents the source for transpiration, which is translated into a proportional amount of biomass produced through the normalized WP. The choice of a water-driven engine instead of the more common radiation-driven engine now used by most established crop simulation models (e.g., Keating et al., 2003; Jones et al., 2003) is based on a recent analysis of the conservativeness of normalized WP (Steduto et al., 2007), and on the focus that AquaCrop has on simulating attainable yields in response to water. Because WP is strongly influenced by evaporative demand, its normalization for different climates is critical. In *AquaCrop*, the normalization is achieved through ET_o, which was found to be more consistent than through the atmospheric Vapor Pressure Deficit (VPD) (Steduto and Albrizio, 2005; Steduto et al., 2007), and the theoretical basis for this has been elaborated (Asseng and Hsiao, 2000). The CO_2 concentration normalization procedure is based on gas exchange principles and supporting data (Hsiao, 1993; Steduto et al., 2007; Xu and Hsiao, 2004). To account for the higher energy content of the biomass produced during yield formation of seed crops high in oil content (Penning de Vries et al., 1983; Azam-Ali and Squire, 2002), WP is adjustable in *AquaCrop* for the yield formation (reproductive) phase. After calculating B, its harvestable portion, the yield (Y), is determined via harvest index (HI), using Eq. (3).

Though *AquaCrop* uses HI as a key parameter, it does not calculate the partitioning of biomass into various organs (e.g., leaves, roots, etc.), i.e., biomass production is decoupled from its allocation to leaves and roots. This choice avoids dealing with the complexity and uncertainties associated with the partitioning processes, which remain among the least understood in crop physiology and are most difficult to model. In *AquaCrop*, a reference HI must be provided for each crop (and cultivar when warranted). HI increases linearly after a lag-phase, starting from the time of anthesis or the beginning of yield formation period, similarly to the approach followed by Amir and Sinclair (1991) and Wheeler et al (1996). Water deficits may affect the final HI value, as discussed below. The relationship between shoot and root is maintained by empirical procedures which are based on the functional balance between canopy development and root deepening (Raes et al., 2008a).

AquaCrop uses thermal time (GDD) as the default driver, and offers calendar time as an alternative when data are not available to derive GDD. GDD is computed following the procedure of McMaster

and Wilhelm (1997), with the additional incorporation of an upper temperature threshold above which crop development no longer increases with increases in air temperature. In addition, a special procedure is found to be necessary for the computation when dealing with winter crops that go through a period of freezing weather. The genetic variation among species and cultivars is implemented in the model through the variation in timing and duration of the various developmental stages, the initial canopy size per seedling, canopy growth and decline coefficients, rate of root deepening and potential maximum depth, normalized WP, and the response factors to environmental conditions.

2.6 Transpiration

As the canopy develops, transpiration (Tr) is simulated separated from soil evaporation (E) because it is the basis for biomass production (Eq. (2)). The model attempts to provide accurate estimations of Tr by accounting for the extent of CC, effects of inter-row micro-advection, and effects on stomata.

Transpiration is calculated as a function of a specific crop coefficient Kc_{tr}, which is the Tr/ET_o ratio of the full canopy of the crop under optimal conditions ($Kc_{tr\,x}$), adjusted for effects of stresses on stomata and for canopy aging and senescence, as follows:

$$Tr = Ks_{sto} * Kc_{tr} * CC_{adj} * ET_o \quad (7)$$

Where CC_{adj} is CC adjusted to account for the interactions between Tr and E, which are particularly relevant under partial canopy cover (Ritchie 1983) and enhances Tr, and Ks_{sto} is the water stress coefficient for stomatal closure. After CC_x is reached, $Kc_{tr\,x}$ is adjusted slightly downward per day as the canopy ages until the onset of senescence. When senescence starts and CC declines following the trend indicated by Eq. (6), $Kc_{tr\,x}$ is adjusted further downward. If water stress affects Tr by reducing stomatal opening, then Ks_{sto} becomes smaller than 1.

For specifics on all the adjustments, see Raes et al., (2008a). Water stress also may affect Tr indirectly by reducing CC, as discussed below.

2.7 Responses to Water Stress

Since the focus of *AquaCrop* is the simulation of water-limited yield, efforts were made to include all the responses underpinning the effects of water stress on crop yield. Other models dealing with water stress have placed more emphasis on simulating stress effects on photosynthesis than on canopy expansion or senescence (van Ittersum et al., 2003; Jones and Kiniry, 1986). *AquaCrop* presents a novel approach by segregating the canopy response to water deficits (Fig. 1) into three components, namely, ① reduction in expansion rate, i.e., reducing the canopy growth coefficient (CGC), ② reduction in stomatal conductance (g_s), and ③ acceleration of senescence, i.e., triggering the early start of senescence and adjusting the canopy decline coefficient (CDC) to the level of water stress. All three major canopy responses are formalized with the same conceptualization and algorithms. Water deficits are quantified through a water stress coefficient (*Ks*) for each response that varies from 1 (no stress) to zero (full stress). Stress occurs when the depletion in the relative soil water content of the root zone reaches an upper threshold value, p, varying between 0 and 1. When that threshold value for a specific response is reached, *Ks* for that response is computed through the following equation:

$$Ks = 1 - \frac{(e^{D_{rel} \cdot f_{shape}} - 1)}{(e^{f_{shape}} - 1)} \quad (8)$$

Where the parameter f_{shape} influences the shape of the function *Ks* and D_{rel} is the relative depletion between the upper and lower threshold. A sample of response functions of *Ks* is presented in Fig. 2.

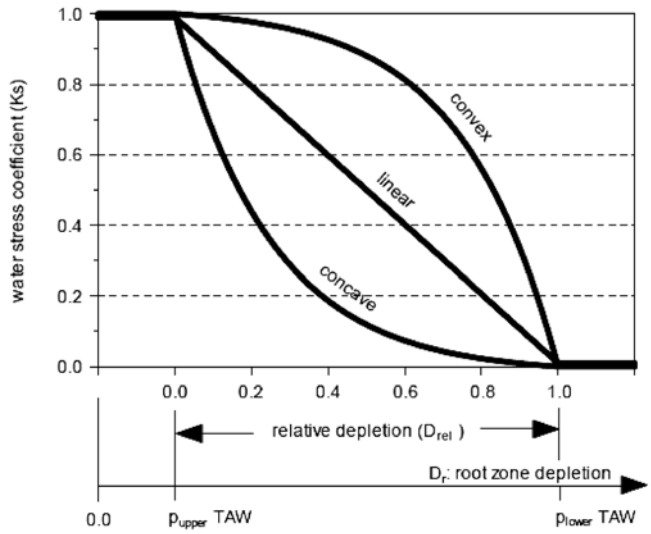

Figure 2 Examples of K_s response function to the relative depletion in soil water content. The function assumes linear shape when f_{shape}=1, concave shape when f_{shape}<0, and convex shape when f_{shape}>0. The initial and final values of p are arbitrarily taken at 0 and 1, respectively just as examples

This relatively high level of refinement for a simple model in the simulation of canopy responses to water stress is extended to the modeling of the responses of HI to water deficits. Empirical equations, but based on the competition between vegetative and reproductive growth, are used in *AquaCrop* to simulate the changes in HI when water deficits occur during the vegetative and/or the reproductive phases. Additionally, the well-known detrimental effects on HI of severe water stress during pollination and fruit set are simulated in a novel way. Pollination failure is calculated according to the fraction of total flowers that would be pollinated each day when stress of a certain level occurs, but its impact on HI is modulated by the extent that excessive potential fruits are present. This model component is still under testing against the limited datasets that exist on this important response. For further insight on the algorithms for simulating the HI responses to water deficits, the reader is referred to Raes et al (2008a).

2.8 The Soil-Root System

The root system in *AquaCrop* is simulated through the *effective rooting depth* (ERD) and its *water extraction pattern*. ERD is defined as the soil depth where most of the root water uptake is taking place, even though some crops may have a few roots beyond that depth. Water extraction pattern follows by default the standard 40%, 30%, 20%, and 10% for each quarter of the ERD starting with the top quarter, and may be established by the user in cases where different patterns are inferred from soil physical or chemical limitations. For the soil profile explored by the root system, the model performs a water balance that includes the processes of infiltration, runoff, drainage within the root zone, deep percolation, plant uptake, evaporation, and transpiration. Capillary rise is not yet included in the current version of *AquaCrop*. A daily soil water balance keeps track of the incoming and outgoing water fluxes at the boundaries of the root zone and of the water retained within it.

The distinctive features of the soil model component of *AquaCrop* are the adaptation of the *BUDGET* (Raes et al., 2006) approach to compute the soil water balance, and the procedures followed to

simulate soil E. Briefly, the soil is divided into 12 compartments of variable depth, a requirement for the detailed simulation of E and of root water uptake. A set of finite differential equations compute the water movement between compartments, while crop water uptake is calculated with a root extraction term (Belmans et al., 1983). The model simulates unsaturated flow by comparing the drainage ability of the different soil horizons (Raes et al., 2006).

The simulation of E from soil is based on the principle of Stage I and Stage II drying (Philip, 1957; Ritchie, 1983) often used by models but relies on a new equation to simulate E during the Stage II drying phase (Raes et al., 2008a) with soil water content of the surface layer as the driver of the E process, instead of using the more common time function (Ritchie, 1972).

2.9 The Management

The management component of *AquaCrop* has two main categories: one on the more general *field* management, and one more specifically on *water* management. Under *field* management are options to select or define the fertility level or regime of the soil, to select and define field-surface practices of mulching to reduce soil E, or the use of soil bunds to control run-off and infiltration, and to define the time of cuttings of forage crops. The model does not compute nutrient balances; instead, parameterization is done for several fertility levels, ranging from optimal to poor. In addition the user may parameterize and define his/her own fertility level. These fertility levels affect CGC, CC_x, the onset of canopy senescence and rate of decline in CC, and the normalized WP. In addition, fertility may also affect stomata. Thus, *AquaCrop* provides general options to account for variations in fertility regime on the overall yield response, but does not simulate the nutrient cycles and dynamics.

Under *water* management are options to select ① rainfed-agriculture (no irrigation) or ② irrigation. Under irrigation one selects the application method (sprinkler, drip, or surface either by furrow or flood irrigation). The user can define his/her own schedule on the basis of applied water depth, or timing criteria, or let the model automatically generate the scheduling on the basis of fixed interval, fixed depth, or fixed percentage of soil water content criteria. With weather data as input, the model can either run the simulation automatically over the whole season, or run in time steps of 1 day or longer as defined by the user. The latter option is particularly suitable for trying out different irrigation schedules by adding water of selected amounts at selected times over the crop development cycle. The user interface offers several options of instant display of the simulated results in terms of crop production parameters or soil water balance. Thus, *AquaCrop* is particularly suited for optimizing a schedule of supplemental or deficit irrigation.

3 Model Performance

AquaCrop has recently been parameterized and calibrated for several crops, and validated against experimental data obtained either in other locations under different climate and water treatments, or in other years. We report here some results of *AquaCrop* performance to show its predictive capabilities for maize, cotton, soybean, and quinoa. In all the results presented here, the "measured" canopy cover was derived from the measured LAI, using a regression equation based on a number of data sets where both CC and LAI were measured.

3.1 Maize

The most extensive efforts on calibration and validation of *AquaCrop* have been carried out in maize (Hsiao et al., 2008; Heng et al., 2008). The maize crop parameters of *AquaCrop* were initially calibrated with an extensive dataset obtained in 6 field experiments conducted at the University of

California, Davis in 6 different years (Hsiao et al., 2008). Instead of calibrating the model with 1 or 2 years of measured data and then test the calibrated model with data measured in other years, the calibration was performed to fit the simulations of all 6 years of Davis data (Hsiao et al., 2008). The soil of the experimental area is dominantly Yolo silty clay loam, high in water holding capacity, deep and with no restrictive layers, allowing roots to reach 2.7 m depth near the end of the season. The climate is Mediterranean, with an annual average rainfall of 440 mm confined mostly to the winter-early-spring period. The 6 experiments involved 4 different cultivars. In the simulation, it was assumed that the cultivars differed only in their phenology, i.e., in their time to flower, senescence and maximum rooting depth, and physiological maturity. The same stress response functions were used regardless of the cultivar or year, or the stress treatment.

All treatments were irrigated around planting time. Thereafter the control treatment was irrigated regularly to ensure maximum production. The stress treatments were rainfed, irrigated regularly only for the first 40% or only for the last 55% of the life cycle, or irrigated lightly 2 or 3 times during the season. Model calibration was performed by comparing the simulated against the measured results for each simulation run, and a common set of parameters were selected which fitted best all the 6 years of experimental data used in this calibration. These parameters were then used to simulate maize data sets collected from 3 locations in other parts of the world, 2 of which were climatically very different from that of Davis (Heng et al., 2008). The parameters values obtained in the calibration of AquaCrop with the experiments conducted in Davis are given in Hsiao et al., (2008).

Model validation for maize was carried out with datasets from Bushland, Texas, Gainsville, Florida, and Zaragoza, Spain, largely differing in soil and climatic conditions (Heng et al., 2008). The Gainsville and Zaragoza datasets were obtained from ICASA Data Exchange (IDE) at http://www.icasa.net, while the Bushland datasets were originally reported by Howell et al (1996). An example of the degree of agreement between measured and simulated values with *AquaCrop* is shown in Fig. 3 for the canopy development and biomass accumulation collected in three experiments in Bushland. *AquaCrop* simulated very well the canopy cover development of 1989 and both the full and short seasons irrigated treatments in 1994 (Fig. 3). In 1990 the simulation of CC was also very good, although the maximum canopy cover in the irrigated treatment was slightly under-estimated (Fig. 3). On the other hand, the CC of the non-irrigated short-season treatment in 1994 was not well simulated after day 70; the simulated canopy cover declined faster than the measured values (Fig. 3).

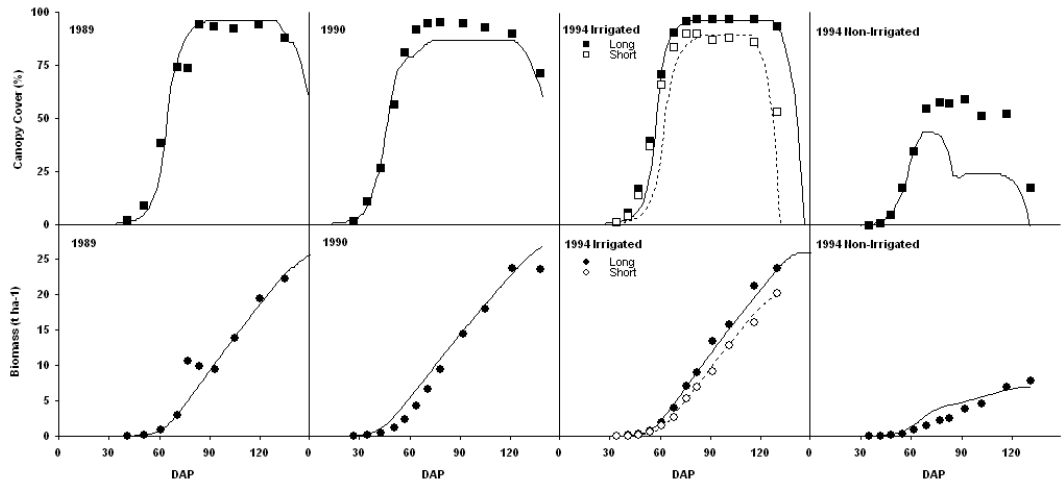

Figure 3 Simulated (line) and measured canopy cover (■) (top) and biomass (●) (bottom) accumulation of maize for the 1989, 1990 and the 1994 fully irrigated and non-irrigated treatments in Bushland, Texas

The time course of biomass production for the three seasons' irrigated treatments in Bushland was simulated accurately (Fig. 3b). The model was able to properly simulate the 1989, 1990 and both the full and short seasons irrigated biomass in 1994. Contrary to the under-prediction in the canopy cover in the non-irrigated short-season treatment in 1994 (Fig. 3a), the model simulated the biomass production that year fairly well (Fig. 3b). The values of simulated and observed total biomass and grain yield are given in Table 1. The biomass comparison shows that the majority of values had a deviation of less than 5%, while the comparison between measured and simulated grain yield was also within 3% in three out of the four cases (no grain yield was given in the non-irrigated treatment in 1994). Excellent match in grain yield was observed in 1989 while grain yield simulation was off by 12.4% in the 1994 irrigated full-season hybrid, even though final biomass was accurately simulated.

Table 1 Comparison between measured and simulated total biomass, grain yield and seasonal evapotranspiration (ET) for Bushland, Texas

Treatment	Final Biomass (Mg ha^{-1})		Grain Yield (Mg ha^{-1})		Total ET (mm)	
	Measured	Simulated	Measured	Simulated	Measured	Simulated
1989 – FI	22.3	25.6	12.4	12.1	625.0	598.0
1990 – FI	26.2	26.8	13.1	12.7	730.8	778.3
1994 – FI (Full Season)	27.8	26.2	13.2	12.3	882.1	808.0
1994 – FI (Short Season)	20.4	19.9	11.3	9.5	696.0	687.0
1994 – NI (Short Season)	7.8	7.0	NA	3.4	NA	—

Model validation results for the experiments located in Gainesville (Florida) and Zaragoza, (Spain), were also quite good, although with less satisfactory results when simulating severe water-stress treatments, especially when stress occurred during senescence (Heng et al., 2008). Overall, considering that parameterization and calibration was done using data collected only in Davis, California, the results of the validation in Texas, Spain and Florida were quite satisfactory.

3.2 Cotton

Parameterization and calibration of *AquaCrop* for cotton under full and deficit irrigation was performed by Farahani et al., (2008) in the eastern Mediterranean environment of northern Syria. The experimental site (Tel-Hadya) is characterized by an annual average rainfall of 350 mm concentrated in the fall to early spring, with no rainfall during the hot and windy summer. Soil at the site is over 1.5 m deep, well-drained, and of clay texture. Experimental results from 3 sequential years (2004 to 2006) were used for the investigation.

The short season cotton cultivar *Aleppo-118* was sown beginning May. Cotton was drip irrigated. Four levels of irrigation were applied and measured by flow meters, namely 40, 60, 80, and 100% of the estimated full water requirements.

AquaCrop was parameterized for cotton using data of 2006 and the parameters were then used to validate the model for the 2004 and 2005 experiments. The model was used to predict ET and seed yield. Validation results for 2004 and 2005 are shown in Fig. 4. *AquaCrop* simulated total ET across irrigation treatments and years with a RMSE of 38 mm, and cotton seed yield with a RMSE of 0.36 t ha^{-1}.

Cotton, being an indeterminate crop with a detrimental tendency to go highly vegetative when water supply is ample, has a complex response to the environment variations and its behavior is

difficult to simulate. Current cotton simulation models such as *GOSSYM* (Baker et al., 1983; Whisler et al., 1986) are amongst the more elaborate mechanistic crop simulation models. The results from Farahani et al. (2008) with *AquaCrop* provide a set of first estimates for the difficult-to-determine parameters for further testing of the model for cotton at other locations. Obviously, this parameterization and testing are preliminary and further work is needed at other geographical locations and under different water deficit regimes. *AquaCrop* has been used to develop optimal strategies for deficit irrigation of cotton under conditions of Southern Spain (Garcia-Vila et al., 2008).

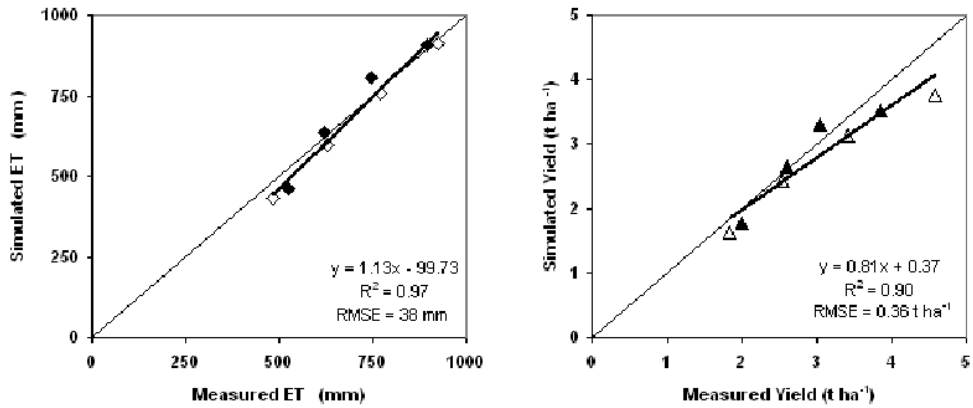

Figure 4 Simulated (line) and measured evapotranspiration (♦) and seed yield (▲) of cotton for the 2004 (solid) and 2005 (open) growing seasons in Tel Hadya, Syria

3.3 Soybean

The evaluation of *AquaCrop* for simulating soybean growth, development and yield was conducted using data from experiments over a seven-year period (1995 – 2001), conducted on a 4.7 ha watershed at the ICRISAT Center, Patancheru, Andhra Pradesh in India. The cropping system was a sequence of soybean-chickpea rotated every year on the same field, with soybean sown during the rainy season and chickpea during the post-rainy season. The soybean cultivar PK 472 was planted with a density of 30 plants/m^2 around 25 June each year, depending on the onset of rainy season. The soil is a Vertic Inceptisol with depth varying between 110 and 125 cm and a extractable soil water around 150 mm/m. Five replicated plant samples were collected over an area of 0.5 m^2 every 7 to ten days throughout the season. Leaf area index and biomass, separated into stems, leaves and pods, were measured on each sample. Final yield was determined on a 45 m^2 area per plot.

The phenology, growth and productivity data of 1996 were used to calibrate the model. Using the planting density, sowing date and measured initial soil water content for that year to initiate the model, WP* was parameterized as 12 g m^{-2} before anthesis, and was reduced by 20% during yield formation, because of the high lipid and protein content of soybean seeds. The model parameters calibrated with the 1996 data were then used to validate *AquaCrop* using the independent dataset from the other six years. A summary of the results comparing the simulated and measured trends of biomass and seed weight for 1996 through 2001 is given in Fig. 5.

Good agreement was observed between measured and simulated values. This result was particularly significant given the variability in rainfall observed over the six years of validation (Fig. 6).

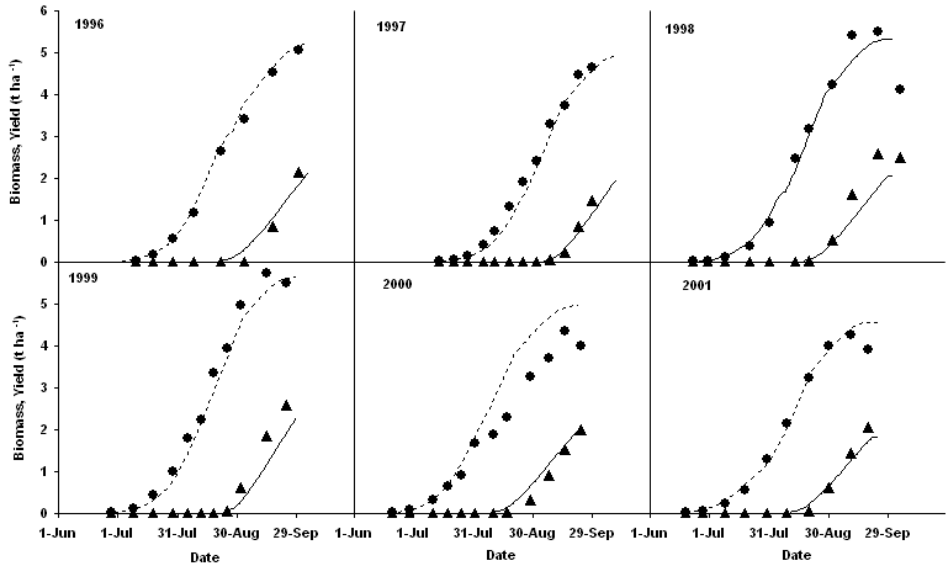

Figure 5 Simulated (line) and measured biomass (●) and yield (▲) of soybean for the 1996 – 2001 crop seasons in Patancheru, India

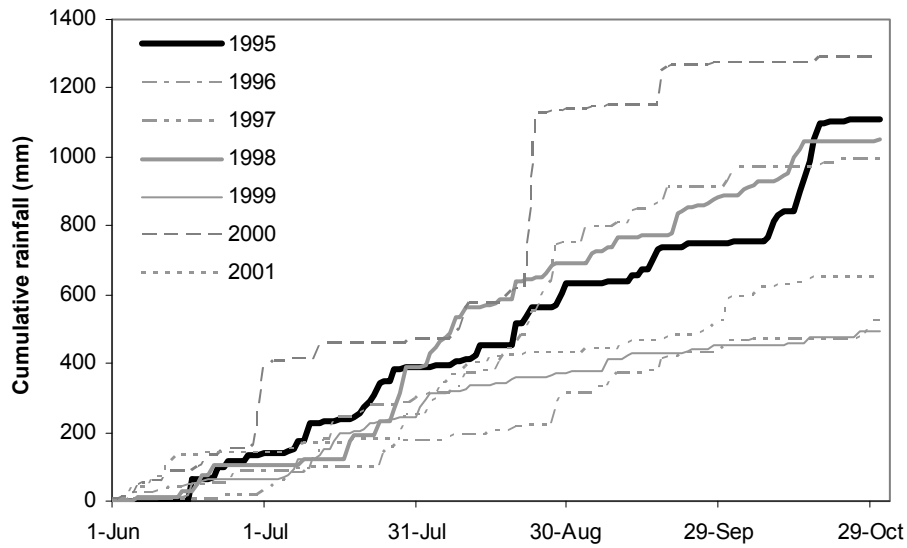

Figure 6 Cumulative rainfall during soybean cropping cycles for the 1995 – 2001 seasons in Patancheru, India

In 2000, *AquaCrop* over-predicted biomass in the second half of the crop cycle. The reason for the apparent over-estimation is not clear. It is possible that due to the unusually high rainfall recorded in that particular season (over 1200 mm between June and September) there might have been some problems either with experimental data collection or with the crop behavior. In fact, close examination of the measured trend reveals a downward shift in biomass production starting from the middle of August up to harvest. The simulations of canopy cover for the six years (Fig. 7) were also satisfactory, except during the early parts of some years when the simulations delayed emergence by 3-5 days as compared to the measured data. That resulted in a discrepancy in the predicted date of maximum canopy cover, as showed in Fig. 7.

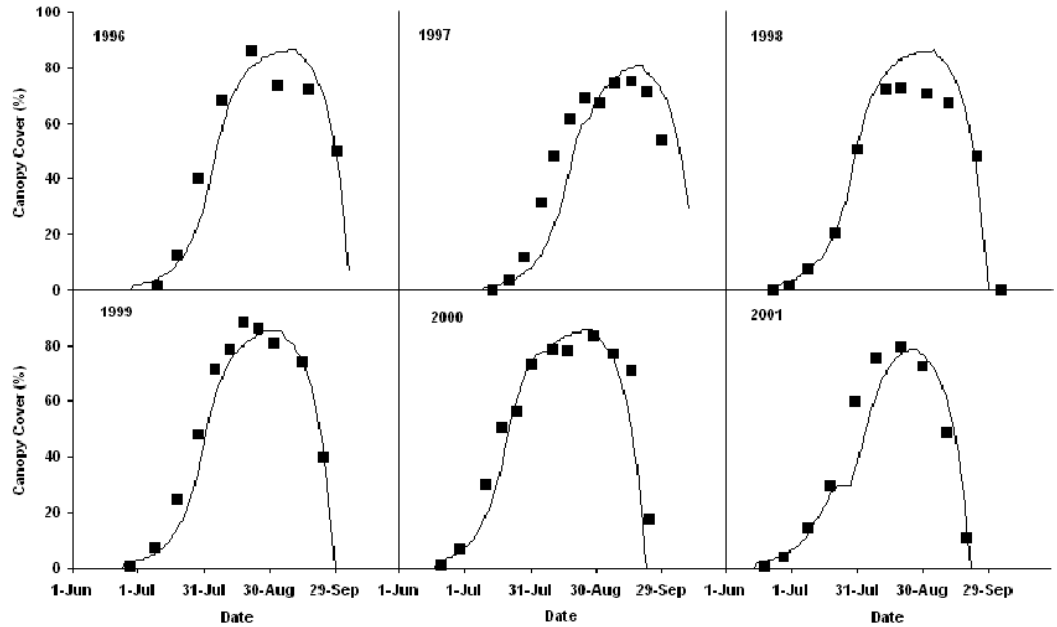

Figure 7 Comparison of AquaCrop simulated (lines) and observed (symbols) canopy cover of soybean during the 1996 – 2001 crop seasons in Patancheru, India

The comparison of simulated against observed biomass and grain yield for the six soybean seasons were in close agreement (Table 2). The excellent overall performance of *AquaCrop* in this case is demonstrated by the fact that only 1 in 6 predictions of biomass and grain yields was outside the 5% deviation of the observed values.

Table 2 Measured and simulated final grain and biomass yields, absolute difference between simulated and measured, maximum and minimum absolute difference, and Root Mean Square Error (RMSE) of soybean during the 1996 – 2001 crop seasons in Patancheru, India

	Biomass at Harvest (t ha^{-1})			Yield (t ha^{-1})		
	Measured	Simulated	|Δ|	Measured	Simulated	|Δ|
1996	5.1	5.2	0.1	2.4	2.1	0.3
1997	4.6	4.9	0.3	1.5	2.0	0.5
1998	5.5	5.3	0.2	2.6	2.1	0.5
1999	5.7	5.6	0.1	2.6	2.3	0.3
2000	5.1	5.8	0.7	2.3	2.3	0.0
2001	4.3	4.6	0.3	2.1	1.8	0.3
Δmax	—	—	0.7	—	—	0.5
Δmin	—	—	0.1	—	—	0.0
RMSE	—	—	0.3	—	—	0.4

AquaCrop has shown sensitivity to initial soil moisture conditions. These were quite variable and difficult to characterize in this case due to the cracking features of the soils of the experimental field (Vertisols and Vertic intergrades). While the very good performance of *AquaCrop* for this dataset is quite encouraging, there is a need to verify the validity of the soybean crop parameters, derived in the semi-arid tropics of India, in other regions.

3.4 Quinoa

AquaCrop has also been calibrated and validated by Geerts et al (2008) for the simulation of ① the soil water balance, ② biomass and ③ seed yield of quinoa (Chenopodium quinoa Willd.) in the Bolivian Altiplano. To calibrate and validate *AquaCrop*, the data of a mini-lysimeter experiment (2004 – 2005) and several field experiments (2005 – 2006 and 2006 – 2007) in 4 locations in the Central and Southern Bolivian Altiplano, described in Geerts et al (2006 and 2008), were used. In each location, the irrigation treatments included: rainfed, different strategies of deficit irrigation, and full irrigation. Quinoa land races fitting best the eco-regions in the study area were selected. The crop parameters of quinoa were calibrated using data from 8 out of the 22 monitored fields, in different years and locations, in order to obtain various environmental and boundary conditions. Excellent results were obtained for the simulation of the soil water balance transpiration, biomass and final yield, as reported in Geerts et al. (2008). An example of the simulation of the soil water content is shown in Fig. 8, where simulated values agreed very well with the measurements throughout the crop cycle. For the 14 validation fields the relation between simulated and observed biomass yielded a coefficient of determination (R^2) of 0.87, a Nash efficiency (EF) of 0.83 and a relative root mean square error (RRMSE) of 16 %. For the relation between simulated and observed yield, the statistics are $R^2 = 0.82$, EF = 0.79, and RRMSE = 18% (Geerts et al 2008).

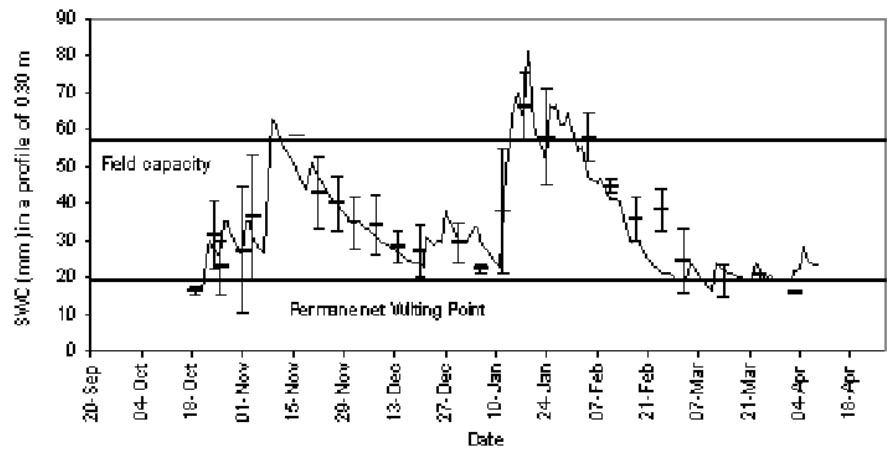

Figure 8 Simulated (line) and observed (— with error bars) soil water content (SWC) for quinoa under deficit irrigation during the 2005-2006 growing season in Patacamaya, Bolivia

4 Concluding Discussion

The conceptual framework, design, structure and key algorithms of *AquaCrop* have been described to highlight its distinctive features. *AquaCrop* is a water-driven simulation model that requires a relatively low number of parameters and input data to simulate the yield response to water of most major field and vegetable crops cultivated worldwide. When compared to other crop simulation models, its parameters are explicit and mostly intuitive and the model was built to achieve a balance between accuracy, simplicity, and robustness. The goal was to make the model as transparent as possible to users that generally do not belong to the research community and are not very familiar with the discipline of crop physiology. Since the development of the first simulation models several decades ago, modelers have attempted to incorporate all the relevant advances in crop physiology and that has resulted in relatively complex, research oriented tools that have a significantly higher number of parameters than *AquaCrop*. For instance, one of the models of the Wageningen school,

uses 27 crop-specific parameters to simulate aboveground growth and production, plus ten genetic coefficients to deal with specific traits (Yin and Van Laar, 2005). The main simulation models currently in use have also been designed to incorporate many physiological processes at a level that requires the use of a relatively large number of parameters (Wang et al., 2002).

Hammer et al. (2002) reviewed the contributions of crop modeling and focused on two areas where models may contribute in the future. One area dealt with improving the understanding of genetic regulation, and with simulating the role of different genetic traits in determining crop productivity (Hammer et al., 2002). For that purpose, crop models require the highest possible level of process physiology, and to be as mechanistic as feasible. The other area where new developments were anticipated is an enhanced role for models in assisting in management decisions, policy actions, and in education and research (Hammer et al., 2002). *AquaCrop* clearly attempts to contribute in this second area. The model is aimed at a broad range of users, from field engineers and extension specialists to water managers at the farm, district, and higher levels. It can be used as a planning tool or to assist in making management decisions, whether strategic, tactical or operational. Even though *AquaCrop* uses a limited number of parameters, it represents an effort to incorporate current knowledge of crop physiological responses to water deficits into a tool that can predict the attainable yield of a crop based on the water supply available. One important application of *AquaCrop* would be to compare the attainable against actual yields in a field, farm, or a region, to identify the constraints limiting crop production and the water productivity levels (benchmarking tool). It can also be used by economists, water agencies, and managers for scenario analysis and for planning purposes. It is suited for prospective studies such as those of future climate change scenarios. Overall, it is particularly suited to develop agricultural water management strategies for a variety of objectives and applications.

The particular features that distinguishes *AquaCrop* from other crop models are its focus on water, the use of ground canopy cover instead of leaf area index, and the use of water productivity values normalized for atmospheric evaporative demand and for carbon dioxide concentration that confer the model an extended extrapolation capacity to diverse locations and seasons, including future climate scenarios. Moreover, although the model is relatively simple, it gives particular attention to the fundamental processes involved in crop productivity and in its responses to water deficits, both from physiological and agronomic background perspectives. The fact that the simulated results agreed generally well with the measured data in the examples presented suggests that *AquaCrop* may be successful in achieving a good balance in simplicity, robustness, accuracy, and ease of use. These findings are particularly promising as they have been obtained with only limited calibration of the model. For further details on the conceptual design of the model, and for the specific algorithms and calculation procedures of *AquaCrop*, the reader is referred to Steduto et al. (2008), and to Raes et al. (2008b).

Acknowledgements

The Authors would like to acknowledge: Arianna Facchi, V. Nageswara Rao, and Piara Singh, for their contribution of the soybean data for *AquaCrop* calibration; Magali Garcia, Roberto Miranda, Jorge A. Cusicanqui, Cristal Taboada, Richard Mamani, Jorge Mendoza, Ruben Huanca, and Teddious Mhizha for their contribution to the quinoa *AquaCrop* calibration and testing.

References

Allen RG, Pereira LS, Raes D, Smith M (1998) Crop evapotranspiration: guidelines for computing crop water requirements. Irrigation and Drainage Paper n. 56. FAO, Rome, Italy.

Amir J and Sinclair TR (1991) A Model of Water Limitation on Spring Wheat Growth and Yield. Field Crop Res 28:59 – 69.

Asseng S and Hsiao TC (2000) Canopy CO_2 assimilation, energy balance, and water use efficiency of an alfalfa crop before and after cutting. Field Crop Res 67:191 – 206.

Azam-Ali SN and Squire GR (2002) Principles of Tropical Agronomy, CABI Publishing, Wallingford, UK.

Baker DN, Lambert JR, McKinion JM (1983). GOSSYM: A simulator of cotton crop growth and yield. South Carolina Agr. Expt. Sta. Tech. Bull. 1089.

Belmans C, Wesseling JG, Feddes RA (1983) Simulation of the water balance of a cropped soil: SWATRE. J Hydrol 63:271 – 286.

Cavero JI, Farre I, Debaeke P, Faci JM (2000) Simulation of maize yield under water stress with the EPICphase and CROPWAT models. Agron J 92:679 – 690.

Doorenbos J and Kassam AH (1979) Yield response to water. Irrigation and Drainage Paper n. 33. FAO, Rome, Italy

Farahani HJ, Izzi G, Oweis TY (2008). Parameterization and evaluation of AquaCrop for full and deficit irrigated cotton. Agron J special issue (under publication).

García-Vila M, Fereres E, Mateos L, Orgaz F, Steduto P (2008) Deficit Irrigation Optimization of Cotton with AquaCrop. Agron J special issue (under publication).

Geerts S, Raes D, Garcia M, Del Castillo C, Buytaert W (2006) Agro-climatic suitability mapping for crop production in the Bolivian Altiplano: A case study for quinoa. Agric Forest Meteorol 139:399 – 412.

Geerts S, Raes D, Garcia M, Miranda R, Cusicanqui JA, Taboada C, Mendoza J, Huanca R, Mamani A, Condori O, Mamani J, Morales B, Osco V, Steduto P (2008) Simulating Yield Response to Water of Quinoa (Chenopodium quinoa Willd.) with FAO-AquaCrop. Agron J special issue (under publication).

Gommes RA (1983). Pocket computers in agrometeorology. *Plant production and Protection Paper* n. 45. FAO, Rome, Italy.

Hammer GL, Kropff MJ, Sinclair TR, Porter JR (2002) Future contributions of crop modeling:/from heuristics and supporting decision making to understanding genetic regulation and aiding crop improvement. Eur J Agron 18:15 – 31.

Heng LK, Hsiao TC, Steduto P, Evett SR, Howell TA, Raes D, Fereres E (2008) Validating the FAO AquaCrop Model on Irrigated and Water Deficient Field Maize. Agron J special issue (under publication).

Hsiao TC (1993) Effects of drought and elevated CO_2 on plant water use efficiency and productivity. In: Jackson MD Black CR (eds) Global environmental change. Interacting stresses on plants in a changing climate. NATO ASI series. Springer, New York.

Hsiao TC, Heng LK, Steduto P, Raes D, Fereres E (2008) AquaCrop — Model Parameterization and Testing for Maize. Agron J special issue (under publication).

Jones CA and Kiniry JR (ed.) (1986) CERES-Maize: A simulation model of maize growth and development. Texas A&M University Press, College Station, TX.

Jones JW, Hoogenboom G, Porter CH, Boote KJ, Batchelor WD, Hunt LA, Wilkens PW, Singh U, Gijsman AJ, Ritchie JT (2003) The DSSAT cropping system model. Eur J Agron 18:235 – 265.

Keating BA, Carberry PS, Hammer GL, Probert ME, Robertson MJ, Holzworth D, Huth NI, Hargreaves JNG, Meinke H, Hochman Z, McLean G, Verburg K, Snow V, Dimes JP, Silburn M, Wang E, Brown S, Bristow KL, Asseng S, Chapman S, McCown RL, Freebairn DM, Smith CJ (2003) An overview of APSIM; a model designed for farming systems simulation. Eur J Agron 18:267 – 288.

McMaster GS and Wilhelm WW (1997) Growing degree-days: one equation, two interpretations. Agric Forest Meteorol 87:291 – 300.

Penning de Vries FWT, van Laar HH, Chardon MCM (1983) Bioenergetics of growth of seeds, fruits and storage organs. In: Smith WH and Banta SJ (eds): Productivity of Field Crops Under Different Environments. IRRI, Los Baños, The Philippines.

Philip JR (1957) Evaporation, and moisture and heat fields in the soil. J Meteorol 14:354 – 366.

Raes D, Geerts S, Kipkorir E, Wellens J, Sahli A (2006) Simulation of yield decline as a result of water stress with a robust soil water balance model. Agr Water Manage 81:335 – 357.

Raes D, Steduto P, Hsiao TC, Fereres E, Heng L (2008a) AquaCrop Calculation Procedures, Prototype Version 2.4. FAO, Rome, Italy.

Raes D, Steduto P, Hsiao TC, Fereres E (2008b) AquaCrop — The FAO crop model for predicting yield response to water: II. Main algorithms and software description. Agron J special issue (under publication).

Ritchie JT (1972) Model for predicting evaporation from a row crop with incomplete cover. Water Resources Research 8, 1204-1213Ritchie JT (1983). Efficient water use in crop production: Discussion on the generality of relations between biomass production and evapotranspiration. In: HM Taylor et al. (ed.) Limitations to efficient water use in production. ASA, CSSA, and SSSA, Madison, WI.

SCS (1993). 'Irrigation water requirements' National Engineering Handbook, part 623. *Soil Conservation Service*, US Dept. of Agriculture. Washington, USA.

Steduto P (2003). Biomass Water-Productivity. Comparing the Growth-Engines of Crop Models. FAO Expert Consultation on Crop Water Productivity Under Deficient Water Supply, 26 - 28 February 2003, Rome, Italy.

Steduto P and Albrizio R (2005). Resource use efficiency of field-grown sunflower, sorghum, wheat and chickpea. II. Water Use Efficiency and comparison with Radiation Use Efficiency. Agric Forest Meteorol 130:269 – 281.

Steduto P, Hsiao TC, Fereres E (2007) On the conservative behaviour of biomass water productivity. Irrigation Science 25, 189 – 207.

Steduto P, Hsiao TC, Raes D, Fereres E (2008) AquaCrop - The FAO Crop Model to Predict Yield Response to Water: I Concepts. Agron J special issue (under publication).

Stewart JI, Hagan RM, Pruitt WO (1974) Functions to predict optimal irrigation programs. J. Irr. Drain. Div. ASCE 100:179 – 199.

Tanner CB and Sinclair TR (1983) Efficient water use in crop production: research or re-search? In: Eds Taylor HM, Jordan WR, Sinclair TR Limitations to efficient water use in crop production. ASA, CSSA, SSSA, Madison, Wisconsin, USA.

van Ittersum MK, Leffelaar PA, van Keulen H, Kropff MJ, Bastiaans L, Goudriaan J (2003) On approaches and applications of the Wageningen crop models. Eur J Agron 18:201 – 234.

Wang E, Robertson MJ, Hammer GL, Carberry PS, Holzworth D, Meinke H, Chapman SC, Hargreaves JNG, Huth NI, McLean G (2002) Development of a generic crop model template in the cropping system model APSIM. Eur J Agron 18:121 – 140.

Whisler FD, Acock B, Baker DN, Fye RE, Hodges HF, Lambert JR, Lemmon HE, Mckinion JM, Reddy VR (1986) Crop simulation models in agronomic systems. Adv Agron 40:141 – 208.

Wheeler TR, Hong TD, Ellis RH, Batts GR, Morison JIL, Hadley P (1996) The duration and rate of grain growth, and harvest index, of wheat (Triticum aestivum L.) in response to temperature and CO2. J Exp Bot 47:623 – 630.

Xu LK and Hsiao TC (2004) Predicted vs. measured photosynthetic water use efficiency of crops stands under dynamically changing field environments. J Exp Bot 55:2395 – 2411.

Yin X and Van Laar HH (2005) Crop Systems Dynamics: An Ecophysiological Simulation Model for Genotype-by-Environment Interactions. Wageningen Academic Publishers, Wageningen, The Netherlands.

Simulating Biomass and Grain Yields of Barley and Oat Crops with the Sirius Wheat Model

A.L. Fletcher, R.J. Martin, J.M. de Ruiter, P.D. Jamieson, R.F. Zyskowski

(New Zealand Institute for Crop & Food Research Limited
Private Bag 4704
Christchurch 8140
New Zealand, E-mail: fletchera@crop.cri.nz)

Abstract: Mechanistic crop models have been used widely to simulate wheat crop responses to the environment. In contrast, there have been few attempts to model barley or oat responses using crop simulation models. This study used Sirius to simulate barley and oat crops from a range of sowing dates under good growing conditions. Simulations were conducted using Sirius, a crop model that was originally conceived for wheat but has a mechanistic framework that is sufficiently robust to be applied to other temperate cereals. The objective of this research was to test the processes operating within the model rather than simply applying it to predict final yields. Therefore, data sets were chosen that had intensive within-season measurements of leaf area index (LAI), biomass and grain yield.

All observed crops were grown at Lincoln, New Zealand, with water and nitrogen supply presumed to be non-limiting. The barley cultivars grown were 'Triumph', 'Dash', and 'Valetta' at five sowing dates and the oat cultivar grown was 'Drummond' at seven sowing dates. Sirius requires a small set of cultivar-specific parameters. Cultivar parameters for the phenology of 'Drummond' oats were taken from a previous experiment. A single cultivar description for 'Triumph' was used for all barley simulations. This cultivar description was based on wheat but with a more rapid phyllochron and a slightly modified LAI relationship with thermal conditions. Otherwise no modification was made to the model structure.

Time courses of crop and grain growth were generally well simulated by Sirius. Root mean squared deviations for final grain yield were 1.3 t ha^{-1} for barley and 1.0 t ha^{-1} for oats. Although there were some small errors in the simulation of LAI, these had only minor effects on simulated biomass and grain yields. However, for late autumn and early spring sowings of 'Drummond' oats LAI and biomass were over-predicted and for a mid spring sowing these parameters were under predicted. This error suggested that there is an aspect of phenological or canopy development not accounted for in Sirius. Overall, Sirius gave good predictions of biomass and grain yield of barley and oat crops under good growing conditions with little or no modification.

Keywords: cereal, crop modeling, leaf area index

Abbreviations

DAS	Days after sowing
DSS	Decision support system
LAI	Leaf area index
RMSD	Root mean squared deviations
RUE	Radiation use efficiency

1 Introduction

Mechanistic crop simulation models are important tools in crop research. They are routinely used to extrapolate results across a wide range of environments and locations, and are capable of examining the effect on multiple crop processes caused by changes in environmental conditions or genetics. Simulation models have been used to examine crop responses to sowing date and location when nutrients and water are non-limiting (Jamieson et al., 1998a; Jamieson et al., 1998c; Porter et al., 1993). These predicted potential yields are then restricted by soil water and nutrient supply (Jamieson and Ewert, 1999; Jamieson and Semenov, 2000; Jamieson et al., 1998c). In this way, simulation models can be applied to create on-farm decision support systems (DSS) (e.g. Armour et al., 2002; Armour et al., 2004a).

Wheat (*Triticum aestivum*) is the most widely grown cereal covering ~216 million ha (FAO, 2008). Therefore, it is not surprising that the bulk of simulation model development and implementation studies with cereals have focused on wheat (e.g. Porter, 1984; Weir et al., 1984). An example of one of these simulation models is the Sirius-wheat model (Jamieson et al., 1998a). Sirius uses readily available weather data (air temperature, rainfall, and solar radiation) to simulate development, growth and yield. In Sirius phenological and canopy development are driven by thermal time (Tt, °Cd). Phenology is modified by photoperiod and vernalization. However, the crop cultivars described in this paper did not have any vernalization requirement. Solar radiation interception is calculated using a modified version of Beer's law (Monsi and Saeki, 1953) with an extinction coefficient of 0.45. Crop growth is simulated using a radiation use efficiency (RUE) of 1.1 g MJ^{-1} (solar radiation), which is modified by temperature. Grain growth is simulated by assuming that ① all growth during grain filling is partitioned to grains, and ② 25% of crop biomass at the beginning of grain filling is remobilized to grains. Nitrogen and water limitations affect these model processes; however the focus in this paper is on potential yield, and therefore water and nutrients are assumed to be non limiting.

Barley (*Hordeum vulgare*) and oats (*Avena sativa*) are the next most important temperate cereals after wheat. Barley is grown on ~56 million ha and oats on 11.3 million ha (FAO, 2008). Both are used for both human consumption and animal feed, as either grain or whole crop silage. In contrast to wheat there are comparatively few studies where simulation models have been used to examine the development and yield of either barley or oats. Previous studies using simulation models to examine barley yield (de Ruiter et al., 1993; Goyne et al., 1996; Travasso and Magrin, 1998; Wahbi and Sinclair, 2005) have focused on areas where observed yields were relatively low (0-5 t ha^{-1}) because of water or nitrogen limitations.

Furthermore, these previous tests of barley models focused on final grain and biomass yields, but comparisons of model processes (i.e. how the yield was formed) are just as important as the tests of final yield (e.g. Jamieson et al., 1998c). For cereal silage production the crop will be harvested before grain maturity. Therefore, simulations of intermediate yields are vitally important.

Phenology of barley and oats (e.g. Sonego, 2000; Sonego et al., 2000) respond to temperature and daylength in a similar manner to wheat, and reported maximum RUE values are comparable to wheat (Goyne et al., 1993; Jamieson et al., 1995b; Kemanian et al., 2004; Muurinen and Peltonen-Sainio, 2006). These similarities suggest that the framework of a wheat simulation model, such as Sirius, could be used to simulate potential growth and yield responses to environment in either barley or oats.

The objective of this research was to determine if the Sirius wheat model could be used to simulate barley and oat crops from a range of sowing dates at Lincoln, New Zealand. This location is capable of producing very high cereal yields when water and nitrogen are non-limiting. In 2006 average barley and oat grain yields in New Zealand were 5.8 t ha^{-1} (10^{th} out of 101 reported countries) and 5 t ha^{-1} (5^{th} out of 75 reported countries) respectively (FAO, 2008). These high

yields are a product of the high incoming solar radiation and relatively cool temperatures during the grain growth period (Armour et al., 2004b). Therefore, this location is well suited to testing simulations of potential yields.

2 Materials and Methods

2.1 Observed Data

All of the observed crops were sown at Lincoln, New Zealand (43°38' S, 172°27' E). The observed data consisted of five experimental barley (B1 – B5) crops and seven experimental oat crops (O1 – O7) (Table 1). For B1 and B2 crops there were no intermediate measurements of grain yield. The data from the unpublished barley experiment (B3 – B5) included sowing date and population treatments. In this analysis only the data for the highest sowing rate (400 plants m^{-2}) were used, because these best represented the maximum potential yield. Data from the B1, B2 and O7 crops were from drought experiments grown under a mobile rain shelter and in one case (B2) there was also variation in N supply. The rain shelter and its operation are described in detail by Martin et al. (1992). The data used in this analysis were from the fully irrigated treatments with maximum N supply.

Table 1 Experimental details of barley and oat data sets

Treatment Code	Sowing Date	Harvest Date	Cultivar	Reference
		Barley		
B1	7 Sep 1988	9 Jan 1989	Triumph	(Jamieson et al., 1995a)
B2	20 Oct 1995	10 Feb 1996	Valetta	(de Ruiter, 1999)
B3	28 May 1999	23 Dec 1999	Dash	Unpublished
B4	30 Aug 1999	8 Feb 2000	Dash	Unpublished
B5	24 Nov 1999	17 Mar 2000	Dash	Unpublished
		Oats		
O1	16 Sep 1994	8 Feb 1995	Drummond	(Martin, 1996)
O2	2 Nov 1994	8 Feb 1995	Drummond	(Martin, 1996)
O3	21 Dec 1994	11 Apr 1995	Drummond	(Martin, 1996)
O4	7 Feb 1995	crop died	Drummond	(Martin, 1996)
O5	3 April 1995	13 Feb 1996	Drummond	(Martin, 1996)
O6	16 May 1995	13 Feb 1996	Drummond	(Martin, 1996)
O7	29 Sep 1998	3 Mar 1999	Drummond	(Martin et al., 2001)

The O4 crop died during winter 1995, therefore only biomass and LAI for the first few months of crop growth were used. For the O1 – O6 oat crops, only measurements of intermediate panicle yield were made (i.e. intermediate grain yields were not measured). These were converted to grain yields by assuming that 7% of the final panicle yield was made up of non-grain parts. These values were then subtracted from the earlier intermediate panicle yields. The error this assumption introduced was assumed to be negligible.

For the B3 – B5 barley crops there were no LAI measurements. Instead the proportion of solar radiation intercepted by the canopy was measured using a ceptometer. These values were compared with the simulated solar radiation interception values.

2.2 Simulations

The Sirius wheat model (Jamieson et al., 1998a) was used to simulate canopy development, biomass

and grain yield for each of the experimental crops. In each case observed weather data (daily minimum and maximum air temperature and incident solar radiation) were collected less than 500 m from the experimental site. In each simulation it was assumed that soil N and water were not limiting crop growth.

Sirius requires a few cultivar-specific input parameters to describe each wheat cultivar. These are principally the parameters that describe phenology responses to temperature and photoperiod (Brooking et al., 1995; Jamieson and Munro, 2000; Jamieson et al., 1995c; Jamieson et al., 1998b). For the barley crops these parameters were determined by calibration with the B1 data set. This resulted in a phyllochron of 87°Cd, no response to photoperiod, a fixed number of leaves (9) and a slower rate of canopy development than a typical wheat crop. The same cultivar description was used for the other two varieties. For the oat crops these parameters were determined by examining phenology results from a previous experiment (Sonego et al., 1997; Sonego et al., 2000). This gave a phyllochron of 99°Cd, a minimum leaf number of 8 and a maximum of 11, and a response to photoperiod of 0.75 leaves hr^{-1}. Neither the barley or oat crops had a vernalization requirement. Otherwise all other parameters were the same as for the spring wheat cultivar 'Batten' (Table 2).

Table 2 Cultivar-specific parameters used for barley and oats in the Sirius wheat model. Parameters for a typical wheat cultivar are included for comparison

Cultivar Parameter	Barley	Oats	Wheat Cultivar[1]
Phyllochron	87℃d	99℃d	100℃d
Response to vernalization	none	none	none
Response to photoperiod[2]	0 leaves hr^{-1}	0.75 leaves hr^{-1}	0.5 leaves hr^{-1}
Minimum leaf final leaf number	9	8	7.5
Maximum leaf final leaf number	9	11	12
Canopy development[3]	1.20	1.79	1.79

[1] The example is for the wheat cultivar 'Batten' used in a previous paper (Jamieson et al., 1998a).
[2] Leaves per hour of photoperiod.
[3] Factor for relative LAI growth rate in thermal time.

Simulated values of final biomass and grain yield were compared with observed data using root mean squared deviations (RMSD, Eq. (1)).

$$\mathrm{RMSD} = \sqrt{\frac{\sum (\mathrm{Observed} - \mathrm{Predicted})^2}{n}} \tag{1}$$

where n is the number of observations.

3 Results and Discussion

3.1 Final Grain and Crop Biomass Yields

There was substantial variation in final grain yields caused by the different sowing date treatments for both barley and oats. Observed barley grain yields ranged from 7.2 t ha^{-1} for a spring-sown crop (B2) to 12.1 t ha^{-1} for the late autumn-sown crop (B3). Observed oat grain yields ranged from 5.4 t ha^{-1} for a summer-sown crop (O3) to 10.9 t ha^{-1} for an autumn-sown crop (O5). The simulated grain yields agreed closely with the observed yields for both barley and oats (Figure 1a). The RMSD was 1.3 t ha^{-1} for barley and 1.0 t ha^{-1} for oats. This represented 14 and 13% of the mean observed yields respectively.

The variation in final biomass yields reflected the differences in grain yield between sowing date treatments. Observed biomass for barley ranged from 12.7 t ha^{-1} for a spring-sown crop to 18.3 t ha^{-1} for late autumn-sown crop. Observed oat biomass was 9.8 t ha^{-1} for a summer-sown crop and 24.9 t ha^{-1} for the autumn-sown crop. Again the simulated values closely fitted the observed final biomass data (Fig. 1b). The RMSDs for final biomass yields were 1.4 t ha^{-1} (9%) for the barley crops and 3.8 t ha^{-1} (25%) for the oat crops.

These values of RMSD for both grain and biomass yields are similar to estimates for 'Rongotea' and 'Avalon' wheat using Sirius from a range of sowing dates drought treatments (Jamieson et al., 1998a). This indicates that the simulations have comparable accuracy for barley and oat grain and biomass yields as they have for wheat.

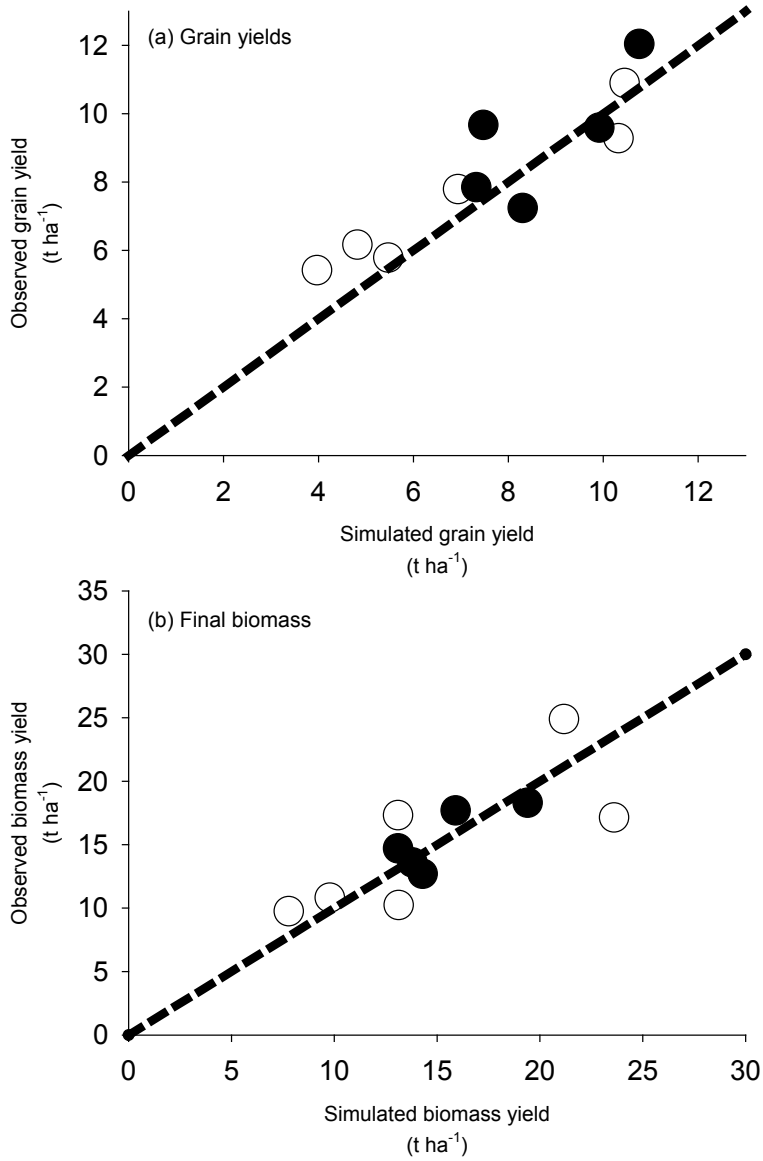

Figure 1 Comparison of simulated and observed, grain yield (a) and total biomass (b) for barley (●) and oat (○) crops. The dotted line, $y = x$, is provided for comparison

3.2 Biomass Accumulation, Partitioning and Canopy Development

Although it is important that the model accurately simulated final barley and oat yields, it is pivotal that the yields were simulated using the correct processes. Therefore, it is also important that simulated intermediate biomass and grain yields, and LAI, match closely measured values.

3.2.1 Barley

The simulations of barley total biomass growth matched the observed values closely (Fig. 2). This was despite there being markedly different patterns of growth between the five barley crops. For example, in the B3 crop rapid biomass growth of 190 kg/ha/day started about 100 days after sowing (DAS), and maximum biomass of 18.3 t/ha was reached 199 DAS. In contrast, the B5 crop began rapid biomass growth of 230 kg/ha/day about 20 DAS and reached maximum biomass of 14.3 t ha^{-1} at 96 DAS.

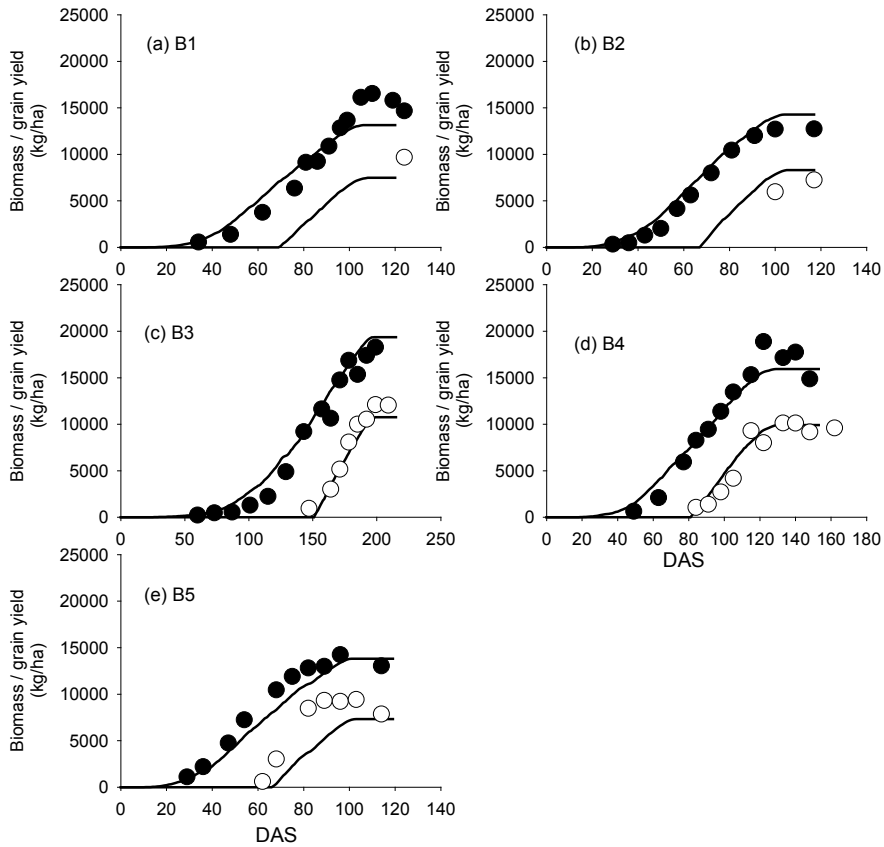

Figure 2 Comparison of simulated (solid line) and observed grain (○) and total biomass yields (●) for five barley crops

Sirius was able to simulate these differences in barley crop growth closely due to its mechanistic treatment of canopy development (Fig. 3). Canopy development was slower in the B3 crop than in the B5 crop due to its winter sowing date. Cool temperatures during early development meant that canopy establishment and the onset of rapid crop growth were delayed. On the other hand, the faster canopy establishment of the B5 crop was due to its late spring sowing date, resulting in warmer temperatures and faster canopy development. Similarly, the different duration of rapid crop

growth was also due to the different temperatures experienced by each crop during this phase. For the B1 and B2 crop Sirius under and over predicted LAI respectively (Figure 3 a and b). However, because in each case both observed and simulated LAIs were close to or greater than 4.0, the impact on simulated radiation interception was small. Assuming an extinction coefficient of 0.45, a LAI of 4.0 would intercept 83% of incoming solar radiation. In these cases it is important only that the model mimics the initial increase in LAI, the time that LAI is greater than 4.0 and the decline in LAI during crop maturation. Sirius simulated this sufficiently well for the B1 and B2 crops to produce good estimates of crop growth.

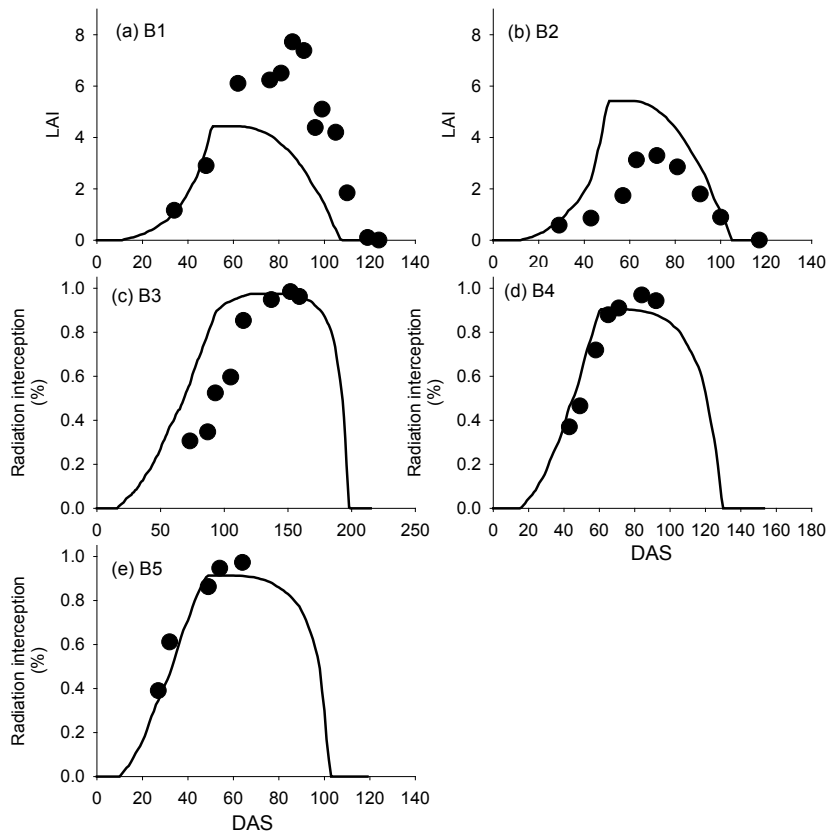

Figure 3 Comparison of simulated (solid line) and observed LAI ((a) and (b)) or radiation interception values ((c), (d) and (e)) for five barley crops

Sirius also closely matched simulated intermediate barley grain yields for the B3 and B4 crops (Figs. 2(c) and (d)). For the B5 crop, Sirius simulated final grain yield closely but predicted initial grain growth rate much slower than it actually occurred, though it closely matched intermediate biomass (Fig. 2(e)). This suggests that model under predicted the rate of remobilization of stored carbohydrate to the growing grain. However, the absolute amount of remobilized biomass appeared to be correct.

3.2.2 Oats

Sirius also gave reasonable estimates of intermediate total biomass and grain yield for the seven 'Drummond' oat crops tested (Fig. 4). Again, this was despite marked differences in crop growth rate and duration across the sowing dates. For example, in the O3 crop rapid biomass growth started

about 30 DAS, and maximum biomass of 8.7 t ha^{-1} was reached 90 DAS (Fig. 4(c)). In contrast, the O5 crop began rapid biomass growth between 100 and 150 DAS and reached maximum biomass of 24.5 t ha^{-1} at 259 DAS (Fig. 4(e)). However, Sirius did over predict intermediate total crop biomass for the O1 and O6 crops and under predict biomass for the O7 crop. Furthermore, the simulations did not match crop growth for the O4 crop from 100 DAS because the crop died during winter. However, Sirius gave excellent predictions of intermediate grain yields for the other three oat crops (Fig. 4).

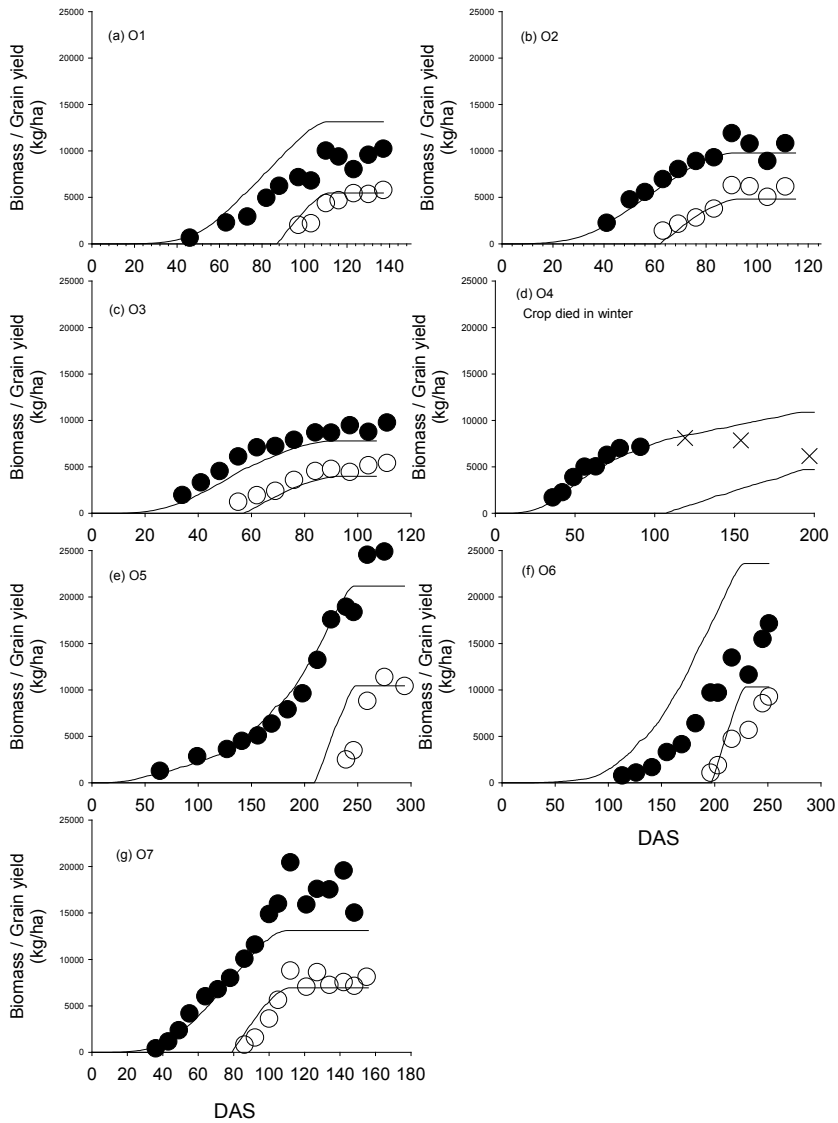

Figure 4 Comparison of simulated (solid line) and observed grain (○) and total biomass yields (●) for seven oat crops. The O4 crop (d) died in mid winter and the final three biomass points (×) are after crop senescence began. Consequently there were no observed grain yield data for O4

Sirius also generally matched the observed values of LAI well (Fig. 5). However, for the O1 and O6 crops Sirius over predicted maximum LAI values (Figs. 5(a) and (f)). This resulted in the over prediction of biomass for these two crops (Figs. 4(a) and (f)). LAI was also over predicted for the O5 crop. However, because both simulated and observed LAIs exceeded 4.0, this had minimal

impact on the simulated biomass. LAI for the O7 crop was under predicted by Sirius. Furthermore, canopy senescence was simulated about 30 days earlier by Sirius than when it actually occurred. This led to underestimates of biomass production. It is surprising then that simulated and observed grain yields matched so closely (Fig. 4(g)). For the O4 crop LAI was simulated well until about 100 DAS, when the crop died and observed LAI declined rapidly compared with the simulations. The over prediction of LAI for O1 and O6 and the under prediction of LAI for the O7 crop suggest that there is some aspect of crop phenological or canopy development of oat crops that is not fully encapsulated in the model. This warrants further investigation.

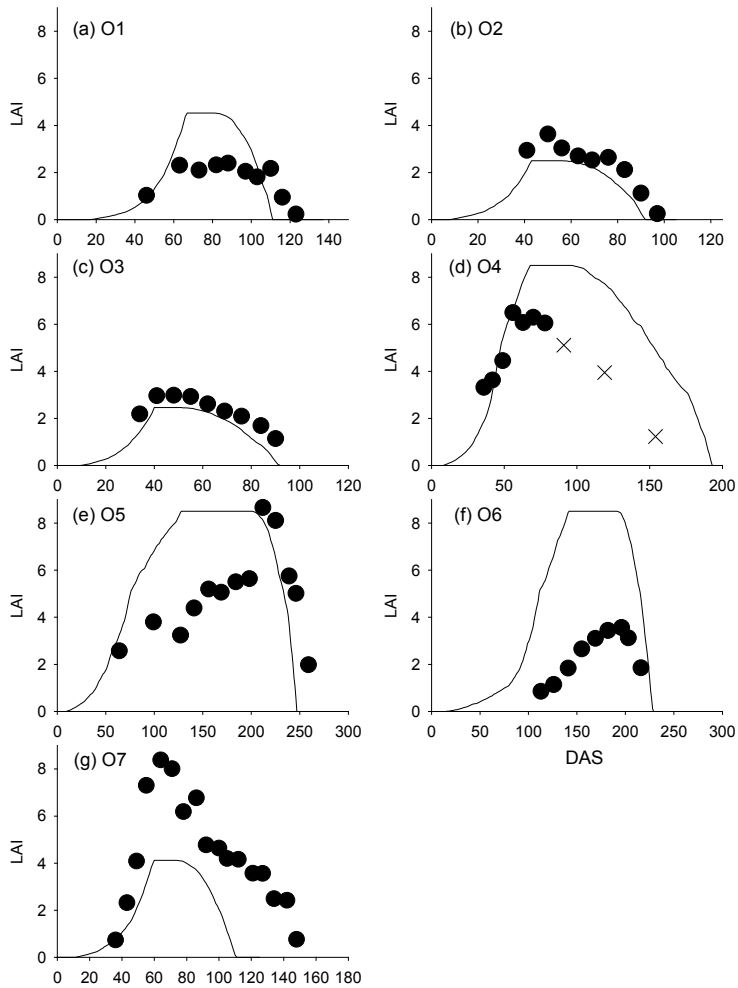

Figure 5 Comparison of simulated (solid line) and observed LAI for seven oat crops. The final three LAI points (×) for the O4 crop (d) are after crop senescence began

4 Summary and Conclusions

The research outlined in this paper demonstrated that a simple mechanistic wheat model such as Sirius simulated grain and total biomass of barley and oat crops provided the correct cultivar-specific parameters were used. This makes it possible to use Sirius as a tool for analyzing various crop management (sowing date and location) scenarios for these crops.

However, there was substantial room for improvement in some aspects of the model. For

example there was disagreement between simulated and observed leaf area index for some sowing dates, particularly for the oat crops. For all of the crops this had very little impact on simulated grain yields but it did cause substantial over (Figs. 4(a) and (f)) and under (Fig. 4 (g)) predictions of biomass. The process of canopy development and subsequent oat growth warrants further investigation and refinement.

This research has focused on simulations of barley and oat crops under optimum conditions. Sirius has a mechanistic framework for simulating responses to water and nitrogen supply in wheat (Jamieson and Ewert, 1999; Jamieson and Semenov, 2000). This framework needs to be tested against barley and oat crops where soil water and nitrogen supply are limited.

Acknowledgements

This work was carried out using resources from the "**L**and **U**se **C**hange and **I**ntensification" and "Pastoral21 Feed" programs funded by New Zealand Foundation for Research, Science and Technology.

References

Armour T, Jamieson P, Zyskowski R (2002) Testing the Sirius Wheat Calculator. Agron. NZ 32/33:1 – 6.

Armour T, Jamieson P, Zyskowski R (2004a) Using the Sirius Wheat Calculator to manage wheat quality - The Canterbury experience. Agron NZ 34:171 – 176.

Armour, T, Jamieson PD, Nicholls A, ZyskowskiR (2004b) Breaking the 15 t/ha wheat yield barrier. Proceedings of the 14th International Crop Science Congress, "New directions for a diverse planet", Brisbane, Australia, 26 Sep – 1 Oct 2004.

Brooking IR, Jamieson PD, Porter JR (1995) The Influence of Daylength on Final Leaf Number in Spring Wheat. Field Crops Res. 41:155 – 165.

de Ruiter JM (1999) Yield and quality of malting barley (*Hordeum vulgare* L-'Valetta') in response to irrigation and nitrogen fertilisation. NZ J. Crop Hort. Sci. 27:307 – 317.

de Ruiter JM, Stol W, van Keulen H (1993) Simulation of yield and quality of malting barley. Agron. NZ 23:11 – 19.

FAO (2008) FAOSTAT [Online] http://FAOstat.fao.org.

Goyne PJ, Milroy SP, Lilley JM, Hare JM (1993) Radiation Interception, Radiation Use Efficiency and Growth of Barley Cultivars. Aus. J. Agr. Res. 44:1351 – 1366.

Goyne PJ, Hammer GL, Meinke H, Milroy SP, Hare JM (1996). Development and use of a barley crop simulation model to evaluate production management strategies in north-eastern Australia. Aus. J. Agr. Res. 47:997 – 1015.

Jamieson PD, Ewert F (1999) The role of roots in controlling soil water extraction during drought: an analysis by simulation. Field Crops Res. 60:267 – 280.

Jamieson PD, Semenov MA (2000) Modeling nitrogen uptake and redistribution in wheat. Field Crops Res. 68:21 – 29.

Jamieson PD, Munro CA (2000) The calibration of a model for daylength responses in spring wheat for large numbers of cultivars. Agron. NZ 30:25 – 28.

Jamieson PD, Martin RJ, Francis GS (1995a) Drought Influences on Grain-Yield of Barley, Wheat, and Maize. NZ J. Crop Hort. Sci. 23:55 – 66.

Jamieson PD, Martin RJ, Francis GS, Wilson DR (1995b) Drought Effects on Biomass Production and Radiation-Use Efficiency in Barley. Field Crops Res. 43:77 – 86.

Jamieson PD, Brooking IR, Porter JR, Wilson DR (1995c) Prediction of Leaf Appearance in Wheat - a Question of Temperature. Field Crops Res. 41:35 – 44.

Jamieson PD, Semenov MA, Brooking IR, Francis GS (1998a) Sirius: a mechanistic model of wheat response to environmental variation. Eur. J. Agron. 8:161 – 179.

Jamieson PD, Brooking IR, Semenov MA, Porter JR (1998b) Making sense of wheat development: a critique of methodology. Field Crops Res. 55:117 – 127.

Jamieson PD, Porter JR, Goudriaan J, Ritchie JT, van Keulen H, Stol W (1998c) A comparison of the models AFRCWHEAT2, CERES-wheat, Sirius, SUCROS2 and SWHEAT with measurements from wheat grown under drought. Field Crops Res. 55:23 – 44.

Kemanian AR, Stockle CO, Huggins DR (2004) Variability of barley radiation-use efficiency. Crop Sci. 44:1662 – 1672.

Martin RJ (1996) The effect of sowing date on growth and yield of two cultivars of oats. Agron. NZ 26:51 – 59.

Martin RJ, Jamieson PD, Wilson DR, Francis GS (1992) Effects of soil moisture deficits on yield and quality of 'Russet Burbank' potatoes. NZ J. Crop Hort. Sci. 20:1 – 9.

Martin RJ, Jamieson PD, Gillespie RN, Maley S (2001) Effect of timing and intensity of drought on the yield of oats (*Avena sativa* L.). Proceedings of the 10th Australian Agronomy Conference, "Science and Technology: Delivering Results for Agriculture".

Monsi M, Saeki T (1953). Über den Lichtfaktor in den Pflanzengesellschaften und seine Bedeutung für die Stoffproduktion. Jap. J. Bot. 14:22 – 52.

Muurinen S, Peltonen-Sainio P (2006) Radiation-use efficiency of modern and old spring cereal cultivars and its response to nitrogen in northern growing conditions. Field Crops Res. 96:363 – 373.

Porter JR (1984) A Model of Canopy Development in Winter-Wheat. J. Agr. Sci. 102:383 – 392.

Porter JR, Jamieson PD, Wilson DR (1993) Comparison of the Wheat Simulation-Models Afrcwheat2, Ceres-Wheat and Swheat for Nonlimiting Conditions of Crop Growth. Field Crops Res. 33:131 – 157.

Sonego M (2000) Effect of temperature and daylength on phenological development of oats (*Avena sativa* L.), Lincoln University, Canterbury.

Sonego M, Jamieson PD, Moot DJ, Martin RJ (1997) Phenological development of oat crops in response to sowing dates. Agron. NZ 27:115 – 118.

Sonego M, Moot DJ, Jamieson PD, Martin RJ, Scott WR (2000) Apical development in oats predicted by leaf stage. Field Crops Res. 65:79 – 86.

Travasso MI, Magrin GO (1998) Utility of CERES-barley under Argentine conditions. Field Crops Res. 57:329 – 333.

Wahbi A, Sinclair TR (2005) Simulation analysis of relative yield advantage of barley and wheat in an eastern Mediterranean climate. Field Crops Res. 91:287 – 296.

Weir AH, Bragg PL, Porter JR, Rayner JH (1984) A Winter-Wheat Crop Simulation-Model without Water or Nutrient Limitations. J. Agr. Sci. 102:371 – 382.

Application of the CERES-Wheat Model to Winter Wheat Yield Forecast in Beijing

Xian Wang [1,2], Cun-Jun Li [1], Liang-Yun Liu[1], Wen-Jiang Huang[1], Peng-Xin Wang[2]

(1 National Engineering Research Center for Information Technology in Agriculture: 100097, China)
(2 China agricultural University: 100083, China)

Abstract: Wheat yield is important for the economy and food requirements of the state, so there is a need for reliable estimates of wheat production under varied environments. On the basis of early-warning information of successive yield predictions, producers and marketing boards could, for example: adjust use of fertilizers, revise marketing plans, and decide on options for following seasons. The dynamic simulation model CERES-Wheat (crop estimation through resource and environment synthesis-wheat) was applied to simulate yields from 2005 to 2007 at Xiaotangshan, which located in Changping of northern Beijing. Experiment datum required of CERES-Wheat model such as soil data, weather data and management data were all collected and checked. Simulation results of 2005 were used to calibrate Model and which of the other two years were gained for validation. Model calibration was made through comparing the field-observed and model-simulated results of five stages: ① dates of anthesis and maturity; ② values of LAI (leaf area index); ③ biomass yields of anthesis and maturity; ④ dry matter of leaf, stem, and grain; ⑤ final wheat yield. The difference of simulated and actual dates of anthesis is less than 6 days, which of the autumn is less than 5 days. The values of LAI and yield also agree well with measured data. This study revealed that the calibration of CERES-Wheat can be used for the prediction of wheat growth and yield in Beijing.

Keywords: crop simulation model, wheat, yield forecast

1 Introduction

China has turned to be the largest producer of wheat in the world (FAO 2004), and nearly 95% of which is winter wheat. Considering the importance of wheat for the economy, government policy and food requirements of the state, there is a need for reliable estimates of wheat production under varied environments. On the basis of early-warning information of successive yield predictions during the growing season, producers and marketing boards could, for example: adjust use of fertilizers and herbicides, revise marketing plans, and decide on options for following seasons.

The official estimates of crop production in China are based on three methods at present. The first is statistical method, which works through complete enumeration for crop acreage and sample crop cutting experiments for yield. Crop sampling leads to large labor force-, material resources- and money-consuming; the second way calculates crop yield through weather model, which can get a accurate result but with a disadvantage that short of acreage information; the last method is using remote sensing (RS) to estimate grain outputs.

Crop simulation model is a process based model (de Wit, 1982), which simulates crop growth and development combine with changing climate stages and varied environmental conditions. In many cases, quantitative information on production can only be obtained through crop simulation studies and long-term climatic records (MacDonald and Hall, 1980; Bouman et al., 1995). Providing

accurate estimates of the benefits and risks of alternative crop management systems with expected yield before final harvest has placed an increasing demand on crop simulation models. The use of crop simulation models for predicting crop yield has been studied extensively and there has been an increased interest in associatio2n with spatial variability and precision farming (Hoogenboom, 2000; Sadler et al., 2000; Paz et al., 2001; M. Bannayan et al., 2004). As a further extension of this approach, the predicted results can be used to determine certain management decisions.

The objective of this study was to evaluate the application of the dynamic crop process model CERES (crop estimation through resource and environment synthesis)-Wheat for forecasting final grain yield for winter wheat under growing conditions in Beijing.

2 Materials and Methods

2.1 Experiment Data

Site Description

Winter wheat ('Jingdong 12') was sown during the autumn of 2004/2005, 2005/2006 and 2006/2007 at Xiaotangshan, which located in Changping of northern Beijing (N40° 10'56", E116° 26'29").This area, which is representative of the irrigated fields of Beijing, is characterized by a semi-arid climate. At this place, winter wheat is the major crop sowed by farms, and the mean air temperature yearly is 12.6℃.

Data Description

The CERES-Wheat model uses daily weather data, together with a set of parameters describing crop, soil and management factors, to simulate wheat growth over the growing season (Hunt et al., 2001). To use the model in Beijing, it was necessary to obtain local values of the above parameters. Experimental information, including latitude, longitude, sowing date, descriptions of the soil series, the number of collected samples, and climate information (table 1) are all collected from2004 to 2007.

Table 1 Distribution of precipitation

Season	Spring			Summer			Autumn			Winter			Total
Month	3	4	5	6	7	8	9	10	11	12	1	2	
Rain(mm)	9.7	16.6	26.8	87.9	194.1	181.4	48.8	24.6	5.6	1.3	2.7	4.9	584.2
Rain/Season	53.1			443.4			78.8			8.9			584.2
%	9.1%			75.9%			13.5%			1.5%			100%

Standard meteorological data with the exception of solar radiation were obtained using DAVIS station from 2004 to 2007. This station provided daily values of the maximum and minimum air temperature (℃), rainfall (mm) and total wind run (m/s). Sunshine hours were gained from China Meteorological data Sharing Service System, and they were converted to daily total radiation (MJ/M^2) using the method of dumin Weng (1997). Besides those, 30 years (1975 – 2006) of daily weather data (maximum and minimum air temperature, ℃; rainfall, mm; sunshine hours, hr) were taken from China Meteorological data Sharing Service System as an input for yield forecasting. Soil inputs include drainage and runoff coefficients, first-stage evaporation and soil albedo, water-holding characteristics for each individual soil layer, and rooting preference coefficients at several depth increments. The model also requires saturated soil water content and initial soil water content for the first day of simulation. The description of the soil characteristics were shown as Fig. 1 (Xuzhang Xue et al., 2003). The brown soils have characteristically light textures with water holding capacities to a depth of 1 m of 150mm or less, so the sampling of the soil deep to 1m and

separated into 6 layers. The crop management data were obtained from field experiments, including plant population, planting depth, and date of planting. If the crop is irrigated, the date of application and amount is also required.

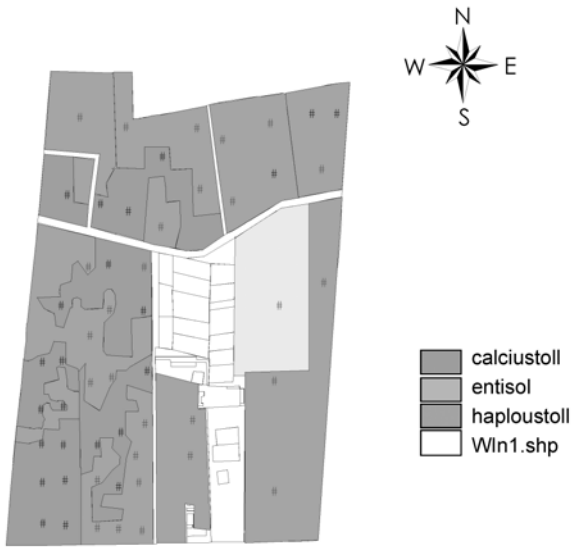

Figure 1 The soil characteristics of Xiaotangshan

2.2 CERES-Wheat Model

Current major crop model systems include DSSAT (Decision Support System for Agrotechnology Transfer; USA, Canada), SUCROS (Netherland) and APSIM (Australia) etc. CERES-Wheat model, as a process-oriented crop model provides some benefits over purely empirical models, is one of the main models that have been incorporated in DSSAT (Hoogenboom et al., 1994). The study works with CERES-Wheat Model through DSSAT 4.

CERES-Wheat is a dynamic crop simulation model that was originally developed under the auspices of the USDA-ARS Wheat Yield Project and the U.S. government multiagency AGRISTARS program (Ritchie and Otter, 1985; Ritchie, 1986). It forms the basis of IBSNAT, the International Benchmark Sites Network for Agrotechnology Transfer (Uehara, 1985), can be used to simulate the growth and yield of wheat under different environments. The model has been tested successfully with data from around the world. Output results could be biomass accumulation and partitioning, leaf area index (LAI), water and N balance, crop growth and yield based on daily time steps etc (Godwin and Singh, 1998; Ritchie, 1998; Ritchie et al., 1998).

2.3 Cultivar Calibration

In order to evaluate the applicability of the CERES-Wheat model to Beijing, calibration of the model was required. The key process of model calibration was adjusting six variety-specific genetic parameters of Jingdong12. Three of these are related to developmental aspects and the others related to the growth of the crop. P1V and P1D define the sensitivity of a variety to vernalization and photoperiod. The third developmental parameter, P5, is the grain-filling duration coefficient. G1, G2 and G3 are the kernel number coefficient, kernel weight coefficient and spike number coefficient, respectively (HUNDAL, 1997). When the predicted values of the relevant growth and yield were

compared with the observed values, the six genetic coefficients were increased or decreased from the initial values. After an iterative process, those values of the coefficients which most realistically simulated the growth and yield of wheat were selected.

Model calibration was made by comparing the field-observed and model-simulated results of five stages: ① dates of anthesis and maturity; ② values of LAI (leaf area index); ③ biomass yields of anthesis and maturity; ④ dry matter of leaf, stem, and grain; ⑤ final wheat yield. The CERES-Wheat model was calibrated to simulate the growth and development of winter wheat using the field-observed crop data of the 2004/2005 season experiment. The comparison of model-simulated and field-observed data was gained for validation at the period 2005/2006 and 2006/2007. In addition, 30 years (1975 – 2006) historical weather information was taken as statistical weather result to predict yield.

3 Result and Discussion

3.1 Simulation Results and Prediction Results Evaluation

The CERES-Wheat model simulated from realistic weather conditions, crop genotypes, soil properties and crop management practices got simulated-results. The values derived from statistic weather data (1975 – 2006), which used as input variables of model, were called predicted-values. All inputs except weather data were prescribed as discussed in the previous sections. The experiment conducted during the 2004/2005 growing seasons was used to calibrate the model, and the experiment conducted during the 2005/2006 and 2006/2007 growing seasons were used for model evaluation. Forecasts of wheat yield were generated for the period 2006/2007.

Overall, the field-observed and model-simulated anthesis dates were in close agreement (Table 2). The difference of simulated and actual dates of anthesis is less than 6 days, which of the autumn is less than 5 days.

Table 2 Comparison of observed and simulated anthesis and physiological maturity dates of winter wheat for different crop years

Crop Year	Sowing Date	Anthesis Date (Days after sowing)		Deviation (No.of days)	Physiological Maturity Date(Days after sowing)		Deviation (No. of days)
		Observed	Simulated		Observed	Simulated	
2004/05	27/9/2004	223	225	2	262	263	1
2005/06	28/9/2005	229	233	6	265	269	4
2006/07	27/9/2006	226	232	6	263	264	5

Experiment data of 2006/2007 season was taken as an example for evaluation. Comparison of simulated-values, observed-values and predicted-values (2006/2007) of LAI was shown as Fig. 2. LAI simulated by the model corresponded reasonably well with that actually observed in the field, although simulated values a little higher at the last 35 days. Similarly, predicted wheat LAI has also shown negative trends in the period of subsequent period. While predicted values delayed much from that of actual, especially at the period of end Anthesis and maturity. The maturity date of forecasted is 270, 6 days later than simulated date. The reason may be attributed to uncertain weather conditions in the region.

Simulated wheat yield (7525kg/ha) and predicted yield (7736kg/ha) was much higher than the actual wheat yields (6992kg/ha). The deviation may be on account of dissatisfactory environment conditions, for instance water stress, N deficiency or unbalance of nutrient at subsequent period.

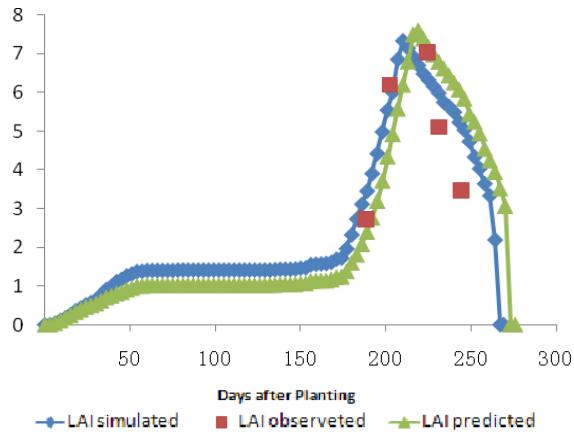

Figure 2 Comparison of simulated-values, observed-values and predicted-values of LAI for 2006

4 Summary and Conclusion

As wheat is a staple crop in China, pre-harvest forecast of wheat yield is necessary to allow policy makers in the government to design policies for export/import, price fixing, storage and transportation. Crop simulation models are process based and consider almost all factors affecting the crop growth and development. With their obvious advantages, crop simulation models have become a favorite tool for yield forecasting.

The crop simulation model was run on recommended levels of inputs for the fields, but simulated and predicted yields are high. This could be due to following reasons: ① farmers are not following the appropriate recommendation; ② around 1 – 5% of the standing crop is lost during various agronomical practices such as fertilizer applications, pesticide applications, herbicide applications, tillage, irrigation etc. (A. S. NAIN 2004); ③ 8 – 10% of the crop yield in fields is damaged during threshing and transportation; ④ some loss also occurs due to pests. Some assumptions made in the CERES-Wheat model may not be realistic in certain situations and these could be addressed in future investigations.

Though the approach released in the present study for wheat yield estimation and prediction showed reasonably good accuracy, it can be further improved by considering issues such as: ① affects of plant diseases and insect pests; ② spatial variability in soil properties; ③ spatial variability of weather; ④ interaction between rotated crops. Future research for yield forecasting can carry through by adopting the use of GIS (geographic information system) and RS (remote sensing).

The present study demonstrates the ability of the CERES-Wheat model to provide regular pre-harvest forecasting of wheat yields in Beijing. Although there is diversity, the total variety trend was corresponded reasonably well with that actually value. The model can act as a useful tool for Winter Wheat yield forecast in Beijing.

References

NAIN1 AS, DADHWAL VK, SINGH TP (2004) Use of CERES-Wheat model for wheat yield forecast in central Indo-Gangetic Plains of India. Journal of Agricultural Science 142: 59 – 70.

Chipanshi AC, Ripley EA, Lawford RG (1997) Early prediction of spring wheat yields in Saskatchewan from current and historical weather data using the CERES-Wheat model. Agricultural and Forest Meteorology 84: 223 – 232.

Bouman BAM, van Diepen CA, Vosen P et al. (1995). Application of systems approaches at the farm and regional levels. Simulation and system analysis tools for crop yield forecasting 325 – 340.

Fraisse CW, Sudduth KA, Kitchen NR. Calibration of the CERES-MAIZE model for simulation site-specific crop development and yield on claypan soils. Applied Engineering in Agriculture 17(4): 547 – 556.

DE WIT, C. T (1982) Simulation of living systems In Simulation of Plant Growth and Crop Production, Simulation Monographs 1 – 24.

Hoogenboom G, Jones JW, Wilkens PW et al. (1994) Crop models 95 – 244.

Hoogenboom G (2000) Contribution of agrometeorology to the simulation of crop production and its applications. Agric. For. Meteorol 103: 137 – 157.

Hunt LA, White JW et al. (2001) Agronomic data: Advances in documentation and protocols for exchange and use. Agric. Syst 70:477 – 492.

JiangMin, Jin Zhiqing, Ge Daokuo et al. Validation and modification of CERES-WHEAT model in winter wheat production region of China. Journal of JiangSu agricultural college 64 – 67.

Ritchie JT , Otter S (1985) Description and performance of CERES-Wheat: a user-oriented wheat yield model. Crop husbandry 159 – 175.

Ma Yuping, Wang Shili, Wang Futang (2005) A Prelim Inary Study On the Application of Crop Simulation models In Agrometeorological Services. Journal of applied meteorological science 293 – 303.

Bannayan M, Crout NMJ, Gerrit Hoogenboom (2004) Application of the CERES-Wheat Model for Within-Season Prediction of Winter Wheat Yield in the United Kingdom. MODELING.

MacDonald RB, Hall FG (1980) Global crop forecasting. Science 208 – 670.

Ritchie JT, Singh U, Godwin DC et al. (1998) Cereal growth, development and yield 79 – 97.

Royce FS, Jones JW, Hansen JW (2001) Model-based optimization of crop management for climate forecast applications. Trans.ASAE 44:1319 – 1327.

John Sadler E, Philip Bauer J, Warren J et al. (2000) Site-specific analysis of a droughted corn crop: II. Water use and stress. Agronomy Journal.

HUNDAL SS, PRABHJYOT-KAUR (1997) Application of the ceres-Wheat model to yield predictions in the irrigated plains of the Indian Punjab. Journal of Agricultural Science, Cambridge 129:13 – 18.

Uehara G (1985) The International Benchmark Sites Network for Agrotechnology Transfer (IBSNAT). Wheat Growth and Modeling 271 – 274.

Xuzhang Xue, Larry C Munn (2003) Soil Survey Results in Xiaotangshan Station.

XIE Wenxia,YAN Lijiao,WANG Guanghuo (2006) Simulation and Validation of Rice Potential rowth Process in Zhejiang by Utilizing WOFOST Model. Chinese Rice Sci 20(3):319 – 32.

Improving the Calibration Process of GreenLab Model on the Cotton Plant

Dong Li, Zhi-Gang Zhan, Yan Guo

(Key Laboratory of Plant-Soil Interactions, Ministry of Education, College of Resources and Environmental Sciences, China Agricultural University, Beijing 100094;
Corresponding author E-mail: zhigang.zhan@cau.edu.cn)

Abstract: The functional-structural GreenLab model uses a set of recurrence equations to simulate plant development and eco-physiological processes. The parameters of the source and sink functions are calibrated by fitting the model to plant architectural data using the nonlinear least squares method. Starting from good initial values is a key issue for the iterative fitting algorithm to converge to the global optimal solution. For the case of single-stemmed cotton (*Gossypium hirsutum* L.) plant, we present a method to retrieve plant functional parameters directly from interpolated measurement data. The advantage of this method is that not only the calculations of source parameters are independent of the sink parameters, but the sink parameters are also separately estimated with respect to organ type. The method is tested to be practical on two years of experimental data of cotton plants.

Keywords: functional-structural model, parameter estimation, *Gossypium hirsutum* L.

1 Introduction

The functional-structural plant models simulate plant architectural development, physiological functioning and their reciprocity. For example, the L-OZCOT model links the L-Cotton (a structure model) and OZCOT (a process based model) (Hanan and Hearn, 2003). The GREENLAB model, which is developed for general plant (de Reffye and Hu, 2003), consists of a set of recurrence equations describing the process of plant biomass production and partitioning among individual growing organs (Yan et al., 2004). This model has been applied to several different plants on various aspects, e.g., parameter optimization and field validation for maize (Guo et al., 2006; Ma et., al., 2007), defoliation effects on cotton plants (Zhan et al., 2007), simulation of wheat and tomato growth (Kang et al 2008; Dong et al., 2008).

For the GreenLab model, the parameters of the source and sink functions are estimated by fitting the model to plant architectural data using the least squares method (Zhan et al., 2003). Because of the nonlinear dependency of the model output on these parameters in an implicit manner, the fitting algorithm works in an iterative way, by starting from a set of initial values. Fitting several parameters simultaneously to one group of target items requires quality initial parameter values. If the initial parameter values are not appropriately set, the iteration process may not converge, or even worse, it may converge to some non-global optimal solution. In this paper, we first explore the GreenLab formulation for the case of single-stemmed cotton plant, and then establish the link between the model output and parameters for the plant at the stable growth stage in term of plant biomass production. Based on these relationships, we give a method of calculating parameter values from interpolated data. The testing results of the method on real data will be presented.

2 Materials and Methods

2.1 The GREENLAB Model Description

The GREENLAB model has been previously described in detail (Yan et al., 2004; Guo et al., 2006; Zhan et al., 2007). We will present here the main principles and specific options for the single-stemmed cotton plant.

2.1.1 Modeling Concepts

For the GreenLab model, the simulation time step is growth cycle (GC), which is the phyllochron corresponding to accumulated thermal time needed for the apical meristem to generate a new metamer (the architectural unit comprising a node, an internode and a leaf including a blade and a petiole for the cotton plant). The plant biomass production and partitioning, organ expansion time, and leaf functional time, as well as metamer appearance, are expressed in GC. At each GC, total biomass production is calculated from the sum of functional blade area by an empirical nonlinear function of intercepted light. The biomass of the 1st GC comes from the seed. Biomass is shared among the growing organs according to their relative sink strength. Organs can expand several GCs and the weight results from accumulation of biomass increments. Architectural development such as blade area, internode length and diameter is computed according to allometric rules (de Reffye et al., 1999).

Fresh biomass acquisition at GC(i) is computed by the following equation:

$$Q(i) = \frac{E(i)\,S_{\mathrm{p}}}{R}\left(1 - \exp\left(-\frac{\sum_{k=1}^{n_{\mathrm{b}}(i)} S_{\mathrm{b}}(k)}{S_{\mathrm{p}}}\right)\right) \tag{1}$$

where $Q(i)$ is the biomass production during GC(i); $E(i)$ is the average potential of biomass production during GC(i) that generally depends on environmental factors (e.g., temperature, wind, and light) and it is assumed constant through all the growth cycles in this study; $n_{\mathrm{b}}(i)$ is the number of functional leaves at the beginning of GC(i) (the maximum is set to 15 for single-stemmed cotton); $S_{\mathrm{b}}(k)$ is the blade area of the kth green leaf; R is an empirical resistance parameter of the plant which also serves as the scaling coefficient so as to produce proper result with given E; S_{p} is the ground projection area of the plant leaves.

Fresh biomass feeds all growing organs (sinks) through a globally shared reserve pool. The amount of biomass partitioned to individual organs is proportional to its relative sink strength that is a function of organ age in terms of GCs, with respect to the type of organ:

$$D_o(i,j) = P_o\, f_o(k), \quad k = i - j + 1 \tag{2}$$

where the subscript o denotes organ type: b, blade; p, petiole; e, pith; D_o is the relative sink strength of the organ; P_o is the coefficient of relative sink strength (potential sink strength, for leaf blade P_{b} = 1 is set as reference); i is the growth cycle; j is the organ position along the main stem and k is the organ age; $f_o(k)$ is an organ type specific function of sink variation in GC(i), taking the beta-like form:

$$f_o(k) = \begin{cases} g_o(k)/M_o & (1 \le k \le t_o) \\ 0 & (k > t_o) \end{cases} \tag{3a}$$

where

$$g_o(k) = \left((k-0.5)/t_o\right)^{\alpha_o - 1} \left(1-(k-0.5)/t_o\right)^{\beta_o - 1} \tag{3b}$$

$$M_o = \max\{g_o(k) \mid 1 \le k \le t_o\} \tag{3c}$$

α_o and β_o are parameters associated with the organ type o; t_o is the organ expansion time which can directly measured. These six parameters can be obtained simultaneously by fitting the model to observation data, as well as other parameters (R, S_p, and P_o).

We define the secondary growth as virtual ring and the ring's growth rate was found tightly dependent on the number of functional leaves of the plants. A linear relationship between the sink strength of the secondary growth and the number of functional leaves $n_b(i)$ is used (Zhan et al., 2007):

$$D_c(i) = P_c \, n_b(i) \tag{4}$$

where P_c is the coefficient of the relative sink strength of the ring initiated at the end of GC(i). A new ring corresponds to a new growth cycle. In GC(i), the total sink strength is calculated by the following equation:

$$D(i) = \sum_{o=b,p,e} \sum_{j=1}^{i} D_o(i,j) + D_c(i) \tag{5}$$

Organ expansion in fresh weight depends on both their relative sink and the total biomass increment for the plant. For the organ of type o and position j, its biomass is acquired through Equation (6):

$$Q_o(i,j) = Q(i-1)\frac{D_o(i,j)}{D(i)} + Q_o(i-1,j) \tag{6}$$

2.1.2 Summary of Plant Parameters Used in the GREENLAB Model

Twelve plant parameters that are not accessible by direct measurement (called hidden parameters) are optimized by fitting procedures. Four coefficients of relative sink strength correspond to four organ types (i.e., P_b, P_p, P_e, P_c for leaf blade, petiole, pith, and ring, respectively); six beta function parameters are used to define the relative sink strength variation while aging for expanding organs (i.e., α_b, β_b, α_p, β_p and α_e, β_e for leaf blade, petiole and pith, respectively); two parameters (i.e., R and S_p) for biomass acquisition related to internal plant resistance to transpiration and Beer-Lambert's law. The initial values of these parameters are estimated in this study.

2.2 The Method of Estimating Model Parameters

2.2.1 The Single-Stemmed Cotton Plant

We take the single-stemmed cotton plant as an example to introduce and test the methods of estimating the model parameters. The cotton plant can grow in a perennial way. The plant with all the axillary buds removed at appearance produces simple plant architecture. Each metamer consists of a few components: a node, an internode, and a leaf (except the first metamer with two cotyledons) including a blade and a petiole. The nodes are not split from internodes. The pith is defined as the internal part of the internode once the secondary growth (rings) is removed.

2.2.2 Estimating the Ground Projection Area (S_p)

The ground projection area (S_p) of the plant can be estimated from the observed the largest blade area. For the single-stemmed cotton, the phyllotaxy angle is assumed to be 120º (actually about 137.5º), and the axillary angle is about 60º (Fig. 1). Three largest blades build up an equilateral triangle. The largest ground projection area (S_p) should be limited in the circum circle of the triangle. We use the area of the inscribed circle of the triangle as the estimation of minimum S_p. Area of the equilateral triangle and its circum circle and inscribed circle are three important data for estimating ground projection area. For large blades are always flexural, the area of the triangle area will be used as the initial value of S_p to start the fitting. Once the projection area (S_p) is estimated, the parameter R can be obtained from Eq. (1).

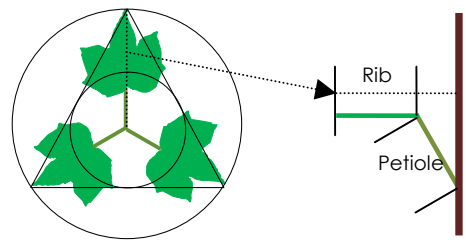

Figure 1 The sketch map of the method to estimate the ground projection area (S_p)

2.2.3 Estimating Sink Strength Parameters for the Leaf

For a certain plant (single-stem cotton in this study), the projection ground area (S_p in Eq. (1)), which can be estimated from the observed data, is limited by plant genotype and density. If the total area of functional leaves is big enough, according to Eq. (1) the biomass produced at each GC will be close to a constant value:

$$Q_m = E\, S_p / R \tag{7}$$

where Q_m is the largest biomass produced at each cycle. If the plant is big enough, the total relative sink strength value of all the organs is denoted as D_m:

$$D_m = \sum_{o=b,e,p} P_o \sum_{k=1}^{t_o} f_o(k) + P_c\, n_b(i) \tag{8}$$

The biomass increment for the organ at the ith GC after its emergence is:

$$Q_o(i) = P_o Q_m / D_m\, f_o(i) \tag{9}$$

Therefore, we can obtain the variation of sink strength from the biomass increment data. And the organ age i_1 when the $f_o(i)$ reaches its maximum can also be directly obtained from the variation data. Equation (3a) is transformed into Eq. (10):

$$f_o(i) = \frac{(i-0.5)^{\alpha_o-1}\,(t_o-(i-0.5))^{\beta_o-1}}{(i_1-0.5)^{\alpha_o-1}\,(t_o-(i_1-0.5))^{\beta_o-1}} \tag{10}$$

The parameters α_o and β_o can be obtained by a linear fitting of logarithmly transformed Eq. (10) to the derived data.

As the biomass increment of an organ at GC(i) is:

$$Q_o(i) = \begin{cases} \dfrac{Q_{\mathrm{m}}}{D_{\mathrm{m}}} P_o \sum_{j=1}^{i} f_o(j) & \left(1 \le i \le t_o\right) \\ \dfrac{Q_{\mathrm{m}}}{D_{\mathrm{m}}} P_o \sum_{j=1}^{t_o} f_o(j) & \left(i > t_o\right) \end{cases} \tag{11}$$

the potential relative sink strength P_o can be calculated from measured data of organ biomass.

2.2.4 Estimating Sink Strength Parameters for the Internode

The secondary growth of the last several internodes at top is very weak and can be ignored, and the parameters α_{e}, β_{e} and P_{e} for pith can be estimated in the same way as for the leaf.

For a given cycle, the biomass of a new ring (denoted by Q_{c}) can be obtained by subtracting the biomass increment for leaves and pith from the increment in plant biomass. From Eqs. (2), (4) and (6), we have the following equation to compute the sink strength coefficient of secondary growth:

$$P_{\mathrm{c}} = Q_{\mathrm{c}} \sum_{i=1}^{t_{\mathrm{b}}} D_{\mathrm{b}}(i) \Big/ \sum_{i=1}^{t_{\mathrm{b}}} Q_{\mathrm{b}}(i) n_{\mathrm{b}}(i) \tag{12}$$

2.3 Testing the Method with Real Data

2.3.1 Source of Data for the Test

The data used to test the methods come from the field experiments of two different years, i.e., 2003 and 2006. The first experiment was conducted at China Agricultural University in Beijing. The cotton (*Gossypium hirsutum* L., cv. G33B) seeds were sown at a spacing of 0.6 m × 0.6 m. The other experiment was at Quzhou experiment station in North China Plain where the cotton (cv. DP99B) plants were at a spacing of 0.8 m × 0.8 m. In both experiments, fertilizer inputs and irrigation were conducted so as to avoid any mineral and water limitations to plant growth. The branches were removed immediately after their initiation and only leaves (including petioles and blades) were kept on the main stem. Each time (once a week for 2003, and two weeks for 2006) four plants were measured on fresh weight and area for leaf blades, as well as the fresh weight, length and diameter for internode and petiole. Root was not considered.

2.3.2 Data Processing

The measurements were conducted between several GCs. The complete data for each GC were approximated through linear interpolation of the observed data. Then the total biomass increment for each GC can be obtained.

2.3.3 Evaluation of the Proposed Method

The calculated parameter values were input Digiplant software as initial values to start the full fitting to obtain the final values. The target consisted of plant architectural and biomass data. The relative error (RE) between the final values (denoted by x_{F}) and the initial values (x_{I}) of fitted parameters is used to evaluate the applicability of the method:

$$\mathrm{RE} = (x_F - x_{\mathrm{I}}) / x_F \tag{13}$$

3 Results

3.1 Calculated Parameter Values from Real Data

The largest blade area of the single-stemmed plant was 450±17 cm^2 (mean±SE) in 2003 and 684 ±18 cm^2 (mean±SE) in 2006. The length of the equilateral triangle side was about 64.95 cm (2006 as an example) because the largest petiole length and blade mid rib were approximately 25 cm. In 2006, the area of the big circle, triangle and small circle were about 4418, 1827 and 1104 cm^2, respectively. The triangle's area (1827 cm^2) is an estimation of S_p. The value of S_p for 2003 was 1174 cm^2 and ranged from 710 to 2840 cm^2.

Fresh biomass in 2003 was much smaller than 2006. After 28 growth cycles, the cumulated biomass of the whole plant increased linearly (Fig. 2), which indicated a constant value of biomass production at each cycle.

The organs (blade, petiole and internode) of the 25th metamer were used to calculate the variation of sink strength. All the cumulated biomass of organs including internode, petiole and blade in 2003 was directly observed and the data in 2006 were obtained by interpolation of the observed data on age 1, 5, 6, 7 and 12. Then biomass increment and variation of sink strength of different organ were achieved (Fig.3). The observed data showed the beta function curve like trend for 2003 (Fig.4).

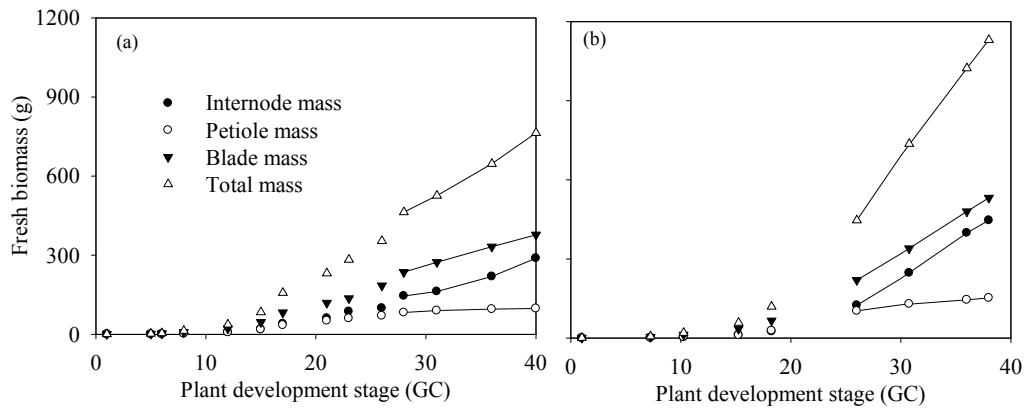

Figure 2 Interpolated total biomass of the single-stemmed cotton plant for 2003 (a) and 2006 (b), respectively

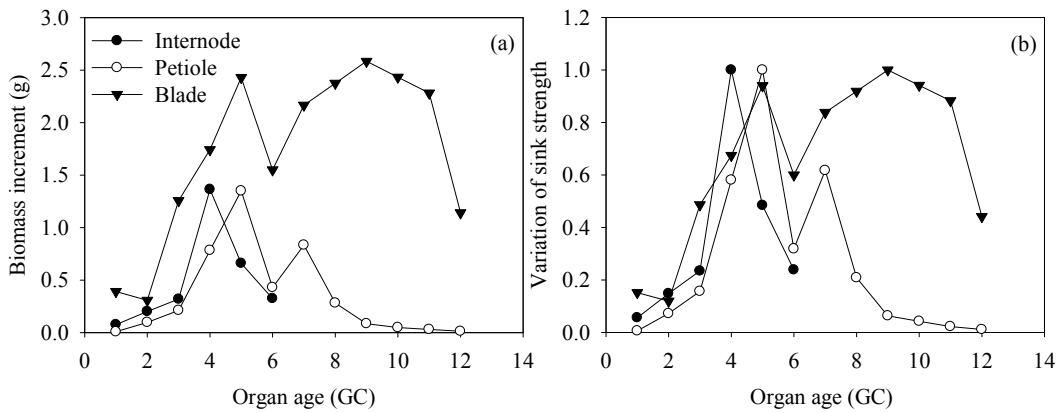

Figure 3 Biomass increment (a) and the variation of relative sink strength for internode, leaf blade and petiole, respectvely. The data are from Exp. 2003

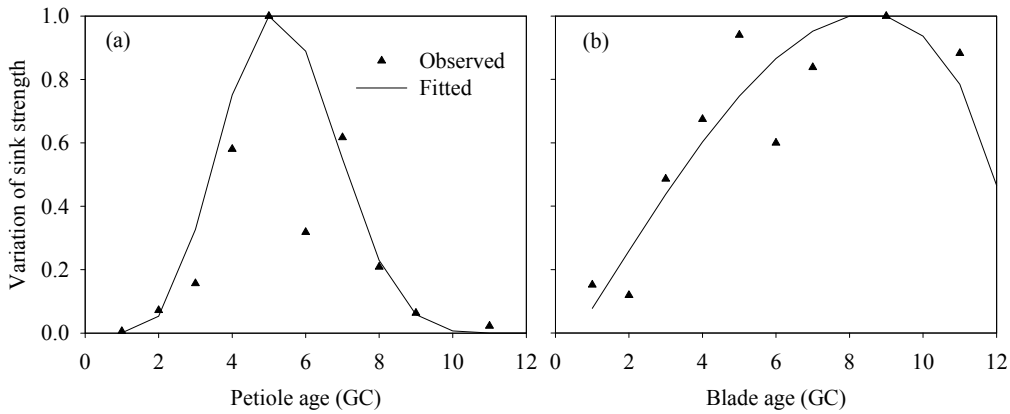

Figure 4 Variation of sink strength for the leaf petiole and blade in 2003

3.2 Fitting the GreenLab Model to Measured Data

The final parameter values (listed in Table 1) were obtained by the DigiPlant software with the previously calculated parameter values as initial to start the fitting. Figures 5 and 6 showed the fitting results for 2003 and 2006, respectively.

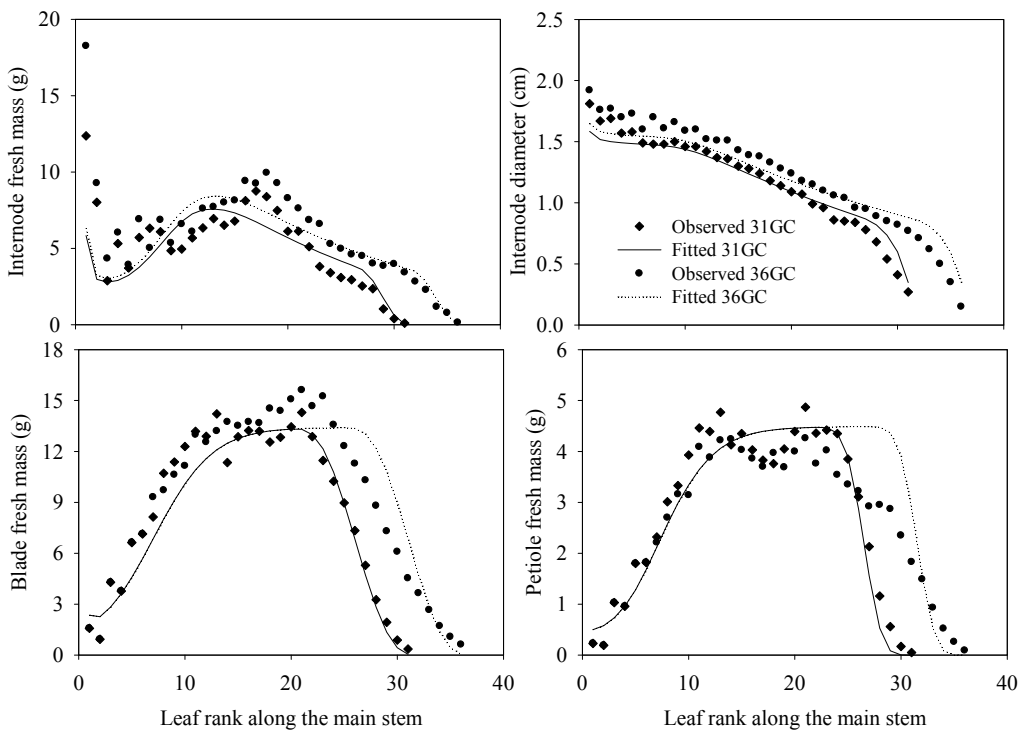

Figure 5 Fitting the GreenLab model to two-stage data of the single-stemmed cotton plant. The target items include fresh mass and diameter of internode, fresh mass of leaf blade and petiole. Data are from Exp. 2003

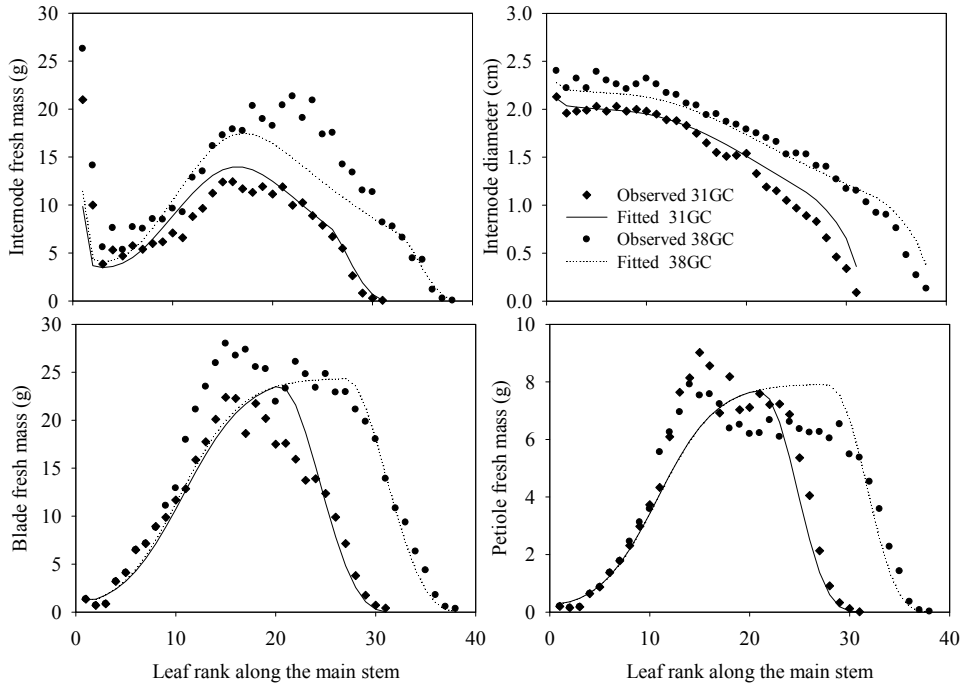

Figure 6 Fitting the GreenLab model to two-stage data of the single-stemmed cotton plant. The target items include fresh mass and diameter of internode, fresh mass of leaf blade and petiole. Data are from Exp. 2006

3.3 Comparison of the Initial and Final Values of Model Parameters

In both years the potential sink strength (coefficient of sink strength) of the petiole was much smaller than the blade. The sink variation parameters of the petiole were larger than other organs (shown in Tab. 1).

We found RE of sink strength coefficients was smaller than 20% for all the three types of organs. For the ground projection area, the initial values in both years were a little larger than the final ones. As a result, the R was estimated well and less than the final values.

Table 1 Comparison of the initial and final parameter values for single-stemmed cotton plants in two years

	Parameter (2003)			Parameter (2006)		
	Initial	Final	RE	Initial	Final	RE
P_b	1	1		1	1	
P_p	0.52	0.62	0.16	0.54	0.48	−0.13
P_e	0.53	0.45	−0.18	0.40	0.35	−0.14
P_c	0.21	0.19	−0.11	0.24	0.28	0.14
α_b	2.14	3.12	0.31	1.19	3.37	0.65
β_b	1.57	3.18	0.51	0.54	2.36	0.77
α_p	6.12	9.25	0.34	4.31	6.36	0.32
β_p	9.00	10.81	0.17	3.11	4.62	0.33
α_e	3.30	3.56	0.07	2.57	2.71	0.05
β_e	2.45	3.61	0.32	1.21	1.63	0.26
R	32.67	29.59	−0.10	30.46	27.52	−0.11
S_p	1209	788.9	−0.53	1827	1514	−0.21

4 Discussion and Conclusions

In the case of calibrating the GreenLab model for the single-stemmed cotton plant, the results show that the parameters of source and sink functions are possible to be estimated from plant data at the stable stage (when the plant biomass production at each GC becomes nearly constant). On one hand, these parameters values may serve as good initial for the iterative optimization algorithm to accomplish the full fitting using specific software such as Digiplant. The directly calculated values of potential sink strength from measured data were very close to the finally fitted ones. On the other hand, the calculated parameter values are also physically meaningful by themselves standalone. Since the proposed methods for parameter estimation are derived from the GreenLab model equations (with a few simplifications), the resulting parameter values and the consequent functions may be used to test the hypothesis in the model.

The model parameters are classified into two groups: one group is for the biomass production, and the other for biomass partitioning. The advantage of our method is that not only the calculations of source parameters are independent of the sink parameters, but the sink parameters are also separately calculated with respect to organ types. The estimated parameter values from direct calculation are also reasonable references to verify the results of the fitting software where all the parameters are optimized together.

The application of the methods given in this paper is limited to the plant that has a stable stage both for biomass production and development of topological structure. But for some specific plant, it seems possible to decompose the full fitting problem into several simpler inverse problems, based on the exploration of plant structure and functions. We believe such kind of work is relevant for the model calibration, and will improve the full fitting that is normally difficult with multiple parameters to estimate.

Acknowledgements

We thank the Digiplant team for the software. This research has been partly supported by the Hi-Tech Research and Development (863) Program of China (2006AA10Z229).

References

de Reffye P, Blaise F, Chemouny S et al. (1999) Calibration of a hydraulic architecture-based growth model of cotton plants. Agronomie 19: 265 – 231.

de Reffye P, Hu BG (2003) Relevant Qualitative and Quantitative choices for building an efficient dynamic plant growth model: Greenlab Case. In Hu B-G, Jaeger M (eds.) Plant Growth Modeling and Applications, Proceedings of PMA03, Beijing, China, Oct. 13-16, 2003. Tsinghua University Press and Springer, 87 – 107.

Dong QX, Louarn G, Wang YM et al. (2008) Does the Structure Function Model GREENLAB Deal with Crop Phenotypic Plasticity Induced by Plant Spacing? A Case Study on Tomato. Ann Bot 101: 1195 – 1206.

Guo Y, Ma YT, Zhan ZG et al. (2006) Parameter Optimization and Field Validation of the Functional-Structural Model GREENLAB for Maize. Ann Bot 97: 217 – 230.

Hanan JS, Hearn AB (2003) Linking physiological and architectural models of cotton. Agr Syst 75: 47 – 77.

Kang MZ, Evers JB, Vos J et al. (2008) The Derivation of Sink Functions of Wheat Organs Using the GreenLab Model. Ann Bot 101: 1099 – 1108.

Ma YT, Li BG, Zhan ZG et al. (2007) Parameter Stability of the Functional-Structural Plant Model GREENLAB as Affected by Variation within Populations, among Seasons and among Growth Stages. Ann Bot 99: 61 – 73.

Yan HP, Kang MZ, De Reffye P et al. (2004) A Dynamic, Architectural Plant Model Simulating Resource-dependent Growth. Ann Bot 93: 591 – 602.

Zhan ZG, de Reffye P, Houllier F et al. (2003) Fitting a Functional-Structural Growth Model with Plant Architectural Data. In Hu BG, Jaeger M (eds.) Plant Growth Modeling and Applications, Proceedings of PMA03, Beijing, China, Oct. 13-16, 2003. Tsinghua University Press and Springer, 236 – 249.

Zhan ZG, Rey H, Li D et al. (2007) Study on the Effects of Defoliation on the Growth of Cotton Plant Using the Functional Structural Model GREENLAB. In Fourcaud T, Zhang XP (eds.) Plant Growth Modeling and Applications, Proceedings of PMA06, Beijing, China, Nov. 13-17, 2006. Los Alamitos: IEEE Computer Society, 194 – 201.

Dry Matter Production and Partitioning in Tomato: Evaluation of a General Crop Growth Model

Ling-Zhi Li[1], P.H.B. de Visser[2], Ya-Ling Li[1], Hai-Ping Li[1]

(1 Shanxi Agricultural University, College of Horticulture, 030801, Shanxi, P. R. China,
Corresponding author, E-mail: yalingli@sxau.edu.cn)
(2 Wageningen University, Plant Research International, 6700 AA, Wageningen, the Netherlands)

Abstract: An existing mechanistic model for the growth, development and production of tomato was calibrated and used to simulate crop growth in China. The model simulates dry matter production of the crop following SUCROS87 as well as transpiration and nutrient uptake. Growth experiments (periodic destructive harvests) from China were used for model validation. Hourly averages for global radiation outside the greenhouse, greenhouse temperature, heating pipe temperature, air humidity and CO_2 concentration, together with measured leaf area index, dry matter distribution and organ dry weights were the inputs to the model. Leaf and stem dry matter production was simulated reasonably well for the experiment. Fruit and root dry matter production was simulated badly for the experiment. LAI, individual leaf area and truss appearance were simulated adequately in the experiment. It is concluded that INTKAM is a robust model for simulating dry matter production in a tomato crop.

Keywords: crop growth, dry matter production and partitioning, greenhouse, *Lycopersicon esculentum*, simulation model, tomato

1 Introduction

Simulation models of crop growth and production provide a widely accepted tool for assessing agricultural production opportunities in different agro-ecological zones in response to weather and management, for identifying ideotypes that are well adapted to certain agro-ecological conditions, for better understanding interactions between genotypes, environment and management (Kropff and Goudriaan, 1994; Yin et al., 2004), and for deriving optimal management strategies in adaptation to uncertain weather and changing climate (Meinke et al., 2001).

Before a model can be used it must be calibrated and validated. Models are often validated with some of the data already used for model development or calibration (Jones et al., 1991; Bertin and Gary, 1993), yet wider validation would better indicate the applicability of the model.

The aim of the present study is to evaluate the INTKAM model, developed at Wageningen University and Research Centre (WUR), for its application to Chinese tomato crop production. Emphasis is put on the interactions between dry matter production and dry matter distribution.

2 Model Description

The INTKAM crop growth model for tomato (Marcelis et al., 2000) simulates crop growth, plant-water relations and plant-nutrient relations. Leaf photosynthesis is computed with a biochemical model (Farquhar et al., 1980). Leaf transpiration rate is calculated with the Penman-Montheith equation, and makes use of the stomatal conductance model described by Nederhoff and de Graaf

(1993). Water requirements for fresh mass growth are based on fixed values for dry matter content of roots, shoot and leaves, and a fruit dry matter content as a function of EC and day number (de Koning, 1994).

3 Materials and Methods

3.1 Experiment

Experiment was conducted in 6 m × 20 m compartments of a trispan greenhouse in Shanxi Agricultural University, the People's Republic of China. Plants were grown in soil at a plant density of 3.3 m^{-2} (one way is 0.2 m within-row plant distance, 1.5 m between rows; the other way is 0.3 m within-row plant distance, 1.0 m between rows). Plants were grown by the high-wire system (Lingzhi Li et al., 2003). Plant nutrition and chemical pest and disease control were described (Lingzhi Li, 2002). Flowers were self-pollinated. Trusses were not pruned after anthesis. Harvests were done two times a week, the fruits being picked when they started to colour. Leaves and side shoot were picked once per week. Leaves below the lowest truss were removed during the experiment.

Periodically (every 2 weeks) three plants per treatment were measured destructively. Leaves (including petioles), stem, root, individual fruit trusses (including peduncles), removed leaves and picked fruits were dried in a ventilated oven at 60℃ for at least one week. The plants used for destructive measurements were always surrounded by guard plants (plants not used in the experiment).

Periodically (every week) seven labeled plants per treatment were measured on height of plant, stem diameter, length between two nodes, length and width of every leaf. Leaf area index in the experiment was calculated using the relationship individual plant leaf area times plant number per square meter field. Periodically (every 2 days) three given plants per treatment were measured on length and width of every leaf in the different seasons.

3.2 Model Validation

The crop growth model INTKAM was validated on greenhouse experiment *Lycopersicon esculentum* in 2001. Climatic data, hourly averages instead of daily values were used in the procedure. Hourly averages for measured global radiation and temperature outside the greenhouse, greenhouse temperature and CO_2 concentration, temperature of heating pipe, VPD of air were input to the model. In order to compare measured and simulated crop growth, the model was also run with LAI, dry matter distribution measured as inputs.

4 Results and Discussion

4.1 Dry Matter Production and Distribution

Cumulative leaf and stem dry matter production was simulated reasonably well in the experiment (Figs. 1 (a) and (b)). The error was bigger on the simulated and measured value of cumulative fruit production (Fig. 1 (c)). The model over-estimates the partitioning into the fruits at high temperatures, which mainly because of an over-estimation of fruit set in the experiment. The heat stress wasn't taken into account in the model. The high temperature had a strong effect on the rate of fruit set in the summer (Gong Zhiqing, 2003). Effects of heat stress on abortion might also be the result of reduced assimilate availability, but heat stress may specifically reduce the metabolic activity of the flower or the flower bud as well (Aloni et al., 1991). Under temperature climate conditions, without

flower or fruit pruning, only a small fraction of tomato flowers sets fruit, indicating that flower initiation does not limit the number of fruits produced. Other authors have reported low fractions of flower sett-ing fruit in pepper (Bakker, 1989; Marcelis, 2004). The measured value of root mass was lower than the simulated value (Fig.1 (d)). We sampled only part of the roots because plants were grown in soil.

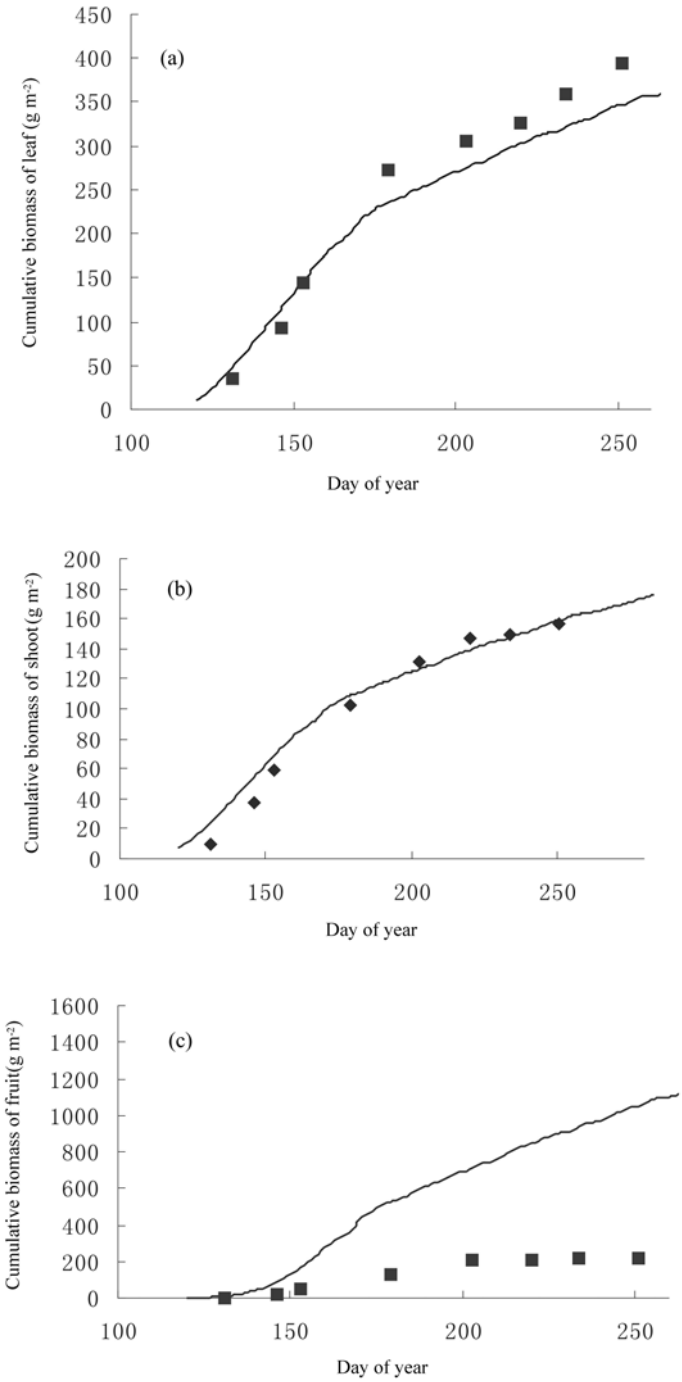

Figure 1 Measured (■) and simulated (—) cumulative biomass

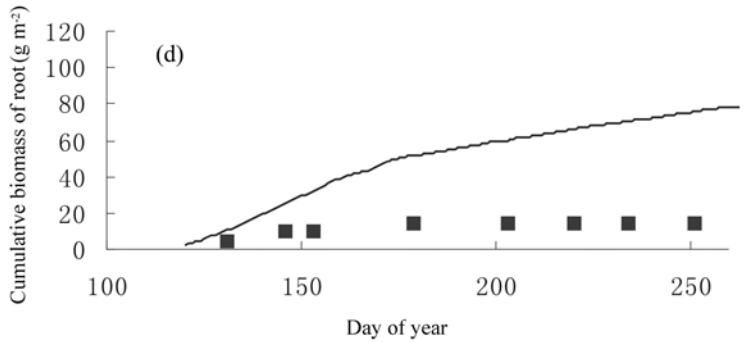

Figure 1 (Continued)

As validation of the model was done in China, it indicates that the model can simulate plant dry matter production and partitioning into the organ when hourly climate data are available.

4.2 Leaf Area Index

LAI was simulated well in the first 40 days of growth (Fig.2). However, LAI was overestimated between days 163 and 191. The main reason was the leaves under the first truss which should be removed early but they retained on the plant. The measured values lowered in comparison to the simulated values after day 200, probably due to maximum air temperatures in the greenhouse that exceeded 38℃. The high temperature had a strong effect on the growth of individual leaf. A lot of energy was lost at high temperature because of the high maintenance respiration.

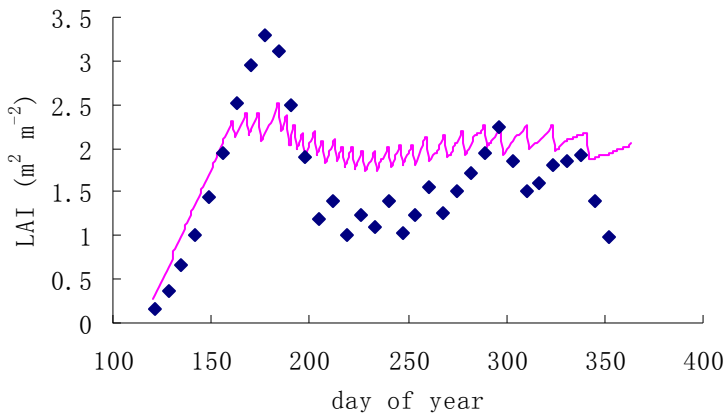

Figure 2 Measured (◆) and simulated (—) leaf area index

4.3 Individual Leaf Area

The observed area of individual leaves was bigger than the simulated leaf area when the leaf grew in May to June. The leaf area grew more quickly in August but the final individual leaf area was smaller than the simulated leaf area in September. It grew slower and smaller than the simulated leaf area in the winter (Fig. 3). Maybe the plant was subject to heat stress in the summer and cool stress in the winter. At the same time the leaf had more maintenance respiration in the summer and less assimilate production in the winter.

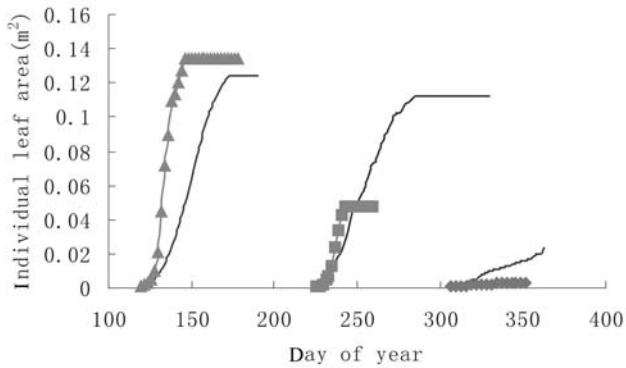

Figure 3 Measured (▲,■,◆) and simulated (—) leaf growth in the different seasons

4.4 Truss Appearance and Node Number

The first truss appearance node was 9 in the simulation (Fig. 4). The plants grew slowly in the experiment. The node number of measured and simulated was 17 and 19, respectively, when the day of year was 184 in July. And it was 26 and 31, respectively, when the day of year was 247 in September. Maybe the heat stress and the energy consumption is also the reason during July and August. The node number of measured and simulated was 31 and 40, respectively, when the day of year was 338 in December since the low temperature during late autumn restrained the plant growth.

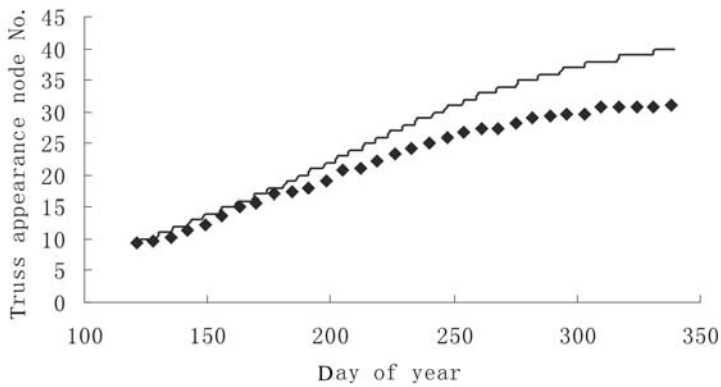

Figure 4 Measured (◆) and simulated (—) truss appearance

5 Conclusion

A greenhouse experiment with tomato was carried out in China. Vegetative development was considered normal, but fruit production was hampered due to heat stress in summer. Simulation of leaf growth with a mechanistic growth model validated for West-European conditions agreed reasonably well with the observations. The model predicted much high fruit production, resulting from a high fruit set and low abortion rate. It is recommended to add mechanisms related to heat stress in the model to be able to simulate growth conditions relevant for China.

Acknowledgements

The study was carried out with financial support from the Shanxi natural scientific fund program (No. 20021086), National Agricultural Department of China '948' program (No. 2003-Z64), Shanxi

scientific technique department program (No. 041018-2) and Shanxi Agricultural University innovative fund program (No. 200218). During the experiment great help and guidance from professor Wen Xiangzhen are gratefully acknowledged.

References

Aloni B, Pashkar T, Karni L (1991) Partitioning of [^{14}C] sucrose and acid invertase activity in reproductive organs of pepper plants in relation to their abscission under heat stress. *Annals of Botany* 67: 371 – 377.

Bakker JC (1989) The effects of temperature on flowering , fruit set and fruit development of glasshouse sweet pepper (*Capsicum annuum* L.). *Journal of Horticultural Science* 64: 313 – 320

Bertin N, Gary C (1993) Tomato fruit-set: a case study for validation of the model TOMGRO. *Acta Horticulturae* 328: 185 – 193.

Elings AM, Heinen BE, Pieter de Visser, et al. (2004) Feed-Forward Control of Water and Nutrient Supply in Greenhouse Horticulture: Development of a System. Acta Hort. 654: 195 – 202.

Farquhar GD, Caemmerer S von, Berry JA (1980) A biochemical model of photosynthetic CO_2 assimilation in leaves of C_3 species. Planta 149: 78 – 90.

Gong Zhiqing (2003) Analysis between greenhouse temperature and growth and production of tomato. MsC dissertation, Taigu: Shanxi Agricultural University (in Chinese with English abstract).

Jones JW, Dayan E, Allen LH,et al. (1991) A dynamic tomato growth and yield model (TOMGRO). *Transactions of the American Society of Agricultural Engineers*, 34: 663 – 672.

Koning ANM de (1994) Development and dry matter distribution in glasshouse tomato: a quantitative approach. Thesis, Wageningen Agricultural University.

Kropff MJ, Goudriaan J (1994) Competition for resource capture in agricultural crops. In: Gresource capture by crops. Eds J.L. Monteith, R.K. Scott & M.H. Unsworth, Nottingham University Press, Loughborough, Leicestershire, 233 – 253.

Li Lingzhi (2002) Growth analysis of the tomato in a greenhouse: A quantitative relation between leaves and fruits and greenhouse environment. MsC dissertation, Taigu: Shanxi Agricultural University, 35pp (in Chinese with English abstract).

Li Lingzhi, Gong Zhiqing, Li Yaling, et al. (2003) The growth and development characteristic of tomato in greenhouse long-season cultivation. Journal of Huazhong Agricultural University, 22 (4): 395-398 (in Chinese with English abstract).

Marcelis LFM, Boogaard HAGM van den, Meinen E (2000) Control of crop growth and nutrient supply by the combined use of crop models and plant sensors. In: Proc. Int. Conf. Modeling and Control in Agriculture, Horticulture and Post-Harvested Processing. IFAC, 351 – 356.

Marcelis LFM, Heuvelink E, Baan Hofman-Eijer LR, et al. (2004) Flower and fruit abortion in sweet pepper in relation to source and sink strength. *Journal of Experimental Botany* 406, 55: 2261 – 2268.

Meinke H, Baethgen WE, Carberry, et al. (2001) Increasing profits and reducing risks in crop production using participatory systems simulation approaches. Agricultural Systems 70, 493 – 513.

Nederhoff EM, Graaf R de (1993) Effects of CO_2 on leaf conductance and canopy transpiration of greenhouse grown cucumber and tomato. J. of Hort. Science 68: 925 – 937.

Spitters CJT, Van Keulen H, Van Kraalingen DWG (1989) A simple and universal crop growth simulator: SUCROS 87. In: Rabbinge R, Ward SA, Van Laar HH, eds. Simulation and systems management in crop protection. Wageningen: Pudoc, 147 – 181.

Yin X, Struik PC, Kropff MJ (2004) Role of crop physiology in predicting gene-to-phenotype relationships. Trends in Plant Science 9, 426 – 432.

Spatial and Seasonal Simulations of Irrigated Processing Tomato

M. Rinaldi, R. Ubaldo, S. Ruggieri

(Agricultural Research Council – Research Unit for cropping systems in dry environments, via Celso Ulpiani, 5, 70125 Bari , Italy)

Abstract: Crop simulation models are used to compare crop management techniques, allowing for multi-year and multi-location runs over minimum time intervals. In Southern Italy, where water-limited conditions are common, it is important to identify irrigation scenarios which allow for a more efficient transformation of water (and irrigation water) into commercial yield. In this research project, a spatial analysis of a long-term simulation was carried out with AEGIS/WIN, a GIS interface of the DSSAT crop simulation package. The case-study refers to a 1000 km^2 area, characterized by 481 soil samples collected over a regular grid. The processing tomato was simulated punctual-based using long-term weather data. The evaluated crop management scenarios were a) rainfed and b) 13 automatic irrigation levels based on soil CAW thresholds. Commercial yield, water and irrigation water use efficiencies (WUE and IRRWUE respectively), and NR were evaluated for each soil sample in order to select the optimum irrigation scenario. This choice was based on different criteria which were defined taking into account the objectives of different stakeholders involved in the tomato crop chain. All the above variables were visualised and mapped with GIS. According to the criteria, the results of the rainfed scenario were not useful, showing low values for fruit yield and negative net returns for WUE. An increase in the threshold of soil water content in order to start irrigation improved the fruit yield, its temporal stability and the WUE. The overall mean of the IRRWUE decreased for thresholds of CAW higher than 50%. Results showed that the optimum CAW threshold was on average 45% for the different criteria parameters. The selection of the optimum scenarios based on yield and profitability were affected by the hydrological properties of the soils. The option criterion based on WUE maximisation proved to be suitable from different points of view and matched the interests of several stakeholders. In this work, a methodological approach is proposed for the spatial and temporal evaluation of irrigation scenarios, developing a support decision system for different stakeholders in planning irrigation water distribution. Some relationships among the stakeholders are also discussed, based on simulated results.

Keywords: DSSAT, simulation model, criteria choice, WUE, yield, net return

1 Introduction

The ever-decreasing availability of water for irrigation and the problem of water resource allocation at district and basin scales are important issues faced by several research projects using crop models and remote sensing information (http://www.demeter-ec.net/index.html; http://www.inea.it/aquater/; http://wasamed.iamb.it/programmi/home.php; http://www.attempto-projects.de/aquaterra/1.0.html). In order to develop a decision support system, biophysical processes and human intervention need to be modelled, such as changes in agricultural to external conditions like water scarcity. CM, if

calibrated and accurately validated, are able to simulate potential crop yield, climate change influence on crop yield, the effect of changes in cropping patterns (crops, cultivars and sowing times), cultivation intensity (rotations) and management practices (irrigation, fertilisation) on yield, profitability and soil fertility (Matthews, 2002). CM should appreciate "soil-climate-crop" interaction, offering stakeholders suggestions for better water allocation and advising farmers on the best irrigation scheduling from an economic point of view.

The applicability of these models can be extended to much boarder spatial scales by combining them with GIS, with layers providing information on soil, climate and crop management data. Several researchers have demonstrated or discussed the strength of this concept for agricultural management decision and planning at various spatial scales (Dent and Thornton, 1988; Hartkamp et al., 1999**a**; Hoogenboom and Thornton, 1990; Thornton et al., 1995).

Climatic variability, in particular rainfall amount and distribution, is very wide in Mediterranean environments; rainfed crop yield is largely dependent on yearly rainfall and in-field experiments and their interaction with other treatments often show significant statistical analysis results. The capability of CM to simulate multi-year crop sequences with daily recorded or generated weather data allows us to examine the yearly variability and to display the output on a frequency distribution base.

Experiences of DSSAT application at spatial scale are reported by Hoongenboom and Thornton (1990) who applied GIS to bean, maize and sorghum CM in Guatemala. Calixte et al. (1992) developed an Agricultural and Environmental Geographic Information System (AEGIS), which combined DSSAT crop models with GIS to assess the impact of different agricultural practices in Puerto Rico. Georgiev et al. (1998), Heinemann et al. (2002), Batchelor et al. (2002) and Nijbroek et al. (2003) reported further applications of DSSAT at spatial scale, especially for water requirement estimates. This permits an upscale of CM use at irrigation district or regional level.

In previous studies, the CM embedded in DSSAT software were calibrated and validated for Southern Italy conditions for wheat (Rinaldi, 2001; Rinaldi, 2004), sunflower (Rinaldi et al., 2003) and tomato (Rinaldi et al., 2007): it proved to be a useful tool in the simulation of field crops in several soil and climatic conditions; the reasons for the selection of DSSAT software include its large number of users, a user-friendly interface and an improved version with further applications.

The seasonal analysis tool (Thornton and Hoogenboom, 1994) allows for multi-year simulations with real or generated daily weather data; it also has an economic module that is useful in comparing management scenarios and geographical areas from an economic point of view. Spatial analysis and interface with GIS is a tool embedded in the latest versions of DSSAT (v.3.5 and the subsequent upgrades) for the simulation of a large number of combinations "soils x climate x management" and to display the output.

The objective of this paper is to apply a GIS-based CM to compare irrigation strategies for processing tomato, an important field crop in Southern Italy. Crop yield, crop water and irrigation water use efficiency and net return were predicted and calculated over a long-term time scale. For each "soil x climate" interaction, optimum irrigation strategies were then estimated and discussed according to the needs of different stakeholders.

2 Materials and Methods

The "Capitanata" is a plain of about 4000 km^2 in South-Eastern Italy, mainly cropped with durum wheat, tomato, sugar beet, olives and grape orchards. Irrigation is managed by the local authority "Consorzio per la Bonifica della Capitanata" of Foggia, that provides irrigation water on demand at low pressure (2-3 bar) for a large part of the plain (1800 km^2). Part of this plain (about 1000 km^2, in the 0 – 180 m a.s.l. altitude range) was studied from pedological and climatic points of view. A

large number of soil samples (481) were collected at the nodes of a georeferenced regular grid, at 0 – 20 and 20 – 40 cm depth and 115 soil profiles were examined up to 2.5 m in depth. The main chemical and physical characteristics were then recorded (texture, hydrological characteristics, nitrogen and phosphorus content, organic matter, bulk density). The 481 points were converted into polygons by the Thiessen method (threshold value = 5) (Hartkamp et al., 1999**a**) and then intersected with a soil map, in order to ensure more homogeneous pedological conditions inside each polygon (Fig. 1).

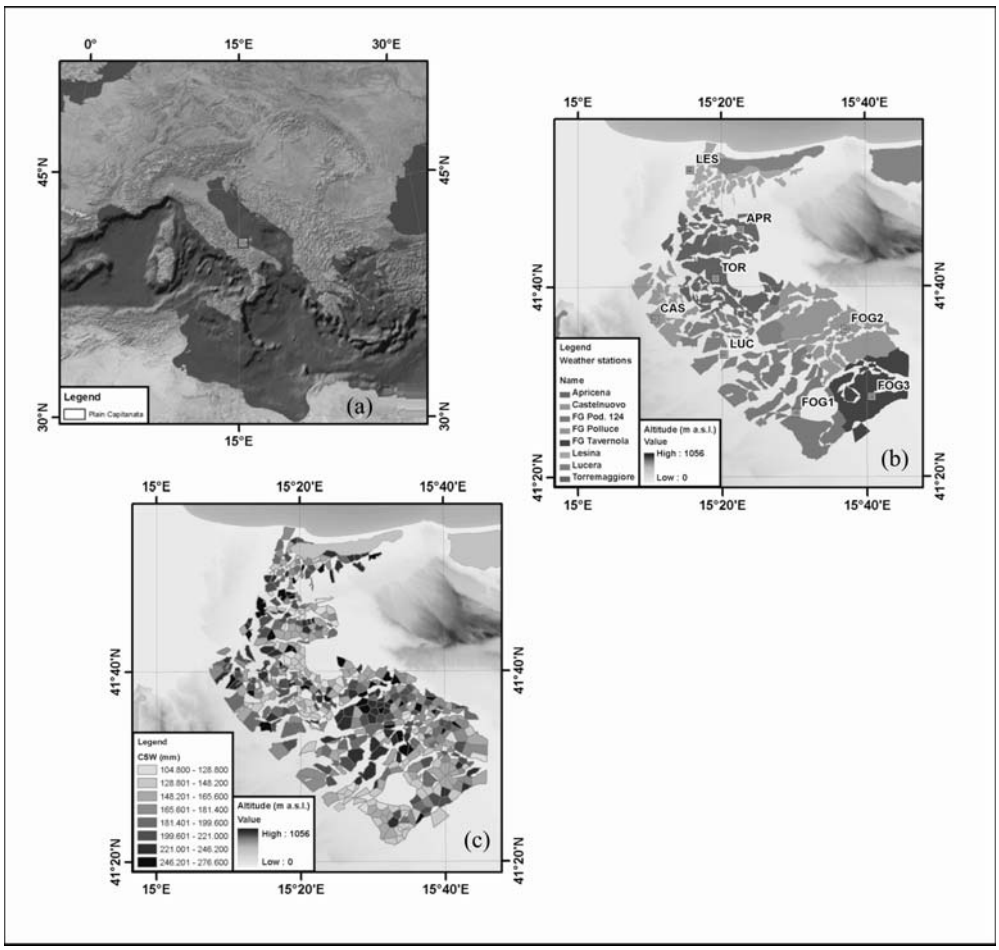

Figure 1 (a) Localization of the test area in Southern Italy; (b) clustering of the 481 soil polygons around the nearest weather stations and Digital Elevation Model (DEM) of the area as background; weather stations: LES (Lesina), APR (Apricena), TOR (Torremaggiore), CAS (Castelnuovo), LUC (Lucera), FOG1 (Foggia Pod. 124), FOG2 (Foggia Polluce), FOG3 (Foggia Tavernola); (c) map of the crop soil water availability (CSW, mm) in the 1 m top layer

Daily climatic data (maximum and minimum temperature, solar radiation and rainfall) were taken from eight meteorological stations located in the area and managed by the "Consorzio" referred to above. Each soil polygon was assigned to the nearest weather station. The climatic characteristics of the 8 stations were calculated based on long-term data during the tomato crop cycle (1st May – 8th August).

The CROPGRO model, embedded in the DSSAT program (Jones et al., 2003), was calibrated and validated in the test area for a processing, self pruning, globe shape, tomato variety (PS 1296,

Rinaldi et al., 2007). The model was used in a seasonal (45 cropping cycles, from 1955 to 1999) and spatial analysis, comparing irrigation scenarios, one not irrigated (rainfed) and 13 automatically irrigated at different rates of soil CAW in the 0.3 m top soil layer. Irrigation was simulated until fruit maturity, with water amount refilling up to field capacity; a drip irrigation method was set. The simulated scenarios are indicated with "IRRn", where n is the percentage of CAW.

The tomato crop, in accordance with local management, was simulated with a fixed sowing date (30^{th} April), fertilisation with 278 kg ha^{-1} of ammonium phosphate pre-sowing and 147 kg ha^{-1} of ammonium nitrate at fruit formation (30^{th} May). The harvest date was simulated by the model at crop maturity. Output variables were analyzed: fresh fruit yield (t ha^{-1}), seasonal irrigation water (mm) and number of irrigation applications and water drainage (mm).

WUE (kg m^{-3}) was calculated as the ratio between the dry fruit matter at harvest and actual seasonal evapotranspiration estimated by the model. IRRWUE (kg m^{-3}) was calculated as the ratio between the dry fruit matter increase compared to the yield of the rainfed scenario and the applied seasonal irrigation volume.

The interface with a GIS program, AEGIS/WIN, allowed us to run the model in 481 polygons and to display the outputs of the model using map visualization (Engel et al., 1997; Hartkamp et al., 1999b). The total number of runs per simulation was 21645 and an average of 45 yearly values were assigned to each polygon (soil-climate interaction). The temporal variability of yield was also analysed computing the related coefficient of variation (%).

The economic evaluation of the simulated tomato was performed by means of the Seasonal Analysis tool of DSSAT, calculating NR (€ ha^{-1}) with reference to prices and costs reported in Table 1.

Table 1 Prices and costs of processing tomato field crop in Southern Italy (referred to 2006)

	Unit	Cost/Price
Fresh fruit price	(€ t^{-1})	60,00
Base production cost	(€ ha^{-1})	5500,00
Water irrigation cost	(€ mm^{-1})	1,00
Irrigation application cost	(€ $application^{-1}$)	15,00

The model outputs and the outputs-derived variables mentioned above were then compared for each soil polygon based on their long-term averages, in order to assess the irrigation strategies that are more in line with the prior targets of the various stakeholders involved in the tomato crop chain. Analysed in greater detail, five criteria options were adopted:

Based on maximisation of net returns (MAX_{NR}), prior target for farmers;

Based on water use efficiency (MAX_{WUE}), prior target for plant physiologists;

Based on maximisation of irrigation water use efficiency (MAX_{IRRWUE}), prior target for the local irrigation authority;

Based on maximisation of fresh fruit yield (MAX_{FY}), prior target for industrialists;

Based on temporal stability of yield, minimising the coefficient of variation (MIN_{CV}), that directly or indirectly affects the interests of all stakeholders.

For each option criterion, the main tomato variables associated with the selected scenarios were mapped, separating them into eight classes by means of the Jenks Natural Breaks method, which identifies breakpoints between classes based on a statistical formula (Jenk's optimization), minimizing the sum of the within-class variance (Jenks 1967). The same clustering method was used for mapping the outputs of the rainfed and the irrigated scenarios, respectively.

3 Results and Discussion

Area description

The climatic stations (Tab. 2) were located in a flat, plain area: only CAS was placed on a smooth hill (177 m a.s.l.), while LES was very close to a lake and the Adriatic sea coast (Fig. 1). Based on weather data during the tomato crop cycle (1st May – 8th August) CAS and LES were the coldest places, CAS and FOG1 the rainiest ones, FOG2, FOG3 and LUC the warmest ones, FOG3 the least rainy location. The CAS station was also the place characterised by lowest solar radiation due to cloud influence.

Table 2 Averages ± standard deviations (coefficients of variation, %, in brackets) of long-term climatic data during tomato crop cycle (1st May – 8th August) for the eight meteorological stations used in this case-study in Southern Italy. The location of stations is mapped in Fig. 1

Agrometeorological Stations	Altitude (m a.s.l.)	Maximum Temp. (°C)	Minimum Temp. (°C)	Rainfall (mm)	Solar Radiation (MJ $m^{-2}d^{-1}$)
APR (Apricena)	55	29.4 ± 1.5 (5.2)	15.6 ± 1.1 (7.2)	97.0 ± 43.4 (44.8)	22.7 ± 2.4 (10.6)
CAS (Castelnuovo)	177	28.1 ± 1.8 (6.6)	15.5 ± 1.1 (7.0)	116.3 ± 41.8 (35.9)	21.0 ± 3.9 (18.7)
FOG1 (Foggia Pod. 124)	92	29.5 ± 1.3 (4.4)	15.8 ± 0.9 (5.7)	112.5 ± 61.0 (54.2)	21.5 ± 2.0 (9.4)
FOG2 (Foggia Polluce)	21	31.6 ± 1.4 (4.5)	15.9 ± 1.5 (9.5)	89.5 ± 46.2 (51.6)	24.3 ± 2.6 (10.7)
FOG3 (Foggia Tavernola)	36	32.0 ± 1.4 (4.5)	15.5 ± 1.7 (10.8)	79.0 ± 45.6 (57.7)	23.5 ± 3.1 (13.3)
LES (Lesina)	13	28.4 ± 1.6 (5.8)	14.6 ± 1.2 (7.9)	97.6 ± 51.0 (52.2)	21.8 ± 2.3 (10.5)
LUC (Lucera)	102	31.1 ± 2.1 (6.8)	15.3 ± 1.1 (7.0)	100.1 ± 40.7 (40.7)	22.2 ± 3.0 (13.7)
TOR (Torremaggiore)	110	30.3 ± 1.3 (4.2)	16.0 ± 1.1 (7.0)	96.2 ± 40.1 (41.7)	24.1 ± 2.7 (11.1)

The main differences among the 481 polygons derived from the soil texture that influenced the hydrological characteristics (wilting point and field capacity). The CSW (mm) resulting from the difference between field capacity and wilting point for the 1 m top soil layer is mapped in Fig. 1. A distribution of soils with greater CSW in the middle part of the tested area was noted, close to FOG2 and LUC (mainly clay soils) and the CAS weather stations, while sandy soils, with lower CSW, were located in the southern part (FOG1 and FOG3) and close to TOR and APR stations (Fig. 1).

Tomato crop is usually irrigated in the test area with sprinklers and, more commonly, with drip irrigation methods; seasonal irrigation volumes range between 300 and 500 mm. The simulated irrigation volumes ranged from 130 up to 460 mm, showing lower values than those recorded in the area (300 – 600 mm), for the tendency of farmers to use more water than real water requirements.

FY simulated in the irrigated scenarios (from 100 up to almost 200 t ha^{-1}) were generally higher than those recorded in the test area (from 70 up to 140 t ha^{-1}), but this overestimation can be explained considering that the model does not take into account the effect of pest damage and weeds.

Rainfed scenario

The fruit yield of the rainfed scenario was very low, 54 t ha^{-1} on average, and with a very large variability, depending on the rainfall, which was very erratic in the test area during the crop growing period (May – August).

In the rainfed scenario, a slightly above-average yield was observed for soils belonging to LES and FOG1 stations (Fig. 2). In the first case, the effect is due to the climate (especially during the summer) produced by proximity to the lake and sea; in the second, rainfed tomatoes may have taken advantage of higher values of rainfall which occurred during the growing season (Table 2).

The areas with larger temporal fruit yield variability in the rainfed scenario were located in the south-eastern part, mainly soils belonging to FOG2 (Fig. 2). This parameter showed a tendency to decrease with the altitude of the reference station; in higher locations (CAS, LUC and TOR) rainfed tomatoes may have taken advantage of the smaller temporal variation of rainfall during the growing season (Table 2).

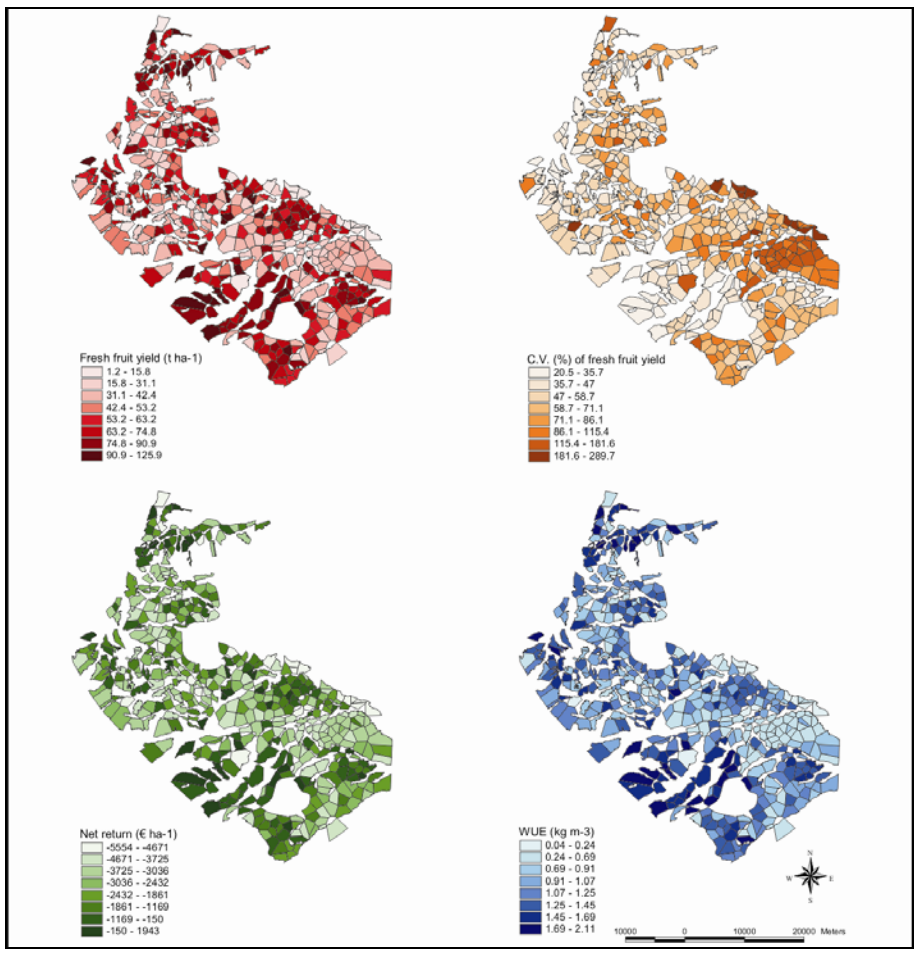

Figure 2 Fresh fruit yield (t ha^{-1}), coefficient of variation (%) of fresh fruit yield, net return (€ ha^{-1}) and water use efficiency (kg m^{-3}) of processing tomato simulated by CROPGRO model in the Rainfed scenario and mapped for the 481 soil polygons

The WUE was very low in the rainfed scenario (1.08 kg m^{-3}) and a large variability of WUE emerged from the spatial analysis, with higher values at FOG1, LES and CAS, where the lowest plant evapo-transpiration values occurred. Lower values of WUE were observed in the area close to the FOG2

station, characterised by large soil CSW (Fig. 1) and consequently greater crop evapotranspiration.

The rainfed scenario proved to be of scarce interest as it showed negative values of NR in every cropping cycle and in more than 80% of the soils (Fig. 2). The NR of the rainfed tomato, only depending on productivity and fixed production costs, followed the yield spatial variability.

Comparison among irrigation scenarios

The effects of automatic irrigation on some model output variables at increasing CAW thresholds are showed in Fig. 3. In the same figure, the values obtained for the rainfed scenario are also reported.

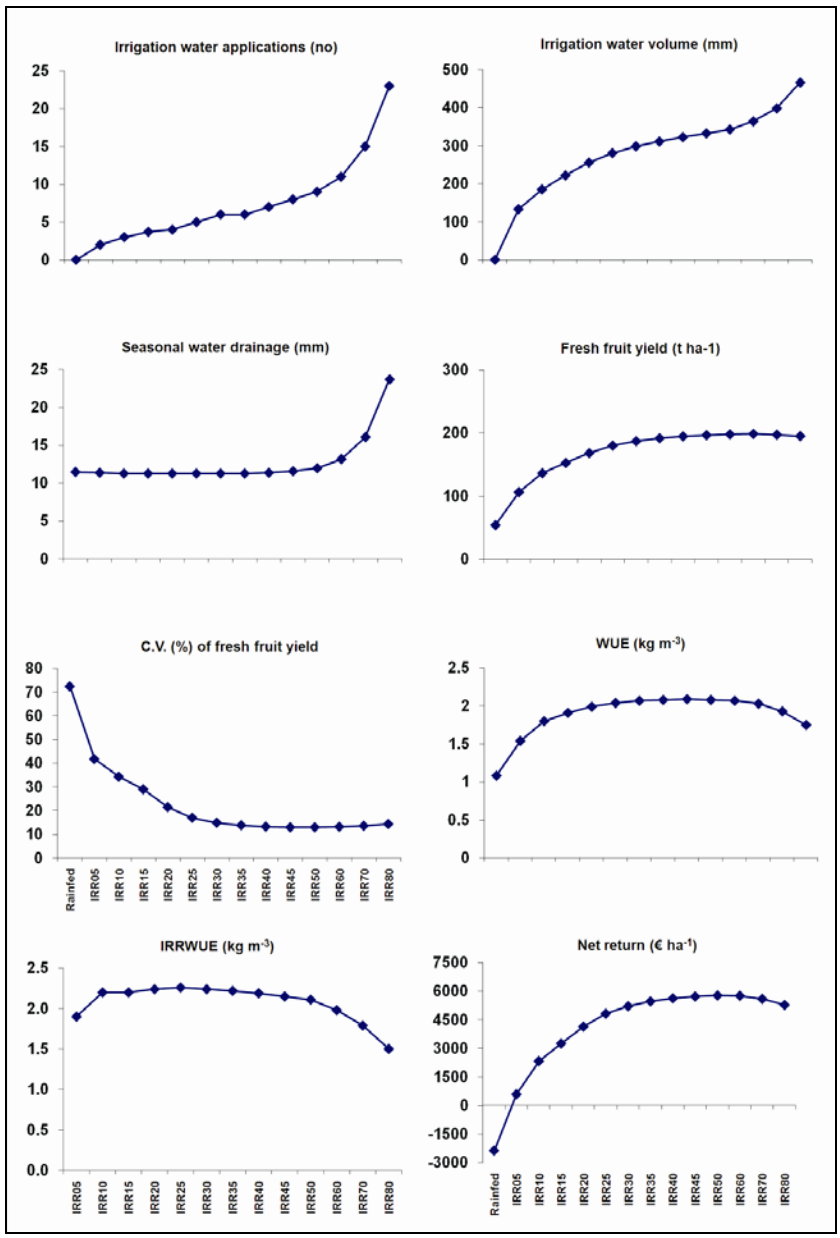

Figure 3 Comparison among 14 automatic irrigation scenarios of tomato simulated by CROPGRO model for 45 years in the 481 soil-polygons, based on overall averages of outputs and derived variables

The number of irrigation applications increased gradually with the level of CAW, with two irrigations applied with IRR05 and with larger increases at IRR70 and IRR80 levels. The thresholds of CAW established for these latter scenarios were often and easily reached; moreover, the soil water content was almost maintained at the level of field capacity, which was set as the threshold for stopping irrigation.

Accordingly to the number of irrigation applications, the amount of water supplied increased with the CAW level, more rapidly with the lowest (from IRR05 up to IRR20) and the highest (IRR70 and IRR80) levels of CAW. Restoration of field capacity at each irrigation explains the significant amount of water (about 130 mm) supplied with the lowest threshold of CAW (IRR05).

Consequently, the effect of irrigation due to the application of the IRR05 scenario was particularly evident on the FY (on average twice that of the rainfed scenario). Furthermore, for the IRR10-IRR30 scenarios, the range yields increased with the CAW auto level, up to approximately 3.5 times greater than in the rainfed scenario. The mean value of the yield remained fairly constant for subsequent increase in the CAW, in spite of the growing water irrigation volume and number of irrigation applications, especially inside the IRR60-IRR80 range. In this range, as the soil water is almost maintained at field capacity, an increase in seasonal water drainage was observed, causing nitrogen leaching.

Nevertheless, the seasonal drainage was minimal (on average lower than 25 mm per year), as was also observed in other studies carried out in the same area (Rinaldi et al., 2007; Rinaldi and Borneo, 2006) and this low quantity of drained water indicates that the water applied during the growing season using automatic irrigation methods driven by soil moisture monitoring is suitable for tomato water requirements (Rinaldi et al., 2007).

Irrigation improved the temporal stability of the FY, strongly reducing the CV compared to the rainfed scenario even at the lowest levels of CAW (IRR05 and IRR10) and was fairly constant at small values (CV = 7 – 9 %) for the other scenarios. Thus, the irrigation amount supplied with IRR05 was enough to preserve tomato plants from water stress that affected fruit yield and its temporal stability in the rainfed scenario.

The WUE increased by 40% with IRR05 and then showed similar results (about twice compared to rainfed tomatoes) for the other irrigation scenarios; only the highest CAW levels (IRR70 and IRR80) showed a slight decrease in WUE due to the growing drainage and subsequent nitrogen loss due to deep percolation.

Mean IRRWUE was 1.90 kg m^{-3} for IRR05 and was similar (higher than 2.00 kg m^{-3}, 2.26 kg m^{-3} maximum) for the scenarios from IRR10 up to IRR50; this parameter subsequently decreased with the CAW level (and water irrigation volume), becoming lower than the value of IRR05 with IRR70 and IRR80. This variation is explained considering the trends reported above for yield and irrigation volume.

A remarkable economic benefit of irrigation practice on the tomato crop was noted. Simulated NR for irrigated scenarios was markedly higher with respect to the rainfed scenario. NR slightly decreased for CAW thresholds higher than 60%, due to the increase of irrigation costs which were not compensated by a proportional increase in yield.

Comparison among Criteria to Identify Optimum Irrigation Scenarios

Irrigation had benefits on tomato crops from different points of view, improving each of the variables used as the criteria in selecting the optimum irrigation scenario; on the contrary, the rainfed scenario was never chosen as the optimum one (Table 3).

The application of different option criteria had different effects on the outputs, shown numerically (Table 4) and graphically (Figs. 4 – 8).

$MAX_{NR.}$ In most soils (73%) NR maximisation was gained by CAW levels higher than or equal

to 50% (Fig. 4a). The optimum CAW threshold was positively related to the soil CSW; indeed, based on MAX_{NR}, IRR35 and IRR40 strategies were assigned only to soils with low values of CSW (150 mm on average), whereas IRR80 was assigned to soils with high values of CSW (240 mm on average). The CSW values of soils attributed to the other were more dispersed.

Table 3 Statistics of optimum CAW_{auto} (%) level for each of the five criterion of option referred to the 481 soils

Criterion	Optimum CAW_{auto} (%) level				
	Mean (†)	Min.	Max.	Mode	Median
MAX_{NR}	60	35	80	60	50
MAX_{IRRWUE}	20	5	45	10	15
MAX_{WUE}	35	15	60	40	40
MAX_{FY}	60	35	80	80	60
MIN_{CV}	45	5	80	40	40

(†) Approximated to the nearest simulated scenario.

Table 4 Averages of output variables of processing tomato simulated by CROPGRO model, referred to the 45 crop cycles of simulation and to the 481 soils, for different criteria of optimal scenario selecting

Criterion	Fresh Fruit Yield (t ha^{-1})	CV of Fresh Fruit Yield (%)	Irrigation Water Volume (mm)	Water Use Efficiency (kg m^{-3})	Irrigation Water Use Efficiency (kg m^{-3})	Net Return (€ ha^{-1})
MAX_{NR}	200.4	11.0	359	2.06	2.07	5882
MAX_{IRRWUE}	174.0	13.0	257	2.03	2.41	4489
MAX_{WUE}	194.7	10.7	314	2.11	2.28	5638
MAX_{FY}	200.9	11.3	383	2.00	1.96	5846
MIN_{CV}	193.8	9.95	338	2.05	2.14	5527

The main impact of the MAX_{NR} criterion was observed on the irrigation water volume and IRRWUE, respectively 39% higher and 14% smaller compared to the MAX_{IRRWUE} criterion (Table 4).

$MAX_{IRRWUE.}$ The maximum water saving was gained by the application of the MAX_{IRRWUE} criterion, which implied the use of the minimum amount of irrigation water, both on average and in nearly every soil type.

The adoption of the MAX_{IRRWUE} criterion caused the major effect on NR, reducing it by 24% on average with respect to MAX_{NR}. This reduction was lower than 20% in about half of the soils, but exceeded 50% in more than 10% of the soils (Figs. 5(b) – 5(f)).

The MAX_{IRRWUE} criterion led to a selection of CAW levels lower than MAX_{NR} (from 5% up to 45%) (Table 3). IRR10 was the prevalent strategy in the area (27% of soils) and the highest thresholds of CAW were assigned to soils located in the central part of the test area (mainly CAS and FOG 2) and in the southern part (Fig. 5(a)).

MAX_{WUE}. The application of the MAX_{WUE} option criterion produced an average net return ranging between 3432 and 7364 € ha^{-1}, preserving levels of profitability very close to the maximum ones in nearly the whole test area and reaching a maximum relative decrease of 20% (Fig. 6(d)).

Optimisation of WUE not only had a relatively weak impact on profitability (-4% on average respect to MAX_{NR}), but it was also gained with CAW thresholds and irrigation volumes lower than MAX_{NR} in nearly the whole area (87% of soils) (Fig. 6(a)). Resulting water saving was only about 12% (45 mm) on average (Tab. 4), but this benefit was not uniform across the area, ranging from less than 10% (in nearly half of the soils) up to 50%.

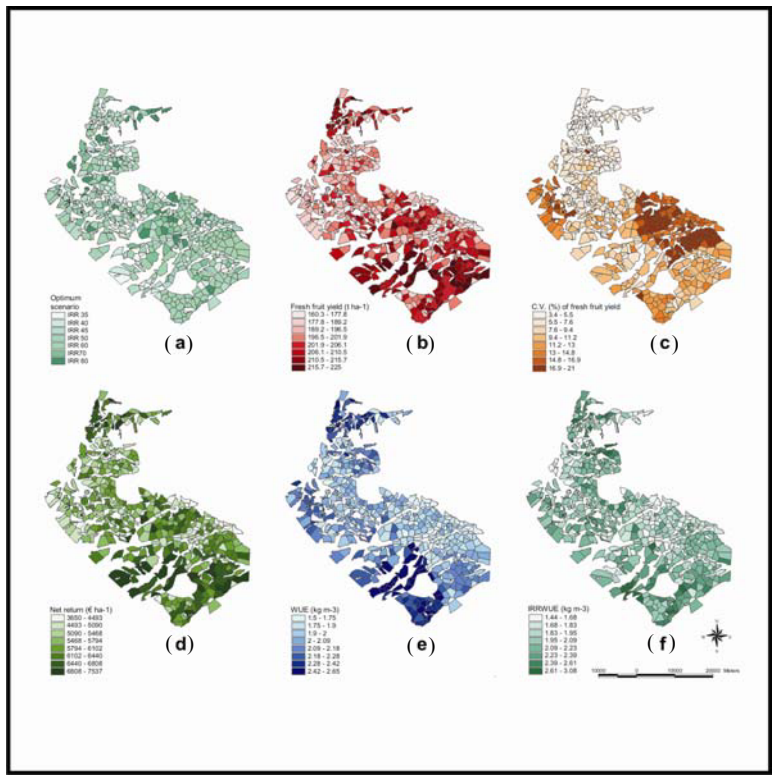

Figure 4 Optimum scenario for net return (a) and related tomato output variables ((b) − (f))

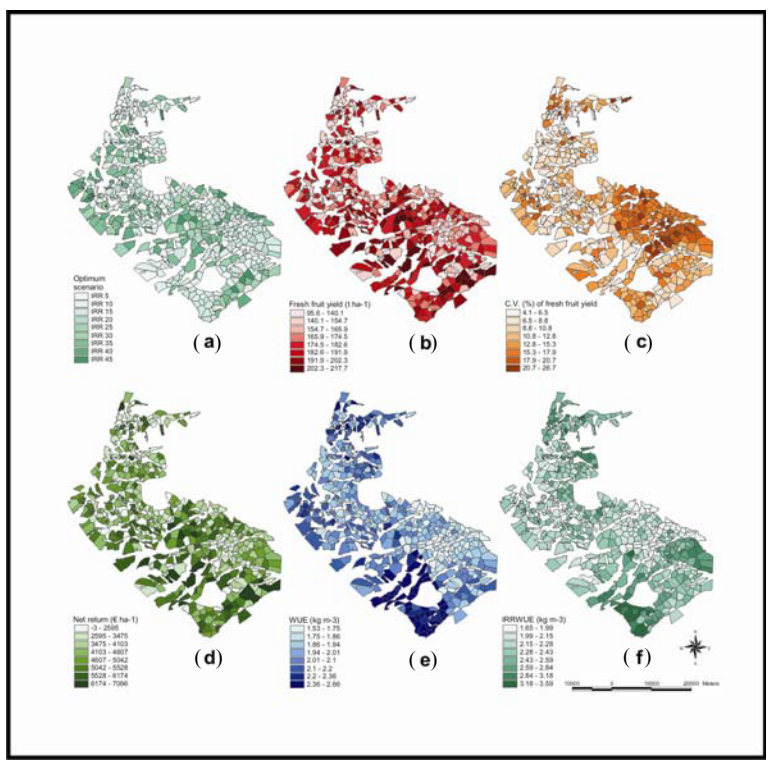

Figure 5 Optimum scenario for irrigation water use efficiency (a) and related tomato output variables ((b)− (f))

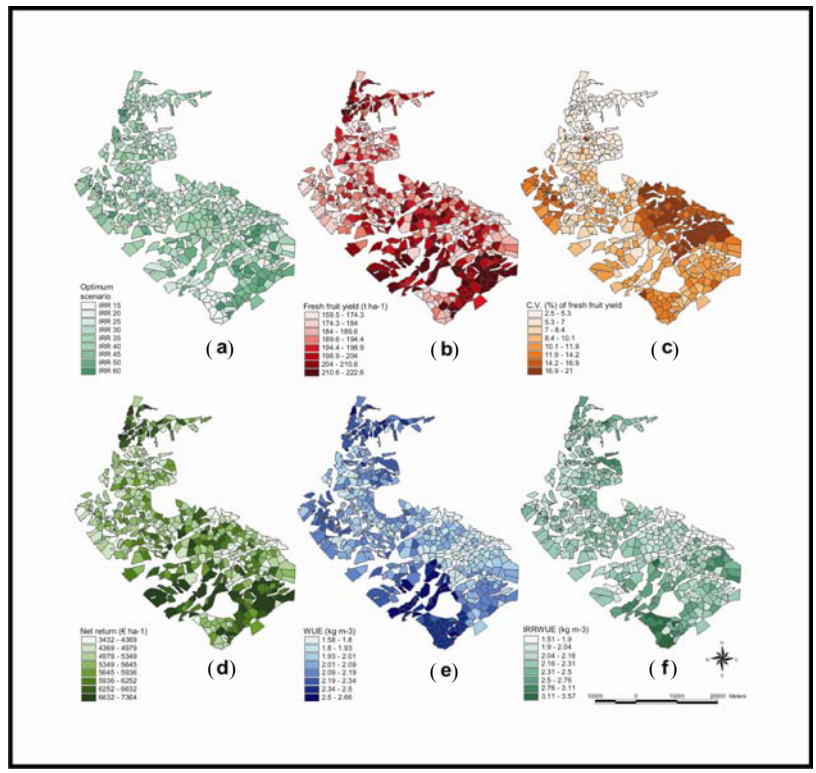

Figure 6 Optimum scenario for water use efficiency (a) and related tomato output variables ((b) – (f))

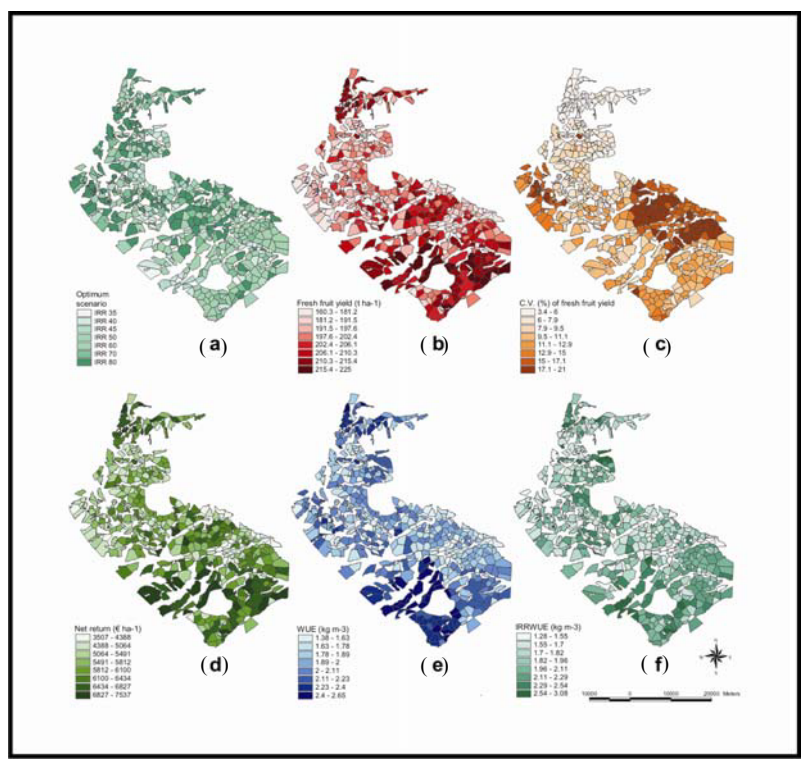

Figure 7 Optimum scenario for fresh fruit yield (a) and related tomato output variables ((b) – (f))

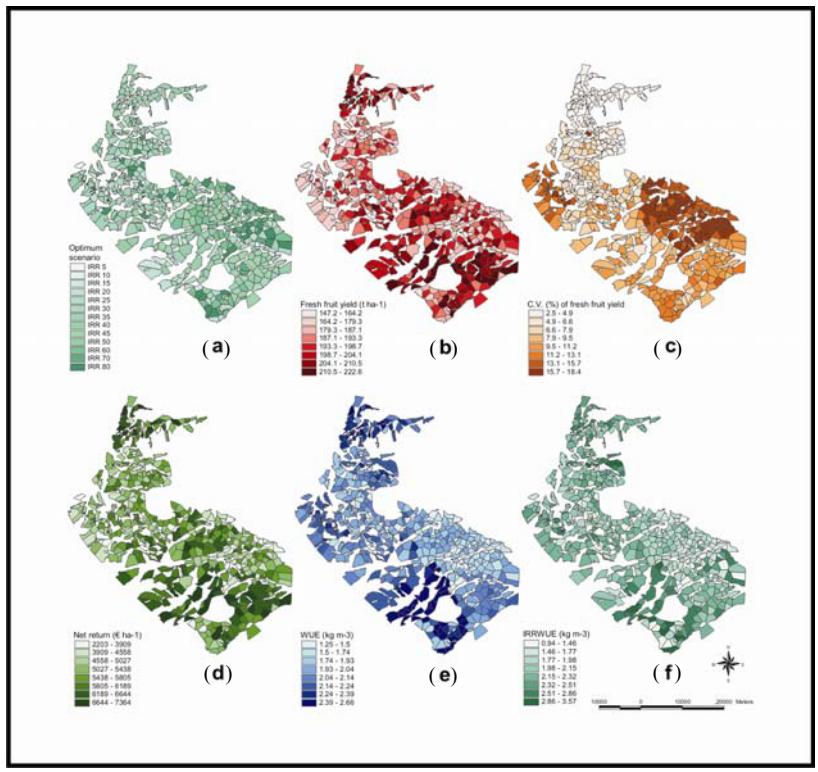

Figure 8 Optimum scenario for coefficient of variation of fresh fruit yield (a) and related tomato output variables ((b) – (f))

The MAX_{WUE} criterion led to only a 5% reduction of IRRWUE (0.1 kg m^{-3}) with respect to MAX_{IRRWUE} (Table 4); this reduction was less than 20% in nearly all the soils and did not exceed 0.6 kg m^{-3} (Fig. 6(f)).

The maximisation of WUE implied the use of an irrigation water amount 30% (57 mm) higher than MAX_{IRRWUE} (Table 4). However, also in this case the effect was not homogeneous across the area, the relative difference in water volume ranging from 0% up to more than 100%. This indicated that in some soils the application of the MAX_{WUE} criterion can be disadvantageous from a water saving point of view compared to MAX_{IRRWUE}.

MAX_{FY}. A maximisation in FY was obtained in the same range of CAW as MAX_{NR} (due to the strong relation between FY and NR) and also in this case many soils (84%) were assigned to CAW levels higher or equal to 50%. Following this criterion, IRR80 was the optimum strategy for more than 30% of soils (Table 3 and Fig. 7(a)). In a previous study to select the most productive scenario for each soil type (Rinaldi and Ubaldo, 2007), the IRR50 and IRR70 scenarios were generally the most productive ones, providing yields on average similar to the overall mean obtained in this study.

When the prior objective of irrigation scheduling was MAX_{FY}, the simulated FY and NR were very similar to the mean values resulting from MAX_{NR} (Table 4). The range of variation of yield in the area was also the same for these two criteria and more than half of the soils were assigned to the same irrigation scenario; in the other soils, the decrease of NR due to the adoption of MAX_{FY} was a maximum of 8% (Fig. 7(b)).

The difference in assignment of CAWauto thresholds between MAX_{NR} and MAX_{FY} showed a mean increase of just 24 mm of irrigation water with the second criterion (Table 4), but it is worth noting that this increase exceeded 100 mm in some soils. In fact, the irrigation water amount was the output which was most affected by fresh yield optimisation (+49% with respect to the MAX_{IRRWUE} criterion).

MIN_{CV} of fruit yield. The selection of an automatic irrigation strategy based on temporal stability of yields (MIN_{CV}) involved the whole range of simulated scenarios (Tab. 3). Only in a small proportion (2%) of soils was optimum CAW lower than 20%, while values from 35 up to 40% were most frequent. The more irrigated soils were located in the south-eastern part of the area (FOG1 and FOG2) (Fig. 8a).

The MIN_{CV} criterion generally provided a mean NR just slightly lower than profitability obtained with the other criteria (except MAX_{IRRWUE}, for which the lowest NR was observed). Nevertheless, in some soils this criterion proved to be more disadvantageous compared to the other criteria from an economic point of view.

From a comparison among the different option criteria and the impacts of the choices of the different stakeholders, the WUE was the most constant output variable, only slightly reduced by the application of the other criteria (on average, from 2% with MAX_{NR} up to 5% with MAX_{FY}) other than MAX_{WUE}. Conversely, water irrigation amount was shown to be the output most influenced by irrigation management; indeed, all the criteria heavily affected the amount of irrigation water with respect to MAX_{IRRWUE} (from a 20% relative decrease with MAX_{WUE} up to 50% with MAX_{FY}) (Tab. 4).

Spatial Distribution of Irrigation Effects

The outputs of the IRR45 scenario are shown in the maps of Fig. 9. IRR45 was chosen as an example of an irrigated scenario as 45% was the CAW threshold that on average proved to be optimum when considering all five option criteria simultaneously. Comparing the maps of Fig. 9 with those shown in Fig. 2, we can analyse changes in the spatial distribution of outputs due to irrigation compared to the rainfed scenario.

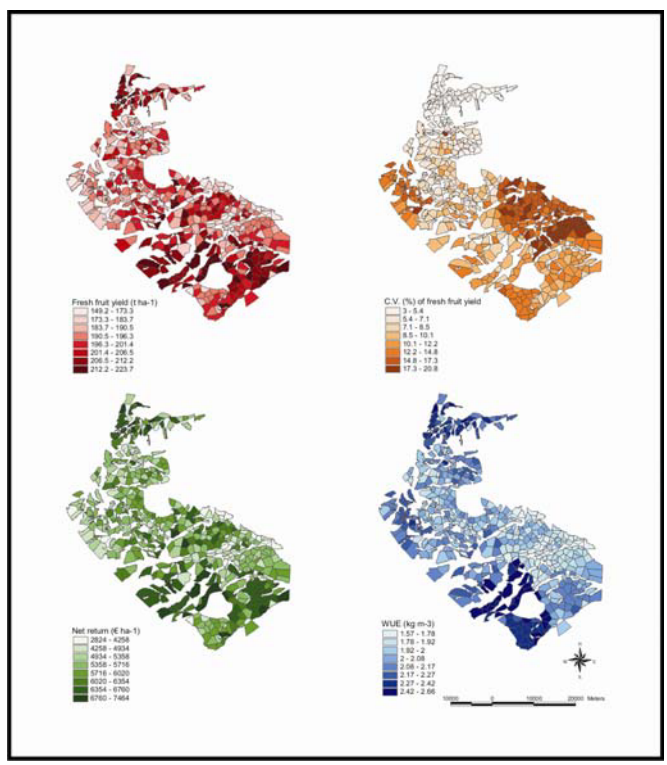

Figure 9 Fresh fruit yield (t ha^{-1}), coefficient of variation (%) of fresh fruit yield, net return (€ ha^{-1}) and water use efficiency (kg m^{-3}) of processing tomato simulated by CROPGRO model in the IRR45 automatic irrigation scenario and mapped for the 481 soil polygons

Irrigation provided an improvement of the main outputs in the whole area, according to the trends shown in Fig. 3.

Irrigation produced an increase of fresh yield inversely related to the productivity of rainfed tomatoes, thus reducing the differences among the soils. Moreover, the increment of yield due to irrigation was less marked in the soils assigned to the less rainy stations (the least yielding were in the rainfed scenario) and directly related to solar radiation during the crop growth period. Indeed, as CROPGRO is a "radiation-driven" model, when the limiting effects of rainfall on productivity are mitigated by irrigation, simulated yield can increase with the availability of solar radiation. Consequently, the soils close to the CAS weather station, that in the rainfed scenario gained a productive benefit from the higher summer rainfall with respect to other areas, were among the less productive in irrigated scenarios. On the contrary, the soils located near the LES station and in the southern part of the area provided yields only slightly higher than the rest of the area both in the rainfed and irrigated scenarios (Figs. 2 and 9).

Irrigation also caused some changes in the spatial distribution of variability of FY. As in the irrigation scenario, the stabilizing effects of irrigation on yields was not homogeneous over the area, but was directly proportional to the variability of yield in the rainfed scenario. Therefore, as observed for FY, irrigation mitigated the differences in CV among the soils. In the IRR45 scenario, the soils with larger temporal fruit yield variability were concentrated in the south-eastern part of the area (similar to the rainfed scenario) and close to the CAS, the station characterized by the largest temporal variability of solar radiation, on which irrigation had no effect; the least variable soils were the northern ones (LES, APR and TOR) (Fig. 9).

The effects of irrigation in terms of WUE reduced the differences among soils but, being a parameter that is only slightly affected by the amount of irrigation, it maintained a spatial distribution similar to the rainfed scenario, with a relative superiority of soils close to FOG1 and LES (Figs. 2 and 9).

The incidence of irrigation in tomato production cost is low (3÷13% of total cost) and for this reason the NR followed the yield spatial variability, depending largely on the productivity in both the irrigated and rainfed scenarios. (Figs. 2 and 9).

4 Conclusions

In this work a methodological approach based on a simulation model has been described for the spatial and temporal evaluation of irrigation scenarios of processing tomatoes. The application of such an approach also allowed for a selection of the optimum scenario based on different criteria, each associated with the prior objectives of a stakeholder.The applied combination of CM and GIS proved to be efficient in providing a fast comparison of irrigation scenarios for a large number of "year/soil/climate" combinations and from different points of view. The short time required for this analysis is a value-added result if we consider that the product price, as well as the water and labour cost, can change from year to year, and so modify the optimum scenario in the different areas.

Spatial and seasonal analysis carried out for different irrigation scenarios allowed us to visualize the most productive and least variable pedo-climatic areas for tomatoes and to assess where the best water use efficiency can be achieved. Moreover, the results of the comparison among the scenarios, visualised on maps, showed the optimum irrigation strategy for each site and the consequences of this choice on the main variables of the tomato.

Positive responses to irrigation practice were observed even at the lowest thresholds of CAW, although the optimum values of outputs (except for IRRWUE and WUE) were generally obtained with higher levels of CAW.

The optimum CAW threshold for the different choice criteria was shown to be on average 45%, with differences among the 481 soils mainly related to the hydrological characteristics, with

particular reference to the CSW. Climatic characteristics slightly affected the crop, with a more limiting effect related to the amount and variability of rainfall on the rainfed crop and a positive effect of the global solar radiation on the irrigated crop. Thus, the less yielding areas and those more characterized by temporal instability of yield were the principal beneficiaries of irrigation practice.

The analysis of impacts on the outputs, derived from the application of different option criteria, highlighted some conflicts and similarities among the criteria and the related stakeholders. The main conflicts were observed between MAX_{IRRWUE} (which markedly reduced the yields and NR) on one hand and MAX_{NR} and MAX_{FY} (which increased irrigation water application and decreased the IRRWUE) on the other. Conversely, there are many similarities between these last two criteria, although the maximisation of profitability allows for a degree of conservation in irrigation water and, consequently, a higher IRRWUE, with respect to MAX_{FY}.

The option of the water distribution authority, oriented towards IRRWUE maximisation, led to a minimum need for irrigation water, and was thus the most sustainable criterion from environmental and energy points of view but not from the economic one. On the contrary, MAX_{FY} was the option criterion that involved the largest amount of irrigation water.

The WUE, being only slightly affected by the CAW level (for thresholds higher than 20%), was also the parameter least affected by the criterion adopted for the selection of scenarios. On the other hand, the gain in WUE due to the application of the MAX_{WUE} criterion compared to the other ones was slight; thus, this physiological criterion might be considered of minor importance in decision-making concerning irrigation management. However, the MAX_{WUE} criterion may be considered generally suitable from different points of view, as it matched interests of several stakeholders: it was the best criterion from a physiological point of view and at the same time allows us to obtain mean values of NR, yield and IRRWUE close to the optimum ones. Furthermore, the application of this criterion also poses the problem of irrigation water conservation, but the increase of water use compared to the minimum (due to the application of the MAX_{IRRWUE} criterion) is less marked with respect to the other criteria.

The results of this case-study highlighted the general relationships among stakeholders, but also drew attention to the spatial variability of these relationships; moreover, the application of scenarios selected for one stakeholder had an impact on tomato output (and subsequently on the interests of the other stakeholders) with variable weights right across the test area, although in many cases these differences concerned only a few soils. This fact raises the problem of how to approach such variability in tomato responses when the results of simulations are to be used as a tool in addressing the general planning of irrigation water distribution at a regional level, with the general aim of sustainable use of water resources. In this case, the needs of different stakeholders should be considered simultaneously according to their relative merits. These concepts are taken into account by multicriteria analysis methods (Sumpsi et al., 1996; Hayashi, 2000), the application of which, performed separately for each soil area in our results, may well provide for further development in this area of study.

Acknowledgements

This work was supported by the Italian Ministry of Agriculture, Food and Forestry Policies (AQUATER project, contract nr. 209/7303/05).

References

Batchelor W D, Basso B, Paz J O (2002) Examples of strategies to analyze spatial and temporal variability using crop models. Eur J of Agron 18:141 – 158.

Calixte J P, Beinroth F H, Jones J W, Lal H (1992) Linking DSSAT to a GIS. Agrotechnology Transfer 15:1 – 7.

Dent J B, Thornton P K (1988) The role of Biological Simulation Models in Farming Systems Research. Agricultural Administration and Extension 29:111 – 122.

Engel T, Hoogenboom G, James W J, Paul W W (1997) AEGIS/WIN: A computer program for the application of crop simulation models across geographic areas. Agron J 89:919 – 928.

Georgiev G A, Hoogenboom G, Ragupathy K (1998) Regional yield estimation using a linked geographic information system, crop application of crop models and GIS. Agronomy abstracts Biol Eng 1st IBE Publ Athens GA 63.

Hartkamp A D, de Beurs K, Stein A, White J W (1999b**)** Interpolation techniques for climate variables. CIMMyt, Mexico DF, NRG-GIS Series 99 – 01.

Hartkamp A D, White J W, Hoogenboom G (1999a**)** Interfacing geographic information systems with agronomic modeling. A review. Agron J 91:761 – 772.

Hayashi K (2000) Multicriteria analysis for agricultural resource management: a critical survey and future perspectives. Eur J of Oper Res 122:486 – 500.

Heinemann A B, Hoogenboom G, de Faria R T (2002) Determination of spatial water requirements at county and regional levels using crop models and GIS. An example for the State of Parana, Brazil. Agric Water Manag 52:177 – 196.

Hoogenboom G, Thornton P K (1990) A GIS for agrotechnology transfer in Guatemala.. In Proc. Application of Geographic Information System, Simulation Models, and Knowledge-based Systems for land use management Blacksburg VA. 12-14 Nov 1990 Va Polytechnic Inst. & State Univ Blacksburg 61 – 70.

Jenks G F (1967) The Data Model Concept in Statistical Mapping. International Yearbook of Cartography 7:186 – 190.

Jones J W, Hoogenboom G, Porter C H, Boote K J, Batchelor W D, Hunt L A, Wilkens P W, Singh U, Gijsman A J, Ritchie J T (2003) The DSSAT cropping system model. Eur J of Agron 18:235 – 265.

Matthews R (2002) Crop-soil simulation models: Applications in developing countries. CABI Publishing Matthews R and Stephens W editors, Wallingford

Nijbroek R, Hoogenboom G, Jones J W (2003) Optimizing irrigation management for a spatially variable soybean field. Agric Systems 76:359 – 377.

Rinaldi M (2001) Durum wheat simulation in Southern Italy using CERES-Wheat model. I. Calibration and validation. In Proc of 2nd International Symposium “Modeling Cropping Systems” Florence (Italy) 16-18 July 81 – 82.

Rinaldi M (2004) Water availability at sowing and nitrogen management of durum wheat: a seasonal analysis with CERES-Wheat model. Field Crops Res 89:27 – 37.

Rinaldi M, Borneo V (2006). Descrizione delle funzionalità di AEGIS/WIN, interfaccia GIS del software di simulazione colturale DSSAT. Un caso studio in Capitanata. Rivista Italiana di Agrometeorologia 2:34 – 47.

Rinaldi M, Flagella Z, Losavio N (2003) Evaluation and application of the OILCROP-SUN model for sunflower in Southern Italy. Agric Systems 78:17 – 30.

Rinaldi M, Ventrella D, Gagliano C (2007) Comparison of nitrogen and irrigation strategies in tomato using CROPGRO model. A case study from Southern Italy. Agric Water Manag 87:91 – 105.

Rinaldi M, Ubaldo R (2007) Simulation at regional level of irrigated wheat and tomato in a Mediterranean environment. In “Water Resource Management IV” CA Brebbia & AG Kungolos (Editors) WIT Press (UK) WIT Transaction on Ecology and the Environment 103:569 – 581.

Sumpsi J M, Amador F, Romero C (1996) Theory and methodology On farmers’ objectives: a multicriteria approach. Eur J of Oper Res 96:64 – 71.

Thornton P K, Saka A R, Singh U, Kumwenda J D T, Brink J E, Brisson N (1995) Application of a maize crop simulation model in the central region of Malawi. Exp Agric 31:213 – 226.

Thornton P K, Hoogenboom G (1994) A computer program to analyze single-season crop model outputs. Agron J 86 (5):860 – 868.

Development of Feeding Strategies for Cows in Small Scale Dairy Farming Systems in the Highlands of Central Mexico by a Simulation Model and On-Farm Experiments. Phase Ⅰ: Development of a Novel Framework

Virgilio Ambriz-Vilchis, Julieta G. Estrada-Flores, Martha Hernández-Ortega, María A. Rojas-Garduño[1], Ernesto Sánchez-Vera[1], Angélica Espinoza-Ortega, Octavio A. Castelán-Ortega

(Centro de Investigacion en Ciencias Agropecuarias. Universidad Autonoma del Estado de Mexico. Instituto Literario # 100, CP 50000. Toluca, Estado de Mexico, Mexico)

Abstract: The small scale dairy farming systems (SSDFS) contributes to maintain the rural environment and livelihoods in the highlands of central Mexico. However, their viability is compromised due to the high costs of feeds and deficient feeding strategies used by farmers. Simulation models in animal production are important tools for decision making, technology transfer and research. The aim of the present work was: develop a methodological framework for using a simulation model as a decision support tool to develop alternative feeding strategies for cows in SSDFS in the highlands of central Mexico. Local and alternative strategies were simulated (900 feeding strategies). The *Buttercup* model (BCM) predictions were compared with those reported in a previous work. Deficiencies in the local feeding strategies were identified in terms of metabolizable protein (MP). Alternative strategies were designed to cover these deficiencies by the use of concentrate supplementation. Three concentrates (C1= maize grain 610, soybean meal 310, urea 30, and cane molasses 50g kg^{-1} DM; C2= maize grain 630, soybean meal 320 and cane molasses 50g kg^{-1} DM; and C3= maize grain 900, urea 50 and cane molasses 50g kg^{-1} DM) where tested in order to meet the MP and metabolizable energy (ME) requirements and to evaluate the productive response of dairy cattle through on-farm experiments. For the BCM validation results data of milk yield from the on-farm experiments were compared with the BCM data predictions. The present methodology is aimed to simplify the use of simulation models in situations, places, and systems similar to the one reported here.

Keywords: simulation model, calibration, dairy cows, feeding strategies

1 Introduction

The SSDFS contributes to maintain the rural environment and livelihoods in the highlands of central Mexico. These systems are present in 80% of the Mexican farming land, and contribute with 28% of the national milk production. However, their viability is compromised due to the high costs of feeds and the deficient feeding strategies implemented (Castelán-Ortega et al., 2008). The use of simulation models may contribute to develop more efficient feeding systems, based on strategies that fulfill the cattle nutrient requirements, basically in terms of metabolizable protein (MP) and metabolizable energy (ME). Models can be used to develop strategies to improve performance, reduce cost of production or reduce nutrient excretion (Orlindo et al., 2005). Models have become the basis of modern feeding systems. They can be valuable tools for estimating

animal requirements and nutrients derived from feeds in each unique farm production scenario and thus can have an important role in providing information that can be used in the decision-making process to enhance the feeding system (Tedeschi et al., 2005; Herrero et al., 2007). Model evolution and development have more than 40 years of experiences, in developed countries are widely known but in the developing world their use and impact are scarce. Therefore the aim of the present work was to create a methodological framework to use a simulation model, as a decision support tool, to develop alternative feeding strategies for cows in SSDFS in the highlands of central Mexico, trough a multiple criteria approach that uses a simulation model, *Buttercup* model (BCM), (Herrero, 1997) and on-farm experiments.

2 Materials and Methods

The methodological approach of this investigation includes two phases (Phase I= PI and Phase II= PII, Fig. 1). PI Simulation: ① calibration of the *Buttercup* model (BCM) with input data collected from previous works and literature references; ② simulation of local feeding strategies; ③ evaluation of the simulated strategies based on the metabolizable energy (ME) and protein (MP) supply and based on the identification of MP and ME unbalances and; ④ selection of the best feeding strategies. PII On-farm evaluation: ① implementation of the best feeding strategies developed in Phase I and PII ② evaluation of the feeding strategies with two on farm experiments, the data obtained from the on-farm experiments were used to validate the model predictions and perform a sensitivity analyses by comparing milk yield observed *vs*. predicted data. Observed values of milk yield were compared with model predictions and a new input data set were obtained. The results from Phase II are reported in the second part of this paper (Ambriz-Vilchis et al., 2008).

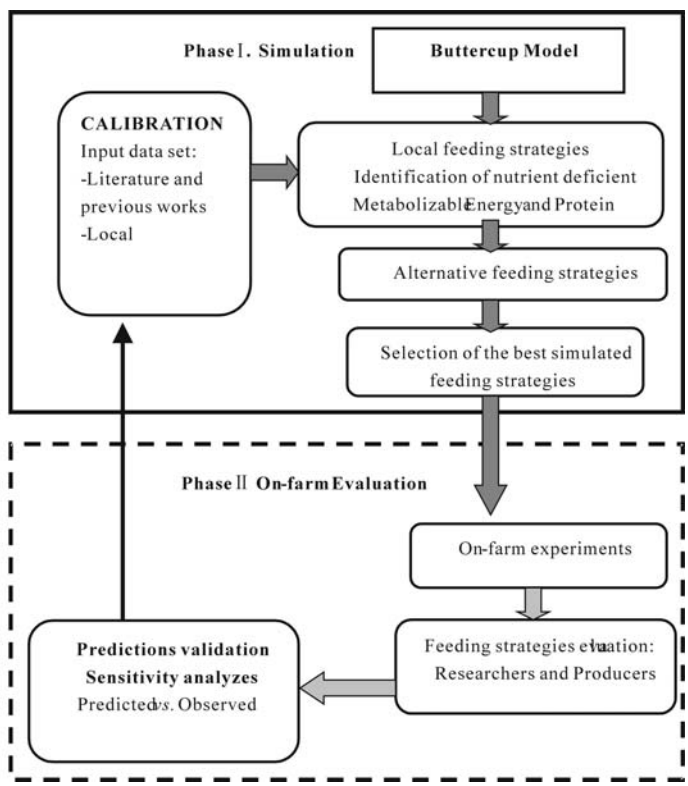

Figure 1 Methodological framework to develop feeding strategies in small scale dairy farming systems

Simulation. In this phase the *Buttercup* model (BCM) was calibrated; BCM is a simulation model developed and validated by Herrero (1997), the model was designed to predict potential intake, digestion and animal performance of individual ruminants, in this case dairy cows, consuming forages, grains and other supplements. The rationale behind the model is that a ruminant of a given body size, in a known physiological state, and with a target production level, will have a potential forage intake determined by physical or metabolic constrains imposed both by plant and animal characteristics. The result is a "hybrid dynamic model", based on a mechanistic platform with specific adaptable parameters which are site specific. This model is largely based on the work of Illius and Gordon (1991 and 1992) and Sniffen et al. (1992) and AFRC (1995).

Local and alternative feeding strategies were simulated; input data set needed to calibrate the BCM, are shown in Table 1, which contains data on chemical and fermentation characteristics of the feedstuffs tested with the model. Table 2 contains data on the characteristics of the local cows that were used to calibrate the BCM.

The BCM was validated ($R^2 = 0.75$) by Herrero (1997); however it was decided to make a calibration exercise to validate the model for local conditions, data from the experiment of García (2002) was used for this purpose. This author used on farm experiments to compare the milk yield of cows fed with maize straw (MS) treated with urea (U) and MS without any treatment, but with urea or soybean meal (SBM) added to the diet during concentrate feeding. Thus three feeding

Table 1 Minimum input data set used for the Buttercup model (MBC) calibration. Nutritive characteristics of the main feed ingredients used in small scale dairy farming systems in the highlands of central Mexico. Simulation exercise phase 1, local ingredients

VARIABLE	MS	GMF	Alf	O	PT	CCo	PC	MG	PoM
DM g kg^{-1}	85.8	22.9	86.5	86.0	27.0	87.4	91.5	86.0	89.0
NDF g kg^{-1} DM	695	629	474	581	582	280	201	119	380
Acho g kg^{-1} DM	267	296	106	250	160	411	600	301	256
A cho rate	0.21	0.26	0.15	0.26	0.3	0.21	0.20	0.17	0.16
B cho g kg^{-1} DM	0.69	0.71	0.49	0.30	0.76	0.67	0.59	0.95	0.63
B cho rate	0.05	0.06	0.10	0.07	0.09	0.15	0.07	0.11	0.06
Lag B h	7.0	7.0	4.7	5.5	NV	3.4	4.0	5.8	4.5
Starch g kg^{-1} MS	0	0	0.45	9	0	0.71	0.77	0.68	0.9
CP g kg^{-1} DM	59.3	87.5	190.0	90.9	156.0	216.0	129.6	93.4	335.3
A CP g kg^{-1} DM	0.30	0.20	0.50	0.14	0.20	0.33	0.22	0.26	0.33
A CP rate	0.27	1.50	1.50	1.20	1.50	1.50	0.15	0.15	1.50
B CP g kg^{-1} DM	0.51	0.71	0.40	0.11	0.71	0.56	0.46	0.69	0.56
B CP rate	0.11	0.12	0.24	0.10	0.12	0.12	0.01	0.01	0.12
Fat g kg^{-1} DM	13.2	32.7	30.0	24.0	21.0	71.0	46.2	43.0	0.5
Ash g kg^{-1} DM	65.0	57.7	107.0	79.0	70.0	75.0	23.6	17.5	49.8

MS= maize stover, GMF= Green maize fodder, Alf= alfalfa hay, O= oat hay, PT= Prairie (grass Rye grass *Lolium perenne* and white clover *Trifolium repens*), CCo= commercial concentrate, PC= producers concentrate, MG= maize grain, PoM= poultry manure. DM= dry matter, NDF= Neutro detergent fiber g kg^{-1} DM, A cho= soluble fraction of the cellular content g kg^{-1}, Rate A cho= degradation rate of the cellular content h^{-1}, B cho= potentially degradable cell wall fraction g kg^{-1} DM, Rate B cho= degradation rate of the potentially degradable cell wall fraction g kg^{-1}, Lag B = lag phase of the potentially degradable fraction h^{-1}, CP= crude protein g kg^{-1} DM, a CP= soluble fraction of de CP g kg^{-1} DM, Rate aPC= degradation rate of the soluble CP fraction h^{-1}, b CP= slowly degradable CP g kg^{-1} DM, Rate b PC= degradation rate of the slowly degradable CP fraction h^{-1}, Fat= g kg^{-1} DM, Ash= g kg^{-1} DM.

Table 2 Minimum input data set on cow characteristics used to calibrate the Buttercup model (BCM). Simulation exercise Phase I, local animals

Variable	Cows first calving	Cows second calving	Cows three or more calving
Live weight, kg	313	355	391
Body condition score	2.0	2.4	1.8
Fat in milk, %	2.8	2.8	2.6
Milk protein, %	3.1	3.1	3.0
Milk yield,kg 305 d	4383	3519	4610

strategies were tested by Garcia (2002), T1= MS with U (40 g kg^{-1} MS) + 1kg maize grain (MG), T2 = MS sprayed with a solution of 10% U (26 g kg^{-1} MS) + 1 kg of MG and T3 = MS without treatment + 760 g SBM. In every feeding strategy cows were supplemented with 3 kg cow $^{-1}$ d^{-1} of commercial concentrate (CC, 18% crude protein). Observed data of milk yield from this on-farm experiment were compared with the predicted milk yield data output of the BCM simulation by a Pearson correlation (R=0.85 $P < 0.05$) and lineal regression (R^2= 0.73) (Fig. 2).

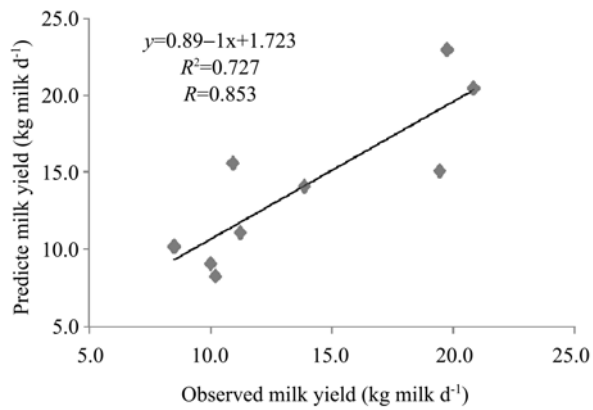

Figure 2 Relation between predicted *vs*. observed values for milk yield (kg d^{-1}), reported by Garcia (2002)

Simulation of the local feeding strategies. In these systems and through the year the feeding strategies tend to vary in their composition, a large variety of ingredients and in different amounts are observed, which results in a long list of different feeding strategies. Using the BCM we try to evaluate as much as we can to achieve this, a factorial arrangement 3 × 3 ×4 × 4 × 5 was designed as shown in Table 3. This arrangement includes forages: maize straw (*Zea mays*) (MS), green maize forage (GMF), oat (*Avena sativa*) (AV), alfalfa (*Medicago sativa*) (ALF) and grass (PT) (Ryegrass *Lolium perenne* associated with white clover *Trifolium repens*); concentrates included: commercial concentrate (CCO), producers concentrate (PCO, ground maize grain 670 g kg^{-1} and wheat bran 330 g kg^{-1}) (Castelán, 1999), maize grain (MG) and poultry manure (PM). The concentrate was administrated in five different levels of supplementation 0, 2, 4, 6 and 8 kg cow^{-1} d. These feeding strategies were tested with the model in cows of different calving number (one, two and three or more) and in different periods of lactation; a total of 720 feeding strategies were simulated.

Simulation of alternative feeding strategies. The alternative feeding strategies simulated were developed and intended to fulfill the ME and MP requirements of the cows in different production stages and with different levels of milk yield. Due to the extended use of maize among local dairy farmers (as grain and forage) it was decided to be used in all the alternative feeding strategies to avoid the costs of including external ingredients and considering the high quality of maize grain in

Table 3 Local feeding strategies used by Small Scale Dairy Farming System producers, simulated with the *Buttercup* model (factorial arrangement 3x3x4x4x5=720 strategies)

Calving *N*	Lactation Stage	Forage	Concentrate	Supplementation Level
C = 1:3	*L*x =1:3	*F* =1:4	*C* = 1:4	*N* =1:5
C = 1	*L*x = 1/3	*F*1 = 70:30 MS: GMF	*C* = CCo	*L* 1 = 0 kg c^{-1} d
C =2	*L*x = 2/3	*F*2 = 70:30 MS : Alf	*C* = PrC	*L* 2= 2 kg c^{-1} d
C = 3 ≤	*L*x = 3/3	*F*3 = 70:30 MS: O	*C* = MG	*L* 3= 4 kg c^{-1} d
		*F*4 = 70:30 MS: Sw	*C* = PoM	*L* 4= 6 kg c^{-1} d
				L 5= 8 kg c^{-1} d

MS= maize straw (*Zea mays*), GMF= green maize fodder, Alf= alfalfa (*Medicago sativa*), O= oat (*Avena sativa*), Sw= sward (Ryegrass (*Lolium perenne*) associated with white clover (*Trifolium repens*), CCo= commercial concentrate, PrC= producers concentrate (maize grain 670 g kg^{-1} and wheat bran 330 g kg^{-1}), MG= maize grain, PoM= poultry manure.

terms of ME. PT was also included. Four sources of CP or non protein nitrogen were selected; three of low cost and accessible for producers: urea (U), canola meal (*Brassica napus*) (CM) and soybean meal (*Glycine max*) (CM); and one of high price: fish meal (FM). The same factorial arrangement approximation described above for the local feeding strategies was used to simulate the effect of the alternative strategies on the milk yield, Table 4 shown the factorial arrangement.

Table 4 Alternative feeding strategies simulated with the *Buttercup* model (factorial arrangement 3×3×1 ×4×5=180 strategies)

Calving *N*	Lactation Stage	Forage	Concentrate	Supplementation Level
C = 1:3	*L*x =1:3	*F* =1	*C* = 1:4	*N* =1:5
P = 1	*L*x = 1/3	*F*1 = 70:30 RM: PT	*C* = GM:U	*L* 1
P =2	*L*x = 2/3		*C* = GM: CM	*L* 2
P = 3 ≤	*L*x = 3/3		*C* = GM:SBM	*L* 3
			C = GM:FM	*L* 4
				L 5

MS= maize straw (*Zea mays*), SwPT= Sw= sward (Ryegrass (*Lolium perenne*) associated with white clover (*Trifolium repens*), MG= maize grain *L*1=0, *L*2=2, *L*3=4, *L*4=6 and *L*5=8 kg d^{-1}, *U*= Urea *L*1=0, *L*2=0.1, *L*3=0.2, *L*4=0.3 and *L*5=0.4 kg d^{-1}, CM= Canola Meal (*Brassica napus, B. campestris*) *L*1=0, *L*2=0.5, *L*3=1.0, *L*4=1.5 and *L*5=2 kg d^{-1}, SBM= Soybean meal (*Glycine max*) *L*1=0, *L*2=0.5, *L*3=1.0, *L*4=1.5 and *L*5=2 kg d^{-1} and FM= Fish meal *L*1=0, *L*2=0.2, *L*3=0.4, *L*4=0.6 and *L*5=0.8 kg d^{-1}.

On-farm implementation of the best feeding strategies obtained. As a result of the simulation process of the local feeding strategies it was observed that these strategies only allow the cows to express their potential milk yield in terms of ME supply but the potential milk yield was not achieve due to a limitation in the MP supply from diet (Fig. 3). Therefore alternative feeding strategies were developed to fulfill this deficiency (Tab. 4). The best results were obtained with SBM and U (Fig. 4), therefore the strategies selected for the on-farm trials include SBM, U and MG as concentrates, Table 5 shows the composition of the alternative feeding strategies based on the supplement developed.

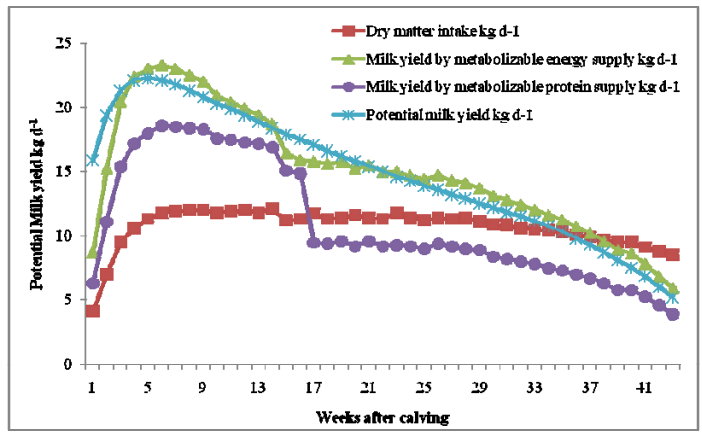

Figure 3 Output of one local feeding strategy simulated with the *Buttercup* model that meet the ME requirements but not the MP requirements of a third calving cow

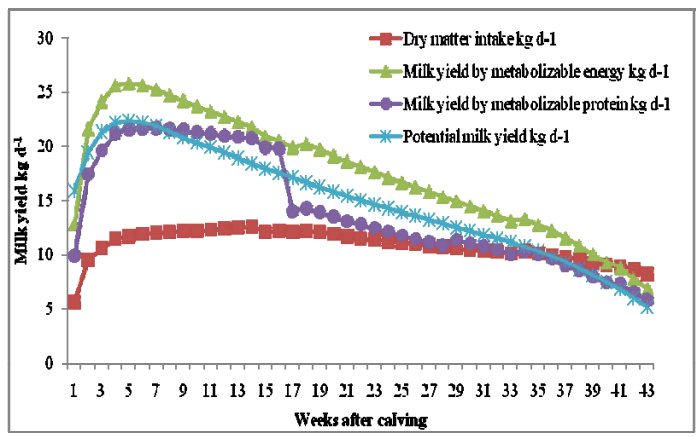

Figure 4 Output of one alternative feeding strategy simulated with the *Buttercup* model that meet the MP and ME requirements of a third calving cow

Table 5 Concentrate composition for on farm experiments (g kg^{-1})

Ingredient	C1	C2	C3
Maize grain	610	630	900
Soy bean meal	310	320	0
Urea	30	0	50
Molasses	50	50	50

Because of the difficulty of the on-farm experimentation, the normal variation in the forage supply, and common practices, the forage availability can´t be fully controlled by researchers it was decided to control ME and MP supply by the use of a concentrate and assume a standard quality of forages used by farmers. Nevertheless the forage diet composition was very similar during the periods and through the on-farm experiments.

The best feeding strategies developed in PI of this work (Table 5), were evaluated with two on-farm experiments carried out in two communities of the State of Mexico, in the highlands central Mexico. In each experiment three concentrates were evaluated by a Double Latin Square Design (3×3), three cows (rows) and three experimental periods (columns) in each Square. The concentrates fulfill the metabolizable energy (ME) and protein (MP) requirements of the experimental cows:

concentrate one (C1): maize grain (MG) 610, soybean meal (SBM) 310, urea (U) 30, and cane molasses (MOL) 50g kg^{-1} DM; concentrate two (C2): MG 630, SBM 320, and MOL 50g kg^{-1} DM; and concentrate three (C3): MG 900, U 50, and MOL 50g kg^{-1} DM. The results of these experiments are shown in the second part of this paper (Ambriz-Vilchis et al., 2008).

A Double Latin Square Design (3×3) was used aiming to evaluate the effect of the feeding strategies, in each Square: three cows (rows) and three experimental periods (columns) were used as fitted factors. The general linear model command of MINITABv14 (2003) was used for the statistical analysis of the animal and feed variables. Results were analyzed according to the model:

$$Y_{ijkl} = \mu + C_i + V_{(i)j} + P_l + T_k + \varepsilon_{ijkl},$$

Where:

Y_{ijkl} = answer variable
μ = general mean
C_i = effect due to square i= 1,2
$V_{(i)j}$ = effect due to cow within square $(i)j$= 1,2,3
P_l = effect due to experimental period l= 1,2,3
T_k = effect due to treatment k= 1,2,3
ε_{ijkl} = residual error term

The milk yield data were compared using correlation analysis and linear regression between milk yields observed *vs*. milk yield predicted values. BCM predicted values of milk yield were obtained with input data set with site specific data obtained from the on-farm experiments carried out. The results are shown in the second part of this paper (Ambriz-Vilchis et al., 2008).

3 Conclusions

The methodology present will simplify the use of simulation models in situations, places and systems similar to the one reported; it represents a simple and tidy way to use simulation models. To design alternative feeding strategies in Small Scale Dairy Farming Systems the methodological framework developed allow the use of Buttercup Model with acceptable results. The model is an efficient tool for developing alternative management strategies *ex ante* and the design of on farm experiments and research.

References

AFRC (1995) Energy and Protein Requirements of Ruminants. An advisory manual prepared by the AFRC Technical Committee on Responses to Nutrients. CAB International, Wallingford.

Ambriz-Vilchis V, Estrada-Flores J G, Hernández-Ortega M, Rojas-Garduño A, Castelán-Ortega O A (2008) Development of feeding strategies for cows in Small Scale Dairy Farming Systems in the Highlands of Central Mexico by a simulation model and on farm experiments. Phase II: On-farm experiments and validation of a simulation model.

Castelán-Ortega O A (1999) A decision support system for campesino maize-cattle production systems of the Toluca Valley in Central Mexico (PhD thesis) University of Edinburgh, Edinburgh.

Castelán-Ortega OA, Estrada-Flores J, Espinoza-Ortega A, Sánchez-Vera E, Ambriz-Vilchis V, Hernández-Ortega M (2008) Estrategias de manejo de recursos en agro-ecosistemas de zonas templadas de México: el caso de los productores campesinos de leche del altiplano central. In: Castelán-Ortega OA, Bernués JA, Ruiz SR., Mould FL. (Eds.), Oportunidades y retos para los sistemas campesinos de rumiantes en Latinoamérica. Manejo de recursos, seguridad alimentaria, calidad y acceso a mercados. 1st ed. Universidad Autónoma del Estado de México, México.

García MA (2002) Tratamiento de Rastrojo de Maíz con Urea como una alternativa para la alimentación de vacas lecheras en sistemas de producción de leche en pequeña escala en el valle de Toluca (tesis de maestría). Universidad Nacional Autónoma de México, México.

Herrero M (1997) Modeling Dairy Grazing Systems: An Integrated Approach (PhD thesis). University of Edinburgh, Edinburgh.

Herrero M, González-Estrada E, Thornton PK, Quirós C, Waithaka NM, Ruiz R, Hoogenboom G (2007) IMPACT: Generic household-level data bases and diagnostics tools for integrated crop-livestock systems analysis. Agric Syst 92:240 – 265.

Illius AW, Gordon IJ (1991) Prediction of intake and digestion in ruminants by a model of rumen kinetics integrating animal size and plant characteristics. Jour Agric Sci 116:145 – 157.

Illius AW, Gordon IJ (1992) Modeling the nutritional ecology of ungulate herbivores: evolution of body size and competitive interactions. Oec 89:428 – 434.

Minitab v14 (2003) Users guide: Data Analysis and Quality Tools. Minitab, Pennsylvania.

Orlindo TL, Fox FD, Sainz RD, Barioni LG, de Medeiros SR, Boin C (2005) Mathematical models in ruminant nutrition. Sci Agric 62:76 – 91.

Tedeschi LO, PAS, Fox DG, Doane PH (2005) Evaluation of the tabular feed energy and protein undegradability values of the National Research Council Nutrient Requirements of Beef cattle. The Prof Anim Sci 21:403 – 415.

Sniffen CJ, O'Connor JD, van Soest PJ, Fox DG, Russell JB (1992) A Net Carbohydrate and Protein System for evaluating cattle diets: II Carbohydrate and Protein availability. Jour Anim Sci 70:3562 – 3577.

Development of Feeding Strategies for Cows in Small Scale Dairy Farming Systems in the Highlands of Central Mexico by a Simulation Model and On-Farm Experiments. Phase Ⅱ: On-farm Experiments and Validation of a Simulation Model

Virgilio Ambriz-Vilchis, Julieta G. Estrada-Flores, Martha Hernández-Ortega, María de los Angeles Rojas-Garduño, Octavio A. Castelán-Ortega

(Centro de Investigación en Ciencias Agropecuarias. Universidad Autónoma del Estado de México. Instituto Literario 100, CP 50000. Toluca, Estado de México, México)

Abstract: The evaluation and validation of simulation models are important stages of model development. The aim of this work was to validate the *Buttercup* model (BCM) with experimental data from on-farm trials. Two on-farm experiments (Experiment 1 E1 and Experiment 2 E2) were carried out to evaluate the effect of supplementing dairy cattle with different sources of protein in Small Scale Dairy Farming Systems. Three concentrates (C1= maize grain 610, soybean meal 310, urea 30, and cane molasses 50g kg^{-1} DM; C2= maize grain 630, soybean meal 320 and cane molasses 50g kg^{-1} DM; and C3= maize grain 900, urea 50 and cane molasses 50g kg^{-1} DM) were developed using the BCM. The effect of the concentrates on milk yield, body condition score and live weight was evaluated using a double Latin Square experimental design. In E1 there were no significant differences ($P> 0.05$) for the variables evaluated. In E2, significant differences ($P<0.05$) were observed in milk fat content, for C2 (33.8g kg^{-1}) was higher than C1 and C3 (26.2 and 26.0g kg^{-1}). The results suggest that it was possible to fulfil the metabolisable protein requirements of the cows in these systems with low cost sources of non-protein nitrogen like the urea used in C3; and that the synthesis of microbial protein (from non-protein nitrogen and fermentable metabolisable energy of the concentrates) was enough to fulfil the cows' requirements of MP for the milk yield levels observed in both experiments. The results also indicate that when specific input data set from the experiments was used the model predictions are acceptable, when comparing predicted *vs.* observed data as a very significant correlation was observed ($P<0.01$).

Keywords: simulation model, validation, feeding strategies, small scale dairy farming system

1 Introduction

The aim of the present work was: develop a methodological framework to generate feeding strategies for cows in Small Scale Dairy Farming Systems (SSDFS), using a simulation model and on-farm experiments. Most examples of the use of simulation models to develop feeding strategies describe the approach used under controlled conditions and in very specialized systems like those observed in developed countries (Fox et al., 2004; Orlindo et al., 2005; Chaves et al., 2006), while there are few examples of their application in smallholder systems and in on-farm circumstances (Molina et al., 2004). This paper describes the Phase II (PII) of the methodological framework addressed in the first part of the paper, and is composed ① on-farm evaluation where two experiments were carried out with smallholder dairy farmers of central Mexico in order to test the best feeding strategies developed by the modeling approach of Phase I (PI); and ② a sensitivity analyses where

the results of the experiments were compared with the model predictions for milk yield.

2 Materials and Methods

On-farm experiments and BCM validation. The methodological approach used was described in the first part of this article (Ambriz-Vilchis et al., 2008), in general it includes two phases: Phase I of model calibration and simulation, and Phase II of on-farm experiments and model evaluation (comparison of BCM predictions *vs.* observed data) which is presented in this paper.

On-farm implementation of the best feeding strategies. The best feeding strategies based on the use of concentrates with high contents of MP developed in the Phase I, as described in Ambriz-Vilchis et al. (2008), were evaluated with two on farm experiments carried out in two communities of the highlands of the State of Mexico (central Mexico). Experiment 1 (E1) took place in the northern region of the State (N) in the municipality of Aculco (20°06'N y 99°50'O, 2440 m), smallholder dairy systems in this region are more specialized i.e. cattle genetics is better than in other regions as well as feeding and management practices. Experiment 2 (E2) was held in the central region (C) of the State in the municipality of Temoaya (19°28'N y 99°35'O, 2680 m) dairy systems there are less specialized and more similar to dual purpose systems. Both experiments were carried out from September to December of 2005. The average temperature in both municipalities was 14℃ with a mean annual rainfall of 800 mm. In each experiment three concentrates were evaluated using a Double Latin Square experimental design (3×3); three multiparous Holstein type cows were allocated to each square (rows) in three experimental periods (columns) of twenty one days each. Animals in each square were grouped by calving number and similar days in milk. The concentrates fulfil the metabolizable energy (ME) and protein (MP) requirements of experimental cows: concentrate one (C1): maize grain (MG) 610, soybean meal (SBM) 310, urea (U) 30, and cane molasses (MOL) 50g kg^{-1} DM; concentrate two (C2): MG 630, SBM 320 and MOL 50g kg^{-1} DM, and concentrate three (C3): MG 900, U 50 and MOL 50g kg^{-1} DM. All cows were fed also with fresh forages produced by farmers.

Each period consisted of twenty one days divided in an adaptation period of 14 days followed by a measuring period of seven consecutive days. At the beginning of each period live weight (LW) and body condition score (BCS) from each cow were recorded. Samples of milk and feed ingredients (forages, by products and concentrates) were taken for laboratory analysis. During the measuring period daily milk yield was recorded (kg of milk d^{-1}). In E1 square 1 the average LW and milk yield (MY) of cows was 555.3 ± 63kg and 21 ± 3.9kg d^{-1} respectively, and for square 2, LW: 546 ± 30.2 kg and MY: 17.7 ± 0.5 kg d^{-1}. In the case of E2 average LW of cows in square 1 was 459.3 ± 56.9 kg and MY: 6.7 ± 0.6 kg d^{-1}, while in square 2 LW: 483 ± 35.6 kg and MY: 6.3 ± 0.6 kg d^{-1}.

Animal management. As the experiments were carry out in on-farm conditions, the feeding systems of the cattle differed slightly so the experiments were adapted to the management the small holder farmers normally give to their cows. In E1, the daily forage supply was by "cut and carry", animals were in total confinement without any grazing time, milking was twice a day (6am – 5pm) and the calves were artificially raised. The concentrate supply was after the milking (half in the morning half in the afternoon). In E2, animals were in semi confinement; forage diet was offered in the pen and had a 5h (+/-2) grazing period in native swards of Kikuyo grass (*Pennisetum clandestinum*), cows were milked only once a day (in the morning) and calves stays with their dam during the grazing period, concentrate supply was offered twice a day, half during the milking and half after the grazing period. In both experiments animals were weighted and BCS was evaluated weekly, milk samples were taken for protein, fat and lactose content determination; protein and fat were measured by an ultrasonic device (Ekomilk, EON Trading LLC, Bulgaria). Lactose was

determined by the Lane Eynon method (SCFI NOM-2003). During the measuring period milk yield was recorded daily, in E1 milk was weighted after milking (morning-afternoon); in E2 milk yield was weighted once a day after the milking and calves were weighted weekly to estimate the daily weight gain of the calves due to the milk intake.

Chemical analysis of the feeds. dry matter (DM) was determined by oven drying samples at 60°C to a constant weight; ash was determined by igniting samples in a muffle furnace at 550°C for 4h; organic matter (OM) by difference between DM content and ash content; nitrogen content (N) by Kjeldahl method and crude protein (CP) content was calculated as N × 6.25. Nutro-detergent fiber (NDF), Acid-detergent fiber (ADF) and lignin (Lig) were determined by the Ankom (2005) method. In order to get the parameters to run the BCM for the sensitivity analyses samples were analyzed by the gas production technique as described by Menke and Steingas (1988) and modified by Theodorou et al. (1994), then fitted to the triple exponential equation (Equation 1), using the Grafit (1992) software.

$$\begin{aligned} GP= \text{ ta: } & a*(1-\exp(-ca*t)) \text{ tb: } b*(1-\exp(-cb*(t-lag)))*(t>lag)*-1 \text{ tc: } m*(1-\exp(-cm*(t-lagm)))* \\ & (t>lagm)*-1(ta+tb+tc) \text{ '} a*(1-\exp(-ca*t))+b*(1-\exp(-cb*(t-lag)))*((t>lag)*-1+m(1- \\ & \exp(-cm*(t \text{ lagm})))*(t>lagm)*-1 \end{aligned} \quad (1)$$

Where GP= total gas production a = soluble fraction, ca = fractional rate of gas production (per h) from fermentation of the soluble fraction, b= gas production from the fermentation of the neutral-detergent fiber (NDF), m= gas production from the fermentation of the microbes, **lag** = phase before fermentation of NDF begins (h), t = time h (hour).

NDF digestibility; OM digestibility and DM digestibility were determined by the micro-technique described by Pell and Schoefield (1993), applied to the residue of fermentation process after the gas production technique. The gas production at 24h of incubation was used to estimate metabolizable energy (ME) content in forages and concentrates as described by Menke and Steingass (1988), equations 2 and 3 respectively.

$$ME= 3.16+0.0695\ GP+0.000730\ GP^2 + 0.00732\ XP + 0.01325\ XL \quad (2)$$

$$ME= 2.04 + 0.1448\ GP + 0.0036\ XP + 0.0243\ XL. \quad (3)$$

In both equations: GP is the volume of gas (ml gas per 200 mg initial DM), XP is the crude protein content (g kg^{-1} DM) and XL is the fat content (g kg^{-1} DM).

Analyses of results. A Double Latin Square experimental design was used, with three cows and three experimental periods per square as fitted factors. The general linear model command of MINITABv14 (2003) was used for the statistical analysis of the variables: animal and feed characteristics. Results were analyzed according to the model:

$Y_{ijkl}=\mu+C_i+V_{(i)j}+P_l+T_k+\varepsilon_{ijkl}$,

Where:

Y_{ijkl} = answer variable

μ = general mean

C_i = effect due to square i= 1,2

$V_{(i)j}$ = effect due to cow within square $(i)j$= 1,2,3

P_l = effect due to experimental period l= 1,2,3

T_k = effect due to treatment k= 1,2,3

ε_{ijkl} = residual error term

The observed milk yield data were compared with model predicted values using correlation analysis and linear regression. BCM predicted values for milk yield were obtained from the on farm

experiments carried out; feeding strategies for each trial animal and period were then simulated. Observed milk yield data (on farm experiments) were compared with the output BCM predictions for milk yield in terms of ME and MP supply from diet.

3 Results

Table 1 shows chemical characteristics and fermentation kinetics of the three concentrates developed by the modeling approach to match the ME and MP requirements of the cows in SSDFS, and thus allow the expression of the potential milk yield during the on-farm trials. Note that all concentrates have high contents of CP because the modeling exercise showed that farmers´ feeding strategies were low in this nutrient and therefore limited the expression of the potential yield in local cows. The high content of soluble carbohydrates in the concentrates (Tab. 1) probably contributed to make an adequate utilization of the extra protein in the rumen.

Table 1 Fermentation kinetics and nutritive values of the concentrates used in the on-farm experiments

Variable	Concentrates		
	C 1	C 2	C 3
DM %	89.18	89.46	89.56
NDF g kg^{-1} DM	113.60	156.00	163.30
Acho g kg^{-1}	472.50	498.50	470.90
Acho rate	0.40	0.50	0.40
B cho g kg^{-1} DM	0.27	0.29	0.30
Bcho rate kg^{-1} DM	0.10	0.10	0.10
Lag B h^{-1}	5.10	5.60	5.90
CP g kg^{-1} DM	267.90	208.50	219.80
A CP g kg^{-1} DM	0.33	0.33	0.33
A CP rate h^{-1}	1.50	1.50	1.50
B CP g kg^{-1} DM	0.56	0.56	0.56
B PC rate h^{-1}	0.12	0.12	0.12
Fat g kg^{-1} DM	71.00	71.00	71.00
Ash g kg^{-1} DM	75.00	75.00	75.00

C1= maize grain 610, soybean meal 310, urea 30, and cane molasses 50g kg^{-1} DM, C2= maize grain 630, soybean meal 320 and cane molasses 50g kg^{-1} DM, and C3= maize grain 900, urea 50 and cane molasses 50g kg^{-1} DM; DM= dry matter, NDF= Neutro detergent fibre, Acho= soluble fraction of the cellular content, Acho rate = degradation rate of the cellular content, Bcho= potentially degradable cell wall fraction, B cho rate = degradation rate of the potentially degradable cell wall fraction, lag B= lag phase of the potentially degradable fraction, CP= crude protein, A CP= soluble fraction of de CP, A CP rate= degradation rate of the soluble CP fraction, B CP= slowly degradable CP, B CP rate= degradation rate of the slowly degradable CP fraction, Fat, Ash.

Animal response. There were no significant differences ($P > 0.05$) in milk yield, milk protein and milk lactose content between concentrates in none of the experiments (Table 2). In E2 significant differences ($P<0.05$) were observed in milk fat content, C2 was higher (33.8g kg^{-1}) than C1 and C3 (26.2 and 26.0g kg^{-1} respectively). It is important to note that the statistical model wasn't able to detect differences in milk yield, but there was up to 0.9 kg cow^{-1} d of extra milk yielded in cows fed C1 *vs*. cows fed C2 in E1, however this difference was not observed in E2.

There were no significant differences ($P>0.05$) in LW and BCS among treatments in none of the experiments (Tab. 3), and there were no differences between periods too.

Table 2 Milk yield (kg), protein, milk fat and lactose contents (g kg $^{-1}$) in experiments 1 and 2

Variable	Experiment 1				Experiment 2			
	C1	C2	C3	sem	C1	C2	C3	sem
Milk Yield (kg d^{-1})	19.8^{a}	18.9^{a}	19.2^{a}	0.46	7.8 ^{a}	7.8 ^{a}	7.5 ^{a}	0.2
Milk Protein (g kg^{-1})	31.7^{a}	32.0^{a}	31.3^{a}	0.05	31.1^{a}	31.5^{a}	31.0^{a}	0.05
Milk Fat (g kg^{-1})	39.7^{a}	39.9^{a}	38.7^{a}	0.17	26.2^{a}	33.8^{b}	26.0^{a}	0.1
Milk Lactose (g kg^{-1})	47.2^{a}	46.9^{a}	47.0^{a}	1.31	46.4^{a}	47.8^{a}	46.9^{a}	1.3

C1= maize grain, soybean meal urea and cane molasses; C2= maize grain, soybean meal and cane molasses; C3= maize grain urea and cane molasses; *sem* = standard error of the mean. Means within the same row without a common superscript indicate statistical differences ($p < 0.05$).

Table 3 Live weight and body condition score of the cows in experiments 1 and 2

Variable	Experiment 1				Experiment 2			
	C1	C2	C3	sem	C1	C2	C3	sem
Live Weight (kg)	536	528	527	5.30	476	475	474	5.3
Body Condition Score (1-5)	2.0	1.9	1.9	0.10	2.0	2.0	2.0	0.1

C1= maize grain, soybean meal, urea and cane molasses; C2= maize grain, soybean meal and cane molasses; C3= maize grain, urea and cane molasses; sem = standard error of the mean.

In E2, like in dual purpose systems, cows were milked only once a day so calves remain with their dams after the morning milking; thus milk yields shown in Table 2 are nearly half of those observe in E1. Cows in the central region have lower milk yield potential (Castelán et al, 2003) however, if the amount of milk consumed by the calves is calculated from their live weight gains as in Holmes and Wilson (1989) (Tab. 4), and then added to the milk yield from the first milking, it can be seen that milk yields in E2 are close to those observed in E1.

Table 4 Estimation of milk consumed by the calves reared by the experimental cows from their daily live weight gains

Concentrate	LW	DWG	Milk intake (kg d^{-1})
C1	89.3	1.1	8.3
C2	94.5	0.9	7.8
C3	92.0	0.8	7.3

LW= initial live weight of calves; DWG= daily weight gain.

Table 5 shows the chemical composition of the forages mixed rations used in both experiments. Data shows that CP contents declined proportionally with the maturity of the plants, on the contrary (as expected) the NDF content increased as the plants matured. The drop in the CP levels was more dramatic in E2 as it passed from 126.5 in period 1 to 59.1 g kg^{-1} DM in period 3. Despite decreasing protein levels the digestibility of the NDF and DM increased slightly from period 1 to period 3 but figures are similar to those of low quality forages as their ME content also suggest (Table 5).

Figure 1 shows a comparison of the milk yield predicted by the BCM from the ME supplied in the diet of E1 and the observed yield for the same experiment. It can be observed that there is a significant correlation coefficient (r=0.77), however some disperse values can still be observed. The same relationship is closer when milk yield from MP supplied in the diet is compared with model predictions (Fig. 2), it can be seen that the correlation coefficient is significantly higher (r=0.83) than in the Fig. 1. In this case the BCM explained 83% of the observed response suggesting that the initial assumption made in terms that the MP was a restricted nutrient may be correct.

Table 5 Chemical characteristics and fermentation kinetics of the forages used in Experiments 1 and 2

IngredientPeriod	Experiment 1			Experiment 2		
	I	II	III	I	II	III
DM g	263.7	440.0	491.0	438.1	626.4	778.2
NDF g kg^{-1} DM	479.3	520.1	588.1	572.3	641.7	745.6
ADF g kg^{-1} DM	276.9	287.0	324.9	300.6	324.9	433.7
Lig g kg^{-1} DM	100.2	109.8	118.1	62.9	62.0	70.5
CP g kg^{-1} DM	146.4	142.5	127.3	126.5	84.2	59.1
NDFD g kg^{-1} DM	306.1	259.1	369.6	339.5	345.6	523.3
DMD g kg^{-1} DM	438.5	525.0	532.4	513.7	541.7	570.9
ME MJ kg^{-1} DM	6.9	6.8	7.4	6.7	6.3	6.2

DM= dry matter, NDF= nutro detergent fiber, ADF= acid-detergent fiber, LIG= lignin, CP= crude protein, NDFd= nutro detergent digestibility, DMd= dry matter digestibility, ME= Metabolizable energy.

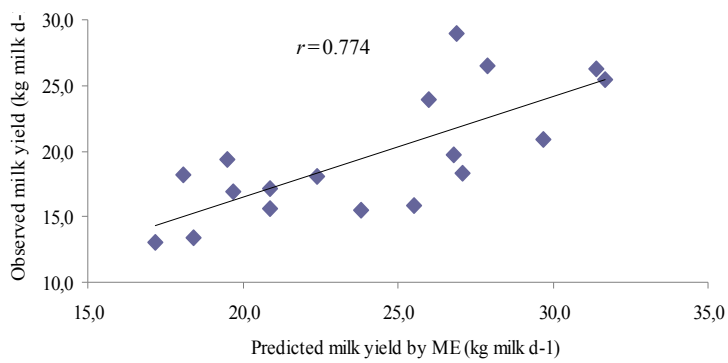

Figure 1 Relationship between predicted *vs.* observed milk yield data (milk yield by metabolizable energy supply) for Experiment 1

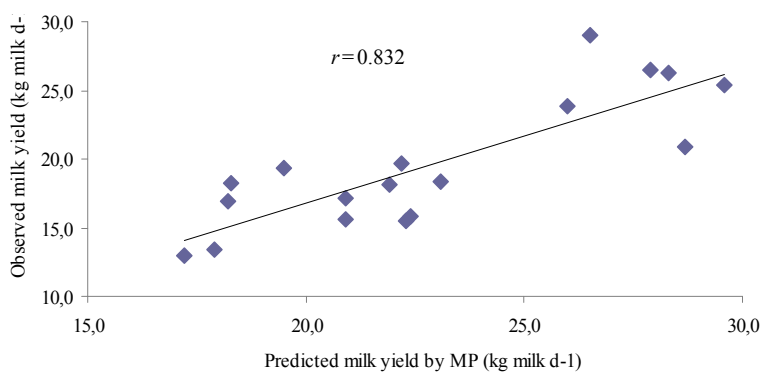

Figure 2 Relationship between predicted *vs.* observed milk yield data (milk yield by metabolizable protein supply) for Experiment 1

Figures 3 and 4 show the same comparison but for E2, it can be observed that the predictions pattern is very similar, BCM explains a larger part of the observed milk yield when the model calculates yield from the MP (r=0.83) supplied in the diet than when ME (r=0.64) is used.

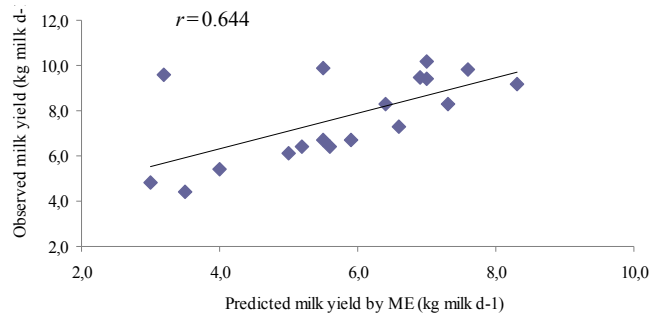

Figure 3 Relationship between predicted *vs.* observed milk yield data (milk yield by metabolizable energy supply) for Experiment 2

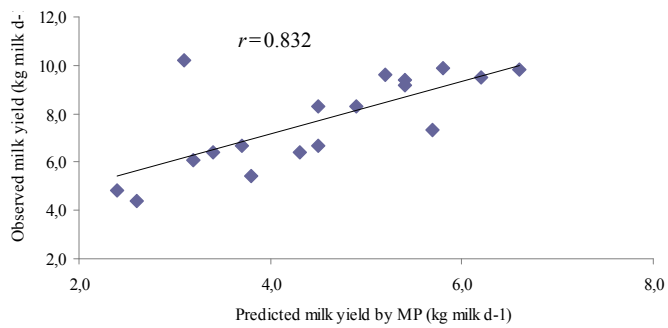

Figure 4 Relationship between predicted *vs.* observed milk yield data (milk yield by metabolizable protein supply) for Experiment 2

4 Discussion

The fact that there were no significant differences among concentrates suggests that it was possible to fulfil the metabolisable protein requirements of the cows in these systems with low cost sources of non-protein nitrogen like the urea used in C3. It is suggested that the synthesis of microbial protein (from non-protein nitrogen and fermentable metabolisable energy of the concentrates) was enough to fulfil the cows' requirements of MP for the milk yield levels observed in both experiments, which in fact are very modest but normal for the region as Castelán et al. (2003) states. Traditional diets of cows in SSDFS are composed of low quality forages such as maize stover and weeds and limited amounts of concentrates and maize grain (Estrada et al., 2006) so, as model predictions suggested in Ambriz-Vilchis et al. (2008), most of the forage mixed rations and supplements used by farmers are deficient in MP thus when a easily available source of nitrogen introduced in the rumen it is rapidly captured by the rumen microbes and transformed into microbial protein provided that there is no lack of fermentable metabolizable energy because as stated in AFRC (1995), energy supply is normally the first limiting factor on microbial protein synthesis. Microbial crude protein is digested by the ruminant and then transformed into MP.

According with the modeling framework described in the first part of this paper (Ambriz-Vilchis et al., 2008) BCM predictions suggested that MP supply by traditional farmer's diets constrained increasing milk yields in cows of SSDFS. The concentrates tested on farm were then formulated to match the MP first and second the ME requirements of dairy cows; results of on-farm experiments indicate that MP and ME supplied by concentrates and forages of the diets allowed the cows to

achieve higher milk yields than normally reported for this type of cattle (Arriaga-Jordean et al., 2001; Castelán et al., 2003, Val-Arreola et al., 2005; Heredia-Nava et al., 2007). This result suggests that the model predictions were partially correct because cows responded well to increasing protein levels in the diet and predicted vs observed values of milk yield were significantly close ($P<0.01$); However it is important to note that milk yield predicted by the model were higher than those observed in the experiments in all cases.

Several reasons may explain the underestimation of milk yields but two are probably the most important ones, first the data on chemical and degradation characteristics of feeds used during the calibration phase may have not resembled properly the actual quality of the ingredients used. When working with simulation models in these particular systems is common to used literature or reported data, ingredients and/or animals that are from temperate climates and intensive production systems that have little to do with SSDFS local ingredients and animals. The low specific information results in less accurate or reliable predictions. It is possible to improve the predictions when specific data is obtained from local animal and ingredients. When a simulation model is going to be used it is necessary that the required input data set are site specific, to obtain reliable predictions (Fox et al., 2004). Even though there is a considerable advance in the nutritional characterization of feed ingredients in SSDFS (Castelán et al., 2003; Estrada-Flores et al., 2006), a bigger effort is needed to achieve a robust feed library, especially in terms of fermentation and degradation rates of the protein and carbohydrates fractions, of the forages and by-products used in these systems. This agreed with the case reported by Chaves et al. (2006), the authors stands out the importance of count with specific feed evaluation of the ingredients that will be used, it is necessary to have specific data to improve the predictions of the model. It is possible that the BCM predictions will be better if we had the whole input data set required for the calibration process and were site specific, especially the values of the CP fractions, the input data set required to use a simulation model had to be precise and easily obtainable on farm, the lack of information about ingredients characteristics in SSDFS complicated the use of simulation models due to the high level of resources required to obtain reliable data, this may be a problem in similar situations.

The second factor that may explain underestimation of milk yield may be attributed to the low genetic merit of cows in SSDFS particularly in E2 (central region) as illustrated by lower milk yields observed here in comparison with the northern region (E1). Many equations of the BCM are based on allometric relationships that were developed using high genetic merit cows which were breed for many generations for efficient use of nutrients like energy and protein for milk synthesis, high dry mater intakes and every time higher milk yields. It is likely that cows in smallholder systems are less efficient in terms of nutrients used with a low intake capacity as there are no genetic improvement programmes (i.e. artificial insemination is seldom used), therefore their intake and efficiency of nutrient utilization for milk yield may be lower than those of the cows used to develop modern feeding systems. Thus it is likely that cows in the experiments were very close to their maximum capacity for milk yield.

5 Conclusions

The approach proposed probed to be an option for feeding strategies development for smallholder dairy systems provided that adequate input data set are available, in particular those related to the degradation of the protein and carbohydrate fraction of the feed ingredients. It is also important to stress the need to modify some of the model equations in order to consider the low efficiency in terms of energy and protein utilization of the low genetic merit dairy cattle like that can find in developing countries, despite this limitations reasonable predictions were obtained that can be used to ex-ante evaluate feeding before their implementation in the field.

References

AFRC, (1995). Energy and Protein Requirements of Ruminants. An advisory manual prepared by the AFRC Technical Committee on Responses to Nutrients. CAB International, Wallingford.

Ambriz-Vilchis V, Estrada-Flores JG, Hernández-Ortega M, et al. (2008) Development of feeding strategies for cows in Small Scale Dairy Farming Systems in the Highlands of Central Mexico by a simulation model and on farm experiments. Phase I: Development of a novel framework.

Ankom Thechnology (2005) Procedures (for NDF, ADF and in vitro Digestibility) ANKOM Technology Method. (http://www.ankom.com/09_procedures.shtml).

Arriaga-Jordán CM, Flores-Gallegos FJ, Peña-Carmona G et al. (2001) Participatory on-farm evaluation of the response to concentrate supplementation by cows in early lactation in smallholder peasant (campesino) dairy production systems in the highlands of central México. The Jour. of Agric Sci 137:97 – 103.

Castelán O, Estrada J, Carretero L et al. (2003) Degradation characteristics of maize weeds, used as forage in smallholder maize-livestock production systems of Central México, in different growing periods. Trop. Subtrop. Agroecosyst. 3:115 – 119.

Chaves AV, Brookes IM, Waghorn GC et al (2006) Evaluation of Cornell Net Carbohydrate and Protein System predictions of milk production, intake and live weight change of grazing dairy cows fed contrast silages. Jour Agric Sci 144:85 – 91.

Estrada-Flores JG, González-Ronquillo M, Mould FL et al. (2006) Chemical composition and fermentation characteristics of grain and different parts of the stover from maize land races harvested at different growing periods in two zones of central México Anim Sci 82:845 – 852.

Fox DG, Tedeschi LO, Tylutki TP et al. (2004) The Cornell net carbohydrate and protein system model for evaluating herd nutrition and nutrient excretion. Anim Feed Sci Tech 112: 29 – 78.

Grafit Erithacus Software Ltd. Grafit: data analysis and graphics program (Computer Program) Version 3 University of Edinburgh Scotland (UK).

Heredia-Nava D, Espinoza-Ortega A, González-Esquivel CE et al. (2007) Feeding strategies for small-scale dairy systems based on perennial (*Lolium perenne*) or anual (*Lolium multiflorum*) ryegrass in the central highlands of Mexico. Trop Anim Health Prod 39:179 – 188.

Holmes CW, Wilson GF (1989) Producción de leche en praderas. Acribia, Madrid.

Menke KH and Steingass H (1988) Estimation of the energetic feed value obtained from chemical analyses and in vitro gas production using rumen fluid Anim Res Dev 28:7 – 55.

Minitab v14., 2003. Users guide: Data Analysis and Quality Tools. Pennsylvania (USA): Minitab.

Molina DO, Matamoros I, Almeida Z et al. (2004) Evaluation of the dry matter intake predictions of the Cornell Net Carbohydrate and Protein System with Holstein and dual-purpose lactating cattle in the tropics Anim Feed Sci Tech 114: 261 – 278.

Orlindo TL, Fox FD, Sainz RD et al. (2005) Mathematical models in ruminant nutrition Sci Agric 1:76 – 91.

Pell AN and Schofield P (1993) Computerized monitoring of gas production to measure forage digestion *in vitro* Jour Dairy Sci 76:1063 – 1073.

Theodorou MK, Williams BA, Dhanoa MS et al. (1994) A simple gas production method using a pressure transducer to determine the fermentation kinetics of ruminant feeds Anim Feed Sci Tech 48:185 – 197.

Secretaría de Comercio y Fomento Industrial Norma Oficial Mexicana NOM-155-SCOFI-2003. México (DF): Secretaría de Economía SE.

Val-Arreola D, Kebreab E, Mills JAN et al. (2005) Analysis of feeding strategies for small-scale dairy systems in central Mexico using linear programming Jour Anim Feed Sci 14:607 – 624.

The Dynamic Model of Crop Growth System under the Multi-Environment External Force Action and Result Simulation

Tao Chi [1,2], Dan-Feng Huang [1]

(1 College of Agriculture and Biology, Shanghai Jiao Tong University: China)
(2 College of Information Technology, Shanghai Ocean University: China)

Abstract: Pot experiments with netted melon (Chunli) were conducted to study the dynamic mechanism of crop growth under the external force action of a variety of environmental factors (light, temperature, water and nutrients, etc). The interactions of environment and crops on construction of the plant morphology were studied in order to establish the dynamic model of crop growth. The paper studied the responses of the crop growth rate to the variation of the external force and its change of biomass saturation value. Comparing the dynamic model with the other plant growth model, the superiority of the former was that it combined macroscopic with microcosmic, which showed the effect of the external forces (including organic nitrogen) on stems, leaves and fruit. The results showed that nitrogen uptake and crop yield were most sensitive to total cumulative temperature and more sensitive to the critical temperature, crop extinction coefficient, the assimilate translocation efficiency to the leaf blade and the maintenance of respiration rate. In addition, crop yield was also sensitive to maximum critical cycling temperature and the leaf area index. Taking the melon growth model as an example, the theory and methodology for regulation and control of the environmental parameters in crop growth process would play important roles in facility agriculture.

Keywords: crop growth, nitrogen use efficiency, water and nitrogen management, external force of environment

1 Introduction

Crop growth system is an artificial zoology system that transforms the environment resource factors (illumination, temperature, water and nutrient content in the substrate and CO_2) to crop fruit from the viewpoint of plant mechanics. Olson (1985) proposed the Serial Markov Model which is used to describe the process of photosynthesis in the plants. A new improved CTM method has been presented in this paper and the corresponding dynamic model of crop growth under multi-environment external force has been established in application.

2 The Influence of Interaction Between Multi-Environment External Forces

2.1 Photosynthesis Efficiency

The influence on photosynthesis is the most remarkable factor in the growth of crops, which is related to many factors such as solar radiation, temperature, CO_2 concentration and so on. It has been reported that the effects of additional CO_2 on crop can increase fruit yield and improve fruit quality in the greenhouse, but the quantitative evaluation is still no substantive breakthrough and

the photosynthesis research still is concentrated on individual plant. The measuring system for photosynthesis has been constructed in the artificial controllable environment and the preliminary quantification of canopy apparent photosynthetic rate has been completed. The experimental results showed that, with the ascension of CO_2 concentration the initial photosynthesis rate and the maximum photosynthesis rate of the plant colonies are increased. At the same time, the CO_2 assimilation ability in the poor light or full sunshine is raised. The light is the key to decide the crops photosynthesis rate, under the different illumination and temperature condition the influence of CO_2 concentration on the photosynthesis rate is obviously different.

On the other hand, the temperature can have an impact on the photosynthesis rate of the plant colonies. When the temperature rises, the initial photosynthesis rate is reduced and the CO_2 assimilation ability of melon colonies in the poor light is being lowered. In the low concentration of CO_2, the saturated photosynthesis rate is raised with the temperature increase; in the high concentration of CO_2, the maximum photosynthesis rate may have a slightly reduces with the temperature increase owing to the interaction between CO_2 and temperature.

2.2 Water Regulation

The water regulation is the key technology in the melon cultivation, the irrigation amounts can influence melon growth, dry mater partitioning, yield and its quality, in particular sugar content. For muskmelon, the water content will affect its appearance quality, such as netted speed, netted quality and esthetics.

The cross-over deign with four treatments in different water condition was used for the study, and medium water content were respectively 0.2357, 0.2713, 0.2974 and 0.3260. In the initial period of fixed field planting (in recovery period or hairy roots period), the difference in the plant height and leaf area of melon under four water treatments was not obviously. After the field planting intermediate stage (10 days after fixed field planting), the gap in the plant height and leaf area of melon under four water treatments was increasing with the root growth. The results showed that, the negative correlation between medium water content and plant height or leaf area was very significant until the planting topping period ($38-40$ days after fixed field planting), so rational drought of medium water content was advantageous to the growth of plant height and leaf area.

2.3 Nitrogen Nutrient Absorption

The nitrogen absorption rate and nitrogen use efficiency of crops is one of important limiting factors in growth, which affects directly the photosynthesis rate, the growth and biomass allocation. The NO_3-N and the NH_4^+-N may provide enough nitrogen nutrient for crops growth, but NH_4^+-N nutrient is safer. In recent years many research all proved that the molecular state amino acid N can be absorbed directly by the crops. It is important to study the inorganic nitrogen and amino acid N uptake kinetics and crop physiological response, which can elaborate amino acid N absorption process and improve nitrogen use efficiency. The test results indicated that, in the concentration range of $0.1\sim2 mmolL^{-1}$ the different nitrogen absorption was in line with Michaelis-menten model, whose maximum absorption efficiency and affinity changed in accordance with the rule as $NO_3-N > NH_4^+-N > Gly-N$. Since the NH_4^+-N nutrient ($1 mmolL^{-1}$) was used, melon's NO_3-N absorption rate can be promoted and may enhance the plasma affinity with the faster pace of nitrogen absorption rate. The growth of seedling, root morphology and nitrogen use efficiency are affected by the use of NO_3-N, NH_4^+-N and $Gly-N$. Compared with NO_3-N treatment, the growth of root system and aboveground was inhibited by NH_4^+-N and $Gly-N$ treatments. Supplied with different ratios of nitrogen forms, the plant height, root volume

and root surface area were shown as $NO_3-N > Gly-N > NH_4^+-N$. There were likely rules in melon's chlorophyll contents, average nitrogen contents and nitrogen absorption. In the NH_4^+-N treatment, a series of ammonia poisoning symptoms may appear, such as root system browning, root necrosis. Compared with NO_3-N treatment, the nitrogen distribution proportion in the root system was improved by NH_4^+-N and $Gly-N$ treatments, the PH value of nutrition solution was obviously reduced by NH_4^+-N treatment and the PH value was increased.

After dealt with different nitrogen treatments, PH value of nutrient solution is of important factor that affected melon growth and nitrogen uptake. Melon is a kind of nitrophile, whose NH_4^+-N absorption rate is higher than amino acid N absorption rate. Since water culture with a single NH_4^+-N treatment can harm to the melon plants and cause significant toxic effects, but the amino acid N can be a good source of nitrogen.

3 Growth Analysis and Quantification

An improved CTM model is established to simulate the dynamics process of crop growth, which is defined as all metabolic components producing live biomass. Biomass growth process is a net accumulation process, which contains all the biomass formation, accumulation and maintenance respiration, such as catabolism. The state of the system is suffered from the effects of multi-environment external force action, such as illumination, temperature, moisture, nutrient matrix and other integrated environment outside factors. The crop growth system can be regard as a iterated result by all action and the state transition process of crop growth dynamics is shown as Fig. 1.

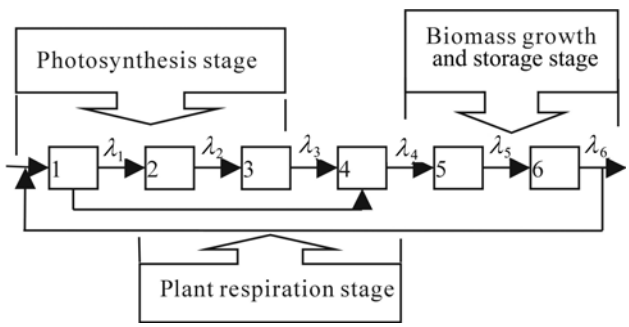

Figure 1 The state transition process of crop growth dynamics

λ_1 represents mean transition probability in consideration of illumination factor, λ_2 represents mean transition probability in consideration of temperature support factor, λ_3 represents mean transition probability in consideration of water use efficiency factor, λ_4 represents mean transition probability in consideration of respiratory demand factor, λ_5 represents mean transition probability in consideration of Nutrient use efficiency, λ_6 represents mean transition probability in consideration of biomass growth and storage factor.

3.1 Photosynthesis Stage Quantification

Most of the establishment of photosynthesis quantification was on the basis of the experience or semi-empirical experience. The relation between the single leaf photosynthesis intensity and the luminous intensity is computed by the Monsi-Sacki formula and the luminous intensity in each level position can be computed by the Beer-Lambert formula.

$$I_i = I_0 e^{-kL} \tag{1}$$

Among them, I_0 indicates solar luminous intensity of the crown level and top surface, *k* represents the community extinction coefficient, *L* represents leaf area index above level *i*. Therefore, integral photosynthetic area is used to define the community photosynthesis intensity.

$$P = (\mathrm{DL} \cdot P_{\max} / k) \cdot L_n \cdot [(P_{\max} + \alpha Q)/(P_{\max} + \alpha Q e^{-k \cdot \mathrm{LAI}})] \tag{2}$$

DL represents daily length (hour), Q represents the mean physiologic radiation intensity $(J/m^2 \cdot h)$, α represents the initial slope of *P*~*I* curve. Since temperature and water contents can impact on photosynthesis, the $P_{\max}$ amendment table is defined as follow:

Table 1 The $P_{\max}$ amendment table

Temperature(C)	Water Content (m^3/m^3)	$P_{\max}$
34.85	0.30451	134
31.93	0.29815	175
31.12	0.29136	103
25.95	0.30366	112
25.17	0.29645	108
20.95	0.24300	95
20.19	0.22773	89
18.66	0.24767	68
16.38	0.24342	71
13.70	0.22264	75
10.99	0.17428	54

3.2 Plant Respiration Stage Quantification

According to the method proposed by McCree, dark breathe process is divided into growth respiratory and maintenance respiratory. Growth respiratory is proportional to photosynthetic rate, almost independent of temperature effect. Maintenance respiratory is greatly influenced by the temperature and dry matter quantity.

$$R_2 = R_1 Q_{10}^{(t_2 - t_1)/10} \tag{3}$$

Among them, R_1 represents respiratory intensity when the temperature is t_1; R_2 represents respiratory intensity when the temperature is t_2; Q_{10} represents temperature coefficient. When $t_1 = 0$, maintenance respiratory can be defined as follow:

$$R = R_0 \mathrm{e}^{k't}, k' = (L_n Q_{10})/10 \tag{4}$$

R represents maintenance respiration when the temperature is t; R_0 is maintenance respiration of 0℃.

3.3 Biomass Growth and Storage Stage Quantification

From the point of view of crop physiology, the remainder that net photosynthetic production in maintenance respiratory minus consumption is used for crop growth. The increment can be computed by “Logistic equation”.

$$W = W_m /(1+\mathrm{e}^{a+bt}) \tag{5}$$

In the formula, W_m is W upper bound of theory, a and b are undetermined coefficients, its revision form is

$$W = W'_m /(1+\mathrm{e}^{a+bt+ct^2}) \tag{6}$$

W'_m is a constant, a, b, c is the undetermined coefficient, t is the time (take day as unit).

4 Example and Result Simulation

According to our the experimental result of greenhouse in the agriculture and biological institute of Shanghai Jiao Tong University, the above-mentioned crops growth model is used in the analog computation and simulation.

4.1 Experiments Setting

With the muskmelon varieties "chunli" for the trial materials, seedlings were cultivated in the 72-holes container on August 18 2003. The seedling age was 24 days and its leaves were bent on colonization in the greenhouse to foster. Container planting was used, 2 plants each flowerpot, matrix for coal cinder, peat, perlite mixture (1:1:1), liquid nutrition of the Polyfeed Israel yuan fertilizer. Pruning was used to keep one fruit each plant. On October 25 the plants which had the similar growing trend, the same number of leaves, the close location of knots and the size of fruit were chosen to move into the climate room, 14 flowerpots each room, altogether 28 flowerpots. All the pruning work had been completed before the flowerpots were moved to the room. After 5 days from then, the plants can adapt to the indoor environment and then photosynthesis determination started, 20, 25, 30℃ for three daytime temperature treatments and 18℃ for a night temperature treatment, CO_2 concentration was set to three levels: 400, 700, 1000μmol · mol^{-1}. Determination was conducted for 16 days in order to ensure the full portfolio.

4.2 The Simulation Result

In the simulation computation, set $\Delta t = 1d$ and $0 \le t \le 123d$, we can obtain crops growth curve under each kind of water fertilizer condition after calculation, its model curve is basically same with the result of water fertilizer configuration manure experiment. Among them, C_1, C_2, C_3 and C_4 represents separately the quantity of biomass in no fertilizer, low fertilizer, middle fertilizer, high fertilizer.

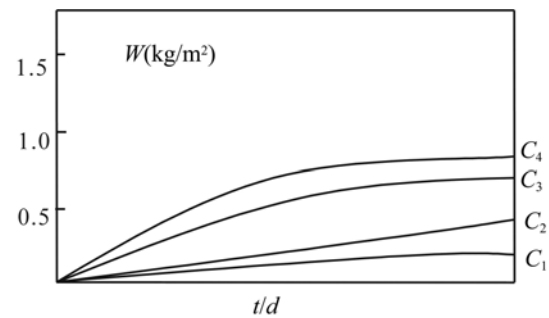

Figure 2 Growth model curve of muskmelon growth

5 Conclusion

According to the growth of muskmelon ecological conditions, the dynamic model had been established to simulate melon growth process with the environment external force factor. The model reflected the combination of objective and microscopic and the melon growth process, which emphasized on the responses of the crop growth rate to the variation of the external force and its change of biomass saturation value. Comparing the dynamic model with the other plant growth model, the superiority of the former was that it combined macroscopic with microcosmic, which showed the effect of the external forces (including organic nitrogen) on stems, leaves and fruit. The results showed that nitrogen uptake and crop yield were most sensitive to total cumulative temperature and more sensitive to the critical temperature, crop extinction coefficient, the assimilate translocation efficiency to the leaf blade and the maintenance of respiration rate. In addition, crop yield was also sensitive to maximum critical cycling temperature and the leaf area index. Taking the melon growth model as an example, the theory and methodology for regulation and control of the environmental parameters in crop growth process would play important roles in facility agriculture.

Acknowledgements

This work were supported by National High Technology Research and Development Program of China (863Program, 2006BAD10A11) and by National Key Technology Research Program, (2006AA10A311) and Shanghai Leading Academic Discipline Project(B209).

References

Lake JV (1966) Measurement and control of the rate of carbon dioxide assimilation by glasshouse crops. Nature, 209,97 – 98.

Korner O (2003) Crop based climate regimes for energy saving in greenhouse cultivation[Dissertation], Wageningen University, the Netherlands.

Farquhar GD, Von S, Caemmerer, Berry IA (1980) A biochemical model of photosynthetic CO2 assimiln leaves of C3 species. Planta, 149: – 90.

Cannel MGR, Thornley JHM (1998) Temperature and CO2 response of leaf and canopy photosynthesis:a clarification using the none-rectangular hyperbola model of photosynthesis. Annals of Botany, 82:883 – 892.

Drake BG, Leadley PW (1999) Canopy photosynthesis of crops and native plant communities exposed to long-term elevated CO2.Plant cell & Environ, 14:853 – 860.

Laing WA (1974) Regulation of soybean net photosynthetic CO2 fixation by the interaction of CO2,O2 and ribulose,Plant Physiology, 54:678 – 685.

Marchlis LFM, Heuvelink E Goudriaan, (1998) Modeling biomass production and yield of horticultural crops: review. Scientia Horticulturate, 74,83 – 111.

Hartz TK (1997) Effects of drip irrigation scheduling on muskmelon yield and quality.Scientia Horticulture, 69: 117 – 122.

Fabeiro C, F Martin de Santa Olalla, de Juan JA (2002) Production of muskmelon under controlled deficit irrigation in a semi-arid climate.Agricultural Water Management, 54:93 – 105.

Villanueva MJ, Tenorio MD, Esteban MA et al. (2003) Compositional changes during ripening of two cultivars of muskmelon fruits.Food chemistry, 87:179 – 185.

McCollum TG,Huber DJ,Cantliffe DJ (1988) Soluble sugar accumulation and activity of related enzymes during muskmelon ruit development,J Amer.Soc.Hort.Sci., 113(3):399 – 403.

Lester GE, Oebker NF,Coons J (1994) Preharvest furrow and drip irrigation schedule-effects on postharvest muskmelon quality.Postharvest Biol.Technol., 4:57 – 63.

Bhella HS (1985) Muskmelon growth,yield and nutrition as influenced by planting method and trickle irrigation.J.Am.Sot.Hort.Sci., 110:793 – 796.

Ibarra L, Flores J, Carlos J et al. (2001) Growth and yield of muskmelon in response to plastic mulch and row covers.Scientia Horticulturae, 87:139 – 145.

Bogle CR, Hartz TK (1986) Comparisons of drip and furrow irrigation for muskmelon production. Hort Science, 21:242 – 244.

Wells JA, Nugent PE (1980) Effect of high soil moisture on quality of muskmelon.Hort Science, 15:258 – 259.

Imtiyaz M, Mgadl NP, Chepete B et al. (2000) Response of six vegetable crops to irrigation schedules.Agricultural Water Management, 45:331 – 342.

A.Halim Orta,Yesim Erd,Tolga Erdem (2003) Crop water stress index for watermelon.Scientia Horticulturae, 1887:1 – 10.

APSIM-Lucerne Validation in the Temperate Climate of New Zealand

D. P. Monks, D. J. Moot, H. E. Brown, E. I. Teixeira

(Agriculture and Life Sciences Division, Lincoln University, Canterbury, New Zealand)

Abstract: Shoot yield data collected from an irrigated lucerne (*Medicago sativa*) crop at Lincoln University, Canterbury, New Zealand (43°38'S, 172°28'E, 11 m a.s.l.) from 1997-01 were used to validate the APSIM-lucerne crop model for a temperate climate. Adjustments to APSIM-lucerne were required to account for autumn shoot death through frosting, defoliation of leaf area as occurs from animal grazing, a change in low temperature response for thermal time accumulation, a reset of stem population as they reduced over time and inclusion of a radiation use efficiency function to account for low temperatures.

Changes were then validated with a separate dataset based on a dryland (670 mm average annual rainfall) crop dataset from the same period. The modified model increased the accuracy of prediction. Root mean squared deviation (RMSD) improved within each season (excluding the first spring regrowth cycle) with averages ranging from 15 to 35% of the mean. The exception was the first autumn regrowth cycle that was underestimated and the mean RMSD was 79%. Further validation was performed using a separate irrigated dataset (2001 – 2004). The modified model generated a distinct pattern of bias within each season, under predicting yield within the first three spring regrowth cycles and over predicting the final three autumn regrowth cycles. These results showed that targeted experimental data to account for storage and remobilization of root reserves in autumn and spring, respectively, are required to further improve accuracy of the model.

Keywords: cardinal temperatures, frost, leaf area removal, *Medicago sativa*, modeling, radiation use efficiency, RMSD, stem population

1 Introduction

Lucerne (*Medicago sativa* L.) has been cultivated for forage since the beginning of recorded history (Michaud et al., 1988) and has been widely promoted and used as a dryland forage in east coast areas of New Zealand (Iversen, 1967; Wynn-Williams, 1982; Moot et al., 2003). However, lucerne has often failed to meet its potential in New Zealand (Langer, 1990) and a steady decline in its use since the 1970s has been associated with the adverse effects of pests, diseases and poor grazing management (Purves and Wynn-Williams, 1989). In New Zealand lucerne is commonly conserved or rotationally grazed throughout summer and autumn. The overall aim of the current research was to provide flexibility in grazing management based on an understanding of lucerne growth and development. APSIM-lucerne was considered an appropriate tool to examine grazing options, but required prior validation in a temperate climate.

2 Materials and Methods

A validation experiment was conducted at Lincoln University, Canterbury, New Zealand (43°38'S, 172°28'E, 11 m a.m.s.l) on a Wakanui silt loam (*Udic Ustochrept*, USDA Soil Taxonomy) with 1.8 – 3.5 m of fine textured material overlying gravels (Cox, 1978). Wakanui soils are imperfectly

drained and display strong mottling which indicates periods of water logging. The experiment was a split plot design with irrigation or dryland as main plots. Three replicate plots (22×6.3 m) of lucerne ('Grasslands Kaituna', 7 kg/ha) were sown as pure swards on 30 November 1996 within a larger experiment (Brown, 2004). The experiment ran over 8 growth seasons (1 July – 30 June) with an establishment season (1996/97) and seven subsequent regrowth seasons (1997/98 – 2003/04).

Complete experimental details were given by Brown (2004). Briefly, the experimental area was prepared with conventional cultivation methods. Soil tests were conducted prior to establishment and annually during the experiment with fertiliser applied to maintain a pH > 6 and Olsen phosphorous > 15 μg/g. Herbicide was applied during establishment and each winter to remove annual grass and broadleaf weeds from all plots. The irrigated treatments were irrigated to maintain the soil water deficit ≤ 200 mm (Brown et al., 2003), with annual irrigation ranging from 65 – 437 mm. The dryland plots were irrigated once on 11 September 1998 to reduce soil water deficit at the start of the 1998/99 growing season.

Comprehensive yield data were only recorded in the first four perennial seasons (1997/98 – 2000/01). Therefore data from these seasons of the fully irrigated lucerne treatment were used to calibrate the APSIM-lucerne model. Data from the first four perennial seasons of the dryland lucerne treatments were then used to validate the changes made.

3 Results

Yield ranged from 28 t DM/ha in the 1997/98 season to 18 t DM/ha in the 1999 – 2000 season. Each year contained at least six defoliation events at the end of an individual 'regrowth' period. These six regrowth cycles fell into three descriptive lots: the initial spring cycle, 4 mid-season cycles and the final, autumn, cycle. The original APSIM-lucerne model over-predicted dry matter yield accumulation by an average of 1.1 t DM/ha/regrowth cycle (Fig. 1). The exception was the initial spring regrowth cycle which was under predicted.

3.1 Frost

The observation that late season frosts terminated lucerne growth and development in seasons 1 and 3 required the addition of a 'frost' function. Dry matter accumulation ceased in the field for the remainder of the season when autumn air temperatures dropped below 0℃. The same effect was not observed in spring and without further controlled environment work on early and mid-season frosting, a mid point was selected at 152 Julian days (1 June) after which a frost would kill the crop. Similar work in the Gansu region, north-west China, noted the need for a 'frost' function in the model (Chen et al., 2003).

3.2 Increased Leaf Area Removal

The model was modified with the aim to reduce the over prediction on the first sampling date within each the regrowth cycles by decreasing the fraction of the stem that remained and minimum LAI after each defoliation. This resulted in each subsequent harvest ithin a regrowth crop being more accurately predicted.

3.3 Cardinal Temperature

Cardinal temperatures from published data based on work from the experimental site (Moot et al., 2001; Brown et al., 2005) increased thermal unit accumulation to 0.71℃d per℃ above T_b of 1℃ for T≤15℃.

3.4 Reducing Stem Populations

Stem populations decreased in response to disease and natural senescence between seasons. Stem populations were stable within a regrowth cycle but decreased between cycles (Brown, 2004). Stem populations were empirically reduced from 850 stems/m^2 in 1997/98 to 600 stems/m^2 in 2000/01 in the model to match observed. The modified stem function gave the greatest improvement in prediction in the four mid-season regrowth cycles. Subsequent experimental investigations have developed a function that could be integrated into further revisions of the model (Teixeira et al., 2007)

3.5 Radiation Use Efficiency

Following analysis of RUE, a simple matrix to increase RUE to a maximum between 18 – 25℃ was implemented (Brown et al., 2005). RUE was subsequently augmented by season so that spring RUE was raised to 130% and autumn RUE was decreased to 55% of original. This improved predictions during the summer and autumn periods (regrowth cycles 2 – 6) from RMSD % 107 to 24.

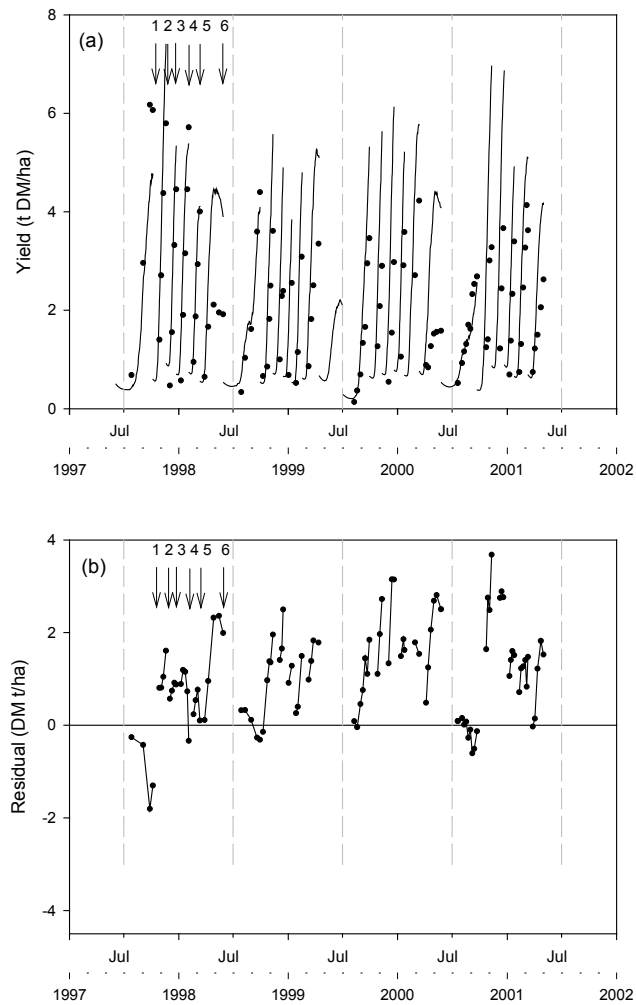

Figure 1 Observed and APSIM-lucerne predicted dry matter (DM) (a), and residuals (b) (predicted minus observed) for a lucerne crop grown at Lincoln University, Canterbury, New Zealand from 1 July 1997 – 1 July 2001. Numbers 1 – 6 indicate the defoliation date for each of the 6 regrowth cycles within the first perennial season (1997/98)

3.6 Validation

Data from the dryland lucerne at the Lincoln University experimental site were then used to validate the changes made to the APSIM-lucerne model. The modified model increased accuracy of prediction of annual DM yield (Fig. 2).

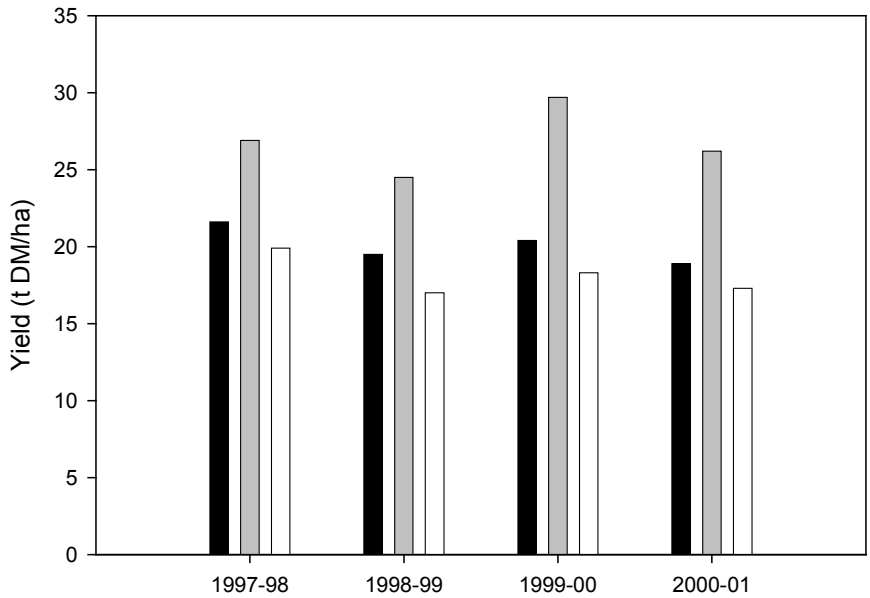

Figure 2 Total observed (■) and predicted ('original' (▒) and 'modified' (□)) annual dry matter yield of a dryland lucerne crop sown in November 1996 at Lincoln University, Canterbury, New Zealand

Prediction of mean dry matter production improved during the mid-season and autumn regrowth periods. Mean annual RMSD % of observed dry matter improved from 35% to 23% (Tab. 1). The spring regrowth period remained inefficiently predicted with the modified model – RMSD% moved further from the observed; 27% for the original model, 79% for the modified model (Fig. 3).

Table 1 Observed and 'modified' (a) and 'original' (b) APSIM-lucerne predicted dry matter (DM) for each measured harvest (per cycle and per year (each year's six cycle average)) for a dryland lucerne crop grown at Lincoln University, Canterbury, New Zealand from 1 July 2001 – 1 July 2004

(a)

Cycle	1	2	3	4	5	6
Mean Observed	2.0	2.8	2.2	2.2	1.8	1.3
Mean Predicted	0.7	2.0	2.1	2.1	2.1	1.3
RMSD	1.81	0.81	0.33	0.33	0.44	0.51
RMSD % of mean	79	30	15	15	22	35

Year	1997/98	1998/99	1999/00	2000/01
Mean Observed	2.4	1.8	2.1	2.1
Mean Predicted	1.9	1.5	1.6	1.5
RMSD	1.02	0.96	0.69	1.05
RMSD % of mean	43	47	33	50

(b)

Cycle	1	2	3	4	5	6
Mean Observed	2.0	2.8	2.2	2.2	1.8	1.3
Mean Predicted	1.4	2.6	2.7	2.7	2.2	1.5
RMSD	1.01	0.68	0.84	0.58	0.63	0.70
RMSD % of mean	51	25	37	26	34	55

Year	1997/98	1998/99	1999/00	2000/01
Mean Observed	2.4	1.8	2.1	2.1
Mean Predicted	2.4	1.9	2.4	2.1
RMSD	0.65	0.83	0.84	0.73
RMSD % of mean	27	45	41	36

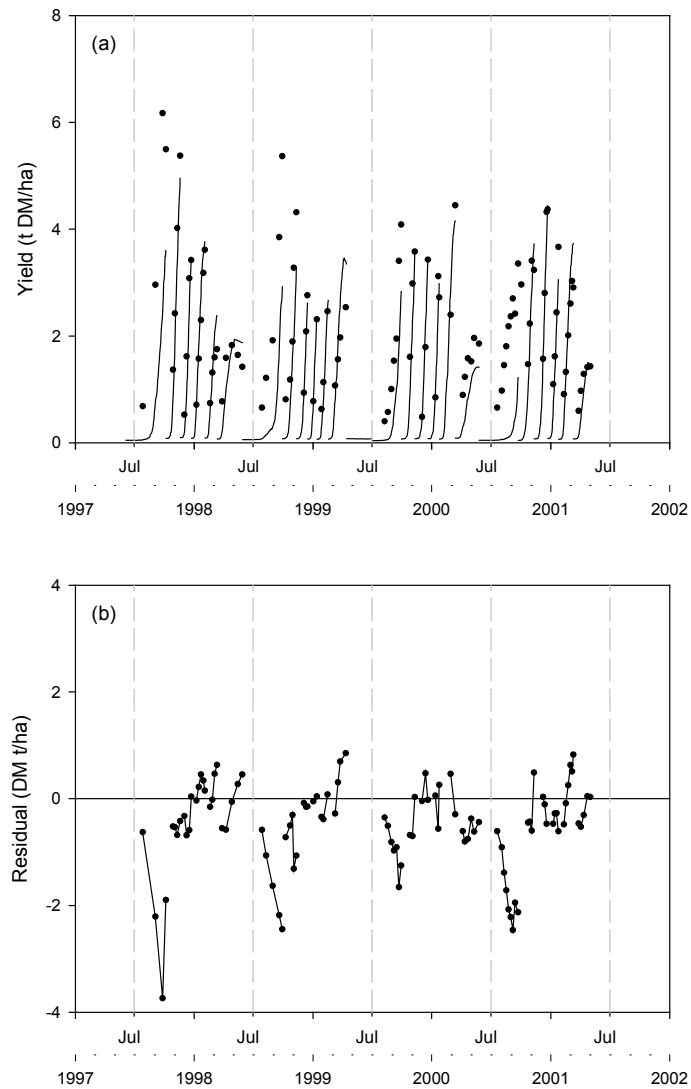

Figure 3 Observed and 'Modified' APSIM-lucerne predicted dry matter (DM) (a), and residuals (b) (predicted minus observed) for a dryland lucerne crop grown at Lincoln University, Canterbury, New Zealand from 1 July 2001 – 1 July 2004

4 Discussion

To confidently predict DM yields and subsequent develop best management protocols for grazing lucerne requires an understanding of the physiological processes that drive crop growth and development. Validating the APSIM-lucerne model for a temperate climate highlighted the strengths and weaknesses in our basic understanding of how the plant adjusts to its biophysical environment.

After modification, APSIM-lucerne was successfully tested against yield data from both an irrigated and a dryland lucerne crop grown at Lincoln University from November 1996 – July 2000. The DM production in the first spring period was consistently under predicted by the model. The model predicted DM yield below the observed by an average of 1.6 t DM/ha per sampling date during the first regrowth period of each year (Tab. 1). This lack of fit highlighted an area where our understanding of above and below ground partitioning was still insufficient to allow accurate simulation. Previously, authors (Dolling et al., 2001; Chen et al., 2003) have 'worked around' this issue by decreasing RUE in the autumn period. Thus, the model has been used to identify areas for strategic experimental investigation to address these issues (Teixeira et al., 2008).

References

Brown H E (2004) Understanding yield and water use of dryland forage crops in New Zealand : a thesis submitted for a degree of Doctor of Philosophy at Lincoln University, New Zealand.

Brown H E, Moot D J, Pollock K M (2003) Long term growth rates and water extraction patterns of dryland chicory, lucerne and red clover. *In*: Legumes for Dryland Pastures. Proc N Z Grassland Assoc symp, 18-19 November 2003, Lincoln University, Grassland Res and Practice Ser Vol. 11. p 91 – 100.

Brown H E, Moot D J, Teixeira E I 2005. The components of lucerne (*Medicago sativa*) leaf area index respond to temperature and photoperiod in a temperate environment. Eur J of Agron, 23, 348 – 358.

Chen W, Bellotti B, Robertson M J, et al (2003) Performance of APSIM-Lucerne in Gansu, north-west China. *In*: Solutions for a better environment. Proc 11th Aust Agron Conf, Geelong, Victoria. Aust Soc of Agron.

Cox J E (1978) Soils and agriculture of part Paparua County, New Zealand. *In:* N Z Soil Bureau Bulletin No. 34. Wellington, New Zealand: D.S.I.R.

Dolling P J, Latta R A, Lyons A M, et al (2001) Adapting APSIM Lucerne to the Western Australian environment. *In*: Proc 10th Aust Agron Conf, Hobart, Tasmania.

Iversen C E (1967) Grazing management of lucerne. *In:* Langer R H M (ed). The lucerne crop. Wellington, New Zealand: A H & A W Reed.

Langer R H M (1990) Pasture Plants. *In:* R H M Langer (ed). Pastures: Their ecology and management. Auckland, New Zealand: Oxford University Press.

Michaud R, Lehman W R, Rumbaugh M D (1988) World distribution and historical development. *In:* Barnes K, Hill Jr R R, (eds). Alfalfa and alfalfa improvement. Madison, U.S.A: Am Soc of Agron.

Moot D J, Brown H E, Teixeira E I et al (2003) Crop growth and development affect seasonal priorities for lucerne management. *In*: Legumes for Dryland Pastures. Proc N Z Grassland Assoc symp, Lincoln University. Grassland Res and Practice Ser. Vol. 11. p 201 – 208.

Moot D J, Robertson M J, Pollock K M (2001) Validation of the APSIM-Lucerne model for phenological development in a cool-temperate climate. *In*: Proc 10th Aust Agron Conf, Hobart, Tasmania.

Purves R G, Wynn-Williams R B (1989) Lucerne - a fresh look. Proc Agron Soc N Z, 19, 95 – 102.

Teixeira E I, Moot D J, Brown H E et al (2007) The dynamics of lucerne (*Medicago sativa* L.) yield components in response to defoliation frequency. Eur J Agron, 26, 394 – 400.

Teixeira E I, Moot D J, Brown H E et al (2008) Modeling shoot and root biomass of lucerne crops – new insights on the seasonality of dry matter partitioning and root maintenance respiration. ibid.

Wynn-Williams R B (1982) Lucerne in the 80s. Christchurch, New Zealand: Agron Soc N Z.

Decision Support System for Greenhouse Environment Control Based on Model

Ji-Zhang Wang, Ping-Ping Li, Yong-Guang Hu, Han-Ping Mao

(Key Laboratory of Modern Agricultural Equipment and Technology, Ministry of Education & Jiangsu Province, Jiangsu University, Jiangsu, 212013, China)

Abstract: Greenhouse environment control and manage mainly emphasize on the growth of crop, and seldom take into account the cost of control. In this research, the decision support system (DSS) of greenhouse environment control based on model is put forward. In this system, models included greenhouse crop growth model, greenhouse control effect model and control cost model. Then knowledge-base, model-base and database are established including the aspects of crop growth, environment control in greenhouse. Based on those, the software of greenhouse environment control decision support system (GHMDS) is developed. With consideration to both crop growth and economic profits, the system combined the advantages of "Model Based Reason (MBR)" and "Knowledge Based Reason (KBR)". By this system, the optimized dynamic parameters of environment control under different weather conditions and crop growth stage can be given. And it also can forecast market period, growth stage. Connected with greenhouse controller, it can realize intelligent control. The simple man-machine interface of GHMDSS makes the user more convenience and more applicable in greenhouse crop and climate management practices.

Keywords: greenhouse, environment control, model, decision support system (DSS)

1 Introduction

Decision support system (DSS), which was presented in 1970s, is a decision support knowledge system based on computer technology and is put into dealing with non-structured problem and semi-structured problem in decision-making. Since 1990s, DSS has been applied to greenhouse manager. Fisher (1997) developed a decision support system The Greenhouse CARE System for recommending night and day temperature settings to control the timing and height of Easter lily. N.D. Clarke et al. (1999) developed the Harrow Greenhouse Manager (HGM)", it is a suit of decision support system tools for integrated crop pest and disease management of greenhouse cucumber and tomato. Sun ZF (2001) developed a real time on line aided decision support system fro greenhouse tomato production. It provides real time decision support and management service based on an on-line date logging system. M. Tchamitchian (2006) developed the decision support system SERRISTE to generate daily climate set points for greenhouse grown tomatoes. The system was based on the mathematical formalization of expert practices and scientific knowledge. it could save energy in the range of 5 – 20%. On model based decision support system research, G. van Straten (1999, 2000) researched the optimal control of greenhouse climate based on crop growth model and temperature integration. It could give long term and short term climate strategies by model based decision support. J.M.Aaslyng et al. (2003) researched a greenhouse component based climate control system (IntelliGrow), the system is based on mathematical model for estimating the absorption of irradiance, leaf photosynthesis and respiration, the result show it could save energy

between 20% and 38%. O. Kornera (2008) created a decision support tool in order to decide at which week of the year to use which climate control regime for the optimal gain of sustainability and plant quality. The greenhouse climate control strategies was made by greenhouse climate and control model, cut chrysanthemum growth model and temperature integration, dynamic humidity control, and negative DIF regimes. The system can be used to quantify the costs in energy or chemicals when using the one or other strategy,

In this paper we established the greenhouse environment control decision support system (GHMDS) based on models, in the system, models included greenhouse crop growth model, greenhouse control effect model and control cost model. By this system, the optimized dynamic parameters of environment control under different weather conditions and crop growth stage can be given.

2 Materials and Methods

2.1 The Principle of Greenhouse Environment Control Based on Model

The greenhouse climate control is aimed at economical optimal, it means how to select the optimal control strategy to get the maximum ratio of the output to investment of greenhouse production.

$$Dn = \int_0^T \frac{w(T_{i1}(t), L_{i1}(t))}{P(t)} \mathrm{d}t \tag{1}$$

The notation *Dn* indicated the ratio value of output to investment of greenhouse production. The notation *P*(*t*) indicated the greenhouse control cost model. The notations indicated the predictive value of temperature and PAR (Photosynthetically available radiation) in greenhouse with the control strategy I (Gu J.N(2001)). The notation i is the control strategy, it includes windows, rolling curtain, shading, fan, and pad and heat system. The notation LAI indicated the leaf area index. The notation indicated the ratio of crop growth; it can be expression as differential equations (Carlos, 2001):

$$\frac{\partial \omega}{\partial t} = \alpha \times P_n \times \mathrm{LAI} \tag{2}$$

The notation indicated the crop growth ratio ($kgm^{-2}s^{-1}$). The notation is the coefficient of dry matter. The notation Pn indicated the photosynthetic ratio of crop. The notation LAI indicated the leaf area index.

The step of optimization of the greenhouse climate control is show as Fig. 1. First, the information of greenhouse climate and greenhouse control device was given, and then the system judged the state of climate whether fit the crop growth. If the result is not, the system would select the optimal control strategy by calculating the maximum ratio of the output to investment of greenhouse production (*Dn*).

2.2 GHMDSS Develop

2.2.1 GHMDS Function

The GHMDS system has online mode and offline mode. With offline mode, the user input information of weather, greenhouse climate and crop growth, the system could give the optimal control strategy. With offline mode, The GHMDS was connected with greenhouse climate collector, and give the real time control strategy.

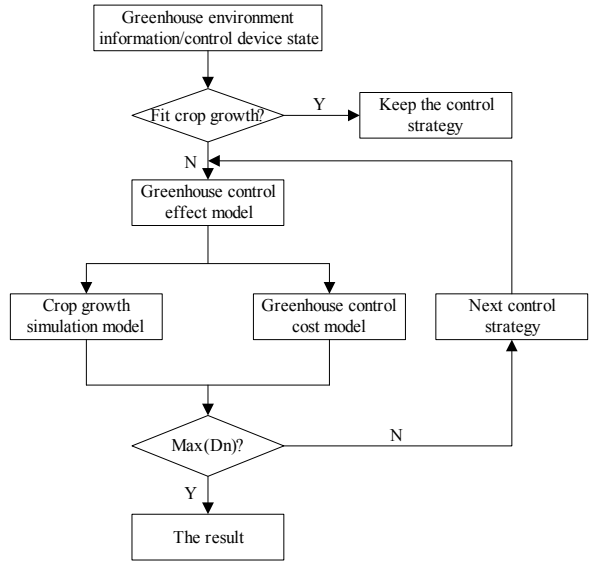

Figure 1 Flow chart of optimize

2.2.2 GHMDS Construction

The system were composed with 6 modules, greenhouse crop growth model module, greenhouse climate control cost model, greenhouse control effect model module, reason and optimal module, system maintenance module and help module. It was show as Fig. 2.

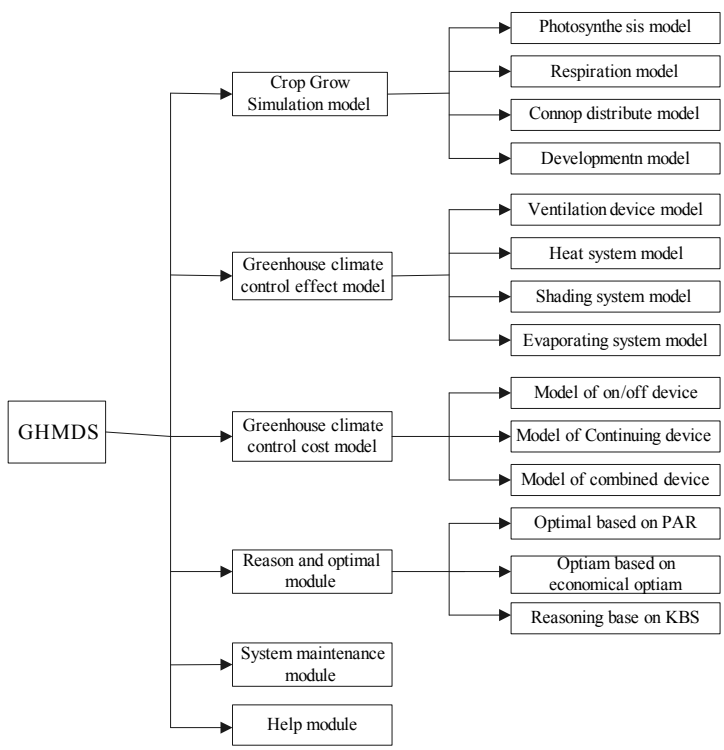

Figure 2 The constructure of GHMDS

2.2.3 Knowledge Base System (KBS)

In this system, the knowledge included crop growth KBS, Greenhouse climate control KBS, Greenhouse climate control rule base. The knowledge was expressed by relational database in this system. Figure 3 is the constructure of the KBS based on database.

Precondition base:	Fact ID	Fact	
Conclusion base:	Conclusion ID	Conclusion	
Rule base:	Rule ID	Fact ID	Conclusion ID

Figure 3 Constructure of the KBS based on database

2.2.4 Model Base System (MBS)

In this system, the model included crop growth simulate model, crop production model, greenhouse climate control effect model and greenhouse climate control cost model. Due to the system was not development on special platform, so the management system was development to manage the model base system. In this system, the models mainly were mathematical function, so the function was stored by database. Figure 4 is the model base management system.

Figure 4 The model base management system

2.2.5 Database System

In this system, the decision support system was based on database system, so the MBS and KBS were expressed by database. The data base of the DSS mainly includes the database of model base, the database of knowledge base, the database of greenhouse climate parameter and the weather, plant, greenhouse type, control device database.

3 Results and Analysis

The GHMDS was developed with BCB 6.0. And the management of model base and KBS was realized with ADO, OOP and database. Figure 5 is the greenhouse state display. Greenhouse climate information and weather information was got through greenhouse information collector on online mode, and it also can be got by manual input. With the information of greenhouse climate and the state of greenhouse control device, the system can make decision the optimal control strategy. Figure 6 is the decision result of GHMDS.

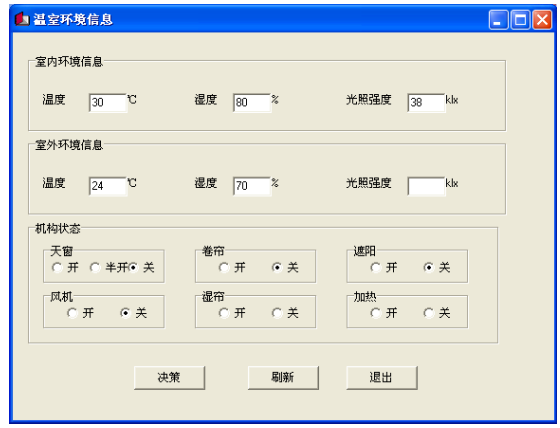

Figure 5 Greenhouse environment information

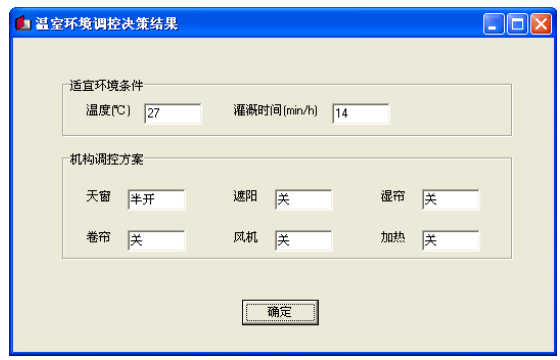

Figure 6 Result of system decision

Acknowledgements

The authors gratefully acknowledge financial support by the National Natural Science Foundation of China (No:30771259) and by the National key technology R&D Program(No:2006BAD11A10) and by the Natural Science Foundation of Jiangsu Province (No:BK2006076) and by the Scientific Research Starting Foundation of Jiangsu University(No: 06JDG038).

References

Carlos Serodio (2001). A networked platform for agricultural management systems, Computers and electronics in agriculture, 31:75 – 90.

Fisher Paul R, Heins Royal D, Ehler Niels et al, (1997). A Decision-support System for Real-time Management of Easter Lily (Lilium longiflorum Thunb.) Scheduling and Height—I. System Description, Agricultural Systems, 54(1) .23 – 37.

Gu JN Mao HP (2001). A mathematical model on intelligent control of greenhouse environment. Transactions of the CSAM 32(6):63 – 66.

van Straten G (1999). Acceptance of optimal operation and control methods for greenhouse for greenhouse. Annual Reviews in Control. 23: 83 – 90.

van Straten G, Challa H, Buwalda F (2000). Towards user accepted optimal control of greenhouse climate. Computers and Electronics in Agriculture. 26 221 – 238.

Aaslyng JM, Lund JB, Ehler N et al. (2003). IntelliGrow: a greenhouse component-based climate control system. Environment Modeling & Software. 18:657 – 666.

Tchamitchian M, Martin-Clouaire R, Lagier J et al. (2006) SERRISTE: A daily set point determination software for glasshouse tomato production. Computers and Electronics in Agriculture. 50, 25 – 47.

Clarke ND, Shipp JL, Papadopoulos AP et al. (1999). Development of the Harrow Greenhouse Manager: a decision-support system for greenhouse cucumber and tomato. Computers and Electronics in Agriculture 24.195 – 204.

Sigrimis NA, Arvanitis KG, Pasgianos GD (2000) Synergism of high and low level systems for the efficient management of greenhouses. Computers and Electronics in Agriculture. 29.21 – 39.

Kornera O, van Straten G (2008). Decision support for dynamic greenhouse climate control strategies. Computers and Electronics in Agriculture. 60,18 – 30.

Sun ZF, Zhang ZB, Tong CF et al. (2001). Development of a Real Time On-line Aided Decision-Making Support System for Greenhouse Tomato Production. Transaction of CSAE. 17 (7),75 – 78.

A Simulation Analysis on Climate Change—Threats or Opportunities for Agriculture

S. Asseng[1], F. Ludwig[1,2], S. Milroy[1], M. I. Travasso[3]

([1]CSIRO Plant Industry, Private Bag No. 5, Wembley, WA 6913, Australia)
([2]Current address: Earth Systems Science and Climate Change Group, Wageningen University, Droevendaalsesteeg 4, Wageningen, The Netherlands)
([3]INTA, Los Reseros y Las Cabanas, 1712 Castelar, Argentina)

Abstract: Our climate is changing and will continue to do so in the future. This has potentially a large impact on agriculture. To study the full impact of a changing climate on agriculture, extensive experimentation would be required. As an alternative, well-tested bio-physical simulation models can be used as a first approximation for such a study. Case studies from major agricultural regions in the world will be presented where a simulation model was used to explore the potential impact of recent and future climate change on wheat production and externalities.

The Pampas of Argentina shows a distinct sub-tropical climate with most rainfall occurring in summer. The main factor limiting wheat production, grown over winter, is rainfall. Rainfall has increased by 100-200 mm/year over the last century in the Pampas, but mainly in summer. In contrast, the wheat-belt of Western Australia shows a distinct Mediterranean climate with most of the rainfall occurring in winter. Also here wheat is grown in winter and again rain is the main factor limiting production. Annual rainfall in the wheat-belt has declined by about 11% since the mid 1970's.

Using the well tested simulation model APSIM-Wheat indicated that the large additional rainfall in the Pampas of Argentina increased some of the yield potential of wheat in the current cropped region and would allow the extension of profitable wheat cropping into currently non-cropped areas. However, soil water storage capacity and managing the stored water over summer will be critical for the wheat crop to benefit from increased summer rainfall. In Western Australia, despite the large decline in rainfall, simulated yields based on the actual weather data did not drop, because rainfall changes occurred mainly in June and July, a period when rainfall often exceeds crop demand and large amounts of water are usually lost by deep drainage. This study highlights that the impact of climate change is often not linearly related to yields and the complexity of the change, the rainfall distribution and the crop water use need to be considered for realistic climate change impact assessments. The examples show that there will be threats and opportunities for agriculture with climate change, depending on the actual change and other systems parameter.

1 Introduction

The global climate is changing and further changes are inevitable regardless of current efforts to reduce global emissions (IPCC, 2007). The accelerating increase of CO2 concentrations in the atmosphere is one of the most certain aspects of global change over the coming decades and recent reports have shown that CO2 is accumulating in the atmosphere faster than recently expected (IPCC, 2007). Because atmospheric CO2 is fundamental to the growth and productivity of terrestrial vegetation, as well as critical for the radiative properties of the atmosphere and hence climate, the

changing atmospheric concentration of CO2 will have far-reaching effects on agricultural production. Projected climate change, such as increased atmospheric concentration of CO2, more severe and more frequent droughts and changing temperatures (IPCC, 2007), will be particularly important for agricultural systems. As these changes can have direct and indirect consequences for crop growth and development with many possible feedback loops, climate change impact might not be the same across agricultural regions.

The Pampas of Argentina shows a temperate humid climate with most rainfall occurring in summer. At the Western bound of the Pampas, the main factor limiting wheat production, grown over winter, is rainfall. Rainfall has increased by 100-200 mm/year over the last century in the Pampas, but mainly in summer (Viglizzo et al., 1995). In contrast, the wheat-belt of Western Australia shows a distinct Mediterranean climate with most of the rainfall occurring in winter. Also here wheat is grown in winter and again rainfall is the main factor limiting production. Annual rainfall in the wheat-belt has declined by about 11% since the mid 1970's (Smith, 2000).

To assess the likely impact of these changes requires well validated simulation models which consider these changes as drivers and capture the main crop physiological functions and other bio-physical aspects of crop-soil-atmosphere systems (Jamieson et al., 2008). We present the impact of these past rainfall changes and possible future changes on wheat production using a simulation modeling approach.

2 Methods

Simulation Model

The Agricultural Production Systems SIMulator (APSIM) (Keating et al., 2003) for wheat (APSIM-Nwheat version 1.55s) is a crop simulation model consisting of modules that incorporate aspects of soil water, nitrogen, crop residues, crop growth and development and their interactions within a crop/soil system that is driven by daily weather data. Documented model source code in hypertext can be viewed at http://www.apsim.info. The model has been successfully tested against data from field experiments across different soil types and Mediterranean and other climatic regions (Asseng et al., 1998a; 1998b; 2001; 2003; 2004) including data from South Queensland, Australia (Asseng et al., 2002), a similar summer dominant climate with wheat growing over winter/early spring mainly on stored water as is the case near the western bound of the Pampas of Argentina.

APSIM-Nwheat calculates potential daily biomass production based on light interception and radiation-use efficiency (RUE). Sub-optimal temperatures, water and N-deficit can reduce the potential growth. Potential water demand is a function of transpiration efficiency (TE) modified by vapour pressure deficit (Monteith, 1988). Simulated plant water uptake is a function of uptake demand, root length density distribution within the soil profile, and available soil water in different soil layers. Rate of rooting depth advance is a function of air temperature, crop water stress, and soil water content in the soil layer with the deepest roots. Vertical soil water movement is simulated using a multi-layered soil model primarily using a cascading approach, with movement both upward and downward also occurring by diffusive flow (Probert et al., 1995). Water (deficit) stress reduces tillering, LAI and photosynthesis, and enhances senescence.

Grain yield is a function of grain number, grain filling and carbohydrate remobilization. In the model, the potential amount of carbohydrates available for remobilization to grain is defined as 75% of biomass growth between 150℃d before grain filling and the commencement of grain filling. Crop phenology is a function of accumulated degree-days, photoperiod and vernalisation requirements.

Simulation Experiments

Argentina: Simulations were carried out for wheat (Triticum aestivum L.) for Chacharramendi, Argentina (about 100 km West of the current central cropping region). Daily rainfall data were partly measured or derived from monthly measured data distributed according measured daily data from Santa Rosa, a location 150 km north-east to Chacharramendi. Maximum and minimum temperatures were derived from three years of measured data at Chacharramendi and correlations with measured data from Santa Rosa. Solar radiation data were used from Santa Rosa. As a fine sandy soil (with about 80 and 110 mm plant-available soil water - PAW to 140 cm depth) is the dominant soil type in this region (INTA, 1990), simulation results can be considered as being representative for the larger region south and north of Chacharramendi.

Western Australia: Nine sites were simulated within the central and northern parts of the wheat-belt (Ludwig et al. 2008). The nine sites covered both the high and low rainfall parts and the warmer and cooler parts of the region. For all sites, daily rainfall data were available from at least 1945 until 2004. Weather data for all sites were downloaded from the from patch point dataset on the Silo website (http://www.bom.gov.au/silo). To analyse the impact of recent climate change on wheat yield and deep drainage two different periods: ① 1945-1974 and ② 1975 – 2004 were compared. These two sets of years were selected because of a large step change in atmospheric circulation that occurred during the mid 1970's (Smith, 2000). Three soil types typical for the region were used for the simulations: ① a sand, ② a loamy sand, and ③ a sand over clay duplex soil. PAWC (Plant-available waster-holding capacity) for the sand was 55 mm to a depth of 150 cm, the maximum rooting depth for this soil. For the loam PAWC was 130 mm to a maximum rooting depth of 230 cm and PAWC was 81 mm for the duplex soil to a maximum rooting depth of 70 cm. Full details of the soils are given by Asseng et al. (2001). The weather data from the last 30 years were then further manipulated by reducing June and July rainfall in steps of 10% to explore the sensitivity of the cropping system to these changes. The reduction assumes that the recent trend in rainfall reduction continues.

3 Results

Argentina: Rainfall at Chacharramendi, a location outside the current cropping region of Argentina, has increased since the period of 1937 – 1965 by about 120 mm for the 1986 – 2005 period. Simulated grain yields over the 70 years increased by 22 – 31 kg/ha per year at Chacharramendi (Fig. 1) as a result of the higher rainfall, but less than expected from the large rainfall increase. As the rainfall increase mainly occurred in summer, soil water storage capacity and summer management (summer crop, weeds or fallow) become critical for having an impact on yield potential of wheat grown over winter. Increased losses of water from deep drainage in the low water storage capacity soils at Chacharramendi (low compared to the main soils in the current wheat growing region) and

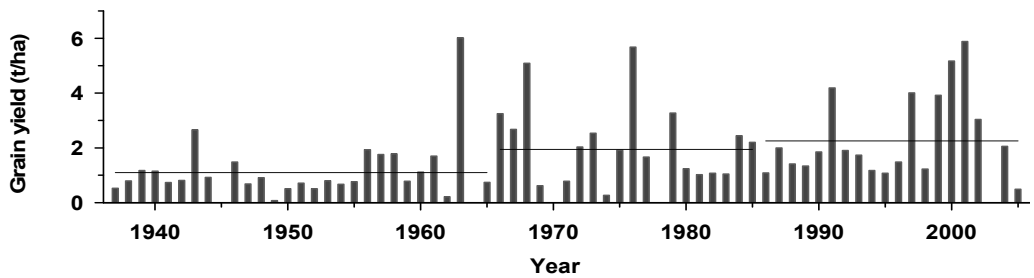

Figure 1 Simulated annual grain yields for Chacharramendi, Argentina

evaporation over summer are the reasons for the lower than expected yield increase in wheat. Summer crops or weeds would further reduce yield benefits for wheat from the increased summer rainfall. Nevertheless, during the last 25 years average wheat grain yields reached about 2.2 t/ha and this average yield and the year-to-year variability of grain yields at Chacharramendi were similar compared to average grain yields and variability at Santa Rosa, a location at the edge of the current cropping region, 50 years ago (data not shown), suggesting new cropping opportunities.

Western Australia: Simulated grain yields based on actual weather records showed no evidence of a systematic reduction between the pre- and post-1975 periods, despite a reduction in rainfall (Ludwig et al., 2008). None of the yield changes were statistically significant. Simulated average grain yields for a loamy sand for the pre- and post-1975 periods are shown for a location in Western Australia in Fig. 2(c), representative for other simulated locations. Simulated average grain yields often tended to be higher (but not statistically significantly) with the reduced rainfall in the post-1975 period due to reduced nitrate leaching on sandy soils and therefore better nitrate availability for crop uptake. However, deep drainage declined significantly in the drier post-1975 period by up to 95% (Ludwig et al., 2008).

Continuing the reduction of rainfall in June–July further reduced deep drainage (data not shown) but indicated that the current cropping systems can absorb even more rainfall decline without affecting grain yields (Figs. 2(a) and 2(b)). However, depending on rainfall location and soil type, further reductions of June-July rainfall beyond 30-50% will eventually cause significant yield declines in an increasing number of seasons (Figs. 2(a) and 2(b)) due to reduced sowing opportunities and increasing water limitations during early growth. Some of this decline might be further delayed by an increasing atmospheric CO2 concentration (Fig. 2(c)).

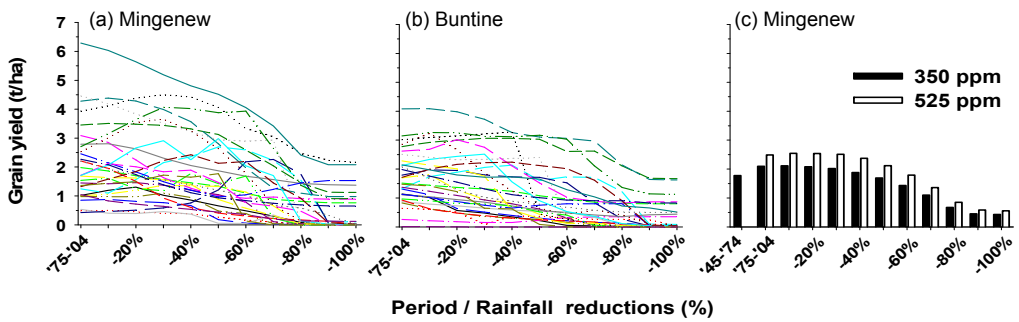

Figure 2 Simulated grain yields for the period 1975 – 2004 and with rainfall reductions (10-100%) for June-July rainfall based on the 1975 – 2004 period for (a) Mingenew (medium rainfall region) and (b) Buntine (low rainfall region) of the Western Australian wheat-belt. Lines indicate individual years. (c) Simulated average grain yields for Mingenew for 1945 – 1974, 1975 – 2004 and with rainfall reductions (10 – 100%) for June-July rainfall based on the 1975 – 2004 for 350 ppm atmospheric CO_2 and elevated atmospheric CO_2 (525 ppm)

4 Conclusion

The simulation results indicated that the large additional rainfall in the currently non-cropped region of Argentina increased some of the yield potential of wheat, but less than anticipated from the large rainfall increase. However, the increased yield potential would allow the extension of profitable wheat cropping into currently non-cropped areas. Soil water storage capacity and managing the stored water over summer will be critical for the wheat crop to benefit from increased summer rainfall. In Western Australia, despite the large decline in rainfall, simulated yields based on the actual weather data did not drop, because rainfall changes occurred mainly in June and July, a period when rainfall often exceeds crop demand and large amounts of water are usually lost by

deep drainage. Further reductions in rainfall during June and July indicated that the current cropping system is resilient to even more rainfall decline until it affects sowing opportunities and early crop survival causing sever reductions in yield potential. These studies highlight that the impact of climate change is often not linearly related to rainfall and the complexity of the change, the rainfall distribution and the crop water use need to be considered for realistic climate change impact assessments. The examples show that there will be both threats and opportunities for agriculture with climate change, depending on the actual change and other systems parameters.

References

Asseng S, Fillery IRP, Anderson GC et al. (1998a) Use of the APSIM wheat model to predict yield, drainage, and NO3- leaching for a deep sand. Australian Journal of Agricultural Research 49: 363 – 377.

Asseng S, Keating BA, Fillery IRP et al. (1998b) Performance of the APSIM-wheat model in Western Australia. Field Crops Research 57: 163 – 179.

Asseng S, Turner NC, Keating BA (2001) Analysis of Water- and Nitrogen-Use Efficiency of Wheat in a Mediterranean Climate. Plant and Soil 233: 127 – 143.

Asseng S, Fillery IRP, Dunin FX et al.(2001) Potential deep drainage under wheat crops in a Mediterranean climate. I. Temporal and spatial variability. Australian Journal Agricultural Research 52: 45 – 56.

Asseng S, van Herwaarden AF (2003) Analysis of the benefits to wheat yield from assimilates stored prior to grain filling in a range of environments. Plant and Soil 256: 217 – 229.

Asseng S (2004) Wheat crop systems—A simulation analysis. CSIRO Publisher, Melbourne, ISBN 064309119X, 275.

Asseng S, Jamieson PD, Kimball B et al. (2004) Simulated wheat growth affected by rising temperature, increased water deficit and elevated atmospheric CO2. Field Crops Research 85, 2-3: 85 – 102.

INTA (1990) - Atlas de suelos de la Republica Argentina. INTA (eds) Buenos Aires, Argentina, 677 pp.

IPCC (2007) Climate Change. 2007. Metz et al. Cambridge Press, UK and New York, USA.

Jamieson PD, Asseng S, Chapman SC et al.(2008). Modeling wheat production. In: World Wheat Book (*in press*).

Keating BA, Carberry PS, Hammer GL et al. (2003) An Overview of APSIM, a model designed for farming systems simulation. Eur. J. Agron. 18, 267 – 288.

Ludwig F, Milroy S, Asseng S (2008) Impacts of Recent Climate Change on Wheat Production Systems in Western Australia. Climatic Change (*in press*).

Monteith JL (1988) Does transpiration limit the growth of vegetation or vice versa? J. Hydrol. 100, 57 – 68.

Probert ME, Keating BA, Thompson JP et al. (1995) Modeling water, nitrogen, and crop yield for a long-term fallow management experiment. Australian Journal of Experimental Agriculture 35: 941 – 950.

Smith IN, McIntosh P, Ansell TJ et al. (2000) Southwest Western Australian winter rainfall and its association with Indian Ocean climate variability. International Journal of Climatology 20: 1913 – 1930.

Viglizzo EF, Roberto ZE, Filippin MC et al. (1995) Climate variability and agroecological change in the central Pampas of Argentina. Agriculture Ecosystems and Environment 55: 7 – 16.

Spatial Analysis of Soil Water Balance in an Agricultural District of Southern Italy

D. Ventrella, E. D. Giacomo, L. Giglio, M. Castellini, D. Palumbo

(CRA - Unità di ricerca per i sistemi colturali degli ambienti caldo-aridi, Bari (Italy))

Abstract: An efficient management of water resources is considered very important for Italy and in particular for Southern areas characterized by a typical Mediterranean climate in order to improve the economical and environmental sustainability of the agricultural activity. The purpose of this study is to analyze the components of soil water balance in an important district of 110 Km2 situated in the Ionical coastal area of Southern Italy and mainly cropped with horticultural crops. The study was performed by using the spatially distributed and physically based model SIMODIS in order to individuate the best irrigation management maximizing the water use efficiency and minimizing water losses by deep percolation and soil evaporation. SIMODIS was applied for 24 soil types distributed in 96 cadastral units for three years characterized by low, normal and high spring summer rainfall. Water melon cultivation was simulated adopting three water supply managements: rainfed and two irrigation strategies based on ① soil water availability and ② plant water status adopting a threshold daily stress value. For each year and management, several water management indicators were calculated and mapped in GIS environment. For seasonal irrigation depth, actual evapotranspiration and irrigation efficiency, the cumulative distribution functions were also determined.

The analysis allowed to individuate the areas particularly sensitive to water losses by deep percolation because of their hydraulic functions characterized by low water retention and large values of saturated hydraulic conductivity. For these areas, the irrigation based on plant water status caused very high water losses by drainage. At the contrary, the irrigation scheduled on soil base allowed to control better this component of soil water balance.

SIMODIS resulted a useful tool to analyse the soil water balance at spatial scale and to support the local irrigation authority for planning the irrigation water distribution not only for economical and productive purposes but also for minimizing the pollution risks of deep soil and groundwater resources.

Keywords: distributed hydrological simulation model, on-demand irrigation system, water use efficiency

1 Introduction

An efficient management of water resources is considered very important for Italy and in particular for Southern areas characterized by a typical Mediterranean climate, where water scarcity and semi-arid climate often cause problems in the agricultural activity.

Different models for the simulation of soil water processes can be used to evaluate the spatial and temporal variations in the soil-plant-atmosphere (SPA) system. The spatially distributed and physically based model SIMODIS (SImulation and Management of On-Demand Irrigation Systems) is a software procedure where the agrohydrological, hydraulic and management aspects of irrigation

are included. This model is based on the integration of different tools such as agrohydrological hydraulic simulation model and GIS techniques (D'Urso, 2001).

For each calculation unit, with homogeneous crop and soil conditions, in which the total area can be divided, the model numerically solves the one-dimensional water flow equation. The spatial distribution of soil water deficit in each unit is computed daily through the soil water model SWAP (Soil Water Atmosphere Plant) (van Dam et al., 1997). The application of SWAP in this distributed form requires the knowledge of the spatial and temporal distribution of the input variables, with special regard to the boundary conditions and the soil hydraulic characteristics.

The objective of this study is to analyze the components of soil water balance through the model SIMODIS for a case study realized in order to optimize the irrigation water use in an important area for agricultural point of view situated in the Ionical coastal area of Southern Italy for two crops: corn (*Zea mais* L.) and water melon (*Citrullus lanatus* Thunb) as typical crop widely cultivated in the studied zone.

2 Materials and Methods

For the application of the model SIMODIS is necessary to set a digital mapping in vectorial form of the area of interest. This work has been developed utilizing a data-set concerning the Ionical coastal area elaborate within the project "CASI 3-SIGRIA 'Studio sull'uso irriguo della risorsa idrica nelle Regioni Obiettivo 1" carried out by the "Istituto Nazionale di Economia Agraria" (INEA) of Rome. In particular we have utilized the data related to the pedology (soil map of scale 1:25.000 and data relating to 24 soil types distributed in 96 cadastral units) and land use (Fig.1).

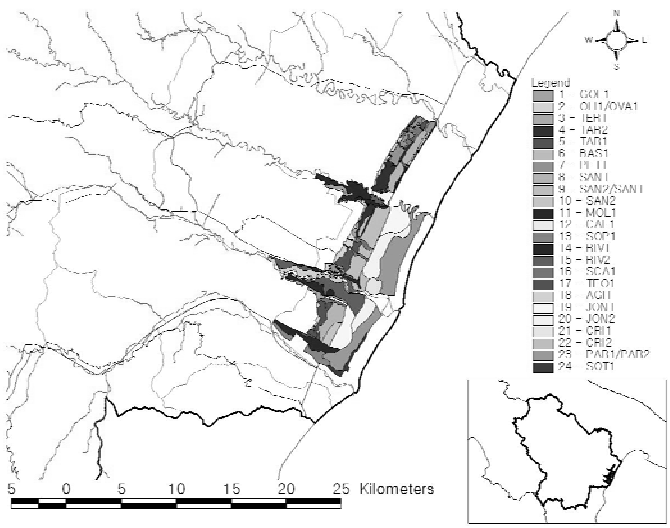

Figure 1 Soil map of the study area

The area of Ionical coastal is located in the Southeast part of the Basilicata region and has an extension of approximately 110 Km^2. The area extends along the coast of Jonical Sea and toward the inside of the territory to an altitude of 60 meters including the basins of four rivers: Sinni, Agri, Cavone and Basento.

The land is mainly cropped with horticultural crops, orchards and vineyards, distributed in relation to the position in the landscape: fruit and vegetable crops prevail in the alluvial deposits, cereals and olive trees predominate in the marine terraces.

The pedological units of the study area are referred to the five main landscapes:

- the hill reliefs (165 hectares), are characterized by coarse sediments alternate with layers of clay;
- the pleistocene marine terraces (3784 hectares) are characterized by coarse and loose sediments;
- the valleys and stream lines (2898 hectares) are characterized by clayey and silty sediments, respectively;
- the coastal retrodunale plain (3993 hectares), is a flat and uniform area mainly formed by alluvial sediments;
- the area in looking on to the costal line with alluvional, marine and eolic sediments (145 hectares).

Figure 2 shows the spatial distribution of the texture classes of the soils (USDA Classification). The dominant soil textures are sandy clay loam, loam and clay loam, with mean values of 39.3%, 35.7% and 25%, respectively for sand, silt and clay. In general, the fraction of sand increases with to increasing depth of the layers.

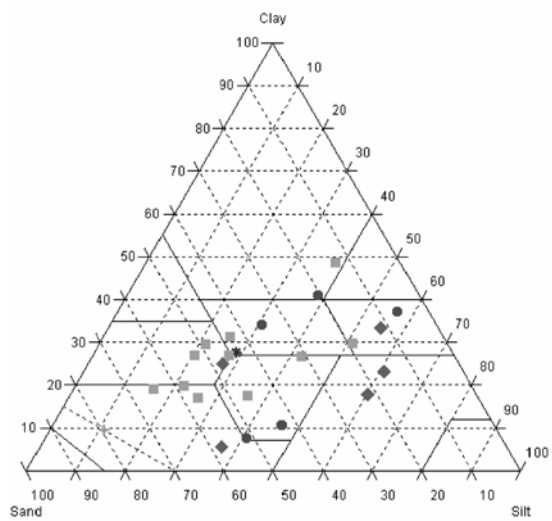

Figure 2 USDA classification of soils used in the model SIMODIS

The soil parameters necessary to use the SIMODIS model are the depth and discretization of each horizon soil profile and the parameters of the function of retention and hydraulic conductivity expressed in the parametric of van Mualem-Genuchten model. In order to calculate the soil parameters, several pedo-transfer functions (PTF) were compared. At the end of this comparison, we have selected the PTF derived from the database European soils HYPRES (Hydraulic PRoperties of European Soils) (Wösten et al., 1999). The choice of this PTF was motivated by the availability and the type of data used. This PTF comes from information collected in the database HYPRES containing information of 5521 soil horizons involving 20 institutions from 12 European countries. HYPRES considers linear regressions of the hydraulic parameters of van Mualem-Genuchten equations (θr, θs, α, n, Ks and l). The inputs required are the percentages of sand and clay, as well as organic matter and bulk density. Also required is a qualitative variable (topsoil and subsoil), which enters in the regression assuming values of 0 or 1.

The parameters relating to the crops necessary for the simulation are the temporal evolution of leaf area index (LAI), the fraction cover (fc) and the crop coefficients (Kc) useful for calculating the actual evapotranspiration (Eta) and the net precipitation rate (P_n).

In the first phase of the work we have simulated the water balance related to cultivation of corn

as a test crop. For the water melon, the LAI and fc were measured directly in several fields during the measurement campaign within the Project AQUATER of 2007. The values *K*c were selected according to those suggested within the OTRIS project ("*L'irrigazione e la fertirrigazione delle colture erbacee ed orticole negli ordinamenti produttivi di Puglia e Basilicata*").

The parameters concerning the temporal evolution of growth roots and the reduction of water uptake under condition of soil water stress, are the others very important crop variables required by SIMODIS. For the first we have utilized the information included in the OTRIS report while regarding the function of water stress we have selected the values suggested for sensitive crops in the SWAP manual.

Three years (1992, 1995 and 2002), representative of low, normal and high condition of spring-summer rainfall, were considered in order to take in account the climate variability of the area.

For the corn the following irrigation scenarios have been compared:

M1 = reference situation without irrigation;

M2 = re-establishment of 100% of soil water reserve when the soil matric pressure head (h) is equal to the threshold value below which the crop water uptake is reduced;

M3 = like M2 with a re-establishment of 70% of soil water reserve.

Water melon cultivation was simulated adopting three water-supply managements:

A1 = reference situation without irrigation;

A2 = like M2, irrigation strategies based on soil water availability

A3 = irrigation strategy based on the plant water status with the irrigation scheduled when the ratio "actual transpiration/potential transpiration" is equal or lower than a critical fraction user defined (0.98 in our case).

For each simulation run the following soil water balance indicators were calculated at seasonal scale: actual values of transpiration (Ta) and evaporation (Ea), height (Irr) and number (n) of irrigations, deep percolation (Perc) and water content (θ) of the surface layer ($0-4$ cm) cm. The irrigation efficiency (Ei) has been calculated by the following expression:

$$E\mathrm{i} = 100 * \frac{ETa_{\mathrm{irr}} - ETa_{\mathrm{noirr}}}{I\mathrm{rr}} \tag{1}$$

where ETa_{irr} and ETa_{noirr} are the actual evapotranspiration calculated with and without irrigation (Irr), respectively.

3 Results and Discussion

In the cultivated area located in the coastal area of Ionical Sea, SIMODIS model allowed to describe the evolution of the components of the soil water balance simulating the cultivations of corn and water melon in the irrigation seasons of 1992, 1995 and 2002.

In general, for the 6 combinations of crop and irrigation management, the actual soil evaporation ranged from 20 to 26% in comparison to Eta. The percentages related to the losses by percolation were significantly lower but with a larger variability ranging between 8 and 18%. The resulting irrigation efficiency, calculated with Eq.(1), was therefore higher than 52% and in the case of M3 it was almost 69%.

Figure 3 shows the soil water balance indicators aggregated for the 5 Landscape Units (LU). Both for the corn and for the melon, the LU were characterized for small differences of Eta. For the other indicators, the first 4 LU showed little variations among them, but the indicator values resulted significantly lower (Percolation and Irrigation) or higher (number of irrigation) than the fifth LU. In the other words, the fifth LU resulted particularly sensitive to water losses by deep percolation because of the related hydraulic functions characterized by low water retention and large values of saturated hydraulic conductivity (52.69 cm d^{-1}). Moreover, for this LU, the

irrigation based on plant water status, for melon cultivation, caused very high water losses by drainage, while such losses were substantially limited when the irrigation was scheduled on the basis of the soil water status. Finally the differences among the LU were more consistent in melon cultivation than corn.

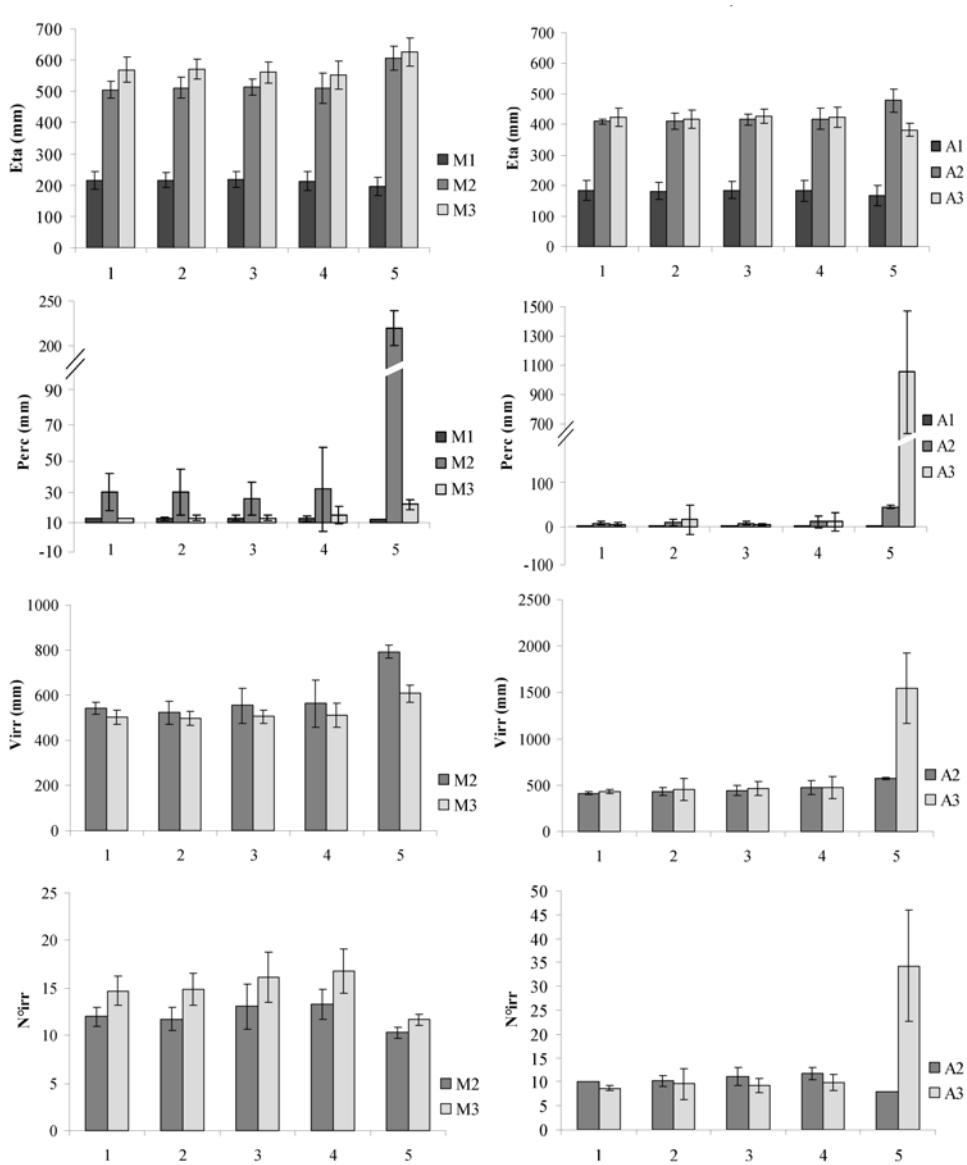

Figure 3 Results for corn (M2 and M3) and melon (A2 and A3) cultivation of actual evapotranspiration (*ETa*), deep percolation (*P*erc), depth (*V*irr) and number (*N*irr) of irrigations estimated for the 5 Landscape Units. The lines indicate the standard deviations

Figures 4 and 5 show the annual weighted distribution functions for *E*ta, *I*rr and *E*i under corn and melon cultivation, respectively. The first result is that the climatic variability impacted above all'Eta. For corn cultivation, the distributions of seasonal irrigation were characterized by a low variability. The same finding was found under A2 scenario for Melon cultivation, but the values of Irr related to A3 scenario were particularly high. Such very high values of *I*rr determined very low values of *E*i particularly evident in Fig. 5.

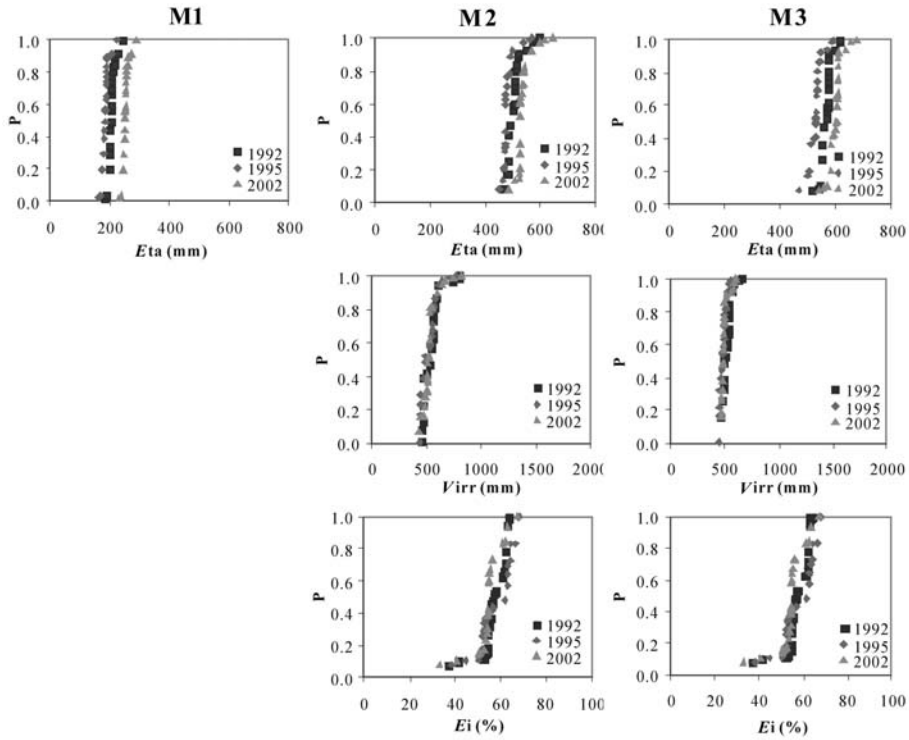

Figure 4 Cumulative distribution functions (*P*) for corn cultivation: actual evapotranspiration (*E*ta), irrigation depth (*V*irr), and irrigation efficiency (*E*i)

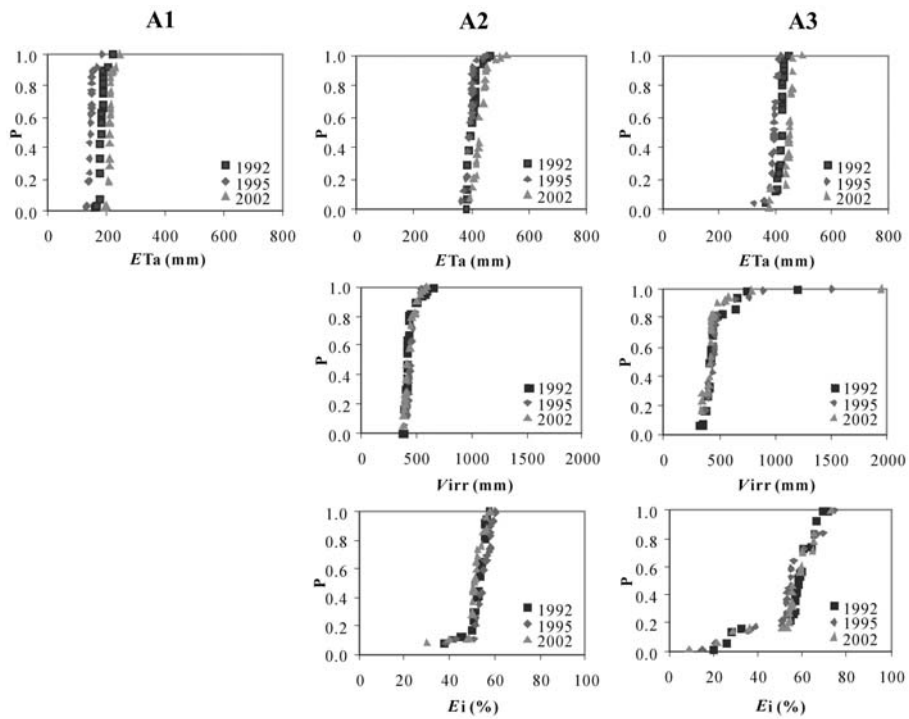

Figure 5 Cumulative distribution functions (*P*) for melon cultivation: actual evapotranspiration (*E*ta), irrigation depth (*V*irr), and irrigation efficiency (*E*i)

Figure 6 reports the spatial distribution of *E*ta, *I*rr, *P*erc and θ for 2002 under A2 scenario. The most sensitive zones to water losses by percolation are located in four well defined area scattered in the basin object of this study. Figure 7 shows an example of temporal evolution of surface soil water availability for which the critical period for water stress, without irrigation, lasted two months from May 15 to July 15.

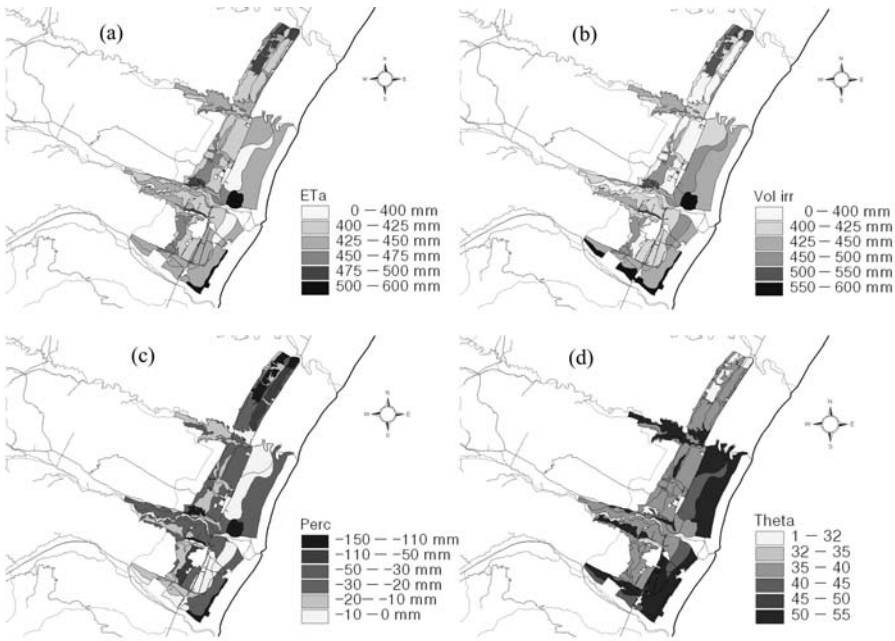

Figure 6 Spatial distributions of actual evapotranspiration (a), irrigation depths (b), deep percolation (c) and surface water content (d). Scenario A2-2002

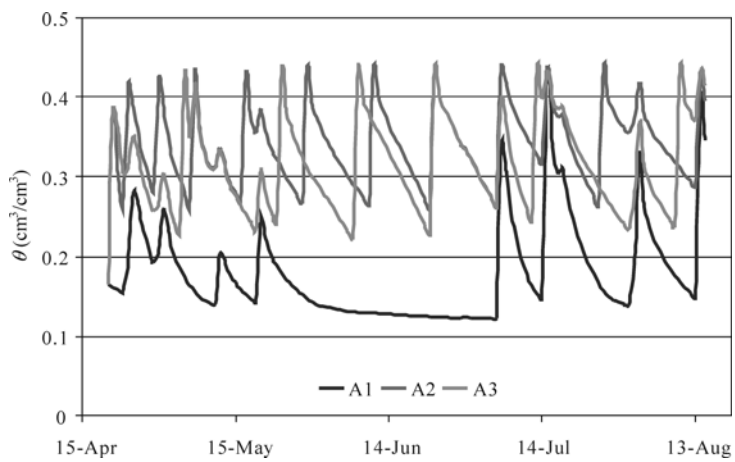

Figure 7 Surface water content (0 – 4 cm): scenarios A1, A2 and A3 - 2002

The comparison of the 5 LU in term of efficiency (*E*i) is reported in Fig. 8. Under corn cultivation the irrigation strategy M3 (re-establishment of 70% of soil water reserve) allowed higher *E*i than M2. However, under melon cultivation, no significant differences of *E*i resulted in the first 4 LU. At the contrary in the last LU, the efficiency of irrigation based on plant water status, A3, was substantially lower than that obtained under A2 scenario.

Finally, the map related to the spatial distribution of *E*i is reported in Fig. 9 with the area most sensitive to water percolation showing the lowest values of *E*i.

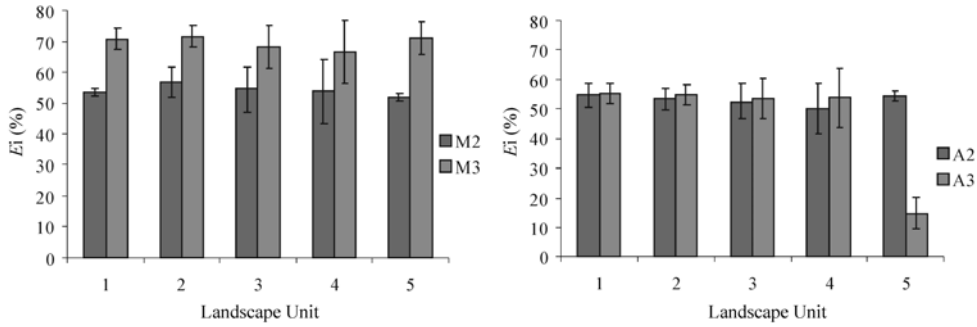

Figure 8 Irrigation efficiency (*E*i) in the landscape units for corn (M2 and M3) and melon (A2 and A3) cultivation. The lines indicate the standard deviations

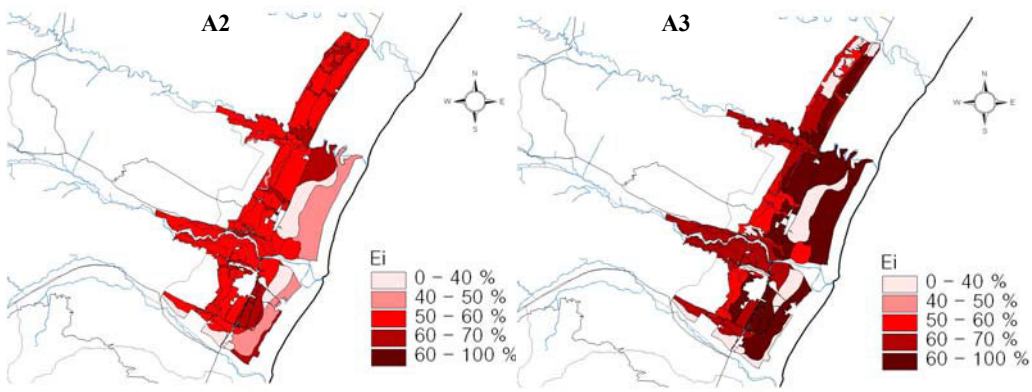

Figure 9 Irrigation efficiency maps: scenarios A2 and A3 - 2002

4 Conclusions

Numerical models are increasingly being used to simulate water and solute movement in the vadose zone for a variety of applications in research and soil/water management.

While a large number of models of various complexity have been developed over the years, relatively few have been tested under field conditions.

The performance and utility of SIMODIS model was assessed by simulating water flow in a distributed scale for an area intensively cultivated in Southern Italy.

The approach described in this study was successful in estimating the principal component of soil water balance under cultivation of corn and water-melon. Analyzing the spatial distribution of these indicators it was possible to individuate the area with higher irrigation requirement. In particular, this case study allowed to identify the most sensitive zones to water losses by deep percolation that require very high volumes of irrigation with low water use efficiency.

In general, the irrigation strategy of melon, based on plant water status, allows to use water in a lightly more efficient way than the irrigation based on soil water status. However, with sand soil, characterized by very large value of saturated hydraulic conductivity, the best way to save water and obtain higher values of water use efficiency is to schedule the irrigation by monitoring the soil water content or adopting the evapotranspirometric method.

Acknowledgements

Funded by Italian Ministry of Agriculture and Forestry Policies (AQUATER Project 209/7303/05).

References

D'Urso G (2001). Simulation and management of on-demand irrigation systems: a combined agrohydrological and remote sensing approach. PhD thesis, Wageningen University, Wageningen, The Netherlands.

D'Urso G, Menenti M, Santini A (1999) Regional application of one-dimensional water flow models for irrigation management. Agric Water Manag 40:291 – 302.

Minacapilli M, Iovino M, D'Urso G (2008) A distributed agro-hydrological model for irrigation water demand assessment. Agric Water Manag 95:123 – 132.

Minacapilli M, Iovino M, D'Urso G (2005) Crop and irrigation water management using high resolution remote sensing and agrohydrological models. In D'Urso G., Osann Jochum M A, Moreno J (Eds), Earth Observation for Vegetation Monitoring and Water Management. AIP Conference Proceedings 852:99 – 106.

AA VV (2002) Studio sull'uso irriguo della risorsa idrica nelle Regioni Obiettivo 1. Carta dei suoli in scala 1:25000 di una porzione di territorio del Consorzio di Bonifica Bradano-Metaponto (MT). Project CASI 3-SIGRIA INEA.

Rizzo V (2000) Ottimizzazione dell'uso delle risorse idriche, convenzionali e non, in sistemi colturali sostenibili. L'irrigazione e la fertirrigazione delle colture erbacee ed orticole negli ordinamenti produttivi di Puglia e Basilicata. Coord. Scientifico E. Tarantino. A cura di. Ecumenica Editrice.

van Dam J C, Huygen J, Wesseling J G., Feddes R A, Kabat P, van Walsum P E V, Groenendijk P, and van Diepen C A (1997). Theory of SWAP version 2.0. Report 71, Dpt. of Water Resources, WAU, Wageningen, The Netherlands.

Wosten J H M, Lilly A, Nemes A, Le Bas C (1999) Development and use of a database of hydraulic properties of European soils. Geoderma 90:169 – 185.

Uncertainty in Multi-Criteria Evaluation Techniques When Used for Land Suitability Analysis

K. K. Benke[1], C. Pelizaro[1], K. E. Lowell[1, 2]

(1 Department of Primary Industries – Parkville Centre, P.O. Box 4166, Parkville, Victoria, 3052, Australia)
(2 CRC for Spatial Information, The University of Melbourne, Ground Floor, 723 Swanston Street, Carlton, Victoria, 3053, Australia)

Abstract: Uncertainty analysis is rarely considered in the application of predictive models in agriculture, resource planning and land suitability analysis. Uncertainty in modeling land suitability for agricultural production arises from a variety of sources. An important source of error is due to uncertainty in model inputs and parameters, especially in the case of multi-criteria analysis requiring data from physical measurements or expert opinion from regional workshops. The concept, scope and taxonomy of uncertainty analysis are discussed in the context of resource planning and land suitability analysis. The model used for land suitability was derived using the Analytic Hierarchy Process (AHP) originally introduced by Saaty in the mid 1970s. The general approach is also appropriate to modeling suitability to pasture and forestry as well as agricultural crops. The deterministic AHP approach produces point estimates only, with no indication of error or confidence in the output. We have integrated the AHP approach with a stochastic simulation model for uncertainty assessment. Since the AHP approach is deterministic, procedural adjustments are required to estimate uncertainty in predictions. The approach taken was to represent expert judgements and ratings by probability distributions and to implement a graded series of stochastic simulations. Variable weight values were subject to constraints of range and unit-sum for each level of the hierarchy in the AHP model. Results for uncertainty analysis are presented for land-use suitability in south-west Victoria in Australia for the crops ryegrass/sub-clover and winter wheat. The work was carried out in the context of a program supporting climate change adaptation funded by the Victorian Government. Estimates of uncertainty for the AHP approach were conservative in nature and a primary objective was to explore and develop further a generalised approach to uncertainty assessment for the AHP model and similar multi-criteria evaluation techniques.

Keywords: AHP, land suitability analysis, multi-criteria decision analysis, uncertainty

1 Introduction

The use of models and quantitative analytical techniques to undertake land management over broad agricultural areas has evolved over time. The advent and widespread availability of high-speed computers accelerated the development of sophisticated decision-support tools that could address multiple inter-related inputs and outputs. When such tools first appeared, there was a sense that the models were so sophisticated, that their outputs were surely accurate—or at least better than anything that could be produced by non-computer-based techniques. Indeed, numerical optimisation techniques such as linear programming were seen as an ideal way to determine the single best land management scenario given a series of inputs and resource constraints.

As consumers of information became more sophisticated, they began to recognise the limits of

such tools and also the quality of the information produced. Part of that growing awareness was recognition that some input data and resource constraints do not readily translate into purely numerical approaches. For example, there is no widely accepted balance for the relative importance of preserving biodiversity whilst protecting against bushfires. In the early 1980s, the appearance of personal computers resulted in a migration of spatially based software to more affordable platforms. This contributed to an adaptation of many previously non-spatial tools to the spatial framework provided by a geographic information system (GIS). While this movement caused increased usage of sophisticated computer-based land management tools, it also increased the scrutiny of spatially explicit data sets.

It now seems inevitable that after powerful analytical tools were linked to spatial datasets, the highly uncertain nature of landscape and agricultural data and models would be revealed. Tool developers and non-numeric end users realised that spatial datasets covering large areas are not as spatially explicit as desired. It was also recognised that the attributes associated with maps of eco-zones, soils, forest type, etc. were across-type averages that could have high variability across a cartographic type. Even the boundaries were recognised as being broad transition zones with undefined characteristics.

Separate from the data issues, uncertainty associated with model predictions also began to receive greater interest. It was recognised that much of this uncertainty is related to natural variability in ecosystem processes. Efforts were thus made to better describe this variability in various phenomena, and acknowledgement of uncertainty inherent in models was enhanced. With the recognition of these factors came a strong desire to have decision-support tools that reflected the associated uncertainties. Although techniques in the past provide a potential structural framework for addressing various types of uncertainties affecting decision-support tools, it remains clear that there is limited understanding of uncertainty-based techniques for decision-making, and little understanding of how the detailed specifications of such techniques can have an impact on outcomes.

2 Land Suitability Analysis

Strategies for resource management, especially in the case of land suitability analysis (LSA), need to be region-based and in the context of a risk management framework. The assessment framework requires integration of intelligent decision support tools with risk analysis in order to provide estimates (in land suitability or production yields) and a measure of uncertainty or error in these estimates. A multi-criteria decision making approach known as the Analytic Hierarchy Process (Saaty, 1994) is one tool used for LSA. It is a deterministic model that produces point estimates without indication of error in predictions. The uncertainty in estimates from such predictive models needs to be addressed in a statistically appropriate manner.

Aside from illustrating the concepts and application of uncertainty analysis, a principal aim of the current paper is to describe how it is possible to produce a conservative estimate of the uncertainty in the output of an AHP-based model when used for land suitability analysis. Multi-criteria decision making analysis is increasingly popular in natural resource management, with applications including land-use suitability analysis and the prediction of agricultural yields (Gamini and Prato, 2006). In the AHP approach, a hierarchy of weightings and ratings is derived from consideration of expert opinion and physical measurements. As a decision making tool, or intelligent decision aid, AHP-based models in particular are popular with natural resource managers. In the AHP method, eigen-value decomposition is applied to a matrix of judgements (given in numerical form) provided by decision makers against a set of alternatives. The procedure yields a set of priorities or relative weights indicating the decision makers' preference for the alternatives (Hahn, 2003). An example of the AHP flowchart is depicted in Figure 1 (Hossain et al., 2006; Sposito, 2006).

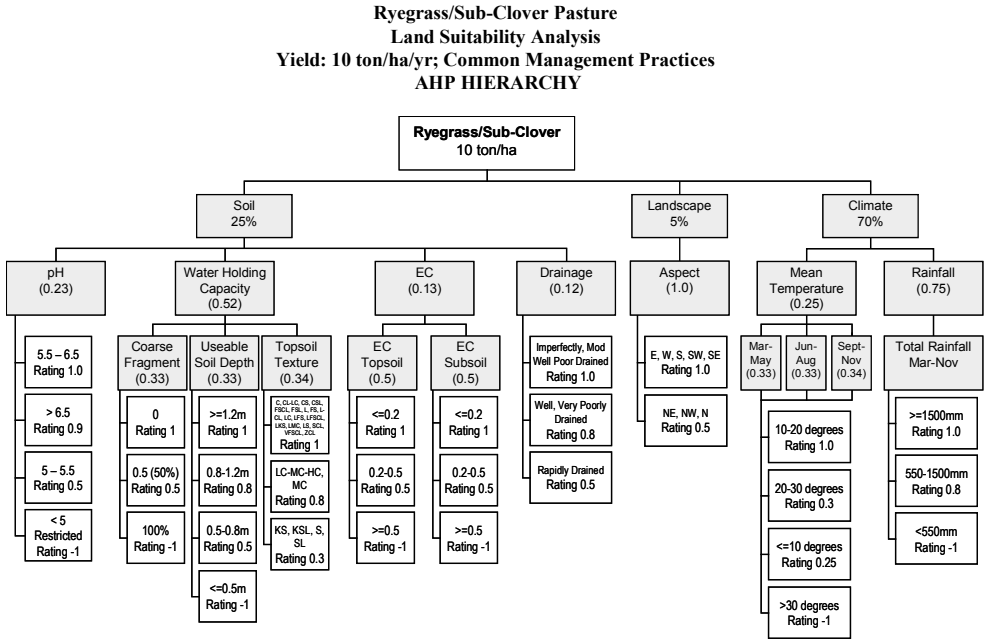

Figure 1 Experimental AHP flowchart structure (interim result for rygrass/subclover)

A problem with the deterministic AHP model is that the weightings represent imprecise point estimates (i.e. with no indication of error or confidence). The model prediction itself is also a point estimate without indication of error or confidence. Limited attempts at stochastic formulations for the AHP decision-making process for weights, have been described in several recent studies (Haines, 1998; Hahn, 2003; Jablonsky, 2005; Mustajoki et al., 2006).

3 Uncertainty Analysis

There are many sources of uncertainty in modeling predictions, including limitations of measurement devices, insufficient data, extrapolations and interpolations, linguistic ambiguity, and variability over space or time (see Table 1). In particular, uncertainty can arise from statistical variation or inherent randomness, systematic errors in judgement, imprecision and lack of agreement amongst experts (Cleaves, 1995).

Table 1 Sources of Uncertainty (Burgman, 2005)

General Uncertainty	Linguistic Uncertainty
Variability (population diversity)	Vagueness (fuzzy delineation)
Incertitude (or lack of knowledge)	Context dependence
Measurement error	Ambiguity (lack of clarity in expression)
Systematic error (bias)	Under-specificity (unwanted generality)
Natural variation (environmental change)	Indeterminacy (usage of terms)
Model uncertainty	—
Subjective judgement	—

Uncertainty is often reduced to a choice between two primary cases: either aleatory uncertainty or epistemic uncertainty (Helton, 1993; Helton, 1996; Hacking, 2001; Oberkampf et al., 2004).

Aleatory uncertainty refers to variability, irreducible uncertainty, inherent or stochastic uncertainty. It is associated with inherent variation in physical systems and is associated with population variability. This type of uncertainty may be modelled using an appropriate technique, such as Monte Carlo simulation (Helton, 1996). The term aleatory originates from the Latin aleator, relating to random choice or "dice player" (Soanes, 2005).

The second type of uncertainty is defined as epistemic uncertainty and refers to reducible uncertainty, or subjective uncertainty. It is associated with ignorance or incomplete information (lack of knowledge) and is a form of qualitative variability. The term is derived from the Greek episteme, relating to knowledge and its methods and scope (Soanes, 2005). The terminology is similar to that proposed by Oberkampf et al and is broadly consistent with that suggested by Helton and Burmaster (1996).

Helton (1993) refers to the two types of uncertainty simply as either stochastic (aleatory) or subjective (epistemic). This primary dichotomy represents convenience in terminology and is also the approach favoured here, although the words irreducible and reducible, respectively, may be even more effective (see Table 2). Ultimately, the most pragmatic distinction may well be simply statistical variability versus lack of knowledge, with linguistic uncertainty added in the appropriate context.

Table 2 Types of Uncertainty (Helton, 1993; Benke et al., 2007)

Aleatory	Type A	Stochastic	Irreducible	Variability
Epistemic	Type B	Subjective	Reducible	State of Knowledge

This dual approach is also favoured in the risk analysis literature by Vose (2000), who uses the terms variability (aleatory) or lack of knowledge (epistemic), but notes that they are often combined in analysis in many situations into "total uncertainty", especially when using Monte Carlo simulation. This lack of separation, however, may in some situations hinder attempts at investigating and reducing sources of uncertainty in a system output. Further division into sub-categories of uncertainty can be grouped under either of these two main types, with variations on this theme provided by Burgman (2005).

At this point, one may ask how does risk management relate to uncertainty? In many applications (such as ecology, hydrology or management of natural resources) one finds that risk is often defined as the product of the likelihood (or probability) of an adverse event and the consequence, i.e. risk = likelihood × consequence. In other applications, such as quantitative microbial risk assessment, risk may be defined simply as the probability of an adverse event (Benke et al., 2008a). Risk management can be viewed as a process dealing with the management of various hazards to the ambient environment. Qualitative risk management as characterised in national standards, such as those of Australia and New Zealand (AS/NZS 4360:2004), is based on subjective estimates of probabilities, whereas quantitative risk assessment is based on probability theory and statistical analysis (Burgman, 2005).

In contrast, uncertainty analysis embraces other issues beyond traditional risk definitions. These broader issues include the propagation of errors in predictive environmental models, which may occur in the inputs, outputs, parameters and model structure. Such issues require analysis of probability distributions rather than a risk specification based on a single imprecise probability or consequence. A deeper insight into the relationship between risk and uncertainty would see risk as the probability and consequence of an adverse event occurring, whilst uncertainty is related to the bound or confidence in the point estimate (of either probability or consequence).

4 AHP Model Predictions

For land suitability analysis, the challenge is to incorporate some measure of uncertainty or confidence in the predictions produced by the AHP model. Since a specific model is under investigation (using the analytic hierarchy process), the uncertainty in this case is treated as aleatory in nature. Aleatory uncertainty or variability is characterised by probability distributions. Metrics for quantification of uncertainty from the output distribution include variance (error), the confidence interval and percentile data. The numerical simulation-based approach adapted for use in this study is based on research in uncertainty associated with non-linear hydrological models and quantitative microbial risk assessment, see Benke et al. (2007, 2008a, 2008b). A feature of the approach taken is the iterative application of Monte. Carlo simulations to produce confidence intervals linked to predictions from a distributed spatial model.

Uncertainty in the AHP model is due to weights and ratings, which affect land suitability estimates. The uncertainty characterisation is possible by ① the use of Monte Carlo simulation in order to model variability in output due to variability in the weights and ratings, and ② statistical representation of weight errors due to expert opinion. The computational aspects of Monte Carlo simulation for risk assessment and uncertainty have been documented in greater detail in recent textbooks (Vose, 2000). The use of AHP for land suitability analysis is described in recent research (Hossain et al., 2006; Sposito, 2006), and invokes GIS-based spatial analysis and multiple criteria modeling.

5 Experimental Results

Workshops for AHP were conducted for ryegrass and winter wheat crops in the south western region of the state of Victoria and involved experts in farming, agricultural science and land-use research. The actual weights for the AHP flowchart for land suitability analysis were derived in the manner described by Hossain et al. (2006). The model output is either a percentage or decimal representing the degree of land suitability.

Monte Carlo simulations were carried out using the software package @RISK (Palisade Corporation, Newfield, New York). Sampling from input probability distributions was subject to the Latin Hypercube method, which executes stratified random sampling without replacement across the full range of each parameter (McKay et al., 1979; Iman and Conover 1983). The Latin Hypercube approach provides more uniform sampling in the tails of the chosen distribution than traditional random sampling and produces much faster convergence (Vose, 2000).

Uncertainty or variability in the weights due to expert opinion was represented using the PERT probability distribution (a variant of the Beta distribution), rather than the triangular distribution, due to its smoothness and continuity, and its greater weighting to the most likely values rather than to the tails (Benke et al., 2008b). Constraint satisfaction requires defined upper and lower bounds on weights and ratings, as defined by the AHP model inputs, and the unit-sum condition on weights to hold for each layer in the AHP hierarchy. Each Monte Carlo simulation experiment in the series was executed over 10,000 iterations. An example of one complete simulation for prediction of land suitability (LS) for the ryegrass/sub-clover workshop is depicted by the histogram in Fig. 2, and the associated cumulative probability distribution is shown in Fig. 3. Monte Carlo simulation outputs can sometimes be skewed, although this has no effect on the estimation of the confidence interval in this study as it is based on using percentile differences from the cumulative probability distribution (Benke et al., 2008b). From the plot shown in Fig. 3, percentiles and confidence intervals can be calculated for a single LS mean value.

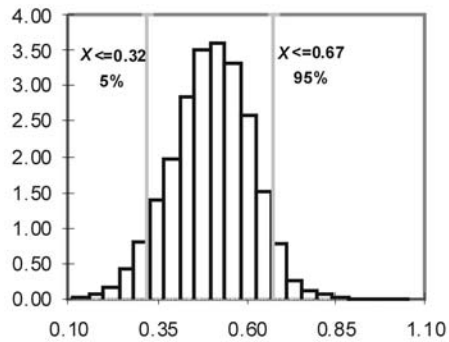

Figure 2 Histogram of output distribution for LS = 0.5 (ryegrass/sub-clover)

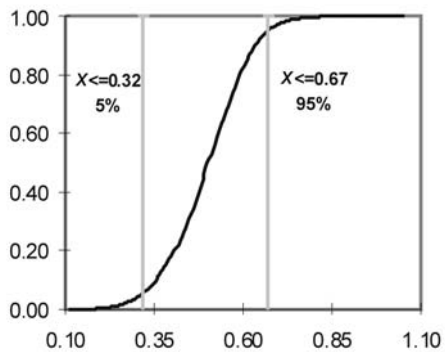

Figure 3 Cumulative probability distribution for LS = 0.5 (ryegrass/sub-clover)

Determination of percentiles and confidence intervals for a range of different LS values is achieved by executing a series of Monte Carlo simulations. In each simulation in the series, a different set of inputs was applied to the model and a corresponding probability distribution produced for land suitability. Both the weightings and ratings were represented by probability distributions. This process provided a set of model predictions for different levels of land suitability together with a corresponding set of probability distributions.

This step provides the required linkage between land suitability estimates and corresponding probability distributions. Once completed, graphical representation can then be used to provide some measure of visualisation of uncertainty. A series of Monte Carlo simulations were used to produce corresponding LS distributions for plotting the percentiles, with all linear regression fits statistically significant, as confirmed by the t-test on all correlation coefficients (r>0.999, p< 0.001). Figure 4 and Figure 5 show variability (uncertainty) about the mean of the LS values, in the form of the plotted percentiles (for ryegrass/sub-clover and winter wheat, respectively). From this calibration data, the 90% confidence intervals (CI) and the 5th, 20th, 80th and 95th percentiles can be extracted and associated with any given land suitability value referenced from the plot. This process therefore produces a numerical measure of error or variability for land suitability estimates, which is information that was not previously available.

6 Summary

The concept of uncertainty has been described and distinguished from traditional risk assessment, with a specific application to land suitability analysis. The predictive model used was based on the

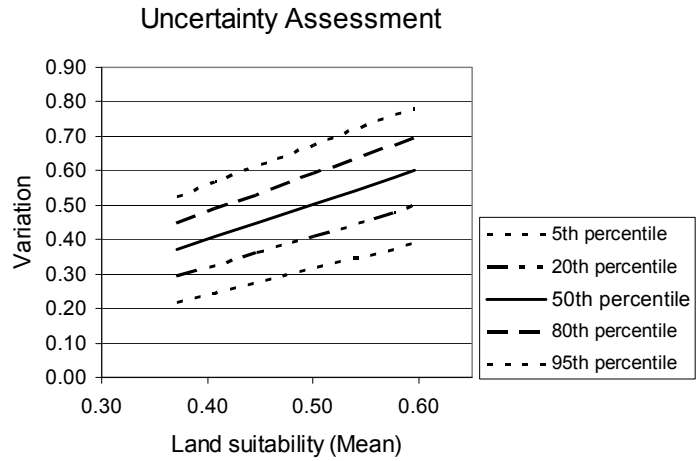

Figure 4 Uncertainty in AHP model land suitability predictions (ryegrass/sub-clover)

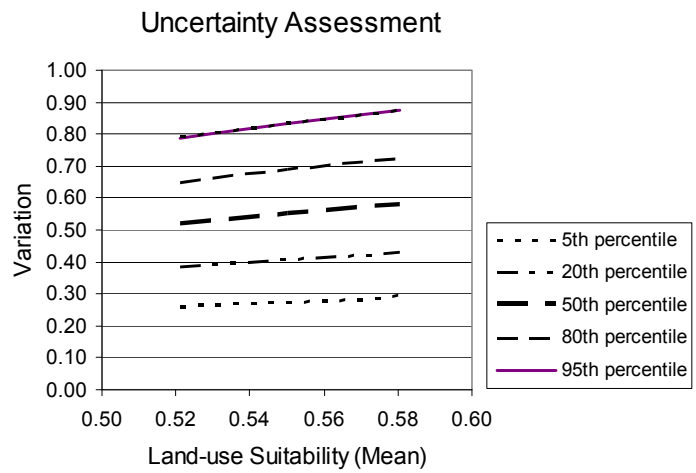

Figure 5 Uncertainty in AHP model land suitability predictions for test data (winter wheat)

AHP approach developed by Saaty (1994), and applied to land suitability analysis by others (Hossain et al., 2006; Sposito, 2006). The original deterministic AHP approach produces point estimates only, with no indication of error or confidence in the output. Uncertainty analysis for the AHP was adapted from various methods described in recent research (Benke et al., 2008a; 2008b).

Uncertainty analysis in the case of data variability requires representation by probability distributions for inputs, outputs or parameters. Variability in model inputs and outputs in this case is referred to as aleatory uncertainty (or statistical variation), as distinct from epistemic uncertainty, which refers to lack of prior knowledge or information on true model structure (Helton and Burmaster, 1996; Benke et al., 2007). The approach taken was to represent weights and ratings by probability distributions and to implement a series of Monte Carlo simulations. Variable weight values were subject to constraints of range and unit-sum for each level of the hierarchy in the AHP model.

Uncertainty in the form of variability is modelled quantitatively by using such metrics as variance, confidence intervals or percentile data. Estimates of the confidence intervals for the AHP approach were conservative due to the range of the feasible region. This approach produces a numerical indication of uncertainty in land suitability analysis that was not previously available from the traditional deterministic model.

References

Benke KK, Hamilton AJ, Lowell KE (2007) Modeling Uncertainty and Risk Assessment in the Management of Environmental Resources. Australasian Journal of Environmental Management 14:16 – 22.

Benke KK, Hamilton AJ (2008a) Quantitative Microbial Risk Assessment: Uncertainty and Measures of Central Tendency for Skewed Distributions. Stochastic Environmental Research and Risk Assessment, 22:533 – 539.

Benke KK, Lowell KE, Hamilton AJ (2008b) Parameter Uncertainty, Sensitivity Analysis and Prediction Error in a Water-Balance Hydrological Model. Mathematical and Computer Modeling, 47:1134 – 1149.

Burgman MA (2001) Flaws in Subjective Assessments of Ecological Risks and Means for Correcting Them. Australian Journal of Environmental Management 8:219 – 226.

Gamini H, Prato T (2006) Using Multi-Criteria Decision Analysis in Natural Resource Management, Ashgate Publishing Limited, Hampshire, England.

Hacking I (2001) An Introduction to Probability and Inductive Logic, Cambridge University Press, Cambridge (UK).

Hahn ED (2003) Decision Making with Uncertain Judgements: A Stochastic Formulation of the Analytic Hierarchy Process. Decision Sciences 34:443 – 466.

Haines LM (1998) A Statistical Approach to the Analytic Hierarchy Process with Interval Judgements. (I). Distributions on Feasible Regions. European Journal of Operational Research 110:112 – 125.

Helton JC (1993) Uncertainty and Sensitivity Analysis Techniques for Use in Performance Assessment for Radioactive Waste Disposal. Reliability Engineering and System Safety 42:327 – 367.

Helton JC, Burmaster DE (1996) Guest Editorial: Treatment of Aleatory and Epistemic Uncertainty in Performance Assessments for Complex Systems. Reliability Engineering and System Safety 54:91 – 94.

Hossain H, Sposito V, Evans C (2006) Sustainable Land Resource Assessment in Regional and Urban Systems. Applied GIS 2(3):24.1 – 24.21.

Iman RL, Conover WJ (1983) A Modern Approach to Statistics. New York, Wiley.

Jablonsky J (2005) Measuring Efficiency of Production Units by AHP Models. ISAHP 2005. Honolulu, Hawaii.

McKay MD, Conover WJ, Beckman RJ (1979) A Comparison of Three Methods for Selecting Values of Input Variables in the Analysis of Output from a Computer Code. Technometrics 21:239 – 245.

Mustajoki J, Hamalainen RP, Lindstedt MRK (2006) Using Intervals for Global Sensitivity and Worst-Case Analyses in Multiattribute Value Trees. European Journal of Operational Research 174:278 – 292.

Oberkampf WL, Helton JC, Joslyn CA, Wojtkiewicz SF, Ferson S (2004) Challenge Problems: Uncertainty in System Response given Uncertain Parameters. Reliability Engineering and System Safety 85:11 – 19.

Saaty TL (1994) Fundamentals of Decision Making, RWS Publications, Pittsburgh, USA. Soanes, C., Hawker, S. Compact Oxford English Dictionary, Oxford University Press, United Kingdom.

Sposito VJ (2006) A Strategic Approach to Climate Change Impacts and Adaptation. Applied GIS 2(3): 23.1 – 23.26.

Vose D (2000) Risk Analysis, John Wiley & Sons, Chichester, England.

Simulation of Spatial Variability of Organic Matter on the Vineyard Area Using the Model of Artificial Neural Networks

M. R. Karaman[1], M. Dursun[2], O. Karkacier[3], S. Şahin[1]

(1 Gaziosmanpaşa University, Agricultural Faculty, Tokat, Turkey, E-mail: rkaraman@gop.edu.tr)
(2 Gazi University, Technical Education Faculty, Ankara, Turkey, E-mail: mdursun@gazi.edu.tr)
(3 Gaziosmanpaşa Univ. Economics and Administrative Sci. Faculty, Tokat, Turkey,
E-mail: oskar@gop.edu.tr)

Abstract: Careful monitoring of an agricultural area has great importance for the managing of three main objectives (economics, society, environment) of sustainable agriculture. Understanding of site specific factors influencing yield will make valuable contributions to these objectives for effective decision-making on the beneficial use of soil resources. On the other hand, easy measuring levels without expensive should be developed for determining of more precise relationships among the site specific factors. In this study, simulations of spatial variability of organic matter contents of soils on the vineyard area were made using the model of Artificial Neural Networks (ANN). ANN is modeling method which is improved by the inspiration of brain physiology of human beings. The method is generally successful in issues such as model selection and classification. For this aim, topsoil ($0-30$ cm), subsoil ($30-60$ cm) and plant samples based on a 20×20 m grids were collected from the plots under the vineyard plants. The study area was modeled with 5 meters period, and generally non linear organic matter value of soil has been modeled by using ANN. A program was build by C++ programming language to solve data by ANN method. As a result, the coefficient of variance (C.V.), kurtosis and skewness values revealed that considerable spatial variability occurred in organic matter contents of soils. Hence, uniform nitrogen (N) fertilizer managements based on an average soil organic matter level will result in increasing unequal soil N distribution and unbalanced plant N consumption. Hence, simulation results showed very good agreement with the measured results. It has been figured out that ANN based modeling will be alternative for other modeling methods. It has also been revealed that the problems for intensive soil samplings depending on site specific variability could be decreased by using the model of ANN. It will be valuable for the sustainability of agro-ecosystems, and more realistic crop nutrition modeling and decision support on farm applications.

Keywords: artificial neural network, simulation, organic matter, vineyard area

1 Introduction

Sustainable agriculture means to protect the environment for the benefit of future generations. Managing of an agricultural area should be included conserving natural resources. Careful monitoring of an agricultural area has great importance for the managing of sustainable agriculture. In this respect, site-specific farming aims to improve crop production efficiency and reduce environmental effects of agricultural chemicals by adjusting farming inputs (e.g., fertilizer, pesticide, and seeds) to the specific conditions within each area of a field (Mermer et al., 2000). Understanding of site

specific soil factors influencing yield will make valuable contributions to effective decision-making on the beneficial use of soil resources.

Local soil fertility status of an agricultural area is one of the important criteria for sustainable agriculture. In this aspect, local nitrogen (N) needs of plants are essential for balanced nutrition of the crops. It is well documented that fertilizers applied to crops are a potential source of nutrient enrichment to surface waters (Myers et al., 1985). Nitrogen fertilizers is also a potential contaminant of groundwaters, it can greatly contribute nitrate to groundwater reservoirs. Fertilizer recovery by crops with conventional farming systems is generally far from complete, with about 50 percent recovery of N (Power, 1983). Thus, all resources of N such as soil organic matter (O.M.) must be considered for environmental aspect and economical gain. One the other hand, it has been revealed that raising the percentage of organic matter from 1% to 2% in sandy soil increased the available water content of that soil by 60% (Hudson, 1994). Water-holding capacity of soils will have a beneficial effect on crop growth, especially during droughty periods. Thus, site specific O.M. status of agricultural area is valuable not only for plant nutrition but also for many parameters required optimal crop production. Hence, accurate determination of site specific O.M. levels is essential for profitable N management decisions and local N needs of crops.

Geostatistic has been used for the design of maps defined the spatial variability of soil properties required for precision agriculture. In precision farming, some mathematical interpolation methods such as local average, contouring or kriging are commonly used for predicting the variables involved with elaboration of fertility maps. However, these methods may present different fertility maps for the same data set (Ulson et al., 2000). Hence, considerable relation has recently been given to the investigation of the studies based on new Technologies. For example, ANN has recently been used to generate soil pedotransfer functions and mapping (Ceddia, 2006).

There are a lot of research about predict of soil nonlinear specials or other agricultural predictions based on Artificial Neural Networks (Fausett, 1994; Drummond et al., 1998; Hurtado et al., 2001; Schmitz et al., 2005; Uno et al., 2005; Delon et al., 2007). In this study, spatial variability of soil O.M. levels on the vineyard area was simulated using the model of Artificial Neural Network. ANN are the computer programs which are improved by the inspiration of brain physiology of human beings. The most important advantage of these predictions based on ANN methods is time saving and cost effective (Behrens et al., 2005). It will also be valuable for the sustainability of agro-ecosystems, and more realistic crop nutrition modeling.

2 Materials and Methods

Simulations of spatial variability of soil O.M. contents on the vineyard area were made using the model of ANNs. For this aim, topsoil (0 – 30 cm) and subsoil (30 – 60 cm) samples based on 20× 20 m grids were taken from the plots under the vineyard plants. The air dried soils were secreened to pass through a 2 mm mesh. Plant samples were also collected from the same plots together with soil samplings. The analysis for N concentration in the top of plant samples was made according to Chapman and Pratt 1961. In the soil samples, O.M. content was determined by the method of Walkley-Black 1947 and available phosphorus analysis was made by the method of Olsen et al., 1954. Saturation percent, electrical conductivity (E.C.) (Richards, 1954), $CaCO_3$ (Allison and Moodie, 1965) and pH (Jackson, 1958) analyses were also made for both topsoil and subsoil samples. Experimental data were subjected to the statistical analysis using StatMost package program (StatMost, 1995).

In ANNs model used for this study; each neuron performs two functions (Dursun and Karaman, 2008). The general concept of this model as below (adopted from general concepts): the first is to

sum all the inputs from lower layer based on their weighting factors as given in Eq. (1). The second is to process this sum by a nonlinear sigmoid function as shown in Eq. (2). The input and output neurons may not contain nonlinear functions. The basic equations describing the dynamics of each neuron are;

$$\text{net}_j = \Sigma_i W_{ij} O_i \tag{1}$$

$$O_j = f(\text{net}_j + \theta_j) \tag{2}$$

Where W_{ij} weight between the jth neuron and the ith neuron in two adjacent layers, θj threshold of the jth neuron, O_i output of the ith neuron, O_j output of the *j*th neuron, $f(.)$ sigmoid function. Such a neural network contains three layers: input layer, hidden layer(s) and output layer. Each layer is composed of several neurons. The number of neurons in the input and output layers depends on the system dynamics and the desired accuracy. All the neurons in adjacent layers are interconnected. The strength of the interconnection was determined by weighting vector of NN (Rumelhart et al., 1986). The most common method of NN training is back error propagation algorithm. The algorithm is based on the gradient search technique that minimisation process is done by adjusting the weighting vector of the NN. Let the objective function (E) could be write as;

$$E = \frac{1}{2} \sum_p \sum_j \left(T_{pj} - O_{pj} \right)^2 \tag{3}$$

Where T_{pj} is the target output of neuron j due to input pattern p. O_{pj} is the NN output of the same neuron and for the same pattern. Minimising Eq. (3) leads to a sequence of update of the weight vector. The weights of the interconnections between two adjacent layers could be updated based on the following formula:

$$W_{ij}(k+1) = W_{ij}(k) + \eta \frac{\delta E}{\delta W_{ij}(k)} + \alpha \Delta W_{ij}(k) \tag{4}$$

Where k is the iteration number, η is the step size, α is the momentum gain and ΔW_{ij} (k) is weight change based on the gradient of the cost function (Maren et al., 1990; Narendra et al., 1990; Yıldırım et al., 1996). In this study, the area was modeled with 5 meters period, and generally non linear O.M. value of soil has been modeled by using ANN (Fig. 1). A packet program has been prepared which can be used for the training of the systems with a input layer of fifteen inputs and a output layer of maximum ten outputs for the training of ANN by using the C++ Program Language. In the prepared program, one input layer, four hidden layers and one output layer are allowed (adopted from general concepts).

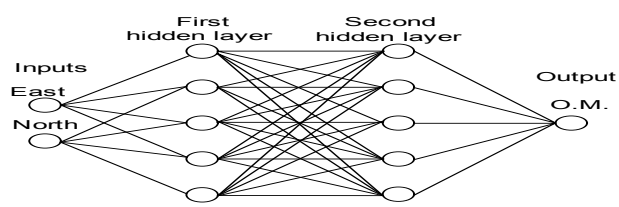

Figure 1 Modeling of soil O.M. by ANN

After the determination of the systems network structure, training of network began with determining learning coefficient which was used for the training, momentum coefficient and entering the numbers of data samples. In order to see the performance of ANN model for simulations, measured data curves have been compared with the curves obtained after the ANN training (Dursun and Karaman, 2008).

3 Results and Discussion

Spatial variability of selected site specific physical and chemical properties such as saturation percent, pH, $CaCO_3$, E.C., O.M. and available phosphorus (P) values for topsoils and subsoils on the vineyard area were presented Tables 1 and 2, respectively.

Table 1 Spatial variability of site specific physical and chemical properties for topsoils

Parameters	Min.	Max.	Mean	C.V. %	Kurtosis	Skewness
Saturation, %	26.00	53.00	40.40	18.85	−0.941	−0.061
pH, 1:5	7.98	8.27	8.12	1.10	−1.320	−0.146
$CaCO_3$, g kg^{-1}	9.58	24.18	17.47	20.79	−0.472	−0.320
E.C., µmhos cm^{-1}	181	479	332	23.50	−0.266	−0.031
O.M., %	1.95	3.49	2.69	14.33	−0.179	−0.015
P, kg P_2O_5 da^{-1}	9.56	41.45	22.74	36.41	−0.487	0.239

Table 2 Spatial variability of site specific physical and chemical properties for subsoils

Parameters	Min.	Max.	Mean	C.V. %	Kurtosis	Skewness
Saturation, %	32	57	46	18.36	–1.337	–0.463
pH, 1:5	7.95	8.37	8.10	1.43	0.085	0.851
$CaCO_3$, g kg^{-1}	13.41	27.71	19.75	20.53	–1.076	0.314
E.C., µmhos cm^{-1}	229	485	365	14.63	1.062	–0.443
O.M., %	0.90	1.96	1.50	17.50	0.386	–0.696
P, kg P_2O_5 da^{-1}	3.95	13.03	8.50	33.06	–1.240	0.023

The coefficient of variance (C.V.), kurtosis and skewness values indicated that a great spatial variability occurred for selected site specific properties of the soils. The maximum C.V. value of 36.41 % was measured for available P value in the top soil. The C.V. value of 33.06 % for P value was less than that of top soil. The C.V. values of O.M. were 14.33 % and 17.50 % for topsoil and subsoil, respectively. The O.M. values were varied from 1.95 to 3.49 % for topsoil, whereas the values were between 0.96 – 1.96 % for subsoil. Three dimensional and contour maps of site specific O.M. for topsoil and subsoil of the vineyard area indicated the importance of spatial variability of soil O.M. (Figs. 2 and 3).

The results have revealed that uniform N fertilizer managements based on an average soil O.M. levels will result in increasing unequal soil N distribution and unbalanced plant N consumption. The findings clearly showed that the site specific O.M. level in the vineyard soil was important factor for maximum N utilization by the vineyard plants. Thus, fertilization programme based on site specific N demands of the plants will increase N use efficiency of the plants with proper N rates. ANN based simulated and measured values for site specific soil O.M. and plant N levels on the vineyard area were presented Table 3. As it is seen from simulated and mesured values, simulation results based on ANN model showed very good agreement with measured results (Table 3). It has been figured out that ANN based modeling could be a good alternative for other methods. It has

also been revealed from similar studies that good results were obtained from ANN models for predicting texture parameters, some chemical components (CaO, K_2O), organic matter and pH (Lahoche, 2002). In other studies, ANN methods have been applied for elaboration and identification of precise fertility maps which can reduce the production costs and environmental impact (Ulson et al., 2000). The results of some other studies based on ANN method for variable-rate fertilization also showed that the model could property describe the fertilizer demand and provide optimum scheme of fertilizer application for every fertilizing unit (ChengLin et al., 2004).

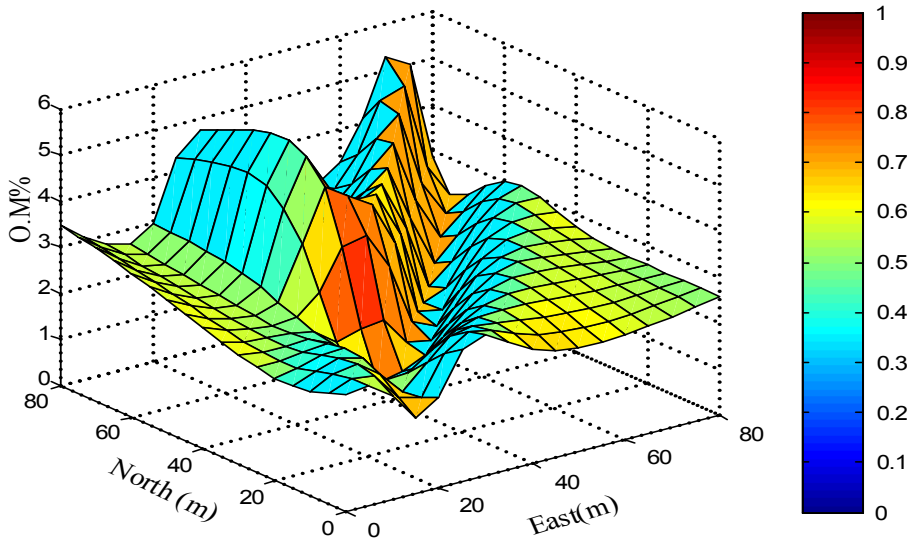

(a) Topsoil

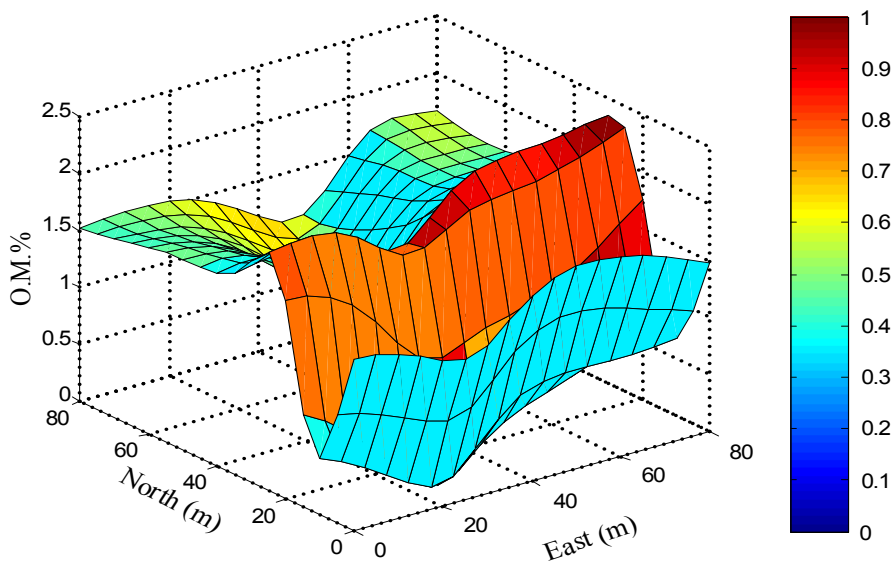

(b) Subsoil

Figure 2 Three-dimensional maps of site specific O.M. levels for topsoil and subsoil, %

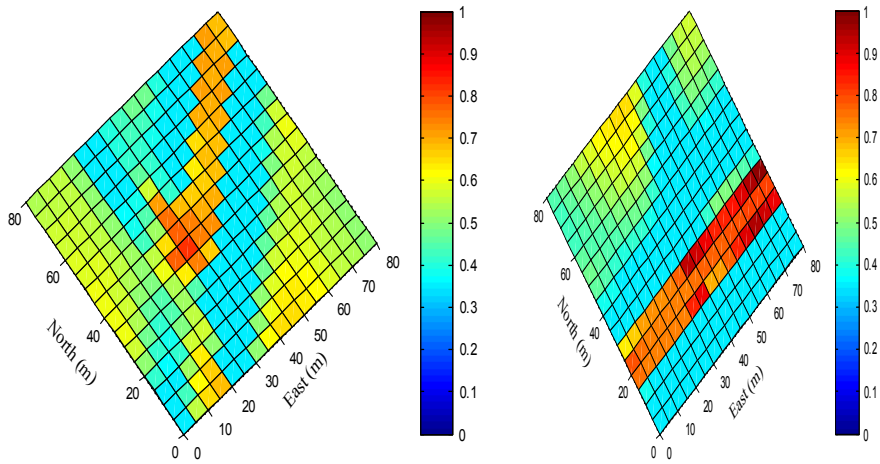

(a) Topsoil (b) Subsoil

Figure 3 Contour maps of site specific O.M. levels for topsoil and subsoil, %

Table 3 Simulated and measured values for site specific soil O.M. and plant N levels, %

East (m)	North (m)	Simulated Topsoil O.M.	Measured Topsoil O.M.	Simulated Subsoil O.M.	Measured Subsoil O.M.	Simulated Plant N	Measured Plant N
0	0	2.539996	2.540000	1.519897	1.520000	2.119900	2.120000
0	20	1.970009	1.970000	1.280095	1.280000	1.852082	1.852000
0	40	2.490035	2.490000	1.629922	1.630000	1.729903	1.730000
0	60	2.280086	2.280000	1.760053	1.760000	2.040242	2.040000
0	80	2.560001	2.560000	1.480022	1.480000	1.919847	1.920000
20	0	2.229761	2.230000	1.750033	1.750000	1.820184	1.820000
20	20	1.949981	1.950000	1.339936	1.340000	2.210027	2.210000
20	40	2.380027	2.380000	0.929999	0.930000	2.159927	2.160000
20	60	2.709950	2.710000	1.200045	1.200000	1.898779	1.900000
20	80	2.570106	2.570000	1.750033	1.750000	1.881396	1.880000
40	0	2.640469	2.640000	1.690327	1.690000	2.059826	2.060000
40	20	2.330011	2.330000	1.559703	1.560000	2.249902	2.250000
40	40	2.920007	2.920000	1.320122	1.320000	2.209680	2.210000
40	60	2.559961	2.560000	1.870058	1.870000	2.135868	2.130000
40	80	2.729928	2.730000	1.959843	1.960000	2.092721	2.100000
60	0	3.139619	3.140000	1.639347	1.640000	2.540028	2.540000
60	20	2.850068	2.850000	1.400962	1.400000	1.999846	2.000000
60	40	3.210026	3.210000	0.899637	0.900000	1.949775	1.950000
60	60	2.760001	2.760000	1.579691	1.580000	2.092760	2.100000
60	80	3.020033	3.020000	1.600298	1.600000	2.098696	2.090000
80	0	3.490145	3.490000	1.520449	1.520000	1.800020	1.800000
80	20	2.999976	3.000000	1.539267	1.540000	1.940193	1.940000
80	40	2.749986	2.750000	1.180184	1.180000	2.149996	2.150000
80	60	3.269990	3.270000	1.490175	1.490000	1.873089	1.870000
80	80	2.879998	2.880000	1.669875	1.670000	1.996665	2.000000

* O.M. values; very low= < 1 %, low = 1–2 %, medium= 2–3 %, sufficient= 3–4 %, and high= >4 %

Hence, the ANN method will be successful for determination of site specific data classifications. It has also been revealed that the problems for intensive soil samplings depending on spatial variability could be decreased by using these methods. It will be valuable for more realistic crop modeling and decision support leading to on-farm applications.

References

Allison L E, Moodie C D (1965) Carbonate, In: Methods of Soil Analysis, Part 2. Agronomy J. 9:1379 – 1400.

Behrens S, Förster H, Scholten T, Steinrücken U, Spies E D, Goldschmitt M (2005). Digital soil mapping using artifical neural networks, Journal of Plant Nutrition and Soil Science 168 (1): 21 – 33.

Caglar N, Arman H (2007) The applicability of neural networks in the determinationof soil profiles, Bull Eng Geol Environ 66:295 – 301.

Ceddia M B, Varella C A, Vieria S, Pinto F A (2006) Artificial Neural Network to Map Spatial Variability of Field Capacity. 18th World Congress of Soil Science, July 9-15, Philadelphia, Pennsylvania, USA.

Chapman H D, Pratt F P (1961) Methods of Analysis for Soils, Plants and Waters, Univ. of California Div. Agr. Sci. USA.

ChengLin M, CaiCong W, ShuHui Z, YinSheng Y, HongWei L, YunXia H (2004) Decision making method for variable-rate fertilization based on data envelopment analysis and artificial neural network. Transactions of the Chinese Society of Agricultural Engineering 20 (2):152 – 155.

Delon C, Serca D, Boissard C, Dupont R, Dutot A, Laville P, Rosnay P, Delmas R (2007) Tellus 59 (3): 502 – 513.

Drummond S T, Joshi A, Sudduth K A (1998) Application of Neural Networks: Precision farming. p. 211 – 215. In Proc. Int. Joint Conf. on Neural Networks, WCCI 98, Anchorage, AK. 4-9 May. IEEE Press, Piscataway, NJ.

Dursun M, Karaman, M R (2008) Artificial neural network based modeling of spatial distribution of phosphorus on the tomato area. Asian Journal of Chemistry. (Accepted for Publication), Manuscript No: 7414 – 2007.

Fausett L V (1994) Fundamentals of neural networks: architectures, algorithms, and applications, Prentice-Hall, Englewood Cliffs.

Hudson B E (1994) Soil organic matter and available water capacity. Journal of Soil and Water Conservation 49 (2):189 – 194.

Hurtado J E, Londonñ o J M, Meza M A (2001) On the applicability of neural networks for soil dynamic amplification analysis, Soil Dyn Earthq Eng. 21 (7):579 – 591.

Jackson M L (1958) Soil Chemical Analysis. Prentica-Hall Inc., Englewood Cliffs, New Jersey, USA.

Lahoche F, Godard C, Fourty T, Lelandais V, and Lepoutre D (2002) An innovative approach based on neural networks for predicting soil component variability. Proceedings of the 6th International Conference on Precision Agriculture and Other Precision Resources Management, Minneapolis, MN, USA, 14-17, July

Lin, CT, and Lee CS (1991) Neural network based fuzzy logic control and decision systems, IEEE Trans.Com, 40, 1320 – 1336.

Maren CH, Pap R (1990) Handbook of Neural Computing Applications, (Academic Press, London) ISBN 0 – 12 – 471260 – 6.

Mermer A, Piant R E, Pettygrove S (2000) Spatial variability of grain yield and soil properties in three wheat fields. ESRI EMEA-2000 European, Middle Eastern and Africian User Conference 18-20 October, Istanbul-Turkey.

Myers C F, Meek J, Tuller S, Weinberg A (1985) Nonpoint sources of water pollution. J. Soil Water Conservation 40:14 – 22.

Narendra K S, Parthasarathy K (1990) Identification and control of dynamical systems using neural networks', IEEE Trans. on. Neural Networks, 1, pp 4 – 27.

Olsen S R, Cole C V, Watanable F S, Dean L A (1954) Estimation of available P in soils by extraction with sodium bicarbonate. Agricultural Handbook, U.S. Soil Dept. 939, Washington D.C.

Power J F (1983) Research in agricultural ecosystems, North Central United States. In: Nutrient Cycling in Agricultural Ecosystems, R. Lowrance, R. L. Todd, L. Ausmussen, and R. Leonard (eds.). p. 121-133. Coll. of Agric. Spec. Publ. 33, University of Georgia, Athens.

Richards L A (1954) Diagnosis and improvement of saline and alkaline soils. USDA Agricultural Handbook, 60, Washington, DC.

Rumelhart D E, McClelland J L (1986) Parallel Distributed Processing. Vol. 1, The MIT Press, Cambridge.

Schmitz G H, Phulmann H, Dröge W, Lennartz F (2005) Artificial neural networks for estimating soil hydraulic parameters from dynamic flow experiments. European Journal of Soil Science 56 (1):19 – 30.

StatMost (1995) Dataxiom Software Inc. User's Guide: StatMost. 5th Ed. Dataxiom Soft. Inc., LA., USA.

Uno Y, Prasher S O, Lacroix R, Grel P K, Karımı Y, Viau A, Patel R M (2005) Artificial neural networks to predict corn yield from compact airborne spectrographic imager data. Computers and Electronics in Agriculture 47 (2):149 – 161.

Ulson J A C, Nunes da Silva I, Benez S H, Boas R L V (2000) Modeling and identification of fertility maps using Artificialneural Networks. IEEE International Conference. Vol:4, pp. 2673 – 2678.

Walkley A (1947) A critical examination of a rapid method for determining organic carbon in soils: effect of variations in digestion conditions and inorganic soil constituents. Soil Sci. 63:251 – 263.

Yıldırım S, Sukkar M F, Demirci R, Aslantas V (1996) 'Design of adaptive NNs-Robust-PID controller for a robot control' Proceedings of IEEE Int. Symposium on Intelligent Control, Michigan, USA, pp.508 – 513.

Youngil L, Young-Sil M, Tae-Wan K (2007) Artificial neural network approach for prediction of ammonia emission from field-applied manure and relative significance assessment of ammonia emission factors, Elseiver European Journal of Agronomy 26:425 – 434.

Ziad R L, Philip K H, Mara J J, Kate M S (2005) Application of PLS and Back-Propagation Neural Networks for the estimation of soil properties, Elseiver Sci. Direct, Chemometrics and Intelligent Laboratory Syst., 75:23 – 30.

Integration of a Crop Simulation Model and Remote Sensing Information

M. Acutis[1], M. Rinaldi[2], F. Mattia[3], A. Perego[1]

(1 University of Milano, Department of Crop Science, Via Celoria, 2 - 20133 Milano, Italy,
Corresponding author E-mail: marco.acutis@unimi.it)
(2 Agricultural Research Conucil (CRA) – Research Unit for cropping systems in dry environments (SCA),
via Celso Ulpiani, 5 – 70125 Bari, Italy; Tel. +39 080 5475016; Fax +39 080 5475023;
E-mail: michele.rinaldi@entecra.it)
(3 ISSIA-CNR, via Amendola, 122/D–70126 Bari, Italy; E-mail: mattia@ba.issia.cnr.it)

Abstract: The monitoring of irrigation requirements at district or regional scale can be based on the use of ecological process-based models and remote sensing data. The former simulates the time evolution (usually at daily scale) of the main biophysical variables which determine crop photosynthesis and water consumption rates; the latter allows to provide the spatial distribution of these variables over a region of interest at a time interval ranging from few days to one month. The evaluation of water balance components and, in particular, the estimate of actual evapotranspiration and the partitioning between soil evaporation and plant transpiration, are crucial issues in semi-arid regions where the scarcity of water resources is becoming an important limiting factor crop growth and yield. The research focused an integrated approach to combine field data, simulation crop model and remote sensing information.

Historic data about topography, soil, climate and land cover were collected and organised into a Geographic Information System, which is routinely updated with remotely sensed images. A mechanistic crop growth model has been coupled with the dynamic soil water balance and root uptake model based on finite difference solution of Richards' equation in order to describe accurately the main crop physiological processes, the soil water fluxes at the interfaces groundwater-soil and soil-atmosphere and water re-distribution in the soil profile. The integration of these two models allows for an improvement of results accuracy for the crop types considered in this study in Mediterranean environmental conditions. Remote sensing images from optical and radar satellite sensors at different spatial scales (from 10 to 50 m) have been collected during crop cycles. Information about land use and leaf area index will be assimilated dynamically by the model, to increase the effectiveness of simulation.

The final product is a Decision Support Systems with the purpose to integrate remote sensing images, to estimate crop and soil variables related to drought, to assimilate these variables into a simulation model at district scale and, finally, to estimate evapotranspiration, plant water status and drought indicators. The structures of the model and Decision Support System are described and the first results of the field and simulation activity are reported.

Keywords: decision support system, leaf area index, simulation model, field crops, data assimilation

1 Introduction

The proper irrigation water management is a hanging requirement, due to the continuous decreasing of the water source availability, especially in Mediterranean environment and in those characterized

by water limited availability (Tuberosa et al., 2007). Precipitation decreasing (Piccarreta et al., 2006) and industrial and civil water demand, especially in development areas, involve a source limited use. Moreover this concern is expected to concern increase according to the climate change forecast (Alcamo et al., 2007). The agricultural economic sustainability mainly in Mediterranean environments, in terms of food production and high quality research, most frequently forces the irrigation water requirement. Among main crops only durum wheat crops and autumn-winter cereals do not require water supply (even if in Northern Africa they are often irrigated, Oweis et al., 1998); in fact, others herbaceous and tree crops provide sufficient economic results only if irrigated.

Further involvements are related to the water cost increasing, due to the competition with other sectors. The reduction of water availability and the increase of its cost can be faced only with rational management of the water resources that includes the prevention of water wasting and losses, but also the use of all the technical resources to increase the global water use efficiency. One of the key points for improving the water use efficiency is to develop a procedure for optimal irrigation scheduling, where irrigation timing and volumes are calculated in a way to avoid at the same time plant water stress and losses due to water percolation below the rooted zone.

At field scale it is possible to obtain an optimal irrigation scheduling through the compilation of hydrologic balance, also with help of simple software (Raes et al., 2006) or through the direct measure of the soil water content or the water potential in soil, it is difficult to extend this methods at lager scales, mainly for the lack of information about land use and crop management. Due to this lack, it is fundamental to employ external information facilities in order to integrate pedological maps and meteorological data available in real time. Therefore remote sensing images are able to provide estimated values of crop biomass (Launay et al., 2005), Leaf Area Index (Hoffmann et al., 2004) and detect planted crops at certain time steps (Blaes et al., 2005). Moreover they are suitable to provide estimated sowing date and shallow soil water content. All these information can be assimilated into a simulation crop model to improve simulation (Dente et al., 2006; 2008)

This research is part of a workpackage of AQUATER project (Rinaldi et al., 2005), which develops an integrated methodological approach in order to improve irrigation water management and provide strategies at territorial scale, employing remote sensing and observed data, in Mediterranean area, characterized by irrigated high-value cropping systems. The developed approach could be deployed in territorial planning as decisional support tool. It is based on innovative technologies such as remote sensing, simulation crop models, GIS (Geographical Information System) to handle distributed meteorological, soil and crop parameters.

The aim of this study is to outline the AQUATER software for the water management optimization in Mediterranean field cropping systems.

2 Materials and Methods

2.1 Software Implementation Technologies

In order to develop a software suitable for actual scenarios, several information requirements are to be respected, besides conceptual accuracy in systems representation, to guarantee reliability, quality, easy updating procedures, maintenance and extensibility of the developed software. At the development beginning, functional requirements are to be identified accurately, according to the standard methodologies of the software architecture definition as the rational unified process (RUP), (Kruchten, 2001). Technologies related to “Agile” (Cohen et al., 2004) development approach are more suitable to be adopted because the software production indeed represents an opportunity of application, test and definition of the scientific knowledge. “Agile” approach allows for frequent releases outflow. The releases are tested deploying real data set, allowing for the scientific concepts

development and also user interaction. The software implementation requires an object oriented language; the software development was based on the Unified Modeling Language (UML) that has demonstrated to be an excellent base for handle complex multiple cell models (Ferrara and Rana, 2006). The software is developed employing, when possible, existing free modules and components. The software frame derives from the integration of interchangeable and extensible components (Rizzoli et al., 2005). The software has been developed for "Net" environment using VBNet and C# programming languages.

2.2 Requirements Analysis

The software has to respect several requirements not yet completely developed. New requirements can be added, while others can get not necessary. The reliability to describe different HRUs (Hydrologic Response Units), characterized by specific soil, crop types and weather data, is the first requirement for a territorial scale software analysis (Flügel, 2006). HRUs, even not geographically contiguous, can be characterized by the same data set. Table 1 shows a set of software requirements, divided in functional categories.

Table 1 Functional requirements of the software

Data access	Modeling	Output report	"What-if" analysis
Specific soil parameters and meteorological data have to be provided to each HRU (Hydrological Response Unit)	Simulation crop water requirement and consumption using FAO56 methodology or trough direct estimation of crop resistance	Water requirement and consumption report at territorial scale	Evaluation of crop and water management based on historical data
Real time updating of meteorological data	Soil water dynamics using Cascading, ISBA or Richards' equation	Production of shape files for the main water and crop variables	—
Real time access to remote detection information for forcing and assimilation	Simulation of development and growth of main Mediterranean field crops	Real time HRU specific alerts of water stress condition	—

2.3 Simulated Processes

The software simulating the crop growth and development implemented here, is based on the STAMINA model (Acutis et al., 2007, Richter et al., 2006). The model is based on gross assimilation of CO_2 and on maintenance and growth respiration to get the final net carbon assimilation. This kind of simulation tools are known as the "School of de Wit" crop models (van Ittersum et al., 2003).

Examples of this type of model are SUCROS (Van Keulen et al., 1982) and the derived WOFOST (Van Keulen and Wolf, 1986; Boogaard et al., 1998). Respect to SUCROS and WOFOST, Stamina model has been improved for the simulation of the seed germination and emergence, implementing the specific software module "GEme" (Bechini et al., 2004) and for better details in the simulation of radiation interception within the canopy. Effect of water stress (1) is simulated according to Sinclair (1986) and Richter et al. (2001), as follows:

$$f_{\text{stress}} = \frac{2}{1+\exp\{-f_{\text{d}}(q_{\text{rel}})\}} - 1 \tag{1}$$

where f_{stress} is a reduction factor of the gross CO_2 assimilation, q_{rel} is the ratio between the actual soil water content and the soil water content at saturation and f_d is a specific factor (range 4 – 14) depending by crop, sensitivity to water stress and development stage.

Root water uptake is simulated in way allowing compensation of the different water availability at different depth in soil. The model has three options to simulate water redistribution into the soil; default option is the finite difference resolution of the Richards' equation according to van Dam and Feddes (2000), as in the SWAP model. This simulation offers the best performance in the soil water content simulation, according to their strong physical basis, and is supported by a high number of researches and application, so can be preferred to others options. The main limitation of this approach is the long time required for simulation; this can create difficulties when the number of hydrologic units to simulate is large and the simulation period is particularly long. The application of the finite difference Richards' equation solution to one hydrologic unit, for one growing season is about 30", using a 2 GHz Pentium dual core processor.

When simulation times become too long, two other approaches are available: the cascading (tipping-bucket model) and the ISBA approach (Noilhan and Planton, 1989). ISBA is based on forcing–restoring of soil water content and can be derived from the Richards' equation with some simplification. Soil is divided in two layers, the first one of few centimetres (usually 10), subject to evaporation process, and the second one of 100 cm. ISBA cannot simulate the effect of root growth in depth and the effects of a shallow water table (usually it is not the case in Mediterranean environments). Cascading approach is the fastest, and even if this approach does not have a strong physical base, can be sufficient in soil where the textural differences among soil horizons are not too much evident. Other limits of cascading approach is the impossibility to simulate water contents greater than the field capacity and the effects of a water table, so is not well suitable in soil with low permeability.

2.4 Real Time Access to Remote Detection Information for Forcing and Assimilation

Different remote detection information can be used in simulation analysis. If it is possible to get information about land cover, LAI and crop sowing (or transplant) date, then remote detection information can be used in forcing procedure, based on LAI detected values. The model computes a new value of leaves weight, function of the specific leaf area (SLA) simulated value; from leaf weight the biomass of the others part of the plant is computed thorough partition coefficients of dry matter among the different plant organs (that model compute for each phenological development stage), and consequently, the total plant biomass. Determination of sowing date from the first value of LAI obtained by remote sensing is under study. In fact, there are no theoretical difficulties in assimilating a LAI data (it is sufficient to restart the growth model in different dates, and, within this interval, to select the data that allows the better simulation of the LAI given by remote sensing), but the effectiveness of this approach is under evaluation, because errors in the remote sensing measure and model approximation reduce the practical value of this approach. The crop pertaining to each HRU is an external input, based on farmer information. Because frequently there are errors in the identification of the crop, model is able to restart when image analysis indicates that the crop effectively present in a specific HRU is not the one declared in input.

3 Results and Discussion

3.1 Model Calibration and Validation

The "Stamina" crop growth model has been used in previous application in Southern Italy conditions and for irrigated field crops, also evaluating the capability to simulate drought conditions. The

following tables, derived by Richter et al. (2006), report good evaluation indexes of the comparison "simulated vs. measured" with the model used in this research for autumnal sugar beet.

Table 2 shows as, for autumnal sugar beet, a not easy to model crop, the modeling efficiencies for plant and root biomass resulted higher than 0.95 and, in general very satisfactory. This consideration is applicable also to the simulation of leaf area expansion. The values reported in Table 3, about sugar beet irrigated according to different irrigation scheduling and with different water stress levels, confirmed the model capability to simulate sugar beet also in water stress conditions, nevertheless modeling efficiency for LAI fall down quickly. Really in this situation the assimilation and forcing of LAI deriving from external information could be very important and effective.

Table 2 Evaluation indexes of "Stamina" simulation model for sugar beet in Foggia, 2000-2002 period

	Total Plant Biomass	Root Yield (g m^{-2})	LAI
Mean Value	10212	6367	3.01
Root Mean Square Error (RMSE)	1746	1146	0.66
General Standard Deviation (GDS)	0.16	0.18	0.22
Modeling Efficiency (EF)	0.96	0.95	0.88
Index of Agreement (d)	0.99	0.98	0.96
Determination Coefficient (CD)	0.81	0.87	0.92
Mean Bias Error (MBE)	− 1109	− 672	0.25
Residual Mass Coefficient (CRM)	0.107	0.106	− 0.093

Table 3 Evaluation indexes of "Stamina" simulation model for sugar beet in Foggia, in different conditions for water availability, 2000-2003 period

	Total Plant Biomass	Root Yield (g m^{-2})	LAI
Mean Value	9843	5008	2.02
Root Mean Square Error (RMSE)	2067	1202	1.11
General Standard Deviation (GDS)	0.21	0.24	0.55
Modeling Efficiency (EF)	0.94	0.93	0.45
Index of Agreement (d)	0.98	0.98	0.90
Determination Coefficient (CD)	0.75	1.00	1.77
Mean Bias Error (MBE)	− 1045	− 234	0.78
Residual Mass Coefficient (CRM)	0.107	0.057	− 0.397

Not shown data (Richter, 2007, personal communication) confirmed, further, the good simulation model responses in a long-term experiment about sunflower and durum wheat, highlighting the validity of proposed approach, not specific for a crop, but that can be used in several cropping systems scenarios. To simulate new crops, the model needs of some input crop parameters (phenological crop length, photosynthesis efficiency, dry matter partition during crop cycle), essential for each new crop the user want simulate.

3.2 LAI Forcing

The available remote sensing images are not yet entirely integrated with a full weather data set and the relationship between LAI and optical indexes needs of further improvement; so, to verify preliminarily the possible improvements of simulation results after LAI forcing, we examined the

experimental data previously used in the calibration phase on autumnal sugar beet. In particular, we used data deriving from several field experiments carried out in Foggia in the 2000/01 and 2001/02 campaigns, used for the calibration and the model was applied with and without LAI forcing.

In the 2000/01 LAI forcing has been applied only at one date, at the end of April, when the first remote sensing image (LANDSAT TM) was available, so it was possible to estimate NDVI and from this index, to derive the LAI value.

In the 2001/02 LAI forcing was applied in two dates, on 9th April and on 6th June, always in periods when the remote sensing data can be available.

In 2000/01, at the date of LAI forcing the LAI was underestimated by the simulation model of about 1.5, while in 2001/02, the model overestimated the LAI in the first date respect to the measured values; on the contrary, in the second date, the simulated LAI values were greatly underestimated. The results are summarized and shown in the Figs. 1 and 2.

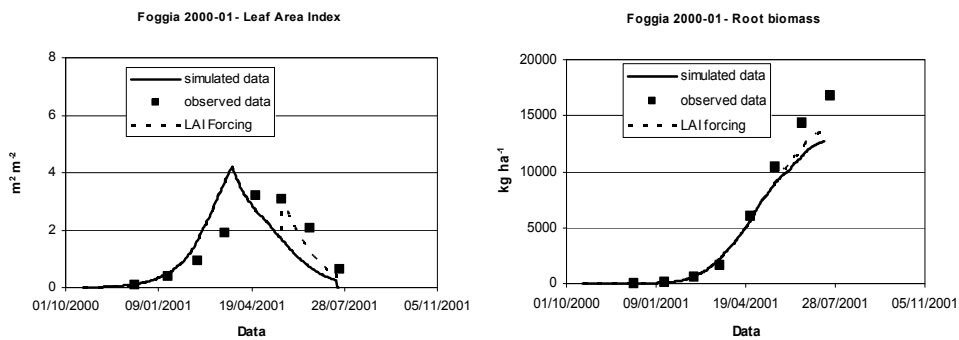

Figure 1 Effects of Leaf Area index (LAI, derived by remote sensing information) forcing into the simulation model on the following LAI and root dry matter behaviours. Foggia, 2000/01

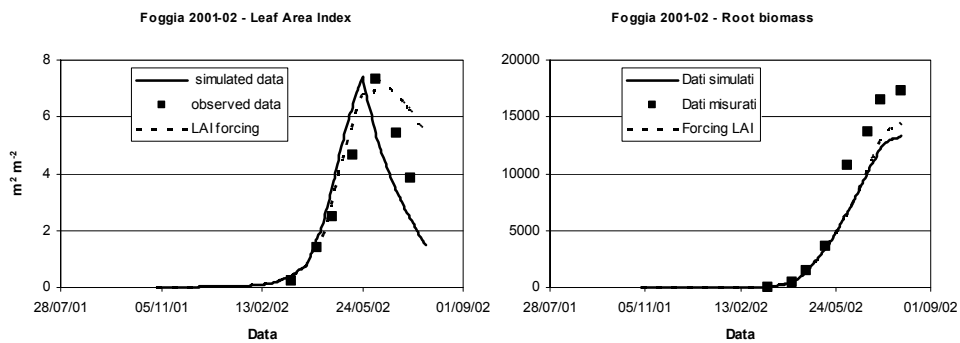

Figure 2 Effects of Leaf area Index (LAI, derived by remote sensing information) forcing into the simulation model on the following LAI and root dry matter behaviours. Foggia, 2001/02

LAI forcing improved significantly model performance in LAI simulation, with positive effects also on the simulation of plant biomass behavior, both total and commercial (root). The results here shown clearly highlighted the useful and positive effects of this assimilation procedure, but also the needs of a simulation model capable of reliable estimation of LAI, on which, the forcing can further improve the results.

Nevertheless, the remote sensing data is fundamental to estimate the start of crop cycle (or emergence time); in fact, assuming averages sowing dates for sugar beet, the simulation results, got worse in early or late sowing times. The importance and usefulness of remote sensing data in this application is great in order to estimate, also in a reasonable range, the field crop sowing time.

3.3 DSS Software

The Decision Support System (DSS) has been structured with the simulation model integrated with a GIS software. At the model has been added all the need components in order to link the model to the GIS software, to map the input and output data and to read the database (soil climate, crop and management). At the moment, the model can read the data stored in shape files (*.SHP format, as defined by ESRI and used in all the GIS softwares) and to update them with the data concerning the different variables. In addition, in the DSS software a tool for the map representation has been included.

The first results here shown, have been obtained by a prototype software version, available at December 2007.

Some examples of the maps attainable with the DSS are shown in the following figures. The maps have been obtained using not real data; in fact, as an example, we report the area of Lucera city (Apulia region, Southern Italy). The examples are referred to the field crops of sugar beet and processing tomato, located in the test area at the date of 10th April and 20th June (Figs. 3 and 4), the phenological phase of sugar beet on 10th April (Fig. 5) and the drought index of processing tomato on 20th June (Fig. 6).

The model is now capable to read the geographic database (shape file format) where, for each simulation unit, the soil characteristics are stored, and further, can use, always for each simulation unit, an agro-climatic station with daily data, as specified by the user.

The model h as been structured in order to read the data deriving from remote sensing images and to force a specific model dynamic variable.

The software is in test and verification phases and the first trial in order to assimilate the remote sensing images to estimate sowing dates are in progress.

The crop sowing date estimation, with images following the sowing itself, is of great importance, because crop water use (ETa) and drought effects are dependent by phenology, and, consequently, are dependent by sowing dates and climatic conditions.

Sowing date prediction is obtained with a process with iterative approximations, re-starting the simulation by different dates, until to find the one obtaining LAI values closer to that derived by remote sensing images (from NDVI index).

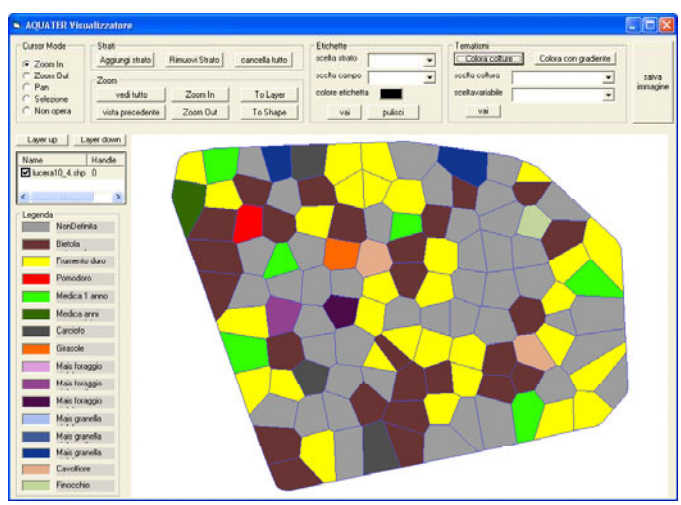

Figure 3 Examples of map attainable with Decision Support System: field crops on 10th April in the Lucera municipality area

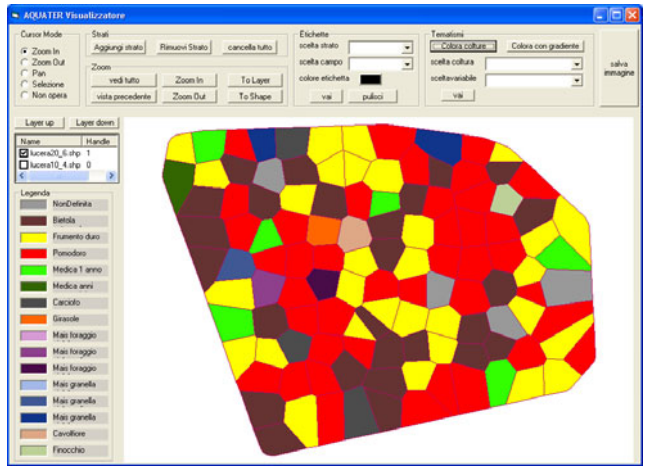

Figure 4 Examples of map attainable with Decision Support System: field crops on 20th June in the Lucera municipality area

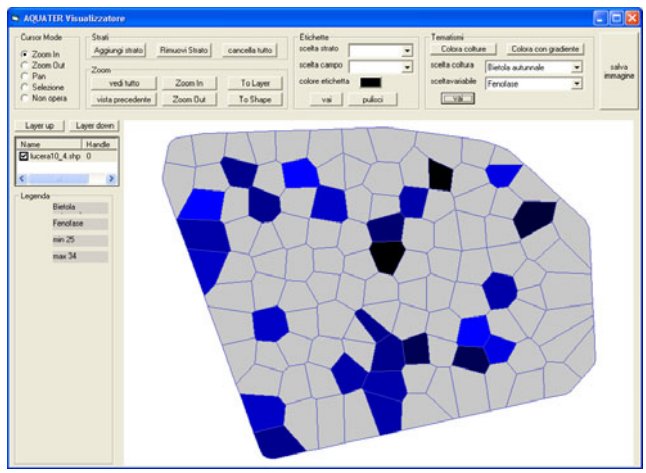

Figure 5 Examples of map attainable with Decision Support System: sugar beet crop phase on 10th April

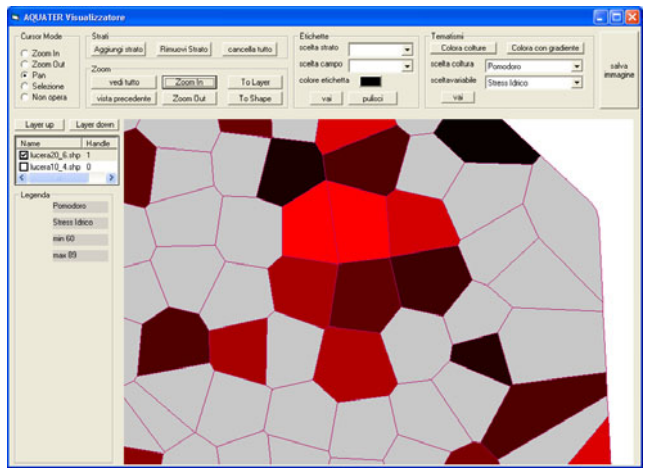

Figure 6 Examples of map attainable with Decision Support System: drought index on processing tomato on 20th June in a part of the Lucera municipality area (Zoom function)

4 Conclusions

A prototype of a Decision System Support has been developed in order to schedule irrigation at district level in a Mediterranean area. The DSS integrates the information deriving from soil and climatic database with a crop simulation model and can simulate the most important field crops in Southern Italy: this information deriving from simulation will be used to estimate the water requirement and irrigation needs at regional level.

A set of input for the DSS are necessary, like the crops and sowing date can be derived by remote sensing images. The Leaf Area Index and plant biomass derived from remote sensing, can be further used in the assimilation procedure into the simulation model, to force the model to fit the values and to obtain an improvement of the simulation results.

The DSS is at first prototype phase, but it is already provided of a GIS visualization tool. The first results obtained show the capabilities of the model, that in the following research, will be further calibrated and validated with plant and soil experimental data. It will be improved also for the user interface, more friendly and easy to use.

References

Acutis M, Rana G, Trevisiol P et al. (2007) Integrating a spatial micrometeorological model into the risk assessment for arable crops in hilly terrain. Modeling water and nutrient dynamics in soil-crop systems. Springer. Edited by: K.C. Kersebaum, J.-M. Hecker, W. Mirschel & M. Wegehenkel.

Alcamo J, Flörke M , Märker M (2007) Future long-term changes in global water resources driven by socio-economic and climatic changes. Hydrol. Sci. J. 49(4), 549 – 562.

Bechini L, Laudato M, Trevisiol P et al. (2004) Dynamic simulation model for seed germination, seedling elongation and emergence. Proceedings of VIII Congress of the European Society for Agronomy, Copenhagen, Denmark, 11-15 July 2004, 217 – 218.

Blaes X, Vanhalleb L, Defournya P (2005) Efficiency of crop identification based on optical and SAR image time series. Remote Sensing of Environment, 96, 3-4: 352 – 365.

Boogaard H L, van Diepen C A, Rötter R P et al. (1998) WOFOST 7.1 User guide for the WOFOST 7.1 crop growth simulation model and WOFOST Control Center 5.1. Techn. Doc. 52, Alterra, WUR, Wageningen, The Netherlands, pp. 144.

Cohen D, Lindvall M, Costa P (2004) An introduction to agile methods. Advances in Computers, 1 – 66.

Dente L, Rinaldi M, Mattia F et al. (2006) Assimilation of polarimetric C-Band Radar data into CERES-Wheat model. Rivista Italiana di Telerilevamento, 35: 21 – 34.

Dente L, Satalino G, Mattia F et al. (2008) Assimilation of Leaf Area Index derived from ASAR and MERIS data into CERES-Wheat model to map wheat yield. Remote Sensing of Environment, 112:1395 – 1407.

Ferrara R M, Rana G (2006) Application of the unified modeling language to a spatially distributed micrometeorological model at catchment scale. Italian Journal of agrometeorology, 1:32 – 40.

Flügel W A (2006) Delineating hydrological response units by geographical information system analyses for regional hydrological modeling using PRMS/MMS in the drainage basin of the River Bröl, Germany. Hydrological Processes 9, 3-4:423 – 436.

Hoffmann C M, Blomberg M (2004) Estimation of leaf area index of Beta vulgaris L. based on optical remote sensing data. Journal of agronomy and crop science, 190, 3:197 – 204.

Kruchten P (2001) “What Is the Rational Unified Process?” The Rational Edge, http://www.ibm.com/developerworks/rational/library/content/RationalEdge/jan01/WhatIstheRationalUnifiedProcessJan01.pdf.

Launay M, Guerif M (2005) Assimilating remote sensing data into a crop model to improve predictive performance for spatial applications. Agriculture ecosystems & enviroment, 111, 1-4:321 – 339.

Noilhan J, Planton S (1989) A simple parameterization of land surface processes for meteorological models, Mon. Wea. Rev. 117:536 – 549.

Oweis T, Pala M, Ryan J (1998) Stabilizing rainfed wheat yields with supplemental irrigation and nitrogen in a Mediterranean climate. Agronomy Journal, 90, 5:672 – 681.

Piccarreta M, Capolongo D, Boenzi F (2006) Trend analysis of precipitation and drought in Basilicata from 1923 to 2000 within a Southern Italy context. Int. J. Climatol. 24:907 – 922.

Raes D, Geerts S, Kipkorir E et al. (2006) Simulation of yield decline as a result of water stress with a robust soil water balance model. Agricultural Water Management, 81, 3:335 – 357.

Richter G M, Rana G, Ferrara R M et al. (2006) Stability and Mitigation of Arable Systems in Hilly Landscapes (EU-QLK-5-CT-2002-01313). Report to the European Commission, Brussels, 280 pp.

Richter G M, Jaggard K W, Mitchell R A C (2001) Modeling radiation interception and radiation use efficiency for sugar beet under variable climatic stress. Agric. Forest Meteorol. 109:13 – 25.

Rinaldi M, Castrignanò A, Mastrorilli M et al. (2005) Decision support systems to manage water resources at irrigation district level in Southern Italy using remote sensing information. An integrated Project (AQUATER). Proc. of Earth Observation, 10-11 December, Napoli (I), 107 – 114.

Rizzoli A E, Athanasiadis I N, Donatelli M et al. (2005) Overall architectural design of SeamFrame. SEAMLESS report no.7.

Sinclair T R (1986) Water and nitrogen limitations in soybean grain production. Part I. Model development. Field Crops Res. 15:125 – 141.

Tuberosa R, Giuliani S, Parry M A J et al. (2007) Improving water use efficiency in Mediterranean agriculture: what limits the adoption of new technologies? Annals of Applied Biology, 150, 2:157 – 162.

van Dam J C, Feddes R A (2000) Numerical simulation of infiltration, evaporation and shallow groundwater levels with the Richards equation. J. Hydrol., 233:72 – 85.

van Ittersum MK, Leffelaar PA, van Keulen H, Kropff MJ, Bastiaans L, Goudriaan J (2003) On approaches and applications of the Wageningen crop models. Eur. J. of Agronomy, 18:201 – 234.

van Keulen H, Penning de Vries F W T, Drees E M (1982) A summary model for crop growth. In: Penning de Vries FWT, van Laar HH (Eds.), Simulation of Plant Growth and Crop Production. Simulation Monographs. Pudoc, Wageningen, The Netherlands, pp. 87 – 98.

van Keulen H, Wolf J (1986) Modeling of agricultural production: weather soils and crops. Simulation Monographs. Pudoc, Wageningen, The Netherlands, pp. 479.

Research of Maize Leaf Disease Identifying Models Based Image Recognition

Yu-Xia Zhao [1, 2], Ke-Ru Wang [1, 3], Zhong-Ying Bai [2], Shao-Kun Li [1, 3*], Rui-Zhi Xie [1], Shi-Ju Gao [1]

(1 Institute of Crop Science, Chinese Academy of Agricultural Sciences/ The National Key Facilities for Crop Genetic Resources and Improvement, NFCRI, Beijing 100081, China, Corresponding author: LI Shao-kun, E-mail: lishk@mail.caas.net.cn)
(2 Beijing Posts and Telecommunications University, Beijing, 100876, China)
(3 Key Laboratory of Oasis Ecology Agriculture of Xinjiang Bingtuan /Research Center of Xinjiang Crop High-Yield, Shihezi University, Shihezi 832000, China)

Abstract: The methods of recognition and diagnosis of main maize leaf diseases using machine vision were studied in the paper. Threshold method was adopted to do image segmentation, and area-marking method was used calculating the num of disease as well as wiping off redundancy dots. And then Freeman link code was used to calculate form feature. Finally diseases were deduced according to bin-tree search method. In the research, the exclusive feature of main maize leaf diseases was presented, and the flow of disease diagnosis was confirmed and the recognition models were developed. The results indicate that the precision of five kinds of maize disease recognition is higher than 80%. It shows that this method is available for recognizing maize disease, and provides technique support for the automatic recognition of disease by compiling the system with reasonable process flow.

Keywords: maize leaf disease, color feature, form feature, image segmentation, area marking

1 Introduction

Machinery vision technology is a new research idea and tool to recognize and diagnose crop diseases and insect pests along with fast developing of computer technique that based on thorough understand and pickup technique progress to object characteristics such as figure, size, color and texture.

In 1995, Tao Y used machinery vision researched the difference of color and luster on apples and potatoes. Zhou (2005) used fuzzy imposed techniques to detect image edge, Shen et al. (2003) applied mathematic morphology method to distinguish image geometric character, and automatically recognizing part of insect pest was done. Leave are vital plant photosynthesis organ and also are the most common part where break disease and insect pest. Serna et al. (2003) presented the severity of corn borer could be distinguished by the shape of leave gnawed by corn borer; Tian Y W (2004), using linearity distinguishing function to segment image; but the study related to image is still less. This paper studied five most common and easily confused maize leaf diseases: Common rust, Curvularia leaf spot, Gray spot (Cerospora zeae-maydis), Brown spot blight (physodermazeze-maydis) and Flyspeck disease(Bipolaris maydis). The study tried to apply machine visual techniques to automatically recognize and diagnose plant disease.

2 Material and Method

2.1 Images of Diseased Leave Acquisition

The images of maize leaf with disease were shot at 2560×1920 pixels with automatic exposure mode using Nikon COOL PIX 5700 digital cameral on the condition of natural light. Unrelated backgrounds of images were removed with Photoshop 6.0 after images were sent to computer.

2.2 Feature Extraction from Images of Disease Spot

Color features extraction

Using RGB and HIS color spaces system, RGB values were acquired by the Get Pixel function provided by Visual C++ 6.0 and HIS values were computed by RGB values (Eq. (1)).

$$\begin{aligned} I &= \frac{1}{3}(R+G+B) \\ S &= I - \frac{3}{(R+G+B)}[\min(R,G,B)] \\ H &= \arccos\left\{\frac{[(R-G)+(R-B)]/2}{[(R-G)^2+(R-B)(G-B)]^{1/2}}\right\} \end{aligned} \tag{1}$$

Note: Value H is from 0 to 180 where $G>B$; if $G<B$, $H=360-H$.

Shape features extraction from images of disease spot

Disease spot shape features including area, girth and circularity were computed with the method of area-marking and Freeman link code.

Area-marking applying recursion method extracted every disease spot feature and stored them to a chain for using to recognize disease.

Using Freeman link code to calculate area, girth and circularity:

(1) Area girth L enclosed by chain code viz. link code length.

$$L=n_e+\sqrt{2}\times n_o \tag{2}$$

Where n_e is No. of even number of chain code number, n_o is No. of odd number of chain code number, or apply approximation viz. L=n, where n which indicated chain code length is chain code number.

(2) Area enclosed by chain code

a_{ix} is the X-axile weight of a_i, a_{iy} is the Y-axile weight of a_i. The range of a_{ix} is from -1 to 1, same as the a_{iy}. As showed in Table 1:

$$S=\sum_{i=1}^{n} a_{ix}(y_{i-1}+\frac{1}{2}a_{iy}), \tag{3}$$

where $y_i = y_{i-1} + a_{iy}$, S is area enclosed by chain code.

(3) Area circularity enclosed by chain code

$$C=\frac{4\pi S}{L^2}, \tag{4}$$

where C is circularity. Theoretically, the value range of C is from 0 to 1, in practice, sometimes C is greater than 1 beacause of noise. It has no effect on recognizing disease. Other signs were the same.

Table 1 Value of a_{ix} and a_{iy}

a_i	a_{ix}	a_{iy}
0	1	0
1	1	1
2	0	1
3	–1	1
4	–1	0
5	–1	–1
6	0	–1
7	1	–1

2.3 System Development Environment

Operating system was Windows 95/98/NT; development tool was Visual C++ 6.0.

3 Results and Analyses

3.1 Image Segmentation

The most distinct change in color feature of diseased leaves was green losing, and the value R in the area of disease spot was markedly greater than other area. So we can choose R as the standard of image segmentation. According to histogram, segmentation threshold R_standard could be computed by the method of Twin Peaks in conjunction with analysis of histogram concave and convexity, and applied statistical method to check it.

Firstly, applying twin peaks method to analyze histogram based on value R of RGB color space after acquiring image. Segmentation effect was the best when threshold in the bottom of valley. But the shape of some histograms of images including objective and background weren't twin peak viz. part of gray of objective was the same as that of background, so valley bottom may be nonexistent. When the area of objective was widely different from background area, one of histogram peak would be lap over the other peak slope viz. only one peak. So analysis of histogram concave and convexity need to be analyze to ascertain threshold.

The study showed R,G, and B were greatly effected by brightness and brightness also effected segmentation results. Applying threshold based on brightness to segment image could resolve the problem of value RGB of image of different brightness unascertained. For increasing computing speed and simplifying judgment complexity, we applied synthetically above methods to segment image and according to brightness to ascertain threshold (Eq. (5)).

$$\text{R\_stander} = \begin{cases} 130, \text{if I\_all} < 0.45 \\ 170, \text{if } 0.45 \le \text{I\_all} < 0.6 \\ 200, \text{if I\_all} \ge 0.6 \end{cases} \tag{5}$$

Where I_all is general image luminance. The result was shown below (Fig.1).

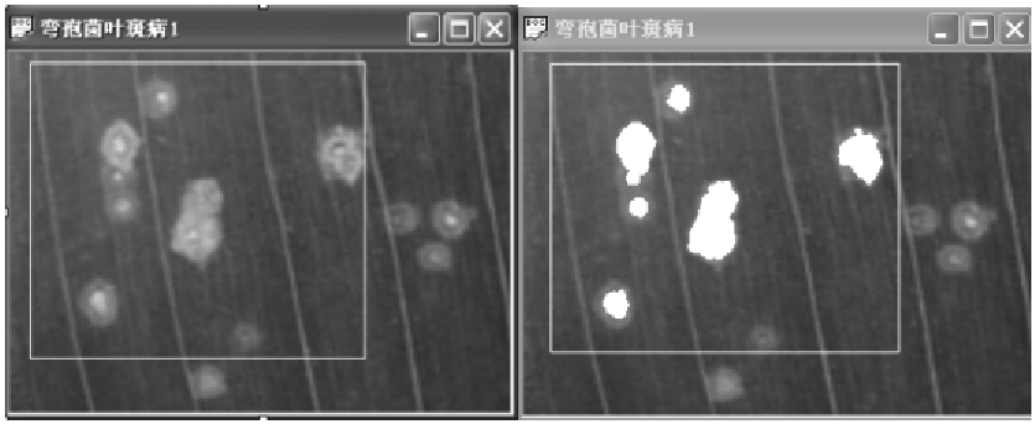

Figure 1 Comparison between original image and segmented image of maize leaf disease

3.2 Disease Spot Features Extraction

Four features of five maize leave diseased spot were extracted by the above method. The feature values were the number of dot whose value *B* less than 30, the number of dot whose value *H* range from 350 to 359 or from 0 to 15 and the disease spot scale of circularity sum less than 50. The result showed only rust has the dot whose value *B* less than 30; the distribution of value H of Curvularia leaf spot and Gray spot were concentrated, and value H in the saturation ring was about 0; but the shape of disease spot were different , Curvularia leaf spot was close to circular and Gray spot was rectangle and the circularity of Curvularia leaf spot was greater than that of Gray spot; the size of speckle disease spot was little and the spots were scattered about in a fairly equal manner. This study applied iterative method and regarded number of dots within disease spot which meet the standards as recognizing feature disposing uncertainty resulting from mean value. Rust disease could be recognized with the feature value B, so other features of rust disease weren't need to extracted.

3.3 Diagnosis Flow

As showed in Table 2 every disease spot had the only recognizing feature and feature range: only the number of dot whose value *B* less than 30 of rust disease spot is more than 3; and the number of dot whose value *H* range from 350 to 359 and from 0 to15 which is more than 15 are Curvularia leaf spot or Gray spot. Then we could distinguish them with circularity, the size of circularity of Curvularia leaf spot is bigger than 0.6 and Gray spot is less than 0.6. The diseases whose disease spot scale of circularity sum less than 50 are speckle. The rest are flyspeck spot. The flow of diagnosis disease spot was presented in Fig. 2.

3.4 Program Development

According to diagnosing flow, maize leave disease diagnosing procedure was programmed with development tool Visual C++ 6.0. Diagnosing result showed that the accuracy of program diagnosing main maize leave disease was up to 80% (Table 3).

Table 2 Character values of maize leaf disease extracted from images

		Rust	Curvularia leaf spot	Gray spot	Brown spot	Flyspeck spot
No of sample		16	16	10	12	10
No of dot whose value B less than 30	minimum	10	0	0	0	0
	maximum	511	0	0	0	0
	mean	188	0	0	0	0
No of dot whose value H range from 350 to 359 or from 0 to 15	minimum	0	24	248	0	0
	maximum	11	204	832	13	8
	mean	1.875	77.625	416.2	2.33	0.8
circularity	minimum	0	0.728	0.251	0.565	0.075
	maximum	0	1.172	0.490	12.566	0.279
	mean	0	0.963	0.351	5.614	0.190
disease spot scale of circularity sum less than 50	minimum	0	0	0	0.929	0
	maximum	0	0	0	1.000	0.5
	mean	0	0	0	0.994	0.1
		Rust	Curvularia leaf spot	Gray spot	Brown spot	Flyspeck spot
No of sample		16	16	10	12	10
No of dot whose value B less than 30	minimum	10	0	0	0	0
	maximum	511	0	0	0	0
	mean	188	0	0	0	0
No of dot whose value H range from 350 to 359 or from 0 to 15	minimum	0	24	248	0	0
	maximum	11	204	832	13	8
	mean	1.875	77.625	416.2	2.33	0.8
circularity	minimum	0	0.728	0.251	0.565	0.075
	maximum	0	1.172	0.490	12.566	0.279
	mean	0	0.963	0.351	5.614	0.190
disease spot scale of circularity sum less than 50	minimum	0	0	0	0.929	0
	maximum	0	0	0	1.000	0.5
	mean	0	0	0	0.994	0.1
		Rust	Curvularia leaf spot	Gray spot	Brown spot	Flyspeck spot
No of sample		16	16	10	12	10
No of dot whose value B less than 30	minimum	10	0	0	0	0
	maximum	511	0	0	0	0
	mean	188	0	0	0	0
No of dot whose value H range from 350 to 359 or from 0 to 15	minimum	0	24	248	0	0
	maximum	11	204	832	13	8
	mean	1.875	77.625	416.2	2.33	0.8
circularity	minimum	0	0.728	0.251	0.565	0.075
	maximum	0	1.172	0.490	12.566	0.279
	mean	0	0.963	0.351	5.614	0.190
disease spot scale of circularity sum less than 50	minimum	0	0	0	0.929	0
	maximum	0	0	0	1.000	0.5
	mean	0	0	0	0.994	0.1

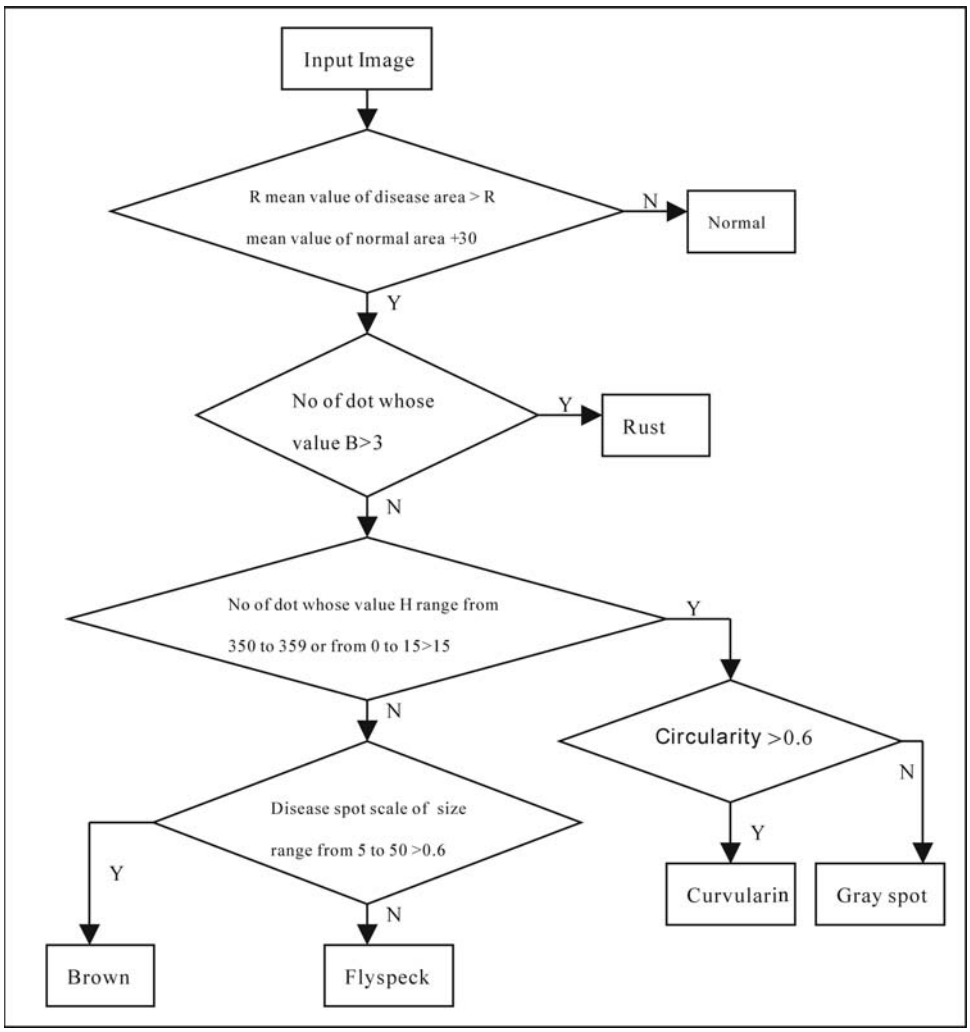

Figure 2 The diagnosis flow of maize leaf disease

Table 3 Results of maize leaf disease diagnosis system based images

Disease name	No of samples	No of recognition	Accuracy of recognition（%）
Rust	20	17	85
Curvularia spot	20	16	80
Gray spot	10	10	100
Brown spot	20	16	80
Flyspeck spot	16	15	87.5

4 Discussions

In the filed of image processing, image segmentation is always hotspot. There is lots of segmentation arithmetic, but most arithmetic is set up based on specific requirement. There are still no arithmetic can be appropriate for all image segmentation. The study of image segmentation was start from gray image segmentation, but gray image only make use of gray information; but color image includes more information and can be expressed by several color models. Lots of corresponding

algorithm has been presented. Tian Y W, using linearity distinguishing function of statistic pattern recognizing to segment color image. American CID Co. developed software CI-110 Plant Canopy Digital Imager to segment image, but disease spot couldn't be automatically segmented because segmentation threshold required several times manual adjustment. The study applied Twin Peaks method in conjunction with analysis of histogram concave and convexity to segment image, and segmentation effect was well. Otherwise, shape features chose in this study were independent which met the independent principle among classifier features. Using least features decreased classifier size and improved classify and identify performance.

The study showed that disease image quality effected disease feature extraction and disease diagnoses, and image brightness and disease spot size also influence disease distinguishing and diagnosis. So the chiefly condition of implementing machine visual technique was image acquiring standard and principle. This study didn't regard this problem when acquiring image and important distinguishing factor viz. disease spot size didn't fully work. The category of plant disease is vast, and disease may vary with the difference of disease time, disease partition and disease severity viz. plant diseases are complicated and changeable. The result of paper and the system of diagnosing and recognition have diagnosed main maize leave disease, which laid the groundwork for automatic diagnosing disease and insect pest and weed, but applying this study results to other plants or other disease need to be studying.

5 Conclusions

This paper studied five common and confusable maize leaf diseases: Common rust, Curvularia leaf spot, Gray spot and Flyspeck spot. Comprehensive utilization of the methods of threshold, area-marking and Freeman link code, we tried to use visual technology to auto recognize and diagnostic plant diseases. The results showed the precision of five diseases recognition is higher than 80% after image processing of image segmentation, disease statistic, redundancy removed and shape feature computed and application of bintree search method. The study has lessons for machine visual technology applying to agricultural production.

Acknowledgement

This works were supported by National High Technology Research and Development Program of China (863 Program, 2007AA10Z237, 2006AA10Z207).

References

Ji S W, Wang R B, Chen J J, Zhao X D (2001) The research on identifying weed in the field when maize is young applying computer process technique. Transactions of the CSAE 17:154 – 156.

Lei Y W, Wei C Z, Ye J, Hou Z A, Li J H, Jia L L (2004) Application of computer-aided cotton leaf-color analysis in nitrogen status diagnosis in cotton plants. Journal of Shihezi University(Natural Science) 22(2):113 – 116.

Li Q Z, Zhang M, Wang M H (2000) Real-Time Apple color grading based on genetic neural network. Journal of Image and Graphics 5:779 – 784.

Qian L F, Liu Y S, Li k (2005) A naive bayes classifier method on terrain evaluation. Computer Engineering and Applications 12:189 – 191.

Serna Jr D G, Pinto F A C, Queiroz D M, Viana P A (2003) Fall Armyworm damaged maize plant identification using digital images. Biosystems Engineering 85:449 – 454.

Shen Z R, Zhao H Q, Yu X W (2003) Use of math-morphological features in insect taxonomy.Ⅲ. At the family level. Acta Entomologica Sinica 46:339 – 344.

Tao Y, Heinemann P H, Varghese Z, Morrow C T, Sommer Ⅲ H J (1995) Machine vision for color inspection of potatoes and apples. Transactions of the ASAE 38:1555 – 1561.
Tian Y W, Li C H (2004) Color image segmentation method based on statistical pattern recognition for plant disease diagnose. Journal of Jilin University (Engineering and Technology Edition) 34:291 – 293.
Wang K R, Li S K, Wang C T, Yang L, Xie R Z, Gao S J, Bai J H (2006) Acquired Chlorophyll Concentration of Cotton Leaves with Technology of Machine Vision. Acta Agronomica Sinica 32: 34 – 40.
Yu X W, Shen Z R, Gao L W, Li Z H (2003) Feature measuring and extraction for digital image of insects. Journal of China Agricultural University 8(3): 47 – 50.
Zhang Y J (2001) Image Segmentation. Science Press, Beijing.
Zhang Y J (1999) Image Process and Analysis. Tsinghua University Press, Beijing.
Zhao H Q, Shen Z R, Yu X W (2002) On computer-aided insect identification through math-morphology features. Journal of China Agricultural University 7(3):38 – 42.
Zhao H Q, Shen Z R, Yu X W (2003) Use of math-morphological features in insect taxonomy. Ⅰ. At the order level. Acta Entomologica Sinica 46(1):45 – 50.
Zhao H Q, Shen Z R, Yu X W (2003) Use of math-morphological features in insect taxonomy. Ⅱ. At superfamily level. Acta Entomologica Sinica 46(2):201 – 208.
Zhou L (2005) Research on fuzzy detection on method of pest's image in store grain based on machine vision. Computer Applications and Software 22(8):24 – 25.

Spectral Characteristics of Cotton Infected with Verticillium Wilt and Severity Level of Disease Estimated Models

Bing Chen [1,2], Ke-Ru Wang [1,2], Shao-Kun Li [1,2*], Xue-Yan Sui [3], Fang-Yong Wang [1,2], Jun-Hua Bai [1,2]

(1 Institute of Crop Science, Chinese Academy of Agricultural Sciences/The state Key Laboratory of Crop Genetics and Germplasm Enhancement, Beijing, P.R. China, 100081, Corresponding author: LI Shao -kun, lishk@mail.caas.net.cn)
(2 Key Laboratory of Oasis Ecology Agriculture of Xinjiang Bingtuan/ the Center of Crop high-Yield Research of Xinjiang, Shihezi University, Shihezi, Xinjiang, P.R. China, 832000)
(3 Institute of Agriculture Sustainable Development, Shandong Academy of Agriculture Sciences, Jinan, 250100, Shandong, P.R.China)

Abstract: In order to elucidated characteristics of spectrum of cotton leaf infected with Verticillium wilt and estimated its severity level (SL) to provide theoretic foundation for further monitoring cotton Verticillium wilt at large scale using airborne and airspace remote sensing. The spectrum reflectance of cotton single leaf infected with Verticillium wilt was measured in cotton disease nursery and field at different growth phases, meanwhile, SL of single leaf infected with Verticillium wilt was investigated. The methods of first derivative spectraum were used to estimate accurately disease of cotton with Verticillium wilt when compared with the reflectance spectrum of different single leaf infected of Verticillium wilt. The results indicated that Spectral characteristic of cotton leaf of Verticillium wilt had better regularity with the increase of SL in different periods and varieties. Spectral reflectance increased significantly at visible light region (400 – 700nm) and near -infrared region (700 – 1300nm) with the increase of the SL, and specially signification at blue - violet to red regions(525 – 680nm). when SL got 25%, cotton leaf of Verticillium wilt could be used as a watershed and diagnosed index in early time. There were evident different characteristics of first derivative spectra in these disease leave, it changed significantly in red edge ranges(680 – 780nm) with different disease level, derivative spectra of red edge swing decreased, and red edge position equal moved to the blue. The thesis indicated that 434 – 724nm and 909 – 1600nm were selected out as sensitive bands region to SL of single leaf. Some inversion models for estimating cotton leaf diseased level of Verticillium wilt all reached the best significantly level. The model in which the first derivative spectra at 723nm could invert accurately the cotton leaf SL, and it may be used to forecasting the position of cotton leaf infected with Verticillium wilt in quantitatively.

Keywords: leaf spectrum, SL, estimating models, verticillium wilt, cotton

1 Introduction

Verticillium wilt of cotton, which is one of the extensive occurrence cotton diseases in China even others countries. Conventional method of monitoring Verticillium wilt was adopted to investigation and sampling in field, which was time -consuming and hard -sledding. Therefore, it is high time found a new method to monitoring cotton disease.

As shown in studies (Chen et al., 2007; Liu & Liu, 1999), some leaf spectrum parameters in crops, such as cell structure, pigment, water and nitrogen content etc, were changed attribute to diseases

and insect pests, leading to spectrum reflectance correspondingly changed too. Therefore, it is may to monitored occurrence and development of Verticillium wilt by remote sensing. There were a great deal of achievements on spectrum characteristics of diseases and insect pests in crops leaf by domestic and overseas scholars (Adams et al., 1999; Yu, 1995; Osborne et al., 2002; Qin & Zhang, 2005; Huang et al., 2004). However, there are few studies fucus on recognizing crop disease (especially to crop disease type and SL) and estimating models with remote sensing (Carter et al., 1996; Demetriades -Shah & Steven, 1998; Zhang et al., 2002; Zhang et al., 2003; Hamid Muhammed & Sarsolle, 2003; Fitzgerald et al., 2004; Moshoua et al., 2004; Kefyalew Girma et al., 2005; Hamid Muhammed, 2005). The spectrum and remote sensing image for Verticillium bacterium stressed provide some diagnoses spectrum characteristics in crops, which are different between leaf and canopy. Therefore, it is possible to monitoring cotton disease and insert pests by remote sensing. How about are spectrum characteristics of Verticillium wilt stress in cotton leaf? How to discern disease and inverse SL in cotton leaf by remote sensing? Up to now, few reports have finished in this field.

The objective of this study were to: ① demonstrate the spectrum characteristics for Verticillium wilt stress, ② find sensitive bands to monitor Verticillium wilt, ③ establish models to predict the disease SL in cotton leaf . Moreover, the studying results will provide theoretic support for further monitoring cotton Verticillium wilt in large area by aviation and spaceflight remote sensing.

2 Material and Methods

2.1 Experiment Field

In 2005 – 2006, the experiments were conducted in Shihezi oasis of Xinjiang, China, which sit the hinterland in the Asia -Europe continent, the northern central section of Tianshan Mountain. The average altitude is 450 meters; and it belongs to the temperate continental arid weather and has 170 – 173 frostless days. The region falls into the premature and sub -suitable planting section for cotton. It is the important base for cotton production in China. And its agricultural mechanization is 80% up. In order to improve the output and the economic interests in the cotton production, the precision management is a key aim which would be put into practice in Xinjiang.

2.2 Design of Experiments

The experiments were including two parts. The plots (a small -scale experimen)was made in cotton disease nursery of institute of Key Laboratory of Oasis Ecology Agriculture in Shihezi university (44°18′N,86°03′E). Initial surface soil test characteristic were grey desert loam with organic matter 1.93%, alkali -hydrolysis nitrogen(N)77.4mg·kg^{-1},available phosphorus (P_2O_5)93mg·kg^{-1} and available potassium (K_2O)315mg·kg^{-1} in 20cm depth, former stubble plant was cotton. The experimental design was a randomized complete block design with three replications,five cotton cultivars were planted with 42.5m^2 in plots, these cultivars were Xin Luza 6(XLZ -6), Xin Luza 7(XLZ -7),Xin Luza 13(XLZ -13), Xin Luza 24(XLZ -24),and Zhong Mian 36(ZM -36). The plant density was 2 40000 plants·hm^{-2} with 60cm+30cm row spacing, the seeding time was in 20, April, 2005 and 2006. Used film cover and drip irrigation. Irrigation quantity carried out 3300m^3·hm^{-2}, fertilizer amounts were pure nitrogen 300 kg·hm^{-2}, P_2O_5 150kg·hm^{-2}, K_2O 75 kg·hm^{-2}. All Phosphorus,Potassium and one -third N were mixed as basis fertilization. Two -thirds N, as growth fertilization, was top -dressed at 28 June, 26 July in 2006 and 2007, respectively. The plot kept from weed, others treatments were applied according to high yield cultivation mode in the local region. The field experiments were performed at three locates: 19 company of 143 regiment, the seed station of 147 regiment and 11company of 148 regiment, where Verticillium wilt have been occurred continuously

in large area in recent years. The soil has middle fertility, and the plant date was 20 – 30 April, others were the same as the plots experiment.

2.3 Sampling and SL Classification

Sample leaves, which were collected from different SL of cotton leaf in fields and plots, were placed in a plastic bag and immediately sent to laboratory to measure spectrum. According to symptoms percent account for whole leaf ,we defined the following five disease SL groups: health (b0):no symptoms, was 0%;slight degree (b1):symptoms was 0% – 25%;medium degree (b2): symptoms was 25% – 50%; severity degree (b3): symptoms was 50% – 75%; extreme severity degree(b4): symptoms was 75% – 100%. The leaves were selected from same place when investigated SL and measured of leaf.

2.4 Data Collections

Leaves spectrum were measured by attaching the ASD Field spec Pro FR 2500 spectrometer (Analytical Spectral Devices, Boulder, CO, USA) to an external ASD Single Leaf Clip (Analytical Spectral Devices, Boulder, CO, USA). External Single Leaf Clip is a self -contained light source that collects spectral manufactured on a 2.5cm diameter circle of the leaf without interference from external light and /or environmental conditions. ASD Field spec Pro FR 2500 spectrometer fitted with a 512 spectrum bands, operating in the 350 – 2500 nm spectrum region with a sampling interval of 1.4 nm between 350 and 1000 nm, and 2 nm between 1000 and 2500 nm, and with spectrum resolution of 3 nm between 350 and 1000 nm, 10 nm between 1000 and 2500 nm. Three spot readings per leaf were taken on the upper and underside of the leaf surface. All reading taken from the leaves were averaged and transformed to percent reflectance using a barium sulfate reference to obtain one representative reading per leaf.

In the year 2005 – 2006, cotton leaves infected with Verticillium wilt (defoliation style)were measured for 15 times. The schedule was as follows, 24th June, 10th August and 20th September at experiment field(XLZ -7, XLZ -13), 20th July and 17th August at 19 company in 143 regiment (XLZ -13) in 2005, and 20th June, 17th July, 3rd August and 10th September at experiment field (XLZ -7, XLZ -8, XLZ -13, XLZ -24, ZM -36), 21 th July and 8th, 12th August at seed station of 147 regiment(602,4432), 12th July, 9th, 25th August at 11 company in 148 regiment (XLZ -24,ZM -36) in 2006 for the four different growth stages.

2. 5 Data Analysis

Reflectance spectral data were performed, using View spec program software (made ASD company, CO,USA). The first derivative spectrum was made using matlab 7.01 software, the formula as follows (Wang et al., 2004):

$$\rho'(\lambda_i) = \frac{[\rho(\lambda_{i+1}) - \rho(\lambda_{i-1})]}{2\Delta\lambda} \quad (1)$$

Where λ_i is wave length come from i wave band, $\rho(\lambda_i)$ is spectrum value from λ_i wave length, Δ_λ denoted space from λ_{i-1} to λ(Decided by sampling interval of spectrum). The correlation between reflectance spectrum, first derivative spectrum and SL was analyzed based on Excel 2003, wave band with characteristic and combination parameters for spectrum red edge were extracted from them (Wang et al., 2003). Including red edge swing (Dr): the maximum first derivative value in red edge region (680 – 780nm); red edge area(SDr): the summation of first derivative value in red edge region; red edge position(REP): the wave length corresponds to Dr; red vale position (Lo): the

wave length valve corresponds to the min first derivative value in red vale scope(640 – 680nm). In addition, statistics analysis applied SPSS 10.0 software, the number of samples used in establishing model and testing were 82 and 61, respectively.

3 Results And Analysis

3.1 Spectral Characteristics for Leaves of Verticillium Wilt with Different SL

The results showed that spectral reflectance of leaves with the increase of the SL decreased from VLR (visible light region)(400 – 700nm) to NIR (near-infrared region) (700 – 1300nm) ,and specially signification at blue-violet to red regions(525 – 680nm)., i.e. spectrum reflectance of health leaf (b0) was the lowest, extreme severity degree(b4) was the highest. Leaves spectrum had analogical change trend for different varieties and growth stages, only value of spectrum reflectance was different (Fig.1). Thereby, SL of Verticillium wilt could be distinguished by using spectrum characteristics discrepancy with different SL in cotton leaves.

In VLR (520 – 680nm), diversity of spectral reflectance with different SL was marked between diseases and health leaves (Fig. 2). With the SL increase, leaf spectral reflectance climbed remarkably. When SL attained b1, reflectance of diseases was higher by 3.2% than normal, when SL attained b2(25%), it higher by 9.2% than normal. Thereby, b2(25%)could be used as a watershed and diagnosed index in early time.

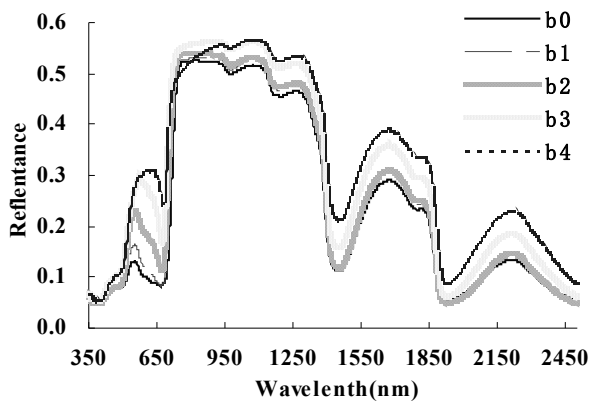

Figure 1 The reflectance spectral curve of cotton leaves with different SL

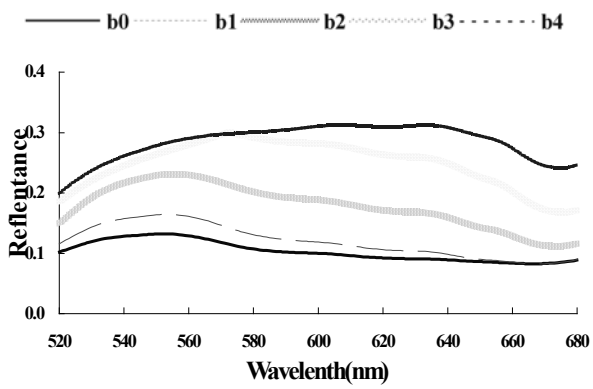

Figure 2 The reflectance spectrum curve of cotton leaf with different SL at 520 – 680nm

The studying demonstrated wave bands which located the red side district in first derivative spectrum were changed biggest (Fig. 3). That was, maximum of the first derivative spectrum and corresponding wavelength between 680nm and 760nm. Comparing with health leaf, all the red edge of cotton leaves of Verticillium wilt with different SL had ‘single swings’, and ‘single swing’ dropped together. Besides, red edge position moved to the short -wave direction. In brief, leaf red edge swing descended, and red edge position happened ‘blue movement’.

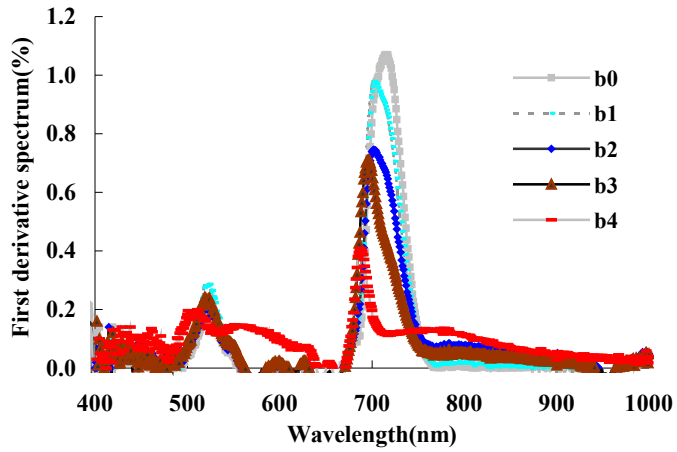

Figure 3 First derivative spectrum curve of cotton leaf with different SL

3.2 Sensitive Wave Band and Spectral Reflectance Predicting Models

The results hint the correlation between spectrum reflectance and SL was positive in 350 – 1600nm, and present significant level between 434 – 724 nm and 909 -1600 nm (Fig. 4). And 434 – 724 nm were selected out as spectrum sensitive wave band for Verticillium wilt leaf. Because the correlations were most significant at 698nm, 825nm, they were selected out. And in view of their combinations, estimates models of leaf infected with Verticillium wilt with SL were established and tested. As shown in table 1, the wave band combinations model, which was established by

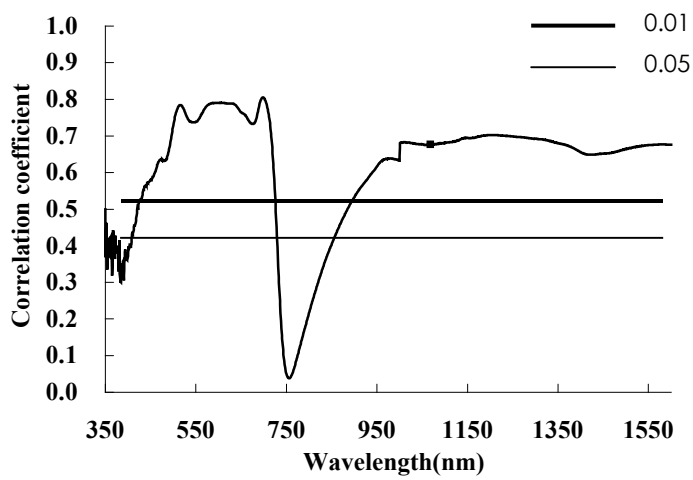

Figure 4 Correlation between SL of leaf and spectrum reflectance of cotton with Verticillium wilt

(R698nm – R825nm) / (R698 nm+R825nm), had higher estimated accuracy, the RMES was the least (0.564).

3.3 Estimating Models for Verticillium Using First Derivative Spectrum

There were strong correlation between disease SL and the first derivative spectrum (Fig.5), farther more, the correlation between first derivative spectrum and SL at 723nm displayed significantly, those bands were selected out.

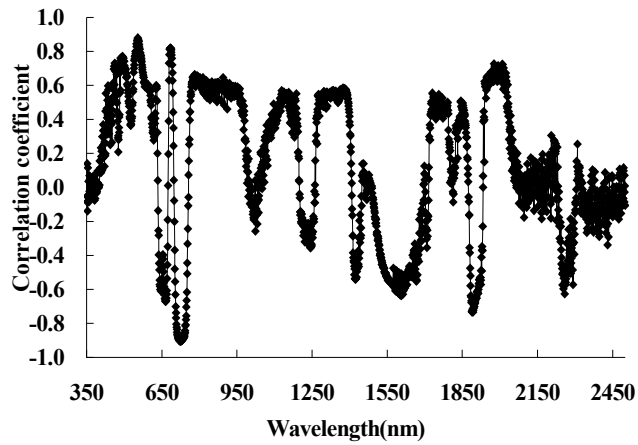

Figure 5 Correlation between SL and first derivative spectrum of cotton leaf with Verticillium wilt

In term of them, monitoring models for Verticillium wilt with SL were founded. The model established by FD723nm had greater estimated accuracy (Table 1), and the highest correlation between estimated and tested value (0.934). SL of cotton leaf could be estimated with first derivative spectrum. Moreover, testing result exhibited that the value b was nonzero in regression model, and reason was possible that samples used in establishing and testing model were come from different years and varieties, and then certain system error was brought.

Table 1 Prediction models for SL of Verticillium wilt infected of cotton leaves

$\lambda^{\dagger}$	Parameters	Diagnostic model(SL)	$R^{2\ddagger}$	RMES§	r¶
698nm	R_{698nm}	SL=13.159x – 0.9561	0.762**	0.649	0.805**
698nm,825nm	R_{698nm}/R_{825nm}	SL=7.0633x – 1.0003	0.776**	0.569	0.848**
698nm,825nm	$R_{825nm} - R_{698nm}$	SL= – 12.819x +5.9048	0.753**	0.593	0.724**
698nm,825nm	$(R_{825nm} - R_{698nm})$ /$(R_{825nm}+R_{698nm})$	SL= – 7.4430x+5.1612	0.798**	0.564	0.861**
723nm	FD_{723}	SL= – 412.84x+4.5149	0.856**	0.542	0.934**
680 – 780nm	D_r	SL= – 2.001Ln(x) – 7.33	—	1.310	0.393 *
680 – 780nm	SD_r	SL = – 0.0441x +4.9538	0.797**	0.623	0.912**
680 – 780nm	REP	SL= – 0.127x+91.109	0.583**	0.974	0.734**
640 – 680nm	Lo	SL= – 0.0704x+ 48.968	0.765**	0.590	0.911**

*Significant at the 0.05 probability level, **Significant at the 0.01 probability level. Number of samples used in establishing model and testing are 82 and 61 respectively.

†, elected wave bands; ‡,Coefficient of determination; §,Root mean square error;

¶,Correlation coefficient.

3.4 Estimating Models for Verticillium Using Red Edge Parameters

The correlation analysis results indicated that all tested parameters of REP, Dr, SDr and Lo, had strong correlation with SL (Table.1). One of the most correlation parameters was SDr. The tested result also illustrated that correlation coefficient between predicting and testing value attained significant level (0.912), the RMSE was less (0.623), which exhibited higher valued precision.

4 Discussions

This study found that spectrum characteristic of cotton leaf of Verticillium wilt had better regularity with the increase of SL in different periods and varieties. As well known, the leaf spectral reflectance is effected mainly subjected to chlorophyll content in VLR. The reflectance is low for health leaf due to strong absorption by chlorophyll and is high in disease leaf due to less absorption by chlorophyll. Whereas the leaf spectral reflectance is determined not only by chlorophyll content, but also by water and dry mater content in each area and the microcellular structures in leaf material (Thomas & oerther, 1972; Chen et al., 2007) in NIR. When cotton leaf was harmed to Verticillium fungus, on the one hand, leaf began with discoloring, withering and chlorophyll concentration dropped quickly. On the other hand, leaf thinned not only because meat cell was destroyed but water content declined. In theory, reflectance descended because of less leaf layers in NIR (Thomas & oerther, 1972). However, influenced by which chlorophyll content reduced and many of cell died were large than by cell was destroyed and water content declined in leaf, leading to reflectance of disease leaf was high than health leaf in NIR without significant comparison with VLR.

The spectrum reflectivity for Verticillium wilt was similar to that stress by insect pests, water and nutrition deficiency in VLR, but was different in NIR of cotton leaf (Feng et al., 2004; Wang et al., 1999). Spectrum reflectance for leaf of Verticillium wilt was higher than normal leaf in NIR. While, reflectance was low contrast stress by insect pests, water and nutrition deficiency with health leaf in NIR. The reasons are probable that cotton leaf infected with Verticillium wilt has different mechanism of bio -chemical physiology compare with insect pest, water and nutrition stress.

After infected the cotton by Verticillium wilt, many callus was created .Because callus could block vascular bundle, prevent water to transport within plant, leaf transpiration was reduced and many poisonous matters were produced, that result bio -chemical physiology changed greatly in leaf. When cotton leaf was invaded by spider, leaf transpiration would accelerate, at the same time, chlorophyll was decompounded and anthocyanin was produced due to sharp release by poisonous matters in leaf organization whereas nutrition shortage would led to N、K of elder leaf into new one, water deficiency would reduce leaf transpiration and increase cell liquid concentration,etc. (Jennifer et al., 2004; Lan et al., 1992; Tilling et al., 2007)Though various stresses including disease would have diversity on physiology bio -chemical mechanism in cotton plant, whether this kind of discrepancy was able to cause the respond on spectral dimensionality or not, which will be an important problem for the future research.

In addition, in this context, models -based reflectance, first derivative spectrum and red edge parameters is seen as better models to predict SL of leaf that is a high accuracy compare with predecessor(Demetriades -Shah and Steven 1990). Especially the model established by 723nm of first derivative spectrum attained most significant level to monitor verticilliunm wilt. However, whether higher precision forecasting models could be established between spectrum eigenvalue and SL, and applied models to aviation and spaceflight remote sensing in large area or not , which need to be researched.

5 Conclusions

The research indicated that with the increase of SL, there is better regularity on spectrum characteristic of cotton leaf with Verticillium wilt in different growth stage. With SL increase, spectrum reflectance increased from VLR (4000 – 700nm) to NIR (700 – 1300nm), and 520 – 680nm are special signification. When SL get b2 (25%), cotton leaf infected with Verticillium wilt could be seen as a watershed and diagnosed index used remote sensing in early time. The studying on first derivative spectrum characteristics for Verticillium wilt showed that, wave bands in red side district (680 – 760nm) changed significantly, and from health to slight to extreme severity disease, DR decreased while REP equal moved to the blue, presented special spectrum characteristics of disease. The results also revealed that spectrum could well reflect the occurrence of verticilliun wilt and SL .the paper proved that 437 – 724nm and 909 -1600nm were selected out as sensitive bands to Verticillium wilt SL in cotton leaf. On the base of the above researches, some forecasting models were established, and models in which at 723nm first derivative spectrum would estimate accurately the SL, and it may be acted as a best predicting model to SL of leaf.

Acknowledgement

This work was supported by National High Technology Research and Development Program of China (863 Program, 2006AA103A302, 2006AA10Z207).

References

Adams M L, Philpot W D, Norvell W A (1999) Yellowness index: An application of spectral second derivatives to estimate chlorosis of leaves in stressed vegetation. Int J Remote Sens 20: 3663 – 3675.

Carter G A, Cibula W G, Miller R L (1996) Narrow -band reflectance imagery compared with thermal imagery for early detection of plant stress. J Plant Physio 148: 515 – 522.

Chen B, LI S -k, Wang K R et al. (2007) Studies of Remote Sensing on Monitoring Crop Diseases and Pests. Cotton Sci 19:57 – 63.

Chen P C, Zhang J H, Li M M et al. (2007) Physiological change and hyperspectral character analysis of cotton leaves infested by Tetranychus turkestani. Chin Bull Entomol 44: 61 – 65.

Demetrialdes-Shan T H, Steven M D, Clark JA (1990) High resolution derivative spectra in remote sensing. Remote Sens Environ 33: 55 – 64.

Feng X W, Chen X, Ba0 A M et al. (2004) Analysis on the cotton physiological change and its hyperspectral response under the water stress condition. Arid Land Geogr Chin 2: 250 – 255.

Fitzgerald G J, Maas S J, Detar W R (2004) Spider mite detection and canopy component mapping in cotton using hyperspectral imagery and spectral mixture analysis. Prec Agric 5: 275 – 289.

Hamed Hamid Muhammed (2005) Hyperspectral crop reflectance data for characterising and estimating fungal disease severity in wheat. Biosyst Eng 91:9 – 20.

Hamid Muhammed H, Larsolle A (2003) Feature-vector based analysis of hyperspectral crop reflectance data for discrimination quantification of fungal disease severity in wheat. Biosyst Eng 86: 125 – 134.

Huang M Y, Huang W J, Huang Y D et al. (2004) Spectral reflectance feature of winter wheat single leaf infected with stripe rust and severity level inversion. Trans CSAS Chin 20:176 – 180.

Jennifer L, Fridgen, Varco J J (2004) Dependency of cotton leaf nitrogen,chlorophyll,and reflectance on nitrogen and potassium availability.Am Soc Agron 96: 63 – 69.

Kefyalew Girma, Mosali J, Raun W R et al. (2005) Identification of Optical Spectral Signatures for Detecting Cheat and Ryegrass in winter wheat.Crop Sci 45: 477 – 485.

Lan J H (1992) Ultrastructural changes in cotton leaves affected by carmine spider mite. Southweast Ageric Univ Chin 14: 528 – 530.

Moshoua D, Bravo C, West J et al. (2004) Automatic detection of ‘yellow rust’ in wheat using reflectance measurements and neural networks. Comput Electro Agric 44:173 – 188.

Osborne S L, Schepers J S, Francis D D et al. (2002) Remote sensing: Detection of phosphorus and nitrogen deficiencies in corn using spectral radiance easurements.Agron J 94:1215 – 1221.
Qin Z H, Zhang M H (2005) Detection of rice sheath blight for in-season disease management using multispectral remote sensing. Int J Appl Earth Obs Geoinf.115 – 128.
Thomas J R, Oerther GF (1972). Estimating Nitrogen Content of Sweet Pepper Leaves by Reflectance Measurements. Agron J 64:11 – 13.
Tilling A K, O, Leary G J, Ferwerda J G et al. (2007) Remote sensing of nitrogen and water stress in wheat . Field Crops Res 104:77 – 85.
Wang K, Shen Z Q, Wang R C (1999) Vegetation nutrient condition and Spectrol feature. Remote Sens Land &Resourse 39: 9 – 14.
Wang X Z, Huang J F, Li Y M et al (2003) Correlation between chemical contents of leaves and characteristic variables of hyperspectral on rice field. Transactions CSAE Chin 19:144 – 148.
Wang X Z, Li J L, Tang Y L (2004) Approach the action of derivative spectral for determining agronomic parameters of cotton. J Huanan Agric Univ Chin 25:17 – 21.
Yu G M (1995) The basic principles and methods of remote sensing application to the Identification of waterlog damage. Remote Sens Envion :10:9 – 14.
Zhang M, Liu X, Oneill M (2002) Spectral Discrimination of Phytophthora infestans infection on tomatoes based on principal component and cluster analyses. Inter J Remote Sens 23:1095 – 1107.
Zhang M, Qin Z, Liu X et al (2003) Hyperspectral remote sensing applications in detecting late blight infection on tomatoes. Int J Appl Earth Obs Geoinf 4: 295 – 310.